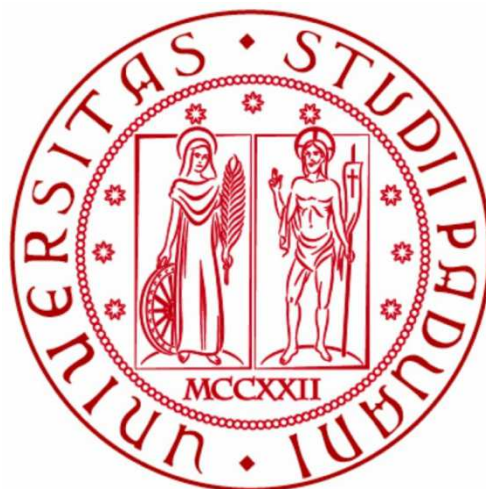


UNIVERSITÀ DEGLI STUDI DI PADOVA

DIPARTIMENTO DI BIOLOGIA

Dottorato in Scienze Molecolari



**DISCOVERY AND CHARACTERIZATION
OF NEW ENE-REDUCTASES**

Relatore: Prof.ssa Elisabetta Bergantino

Dipartimento di Biologia

Tesi Sperimentale di Dottorato
di **Marina Simona Robescu**

Anno Accademico 2017/2018

The research presented in this thesis was carried out in collaboration with F.I.S.-
Fabbrica Italiana Sintetici S.p.A.

30th September 2018

Abstract

Seven new putative ene-reductases (ERs or OYEs) have been identified and selected using bioinformatics tools from different organisms: *Galdieria sulphuraria* (GsOYE), *Chroococcidiopsis thermalis* (CtOYE), *Chloroflexus aggregans* (CaOYE), *Botryotinia fuckeliana* (BfOYE1 and BfOYE4) and *Aspergillus niger* (AnOYE2 and AnOYE8). Based on most updated literature, both the photosynthetic organisms (*Galdieria*, *Chroococcidiopsis* and *Chloroflexus*) and the fungi (*Botryotinia* and *Aspergillus*) result very interesting sources for ERs, that have not been exploited until now.

The cloning and expression strategy used was the same for all the seven putative sequences. After a first trial of expression in *E. coli* BL21(DE3) good over-expression and solubility were obtained for GsOYE, CtOYE, CaOYE and BfOYE1 while for the other three proteins further optimization was necessary. To overcome the low solubility of AnOYE2 and AnOYE8 and the low production of BfOYE4 many strategies have been performed such as lowering the temperature of expression and using chaperons, but also trying other expression hosts (*i.e.* *P. pastoris*).

A biocatalytic characterization was carried out for all proteins. Once verified their activity as ene-reductases *in vitro*, a steady-state study was performed in order to obtain the kinetics parameters. For two enzymes, GsOYE and CtOYE, bioconversions were set-up at the Biocatalysis laboratories of Graz University headed by Prof. Kurt Faber, a main expert of biocatalysis and also of ene-reductases. Finally, a biochemical characterization was carried on in order to determine the thermal stability, pH tolerance and also the three-dimensional structure of the newly discovered enzymes.

Moreover, their application for the hydride-independent isomerization of non-activated C=C-bonds and subsequent reduction is also discussed and the efforts in elucidating this new reactivity are shown in detail.

The work presented in this thesis lead to the discovery of new ERs enlarging the possibility to find out novel and promising biocatalysts for C=C-bond bioreduction but also for other unexpected biocatalytic reactivities.

Riassunto

Sette nuove ene-reduttasi putative sono state identificate attraverso mezzi bioinformatici con un approccio di “genome mining” da diversi organismi: *Galdieria sulphuraria* (GsOYE), *Chroococcidiopsis thermalis* (CtOYE), *Chloroflexus aggregans* (CaOYE), *Botryotinia fuckeliana* (BfOYE1 and BfOYE4) e *Aspergillus niger* (AnOYE2 and AnOYE8). In particolare gli organismi fotosintetici (*Galdieria*, *Chroococcidiopsis* e *Chloroflexus*) e i funghi (*Botryotinia* e *Aspergillus*) sono, ad oggi, fonti di ene-reduttasi rimaste inesplorate.

Per il clonaggio e l'espressione di tutte e sette le sequenze codificanti le proteine di interesse è stata utilizzata una strategia comune. Inizialmente tutte le proteine sono state espresse utilizzando come ospite *E. coli* BL21(DE3); con questa strategia, però, sovraespressione e buona solubilità sono state ottenute solo per quattro delle sette proteine, GsOYE, CtOYE, CaOYE e BfOYE1. Per le altre tre proteine è stata necessaria un'ulteriore ottimizzazione. La bassa solubilità di AnOYE2 e AnOYE8 e la scarsa espressione di BfOYE4 sono state affrontate utilizzando diverse strategie, come la diminuzione della temperatura e l'utilizzo di chaperonine ma anche l'utilizzo di altri ospiti per l'espressione proteica (*P. pastoris*).

Per tutte e sette le proteine ricombinanti è stata condotta una caratterizzazione biocatalitica. Una volta dimostrata la loro attività come ene-reduttasi *in vitro*, sono stati determinati anche i parametri cinetici per i substrati preferiti da ciascun enzima. Nel laboratorio del Professor Kurt Faber dell'Università di Graz, sono state messe a punto bioconversioni per i due enzimi GsOYE e CtOYE, al fine di capirne il profilo di selettività nei confronti di substrati standard.

Infine, è stata condotta anche una caratterizzazione biochimica che ha permesso di determinare la stabilità termica e la tolleranza a diversi pH dei nuovi enzimi identificati; per i quali è stata anche ottenuta la struttura tridimensionale.

Nella tesi è discusso l'utilizzo degli enzimi nell'isomerizzazione NADH-indipendente di substrati con legami C=C non attivati e la loro successiva riduzione, così come gli sforzi per chiarire il meccanismo d'azione di questa nuova reattività scoperta solo di recente.

Il lavoro presentato ha portato alla scoperta di nuove ene-reduttasi, ampliando così il pannello dei biocatalizzatori disponibili per la riduzione del doppio legame C=C ma anche per reattività biocatalitiche inaspettate.

Contents

1. INTRODUCTION	1
1.1 Industrial Biotechnology	2
1.2 Biocatalysis	5
1.3 Asymmetric hydrogenation of C=C-bonds	9
1.3.1 Chemical hydrogenation	9
1.3.2 Enzymatic hydrogenation	10
1.4 Ene-reductases from the family of Old Yellow Enzyme	12
1.4.1 Physiological role	12
1.4.2 Reaction mechanism of OYEs.....	15
1.4.3 OYE subclasses and their structural features.....	21
1.4.4 Synthetic applications.....	31
1.4.5 Versatile catalytic behavior of ene-reductases	34
2. AIM OF THE THESIS	38
3. DISCOVERY, EXPRESSION AND PURIFICATION OF NEW PUTATIVE ERs	40
3.1 Exploring novel putative ERs	42
3.1.1 New putative ERs from prokaryotic organisms	44
3.1.2 New putative ERs from eukaryotic organisms.....	44
3.2 General cloning and expression strategy	50
3.3 GsOYE from <i>Galdieria sulphuraria</i>	52
3.4 CtOYE from <i>Chrococidiopsis thermalis</i>	55
3.5 CaOYE from <i>Chloroflexus aggregans</i>	58
3.6 BfOYE1 and BfOYE4 from <i>Botryotinia fuckeliana</i>	60
3.6.1 Cloning of <i>BfOYE1</i> and <i>BfOYE4</i>	60
3.6.2 Expression and purification of <i>BfOYE1</i> and <i>BfOYE4</i>	61
3.7 AnOYE2 and AnOYE8 from <i>Aspergillus niger</i>	70
3.8 OYE2 and OYE3 expression and purification	74
4. CHARACTERIZATION OF NEWLY DISCOVERED ERs	77
4.1 Preliminary substrate spectrum	78
4.1.1 Substrate spectrum of ERs isolated from photosynthetic organisms.....	80
4.1.2 Substrate spectrum of ERs isolated from fungi	82
4.2 Steady-state kinetics	85
4.3 Conversions	88
4.3.1 GsOYE and CtOYE bioreduction of α,β -unsaturated carbonyl compounds....	88
4.3.2 Kinetic resolution of 5-phenyl-2-cyclohexenone	93
4.3.3 GsOYE and CtOYE bioreduction of α,β -unsaturated nitroalkenes	94
4.4 Oligomeric state investigation	101
4.4.1 Classical OYEs.....	101
4.4.2 Thermophilic-like OYEs	102
4.5 pH optimum	106
4.6 Determining unfolding temperatures	107
4.6.1 Classical OYEs.....	107
4.6.2 Thermophilic-like OYEs	110
5. CRYSTAL STRUCTURE DETERMINATION	114
5.1 General crystallization strategy	115
5.2 GsOYE and CtOYE crystal structure	117
5.2.1 Structural analysis of GsOYE and CtOYE	119
5.2.2 Overall GsOYE and CtOYE structural comparison	131
5.2.3 GsOYE and CtOYE ene-reductase vs nitro-reductase activity.....	134
5.3 BfOYE4 and CaOYE crystallization and refinement	138
5.3.1 Structural analysis of <i>BfOYE4</i> and <i>CaOYE</i>	140

5.3.2	Overall <i>Bf</i> OYE4 and <i>Ca</i> OYE structural comparison.....	- 151 -
5.4	OYE2 and OYE3 crystal structure	- 156 -
5.4.1	Structural analysis of OYE2 and OYE3	- 159 -
5.4.2	Overall OYE2 and OYE3 structural comparison.....	- 164 -
6.	Hydride-independent asymmetric isomerization of non-activated C=C-	bonds mediated by OYEs..... - 167 -
6.1	Stereoselective isomerization of α-AL to β-AL.....	- 169 -
6.2	Role of pH in the isomerization reaction	- 170 -
6.3	Understanding the mechanism of the isomerization reaction.....	- 172 -
6.3.1	Mutagenesis	- 172 -
6.3.2	Mutants crystal structure.....	- 176 -
6.3.3	<i>Gs</i> OYE crystal structure in complex with angelica lactones	- 179 -
6.3.4	Hypothetical mechanism of reaction in <i>Gs</i> OYE.....	- 182 -
6.4	Cascades for the reduction of α-AL to γ-valerolactone.....	- 182 -
6.4.1	Reaction parameters investigation.....	- 182 -
6.4.2	One-pot one-step cascades	- 184 -
6.4.3	One-pot two-step cascades	- 186 -
7.	Summary and Outlooks	- 189 -
7.1	Summing-up.....	- 190 -
7.2	Outlooks	- 192 -
8.	MATERIALS AND METHODS	- 193 -
8.1	Materials	- 194 -
8.1.1	Primers	- 195 -
8.1.2	Nutrition media.....	- 200 -
8.1.3	Bacterial and yeast strains	- 201 -
8.1.4	Expression vectors	- 202 -
8.2	Methods	- 205 -
8.2.1	Cloning	- 205 -
8.2.2	Expression in <i>E. coli</i>	- 207 -
8.2.3	<i>Bf</i> OYE4 expression in <i>Pichia pastoris</i>	- 210 -
8.2.4	SDS-PAGE and UREA-PAGE	- 211 -
8.2.5	Immunoblot assay.....	- 212 -
8.2.6	Purification and enzymes concentration determination	- 212 -
8.2.7	Activity assay and steady- state kinetics.....	- 213 -
8.2.8	Conversions and GC/GC-MS analysis	- 215 -
8.2.9	Angelica lactone isomerization: conversions and enantiomeric excess determination	- 218 -
8.2.10	Oligomeric state determination by SEC chromatography	- 219 -
8.2.11	Oligomeric state determination by native PAGE	- 221 -
8.2.12	ThermoFluor assay	- 221 -
8.2.13	Activity assay to determine the pH <i>optimum</i>	- 221 -
8.2.14	Three-dimensional structure determination	- 222 -
	BIBLIOGRAPHY	223
	APPENDIX.....	237

Abbreviations

A

α -AL	α -Angelica lactone
β -AL	β -Angelica lactone
ADH	Alcohol dehydrogenase
AnOYE2	<i>Aspergillus niger</i> Old Yellow Enzyme 2
AnOYE8	<i>Aspergillus niger</i> Old Yellow Enzyme 8
AOX	Alcohol oxidase
APIs	Active pharmaceutical ingredients
ArOYE6	<i>Ascochyta rabiei</i> Old Yellow Enzyme 6
ASU	Asymmetric unit

B

BfOYE1	<i>Botryotinia fuckeliana</i> Old Yellow Enzyme 1
BfOYE4	<i>Botryotinia fuckeliana</i> Old Yellow Enzyme 4
BiNAP	(2,29-bis(di- phenylphosphanyl)-1,19-binaphthyl)
Blast	Basic Local Alignment Search Tool
BMGY	Buffered Glycerol-complex medium
BMMY	Buffered Methanol-complex medium
BVMO	Baeyer–Villiger-monooxygenase

C

CaOYE	<i>Chloroflexus aggregans</i> Old Yellow Enzyme
CrS	Chromate reductase from <i>Thermus scotoductus</i> SA-01
CtOYE	<i>Chroococcidiopsis thermalis</i> Old Yellow Enzyme
CYPs	Cytochrome P450 monooxygenases

D

De	Diastereoisomeric excess
DMSO	Dimethyl sulphoxide
DrER	<i>Deinococcus radiodurans</i> ene-reductase

E

EasA	Ergot alkaloid synthase from <i>Aspergillus fumigatus</i>
Ee	Enantiomeric excess
E-factor	Environmental factor
EnoRs	Enoate reductases
ERs	Ene-reductases
EtOAc	Ethyl acetate
E-value	Enantioselectivity
EWG	Electron-withdrawing group

F

FAD	Flavin adenine dinucleotide
FMN	Flavin mononucleotide
FOYE	<i>Ferrovum</i> Old Yellow Enzyme

G	
GAP	Glyceraldehyde-3-phosphate-dehydrogenase
GC	Gas chromatography
GC-MS	Gas chromatography-Mass spectrometry
GeoER	<i>Geobacillus</i> sp.30 ene-reductase
GkOYE	<i>Geobacillus kaustophilus</i> Old Yellow Enzyme
GsOYE	<i>Galdieria sulphuraria</i> Old Yellow Enzyme
H	
HPLC	High performance liquid chromatography
I	
IMAC	Immobilized Metal Affinity Chromatography
IPTG	isopropyl- β -D-thiogalactopyranoside
J	
JA	Jasmonic acid
K	
k_{cat}	catalytic constant
Km	Michaelis constant
KYE	<i>Kluyveromyces lactis</i> ene-reductase
L	
LB	Luria broth
LTD	Leukotriene B ₄ dehydrogenase
M	
MCP	2-methyl-cyclopenten-1-one
MDRs	Flavin-independent medium chain dehydrogenase/reductases
MR	Morphinone reductases from <i>Pseudomonas putida</i>
N	
NAD(P)H	Nicotinamide adenine dinucleotide (phosphate)
NADH ₄	1,4,5,6-tetrahydroNADH
NCBs	Nicotiamide coenzyme biomimetics
NemA	N-ethylmaleimide reductase from <i>Escherichia coli</i>
NerA	Glycerol trinitrate reductase from <i>Agrobacterium radiobacter</i>
NoER	Ene-reductase from <i>Nostoc</i> sp. PCC 7120
NtDBR	<i>Nicotiana tabacum</i> flavin-free double bond reductase
O	
OD	Optical density
(9 <i>S</i> ,13 <i>S</i>)-OPDA	cyclopentenone (9 <i>S</i> ,13 <i>S</i>)-12-oxophytodienoate
OPR1	12-Oxophytodienoate reductase 1 from <i>Solanum lycopersicum</i>
OPR3	12-Oxophytodienoate reductase 3 from <i>Solanum lycopersicum</i>
OYEs	Old Yellow Enzymes
OYE1	Old yellow enzyme 1 from <i>Saccharomyces pastorianus</i>
OYE2	Old yellow enzyme 2 from <i>Saccharomyces pastorianus</i>
OYE2.6	Old yellow enzyme from <i>Pichia stipitis</i> 2.6

OYE3	Old yellow enzyme 3 from <i>Saccharomyces pastorianus</i>
OYERo2	<i>Rhodococcus opacus</i> old yellow enzyme 2
P	
Pd/C	Carbon supported palladium catalysts
PETNR	Pentaerythritol tetranitrate reductase from <i>Enterobacter cloacae</i>
PGF _{2α}	Prostaglandin F _{2α}
PGH ₂	9,11-endoperoxide-prostaglandin H ₂
pHBA	para-hydroxybenzaldehyde (4-hydroxybenzoic acid)
Q	
QnoR	Quinone reductase-like ene-reductase
R	
RmER	<i>Ralstonia metallidurans</i> ene-reductase
r.m.s.d.	Root mean square deviation
S	
SDRs	Short chain dehydrogenase/reductases
SDS-PAGE	Sodium dodecyl sulphate polyacrylamide gel electrophoresis
SEC	Size Exclusion Chromatography
SYE1	<i>Shewanella oneidensis</i> Old Yellow Enzyme 1
T	
TcOYE	<i>Trypanosoma cruzi</i> Old Yellow Enzyme
Tm	Temperature of melting
TNT	2,4,6-Trinitrotoluene
TOYE	<i>Thermoanaerobacter pseudethanolicus</i> Old Yellow Enzyme
TsOYE	<i>Thermus scotoductus</i> Old Yellow Enzyme
V	
γ-VL	γ-Valerolactone
X	
XenA	Xenobiotic reductase from <i>Pseudomonas putida</i>
Y	
YersER	<i>Yersinia bercovieri</i> ene-reductase
YPD	Yeast extract Peptone Dextrose medium
YPDS	Yeast extract Peptone Dextrose medium with Sorbitol
YqjM	Old Yellow Enzyme from <i>Bacillus subtilis</i>

1. INTRODUCTION

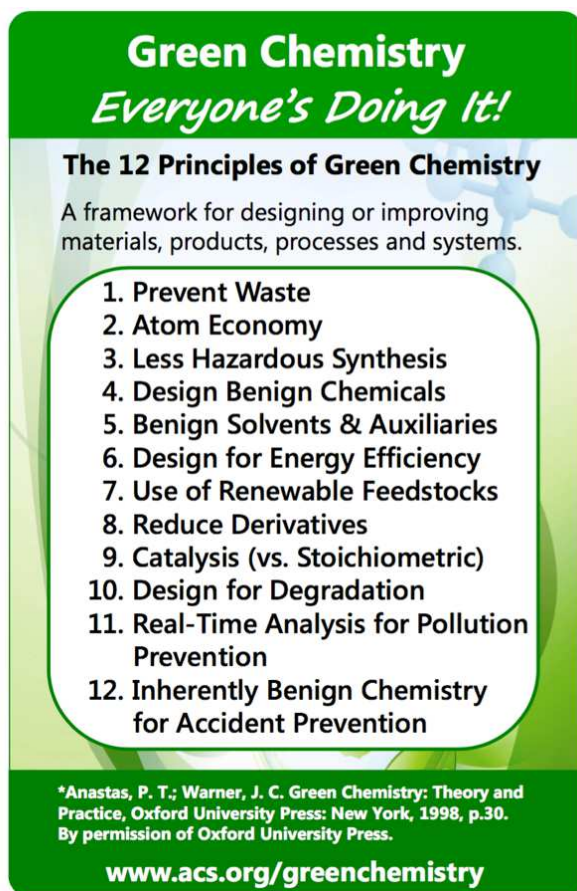
White biotechnology (or industrial biotechnology) comprises all the applications of biotechnology related to industrial processes. White biotechnology is focused onto the design of low resource-consuming processes and products, making them more energy efficient and less polluting than established ones. The use of microorganisms in chemicals production, the design and production of new materials (bioplastics, textiles) and the development of new sustainable energy sources such as biofuels (bioethanol, biodiesel) are only a few examples of white biotechnology [1, 2].

1.1 Industrial Biotechnology

Industrial biotechnology is a multidisciplinary technology, based on the integrated application of biochemistry, microbiology, molecular genetics and process technology to develop useful processes and products, using microbial, animal or plant cells, their organelles or enzymes as biocatalysts. It is also referred to as “white biotechnology” for the positive environmental aspects derived from its application [3]. As a matter of fact, this field of biotechnology is a main contributor to “green chemistry”. Green chemistry attains the design of chemical products and processes that reduce or eliminate the use and generation of hazardous substances; white biotechnology answers many of the so-called “12 principles of Green chemistry” (Fig. 1), postulated by Prof. Anastas in 1998 [4], and is expected to realize, therefore, substantial advantages for the environment, consumers and industry [5].

Nowadays the green chemistry concept is widespread both in industry and in academia. “It is better to prevent the formation of waste rather than to clean it up after the fact” is known as the “1^o principle” of green chemistry. It summarizes very well the rationale and the aim of green chemistry philosophy: to eliminate the problem of waste generation by working on the design of the process itself so that it would produce the least amount of waste. This avoids the necessity for the waste treatment later on. For the same reasons, other principles enhance the necessity to maximize the incorporation of all starting materials into the final product (2^o principle) as well as the choice of raw materials (reagents and solvents) that have not to be toxic for humans and the environment, and that possibly derive from renewable resources (3^o, 4^o and 7^o principles). The reactions should take place in mild conditions, room temperature and pressure (6^o principle), thus contributing to reduce pollution and energy consumption.

Moreover, catalytic processes should be preferred rather than stoichiometric ones, thus reducing also the use of derivatives (8° and 9° principles).



Thanks to the application of the 12 principles of green chemistry is not so hard to imagine that chemistry can turn toward a *green* direction, thus becoming absolutely sustainable [4].

The powerful tools provided by industrial biotechnology and a growing awareness of the environmental issues have recently led to the diffusion of industrial biotechnology in many sectors of the chemical industry, particularly in fine chemicals but equally so for bulk chemicals such as plastics and fuels, with very positive results with regard to sustainability as well as industrial competitiveness [3].

Figure 1. Green Chemistry principles.

Fermentation of microorganisms and/or the use of isolated enzymes for synthetic purposes are perhaps the most representative applications of white biotechnology. The fermentation technology is used to produce a wide variety of bulk and fine chemicals like ethanol, lactic acid, citric acid, vitamins, amino acids, solvents, antibiotics, biopolymers, bio-pesticides, industrial enzymes, bio-colorants, bio-surfactants, alkaloids and steroids. Due to their structural complexity, for several of these products the fermentation is the only possible industrial production method [3]. Table 1 shows the world production amounts and prices for a number of these fermentation products. These products are obtained *via* industrial fermentation by converting raw materials derived from the waste of other industrial sectors (*i. e.* carbohydrates, oils and fats, hydrocarbons) into new, high-added value products, according to the modern concept of “bio-refinery” [6, 7].

Table 1. World production amounts and prices for a number of fermentation products (modified from [3]).

	World production (ton/year)	World market price (euro/kg)
Bio-ethanol	38000000	0,4
L-Glutamic acid (MSG)	1500000	1,5
Citric acid	1500000	0,8
L-Lysine	350000	2
Lactic acid	250000	2
Vitamine C	80000	8
Gluconic acid	50000	1,5
Antibiotics (bulk products)	30000	150
Antibiotics (specialities)	5000	1500
Xanthan	20000	8
L-Hydroxyphenylalanine	10000	10
Dextran	200	80
Vitamin B12	3	25000

Scientists have now different toolsets to specifically manipulate the genetic material of microorganisms. Through metabolic engineering the metabolism of microorganisms can be modified, while through genetic engineering genes derived from higher organisms (plants and animals) or other microorganisms (yeast, bacteria, virus, algae) can be expressed after being inserted into industrial microorganisms. In this way, new gene products can be made or new metabolic pathways can be created to produce chemical substances with high efficiency *via* industrial fermentation processes. Moreover, scientists are now attempting to create *de novo* genomes in synthetic microorganisms easier to manipulate than those available in Nature [8].

Enzymes are an alternative to using microorganisms *in toto*. They are catalytically active proteins able to run very specific and efficient chemical reactions. They work without needing extreme temperatures, high pressures or harsh conditions as often required in chemical synthetic processes. Enzymes have become very important in a wide range of industrial sectors because of the biotransformations that they can carry out [3]. Examples of established applications of enzymes at a large scale involve the starch, detergent and feed sector. A key class of enzymes in starch sector is represented by α -amylases. These enzymes are able to hydrolyze starch to glucose, one of the most important renewable raw material [9]. The detergent sector represents another huge application area for enzymes. Here, proteases and lipases are used to break down protein and fat stains on

clothing [10-12]. The feed industry is another important market. Phytase from the fungus *Aspergillus niger* is a phosphatase that enhances phosphate bioavailability in the gut and therefore has been increasingly employed as animal feed additive to release phosphate from phytic acid from plants seeds and grains. Thus, less additional phosphate has to be added to animal feed, with considerable environmental benefits [13, 14].

Industrial enzymes represent a two billion dollar sector in industrial biotechnology. At industrial scale the use of enzymes as biocatalysts (used in free or immobilized form) is rapidly developing. In fine chemical/APIs production, one or two biotransformation steps are mostly present within complex synthetic schemes of synthesis [3].

1.2 Biocatalysis

Enzymes have been used for thousands of years to produce and preserve foodstuffs such as cheese, beer, vinegar, and wine. So, biocatalysis is anything but a “modern” technology or concept. In 1858 Louis Pasteur placed a milestone in biocatalysis by treating an aqueous solution of racemic tartaric acid ammonium salt with a culture of the mold *Penicillium glaucum*, leading to the consumption of (+)-tartaric acid and concomitant enrichment of the (–)-enantiomer. This can be considered the first enzyme-catalyzed kinetic resolution [15].

In the organic synthesis sector, the use of biocatalysts, as isolated enzymes and also whole cells, is one of the most eco-compatible technology used both in academia and industry (fine chemicals, pharmaceuticals, food, plastics, cosmetics) [16]. This technology often offers major advantages in terms of enhanced reaction selectivity, reduced costs of raw materials, lower energy costs, improved safety and sustainability of production [3]. The diffusion of this technology in the industrial sector and the introduction of the E(nvironmental)-factor [17] have changed the concept of “efficiency” of an industrial process, which is no more focused just on the final yield but takes into account also the reduction of waste generated and the optimization of recyclable biocatalysts [18].

The E-factor was proposed in the late 1980s for assessing the environmental impact of industrial manufacturing processes (kg waste/kg product) and the now well-known Table of E-factors (Table 2) is used to measure the waste in different segments of the chemical industry.

Table 2. E-factors in the chemical industry (modified from [17])

Industry segment	Product tonnage	E-Factor (kg waste/kg product)
Oil refining	10^6 - 10^8	<0.1
Bulk chemicals	10^4 - 10^6	<1-5
Fine chemicals	10^2 - 10^4	5-50
Pharmaceuticals	10 - 10^3	25-100

The E-factor is the actual amount of waste produced in the process, defined as everything but the desired product. It takes the chemical yield into account and includes reagents, solvent losses, all process aids and, in principle, even fuel (although this is often difficult to quantify). A higher E-factor means more waste and, consequently, greater negative environmental impact. The ideal E-factor is zero [17].

Accumulated work during the past decade has shown that there are (surprisingly) few barriers to the use of enzymes and whole cells as biocatalysts in organic synthesis. Isolated enzymes are typically used for hydrolytic or isomerization reactions. Whole cells are often used for synthetic reactions that require cofactors which must be regenerated, because although cofactor regeneration *in vitro* is possible, it is generally easier and less expensive to regenerate cofactors in metabolically active cells. Both isolated enzymes and whole cells are used in industry today, and are an active area of research [19].

The physical state of biocatalysts used for biotransformations can be very different: isolated enzymes, more or less purified, or whole microorganisms, either in free or immobilized form. The choice of their physical state depends on many factors, such as (i) the type of reaction, (ii) if there are cofactors to be recycled and (iii) the scale at which the biotransformation has to be performed [20]. The general *pros* and *cons* of using isolated enzymes rather than whole cell systems are outlined in Table 3.

The use of isolated enzymes guarantees a higher specificity compared to a whole cell system, where side reactions can occur due to uncontrolled cellular metabolism. However, enzyme solubility in water makes more difficult the recovery of the protein or its preparation for continuous processes.

Enzymes are powerful catalysts: they are able of accepting a wide variety of complex molecules as substrates, and are exquisitely selective, catalyzing reactions with high enantio- and regio- selectivities.

Table 3. Isolated enzymes *versus* whole cell systems (modified from [20]).

Biocatalyst	Form	Pros	Cons
Isolated enzymes	Any	Simple apparatus, simple workup, better productivity due to higher concentration tolerance	Cofactor recycling necessary, limited enzyme stabilities
	Dissolved in water	High enzyme activities	Side reactions possible, lipophilic substrates insoluble, workup requires extraction
	Suspended in organic solvents	Easy to perform, easy workup, lipophilic substrates soluble, enzyme recovery easy	Reduced activities
	Immobilized	Enzyme recovery easy	Loss of activity during immobilization
Whole cells	Any	No cofactor recycling necessary, no enzyme purification required	Expensive equipment, tedious workup due to large volumes, low productivity due to lower concentration tolerance, low tolerance of organic solvents, side reactions likely due to uncontrolled metabolism
	Growing culture	Higher activities	Large biomass, enhanced metabolism, more byproducts, process control difficult
	Resting cells	Easier work-up, reduced metabolism, fewer by-products	Lower activities
	Immobilized cells	Cell reuse possible	Lower activities

As a result, these biocatalysts can be used in both simple and complex transformations without the need for tedious protection and deprotection steps that are common in enantio- and regioselective conventional organic synthesis. Due to their high selectivity, enzymes can catalyze reactions with few by-products formation, thus with low waste generation. For these reasons, enzymes often represent an environmentally friendly alternative to conventional chemical catalysts [19]. Nevertheless, industrial application of enzymes is often hampered by a lack of long-term operational stability and difficult recovery and re-use of the biocatalyst. Moreover, the toolbox of (commercially) enzymes available is limited and often their applicability is exclusive for selected reactions. Isolated enzymes are also difficult to recover and re-use and often require costly cofactors for the catalysis [21].

Nowadays, these problems are partially, or almost completely, solved. Thanks to the progress of molecular biology and high-throughput sequencing techniques, an increasing number of enzymes have been produced in recombinant form and have become commercially available. In addition, thanks to protein engineering techniques and/or physical methods (*i.e.* immobilization), their stability towards reaction conditions (*i.e.* temperature, pH, ionic strength and co-solvents) and their substrate specificity, can be modified to encounter the characteristics required by industry [22, 23]. The high cost of cofactors usually prevents from their stoichiometric use in large-scale reaction, thus, enzymatic systems for cofactor regeneration or more economical synthetic biomimetics can be a valid solution [24].

Therefore, enzymes are of great interest from an industrial point of view, enabling the synthesis of a large variety of hard-to-synthesize compounds under mild reaction conditions. Redox reactions are very important at industrial level representing 30% of the industrial biocatalytic applications of enzymes [21].

1.3 Asymmetric hydrogenation of C=C-bonds

The asymmetric reduction of prochiral C=C-double bonds is a powerful tool in synthetic organic chemistry for the preparation of optically active molecules with (up to two) stereogenic centers. The importance of catalyzed asymmetric hydrogenation reactions is highlighted by the Nobel prize in Chemistry awarded in 2001 to William Knowles for its pioneering work on the catalytic asymmetric hydrogenation of α -acylaminoacrylic acid for the production of L-DOPA, a widely used drug for the treatment of Parkinson's disease [25]. Several metal-based or organocatalytic approaches have been developed during the years for the production of a wide range of enantiopure synthons. However, in the last twenty years "greener" methods based on the use of either isolated enzymes or whole-cell biocatalysts have become increasingly important in the production of fine chemicals and pharmaceuticals [26].

1.3.1 Chemical hydrogenation

Historically, the first asymmetric hydrogenation of simple prochiral olefins was performed using chiral phosphine- rhodium complexes in homogeneous solution. However, low enantioselectivities were achieved [27, 28]. Later on, the advent of the chiral ligand BiNAP (2,29-bis(di- phenylphosphanyl)-1,19-binaphthyl) in complex with ruthenium fulfill better performances either in terms of extension of substrate *spectrum* or enantioselectivity [29]. Nowadays, heterogeneous catalysts are widely employed in the selective hydrogenation of C=C-bonds, due to simple recovery and recycling of the precious metal. Carbon supported palladium (Pd/C) catalysts, usually in solution with additives like pyrimidines, amines and diphenylsulfide, are routinely used for the selective reduction of C=C-bond.

Despite outstanding performances have been reported for Pd/C catalysts different drawbacks have also to be considered. The reaction takes place using high pressure H₂ and palladium, which is highly reactive and inflammable, beyond the use of organic solvents. Leaching of Pd from the carbon support is also highly possible due to the weak interactions between the metal and the support, thus with subsequent contamination of the final product. Moreover, protecting groups have to be employed in order to obtain a chemo-selective reaction and just *cis*-addition has been reported [30]. The only example of *trans*-hydrogenation reported in literature, is the metal-free organocatalysis with the

use of iminium catalyst and Hantzsch ester as hydride source. This process suffers from low atom economy as molar amount of catalysts are needed [31, 32].

Therefore, the application of biocatalysts represents a sustainable alternative to metal-based hydrogenation. Biocatalytic hydrogenations avoid the use of metals as well as hazardous and dangerous chemicals. Moreover, as already mentioned, enzymes are stereospecific and operate in mild reaction conditions [33].

1.3.2 Enzymatic hydrogenation

The application of enzymes for the reduction of non-activated C=C-bonds is a highly sought reaction in organic synthesis, although not widely spread in Nature. Few mechanisms that allow this reaction to occur, are naturally present in cells but all of them require several different chemical reactions necessary to functionalize the carbon atoms adjacent to the C=C-bond, thus activating it before the actual reduction takes place. Indeed, enzymes able to catalyze such a reaction in a single step have not yet been isolated and characterized [34].

Contrariwise, the bioreduction of activated C=C-bonds, is extremely widespread in all sorts of organisms. Three main classes of enzymes have been identified and used as biocatalysts for the reduction of activated C=C-bonds (Fig. 2). Ene-reductases (ERs) from the flavin mononucleotide (FMN)-containing Old Yellow Enzyme (OYE) family of oxidoreductases (EC 1.6.99.1) are the main class of enzymes involved in C=C-double bond bioreduction. These enzymes act on double bonds activated by one or more electron withdrawing groups (EWGs), such as α,β -unsaturated carbonyl compounds, nitroolefins and maleimides [35]. The second class of enzymes able to reduce the activated C=C-bond is that of enoate reductases (EnoRs) (EC 1.3.1.31). These enzymes have been firstly isolated from anaerobic *Clostridia* sp. and contain flavin adenine dinucleotide (FAD) and an iron–sulphur cluster [4Fe–4S] in their structure. However, enoate reductase are much more difficult to isolate and employ in preparative chemical transformations compared to ene-reductases, due to their extreme sensitivity to molecular oxygen. Moreover, their substrate scope is generally limited to 2-enoate substrates [36]. Nevertheless, in the last years, different homologues from this family have been identified and employed under anaerobic conditions and as whole cell biocatalysts for the synthesis of dihydrochalcones [37] and adipic acid [38]. Few ene-reductases that do not belong to the OYE family are flavin-independent medium chain dehydrogenase/reductases (MDR; EC 1.3.1.x) and

short chain dehydrogenase/reductases (SDR; EC 1.1.1.207-8). MDR and SDR superfamily have generally narrow substrate spectra and low enzyme activities. Typical substrates include aromatic and monocyclic alkenes containing aldehydes or ketones as activating groups [34].

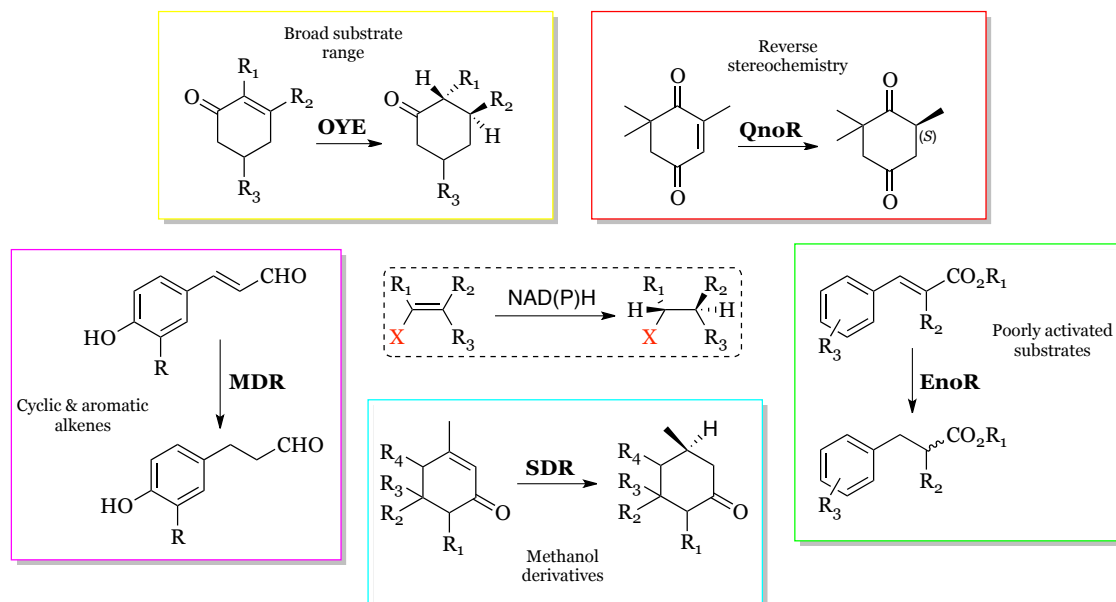


Figure 2. Asymmetric activated alkene reduction catalyzed by ene-reductases (ERs). Enzyme classes: OYE = Old Yellow Enzyme; EnoR = oxygen-sensitive enoate reductases; SDR = short-chain dehydrogenase/reductase salutaridine/menthone reductase-like subfamily; MDR = medium-chain dehydrogenase/reductase leukotriene B₄ dehydrogenase subfamily; QnoR = quinone reductase-like ene-reductase (modified from [39]).

The addition of [2H] occurs with exclusive *anti*-stereochemistry (*trans*-addition), thus showing stereo-complementarity to the heterogeneous metal-catalyzed hydrogenation. There is only one exception reported in literature of enzymatic *syn*-hydrogenation performed by *Nt*D₄BR from *Nicotiana tabacum* on verbenone, carvone, and 2-cyclohexen-1-one. This flavin-independent enzyme belongs to the leukotriene B₄ dehydrogenase (LTD) subfamily of the zinc- independent, medium chain dehydrogenase/reductase superfamily of enzymes [40]. In addition, two active non-OYE homologues possessing completely different protein fold but mirror-image orientation of the critical catalytic active site residues (“catalophore”) were identified through mining of structural databases. These proteins showed inverted stereopreference compared to ene-reductases, allowing the access of the substrate to the opposite (*re-*) face of the flavin, thus, acting as enzyme-enantiomers [41].

1.4 Ene-reductases from the family of Old Yellow Enzyme

Ene-reductases (ERs), from the Old Yellow Enzyme (OYE) family (E.C. 1.6.99.1), have received much attention and have been extensively investigated during the last years for their biocatalytic potential. These nicotinamide-dependent flavoproteins are versatile biocatalysts catalyzing the reduction of α,β -unsaturated ketones, aldehydes, nitroalkenes, carboxylic acids, and derivatives, affording the synthesis of molecules with a variety of biotechnological and pharmaceutical applications. These enzymes have also been employed in the bioremediation of explosive-contaminated soils [42] since they can reduce nitrate esters, nitroglycerin and nitroaromatic explosives [43-45].

1.4.1 Physiological role

OYE-like enzymes are ubiquitous in nature and have been found in yeasts, bacteria, plants and parasitic eukaryotes [46]. Nevertheless, their physiological role is still not elucidated, apart from few homologues. Different studies have suggested a common physiological role for OYE-homologues in the detoxification of electrophilic compounds both endogenous and xenobiotic and in the response to the oxidative stress [46].

It has been demonstrated that the expression of YqjM from *Bacillus subtilis* is strongly induced *in vivo* by the aromatic nitro-compound 2,4,6-trinitrotoluene (TNT) and by hydrogen peroxide with high levels of protein detectable already after few minutes incubation, suggesting a role in detoxification and in the oxidative stress response [47]. OYEs from *Corynebacterium glutamicum* [48] and *Shewanella oneidensis* [49] are also known for their involvement in the oxidative stress response.

However, the involvement of different OYE-homologues in specialized metabolic pathways has also been described in different organisms: jasmonic acid biosynthesis in plants [50], ergot alkaloid biosynthesis in *Aspergillus fumigatus* [51] and prostaglandin F_{2 α} biosynthesis in *Trypanosoma cruzi* [52]. OYEs from plants such as *Arabidopsis thaliana* [53], *Solanum lycopersicum* [50] and *Oryza sativa* (rice) [54] catalyze the reduction of cyclopentenone (9*S*,13*S*)-12-oxophytodienoate [(9*S*,13*S*)-OPDA] to the corresponding cyclopentanone (Fig. 3) in the biosynthesis of the plant hormone jasmonic acid (JA). JA and its derivatives have several roles in plant defense and development such as plant

resistance responses against herbivores and pathogens, male and female reproductive development and seed germination. Moreover, plant OYEs are known to be involved also in the detoxification of oxygenated lipids generated during the oxidative burst in wounded and diseased plant tissues [55], while they seem involved as well as in the metabolism of α,β -unsaturated carbonyl compounds produced during insect attack and bacterial pathogenesis [56].

Ergot alkaloids are secondary metabolites produced by different filamentous fungi species used as drugs thanks to their wide array of pharmacological effects. In *A. fumigatus* cells ergot alkaloids are synthesized starting from the condensation of tryptophan and dimethylallyl diphosphate (DMAPP) to form the intermediate chanoclavine-I aldehyde, which is further transformed in festuclavine (Fig. 4). It has been demonstrated that the conversion of chanoclavine-I aldehyde to dihydrochanoclavine aldehyde in *A. fumigatus* requires an OYE homologue enzyme (EasA) [51]. Moreover, in the parasitic trypanosome *T. cruzi*, the etiological agent of Chagas disease, it has been discovered that an OYE homologue (*TcOYE*) is involved in the reduction of 9,11-endoperoxide PGH_2 to $\text{PGF}_{2\alpha}$ (Fig. 5). Surprisingly, *TcOYE* was also shown to reduce a variety of trypanocidal drugs such as the diterpene komaroviquinone, nifurtimox, and nitrobenzylphosphoramidate mustards, suggesting an important role as a key enzyme in drugs metabolism [57]. These compounds could undergo either one- or two-electron reduction [58].

In addition, Nizam *et al.* [59] have reported that many fungal species contain in their genome more than one gene (from 1 to 22 genes) coding for OYE enzymes with different subcellular localization. This wide subcellular distribution (*e.g.* cytoplasm, mitochondria, cytoskeleton, nucleus, peroxisome and extracellular) could suggest different physiological functions for these enzymes within the same species. The differential expression of these isoenzymes is thought to be triggered by external stimuli such as of toxic substrates or different types of nutrients as well as physico-chemical parameters of the surrounding environment [60]. Finally, several bacterial OYEs, such as pentaerythritol tetranitrate (PETN), are known for their ability to reduce a range of xenobiotic explosive compounds (*e.g.* nitroglycerine and TNT) [45]. Moreover, certain prokaryotic OYEs are active with morphine alkaloids [61] and N-ethylmaleimide [62]. However, these compounds are far from being considered the real substrates for OYE homologues as they are not synthesized *in vivo* by these organisms. In the same way, many OYE members

have been reported as being able to reduce some steroids [63] but although their ability to bind and transform steroids their involvement in sterol metabolism has not yet been proved.

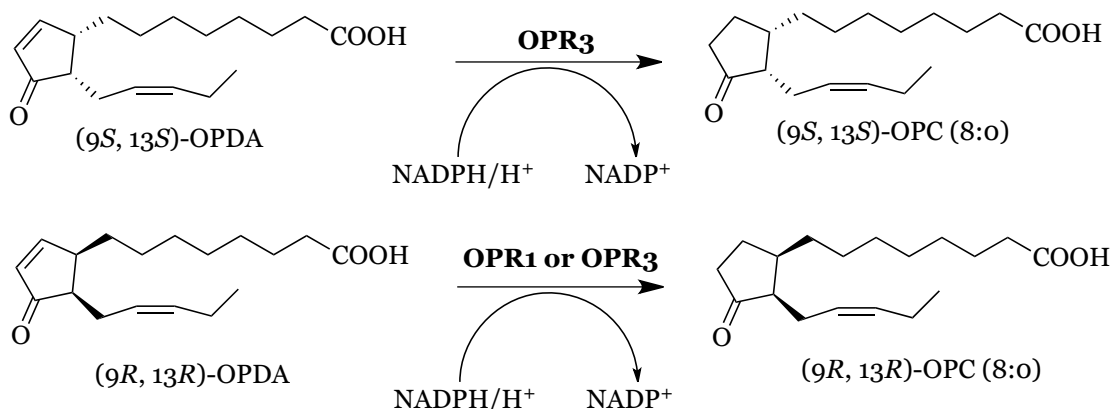


Figure 3. Scheme of the substrate specificity of *SIOPR* isoforms. Whereas OPR3 reduces both *cis*-OPDA enantiomers, OPR1 only reduces (9*R*,13*R*)-OPDA [64].

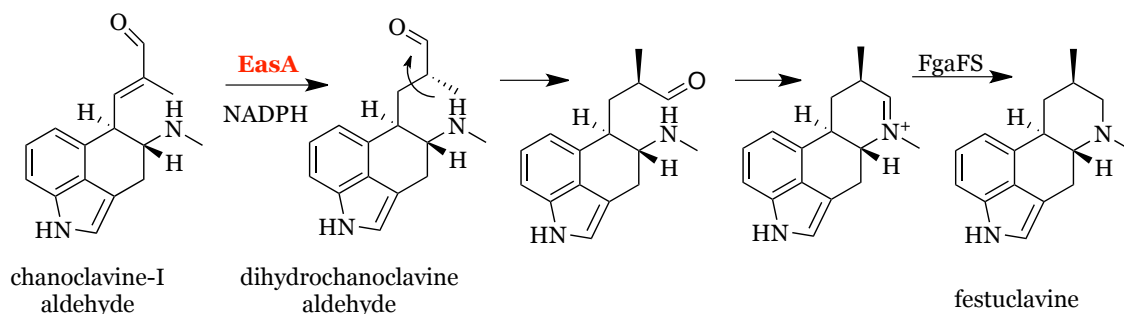


Figure 4. The reaction catalyzed by the Old Yellow Enzyme EasA from *A. fumigatus*, the conversion of chanoclavine-I aldehyde to dihydrochanoclavine, is labeled in red. The next two reactions are hypothesized to be spontaneous. The final reaction for the generation of festuclavine is catalyzed by FgaFS, festuclavine synthase (modified from [65]).

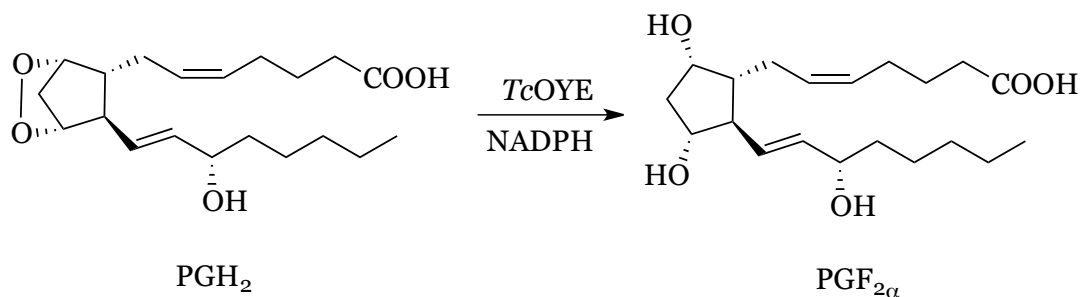


Figure 5. Reduction of PGH₂ to PGF_{2α} mediated by TcOYE [57, 58].

1.4.2 Reaction mechanism of OYEs

The hydrogenation reaction mediated by OYEs proceeds via a hydride transfer mechanism involving two half reactions: a first step in which the flavin is reduced at the expense of NAD(P)H cofactor followed by a second step in which the reduction of the activated alkene occurs with concomitant flavin re-oxidation (Fig. 6) The half-reactions of OYEs have been extensively studied since their discovery enabling a detailed and complete understanding of the reaction mechanism [43, 66, 67].

It has been demonstrated that the reaction has a ping-pong bi-bi mechanism where both the oxidative and reductive substrates share overlapping binding sites [63, 68, 69]. The reaction cycle begins with the reductive half reaction during which the NAD(P)H cofactor enters the active site and interacts through hydrogen bonding with two conserved active-site residues. After this interaction, the nicotinamide C4 atom, the hydride donor, is opportunely positioned above the N5 atom of oxidized FMN, thus the hydride transfer can occur (Fig. 7A) [70]. Different crystal structures of OYEs have been solved in complex with NAD(P)H or its non-functional analogue 1,4,5,6-tetrahydroNADH (NADH₄) (Fig. 7B) [71-73]. Following FMN reduction, NADP⁺ is released from the active site, and the enzyme is now ready for the reduction of the substrate.

Although NAD(P)H is the preferred physiological coenzyme, different nicotinamide coenzyme biomimetics (NCBs) have been used as a relatively inexpensive alternative source of hydride [74]. These compounds retain the pyrimidine ring structure, but possess different substituent functional groups either on N1 nitrogen (NCBs 1-2, 6-7 in Fig. 8) or at the C3 carbon (NCBs 3-5) [75]. As with the natural coenzyme, the correct positioning of the pyridine ring is crucial for optimal hydride transfer [74, 76]. Since NCBs synthesis, several OYEs were found to exhibit high catalytic activities with different NCB analogues and, surprisingly, sometimes the catalytic efficiencies measured were higher with NCBs compared to the natural coenzyme NAD(P)H [77, 78]. Crystallographic studies on XenA from *P. putida* in complex with the non-functional analogue NADPH₄ and different NCBs (**1**, **2**, **3**) showed only minimal variations in the three-dimensional structure. One exception in all three NCBs structures was the alternative conformation of the tryptophan residue (Trp302 in XenA), which reduced the volume of the active site (Fig. 9) [78].

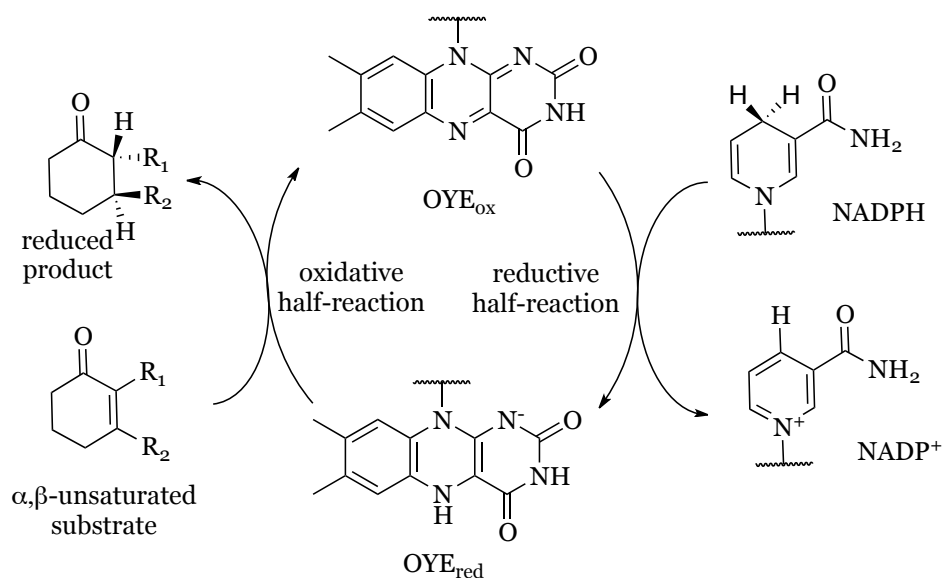


Figure 6. OYE-catalyzed asymmetric hydrogenation of activated alkenes (modified from [33]).

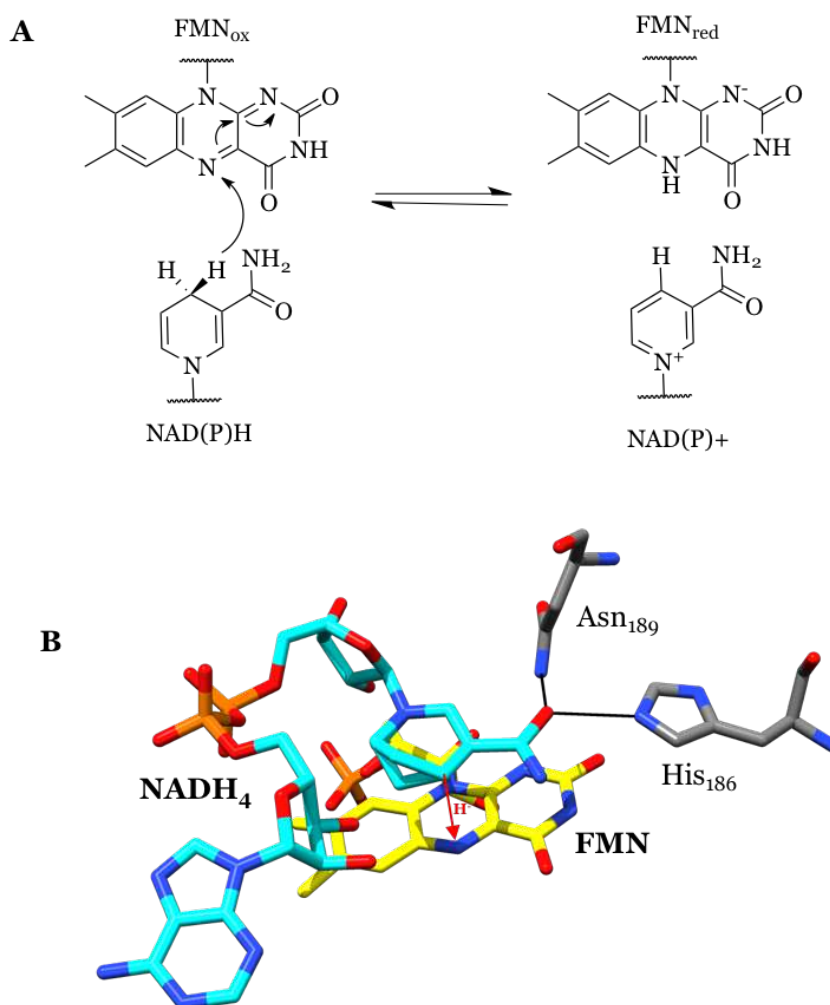


Figure 7. Hydride transfer and FMN reduction in the reductive half-reaction of OYEs. A) Reaction scheme of the stereo-selective oxidation of NADH where the C4 *R*-hydrogen is transferred to N5 of FMN (modified from [79]). B) Crystal structure view of 1,4,5,6-tetrahydro NADH inhibitor bound in the active site of MR (accession code 2r14) [71]. MR residues, FMN and NADH₄ are shown as atom colored sticks with dark grey, yellow and cyan, respectively.

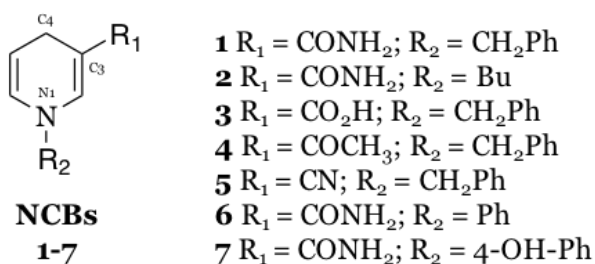


Figure 8. Nicotinamide coenzyme biomimetics (NCBs) previously used in OYE-catalyzed hydrogenations to replace NAD(P)H [74, 75, 77].

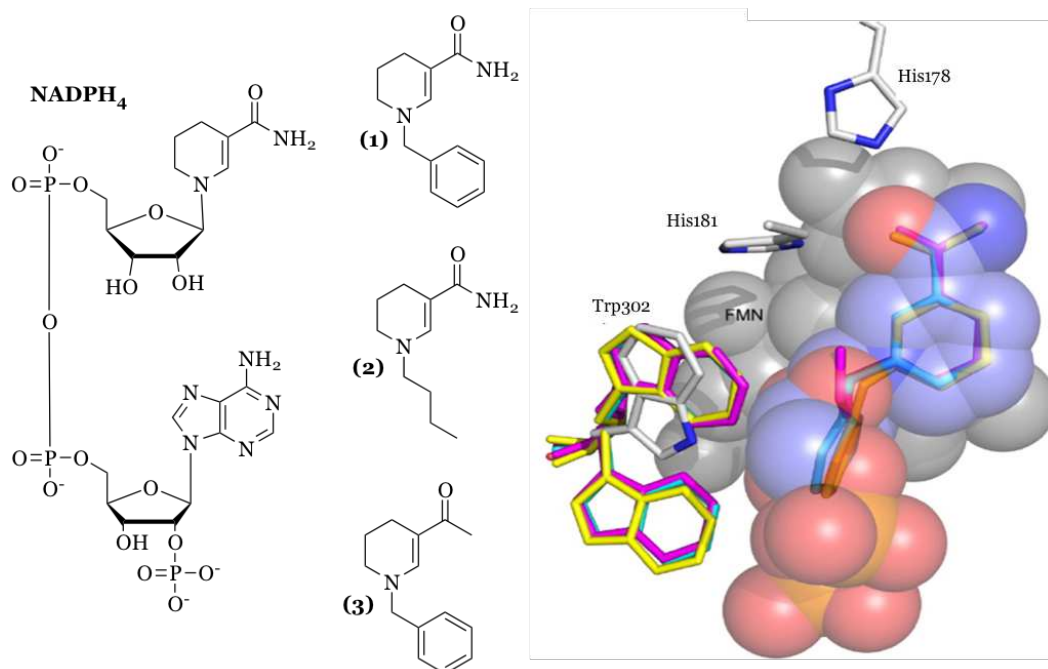


Figure 9. Superimposition showing the highly conserved nature of ligand and biomimetic binding. Residues Trp302, His181, and His178 of XenA are shown in stick representation colored with white carbon atoms and blue nitrogen atoms. These residues correspond to the NADPH₄-bound structure. The ordered portion of the NADPH₄ is shown as semitransparent spheres in all-atom color (carbon, purple; oxygen, red; phosphorus, orange) with its associated underlying FMN cofactor shown as gray spheres. Three biomimetic compounds are shown in stick representation with their respective Trp302 residues colored to match the biomimetic. **1** (cyan); **2** (yellow); and **3** (magenta). Dual occupancies are present for residue Trp302 for each of the three mimics (modified from [78]).

The catalytic cycle is completed with the oxidative half reaction where a number of oxidizing substrates, activated by different electron-withdrawing groups (EWGs) can act as electron acceptors (Fig. 10) [70]. The substrate enters into the active site of the reduced enzyme and binds to the His/Asn (His/His) conserved pair through its activator group. This step enhances the C=C-bond polarization and supports the hydride transfer from N5 of the reduced flavin onto C β of the substrate. Simultaneously, a proton, usually delivered from the opposite side of the hydride attack, is delivered onto the C α by a conserved tyrosine residue (in some cases substituted by a cysteine) or water [80].

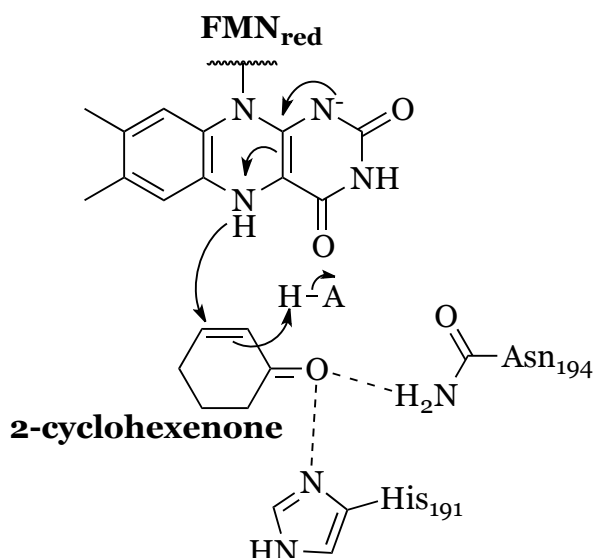


Figure 10. The oxidative half-reaction with 2-cyclohexenone, a common OYE substrate. H-A is a proton donor from either a conserved tyrosine or water. Numbering of the residues is based on OYE1 sequence [81].

The reaction resembles an asymmetric conjugate Michael-type addition of a hydride onto activated alkenes and, as already mentioned, results in exclusively relative *trans*-stereospecificity [46]. However, for some substrates, low enantiomeric excess (ee) values were detected suggesting more than one substrate-binding mode which differ in the exposure of opposite diastereotopic faces of the C=C-bond to hydride attack [63]. Two principal binding modes have been described: the classical binding mode (adopted for example by 2-methyl-cyclohexenone) and the “flipped” mode obtained by a 180° flipping of the substrate (adopted for example by α -methyl-cinnamaldehyde) (Fig. 11).

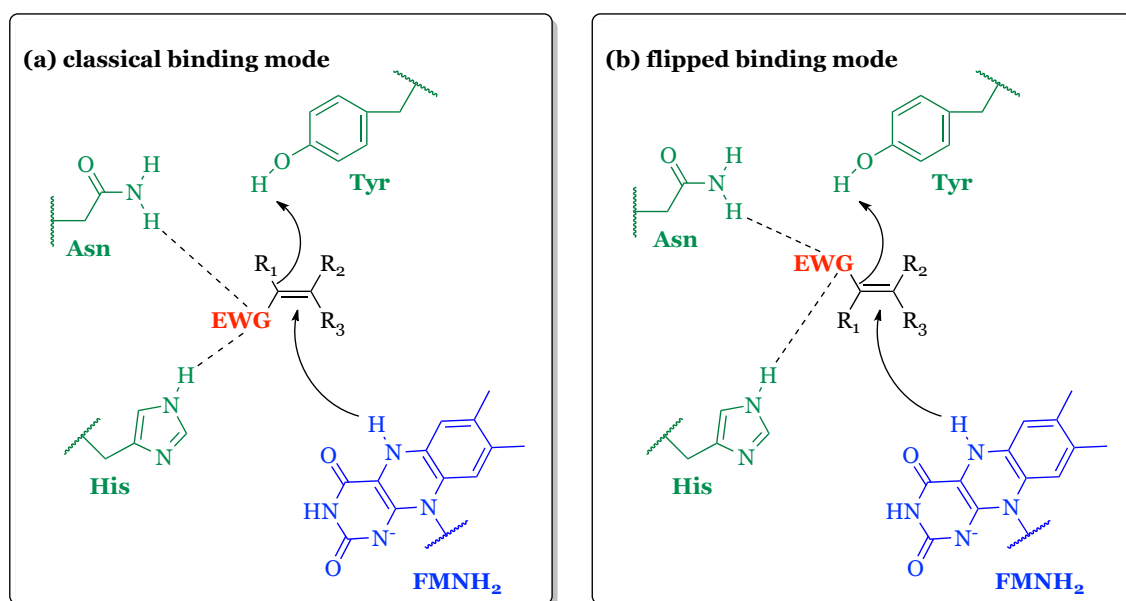


Figure 11. Mechanism of C=C double bond reduction mediated by ERs: (a) classical binding mode; (b) flipped binding mode (modified from [34]).

Although ERs generally show excellent stereoselectivities toward many substrates, natural enzymes are available only in a single enantiomeric form, thus they can catalyze the production of just one enantiomer. One big challenge in the use of ERs in industrial applications is the (almost) complete lack of enantiocomplementare pairs in wild-type enzymes in order to get access to both enantiomers. The isoenzymes OPR1 and OPR3 have been reported to behave in a stereocomplementary fashion in the reduction of (*E*)-1-nitro-2-phenylpropene by producing opposite enantiomeric products with excellent stereoselectivities, despite their highly conserved active site architecture (55% sequence identity, 70% homology) [82]. The same behavior was reported also for OYE1 and OYE2.6 pair with certain Morita– Baylis–Hillman adducts [83].

Since stereocomplementary in wild type ERs is extremely rare and often substrate specific, different strategies have been developed either by substrate- or enzyme-engineering in order to get access to both enantiomers of the desired product with high stereoselectivity (Fig. 12). Substrate-based approaches generally rely on a switch in the (*E*)/(*Z*) geometry of the substrate [84, 85], or on variations in the protection groups [86, 87]. Enzyme-based approaches towards stereocomplementary biocatalytic reactions often rely on mutagenesis of the biocatalyst. There is a growing interest in finding hotspot positions, involved in stereoselectivity control, that can be engineered [88, 89]. During the years, several hotspot positions involved in the selectivity control, activity and also substrate scope have been identified in OYE1 [90], OYE2.6 [91], PETNR [63] and YqjM [92]. For example, a single mutation of residue Tryptophan 116 in OYE1 has been reported to switch the stereopreference of the enzyme towards the industrially relevant carvone substrate. The mutant W116I enzyme converts (*S*)-carvone to *trans*-(1*S*,4*S*)-dihydrocarvone with high conversion (>98%) and good stereoselectivity (88% de) while the wild-type shows moderate activity (48%) and high stereoselectivity (93% de) towards the *cis*-(1*R*, 4*S*)-product [93]. Other examples of stereocomplementary pairs generation through mutagenesis are illustrated in Figure 13.

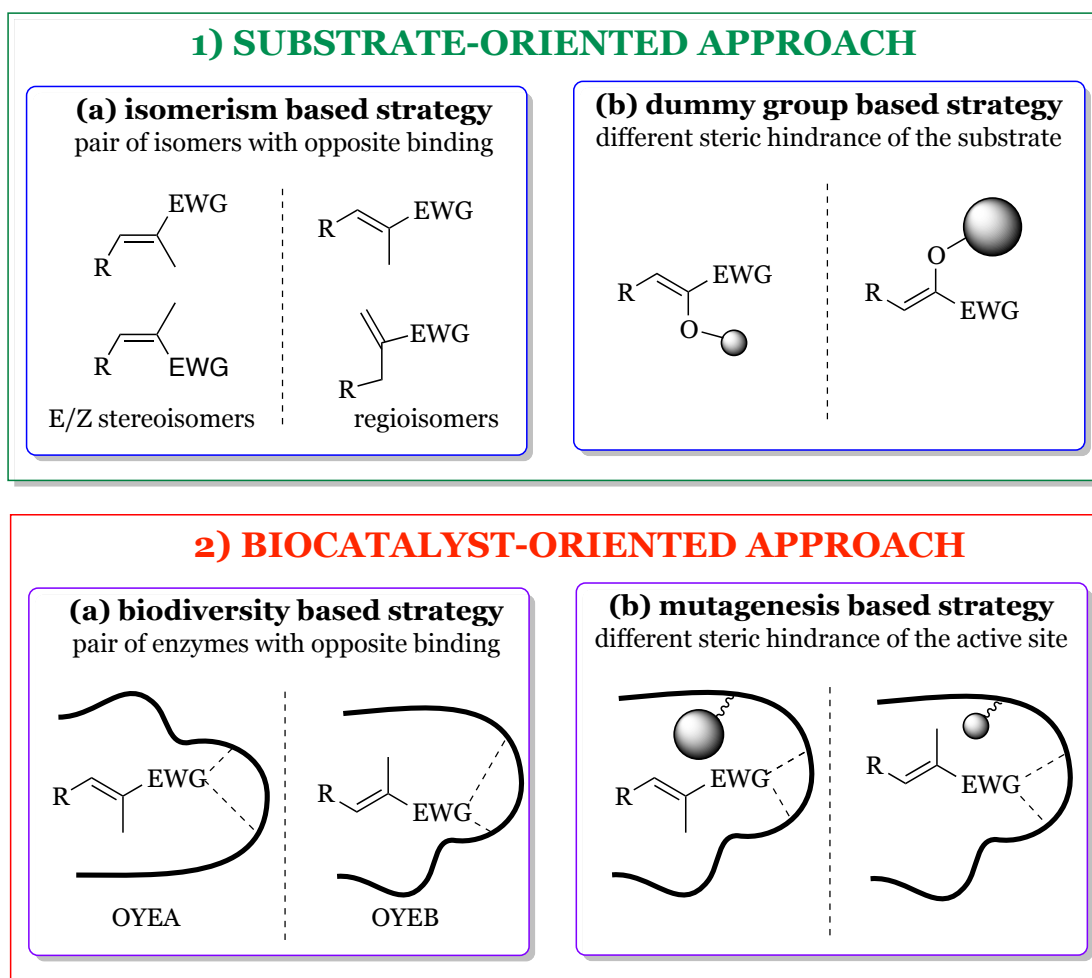


Figure 12. Stereocontrol strategies in the bioreduction of C=C-bonds (modified from [34]).

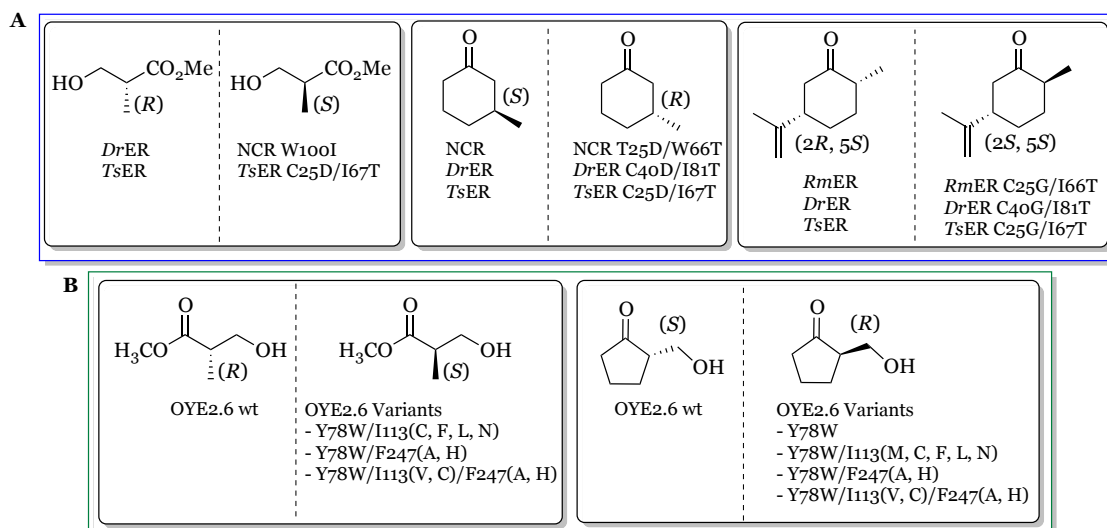


Figure 13. Generation of stereocomplementary pairs of products by engineering of ERs: A) Scaffold sampling and B) Site-saturated mutagenesis approaches (modified from [39]).

1.4.3 OYE subclasses and their structural features

All OYE members have a typical β -barrel (TIM-barrel) topology composed of eight twisted- β -sheet strands surrounded by eight α -helices and with an N-terminal α,β -hairpin lid that covers the bottom of the barrel (Fig. 14). The flavin mononucleotide (FMN) cofactor is bound at the C-terminal edge of the barrel, with its *si* face exposed to substrates and solvent. The loops connecting the central β -strands with the adjacent α -helices determine the architecture of the substrate and the cofactor-binding sites. These loops exhibit significant diversity among OYEs regarding sequence and conformation, thus affecting the activity and stereoselectivity of each enzyme for the different substrates [68, 94].

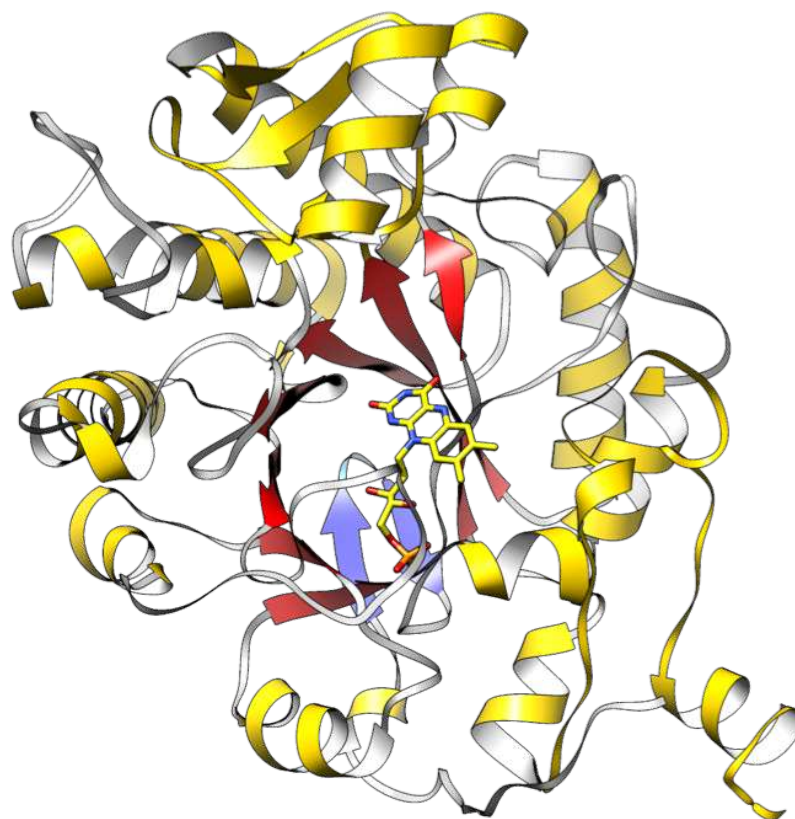


Figure 14. TIM-barrel structure of OYEs. Three-dimensional structure of OYE1 from *Saccharomyces pastorianus* (pdb entry 10ya) [68]. The α -helices and β -strands of the TIM-barrel are indicated in gold and red, respectively. The N-terminal hairpin composed by 2 short β -strands at the bottom of the barrel are colored in blue. The FMN cofactor is displayed as a stick-model and colored in yellow.

Two amino acids residues involved in substrate binding (*i.e.* His191 and Asn194, OYE1 numbering) are highly conserved within OYEs family. OYE1 and Morphinone reductase (MR) contain the histidine-asparagine pair while in 12-oxophytodienoate reductase (OPR3) and pentaerythritol tetranitrate reductase (PETNR) both residues are histidines (Fig. 15) [45]. These residues interact with

the electron withdrawing groups of the substrate through hydrogen bonding and thus, play a crucial role in the correct orientation of the C=C-bond above the N5 of the flavin [63]. The role of the conserved active site histidine and asparagine/histidine pair in ligand binding has been extensively studied and demonstrated by site directed mutagenesis in different OYE homologues [63, 70]. Tyr196 is another highly conserved residue within the OYE-family (except in MR where a Cys residue is present) (Fig. 15) acting as the proton donor in the oxidative half-reaction of OYE with 2-cyclohexen-1-one [80]. It has been demonstrated that the Y196F mutation in OYE1 dramatically decrease (of about 6 orders of magnitude) the rate of the oxidative half-reaction, while it has little effect on substrate binding and reductive half-reaction thus confirming the role of this residue as proton donor [80]. However, the absence of this conserved tyrosine in MR [81], combined with the relatively small effects seen in the activity of the corresponding tyrosine to phenylalanine mutants in PETN reductase and in chromate reductase (CrS) from *Thermus scotoductus*, have demonstrated that this residue is not essential for catalysis in all OYEs as water can potentially act as proton donor [95, 96].

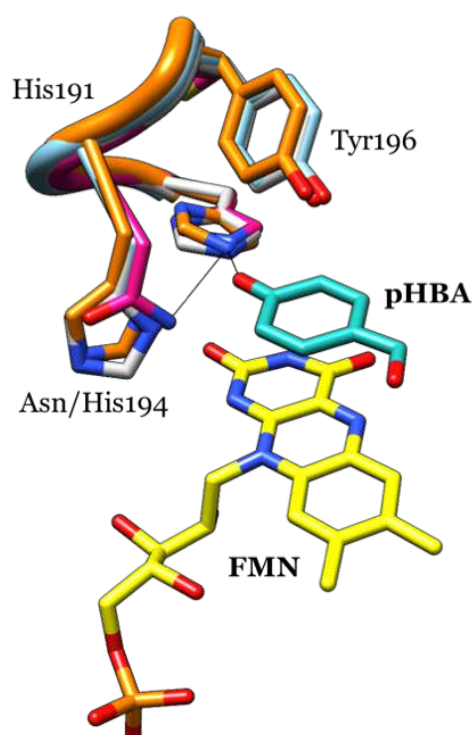


Figure 15. Comparison of active site residues of OYE1 in complex with pHBA (cyan) (pdb entry 1ko3), OPR3 (orange) (pdb entry 2hsa), PETNR (grey) (pdb entry 2aba), MR (pink) (pdb entry 1gwj). FMN is shown as atom colored sticks with yellow carbons. Hydrogen bonding is depicted as black line. Numbering is based on OYE1 sequence.

Around these highly conserved residues involved in substrate binding and catalytic mechanism, in the active site other important amino acids residues are present, playing a role in catalysis and in FMN binding. The latter ones vary within the different OYE classes. The bacterial OYEs have been first divided into two subfamilies, the “classical” and the “thermophilic-like” class (formerly YqjM-like), according to the classification proposed by Toogood *et al.* [33] based on sequence alignment (Fig. 16A) and quaternary structure organization. Enzymes with amino acid sequence alignment similar to OYE1 are clustered in the classical family, while OYEs belonging to the second group exhibit similarities with YqjM, the first thermophilic-like ene-reductase to be discovered. Residues involved in the interaction with the flavin cofactor (T26, Q114, H191, R243, and R348, OYE1 numbering) are highly conserved in both classes of OYEs (Fig. 16B); however, some differences have been reported. Residue T37 in OYE1 is known to influence the flavin redox potential; by interacting with the isoalloxazine ring O4 atom T37 stabilizes the negative charge of the reduced flavin [97]. This residue is highly conserved within the classical subclass, but it is substituted by a conserved cysteine residue in the thermophilic-like family. Finally, another peculiarity of thermophilic-like OYEs are the C-terminal residues R312, Q333, Y334, and R336 (YqjM numbering) that are involved in the formation of the functional dimer–dimer interface [94]. Moreover, the residue Arg336 in YqjM is involved also in substrate binding by protruding into the active site of the adjacent monomer. It also acts in modelling the active site shape cavity [94]. Since classical OYEs are monomeric enzymes their active sites do not have a residue located in the same way as the Arg336 of YqjM.

Based on quaternary structure it has been noted that OYEs from the classical family occur as monomers or dimers in solution, whereas thermophilic-like OYEs usually form homodimers or homotetramers (or even higher oligomeric states such as octamers and dodecamers) through the C-terminal “arginine finger” (*e.g.* Arg336 in YqjM) (Fig. 17A) [33]. In thermophilic-like OYEs generally a wider access channel into the active sites is present compared to classical OYEs that have significantly smaller active sites due to the shortening and reorientation of loop- β 6, that enter into the active site and is positioned in close contact with FMN. Moreover, loop- β 3 differs greatly in length and type of structural units between OYE homologues: in classical OYEs it is generally longer and oriented near the entrance of the active site forming a sort of capping domain (Fig. 17B and 17C).

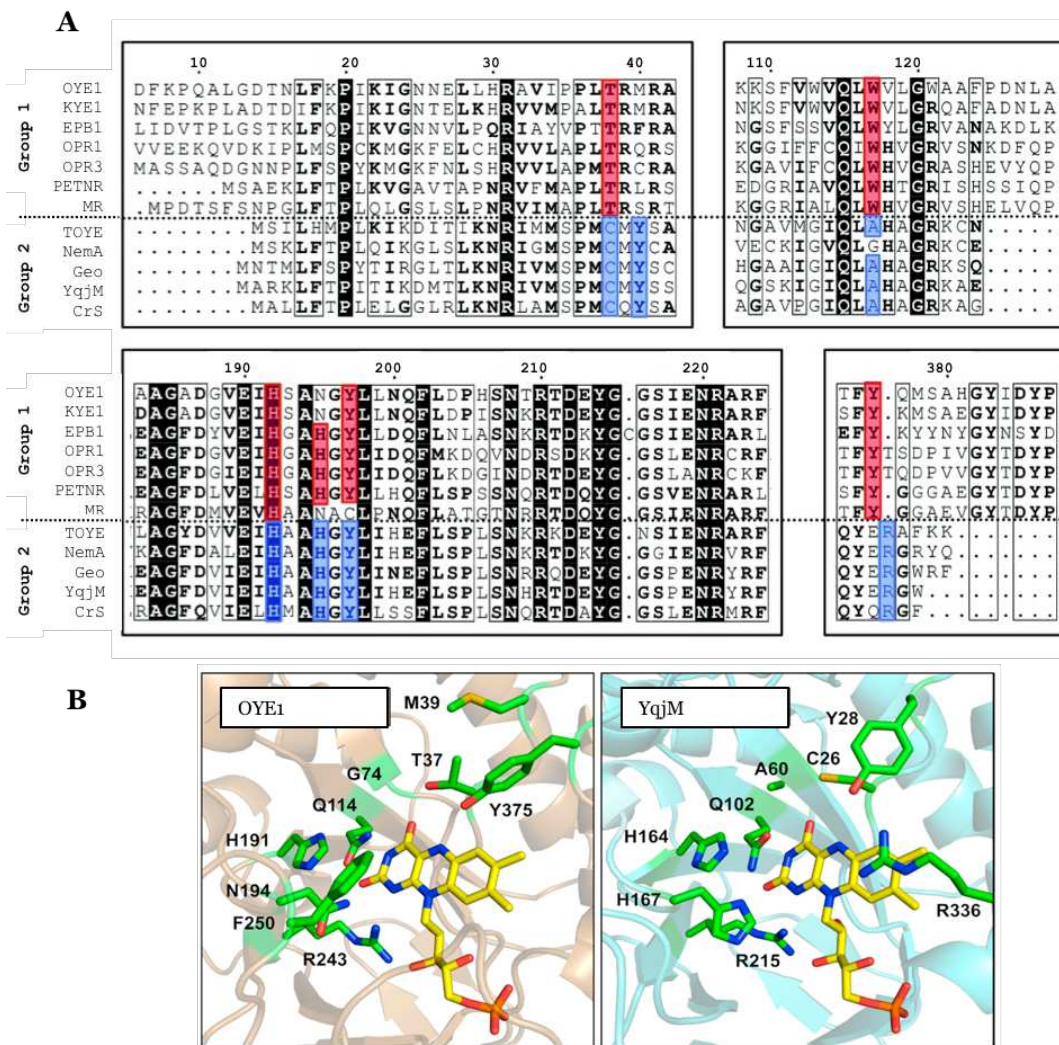


Figure 16. (A) Amino acid sequence alignment between 12 OYE enzymes. Sequence alignment was performed using Multalin [33]. Boxes highlighted in red and blue show the sequence conservation of active site residues T26, Y28, W102, H181, H184, Y186, Y351 (PETN reductase numbering) and R333 (TOYE numbering) for classical OYEs (Group 1) and thermophilic-like OYEs (Group 2), respectively. Alignment numbering refers to the OYE1 sequence. Accession numbers: OYE1 (*S. pastorianus*; Q02899); KYE2 (*Kluyveromyces lactis*; L39452), EPB1 (EBP1; *Candida albicans*; L25759); OPR1 (*S. lycopersicum*; Q9XG54); OPR3 (*S. lycopersicum*; Q9FEW9); PETNR (*Enterobacter cloacae*; U68759); MR (*Pseudomonas putida* M10; AAC43569); TOYE (*T. pseudethanolicus*; YP001664021); NemA (*Coprothermobacter proteolyticus*; B5Y655); GeoOYE (*Geobacillus kaustophilus* HTA426; Q5KXG9); YqjM (*Bacillus subtilis*; P54550); and CrS (*Thermus scotoductus* SA-01; YP143423) [33]; (B) Active sites of OYE1 (metallic brown) (pdb entry 1oya) and YqjM (metallic blue) (pdb entry 1z41). R336 in YqjM belongs to the adjacent subunit [98].

For thermophilic-like OYEs, it has been reported that after purification the proteins are not fully flavinated, suggesting a weaker binding of the cofactor that can be easily released from the structure due to the wider open active site [47]. Generally, thermophilic-like OYEs have some outstanding characteristics with respect to their classical counterparts. They have an average increased thermal stability and enhanced resistance to co-solvents and extreme pH values [73, 96, 99-101].

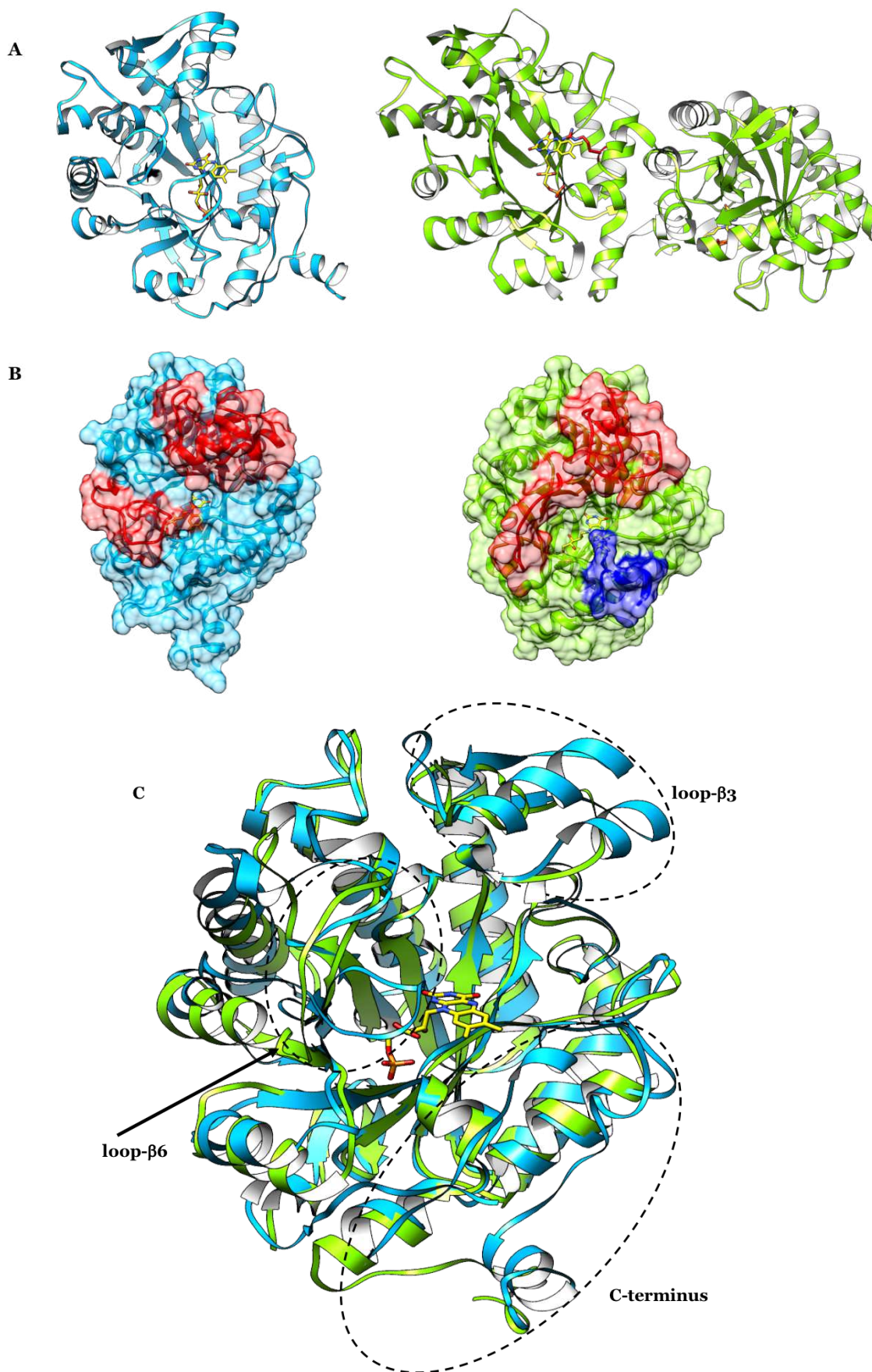


Figure 17. Tertiary structure of OYE1 (pdb accession 1oya) and YqjM (pdb accession 1z41) shown as (A) ribbon and sticks cartoon and (B) surface highlighting the structural differences between classical and thermophilic-like OYEs (red). For YqjM the blue region corresponds to the adjacent monomer. (C) Comparison between OYE1 (classical OYE) and YqjM (thermophilic-like OYE). Circles highlight the structural distinct features of each subclass.

These peculiarities have been ascribed to different structural features such as shorter sequence length (between 337 and 371 amino acids) compared to classical OYEs (between 349 and 412 amino acids), high proline content within loops and turns as well as to strong inter-subunit interactions through hydrogen bonding and complex salt bridge networks at the dimerization interface. It has been observed that the number and type of interactions at the dimerization interface can vary between thermophilic-like members, thus influencing the stability. The incorporation of these salt bridges in the non-thermoresistant OYERo2 homologue isolated from *Rhodococcus opacus* has been reported as a successful tool to increase the thermal stability of the protein and improve its tolerance toward co-solvents [102].

One year later after Toogood's classification, Oberdorfer *et al.* [103] reported some other finger print motifs based on the different OYE subclasses and determined also some sequence patterns involved in the shaping of the active site pockets. Only two highly conserved amino acids called "bounding residues" were identified as responsible for the shaping of the binding pocket: in monomeric OYEs two aromatic residues (*e.g.* Tyr78 and Tyr358 in OPR1 or Phe74 and Tyr370 in OPR3), the first situated on loop β 2 and the second on the C-terminus of the protein, while in dimeric OYEs the first aromatic residue is replaced by a small polar threonine or serine residue (Thr70 in YqjM). The second bounding residue in the dimeric OYEs is again a conserved tyrosine (Tyr28 in YqjM), originating from loop β 1. The two regions in loop- β 1 and loop- β 2 show some conservation patterns based on OYE subclasses. It has been seen that near the first bounding residue in loop- β 2 monomeric OYEs exhibit a G-[FYW]-X(3)-P-G-[ILV]-[FHYW] pattern (Fig. 18A blue shading), while the corresponding motif in dimeric OYEs (Fig. 18A, yellow shading) is significantly different showing a conserved G-R- I-[TS]-X(4)-G-I-W pattern. The second bounding residue in dimeric OYEs (a tyrosine in all structures) originates from loop- β 1 and is the last residue in the conserved sequence pattern P-M-C-[MQ]-Y (Fig.18A, green shading), while a different but well-conserved motif P-[LM]-T-R-X-R was detected in this region also for monomeric OYEs (Fig. 18A, red shading) [103]. A detailed nomenclature of OYEs loops is shown in Figure 18B.

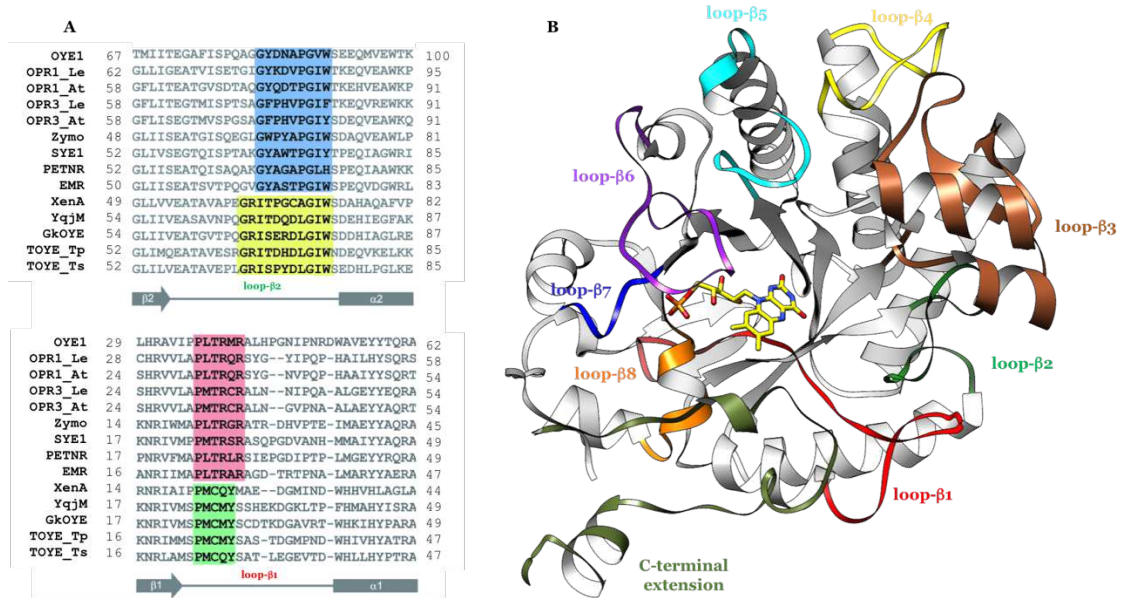


Figure 18. (A) Sequence alignment of OYEs with 3D structures available. Conserved regions correspond to loop β 2 (upper part) and loop β 1 (lower part) in monomeric (blue and red shading) and dimeric (yellow and green shading) OYEs. (B) Overall structure of OYE1 (10ya) showing the loops originating from β -strands 1 to 8 as well as the C-terminal extension, color coded. The FMN cofactor is displayed as a stick-model [103].

In 2016, Nizam *et al.* [59] performed a bioinformatics analysis on 424 putative OYEs from 60 different fungal species detecting a novel group of fungal OYEs, with no conservation of the typical active site residues neither of OYE1 nor YqjM. Out of the 424 sequences studied, 199 sequences belong to Class I (OYE1-like), 127 sequences were clustered in Class II (YqjM-like) and 98 sequences were grouped into the newly discovered Class III. Moreover, another interesting observation was that different OYE homologues (from 2 to 22) clustered in all the three subgroups were found in the same organism. Comparing the sequences of Class I fungal OYE members clearly showed that the active site residues His191, Asn194, Tyr196, Phe250 and Tyr375 of OYE1 were either well conserved or substituted with similar amino acids in almost all the fungal OYE proteins studied. In a similar way, sequence comparison of Class II members was performed, highlighting that the conserved residues Cys26, Tyr28, Lys109, His164, His167, Tyr169 of YqjM were well conserved also in fungal OYE members with only few substitutions with similar amino acids. Sequence alignment of Class III members revealed strict conservation of YGGS motif and the core active site residues (His191, Asn194 and Tyr196 of OYE1 or His164, His167 and Tyr169 of YqjM) but the other typical residues present in the active site of Class I or Class II proteins were not detected in these OYE members. In order to identify the differences between class III and the two already known OYE families, 6 OYE

homologues identified in *Ascochyta rabiei* [104] were analyzed by comparative homology modeling. A unique active site organization of Class III OYEs has been reported, even if these OYEs are related to some extent to Class II OYEs (Table 4). In *ArOYE6* Thr40, Arg42, Asn80, His196, His199, Tyr201 and Arg355 were predicted as the active site residues. The major differences with Class II proteins are the substitution of Cys26 and Tyr28 of YqjM with Thr40 and Arg42 in *ArOYE6*. Another important difference in *ArOYE6* is the non-shared active site architecture. In Class II OYEs it has been demonstrated that the arginine or tryptophan finger protrudes from one monomer into the active site of the adjacent monomer, as already mentioned. In *ArOYE6*, the Arg355 comes from the same monomer, therefore suggesting a monomeric nature of the enzyme. The comparative modeling study also provides insights into a different binding of FMN. The analysis identified eight residues (Ala38, Thr40, Asn80, His196, Lys249, Phe306, Phe328, and Lys328, numbering according to *ArOYE6*) forming hydrogen bonds and six residues (Gly37, Met39, Arg42, His199, Phe305 and Arg355) involved in hydrophobic interactions with FMN [104]. However, despite these interesting features of fungal Class III OYE homologues, none of these enzymes have been characterized thus far.

Table 4. Comparison between the conserved active site residues and FMN binding residues identified in three members from different OYE families [104].

Conserved residues	OYE1	YqjM	ArOYE6
Active site residues	His191 Asn194 Tyr196 Phe250 Tyr375	Cys26 Tyr28 Lys109 His164 His167 Tyr169	Thr40 Arg42 Asn80 His196 His199 Tyr201 Arg355
FMN binding	Pro35 Thr37 Gly72 Gln114 Arg243 Gly324 Asn325 Phe326 Gly345 Gly347 Arg348	Ser23 Pro24 Cys26 Ala60 Gln102 His164 His167 Arg215 Ser249 Gln265 Gly284 Met285 Phe305 Gly307 Arg308 Glu309 Arg310	Gly37 Ala38 Met39 Thr40 Arg42 Asn80 His196 His199 Lys249 Phe305 Phe306 Phe328 Lys329 Arg355

Recently, Scholtissek *et al.* [98] have proposed a new classification based on the phylogenetic analysis of biochemically characterized OYEs. Calculating the phylogenetic distance tree of 63 characterized OYEs, three, instead of the established two, comprehensive groups were identified (Fig. 19). Class I (highlighted in yellow) contains many classical OYEs from plants, bacteria and also cyanobacteria; class II (highlighted in grey) regards exclusively classical enzymes from fungi; to class III (highlighted in green) belong the traditional thermophilic-like OYEs. Several sequences (SYE4, *Chr-OYE1*, Nox, *LacER* and YqiG), however, have not been assigned to any class. They may be evolutionary intermediates or ancestors of Class I and Class III OYEs homologues considering their bacterial origin. The authors have looked also to the differences present in these three clusters evaluating their three-dimensional structure (FMN and substrate binding; oligomeric state), the reactivity with NCBs and the biocatalytic conversions and steady-state parameters. Class I OYEs are monomeric enzymes isolated from plants and bacteria that generally prefer α -methylated cyclic enones as substrates. Class II enzymes have fungal origins and they have evolved in a co-driven evolution from class I. Members of class I and class II are phylogenetically and structurally closely related resulting in similar substrate preferences. Members of Class III are likely driven by a convergent evolution to class I/II and they exhibit different structure organization, biochemical behavior and substrate preference compared to Class I and II homologues. They form oligomers built from homodimers and are often thermostable. Moreover, they highly prefer maleimides as substrates.

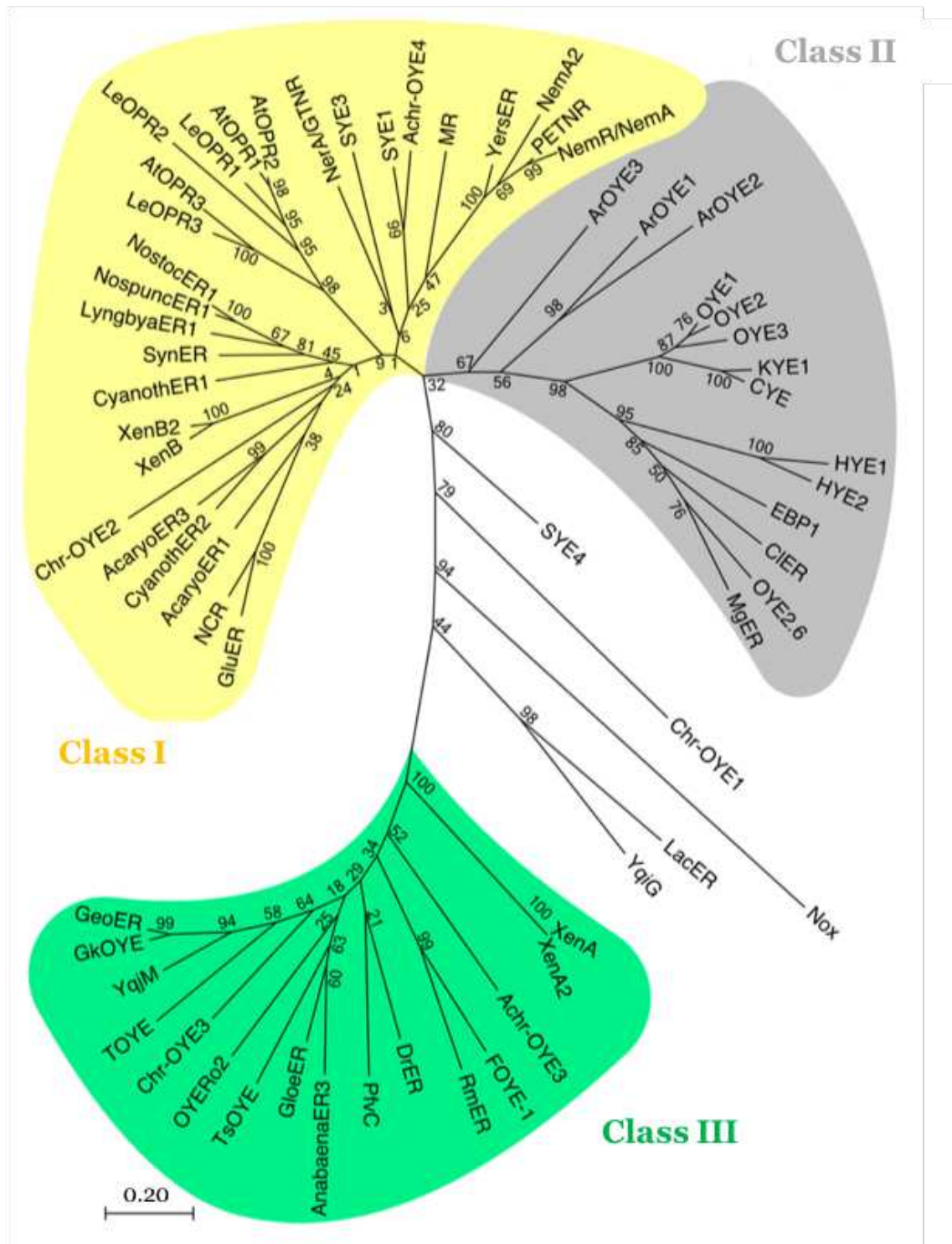


Figure 19. Dendrogram showing the relationship between 63 characterized OYEs and their classification in three different classes: Class I (yellow shading), Class II (grey shading) and Class III (green shading) [98].

1.4.4 Synthetic applications

Since OYEs are active among different types of substrates, they were exploited for the synthesis of a wide range of industrially useful compounds. Ene-reductases, both as isolated enzymes and/or whole cell biocatalysts, have been extensively used for the synthesis of terpenoids, fragrance compounds and chiral building blocks [26, 105]. Just to make some examples, some OYE homologues have been employed in the reduction of citral to citronellal [82, 106-108], a key intermediate in menthol synthesis. In this case the whole cell systems generally lead to the production of the corresponding saturated alcohol due to side reactions compared to the isolated enzymes that furnished exclusively the desired aldehyde product [109, 110]. A quantitative and highly stereoselective enzymatic synthesis of various α -methyl dihydrocinnamaldehyde derivatives, that are widely employed as active ingredient in perfumes, has been developed using an aqueous-organic biphasic system (containing 20% t-BuOMe) and OYE1-3 as biocatalysts [111]. The synthesis of different important chiral building block has been also reported. The reduction of ketoisophorone to the commercially useful (*R*)-levodione, an important key intermediate for the synthesis of various carotenoids, has been reported for the vast majority of OYE homologues yielding exclusively the (*R*)-enantiomer (up to >99% ee) [33]. Another interesting building block (2*R*,5*R*)-dihydrocarvone was produced starting from (*R*)-carvone using recombinant *E. coli* cells expressing the cyanobacterial ER isolated from *Nostoc* sp. PCC 7120 (*NoER*) and an *in situ* substrate supply and product removal strategy [112].

By now the biocatalytic scope of ene-reductases in the reduction of activated C=C-bonds has been well-defined concerning substrate acceptance, stereoselectivity and cofactor dependence. For these reasons in the last years the research is focusing more and more on challenging transformations using more complex substrates that for example incorporate more than one (activating) functional group, such as nitriles and carboxylic esters (Fig. 20). For example, ene-reductases have been used by Pfizer in the asymmetric bioreduction of α,β -cyanoacrylate esters, providing a novel route for the synthesis of pregabalin precursors [113, 114]. Moreover, a panel of functionalized α -chiral phosphonates were recently obtained starting from β -activated vinylphosphonate derivatives [115]. In the same way poorly activated substrates with carboxyl acid groups and

cyclic carboxylic esters have been converted starting from cinammic acid derivatives or unsaturated lactones with very good conversions [116, 117].

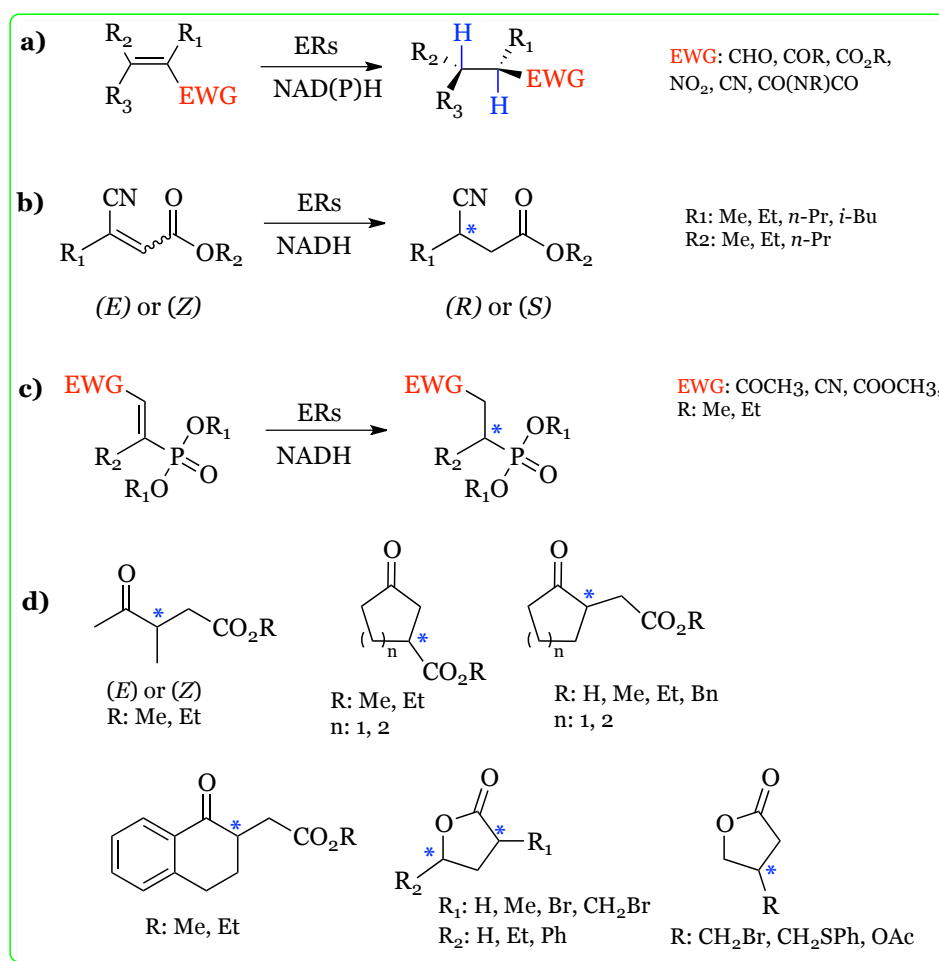


Figure 20. Access to chiral products with increased chemical complexity using ene-reductases through single-step reaction and multi-step reaction (EWG, electron-withdrawing group). (a) OYE-catalyzed *trans*-selective reduction of activated C=C-bonds. Asymmetric bioreduction of (b) α,β -cyanoacrylate esters [113], (c) functionalized α -chiral phosphonates [115] and (d) γ -oxo-esters [118] and α - β - γ -chiral lactones [117].

Moreover, in recent years the coupling of the C=C-bond reduction performed by ene-reductases to the classical chemical reactions (chemoenzymatic processes) or to other enzymatic reactions (multi-enzymatic biotransformation) is attracting great interest (Fig. 21). For example, a two-step one-pot enzymatic process was set-up using an ene-reductase and an alcohol dehydrogenase for the reduction of a suitable unsaturated ketone obtaining the chiral commercial fragrance Muguesia® [119]. Also chiral amines, important building blocks for the preparation of pharmaceuticals, have been synthesized by a one-pot process, coupling the action of ene-reductases and ω -transaminases [120]. Synthetic cascades have also been designed by incorporating different biocatalysts into a single cell (designer bug). A chimeric protein composed by XenB from *P. putida*

fused to a Baeyer–Villiger-monooxygenase (BVMO) has been used together with an ADH inside *E. coli* cells for the production of chiral lactones starting from unsaturated alcohols [121]. Similarly, a sequential process using two different recombinant *E. coli* whole cells expressing a cytochrome P450 monooxygenases (CYPs) from *Bacillus megaterium* and YqjM from *Bacillus subtilis*, was employed for the synthesis of both enantiomers of a cyclic ester [122]. Moreover, an eight-enzyme system was set-up in *Saccharomyces* cells for the production of ergot alkaloid cycloclavine from chanoclavine-I, mimicking the natural pathway occurring in filamentous fungi [123].

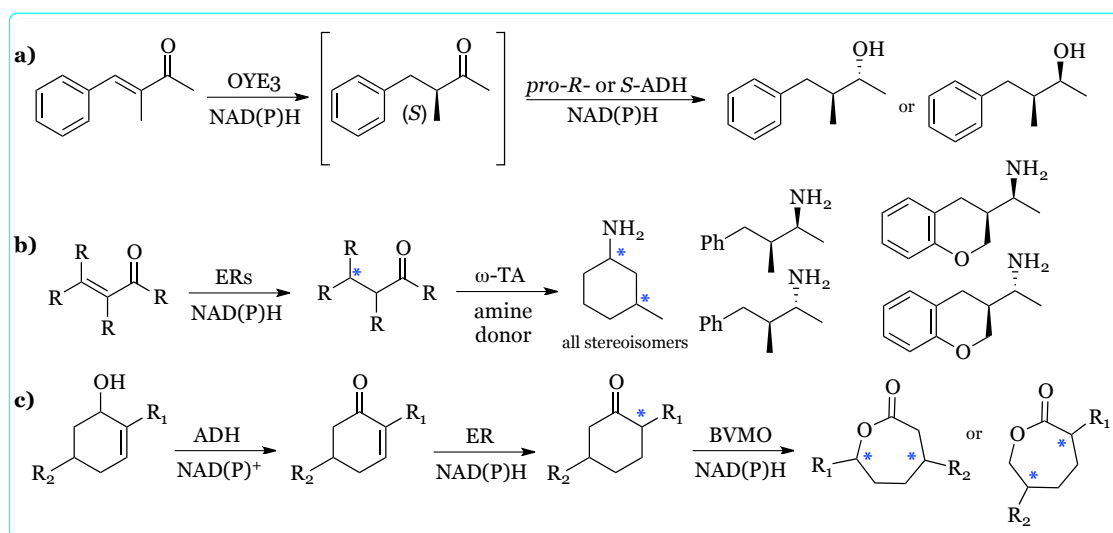


Figure 21. Bi-enzymatic cascades combining ene-reductases (ERs) with (a) alcohol dehydrogenases (ADHs) for the synthesis of Muguesia® [119], (b) ω -transaminases (ω -TAs) [120], (c) Designer bug containing fusion ER-Baeyer–Villiger monooxygenase (BVMO) combined with ADH to produce α,δ -chiral and/or β,ϵ -chiral ϵ -lactones [121].

Furthermore, biocatalysis using OYEs was combined also with classical organocatalysis and transition-metal catalysis. Guerbet alcohols were produced from 1-hexanol via organocatalytic oxidation/ homoaldol-condensation and a subsequent double-reduction sequence catalyzed by a OYE coupled to an alcohol dehydrogenase (ADH) enzymatic step. [124]. Recently, a one-pot two-step chemoenzymatic cascade was reported for the enantioselective synthesis of 2-aryl 1,4-dicarbonyl compounds: a first step of a rhodium-catalyzed diazocoupling was used to produce the substrate for the subsequent stereoselective OYE-catalyzed reduction [125].

Besides the well-known two-electron reductive processes at the expense of a reduced flavin cofactor alternative and, sometimes unexpected reactions have been reported during the years for this intriguing class of enzymes.

1.4.5 Versatile catalytic behavior of ene-reductases

The catalytic promiscuity of flavin cofactors [126] has also been detected in OYEs [127, 128] and all three main electronic states of FMN have been involved in different OYE-mediated reactions (Fig. 22). Over the years, various reductive reactions catalyzed by FMN reduced hydroquinone (FMN-HQ) have been reported, including nitro-reduction and (nitro)arene-reduction, as well as the redox-neutral C=C-bond isomerization of methylene- γ -butyrolactone through intermolecular hydride transfer [127, 128]. Moreover, Hyster *et al.* demonstrated the involvement of FMN semiquinone (FMN-SQ) in a novel radical reductive dehalogenation of α -bromoesters [129]. Finally, acid-base catalysis without hydride transfer (oxidized FMN) was detected with some OYE homologues [130].

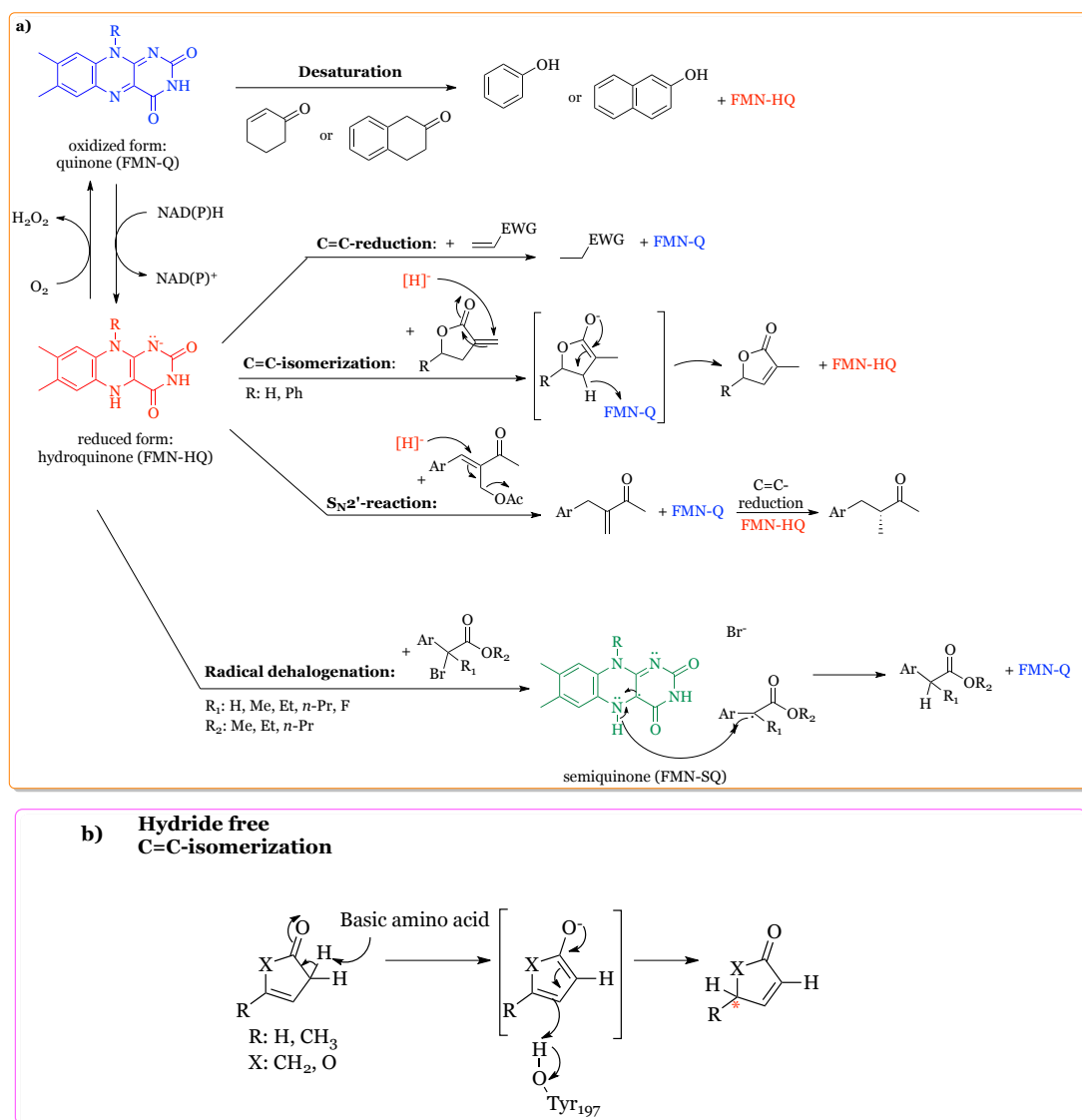


Figure 22. Non-classical reactions catalyzed by OYEs (EWG, electron-withdrawing group). (a) Reactions catalyzed by the oxidized quinone form (FMN-Q) [131], the reduced hydroquinone (FMN-HQ) [127, 132] or *via* the semiquinone of FMN (FMN-SQ) [129], (b) hydride-free acid-base catalyzed isomerization [130].

1.4.5.1 Bio-Nef pathway

The bio-Nef pathway (Fig. 23), was reported in literature on *sec*-nitro-aliphatics compounds. Several ERs have been reported to transfer a hydride directly onto the nitro-group yielding the highly unstable nitroso-derivative, which spontaneously can tautomerize to form the more stable corresponding oxime. This intermediate can be subsequently reduced enzymatically furnishing the water-labile imine, which spontaneously hydrolyzes to the corresponding carbonyl compound and ammonia [133]. XenB and NerA show to be predominantly active in the reduction of the activated C=C-bond of the *sec*-nitro-aliphatic compounds furnishing the corresponding nitroalkanes. While XenaA, MR and PETNR yield substantial amounts of oxime intermediates, thus showing a preponderant nitro-reductase activity.

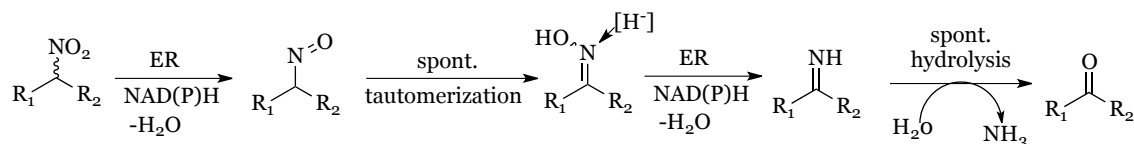


Figure 23. Bio-Nef reaction mediated by ene-reductases on *sec*-nitro-aliphatics [133].

For 1-nitro-2-phenylpropene (Fig. 24), a mixture of 1-nitro-2-phenylpropane (obtained as the initial product from C=C-bond reduction) and of the intermediate oxime or final aldehyde (obtained through the Nef-pathway on the previously produced nitroalkane) were detected with all the enzymes. In this case, the bio-Nef pathway and the C=C-bond reduction seem to occur sequentially [133].

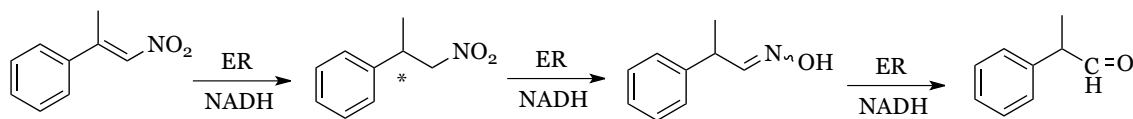


Figure 24. Sequential bioreduction of 1-nitro-2-phenylpropene [133].

1.4.5.2 Hydride-independent isomerization of α -angelica lactone

Very recently a nicotinamide-free and hydride-independent process catalyzed by OYE2 has been reported for the isomerization of α -angelica lactone to β -angelica lactone, which could be further reduced to γ -valerolactone in the presence of NADH, allowing a formal asymmetric reduction of non-activated C=C-bonds [130] (Fig. 25).

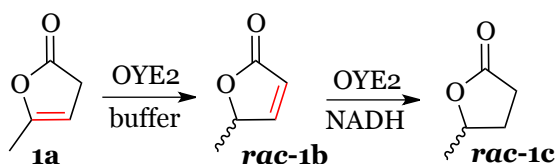


Figure 25. Hydride-independent α -angelica isomerization and subsequent reduction to γ -valerolactone [130].

The isomerization of α -angelica lactone mediated by OYE2 in aqueous buffer was very fast furnishing 6.3 mM of racemic β -isomer in 15 min at 30 °C. Moreover, the reaction was also scaled up using 25 mM initial substrate concentration allowing the isolation of 18 mg of product (32% overall yield and 98% purity) after 45 min of reaction, thus demonstrating the applicability of this sustainable process for the valorization of renewable bio-based chemical platform. α -Angelica lactone is usually produced through dehydration of levulinic acid, which is derived from cellulosic feedstocks. Both α -angelica lactone and γ -valerolactone are two versatile building blocks with a wide range of industrial applications (*e.g.*, precursors of bio-based polymers and natural products, solvents, fuel additives [134]).

The mechanism of action has not yet been elucidated but most likely relies on acid-base catalysis (Fig. 26) as it has been demonstrated that no hydride transfer is involved since FMN is naturally occurring in oxidized form in OYE homologues and the isomerization reaction is performed without addition of NADH [130]. The substrate enters the active site of the enzyme and interacts through its ketone group with the classical residues involved in binding in OYEs (His192 and Asn195). At this point a base, not yet identified, subtracts a proton generating an aromatic anion as intermediate. This aromatic anion resembles a phenolate, that is known from previous data to be an OYE inhibitor which strongly interacts with the oxidized FMN. The enzyme is restored by the proton donor Tyr192 promoting the released of the product after protonation.

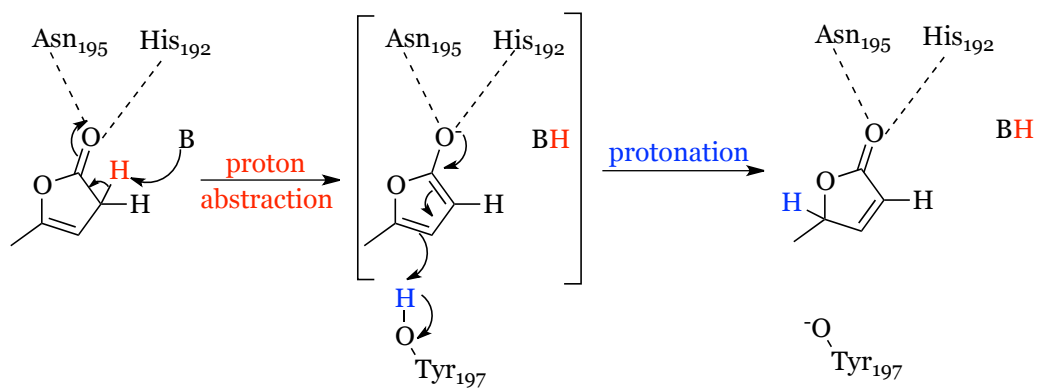


Figure 26. Initial proposed mechanism for the isomerization of α -angelica lactone by OYE2. B= base residue (modified from [130]).

2. AIM OF THE THESIS

The asymmetric reduction of prochiral C=C-bonds is one of the most widely employed synthetic strategy for the preparation of optically active molecules [35, 39]. The classical approaches to perform this reaction involve the use of hazardous agents (*e.g.* palladium and H₂ under pressure) [30]. Biocatalysis represents an environmental friendly alternative that can be employed to carry out this reaction. In this contest, ene-reductases (ERs) are greener catalysts able to catalyze the stereoselective C=C-bond hydrogenation on a wide range of substrates yielding products with a variety of biotechnological and pharmaceutical applications [105]. ERs are flavin- and NAD(P)H-dependent catalysts that have been extensively studied in the last years as attractive tools for alkenes reduction with the potential to generate up to two stereogenic centers [39, 135]. In general, ERs have been identified in a large number of organisms such as bacteria, fungi and plants but nevertheless their toolbox is still reduced [98].

The goal of this project was to discover novel ERs in order to enlarge the toolbox of recombinant biocatalysts able to perform the C=C-bond hydrogenation towards molecules of potential pharmaceutical interest. The research has been accomplished in collaboration with and by the financing of Fabbrica Italiana Sintetici (F.I.S.) S.p.A.

In order to discover novel ERs new sources of enzymes have been exploited such as extremophilic algae, (cyano)-bacteria and fungi organisms. Their biocatalytic potential was investigated by characterizing their substrate *spectrum* and biochemical properties, including thermal and organic solvent tolerance, the pH *optimum*, oligomeric state and three-dimensional structure.

3. DISCOVERY, EXPRESSION AND PURIFICATION OF NEW PUTATIVE ERs

Abstract:

Ene-reductases (ERs) from the Old Yellow Enzyme (OYE) family are versatile flavin-dependent catalysts that have been applied to the asymmetric *trans*-reduction of a broad range of activated C=C-bonds at the expense of NAD(P)H cofactor [35]. During the years, alternative catalytic activities of OYE homologues were also observed [135] such as the most recent hydride-independent isomerization of non-activated C=C-bonds [130]. The number of available ERs has grown significantly thanks to the vast genetic information available from genome sequencing. The conserved “finger print” motifs of ERs were used for a genome mining approach in order to identify new putative ERs in unconventional and extremophilic organisms. By using this approach seven new putative ERs have been identified and selected from different organisms (*i.e.* algae, cyanobacteria, bacteria and fungi). This chapter provides an overview on the discovery of the seven putative ERs and a detailed description on their cloning and heterologous expression and purification.

Over last years the number of available ERs has grown significantly, nevertheless the demand for new ERs keep growing in order to expand the biocatalytic toolbox and to overcome some limitations of this class of enzymes (such as poor substrate tolerance, modest turnover numbers, low stability in the harsh industrial conditions and in some cases low enantioselectivities) [39]. Only few industrial processes have been implemented for the large scale production achieving only recently the space-time yields required by industry [128]. The quantitative production of (2R, 5R)- dihydrocarvone starting from (R)-carvone in a biphasic system was reported using 300 mM substrate concentration (productivity of 7 g L⁻¹ h⁻¹) [112] and the reduction of ketoisophorone to (R)-levodione using 500 mM substrate concentration (productivity of 60 g L⁻¹ h⁻¹) [136]. Johnson Matthey has screened its own collection of ene-reductases with the aim of finding enzymes able to tolerate molar range substrate concentrations [137]. Furthermore, in recent years unexpected reactivity due to the chemical versatility of flavin cofactor, has been reported for this class of enzymes [135, 138]. So, the discovery of new ene-reductases has moved far beyond the classical C=C-bond reductions, driven by curiosity to (completely) understand the potentialities of this class of biocatalysts.

The majority of already known ene-reductases are derived from either bacterial, fungal, or plant sources and generally work under mesophilic reaction conditions. Few examples of ERs with improved thermostability have been isolated from extremophilic organisms and are reported in literature: TOYE isolated from *Thermoanaerobacter pseudethanolicus* [73], the chromate reductase (CrS) from the thermophile *Thermus scotoductus* SA-01 [96], GkOYE from *Geobacillus kaustophilus* [99] and FOYE from the acidophilic iron-oxidizing bacterium *Ferrovum* sp. JA12 [101]. In the last decade, attention to extreme environments has increased in order to find previously unknown extremophilic microorganisms. Microorganisms that live in extreme environments produce extremozymes, enzymes that have developed molecular mechanisms of adaptation to extreme physico-chemical conditions which make them very attractive as biocatalysts in industrial biotransformation processes [139]. Therefore, the discovery of thermophilic ERs has a great industrial potential to expand the ER biocatalytic toolkit.

3.1 Exploring novel putative ERs

All the putative ene-reductases, reported in this thesis, have been identified using a genome mining database approach. OYE1 and YqjM, belonging to the classical and thermophilic-like subclasses of ene-reductases respectively, have been used as probe sequences in the homology alignment performed by tBlastn-search. In order to enlarge the possibility to find out novel and promising biocatalysts, we have looked to unconventional and extremophilic organisms.

Using OYE1 or YqjM as template sequences together with the typical finger print motifs of classical and thermophilic-like ERs, reported by Oberdorfer *et al.* [103] (highlighted in Fig. 27), we have identified and selected seven new putative ERs from five different organisms, as reported in Table 5.

Table 5. Putative ene-reductases selected from different organisms: identity with the probe sequence, class of ene-reductases (I classical, II thermophilic-like), sequence length (AA), molecular weight (MW) and isoelectric point (pI) calculated by the computational tool ProtParam, microorganism source.

ERs	Identity (%)	Class	AA	MW (Da)	pI	Microorganism
GsOYE	38 (YqjM)	I	381	43267	5.75	<i>Galdieria sulphuraria</i>
CtOYE	41 (OYE1)	I	390	42580	5.75	<i>Chroococcidiopsis thermalis</i>
CaOYE	49 (YqjM)	II	374	39913	6.65	<i>Chloroflexus aggregans</i>
BfOYE1	43 (OYE1)	I	373	41379	5.48	<i>Botryotinia fuckeliana</i>
BfOYE4	27 (OYE1)	II	439	47728	6.36	<i>Botryotinia fuckeliana</i>
AnOYE2	42 (OYE1)	I	369	41150	6.02	<i>Aspergillus niger</i>
AnOYE8	30 (OYE1)	II	421	45757	6.68	<i>Aspergillus niger</i>

Four out of the seven sequences identified (*i.e.* GsOYE, CtOYE, BfOYE1 and AnOYE2) belong to the classical ERs family while the remaining three (*i.e.* CaOYE, BfOYE4 and AnOYE8) belong to the thermophilic-like subclass. All the selected sequences possess the conserved finger print motifs specific for each class of ERs: classical OYEs exhibit the well-conserved P-[LM]-T-R-x-R motif in loop β_1 and a G-[FYW]-xxx-P-G-[ILV]-[FHYW] pattern in loop β_2 (Fig. 27, red and cyan shading) while thermophilic OYEs exhibit the P-M-C-[MQ]-Y and G-R-I-[TS]-xxxx-G-I-W conserved motifs (Fig. 27, green and yellow shading). Finally, all selected sequences have the conserved catalytic pattern HxxN/HxY (Fig. 27, bold and red). The pair residues His/Asn or His/His act as H-bonding donors to

the electron-withdrawing group of the substrate and the conserved tyrosine residue is necessary to deliver a proton onto the C α atom of the C=C-bond.

GsOYE	-----MLKLLLE	6
CtOYE	-----MNTNIDLFS	9
BfOYE1	-----MSPSTLFT	8
AnOYE2	-----MCSKLFQ	7
CaOYE	-----MQPHLFT	7
BfOYE4	MSTPTPHQHGVCSTSPRPGLLNTPAGVPFYTPLQSPSPSGTALHL---SPSTPKLFT	57
AnOYE8	-----MKDIKVEPAKGISYFPAQETPAGTAANPQTSKGAI PKLFQ	41
	* :	
GsOYE	PFDLNGLELANRMVMA ELDRN AGPRFVPTKMNALYYAQRSL--GLIITEATQISQQGM	64
CtOYE	PVRLGRYELPNRMVMA ELDRN AGEGNVPRELNAEYYAQRVSA--GLIITEATQVSPQGL	67
BfOYE1	PLKVGTSSELQHRIAM ELDRN ADDNHVPLPMVAEYYAQRASVPGTLLVSEATFIAPRAA	68
AnOYE2	PLQIGKTNLEHRVMA ELDRN ADSQHVPLPMATYYEQRASVPGTLLIAEATLISPSAG	67
CaOYE	PLTIGSVTLRNRIGMS EMCV SAVDGFPTDW-HLMLHGRARAGVGLIILEATAVSPE GR	66
BfOYE4	PLKIRSLTLQNRIMLS EMCV SASNGHFTPW-HMAHLGGIISRGPGLSMVEATSVLPE GR	116
AnOYE8	PITIRGLTFQNLGVS EMCV SAEDGHMTDY-HLAHLGGIAQRGPGLIMIEATAVQPE GR	100
	* . : : : * : : * : : *	
GsOYE	GYPDTFGI ITDEQVDGWRMVTEAVHRRREGCIFLQLWHVGRVSHSSF-----QPN	113
CtOYE	GYPPTFGI HSQEQVEGWRVLTKAVHDRGGKIFLQLWHVGRISHPDL-----QVD	116
BfOYE1	GYANPPGI WNKEQIAGWKKVTDVAHAKKSYIMQLWALGRAADPSV-----L-QQE	118
AnOYE2	GVPHAPGV SEEQVNGWKKITEAVHKKGSFIFCQLIAGRAADPAQ-----L-HAE	117
CaOYE	ISPFDLGI WSDHIAALSRIVKLIESLGAVAGIQLAHAGRKASVGRPWEGGK--PIAPAN	124
BfOYE4	ITPEDSGL WLDSSQDKLKEVVQFAHSQQQLIGIQLSHAGRKASVPAWLD-RSAVATEEA	175
AnOYE8	ISPDVGL WQDSQIAPARVIEFAHSQGGKIGIQLAHAGRKASTTVPWMLNHGSIAIENV	160
	* : . : : : ** ** :	
GsOYE	-GQL--PVAPSAIAPE-GEVMTYDGIKPFETPRALETEEVAHIVEDYRKAAINAKRAGFD	169
CtOYE	-GAL--PVAPSAIAPSEGMATYEGEKPYVTPRALETEAIPGIVEYRQGAKNALAAAGFD	173
BfOYE1	GGYK--LQSSDIAFEGG-----GKPEPLTEAEIKEYIELYTAQAKNAIEAGFD	165
AnOYE2	GGFM--LHAPSPIIEPGM-----PVPKELDEIEVQEIIINDFAMAARNAIRAGFD	165
CaOYE	GGWP--VVGPTAEPPFAGY-----PTPIPLDAAGIARVVADFATATKRARAAGFR	172
BfOYE4	GGWPTKVKGPSAIPYDEHH-----YKPSAMTLEDIQEFKDAWAASLKRALKAGFD	225
AnOYE8	GGWPDNVKGPSDIPFSETF-----PRPRAMTQDDIREFKEAWAAAKRALVAGAD	210
	* . : : : : * : : : : . . * **	
GsOYE	GIEI H SANGYLLHEFLEDGNTKRTDRYGGSIENRTRIVFEVLDAVCKVYPSRRV-GIRLS	228
CtOYE	GVEI H SANGYLLDQFLHDGNSHRTDEYGGSIENRARLLMEVTEAVSVWGAADV-GVRLS	232
BfOYE1	GVEI H SANGYLLIDQFFQDTANQRTDSWGGSVENRAREFGLVAKSVVAAVGAET-SMRLS	224
AnOYE2	GVEI H SANGYLLVDQFLQDVSNKRNDKGGSIENRARFGLVAKAVADAIGADRL-GFRLS	224
CaOYE	WIEI H AHGYLELHNFLSPLGNDRNDEYGGDLRGRVRLLEVTAAVRAEWPDDLPLAVRLS	232
BfOYE4	VIEI H NAHGYLELHEFVSPVSNKRTDQYGGSFENRIRLTLEIVEITRKIIPESMPLFLRIS	285
AnOYE8	FIEI H NAHGYLELASFLTPYANKRTDEYGGSFENRMLPLKIAQLTRDTVGEHVPVFLRLS	270
	:*** *:*** :.* . *.* :* . . * : : :.*	
GsOYE	P--DTEFMSMSDSR-PALYSYLQELSRRELAYLHLIEPRIKGNVDVE--KE-SSLNVK	282
CtOYE	P--SGTFGSVYDSDL-KALFTYVDALNQFELAYLHLVEPRVAGNETVE--NPTSELSK	287
BfOYE1	P--FSPFQGMKADP-IPQFTYIAQELKLNLYLHVVESRIIGNADIE--ATE--KVD	276
AnOYE2	P--WNTWQSMKMVDP-VPQFTYFVERLQLGLAYLHVIESRVINNVCE--KEG--SIK	276
CaOYE	CSDWTF-----EGLTIADTVEVARMLRQG-V--DLIDCSGGIAPGITIPVGEYQVP	283
BfOYE4	ATDWLDYEGFGEESWTVADSARLAGILADRG-V--DLMDVSSGANHPKQKITAGLGYQAP	342
AnOYE8	ASDWLGST--STETWDLQHAVRFAEALADQGAI--DLVDVSSGGLHSSQEVKSGPGFQAP	326
 * : : : :	
GsOYE	FFRPLYK-----G--VLITAG-----GYQKETGEERLQ---KQHADLVAYGR	319
CtOYE	YFRPIYK-----G--TLISAG-----GYDRESGNAVLA---SGDADLVAYGR	324
BfOYE1	FLINIWV-----GTSPIILAG-----GFTAESAKKAVEEYKGDIVIVFGR	318
AnOYE2	FLLDVWG-----KSAFVIVAG-----GYRPNVENALEEYKYDKVAVAFGR	318
CaOYE	FAAQVRREAN--IATAAVGLITRPEHADAIVRN-----GDADLVLLGR	324
BfOYE4	FAKEIKRVVGERMLVGTVMGIGSRQAEGLLSGMGGGERVDEGEEEGKGTLEDLVIVAR	402
AnOYE8	FGIAVKAVGERMLVATVGHIRDGKANRLLEE-----EGLDVLVIVGR	369
	: : : : : : : : : : : . *	
GsOYE	WVIANPDLPSRFEQNALPNPYDRATFYGG-NEKGYTDYPFDPDRDSQEALKEAEAERKW	378
CtOYE	LFITNPDLQRFALNAQLNPDYDRSSFYGG-DKRGYTDYPSLELQAAG-----	370
BfOYE1	YFITNPDLPRVKEGIEFTPYDRDFYNNKKEAEGYTTYPFSEKFEAQRKAIESSA----	373
AnOYE2	HFIANPDLPRIRHDIHLNPDYRESFYTPLENGYTDYFSAEFTKSKTKC-----	369
CaOYE	ELLRDPHWPVLRARALGHDLAPPQYLRAW-----	354
BfOYE4	GFQKNPGLVWEWAEELGVRIMVAHQMRWGRGKAGGH-----	439
AnOYE8	GFQKDFGLVWTFQAHLQDVEVAMPQQIRWGFSGRRGTFVFDVPSYKPSVIE-----	421
	. : *	
GsOYE	RRL	381
CtOYE	---	370
BfOYE1	---	373
AnOYE2	---	369
CaOYE	---	354
BfOYE4	---	439
AnOYE8	---	421

Figure 27. Sequence alignment of the selected seven putative ERs performed by Clustal Omega. The catalytic residues are in bold (red) and the finger print motifs reported by Oberdorfer *et al.* [103] are highlighted in red and cyan for classical ERs and green and yellow for thermophilic-like ERs. GsOYE (XP_005703492.1), CtOYE (WP_015152687.1), CaOYE (WP_015941499.1), BfOYE1 (XP_001558622.1), BfOYE4 (XP_001554780.1), AnOYE2 (XM_001393007.1) and AnOYE8 (NT_166519.1).

3.1.1 New putative ERs from prokaryotic organisms

Bacteria and cyanobacteria are reported in literature as ERs sources (Table 6). The vast majority of ene-reductases have been identified in bacteria. However, to our knowledge, photosynthetic bacteria have not yet been exploited as ERs sources. In the meanwhile, just ten ene-reductases have been identified and characterized from cyanobacteria. These enzymes shown high catalytic efficiency and some of them excellent stereoselectivities in the reduction of (*R*)-carvone. Moreover, AcaryoER1, AcaryoER3 and AnabaenaER3 could accept also NADH instead of the most expensive NADPH, as cofactor [140].

We have identified two new putative ERs from extremophilic photosynthetic bacteria: the cyanobacterium *Chroococcidiopsis thermalis* and the thermophilic phototrophic filamentous bacterium *Chloroflexus aggregans* (Table 5). CtOYE (WP_015152687.1), belonging to the classical class of ene-reductases, was chosen using OYE1 as probe showing 41% identity with this, while CaOYE (WP_015941499.1), belonging to thermophilic-like OYE subclass, was chosen using YqjM as probe sequence and its primary sequence is 49% identical to the probe.

3.1.2 New putative ERs from eukaryotic organisms

Fungi and plants, are also reported as ERs sources but the number of enzymes isolated from these eukaryotic organisms is still limited as shown in Table 7. Nevertheless, different whole-cell screenings with fungi or plant tissues are reported in literature. A functional screening using whole-cell biotransformation was performed by Romagnolo *et al.* [141] using 28 fungi belonging to different phyla in order to detect ER activity towards three representative OYE standard substrates. In most cases, activity towards 2-cyclohexen-1-one, α -methyl- β -nitrostyrene, and (E)- α -methylcinnamaldehyde was detected. Similarly, in another study reported by Romano *et al.* [142] eight OYEs from nonconventional yeasts have been screened by expressing them in a *Saccharomyces cerevisiae* deleted OYE strain (BY4741 Δ Oye2). Target compounds were ketoisophorone, α -methyl-*trans*-cinnamaldehyde, and *trans*- β -methyl- β -nitrostyrene. In parallel to the functional screening a bioinformatic approach was also reported by Nizam *et al.* [59]. Using active site residues and sequence alignments, 424 OYEs proteins from 60 fungal genomes were identified.

Table 6. Sources of biochemically characterized prokaryotic OYEs (modified from [98])

Group/Order	Enzyme	Source	References
Proteobacteria/ α-Proteobacteria	NerA (CAA74280)	<i>Agrobacterium radiobacter</i>	[143]
	NCR (AAV90509)	<i>Zymomonas mobilis</i>	[144]
	GluER (AAW60280)	<i>Glucunobacter oxidans</i> DSM 2343	[145]
Proteobacteria/ β-Proteobacteria	FOYE1 (KRH78075)	<i>Ferrovum</i> sp. JA12	[101]
	RmER (ABF11721)	<i>Cupriavidus metallidurans</i> CH34	[146]
	Achr-OYE3 (AFK73187)	<i>Achromobacter</i> sp. JA81	[147]
	Achr-OYE4 (AFK73188)	<i>Achromobacter</i> sp. JA81	[147, 148]
Proteobacteria/ γ-Proteobacteria	MR (AAC43569)	<i>Pseudomonas putida</i> M10	[149]
	PETNR (AAB38683)	<i>Enterobacter cloacae</i> PB2	[150]
	NemA (BAA13186)	<i>Escherichia coli</i>	[62]
	NemA2 (AHC69715)	<i>Pseudomonas putida</i> ATCC 17453	[151]
	XenA (AAF02538)	<i>Pseudomonas putida</i> II-B	[152]
	XenA2 (AHH54488)	<i>Pseudomonas putida</i> ATCC 17453	[151]
	XenB (AAF02539)	<i>Pseudomonas fluorescens</i> I-C	[152]
	XenB2 (AGS77941)	<i>Pseudomonas putida</i> ATCC 17453	[151]
	YersER (WP_032896199)	<i>Yersinia bercovieri</i>	[153]
	SYE1 (AAN55488)	<i>Shewanella oneidensis</i>	[49]
	SYE3 (AAN57126)	<i>Shewanella oneidensis</i>	[49]
SYE4 (AAN56390)	<i>Shewanella oneidensis</i>	[49]	
Actinobacteria	OYER02 (ALL54975)	<i>Rhodococcus opacus</i> 1CP	[102]
	Nox (ALG03744)	<i>Rhodococcus erythropolis</i>	[154]
	PfvC (AFF18622)	<i>Arthrobacter</i> sp. JBH1	[155]

Bacteroidetes/ Flavobacteria	<i>Chr-OYE1</i> (ALE60336)	<i>Cryseobacterium</i> sp. CA49	[156]
	<i>Chr-OYE2</i> (ALE60337)	<i>Cryseobacterium</i> sp. CA49	[156]
	<i>Chr-OYE3</i> (AHV90721)	<i>Cryseobacterium</i> sp. CA49	[157]
Firmicutes/ (Bacilli, Clostridia)	YqjM (BAA12619)	<i>Bacillus subtilis</i> strain 168	[94]
	YqiG (BAA12582)	<i>Bacillus subtilis</i> strain 168	[158]
	<i>GkOYE</i> (BAD76617)	<i>Geobacillus kaustophilus</i> DSM7263	[99]
	<i>GeoER</i> (BAO37313)	<i>Geobacillus</i> sp. 30	[100]
	<i>LacER</i> (ADK19581)	<i>Lactobacillus casei</i> str. Zhang	[159]
	TOYE (ABY93685)	<i>Thermoanaerobacter pseudethanolicus</i>	[73]
E39			
Deinococcus-Thermus	<i>TsOYE</i> (CAP16840)	<i>Thermus scotoductus</i> SA-01	[160]
	<i>DrER</i> (AAF11740)	<i>Deinococcus radiodurans</i> R1	[146]
Cyanobacteria/ (Gloebacteria, Oscillatoriophycidea, Nostocales)	<i>GleoER</i> (BAC91769)	<i>Gloeobacter violaceus</i> PCC7421	[140]
	<i>CyanoER1</i> (ACK64210)	<i>Cyanothece</i> sp. PCC8801	[140]
	<i>CyanoER2</i> (ACK65723)	<i>Cyanothece</i> sp. PCC8801	[140]
	<i>LyngbyaER1</i> (EAW37813)	<i>Lyngbya</i> sp. PCC8106	[140]
	<i>AcaryoER1</i> (ABW29811)	<i>Acaryochloris marina</i> MBIC11017	[140]
	<i>AcaryoER3</i> (ABW32756)	<i>Acaryochloris marina</i> MBIC11017	[140]
	<i>SynER</i> (ABB56505)	<i>Synechococcus elongatus</i> PCC7942	[161]
	<i>NospuncER1</i> (ACC84535)	<i>Nostoc punctiforme</i> PCC73102	[140]
	<i>NostocER1</i> (BAB73564)	<i>Nostoc</i> sp. PCC7120	[140]
	<i>AnabaenaER3</i> (ABA25236)	<i>Anabaena variabilis</i> ATCC 29413	[140]

Within the analyzed species, the number of OYE homologs found in each genome varies from one to twenty-two, and over a half of the fungi analyzed contain more than five OYEs belonging to both classes of ene-reductases. This evolutionary diversification might be explained thanks to the high versatility of these organisms and to their adaptation to different environments and carbon sources. Moreover, the expression of the different isoenzymes can be triggered by the surrounding environment (*e.g.* nutrients, presence of noxious substrates, physico-chemical parameters). For these reasons, the different isoenzymes may have evolved toward the recognition and reduction of specific substrates, thus, making fungi very attractive as new biocatalyst sources having an enzyme toolbox catalytically fine-tuned toward a wide range of substrates [60]. Finally, functional screening of ER activity has also been described with 13 plant tissue cultures using 2-cyclohexen-1-one as the model substrate [162]. Different plant cultures displayed ER activity also toward β -nitrostyrene and maleimides. Thanks to their complex and unique biosynthetic pathways and enzymatic promiscuity, photosynthetic eukaryotes seem to be good candidate sources in the search of new ERs.

Table 7. Sources of biochemically characterized eukaryotic OYEs (modified from [98])

Kingdom	Enzyme	Source	Ref.
Fungi	OYE1 (CAA37666)	<i>Sacchromyces pastorianus</i>	[163]
	OYE2 (AAA83386)	<i>Sacchromyces cerevisiae</i>	[164]
	OYE3 (AAA18013)	<i>Sacchromyces cerevisiae</i>	[165]
	EBP1 (AAA18013)	<i>Candida albicans</i>	[166]
	HYE1 (AAN09952)	<i>Ogataea angusta</i>	[167]
	HYE2 (AAN09953)	<i>Ogataea angusta</i>	[167]
	CYE (BAD24850)	<i>Kluyveromyces marxianus</i>	[168, 169]
	KYE1 (AAA98815)	<i>Kluyveromyces lactis</i>	[153]
	OYE2.6 (ABN66026)	<i>Scheffersomyces stipitis</i> CBS 6054	[170]
	CIER (EEQ40235)	<i>Clavispora lusitaniae</i> ATCC 42720	[136]
	MgER (EDK41665)	<i>Meyerozyma guilliermondii</i> ATCC 6260	[171]
Plants	<i>LeOPR1</i> (NP_001234781)	<i>Solanum lycopersicum</i>	[172]
	<i>LeOPR2</i> (NP_001233868)	<i>Solanum lycopersicum</i>	[173]
	<i>LeOPR3</i> (NP_001233873)	<i>Solanum lycopersicum</i>	[173]
	<i>AtOPR1</i> (NP_177794)	<i>Arabidopsis thaliana</i>	[174]
	<i>AtOPR2</i> (NP_177795)	<i>Arabidopsis thaliana</i>	[175]
	<i>AtOPR3</i> (NP_001077884)	<i>Arabidopsis thaliana</i>	[176]

Apart from the few enzymes reported in Table 7, fungi and photosynthetic eukaryotes are still an unexplored source of OYEs despite their high potential. Moreover, to our knowledge, until now, just superior photosynthetic eukaryotes such as higher plants have been taken in consideration while simple photosynthetic organisms such as unicellular algae have not yet been explored as ERs sources. We have identified five new putative ERs from eukaryotic organisms: the poly-extremophilic alga *Galdieria sulphuraria* and the fungi *Botryotinia fuckeliana* and *Aspergillus niger*.

GsOYE (XP_005703492.1), isolated from the polyextremophilic alga *Galdieria sulphuraria*, was 38% identical to the probe sequence YqjM, used for its identification.

The Ascomycete *Botryotinia fuckeliana*, identified in parallel by the screening of Nizam [59] and Romagnolo [141], seem to be an interesting source for new putative ene-reductases. In the genome of this fungus, 7 OYEs homologues are present and they belong to different OYEs classes (Table 8). Furthermore, *B. fuckeliana* cells, were able to completely reduce 2-cyclohexen-1-one and moderate activity was detected with α -methylcinnamaldehyde [141]. *BfOYE1* (XP_001558622.1) and *BfOYE4* (XP_001554780.1), belonging to the classical and thermophilic-like class, respectively, were chosen among the 7 sequences retrieved using OYE1 as probe sequence. *BfOYE1* shows 43% identity while *BfOYE4* shows 27% identity with the probe.

The Ascomycete *Aspergillus niger*, identified in parallel by the screening of Nizam [59] and Romagnolo [141], is another interesting source for new putative ene-reductases. In the genome of this fungus, 12 OYEs homologues are present and they belong to different OYEs classes (Table 9). Furthermore, *A. niger* cells were shown to moderately reduce 2-cyclohexen-1-one and completely convert methylnitrostyrene within 2 days [141]. *AnOYE2* (XM_001393007.1) and *AnOYE8* (NT_166519.1), belonging to the classical and thermophilic-like class, respectively, were chosen among the 12 sequences retrieved by using OYE1 as probe sequence for the blast research. *AnOYE2* and *AnOYE8* are 42% and 30% identical to the probe, respectively.

The eukaryotic ene-reductases, especially the one from fungi, were chosen based on the number of exons and of predicted N-glycosylation sites, to facilitate the engineering strategy for expression, which was firstly planned in *E. coli* and in a

second moment in *P. pastoris*.

Table 8. List of OYE genes identified from *Botryotinia fukeliana* along with their corresponding nomenclature, protein sequence ID, Class, protein length and sub-cellular localization (modified from [59]).

OYEs	Sequence ID	OYE class	Aa lenght	sub-cellular localization
BfOYE1	XP_001558622.1	I	373	Cytoplasm
<i>BfOYE2</i>	XP_001556041.1	I	413	Cytoplasm
<i>BfOYE3</i>	XP_001558929.1	II	432	Cytoplasm
BfOYE4	XP_001554780.1	II	439	Mitochondria
<i>BfOYE5</i>	XP_001548368.1	II	365	Cytoplasm
<i>BfOYE6</i>	XP_001547575.1	III	443	Cytoplasm
<i>BfOYE7</i>	XP_001547383.1	III	335	Cytoskeleton

Table 9. List of OYE genes identified from *Aspergillus niger* along with their corresponding nomenclature, protein sequence ID, Class, protein length and sub-cellular localization (modified from [59]).

OYEs	Sequence ID	OYE class	Aa lenght	sub-cellular localization
<i>AnOYE1</i>	XP_001394816.2	I	370	Cytoplasm
AnOYE2	XP_001393044.1	I	369	Cytoplasm
<i>AnOYE3</i>	XP_001390054.1	I	384	Mitochondria
<i>AnOYE4</i>	XP_001401198.1	I	421	Cytoplasm
<i>AnOYE5</i>	XP_001389993.1	II	420	Cytoplasm
<i>AnOYE6</i>	XP_001389551.2	II	419	Cytoplasm
<i>AnOYE7</i>	CAK48758.1	II	415	Cytoplasm
AnOYE8	XP_001399273.1	II	421	Cytoplasm
<i>AnOYE9</i>	XP_001397404.1	II	443	Cytoplasm
<i>AnOYE10</i>	XP_001391174.1	II	422	Cytoplasm
<i>AnOYE11</i>	XP_001390672.2	III	412	Mitochondria
<i>AnOYE12</i>	XP_001395504.2	III	418	Mitochondria

3.2 General cloning and expression strategy

A common strategy was used for the cloning of all seven sequences identified previously (Fig. 28). The expression vectors were created by digestion of pET-28a(+) with NdeI/BamHI (except for *AnOYE8* that was digested with NdeI/HindIII) and ligation of the amplified sequences, cut by the same enzymes. The desired sequences were obtained starting from genomic DNA by two subsequent PCR reactions: a first PCR amplification was performed using external primers in order to produce a preliminary amplicon, and a second mutagenic one utilizing nested primers. In this case, the latter step introduced the NdeI and BamHI/HindIII restriction sites at the 5' and 3' of the coding sequence. The DNA sequence for each newly identified ene-reductase and all the steps employed in their cloning are reported in detail in the appendix. The final recombinant plasmids were checked by sequencing.

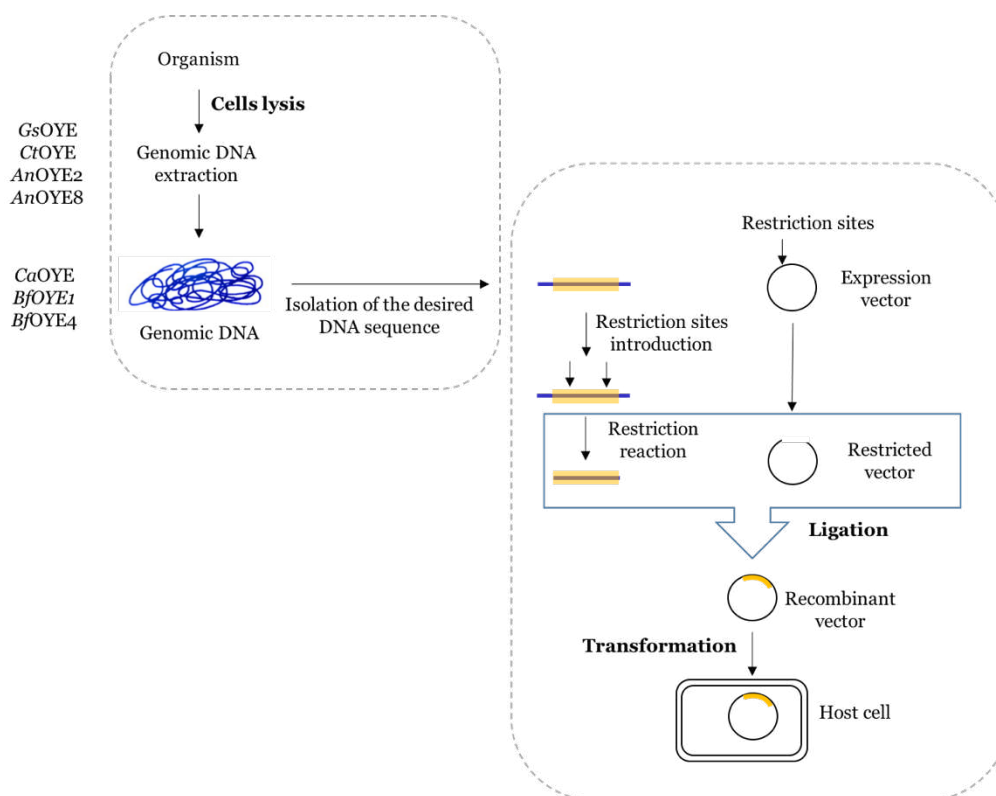


Figure 28. Cloning strategy scheme.

Plasmid pET-28a(+), which carries the T7 promoter, the kanamycin resistance gene and a hexahistidine coding sequence tail fused to the 5' of cloned ORF was used as expression vector. The host cells for this expression system are *E. coli* BL21 (DE3) cells that have the gene for the T7 RNA polymerase stably integrated in their genome and it is controlled by the inducible promoter lac. Thus, the obtained constructs were transformed in *E. coli* BL21 (DE3) and preliminary

expression tests were performed. In order to set up the proper conditions to obtain the desired recombinant proteins in soluble form different parameters such as temperatures and strains of *E. coli* were varied. An SDS-PAGE analysis was used to verify the expression of the proteins at different induction times and their solubility behavior after cell disruption. To confirm the identity of the target proteins an immunoblotting assay was performed using anti His-tag antibodies. Once the best conditions of production were identified the proteins were purified using IMAC chromatography following the standard protocol reported in the section Materials and Methods. The optimized conditions of expression of the proteins are summarized in Table 10.

In addition to the seven putative ene-reductases, other two already reported enzymes, OYE2 and OYE3, respectively, were produced and used for crystallographic studies in collaboration with Dr. Mélanie Hall from Graz University. The expression conditions of these two proteins have been optimized and are also summarized in Table 10.

Table 10. Optimized conditions for putative ERs production: expression vector and host, temperature and final yield.

Enzyme	Cloning vector	Expression host & strain	Temp (°C)	Yield (mg/L)
GsOYE	pET28a(+)	<i>E. coli</i> BL21 (DE3)	25	98
CtOYE	pET28a(+)	<i>E. coli</i> BL21 (DE3)	25	80
CaOYE	pET28a(+)	<i>E. coli</i> BL21 (DE3)	25	75
BfOYE1	pET28a(+)	<i>E. coli</i> BL21 (DE3)	25	42
BfOYE4	pET28a(+)	<i>E. coli</i> BL21 (DE3)	16	7
		<i>E. coli</i> BL21 (DE3) Arctic ®	16	10
AnOYE2	pET28a(+)	<i>E. coli</i> BL21 (DE3) Arctic ®	12	13
AnOYE8	pET28a(+)	<i>E. coli</i> BL21 (DE3) Arctic®	12	9
OYE2	pET28a(+)	<i>E. coli</i> BL21 (DE3)	16	40
OYE3	pET28a(+)	<i>E. coli</i> BL21 (DE3)	16	40

An additional Size Exclusion Chromatography step was performed for crystallization studies in order to obtain highly-pure protein preparations. Finally, enzymes concentration was measured by spectrophotometry, measuring the concentration of free flavin mononucleotide (FMN) in a solution of denatured protein and calculated as previously reported [177]. For more details see Materials and Methods chapter and Appendix for the UV/Vis spectra of each purified enzyme.

3.3 GsOYE from *Galdieria sulphuraria*

Galdieria sulphuraria (Fig. 29) is a unicellular thermoacidophilic red alga able to grow in the extreme conditions of pH (1.5 - 2.0) and temperature (> 56 °C) of volcanic hot springs. Moreover, it displays also high salt and metal tolerance and exhibits extensive metabolic versatility [178, 179]. This microalga is of particular importance in the human nutrition, cosmetics and fine chemicals fields. Heterotrophic cultures of *G. sulphuraria* contain high levels of phycocyanin, a pigment used in the diagnostic field as fluorescent marker and as dye in the cosmetic and food market. Furthermore, the high protein content of its cell wall is a unique feature that can be exploited for nutritional applications [180].

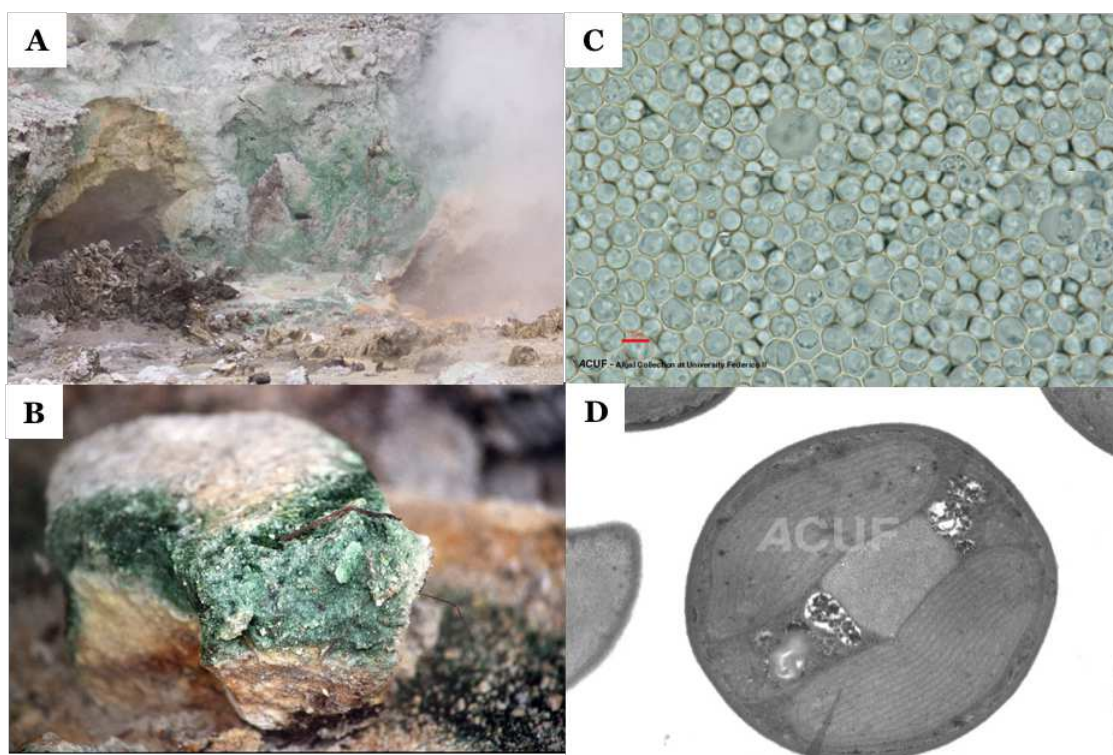


Figure 29. (A) Cyanidiophyceae community near the hot springs; (B) *Galdieria* growing on a rock at Pisciarelli (Italy); (C) *Galdieria sulphuraria* cells in heterotrophic growth; (D) TEM image of *Galdieria* cells. All the pictures are from www.ACUF.net

Galdieria sulphuraria strain 074W was kindly provided by Dr. Antonino Pollio from the ACUF collection of the Biological Science Department of University Federico II, Naples, Italy. Cultures of *G. sulphuraria* were grown at 30 °C in Allen Medium pH 1.0 [181] on a rotatory platform shaker at 70 rpm. Light conditions used were 25 mol photons m⁻² sec⁻¹. The genomic DNA has been extracted following an established protocol [182] and used as starting material for the two consecutive PCR reactions described in section 3.2. Two additional PCR reactions

were performed in order to suppress an internal NdeI restriction site and a predicted N-glycosylation site.

As displayed from the gel in Figure 30A, very good over-expression and solubility were obtained for GsOYE expressed in BL21(DE3) strain at 25 °C. From immunoblotting assay (Fig. 30B) a small (negligible) fraction of the protein has been detected also in the insoluble fractions.

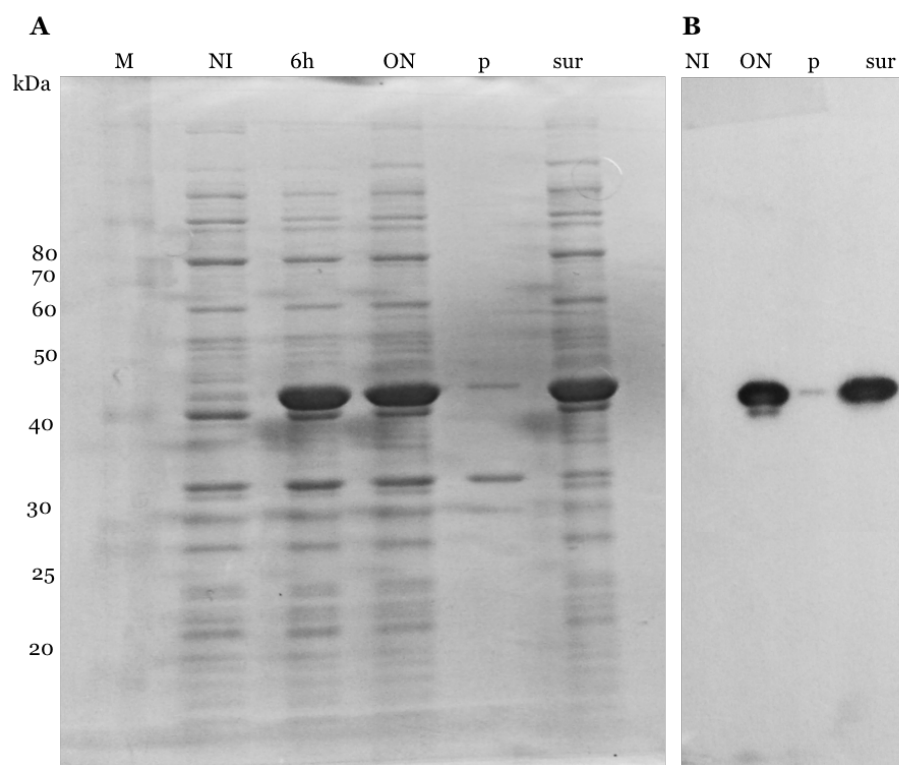


Figure 30. (A) SDS-PAGE 12% acrylamide: BL21(DE3) grown at 25 °C expressing GsOYE: BenchMark™ protein ladder (M), total cell extracts from non-induced (NI) and 6 h and overnight induced cells with IPTG (6h and ON), pellet fraction (p), soluble protein fraction (sur). (B) Western blot assay with anti-His tag antibodies with samples of protein induced at 25 °C.

GsOYE has been purified in the optimized conditions reported in Table 10 with very good yields (98 mg/L). The SDS-PAGE in Figure 31 shows the homogeneity of the recombinant protein preparation after IMAC and SEC purification.

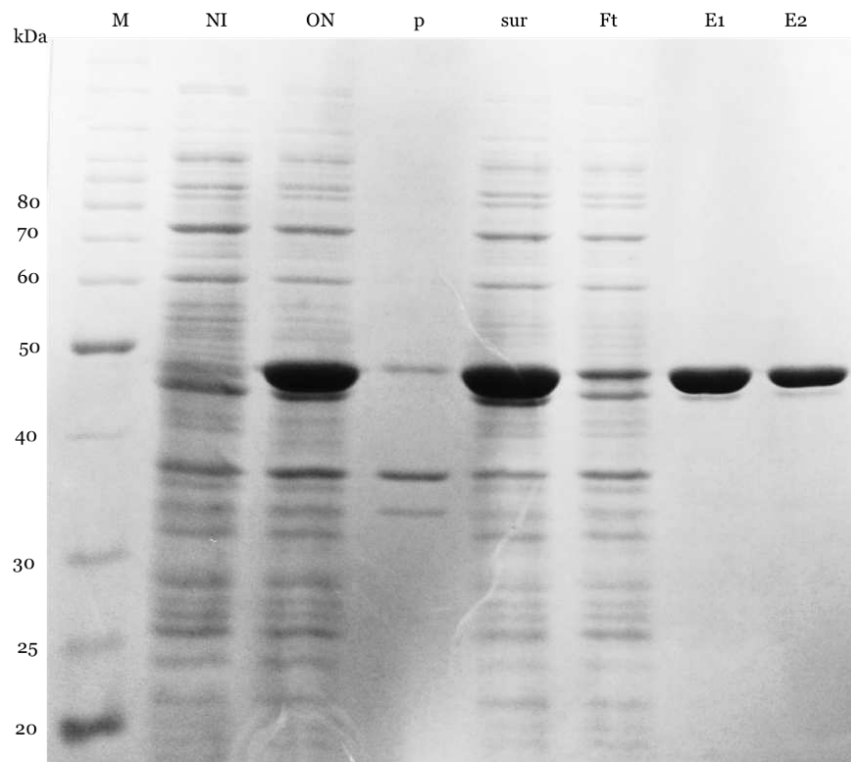


Figure 31. (A) SDS-PAGE 12% acrylamide of *GsOYE* purification using BL21(DE3) cells grown at 25 °C: BenchMark™ protein ladder (M), total cell extracts from non-induced (NI) and overnight induced cells with IPTG (ON), pellet fraction (p), soluble protein fraction (sur), flow-through (Ft), eluted fraction from IMAC (E1) and preparative SEC (E2).

3.4 *CtOYE from Chroococcidiopsis thermalis*

Chroococcidiopsis thermalis (Fig. 32) is a coccoid cyanobacterium, adapted to live in extreme environments such as arid, hot and cold deserts. This organism lives generally on the surface of porous rocks or in biofilms at the stone-soil interface in desert pavements. Most of the time, the cells are desiccated or frozen. The cells are able to resist to desiccation by producing abundant exo-cellular polysaccharides that regulate the loss and uptake of water [183].

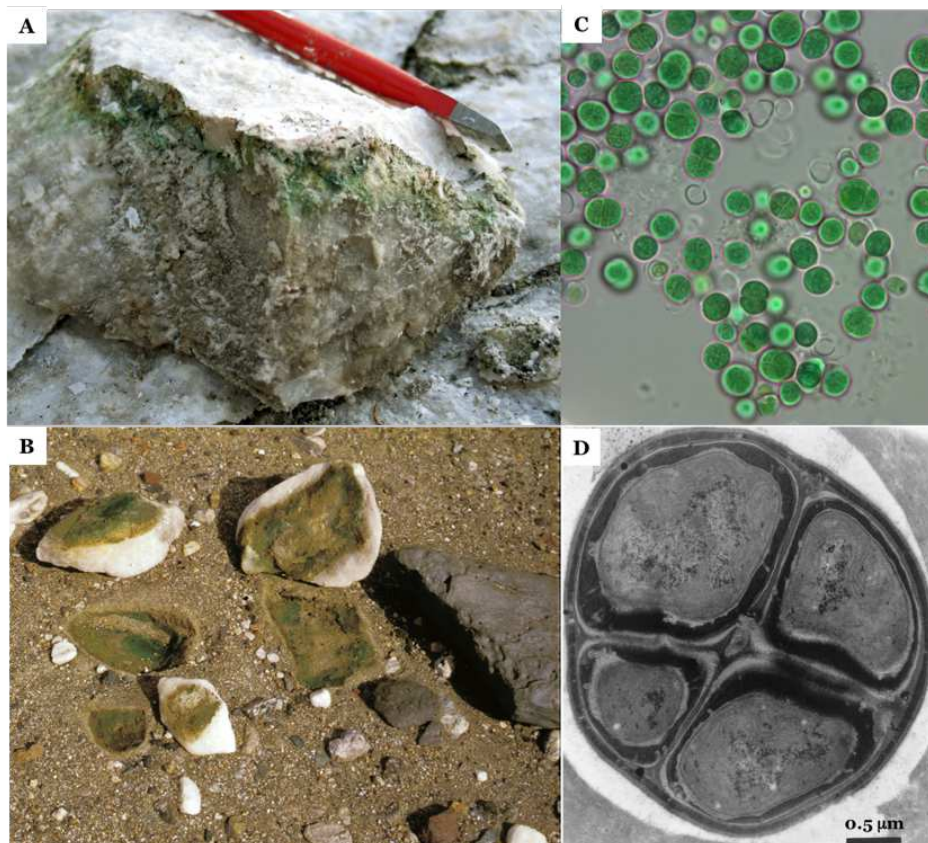


Figure 32. (A) *Chroococcidiopsis* growing on the upper layers of a fractured gypsum rock from the lower Saxony city Bad Sachsa, (B) *Chroococcidiopsis* growing underneath quartz pebbles in the Namib-Desert, (C) Cells of *Chroococcidiopsis thermalis* grown in BG-11 medium (D) Electron micrograph of ultrathin section of 2-month-old *Chroococcidiopsis* strain 029 showing multicellular aggregate containing cells of different sizes. Pictures A and B are from Burkhard Büdel, TU Kaiserslautern (https://dbg-phykologie.de/en/?tx_wwpreset%5Barticle%5D=7924), picture C was kindly provided by Nicoletta LaRocca, while picture D is modified from [183].

Chroococcidiopsis thermalis PCC 7203 from the Pasteur Culture Collection was kindly provided by Prof. Nicoletta LaRocca from Padova University, Italy. Cells were grown photoautotrophically at 20 °C in BG11 medium. Static cultures were continuously illuminated at 25 mol photons m⁻² sec⁻¹. The genomic DNA has been extracted following an established protocol [182] and used as starting material for the two consecutive PCR reactions described in section 3.2.

As shown in the gel depicted in Figure 33A, very good over-expression and solubility were obtained for *CtOYE* expressed at all temperatures tested. At 18 °C the over-expression levels seem higher than that at 25 and 30 °C but more protein is present in the insoluble fraction. The best compromise between over-expression levels and solubility is represented by 25 °C expression. From blot analysis, some shorter polypeptides (likely resulting from proteolysis or from abortive protein synthesis due to the presence of rare codons (22%) in the original sequence), have been detected in the soluble fraction (Fig. 33B).

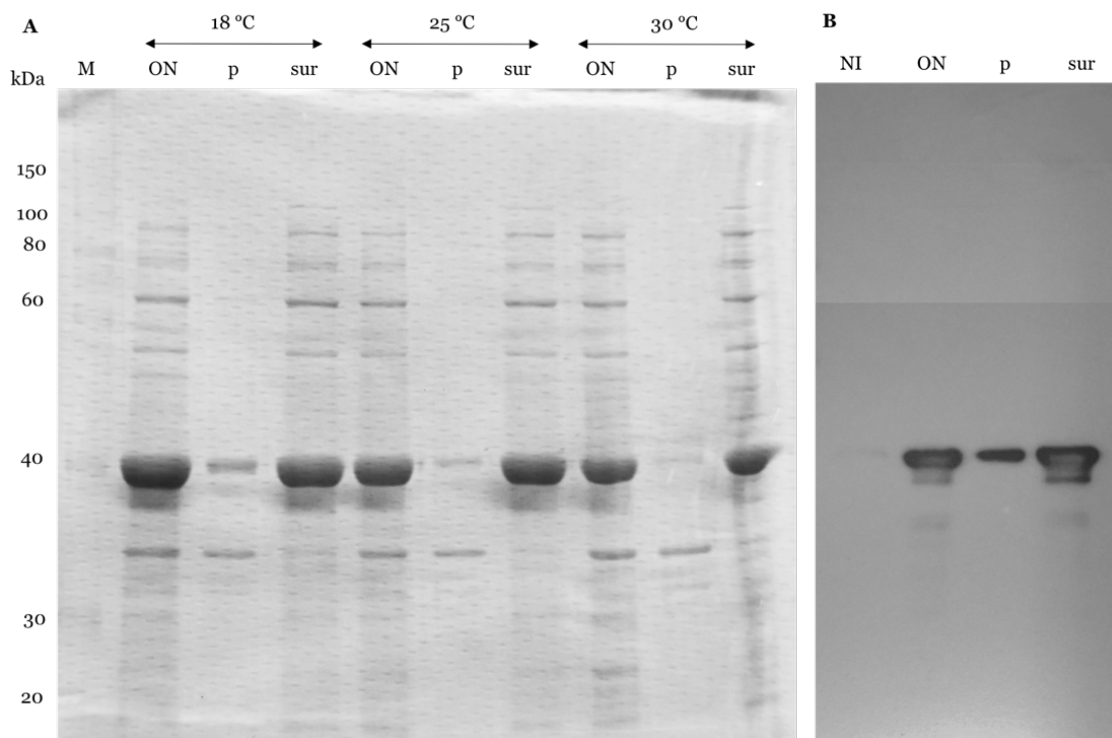


Figure 33. (A) SDS-PAGE 12% acrylamide: BL21(DE3) grown at 18, 25 and 30 °C expressing *CtOYE*: RotiMark™ protein ladder (M), total cell extracts from over-night induced cells with IPTG (ON), pellet fraction (p), soluble protein fraction (sur). (B) Western blot assay with anti-His tag antibodies with samples of protein induced at 25 °C.

CtOYE has been purified with very good yields (80 mg/L). During the purification, some protein was eluted with the flow-through probably due to saturation of the resin (Fig. 34) and the shorter protein impurities, observed in the immune-blot analysis, appear to be almost (completely) eliminated after SEC chromatography.

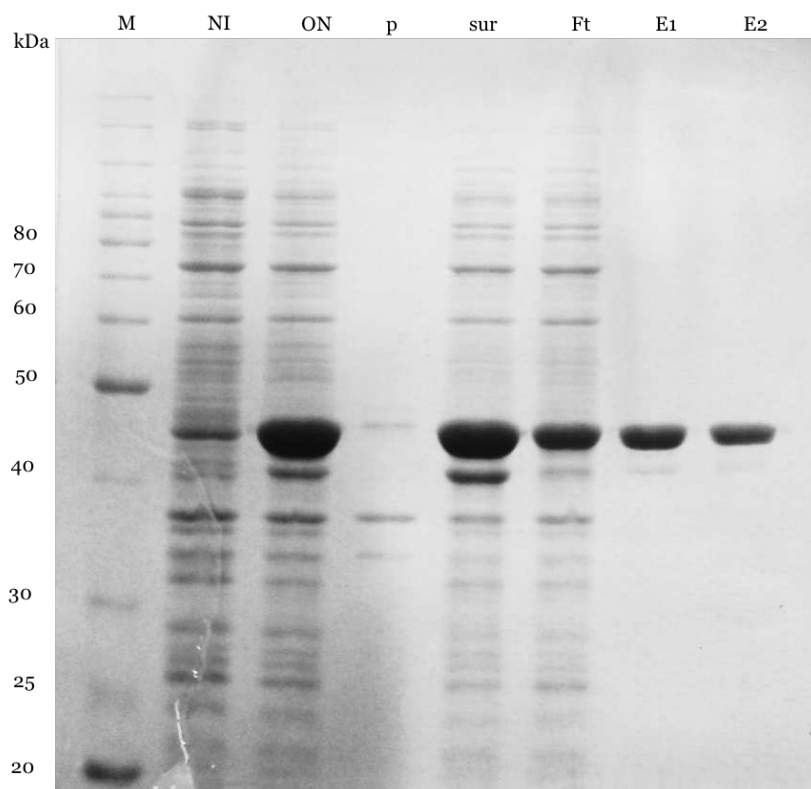


Figure 34. SDS-PAGE 12% acrylamide of *CtOYE* purification using BL21(DE3) cells grown at 25 °C: BenchMark™ protein ladder (M), total cell extracts from non-induced (NI) and over-night induced cells with IPTG (ON), pellet fraction (p), soluble protein fraction (sur), flow-through (Ft), eluted fraction from IMAC (E1) and preparative SEC (E2).

3.5 CaOYE from *Chloroflexus aggregans*

Chloroflexus aggregans is a thermophilic phototrophic filamentous bacterium belonging to the family of *Chloroexaceae*, characterized by gliding motility (Fig. 35). It was first isolated from bacterial mats in Yufuin and Meotobuchi hot springs from Japan. It generally forms dense bacteria mats with other organisms such as thermophilic cyanobacteria, sulphur-oxidizing bacteria and aerobic and anaerobic heterotrophic bacteria. *Chloroflexus* is widely distributed in terrestrial hot springs in the temperature range of 50–70 °C with an optimal temperature of growth of 55 °C [184].

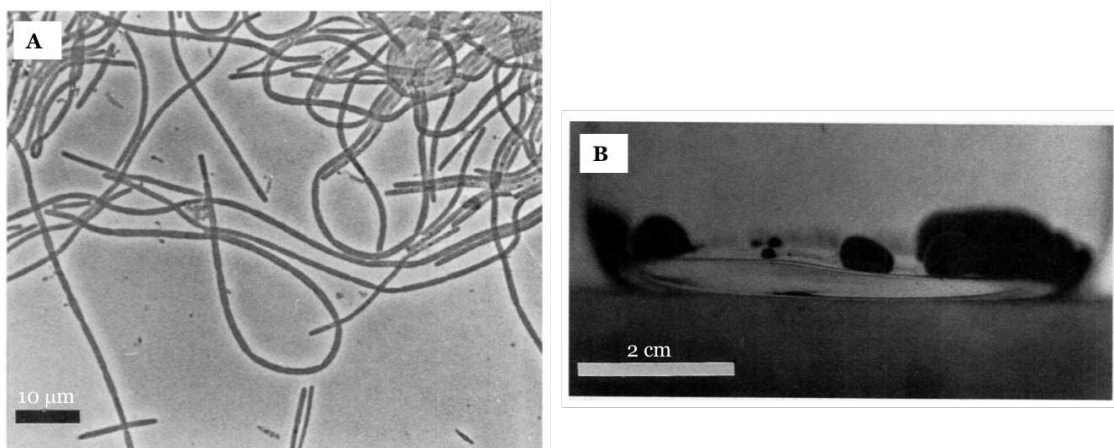


Figure 35. (A) Phase-contrast photomicrograph of *Chloroflexus aggregans* strain DSM 9485 cells showing septa in filaments. Cells in the stationary growth phase were grown phototrophically at 55 °C and 30 W/m² in PE medium. (B) Mat-like dense aggregates of strain DSM 9485 cells growing in the bottom of a 200 ml screw-cap bottle containing PE medium under phototrophic conditions (modified from [184]).

The genomic DNA of *Chloroflexus aggregans* DSM 9485 was purchased from DSMZ culture collection and used as starting material for the cloning strategy described in section 3.2.

CaOYE was highly over-expressed at all different temperatures tested (18 °C, 25 °C and 30°C) (Fig. 36A). As a result of the massive synthesis, at all tested conditions the enzyme was partially accumulated in the form of insoluble inclusions bodies. A good amount of correctly folded protein, sufficient to perform the biochemical and biocatalytic characterization, was found in the soluble fraction (Fig. 36A). The western-blot analysis showed that a (lower) fraction of the recombinant product was produced as shorter, incomplete polypeptides (likely resulting from proteolysis or from abortive protein synthesis due to the presence of rare codons (16%) in the original sequence), that however accumulates in the insoluble fractions (Fig. 36B).

CaOYE has been purified in the optimized conditions reported in Table 10 with very good yields (75 mg/L). The gel of the final purification is not shown.

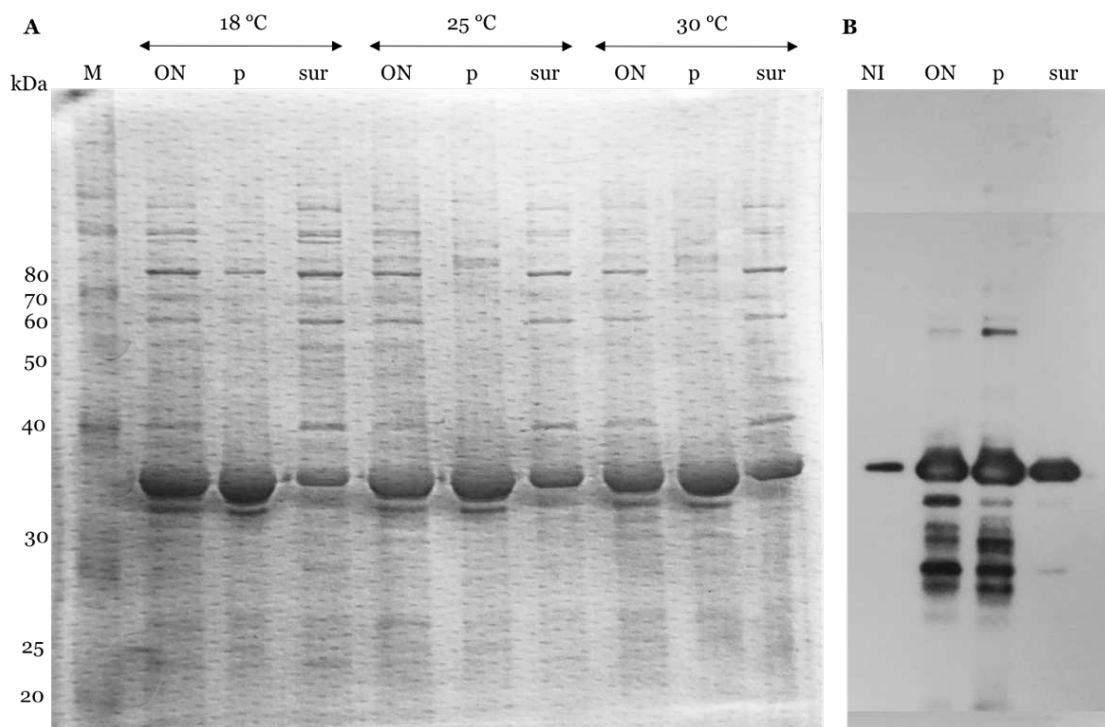


Figure 36 (A) SDS-PAGE 12% acrylamide: BL21(DE3) grown at 18, 25 and 30 °C expressing *CaOYE*: BenchMark™ protein ladder (M), total cell extracts from over-night induced cells with IPTG (ON), pellet fraction (p), soluble protein fraction (sur). (B) Western blot assay with anti-His tag antibodies with samples of protein induced at 25 °C.

3.6 *BfOYE1* and *BfOYE4* from *Botryotinia fuckeliana*

The fungus *Botryotinia fuckeliana* B05.10 (*Botrytis cinerea*) (Fig. 37) belongs to the class of Ascomycetes. It is a plant pathogen (gray mold) and its infections are of considerable economic importance in grapes, vegetables and berries cultivation crops [185].

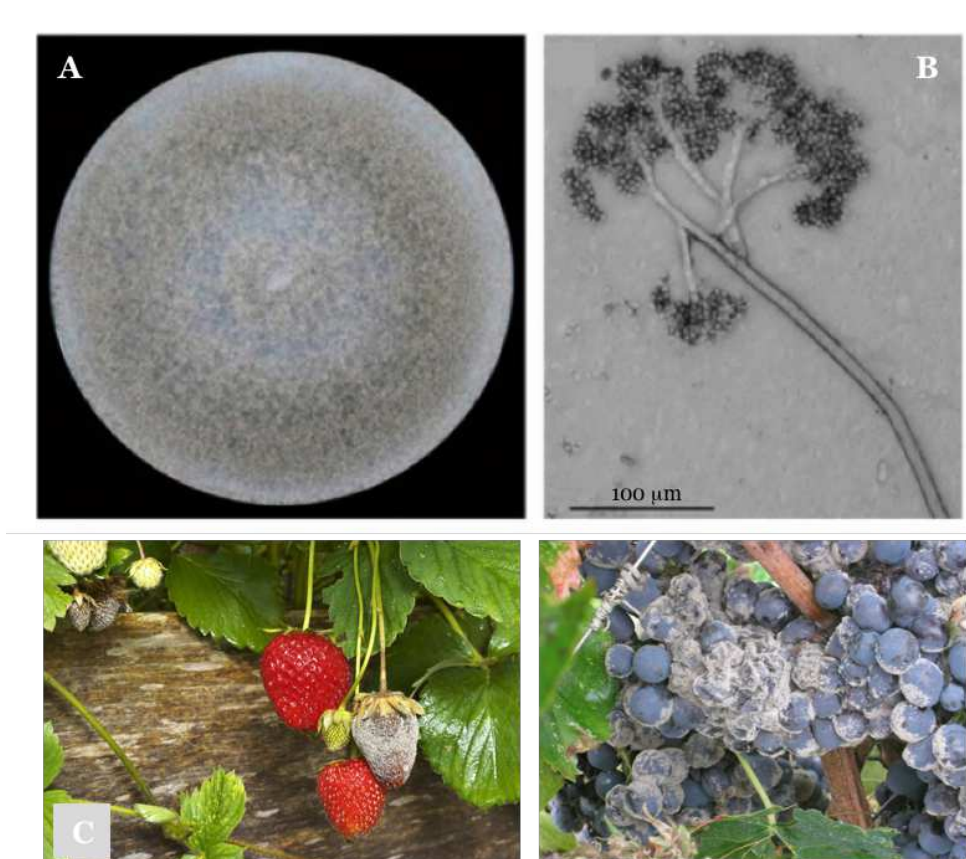


Figure 37. *Botrytis cinerea*. (A) Colony morphology on potato dextrose agar. (B) Conidiophore (modified from [185]). (C) Gray mold symptoms on strawberries and grapes.

3.6.1 Cloning of *BfOYE1* and *BfOYE4*

The genomic DNA of the fungus *Botryotinia fuckeliana* B05.10 was kindly provided by Professor Paul Tudzynski from Münster University and used for the isolation and subsequent cloning of the desired proteins, as already described in section 3.2. For *BfOYE1* an additional PCR reaction was performed in order to suppress a predicted N-glycosylation site. While for *BfOYE4* an additional PCR reaction was performed in order to remove an intronic sequence.

Moreover, *BfOYE4* sequence was also cloned into pPICZ α and pGAPZ α vectors using a strategy similar of that used for pET28a(+) vector. Briefly, the pET28a(+) vector was used as template for the amplification of the desired insert. The amplicon obtained from this first PCR was used for a second mutagenic PCR

amplification driven by nested primers for the insertion of the desired restriction sites PmlI and NotI, respectively at the 5' and 3' of the coding sequence. These vectors were used to transform *P. pastoris* cells

3.6.2 Expression and purification of *BfOYE1* and *BfOYE4*

The expression of both proteins was first tested in *E. coli*, as already mentioned. If for *BfOYE1* good over-expression and yield were obtained using a bacterial host, the level at which *BfOYE4* was produced was very low. Considering that these enzymes derived from a fungus organism, in order to try the over-expression of *BfOYE4*, its heterologous production has been tested also in the yeast *P. pastoris*.

3.6.2.1 Expression and purification of *BfOYE1*

BfOYE1 was the first enzyme expressed during this PhD work. The first over-expression tests have been performed without the addition of riboflavin, the natural precursor of FMN, or FMN itself after cells induction. The enzyme was overexpressed at all temperature tested but, as expected, it was completely insoluble at 37 °C and partially soluble only at temperatures lower than 37 °C (Fig. 38).

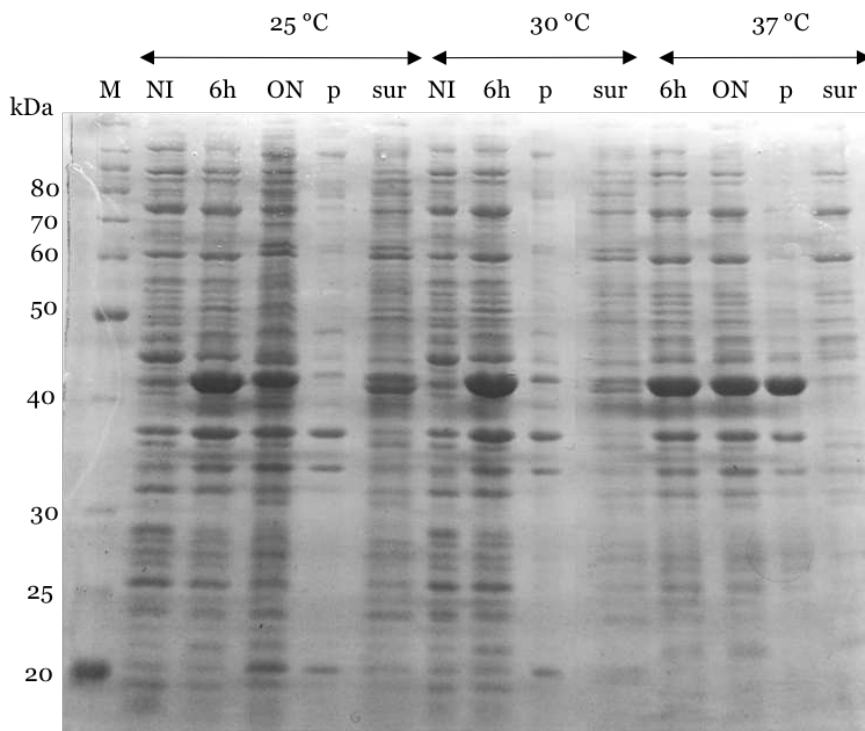


Figure 38. (A) SDS-PAGE 12% acrylamide: BL21(DE3) grown at 25, 30 and 37 °C expressing *BfOYE1* without addition of flavin cofactor: BenchMark™ protein ladder (M), total cell extracts from non-induced (NI) and 6 h and over-night induced cells with IPTG (6h and ON), pellet fraction (p), soluble protein fraction (sur).

In order to enhance the flavination and correct folding of the protein, FMN (100 μM) or riboflavin (25 μM) were added to the cell culture after induction. As shown in Figure 39A, this strategy was successful in promoting the solubility of the protein with just a small fraction still present as insoluble form. Based on these results for the expression of all the other ene-reductases reported in this thesis we decided to always add riboflavin, a FMN precursor, to the culture medium before induction (for more details see Materials and Methods).

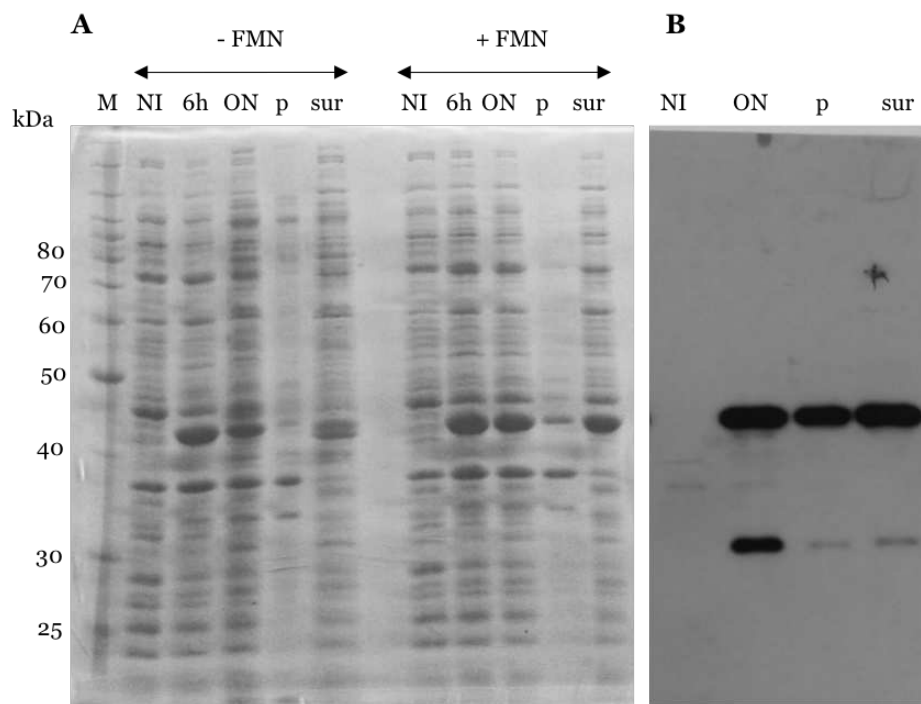


Figure 39. (A) SDS-PAGE 12% acrylamide: BL21(DE3) grown at 25 °C expressing *BfOYE1* without and with the addition of riboflavin: BenchMark™ protein ladder (M), total cell extracts from non-induced (NI) and 6 h and over-night induced cells with IPTG (6h and ON), pellet fraction (p), soluble protein fraction (sur). (B) Western blot assay with anti-His tag antibodies with samples of protein induced at 25 °C.

BfOYE1 has been purified in the optimized conditions reported in Table 10 with very good yields (40 mg/L). The SDS-PAGE in Figure 40 shows the homogeneity of the recombinant protein preparation after IMAC and SEC purification.

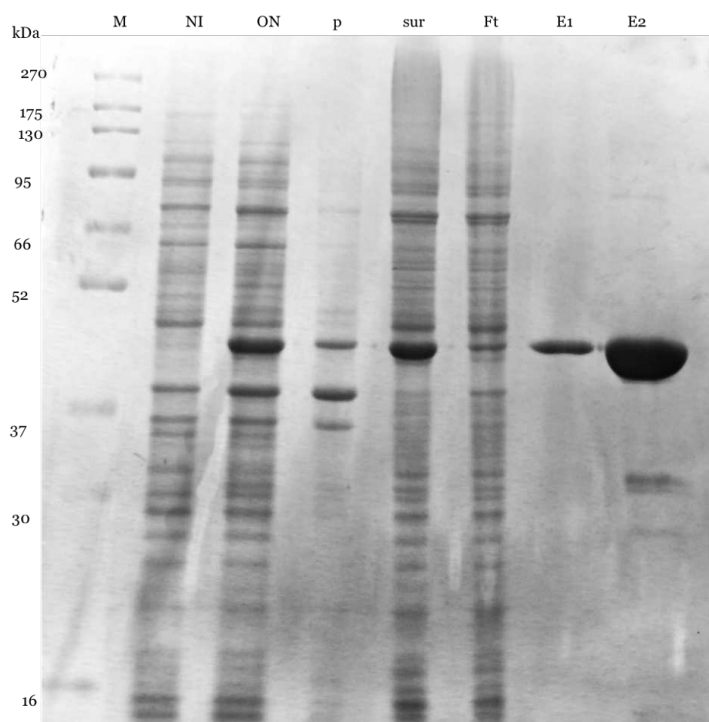


Figure 40. SDS-PAGE 12% acrylamide of *BfOYE1* purification using BL21(DE3) cells grown at 25 °C: Prestained SharpMass™ VII protein ladder (M), total cell extracts from non-induced (NI) and over-night induced cells with IPTG (ON), pellet fraction (p), soluble protein fraction (sur), flow-through (Ft), eluted fraction from IMAC (E1) and preparative SEC (E2).

3.6.2.2 Expression and purification of *BfOYE4*

BfOYE4 was first expressed using *E. coli* BL21 (DE3) cells at different temperatures (16 °C and 25 °C, respectively). As shown in the SDS-PAGE gel in Figure 41A, a band (red box) corresponding to the expected molecular weight (47.7 kDa) was detected but however its level of over-expression was quite low. Moreover, just at lower temperature the protein was completely soluble. The low expression level could be ascribed to the different codon usage between the bacterial host organism and the eukaryotic source organism. Indeed, analysis of the sequence for rare codons in *E. coli* revealed that 26% of sense triplet in *BfOYE4* sequence had less than 10% codon frequency in *E. coli*. The presence of regions with under-represented codons close one another can lead to a dramatic reduction of the expression of heterologous proteins. For these reasons, the expression of the desired protein was tried also in CodonPlus *E. coli* RIL strain. This strain of *E. coli* has been engineered to contain extra copies of the genes that encode the tRNAs that most frequently limit the translation of heterologous proteins such as the arginine (R) codons AGA and AGG, the isoleucine (I) codon AUA and the leucine (L) codon CUA. Nevertheless, also with this engineered strain (Fig. 41B) the levels of over-expression of the desired protein were very low and, additionally, at 25 °C the protein was almost completely found in the

insoluble fraction. The temperature seemed to be the most important parameter for solubility modulation. The identity of the protein was confirmed by immunoblotting assay as it was produced in low amount and it was not easily distinguishable from the other *E.coli* proteins (Fig. 42B).

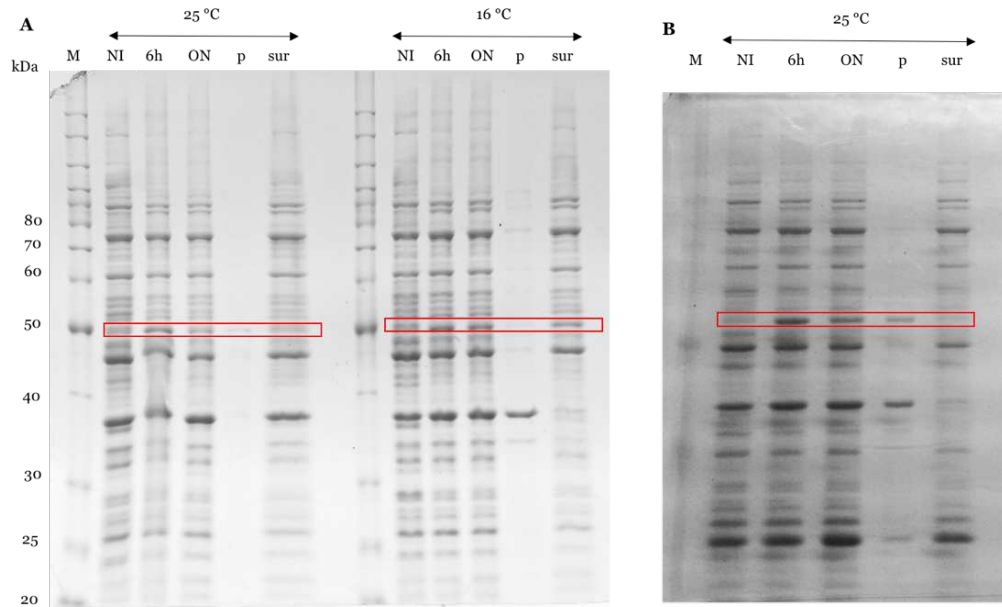


Figure 41. SDS-PAGE 12% acrylamide: (A) BL21(DE3) grown at 25 °C and 16 °C, (B) BL21 (DE3) RIL grown at 25 °C expressing *BfOYE4*: BenchMark™ protein ladder (M), total cell extracts from non-induced (NI) and 6 h and over-night induced cells with IPTG (6h and ON), pellet fraction (p), soluble protein fraction (sur).

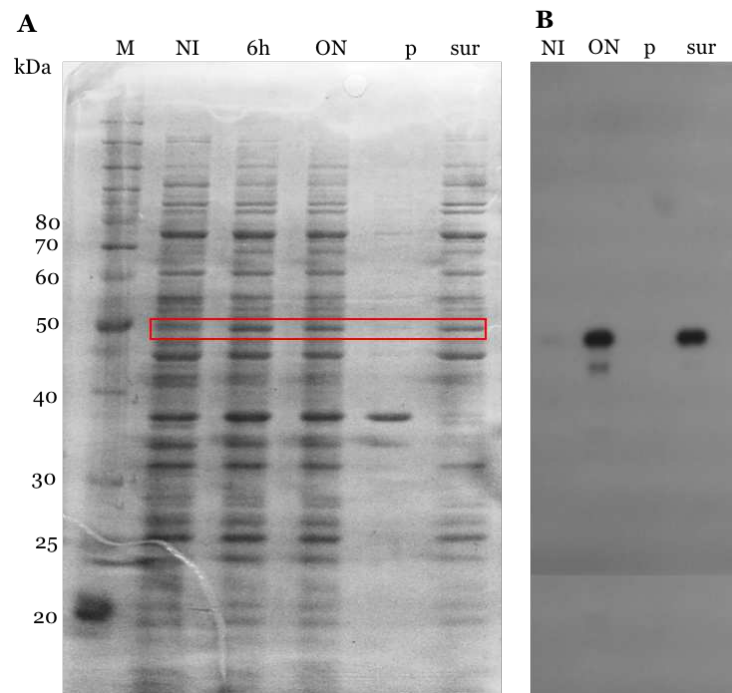


Figure 42. (A) SDS-PAGE 12% acrylamide: BL21(DE3) grown at 16 °C expressing *BfOYE4*: BenchMark™ protein ladder (M), total cell extracts from non-induced (NI) and 6 h and over-night induced cells with IPTG (6h and ON), pellet fraction (p), soluble protein fraction (sur). (B) Western blot assay with anti-His tag antibodies with samples of protein induced at 16 °C.

The expression level of some recombinant proteins may be minimal or not detectable because the heterologous protein, when expressed in an unfolded and insoluble form, is deleterious or lethal to the standardly employed BL21 strains of *E. coli*. Since the expression of *BfOYE4* was quite challenging, we decided to screen different *E. coli* strains that usually are used for the expression of difficult-to-fold proteins such as C41 (DE3), C43 (DE3) and Arctic® BL21 (DE3). C41 (DE3) and C43 (DE3) were derived from BL21 (DE3) and contain different genetic mutations that limit the accumulation of inclusion bodies, so preventing cell death associated with over-expression of many recombinant protein [186]. BL21 (DE3) Arctic® cells are engineered to co-express the cold-adapted chaperonins Cpn10 and Cpn60. These chaperonins confer improved protein processing at lower temperature, potentially increasing the yield of active and soluble recombinant protein [187]. Therefore, *BfOYE4* expression was tested at low temperature (12 °C) using these different *E. coli* strains. After 72 hours for all *E. coli* strains tested, a band at 47.7 kDa, corresponding to *BfOYE4*, was clearly detected as shown in Figure 43 (red box). The protein was prevalently produced in a soluble form even though its over-expression was still low. However, slightly higher amounts, sufficient for a preliminary biochemical characterization, were obtained with *E. coli* Arctic® strain.

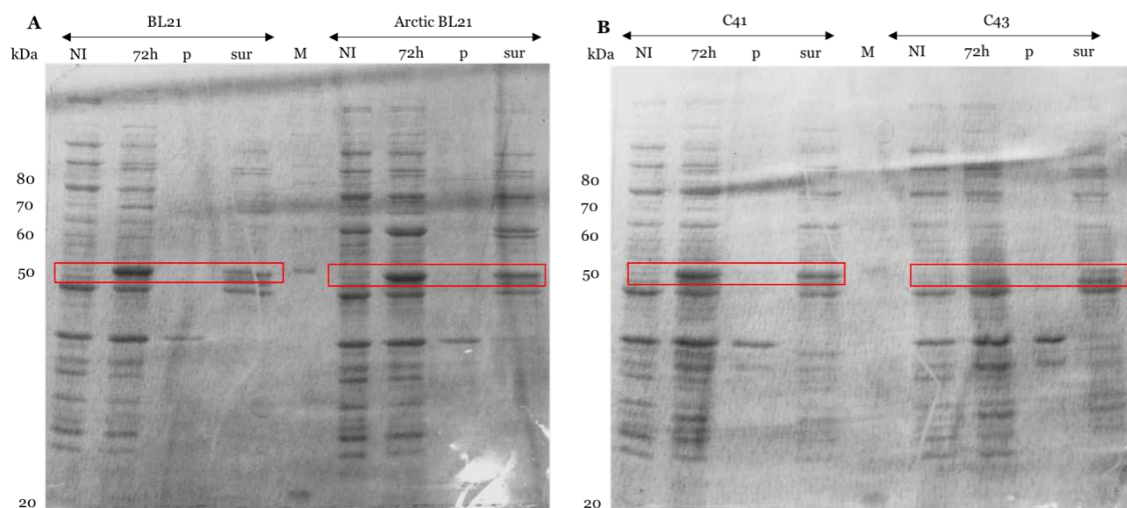


Figure 43. SDS-PAGE 12% acrylamide: (A) BL21(DE3) and BL21(DE3) Arctic® (B) C41(DE3) and C43(DE3) grown at 12 °C expressing *BfOYE4*: BenchMark™ protein ladder (M), total cell extracts from non-induced (NI) and 72 h induced cells with IPTG (72h), pellet fraction (p), soluble protein fraction (sur).

Changing the host organism for the expression, was another strategy adopted in order to enhance the production levels of the desired *BfOYE4*. In fact, keeping in mind that *BfOYE4* was isolated from an Ascomycete, the yeast *P. pastoris* could

represent a better choice for its expression. Two different expression vectors were used: a methanol-inducible system (pPICZ α) and a constitutive expression system (pGAPZ α), both permitting the fusion with a tag for extracellular secretion and easier purification. After yeast transformation by electroporation, recombinant clones were selected using increasing concentration of antibiotic: nine transformants were selected to test the inducible system and eight recombinant clones (six characterized by fast growth and two characterized by slow growth) were selected to test the constitutive system.

Initially, *BfOYE4* protein has been expressed under the control of P_{AOX1} strong inducible promoter. This system allows the generation of biomass in absence of the inducer and only when methanol is available protein expression can start. In the Urea-PAGE shown in Figure 44A, the target protein was not clearly detected even if a change in the expression profile of *P. pastoris* cells transformed with the plasmid is visible compared to the wild-type cells. From literature data, it is known that methanol induction and the temperature of growth can promote the overexpression of various endogenous proteins, and moreover, also the expression of the heterologous protein of interest can further change the expression profile in *P. pastoris* [188]. Western blot assay was also performed: however, even with this technique, there was not a detectable expression of the desired protein (Fig. 44B).

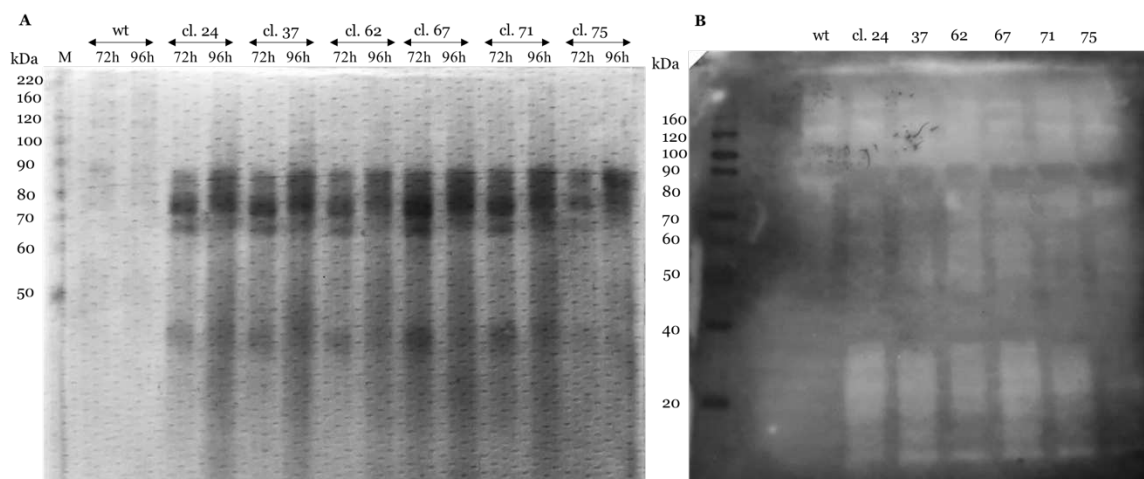


Figure 44. (A) UREA-PAGE 12% acrylamide: X33 grown at 28 °C transformed with pPICZ α -*BfOYE4*: culture medium (ten times concentrated) from clones 24, 37, 62, 67, 71, 75, collected 72 and 96 hours after the expression induced by adding 1% MeOH every 24 h; X-33 wild type cells were also induced with methanol and used as negative control. (B) Western blot assay with anti-His tag antibody of the supernatants (ten times concentrated) from clones 24, 37, 62, 67, 71, 75, collected 72 hours after the expression induced by 1% MeOH.

Further studies were performed lowering the temperature of expression, adding more methanol for the induction and also adding FMN cofactor to the culture *medium* in order to avoid a possible cofactor deficiency and a consequent misfolding of the protein, but the desired protein was not detected in the extracellular *medium* (data not shown). Finally, the expression of the protein was also investigated inside the cells but even in this case no expression of the desired protein was detected as shown in Figure 45.

The expression of *BfOYE4* in *P. pastoris* was also tested using the constitutive promoter GAP. The results are shown in Figure 46. Again, there were no differences between the expression profile of pGAPZα-*BfOYE4* recombinant clones and the expression profile of the negative control, which was transformed with the empty pGAPZα vector. Therefore, the expression of *BfOYE4* in *P. pastoris* was finally considered unsuccessful.

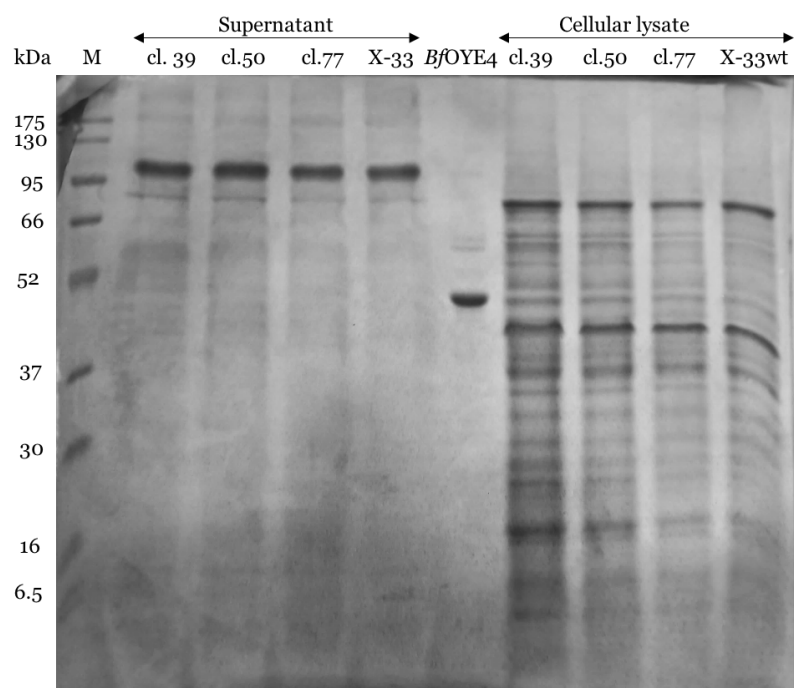


Figure 45. UREA-PAGE 12% acrylamide: X-33 grown at 25 °C transformed with pPICZα-*BfOYE4*: culture *medium* (ten times concentrated) and cellular lysates from clones 39, 50, 77, collected 72 hours after the expression induced by 2% MeOH; purified *BfOYE4* previously expressed from BL21(DE3) Arctic® was used as positive control. X-33 wild type cells were also induced with methanol and used as negative control.

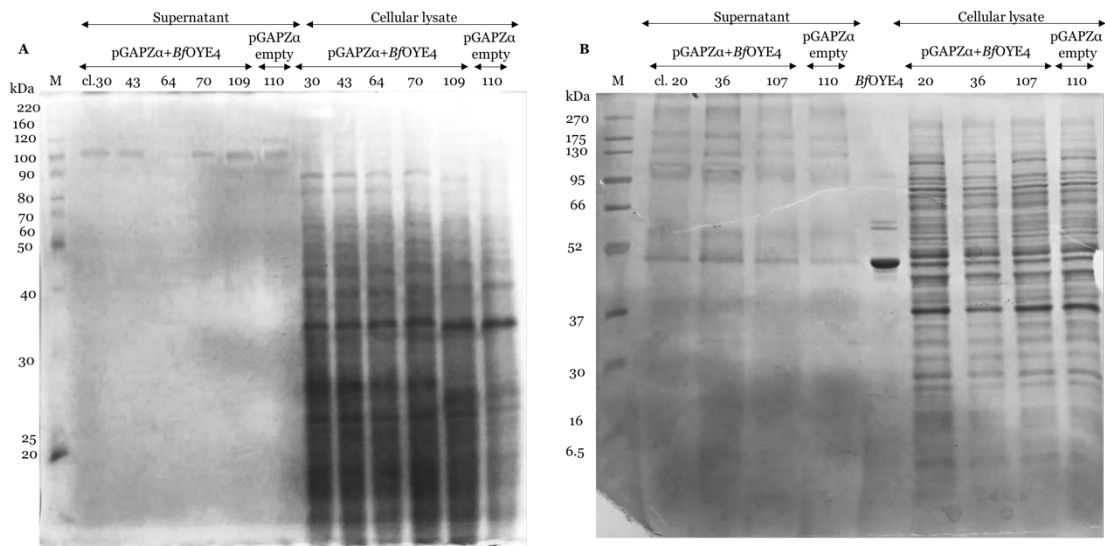


Figure 46. UREA-PAGE 12% acrylamide: X-33 grown at 28 °C transformed with pGAPZα-*BfOYE4* (A) cl. 30, 43, 64, 70, and 109; (B) cl. 20, 36, and 107: culture medium (ten times concentrated) and cellular lysates collected after 72 hours of growth in YPD medium. Purified *BfOYE4* previously expressed from BL21(DE3) Arctic® used as positive control. On both (A) and (B), the culture medium and the cellular lysate of the clone 110 transformed with the empty vector and collected after 72 hours were used as negative control.

After various attempts, *Pichia pastoris* was dismissed since the (over-)expression of the desired protein had not been achieved. Even though the expression of *BfOYE4* in *E. coli* Arctic® strain was low it was considered sufficient for a preliminary biochemical characterization. For these reasons, the protein was purified from *E. coli* using the optimized conditions reported in Table 10 with moderate yields (10 mg/L). The SDS-PAGE in Figure 47 shows the homogeneity of the recombinant protein preparation after IMAC purification. The Arctic strain® produces the heterologous chaperonin Cpn60 and co-chaperonin Cpn10, from the psychrophilic bacterium *Oleispira antarctica*, that are involved in protein refolding also at low temperature (between 4 °C to 12 °C) allowing *E. coli* to grow at significant high rates at these low temperatures [187]. The protein of interest was co-purified with a polypeptide having a molecular mass of about 60 kDa (Fig. 47). This contamination corresponds to the heterologous chaperonin Cpn60 co-expressed by the Arctic® strain, that likely favours the folding of *BfOYE4* by directly interacting with it. The undesired contaminant was removed (Fig. 47, lane Chp.) introducing an additional washing step with MgATP buffer as reported in literature [189]. However, despite this additional step of washing in the final preparation some chaperonin contaminant was still present.

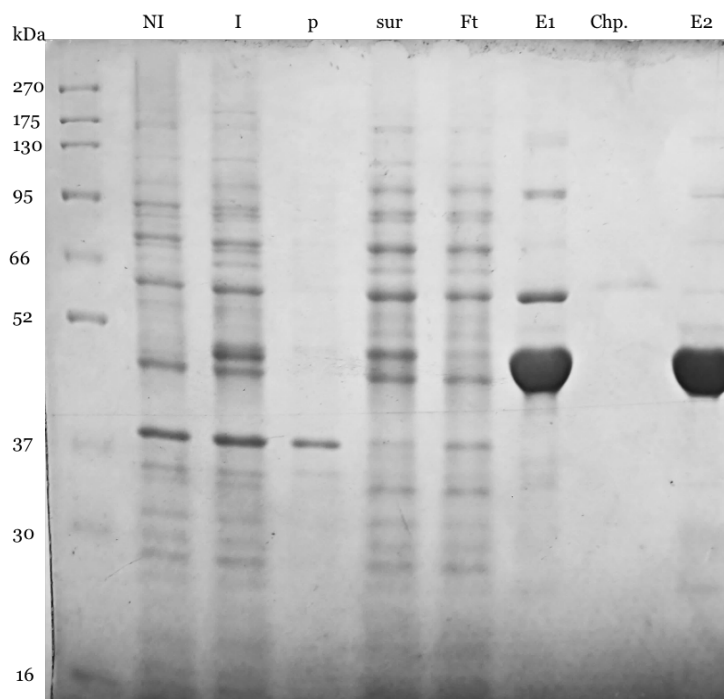


Figure 47. SDS-PAGE 12% acrylamide: BL21(DE3) Arctic® grown at 16 °C expressing *BfOYE4*: SharpMass™ VII protein ladder, total cell extracts from non-induced cells (NI) and from overnight induced cells (ON), pellet fraction (p), soluble protein fraction (sur), flow-through (Ft), eluted fractions from IMAC chromatography (E1), removed chaperonin (Chp.), eluted fractions from IMAC chromatography (E2) after chaperonin removal.

For crystallization studies (see Chapter 5) the protein was purified using BL21 (DE3) cells. Even though the yield of the purification was slightly lower (7 mg/L) the chaperonin impurities were not present leading to a homogeneous preparation suitable for crystallization trials.

3.7 *AnOYE2* and *AnOYE8* from *Aspergillus niger*

The fungus *Aspergillus niger* (Fig. 48) is a cell factory widely used in biotechnology for the production of industrial enzymes, pharmaceuticals and food ingredients. Its high secretory capacity is exploited by industry for the production of heterologous proteins and enzymes. Furthermore, its ability to degrade a wide panel of xenobiotics through various metabolic pathways is exploited in bioremediation [190].

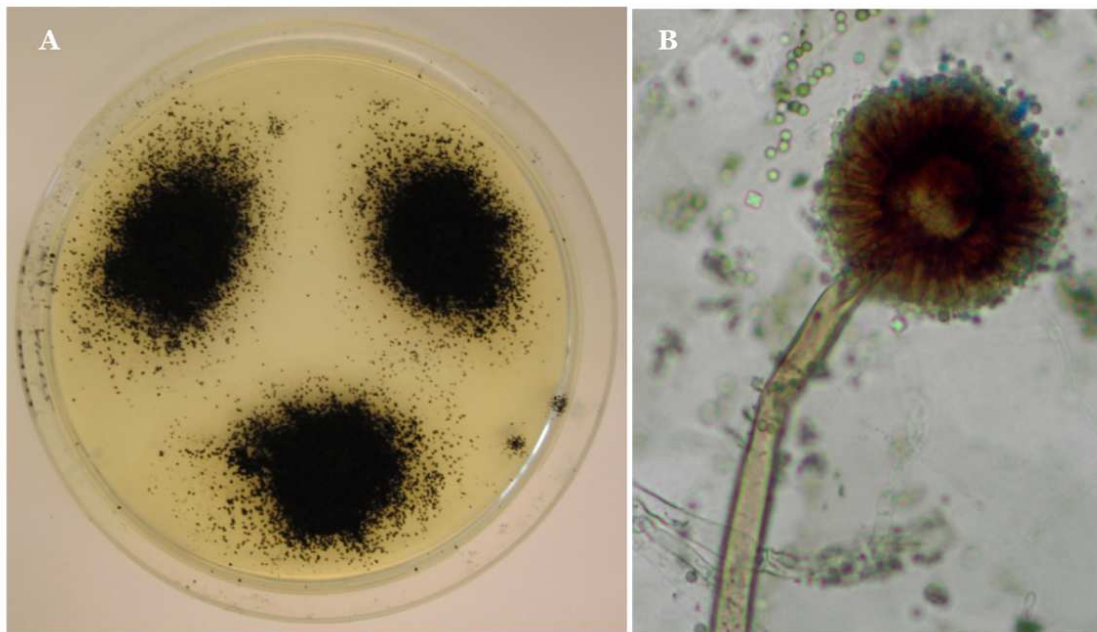


Figure 48. (A) Morphology of *A. niger*: two weeks old colonies growing on minimal media and (B) microscopic picture of a conidiophore, the structure producing asexual spores (modified from [191]).

The strain *Aspergillus niger* CBS 513.88 was purchased from CBS (Centraalbureau voor Schimmelcultures) (*Central Bureau of Fungal Cultures* in English) strain collection (Netherlands). The cells were grown on solid malt extract broth medium and their genomic DNA was extracted following an established protocol [182]. For *AnOYE8* an additional PCR reaction was performed in order to remove an intronic sequence.

The expression of *AnOYE2* was first tried in BL21 (DE3) cells at 25 °C and 16 °C. The protein was highly over-expressed but it was completely insoluble at 25 °C and only a small fraction of the protein was soluble at 16 °C (Fig. 49). The expression in the Arctic® strain resulted more convenient, with a higher amount of soluble protein obtained at 16 than 12°C (Fig. 50A).

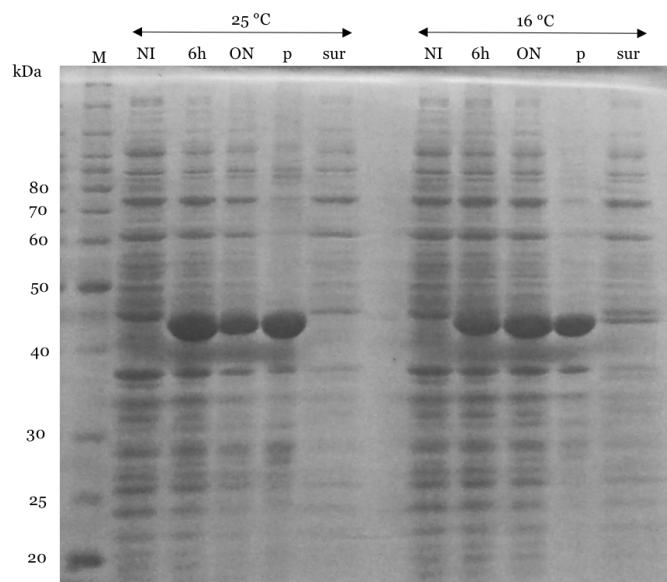


Figure 49. SDS-PAGE 12% acrylamide: BL21(DE3) grown at 25 °C and 16 °C expressing *AnOYE2*: BenchMark™ protein ladder (M), total cell extracts from non-induced cells (NI) and from 6 h and over-night induced cells with IPTG (6h and ON), pellet fraction (p), soluble protein fraction (sur).

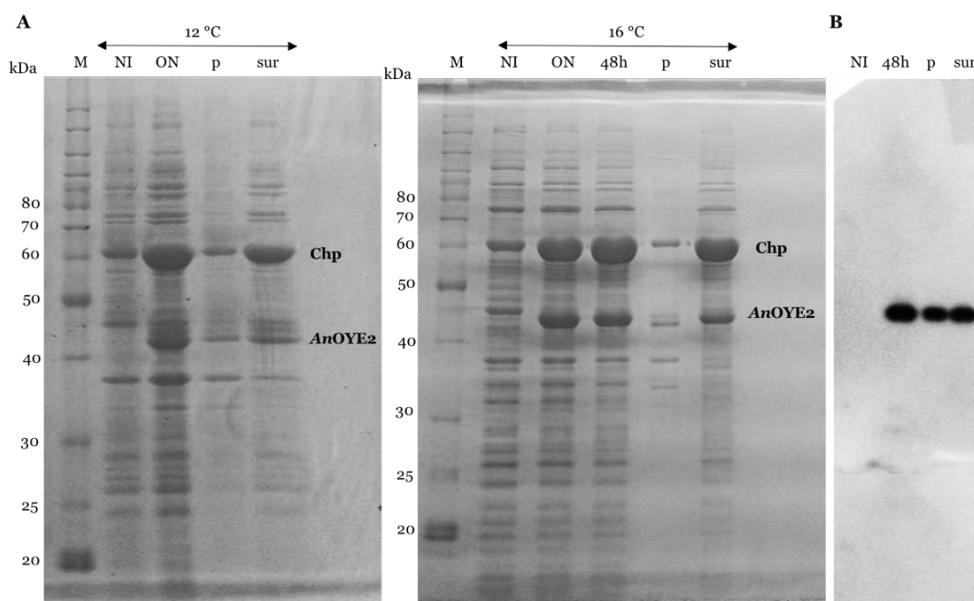


Figure 50. (A) SDS-PAGE 12% acrylamide: BL21(DE3) Arctic® grown at 12 °C and 16 °C expressing *AnOYE2*: BenchMark™ protein ladder (M), total cell extracts from non-induced cells (NI) and from over-night and 48 h induced cells with IPTG (ON and 48h), pellet fraction (p), soluble protein fraction (sur). (B) Western blot assay with anti-His tag antibody with samples of 16 °C induction.

The expression of *AnOYE8* was also tried first in BL21 (DE3) cells at 25 °C. As already reported for *AnOYE2*, its expression was highly induced but its solubility was very low (Fig. 51A). In order to enhance its solubility *E. coli* BL21 (DE3) Arctic® strain was tested at 12 °C. In these conditions, its solubility was clearly enhanced but however a major insoluble fraction was still present (Fig. 51A and 51B). For both proteins the presence (and the activity) of the heterologous chaperonins in the Arctic® cells, more than the low growth temperature, seemed

to play a crucial role for enhancing the correct folding and solubility of the proteins.

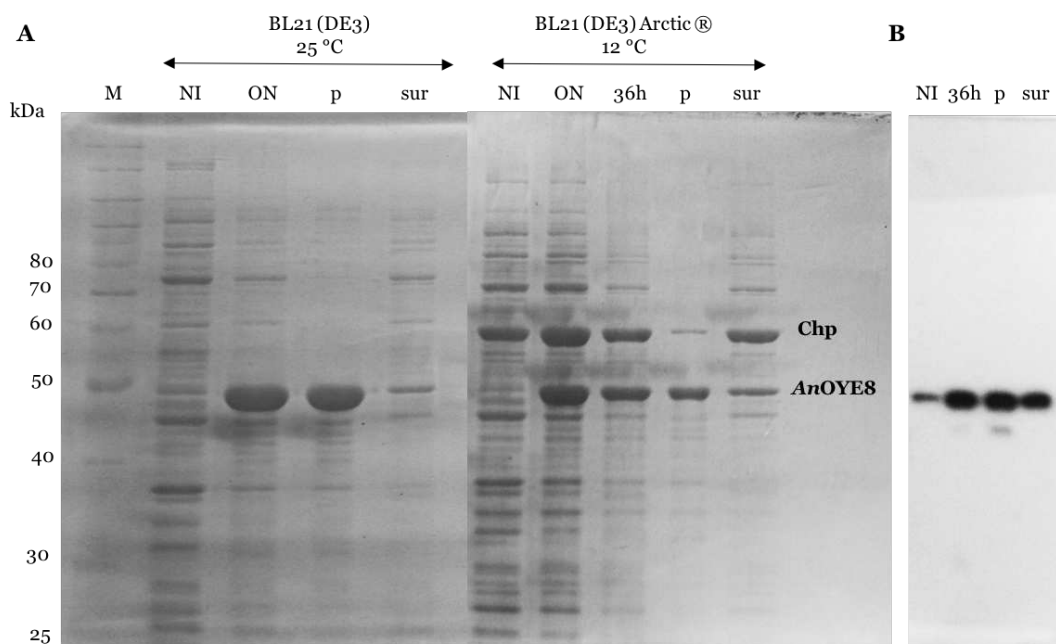


Figure 51. (A) SDS-PAGE 12% acrylamide: BL21(DE3) grown at 25 °C and BL21 (DE3) Arctic ® grown at 12 °C expressing *AnOYE8*: BenchMark™ protein ladder (M), total cell extracts from non-induced cells (NI) and from over-night and 36 h induced cells with IPTG (ON and 36h), pellet fraction (p), soluble protein fraction (sur). (B) Western blot assay with anti-His tag antibody with samples of 12 °C induction.

Both proteins were purified at low temperature from *E. coli* BL21 (DE3) Arctic® cells in moderate yields (13 mg/L *AnOYE2* and 9 mg/L *AnOYE8*). As observed for *BfOYE4*, the chaperonin Cpn60 co-expressed by the Arctic® strain was co-purified as major contaminant of *AnOYE2* and *AnOYE8*. The undesired contaminant was removed (Fig. 52, lane Chp), as already mentioned in section 3.6 following a standard protocol [189]. However, despite this additional step of washing some contaminant chaperonin molecule was still present in the final preparation.

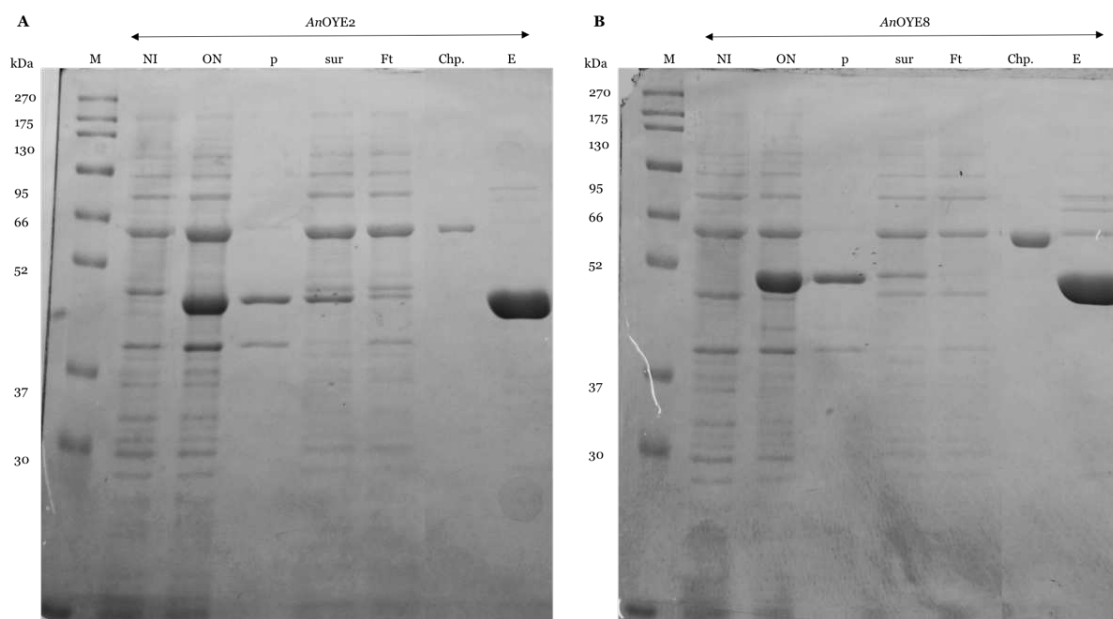


Figure 52. SDS-PAGE 12% acrylamide: BL21(DE3) Arctic® grown at 16 °C and 12 °C expressing *AnOYE2* (A) and *AnOYE8* (B), respectively: SharpMass™ VII protein ladder, total cell extracts from non-induced cells (NI) and from over-night induced cells (ON), pellet fraction (p), soluble protein fraction (sur), flow-through (Ft), removed chaperonin (Chp.), eluted fractions from IMAC chromatography (E).

3.8 OYE2 and OYE3 expression and purification

The expression of both proteins has been tested first at room temperature (Fig. 53) with the addition of riboflavin (25 μ M) after cell induction. The proteins were over-expressed but their solubility was moderate (OYE2) or very low (OYE3). In order to enhance their solubility, the temperature has been lowered to 16 $^{\circ}$ C (Fig. 54). In these conditions both proteins were highly soluble.

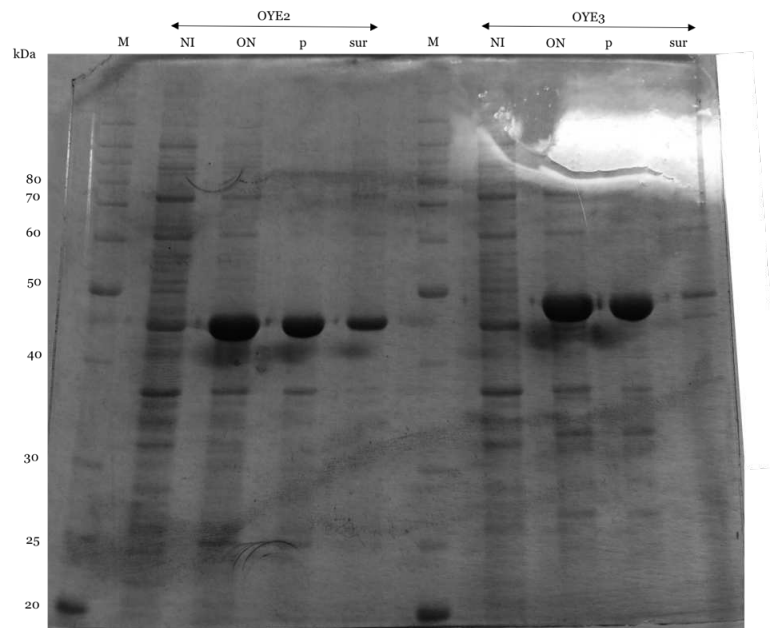


Figure 53. SDS-PAGE 12% acrylamide: BL21(DE3) grown at 25 $^{\circ}$ C expressing OYE2 and OYE3: BenchMark™ protein ladder (M), total cell extracts from non-induced cells (NI) and from over-night induced cells with IPTG (ON), pellet fraction (p), soluble protein fraction (sur).

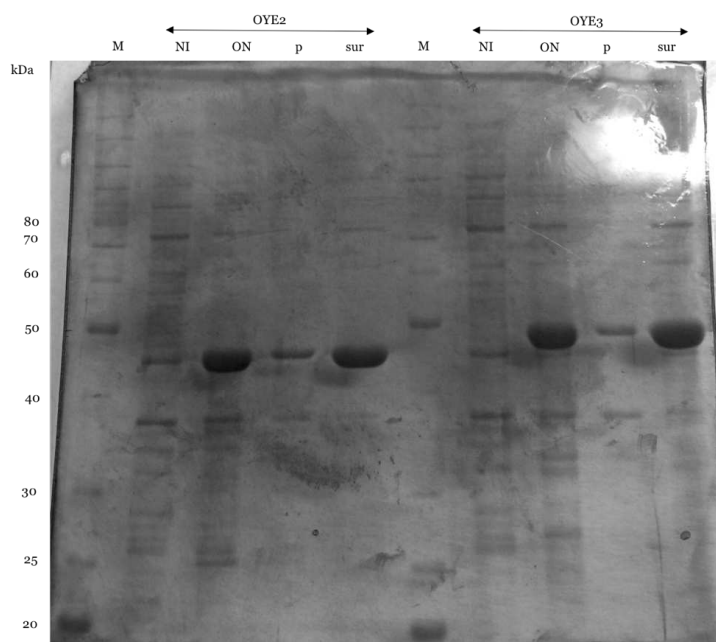


Figure 54. SDS-PAGE 12% acrylamide: BL21(DE3) grown at 16 $^{\circ}$ C expressing OYE2 and OYE3: BenchMark™ protein ladder (M), total cell extracts from non-induced cells (NI) and from over-night induced cells with IPTG (ON), pellet fraction (p), soluble protein fraction (sur).

The recombinant OYE2 and OYE3 were expressed in *E. coli* BL21 (DE3) cells in the optimized conditions reported in Table 10 with good yields (40 mg/L for both proteins). An SDS-PAGE analysis was performed to check all the purification steps and the final purity of both proteins (OYE2, (Fig. 55A) and OYE3, (Fig. 55B). Some low molecular weight impurities were still present in the preparation also after SEC purification.

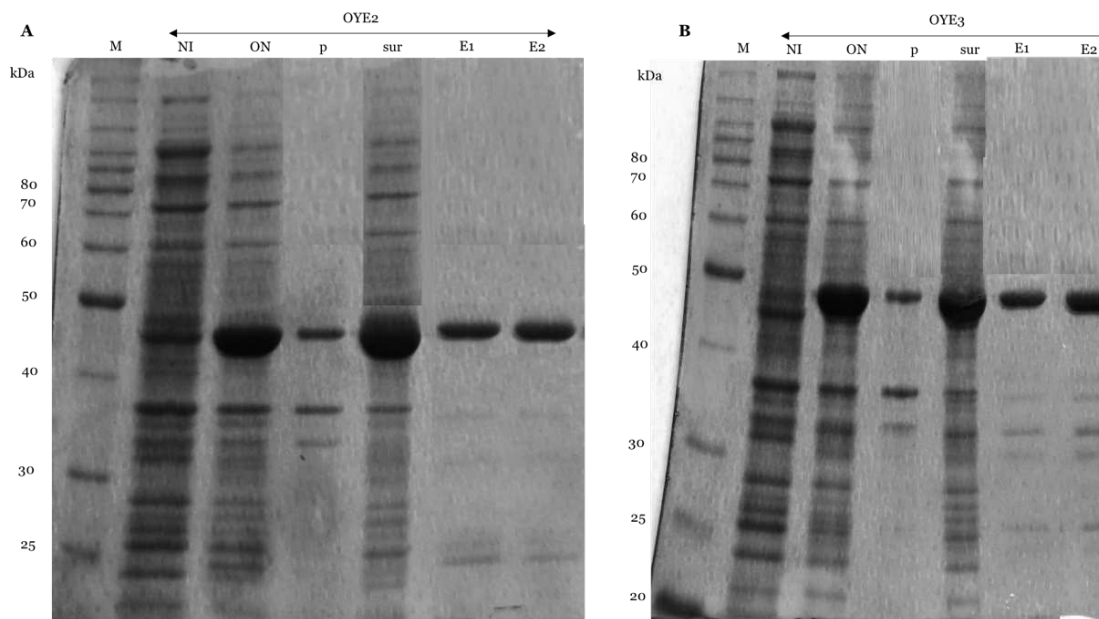


Figure 55. SDS-PAGE 12% acrylamide: BL21(DE3) grown at 16 °C expressing (A) OYE2 and (B) OYE3: BenchMark™ protein ladder (M), total cell extracts from non-induced cells (NI) and from over-night induced cells with IPTG (ON), pellet fraction (p), soluble protein fraction (sur), fractions eluted from IMAC (E1) and SEC (E2).

Concluding remarks

We have identified and selected, by bioinformatic tools, seven new putative ene-reductase from five different unconventional organisms such as fungi, (cyano)-bacteria and algae. The enzymes belong to both classical and thermophilic-like OYE subclass. Based on the literature photosynthetic bacteria and algae result as unexploited sources of ERs while fungi and cyanobacteria are still not so common even though they have great potentialities. The cloning strategy used was the same for all seven putative enzymes. Overexpression tests were performed using different temperatures and *E. coli* strains in order to find the best purification conditions. Moreover, the expression of *BfOYE4* was also tested in *P. pastoris*. However, its expression was not achieved with this host. All the proteins were moderately (at least in sufficient amount for further characterization) to very well over-expressed with a good solubility in *E. coli*.

Furthermore, the expression of two known ene-reductases, OYE2 and OYE3, was optimized in order to obtain good yields for crystallization studies.

4. CHARACTERIZATION OF NEWLY DISCOVERED ERs

Abstract:

After setting up an optimized protocol for the purification of the seven putative ERs, their biocatalytic potential was demonstrated by characterizing their substrate *spectrum*. First their activity as ene-reductases has been demonstrated *in vitro* using a panel of standard substrates. Furthermore, a steady-state kinetic analysis was carried out for the most promising biocatalysts and last, for two of the seven enzymes biotransformations were set-up in order to investigate also the stereoselectivity profile of these newly discovered ERs. Finally, their biochemical properties, including thermal and organic solvent tolerance, the pH *optimum* and the oligomeric state were also determined and are reported in this Chapter.

4.1 Preliminary substrate spectrum

To explore the biocatalytic potential of the new ene-reductases different standard substrates have been tested spectrophotometrically measuring the consumption of NADPH at 340 nm. The standard substrates belong to different types of molecules classes activated by different electron withdrawing groups (*e.g.* linear and cyclic ketones and aldehydes, maleimides) (Fig. 56). The substrate *spectrum* of the newly identified OYE homologues is summarized in Table 11.

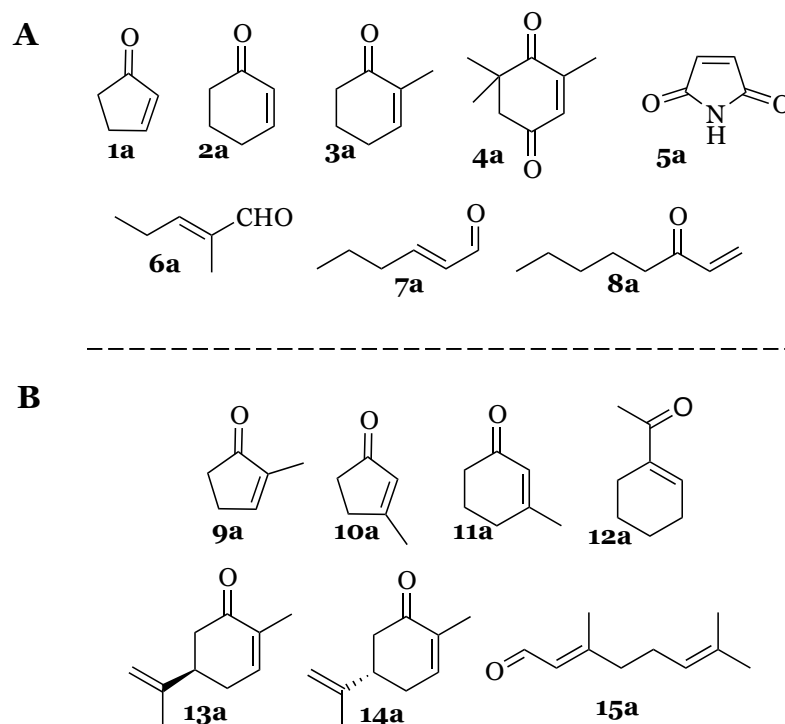


Figure 56. α,β -Unsaturated carbonyl compounds tested as substrates of the newly identified OYEs: (A) substrates for which activity was detected and is reported in Table 12; (B) tested substrates with undetectable activity.

Molecular oxygen can compete with OYEs substrates for the oxidation of the reduced FMNH₂ [46], thus reducing the overall reaction rate [107] and, sometimes, product enantiopurity [192]. It has been demonstrated that during the aerobic biotransformations catalyzed by OYEs, different reactive oxygen species (ROS) are formed such as hydrogen peroxide and superoxide [193-195]. As the reactions were performed aerobically the background oxidase activity was also measured for all enzymes described in this thesis (first row in Table 11). Moreover, it is known that the protein environment can tune the rate of reaction between dioxygen and the reduced flavin in flavoenzymes [196]. Compared to the fungal OYE homologues, for the three OYEs isolated from photosynthetic microorganisms higher background oxidase activities were detected (0.7 – 1.0 U/mg *vs* 0.17 – 0.37 U/mg).

Table 11. Preliminary screening of new putative OYEs.

Substrate	U/mg						
	<i>GsOYE</i>	<i>CtOYE</i>	<i>CaOYE</i>	<i>BfOYE1</i>	<i>BfOYE4</i>	<i>AnOYE2</i>	<i>AnOYE8</i>
O₂	0.98 ± 0.17	0.70 ± 0.15	1.0 ± 0.18	0.32 ± 0.00	0.17 ± 0.00	0.37 ± 0.07	0.28 ± 0.07
1a	2.3 ± 0.26	2.0 ± 0.04	N.D.	3.8 ± 0.22	2.2 ± 0.19	N.D.	1.1 ± 0.08
2a	4.1 ± 0.26	4.8 ± 2.67	5.25 ± 0.22	10.3 ± 0.00	3.3 ± 0.00	N.D.	0.7 ± 0.08
3a	1.7 ± 0.00	3.4 ± 0.25	N.D.	5.7 ± 0.37	1.4 ± 0.31	N.D.	0.8 ± 0.08
4a	N.D.	3.4 ± 0.10	8.3 ± 0.50	10.3 ± 0.30	N.D.	N.D.	N.D.
5a	7.1 ± 0.09	17.5 ± 0.65	2.2 ± 0.37	11.3 ± 0.30	22.5 ± 0.25	16.6 ± 0.53	N.D.
6a	2.4 ± 0.09	6.4 ± 0.30	2.0 ± 0.15	7.5 ± 0.60	0.9 ± 0.06	1.5 ± 0.07	1.0 ± 0.00
7a	4.4 ± 0.78	6.9 ± 1.72	N.D.	9.4 ± 0.50	0.8 ± 0.13	N.D.	1.0 ± 0.08
8a	1.7 ± 0.35	12.3 ± 0.40	9.4 ± 0.40	4.7 ± 0.15	23.4 ± 1.87	N.D.	1.2 ± 0.00

The standard assay (100 µl) was performed at 25°C in 50 mM Tris-HCl, 150 mM NaCl (pH 8.0) containing 100 µM NADPH and 10 mM of substrate. The reaction was started through the addition of enzyme to a final concentration of 200 nM. N.D. not detected. All measurements have been performed at least in duplicate. Background oxidase activity was measured in the absence of alkenes (first row) but it was not subtracted from the specific activity for the other substrates.

4.1.1 Substrate spectrum of ERs isolated from photosynthetic organisms

As illustrated in Chapter 3, three among the new ERs were identified in photosynthetic microorganisms: the red alga *Galdieria sulphuraria* (*Gs*), the cyanobacterium *Chroococcidiopsis thermalis* (*Ct*) and *Chloroflexus aggregans* (*Ca*). Substrate spectra of the three homologous enzymes were shown to be different with *Gs*OYE and *Ct*OYE having a wide substrate *spectrum* (Table 11), with good to moderate activities for (almost) all the substrates tested and *Ca*OYE having a more limited substrate *spectrum* (Table 12), compared to *Gs*OYE and *Ct*OYE homologues, displaying good activity with 3 out of 8 substrates tested and low activity for substrates **5a** and **6a**.

*Gs*OYE and *Ct*OYE show their maximum activity with maleimide (**5a**) (7.1 and 17.5 U/mg, respectively), as already reported in literature for the ERs isolated from cyanobacteria for which activities in a range of 0.90 - 29.58 U/mg were detected [140]. Surprisingly, *Ca*OYE has lower activity with this substrate (2.2 U/mg).

Compared to maleimide, the activities of *Gs*OYE and *Ct*OYE towards enones and aldehydes were lower. The non-substituted six member-ring 2-cyclohexen-1-one (**2a**) was reduced with higher reaction rates by all three ERs compared to the non-substituted five member-ring cyclopenten-1-one (**1a**) (4.1 - 5.25 U/mg *vs* 0 - 2.3 U/mg). The same behavior was also reported for the ERs isolated from cyanobacteria [140].

The α -substituted 2-methyl-cyclohexen-1-one (**3a**) was converted by *Gs*OYE and *Ct*OYE with this last showing a 2-fold higher activity (1.7 *vs* 3.4 U/mg). *Ca*OYE was completely ineffective with this substrate. The α -substituted 2-methyl-cyclopenten-1-one (**9a**) was not converted by none of the biocatalysts.

As for (almost) all ERs reported in literature, the β -substituted cyclic enones (3-methyl-2-cyclopenten-1-one (**10a**) and 3-methyl-2-cyclohexen-1-one (**11a**) were not converted. These substrates have been reported as being “difficult” to convert due to unfavorable steric interactions with active site residues. However, it has been demonstrated that the reduction of the bulkiness of some residues such as Trp 116 in the classical OYE1, and thus the increase of active site volume did not favor the conversion of these substrates [93]. On the contrary, the mutations Cys40Asp - Ile81Thr and Cys25Asp - Ile67Thr in the thermophilic-like *Dr*ER and

RmER greatly enhanced the conversion of the β -substituted alkenes (from 1% to 73% and 95% conversion, respectively) [89].

The reduction of ketoisophorone (**4a**) was catalyzed with activities from 0.0 to 8.3 U/mg with *CaOYE* showing the best activity and *GsOYE* being completely inactive.

With the linear substrates tested, *CaOYE* exhibits modest activity in the presence of 2-methyl-pentenal (**6a**) while no activity was detected in the presence of *trans*-2-hexen-1-al (**7a**). In contrast, *GsOYE* and *CtOYE* actively reduce **6a** and **7a** with rates 2.6 and 1.6 higher for *CtOYE* compared to *GsOYE*, for both substrates respectively.

1-octen-3-one (**8a**) was the preferred linear substrate for *CtOYE* and *CaOYE* (12.3 and 9.4 U/mg, respectively) while moderate activity was registered for *GsOYE* with this substrate (1.7 U/mg).

The terpenoids (*R*)- and (*S*)-carvone (**13a** and **14a**), as well as the highly reactive aldehyde citral (**15a**) were not converted.

ERs isolated from cyanobacteria have been reported to accept NADH as reductive equivalent donor showing identical or up-to 12.3- fold lower activity compared to the preferred NADPH cofactor [140]. As both *GsOYE* and *CtOYE* were isolated from photosynthetic organisms we decided to test their activity using NADH and the preferred substrate maleimide. The results are shown in Table 12, together with the values detected for cyanobacterial ERs for easier comparison. *GsOYE* and *CtOYE* show a good NADH acceptance in the reduction of maleimide. Using 500 μ M NADH, the specific activity of *GsOYE* was 2.3-fold lower than with the preferred cofactor NADPH, while for *CtOYE* the activity was 5 times lower in the same conditions. A more comprehensive study of this behavior is presented in the next section where K_m and k_{cat} values for both NAD(P)H cofactors are reported.

The substrate *spectrum* of the three studied ene-reductases points out some differences in terms of substrate preference. These enzymes have been isolated from different photosynthetic organisms (*i.e.* alga, cyanobacteria and phototrophic bacteria) and they belong to two different OYEs subclasses: *GsOYE* and *CtOYE* are classical OYEs while *CaOYE* belongs to the thermophilic-like family. *CaOYE* has a restricted substrate *spectrum* with generally lower activities compared to *GsOYE* and *CtOYE*. Moreover, this enzyme shows a very low activity in the presence of maleimide which, on the contrary, is the preferred substrate of *GsOYE* and *CtOYE*. The same behavior was reported also for the two

thermophilic-like ERs isolated from cyanobacteria (AnabaenaER3 and GloeoER) [140].

Table 12. Specific activity and cofactor preference of GsOYE and CtOYE and of cyanobacterial ERs reported by Fu *et al.* [140].

	U/mg (500 μ M NADPH)	U/mg (500 μ M NADH)	NADPH:NADH activity ratio 500 μ M (200 or 250 μ M)
GsOYE	14.0 \pm 0.87	6.18 \pm 0.00	2.3 (2.8)
CtOYE	55.0 \pm 0.00	11.0 \pm 0.00	5.0 (7.9)
CyanothER1	1.25 \pm 0.24	1.25 \pm 0.16	1.0 (0.9)
CyanothER2	32.75 \pm 3.12	12.01 \pm 0.34	2.7 (5.3)
AnabaenaER3	3.01 \pm 0.02	2.05 \pm 0.06	1.5 (1.6)
LyngbyaER1	4.26 \pm 0.42	0.38 \pm 0.05	12.3 (39.4)
NostocER1	10.50 \pm 1.22	1.36 \pm 0.04	7.7 (17.2)
NospuncER1	4.26 \pm 0.25	1.28 \pm 0.04	3.3 (5.0)
AcaryoER1	26.33 \pm 2.18	10.45 \pm 0.92	2.5 (3.5)
AcaryoER3	35.53 \pm 1.65	16.73 \pm 0.39	2.3 (4.2)
GloeoER	1.06 \pm 0.08	N.D.	N.D.

Assay conditions for GsOYE and CtOYE 10 mM maleimide, 50 mM Tris buffer (pH 8.0), RT while for cyanobacterial ERs 10 mM maleimide, 100 mM sodium phosphate buffer (pH 7.0), 30 °C. The ratio of the activity with NADPH and NADH used for the estimation of cofactor preference depends on the Km constants of both cofactors. Therefore, the NADPH to NADH activity ratio using 250 μ M cofactor for GsOYE and CtOYE and 200 μ M for cyanobacterial ERs is additionally shown.

To our knowledge, GsOYE and CtOYE are the first ene-reductases isolated from photosynthetic organisms with the highest activity registered until now for **7a** (4.4 - 6.9 U/mg) compared to the cyanobacterial ones (0.27 - 2.32 U/mg) reported by Fu *et al.* [140] Finally their good acceptance of NADH is pointed out by a low NADPH:NADH activity ratio of 2.3 - 5.0 compared to the ratios registered in the range of 7 - 22 for KYE, XenA and YersER, isolated from non-photosynthetic organisms [153].

4.1.2 Substrate spectrum of ERs isolated from fungi

BfOYE1 and BfOYE4 (from *Botryotinia fuckeliana* B05.10) exhibit a wide substrate spectrum compared to AnOYE2 and AnOYE8 (from *Aspergillus niger* CBS 513.88) (Table 11). BfOYE1 and BfOYE4 were active on (almost) all the tested

substrates showing modest to very good reaction rates. While *AnOYE2* is the enzyme with the most limited substrate *spectrum* showing very good activity with maleimide (**5a**) (16.6 U/mg) and moderate rate with 2-methyl-pentenal (**6a**). No activity was detected with all the other substrates tested. *AnOYE8* shows very modest activity with all the substrates tested in the screening (range of activity registered 0.7 - 1.2 U/mg). The non-substituted six member-ring 2-cyclohexen-1-one (**2a**) was reduced with higher reaction rates by *BfOYE* enzymes compared to the non-substituted five member-ring cyclopenten-1-one (**1a**) (3.3 - 10.3 U/mg vs 2.2 - 3.8 U/mg). Conversely, *AnOYE8* has a slightly higher activity with **1a** compared to **2a** (0.7 vs 1.1 U/mg, respectively).

The α -substituted 2-methyl-cyclohexen-1-one (**3a**) was converted by *BfOYE1* and *BfOYE4* with *BfOYE1* showing a 4-fold higher activity (5.7 vs 1.4 U/mg). Very low conversion was detected for this substrate with *AnOYE8*. The α -substituted 2-methyl-cyclopenten-1-one (**9a**) was not converted.

As for (almost) all ERs reported in literature, no enzyme activity was detected using the β -substituted cyclic enones (3-methyl-2-cyclopenten-1-one (**10a**) and 3-methyl-2-cyclohexen-1-one (**11a**)).

The reduction of ketoisophorone (**4a**) was detected just in the presence of *BfOYE1* with very good rates (10.3 U/mg) while all the others ER were completely inactive.

BfOYE1, *BfOYE4* and *AnOYE2* showed very good activities in the presence of maleimide (**5a**) (11.3, 22.5 and 16.6 U/mg, respectively) with *BfOYE4* being the most active enzyme in the presence of this substrate.

With the linear substrate **6a**, differences in substrate preferences were detected between the two classical ERs (*BfOYE1* and *AnOYE2*) compared to their thermophilic-like counterparts (*BfOYE4* and *AnOYE8*). The classical OYEs showed higher activities with this substrate (7.5 and 1.5 U/mg vs 0.9 and 1.0 U/mg, respectively). *BfOYE1* exhibited a 9-fold higher activity with *trans*-2-hexen-1-al (**7a**) compared to *BfOYE4* and *AnOYE8*.

The linear substrate 1-octen-3-one (**8a**) was the preferred substrate for *BfOYE4* and *AnOYE8* (23.4 and 1.2 U/mg, respectively) but good activity was registered also with *BfOYE1* (4.7 and U/mg).

The enzymes isolated from the fungus *Botryotinia fuckeliana* have a wider substrate *spectrum* and higher specific activities compared to the ones isolated from *Aspergillus niger*. Even if *Aspergillus niger* cells were active in the

reduction of 2-cyclohexen-1-one and (Z)- α -methyl-nitrostyrene [141], as already mentioned in Chapter 3, AnOYE2 and AnOYE8 do not seem to be very promising biocatalysts. In the genome of this fungus 12 genes coding putative OYEs were found and it is known that their expression can be triggered by the presence of different substrates or environments, leading to a high substrate specialization of each isoenzyme. From *in silico* predictions performed on the different OYE homologues of *Mucor circinelloides* (10 homologues) [60] and *Ascochyta rabiei* (6 homologues) [104] structural and biochemical differences have been reported between the homologues present in each species suggesting a specific application for each of them. For these reasons, maybe the compounds used during our screening were not mimicking the natural substrates (still unknown) of these enzymes leading to a limited activity *spectrum* and low recovered specific activities. Another possible explanation is that these genes encoding the two ene-reductases could be ancestral (silenced) genes that are not expressed in the cells (pseudogenes) [59, 60].

4.2 Steady-state kinetics

Steady-state kinetic parameters of *GsOYE*, *CtOYE*, *CaOYE*, *BfOYE1* and *BfOYE4* were determined and the results are reported in Table 13. For *GsOYE*, *CtOYE* and *BfOYE4* kinetic parameters for the cofactors NAD(P)H have also been determined and are reported. All the enzymes showed a typical Michaelis-Menten behavior and the kinetics parameters k_{cat} and K_{m} were calculated for a set of substrates identified in the preliminary screening assay.

The highest affinities (K_{m} from 6 to 69 μM) and activities ($k_{\text{cat}} = 6.78$ to 36.35 s^{-1}) for all the enzymes studied (except *CaOYE*) were observed with maleimide (**5a**), resulting in catalytic efficiencies in the range of 399 - 1940 $\text{mM}^{-1} \text{s}^{-1}$. *CtOYE* demonstrated to be the most efficient biocatalyst in the reduction of maleimide. 2-Cyclohexen-1-one (**2a**) was reduced by all the enzymes with catalytic efficiencies in the range 0.69 – 11.5 $\text{mM}^{-1} \text{s}^{-1}$ with *BfOYE1* and *CaOYE* being the best and the worst biocatalyst ($K_{\text{m}} = 5.52$ vs 0.43 mM), respectively.

The introduction of the methyl group in α - position (**3a**) of 2-cyclohexen-1-one reduced the activity of all the enzymes toward the substrate, as already shown in the preliminary screening. Due to the reduced activity registered previously, it was possible to determine the kinetic parameters for this substrate just for *BfOYE1* and *BfOYE4*. The catalytic efficiency of *BfOYE4* for **3a** was 13-fold lower compared to **2a** due both to reduced k_{cat} and to an increased K_{m} value. On the contrary, *BfOYE1* could better tolerate the methyl substitution on the ring showing similar K_{m} and k_{cat} values and catalytic efficiency compared to **2a** (9.3 instead of 11.5 $\text{mM}^{-1} \text{s}^{-1}$).

Other bulkier substitutions such as in ketoisophorone (**4a**) had opposite effects with the catalysts that were able to reduce this substrate. For *BfOYE1* almost a 4-fold lower catalytic efficiency was observed compared to **2a**. Surprisingly, *CaOYE* showed very high affinity (13 μM) for this substrate and thus a very good catalytic efficiency (174.6 $\text{mM}^{-1} \text{s}^{-1}$).

The ring size had a significant effect on the kinetic parameters as the catalytic efficiencies observed for all the enzymes with 2-cyclopenten-1-one (**1a**) were very low (0.14 – 2.1 $\text{mM}^{-1} \text{s}^{-1}$) compared to the ones for 2-cyclohexen-1-one (**2a**) (0.69 – 11.5 $\text{mM}^{-1} \text{s}^{-1}$). *CaOYE* was completely inactive with this substrate.

The aliphatic enal *trans*-2-hexen-1-al (**7a**) was a rather good substrate for *GsOYE*, *CtOYE* and *BfOYE1* with catalytic efficiencies in the range 2.31- 23.6 $\text{mM}^{-1} \text{s}^{-1}$.

¹ s⁻¹; for the aliphatic enone 1-octen-3-one (**8a**) low biocatalytic efficiency was detected for *Ca*OYE compared to *Bf*OYE4 (1.17 vs 8.28 mM⁻¹ s⁻¹).

Finally, for *Gs*OYE, *Ct*OYE and *Bf*OYE4 the kinetic parameters have been determined also for the cofactors NADH and NADPH. Very good affinities ($K_m = 53 - 135 \mu\text{M}$) and activities ($k_{\text{cat}} = 11.41 - 89 \text{ s}^{-1}$) were registered for all three enzymes in the presence of the preferred cofactor NADPH with catalytic efficiencies ranging from 203 to 881 mM⁻¹ s⁻¹. In the presence of NADH a 8.9-fold and 27-fold lower catalytic efficiencies were observed for *Gs*OYE and *Ct*OYE, respectively. No activity was detected in the reduction of maleimide using *Bf*OYE4 and NADH.

Table 13. Steady-state kinetic parameters of OYE homologues.

Enzyme	Substrates	K_m (mM)	k_{cat} (s ⁻¹)	k_{cat}/K_m (mM ⁻¹ s ⁻¹)
GsOYE	NADPH ^a	0.054 ± 0.009	11.41 ± 0.519	203.00
	NADH ^a	0.388 ± 0.098	8.81 ± 0.713	22.70
	1a ^b	15.540 ± 3.630	2.17 ± 0.166	0.14
	2a ^b	1.079 ± 0.224	3.81 ± 0.232	3.53
	5a ^b	0.017 ± 0.020	6.78 ± 0.167	399.00
CtOYE	7a ^b	1.908 ± 0.153	4.41 ± 0.102	2.31
	NADPH ^a	0.053 ± 0.009	46.71 ± 1.948	881.00
	NADH ^a	0.439 ± 0.031	14.27 ± 0.346	32.50
	1a ^b	13.230 ± 2.470	2.09 ± 0.156	0.16
	2a ^b	2.103 ± 0.489	5.65 ± 0.282	2.68
CaOYE	5a ^{b*}	0.006 ± 0.001	12.42 ± 0.282	1940.00
	7a ^b	0.600 ± 0.038	5.43 ± 0.079	9.06
	2a ^b	5.520 ± 0.627	3.82 ± 0.176	0.69
	4a ^b	0.013 ± 0.002	2.27 ± 0.055	174.6
	8a ^b	10.32 ± 1.438	12.13 ± 0.661	1.17
BfOYE1	1a ^b	2.823 ± 0.364	5.979 ± 0.211	2.1
	2a ^b	0.436 ± 0.064	5.001 ± 0.157	11.5
	3a ^b	0.443 ± 0.056	4.133 ± 0.124	9.3
	4a ^b	2.138 ± 0.281	6.320 ± 0.283	2.9
	5a ^{b#}	0.012 ± 0.002	9.912 ± 0.293	826
	6a ^b	0.067 ± 0.008	7.838 ± 0.007	117
	7a ^b	0.449 ± 0.065	10.61 ± 0.473	23.6
BfOYE4	NADPH ^a	0.135 ± 0.019	89.22 ± 3.375	660.88
	1a ^b	1.071 ± 0.121	1.06 ± 0.030	0.99
	2a ^b	0.652 ± 0.087	2.57 ± 0.066	3.94
	3a ^b	1.831 ± 0.182	0.56 ± 0.013	0.30
	5a ^{b*}	0.069 ± 0.009	36.35 ± 1.119	529.20
	8a ^b	2.724 ± 0.501	22.56 ± 1.138	8.28

The standard assay (100-200 µl) was performed at 25 °C in 50 mM Tris-HCl (pH 8.0), 200/#40/*20 nM ERS and ^a1 mM maleimide or ^b100 µM NADPH.

4.3 Conversions

Biotransformations using purified *GsOYE* and *CtOYE* and different types of substrates were investigated using GC and GC-MS analysis in order to detect conversions and stereoselectivities. These two enzymes were chosen for this further characterization step as they were the first biocatalysts purified during this PhD project and thus their biocatalytic and bio-chemical characterization (including their 3D structure) was in an advanced stage. This activity was carried out in the laboratory of Professor Kurt Faber from Graz University during the second year of this PhD.

4.3.1 *GsOYE* and *CtOYE* bioreduction of α,β -unsaturated carbonyl compounds

The reduction of α,β -unsaturated carbonyl compounds by ERs yield a vast variety of chiral (and in some cases enantiopure) products that have a broad range of applications in industry [26, 105]. Cyclic ketones and maleimides are important synthons for organic synthesis and pharmaceutical drug synthesis [197]. (*R*)-levodione, the product of ketoisophorone (**7a**) reduction is an important building block for the synthesis of terpenes and carotenoids, while carvones (**8b** and **9b**) and citronellal (**12b**) are used in the flavor and fragrances industry [198-200].

A panel of α,β -unsaturated carbonyl compounds bearing various substitutions (Fig. 57) were tested as substrates using the standard concentration of 10 mM coupled with a GDH recycling system. The results of these first trials are summarized in Table 14.

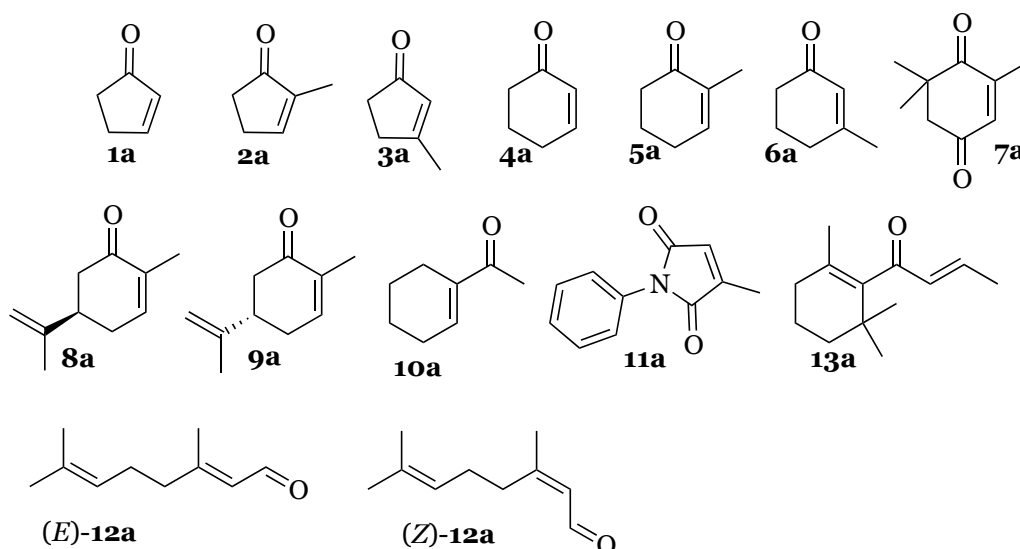


Figure 57. α,β -Unsaturated carbonyl compounds tested as substrates of *GsOYE* and *CtOYE*

In the screening of the carbonyl compounds investigated, *GsOYE* and *CtOYE* displayed similar behaviors in terms of activities and stereoselectivities, as already shown also in the preliminary spectrophotometric screening and from kinetic parameters analysis (see section 4.1 and 4.2 of this Chapter). This is not surprising considering their high sequence identity (63%) and homology (76%) and the fact that they both belong to the classical OYE family.

Table 14. Bioreduction of activated alkenes **1a-13a** catalyzed by ene-reductases *GsOYE* and *CtOYE*

Substrate	<i>GsOYE</i>		<i>CtOYE</i>	
	Conv. (%)	ee (%)	Conv. (%)	ee (%)
1a	97	-	95	-
2a	8	(<i>S</i>) 70	18	(<i>S</i>) 70
3a	2 (6*) [§]	(<i>S</i>) >99	ND (2*) [§]	(<i>S</i>) >99
4a	> 99	-	> 99	-
5a	88	(<i>S</i>) >99	88	(<i>S</i>) >99
6a	5 (9*) [§]	(<i>S</i>) >99	1 (3*) [§]	(<i>S</i>) >99
7a	> 99	(<i>R</i>) 75	> 99	(<i>R</i>) 75
8a	2	(2 <i>R</i> ,5 <i>S</i>) >99	2	(2 <i>R</i> ,5 <i>S</i>) >99
9a	2	(2 <i>R</i> ,5 <i>R</i>) >99	2	(2 <i>R</i> ,5 <i>R</i>) >99
10a	35	-	18	-
11a	> 99	(<i>R</i>) >99	> 99	(<i>R</i>) >99
(E)/(Z)-12a [#]	40 [§]	(<i>S</i>) 37	9 [§]	(<i>S</i>) 22
(Z)-12a [#]	39 [§]	(<i>S</i>) 80	8.5 [§]	(<i>S</i>) 55
13a	-	-	-	-

The standard assay (500 μ l) was performed at 30 °C and 120 rpm in 50 mM Tris-HCl (pH 8.0) containing 100 μ M NAD⁺, 10 U/ml GDH, 20 mM glucose and 10 mM of substrate. The reaction was started through the addition of enzyme to a final concentration of 100 μ g/ml or * 300 μ g/ml and incubated over-night.

The standard assay (500 μ l) was performed at 30 °C and 120 rpm in 50 mM Tris-HCl (pH 8.0) containing 15 mM NADH and 10 mM of substrate. The reaction was started through the addition of enzyme to a final concentration of 100 μ g/ml and incubated for 6 h. All the experiments were performed at least in duplicate. Conversion is based on product formation according to calibration curve; for **10a** and **11a** it is based on substrate consumption according to calibration curve due to the absence of an authenticated GC standard and [§]in some cases apparent conv.% is reported (area product/(area product + area substrate) *100).

Non-substituted five-member ring (**1a**) and six-member ring (**4a**) were fully converted by both enzymes.

GsOYE and *CtOYE* displayed moderate stereoselectivities in the reduction of 2-methylcyclopenten-1-one (**2a**), which was converted to the (*S*)-enantiomer (70% *ee*) with low to moderate conversions (8% and 18% conversion for *GsOYE* and *CtOYE*, respectively). For 2-methyl-cyclopenten-2-one (**2a**), the conversion was lower compared to the six-member ring counterpart and also the stereoselectivity was moderate. This lower stereoselectivity can be explained with the different binding modes that this substrate can adopt inside the active site. The crystal structure of *GsOYE* in complex with **2a** (Fig. 58) indeed clearly shows that **2a** can bind in two different orientations. For more details about the crystal structure of *GsOYE* in complex with **2a** see Chapter 5.

Moreover, compared to the cyanobacterial ERs AnabaenaER3, CyanothER2 and LyngbyaER1 reported by Fu *et al.* [140] for which high conversion (up to 99%) and enantiomeric excess (up to 83% ee (*S*)-**2b**) were reported with **2a**, GsOYE and CtOYE are less performant both in terms of conversion and stereoselectivity. GsOYE and CtOYE have good sequence identity with the classical ene-reductases LyngbyaER1 and CyanothER2 (64 and 51% identity with GsOYE and 75% and 72% with CtOYE, respectively), but moderate identity with the thermophilic-like AnabaenaER3 (roughly 28% identity and 45% homology) for both enzymes.

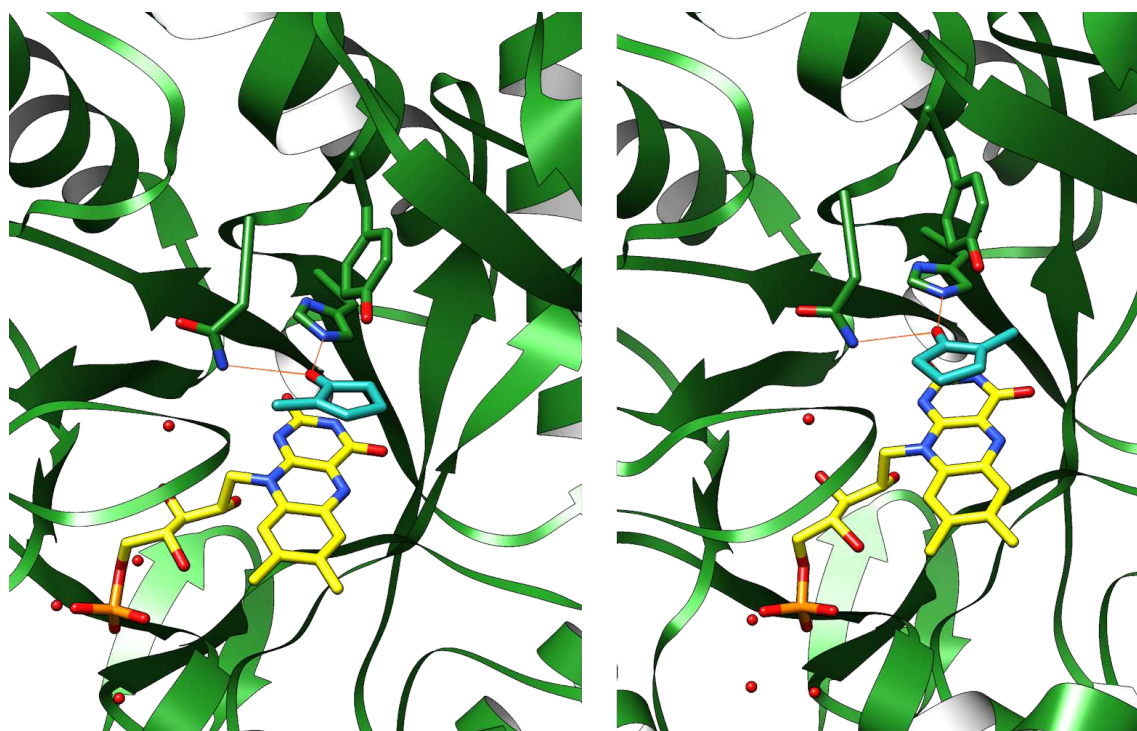


Figure 58. GsOYE soaked with 2-methyl-cyclopenten-1-one (**2a**): 2 different binding modes are observed explaining the moderate stereoselectivity of the enzyme for this substrate. The crystal structure is shown as a green cartoon. The substrate and the important catalytic residues are shown as atom-colored sticks.

A net improvement in conversion and stereoselectivity was observed when the ring size was increased from five (**2a**) to six carbon atoms (**5a**): **5a** was converted into (*S*)-**5b** with excellent stereoselectivity (>99 % ee) and high conversion (88%) by both enzymes. For most OYEs reported in literature, the reduction of 2-methyl-cyclohexen-1-one (**5a**) afforded the (*R*)-enantiomer while for GsOYE and CtOYE, excellent stereoselectivity was detected for the (*S*)-enantiomer. To our knowledge only two other OYEs, KYE from *Kluyveromyces lactis* and YersER from *Yersinia bercovieri* respectively, show >99% stereoselectivity for the (*S*)-enantiomer [201]. Both GsOYE and CtOYE show moderate sequence identity with these already reported ene-reductases (38% and 50% identity and 54% and 65% homology).

In contrast to α -substituted cyclic enones, β -substituted analogues (**3a**, **6a**) were poorly converted, although with high stereoselectivity (>99% *ee*) and furnished exclusively (*S*)-products **3b** and **6b**. A higher amount of enzyme (300 $\mu\text{g/ml}$) was also used in order to boost conversion with these two difficult substrates but just a scarce improvement was registered.

The reduction of ketoisophorone (**7a**) proceeded smoothly to the formation of (*R*)-levodione (**7b**) with moderate stereoselectivity (75% *ee*) and excellent conversion (> 99% conversion). Generally lower optical purities for (*R*)-levodione are reported in literature due to product racemization in aqueous environments [107]. For cyanobacterial OYEs [140], enantiomeric excess in the range 17-46% has been reported, and also for other OYEs (such as PETNR and TOYE) *ee* < 50% have been measured for this product. However, *ee* >90% were also reported in literature for some OYEs homologues [82, 106, 146].

The terpenoids (*S*)-carvone and (*R*)-carvone (**8a** and **9a**) were poorly converted (2% conversion) but with high stereoselectivity (> 99% *de*): (*2R,5S*) and (*2R,5R*)-diastereoisomers were respectively obtained.

1-Acetyl-1-cyclohexene (**10a**) was poorly reduced by both enzymes (35% and 18% conversion for *GsOYE* and *CtOYE* respectively).

N-phenyl-2-methylmaleimide (**11a**) was completely reduced (> 99% conversion) by both enzymes with excellent stereoselectivity furnishing exclusively (*R*)-**11b** (> 99% *ee*), as all the OYEs homologues reported until now [98]. As already discussed in the Introduction two active non-OYE homologues were identified from *Thermus thermophilus* and *Pyrococcus horikoshii* possessing mirror-image orientation of the critical catalytic active site residues (“catalophore”) and thus showing inverted stereopreference for **11a** compared to ene-reductases [41].

In the reduction of α,β -unsaturated aldehyde citral (**12a**), the (*E/Z*)-configuration of the substrate played a crucial role in the stereoselectivity [144]. (*Z*)-configured substrate neral (*Z*)-**12a**, was reduced by *GsOYE* and *CtOYE* to (*S*)-citronellal (**12b**) with poor conversion (39 and 9% conversion, respectively) but higher stereoselectivity (80 % and 55% (*S*)-**12b**) compared to citral (mixture of (*E*)-**12a** and (*Z*)-**12a** 47:53) (37 % and 22% (*S*)-**12b**). These results were obtained using 15 mM NADH in the reaction medium and 6 h reaction time in screw-cap glass vials in order to avoid substrate/product evaporation. Different attempts for using the recycling system with GDH together with *GsOYE* on **12a** have been performed but the conversion was lower (conv. 14 %) maybe due to the

high reactivity of the substrate that could react with the amino groups exposed on the surface of GDH, leading to its inactivation. Moreover, reaction *medium* engineering has been applied using 10% and 20% of TBME as co-solvent in an attempt to increase the conversion rate of GsOYE with this substrate. Nevertheless, the conversion was not further optimized (data not shown).

Finally, no conversion was observed for β -damascone (**13a**). This compound has been investigated here for the first time as possible substrate for ene-reductases. Despite the presence of two C=C-bonds activated by the same electron-withdrawing group, no reaction occurred, most likely due to steric hindrance.

Enzymatic reductions mediated by isolated OYEs in large preparative scale are very scarce due to substrate inhibition effects. A first example of preparative scale OYE mediated bioreduction (70 g) was reported by Mangan and co-workers [202], that achieved 53% conversion after 20 hours of reaction in the reduction of an ester-activated olefin after optimization of reaction *medium*. Low productivities have been overcome using different strategies such as reaction engineering techniques (*e.g. in situ* substrate feeding product removal) [203] or biocatalyst engineering [204]. However, recently Johnson Matthey has screened their wild-type ERs collection reporting substrate tolerance loading to up 1.5 M concentration [137].

Encouraged by Dominguez *et al.* [137] findings, further studies were performed increasing the initial concentration of some substrates to 50 mM in order to investigate the substrate loading capacity of the newly discovered ene-reductases. The results are summarized in Table 15. Both enzymes exhibit approximately 50% conversions for almost all the substrates tested, compared to close to full conversion registered in the biotransformations run on 10 mM substrate. For **2a** and **8a** modest conversion rates were registered, however these substrates were scarcely converted already at 10 mM starting concentration. In contrast, for **4a** good to excellent conversion was still surprisingly detected, thus increasing concentrations (up to 100 mM) were also tested. Higher concentrations of substrate **4a**, however, appeared to result in inhibition or deactivation of both enzymes (lower conversions observed).

Table 15. Bioreduction of selected substrates in 50-100 mM concentration.

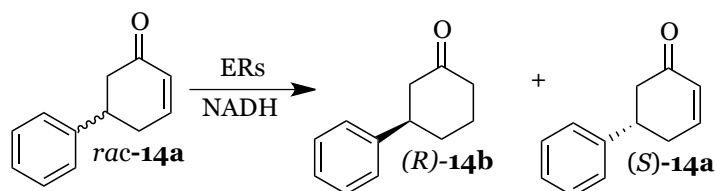
Substrate	GsOYE	CtOYE
	Conv. (%)	Conv.(%)
1a	54	52
2a	1.3	8
4a	96 (#25)	76 (#34)
5a	53	42
7a	52	60
8a	1.8	11
11a	54	46

The standard assay (500 μ l) was performed at 30 °C and 120 rpm in 50 mM Tris-HCl (pH 8.0) containing 100 μ M NAD⁺, 50 U/ml (#100 U/ml) GDH, 100 mM (#200 mM) glucose and 50 mM (#100 mM) of substrate. The reaction was started through the addition of enzyme to a final concentration of 100 μ g/ml or #200 μ g/ml and incubated over-night. The conversion reported is based on product formation or substrate consumption (**11a**) according to calibration curve. The conversions for #**4a** are reported as apparent conversion (area product/(area product + area substrate) *100).

4.3.2 Kinetic resolution of 5-phenyl-2-cyclohexenone

OYEs have been reported to mediate the kinetic resolution of different racemic γ -substituted lactones with excellent enantioselectivities (E-values up to 49), owing to stereorecognition of the distant chiral center. Moreover, a case of dynamic kinetic resolution was also demonstrated for 3-methyl-5-phenylfuran-2(5*H*)-one, thanks to *in situ* racemization of the substrate leading to 73% conversion and >99% ee and 96% de for the formed product [117].

A racemic mixture of 5-phenyl-2-cyclohexenone (**14a**) was used as starting material to test the ability of GsOYE and CtOYE to perform a kinetic resolution. The enantioselectivity values (E-values) obtained are reported in Table 16. Both enzymes displayed low enantioselectivity on **14a** (E-values <12) but they were able to accept and moderately convert this bulky substrate (23% and 60% conversion for GsOYE and CtOYE, respectively). Both enzymes showed the same enantiopreference producing the (*R*)-enantiomer, however GsOYE was more selective than CtOYE.

Table 16. Kinetic resolution of **14a**^a

Enzyme	ee 14b (%)	ee 14a (%)	E	Conv. (%)
GsOYE	72 (<i>R</i>)	22 (<i>S</i>)	8	23
CtOYE	42 (<i>R</i>)	86 (<i>S</i>)	10	60

^a Conversion calculated from $[ee_{\text{substrate}}/(ee_{\text{substrate}}+ee_{\text{product}})]$. Tool for calculation of E-value (enantioselectivity)^[205] available (open access) at <http://biocatalysis.uni-graz.at/enantio/cgi-bin/enantio.pl>

4.3.3 GsOYE and CtOYE bioreduction of α,β -unsaturated nitroalkenes

Reduction of the C=C-bonds of nitroalkenes leads to the formation of nitroalkanes, which can be further modified into high added value compounds such as amines, aldehydes, carboxylic acids, oximes and hydroxylamines [206-208]. Moreover, different OYE homologues have been reported for their ability to catalyze the nitro-group reduction due to their catalytic promiscuity [138]. Often the products formed after NO₂-reduction can further react through spontaneous reactions leading to the formation of unusual and unexpected products as already discussed in the Introduction.

GsOYE and CtOYE activity was tested using the nitroalkenes depicted in Figure 59. The results obtained with this class of strongly activated alkenes are summarized in Table 17.

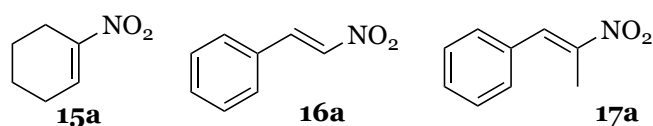
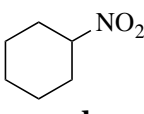
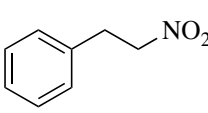
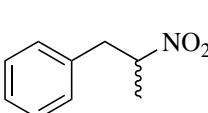
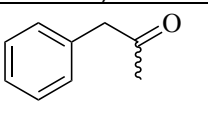


Figure 59. Nitrocompounds tested as substrates of GsOYE and CtOYE.

All nitroalkenes tested were well accepted by both enzymes compared to carbonyl compounds due to the strong activation exerted by the nitro group.

The nitroalkenes (**15a-17a**) were tested at different pH values. In the reduction of **15a**, GsOYE and CtOYE showed completely different behaviours: while GsOYE was extremely sensitive to the pH *medium* and an activity decrease with the increase of pH (73 % of conversion at pH 5.0 *vs* 25% of conversion at pH 8.0) was observed, CtOYE exhibited high activity (> 97% conv.) regardless of the pH *medium*. For **16a** GsOYE showed excellent conversion (> 99%) at all pH values tested while for CtOYE a decrease in the formation of the main product was observed at basic pH due to the formation of other secondary products of higher molecular weights (Fig. 60). The formation of these byproducts was enhanced at slightly higher reaction temperatures (30 °C instead 25 °C) and using higher concentrations of glucose (50 mM instead of 20 mM), and thus of reducing equivalents. In these conditions, besides the classical C=C-bond reduction, CtOYE may also catalyze the nitro-group reduction to the corresponding nitroso- and hydroxylamino products, that could spontaneously condensate to dimeric side-products as observed in the reduction of nitrobenzene [209].

Table 17. Bioreduction of nitrocompounds **15a-16a** at various pH values

Substrate	Main products	pH 8.0		pH 5.0	
		GsOYE conv. (%)	CtOYE conv. (%)	GsOYE conv. (%)	CtOYE conv. (%)
15a	 15b	25	99	73	97
16a	 16b	> 99	89	> 99	95
17a	 17b	> 99	> 95	85	n.t.
	 17f	1	0	10	n.t.

The standard assay (500 μ l) was performed at 30 °C and 120 rpm in 50 mM Tris-HCl (pH 8.0 and pH 5.0) containing 500 μ M NAD⁺, 100 U/ml GDH, 50 mM glucose and 10 mM of substrate. The reaction was started through the addition of enzyme to a final concentration of 100 μ g/ml and incubate over-night. The conversion reported is apparent conv. (area product/(area product + area substrate) *100). n.t. not tested.

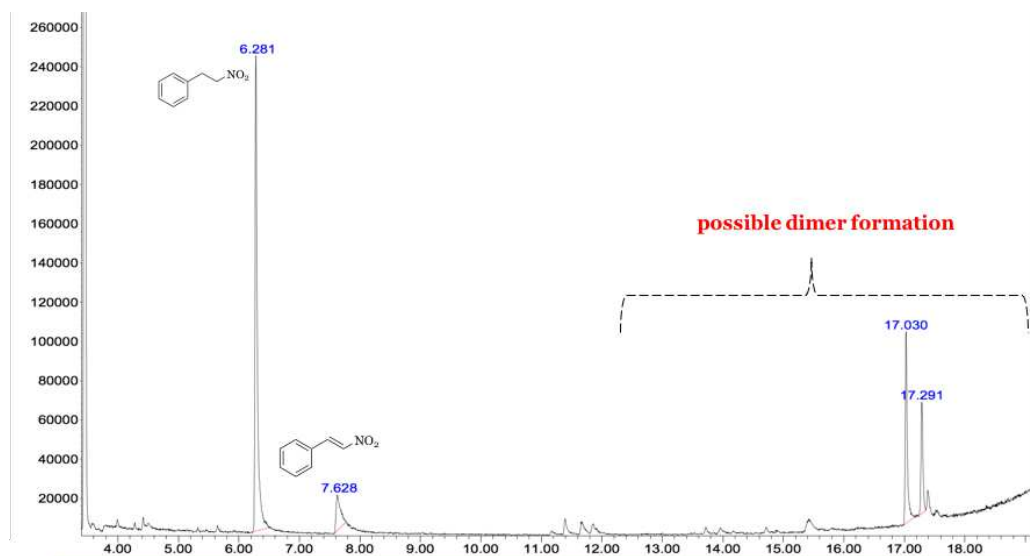


Figure 60. GC-MS chromatogram of β -nitro-styrene reduction by CtOYE at pH 8.0 showing byproduct formation.

For **17a** very good conversions were obtained at pH 8.0 (> 95% conversion) for both enzymes. Moreover, for GsOYE a small peak (< 1% conv.) corresponding to **17f**, a secondary product due to the bio-Nef pathway [133] (Fig. 61), was detected. Surprisingly at pH 5.0 we observed an increase in the bio-Nef pathway (10% conv. to **17f**) and a slight decrease in **17b** formation (85% conv.). Despite various

control reactions, it could not be clearly determined if the Nef pathway occurred directly on **17a** or on **17b** (data not shown).

As the acidic α -proton of product **17b** racemizes spontaneously, we decided to optimize the ee of the product (**17b**) using different temperatures of reaction and different pHs, aiming at slowing down or preventing the racemization [210]. At pH 5.0 and 10 °C, the best ee values were obtained: 50% and 70% (*R*)-**17b** for GsOYE and CtOYE, respectively (Table 18).

Table 18. Influence of reaction conditions on the stereoselectivity of OYE-catalyzed reduction of **17a**. n.d. not detected; n.m. not measured.

pH	Temperature (°C) / reaction time	Enzyme	Conv. %	Conv.%	ee 17b (%)
			17b	17f	
5	25 / ON	GsOYE	85	10	<i>rac</i>
6			83	11	<i>rac</i>
7			93	6.5	<i>rac</i>
8			>99	n.d.	<i>rac</i>
5	10 / 6 h		n.m.	n.m.	50 (<i>R</i>)
6			n.m.	n.m.	43 (<i>R</i>)
7			n.m.	n.m.	22 (<i>R</i>)
8			n.m.	n.m.	<i>rac</i>
5	10 / 6 h	CtOYE	n.m.	n.m.	70 (<i>R</i>)
6			n.m.	n.m.	68 (<i>R</i>)
7			n.m.	n.m.	32 (<i>R</i>)
8			n.m.	n.m.	<i>rac</i>

The bio-Nef pathway, as already reported in Chapter 1, is catalyzed by different OYEs homologues such as XenA, NerA, PETNR, OPR3 and MR [133]. We decided to set-up a time study using GsOYE as biocatalyst at acidic pH and different (generally lower) temperatures and glucose concentrations in order to slow down the reaction and have the chance to isolate more intermediates to better investigate this reaction (Fig. 61). Particularly relevant was the question whether the nitro reduction takes place on the reduced compound (**17b**, such as shown in Fig. 61) or possibly on **17a** directly.

Using 20 mM of glucose and thus just two reducing equivalents, and low temperature (Fig. 62), the reaction was not complete as for the Nef-pathway three hydrides are necessary. However, in the initial stage of the reaction, the substrate **17a** was rapidly consumed and surprisingly both products the one of the C=C-bond reduction (**17b**) and the one formed through the bio-Nef pathway (**17f**) were produced simultaneously. Between 4 h and 6 h of reaction we observed a slight decrease in the amount of **17b** and a simultaneous increase in oxime (**17d**) and ketone (**17f**) formation. A chromatogram showing the intermediates detected by

GC-MS is shown in Figure 64.

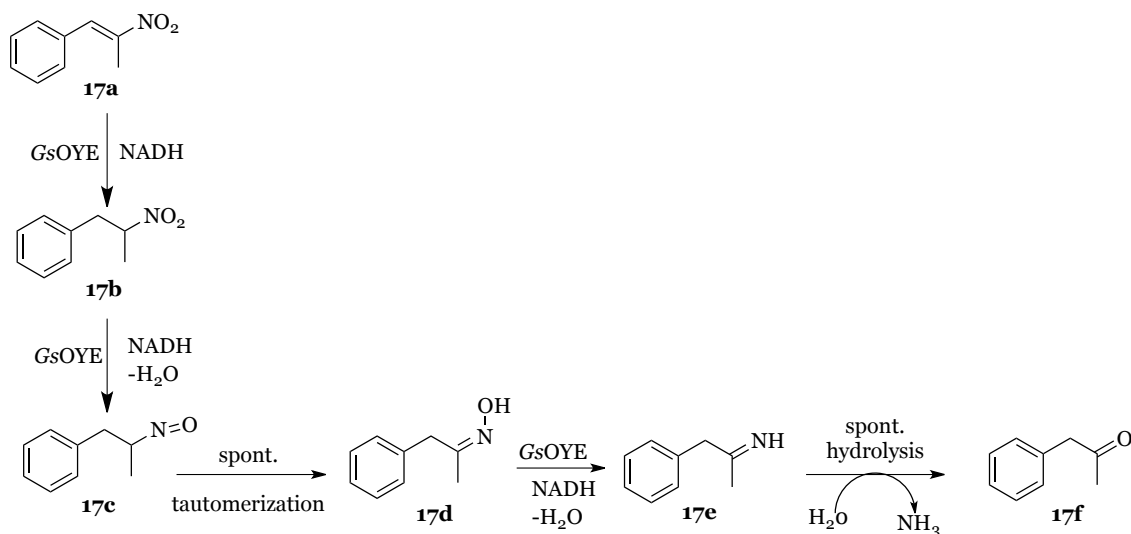


Figure 61. Bio-Nef pathway on *trans*- β -methyl- β -nitrostyrene (**17a**) catalyzed by GsOYE following the reaction mechanism described for 1-nitro-2-phenyl-propene [133].

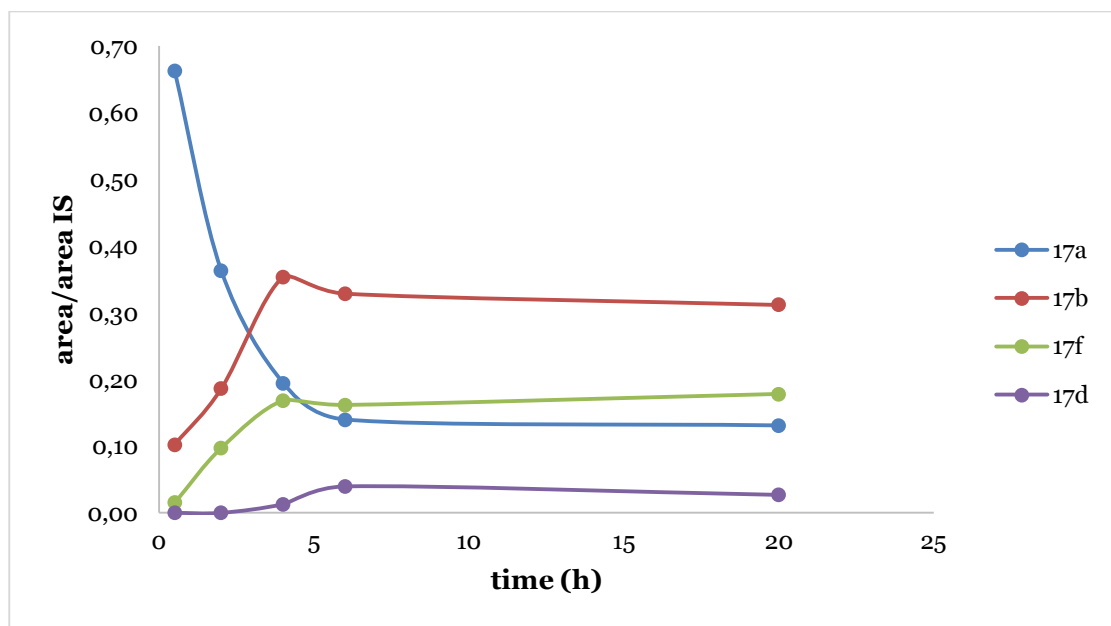


Figure 62. Normalized data from the time study of bio-Nef reaction at pH 5.0 using 20 mM glucose and 10 °C.

Using 50 mM glucose (Fig. 63) the reaction was faster (however still not complete) in the initial 2 hours yielding higher amounts of **17b** compared to the previous study. However, in the following 2 hours a net decrease in **17b** amount was registered together with an increase of **17d** and **17f** amounts.

As from the results of these preliminary time-studies was not so clear if the Nef pathway occurred directly on **17a** or on **17b** and in order to get more insights into this intriguing reaction we have set-up further experiments to try to understand if GsOYE produced **17f** exclusively from **17b** or directly from **17a** or both.

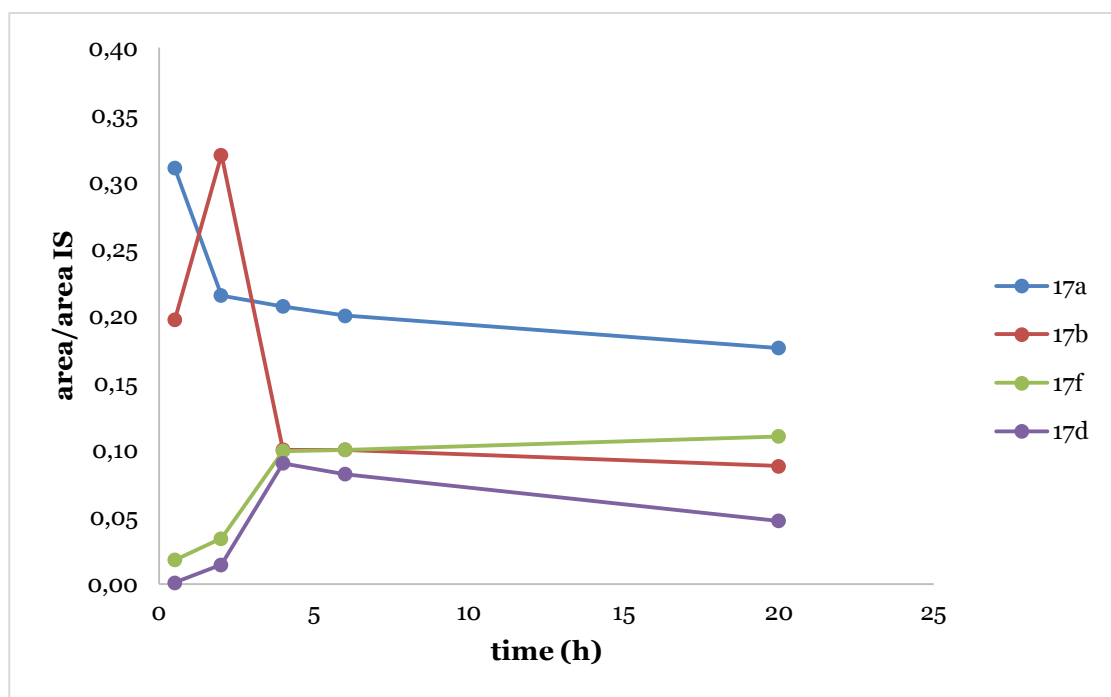


Figure 63. Normalized data from the time study of bio-Nef reaction at pH 5.0 using 50 mM glucose and 10 °C.

17b was produced enzymatically using GsOYE enzyme and pH 8.0 knowing that in these conditions the reaction proceeded just through the C=C-bond reduction with high conversion (> 99%, Table 17). Once **17b** was produced it was extracted from the reaction *medium* following the standard extraction protocol and then dried under reduced pressure and used as starting material. For this second reaction run at pH 5.0, both GDH recycling system and NADH excess were investigated and also different temperatures of incubation (25 °C and 10 °C). To our surprise, at 25 °C no traces of **17f** were detected both with GDH recycling system or NADH excess, while at 10 °C just 5% conv. of **17b** to **17f** was detected using 15 mM NADH. It thus appears that **17f** is preferentially obtained from **17a**, in a competitive reaction with the C=C-bond reduction. Moreover, bio-Nef reaction seems heavily influenced (and promoted) by (low) temperature and reaction *medium* pH. In particular, imines are notoriously unstable at acidic pH, which would explain faster conversion to **17f** through hydrolysis of **17e** at pH 5.0. Taken together, these data prompted us to propose other possible reaction mechanisms that are depicted in Figure 65.

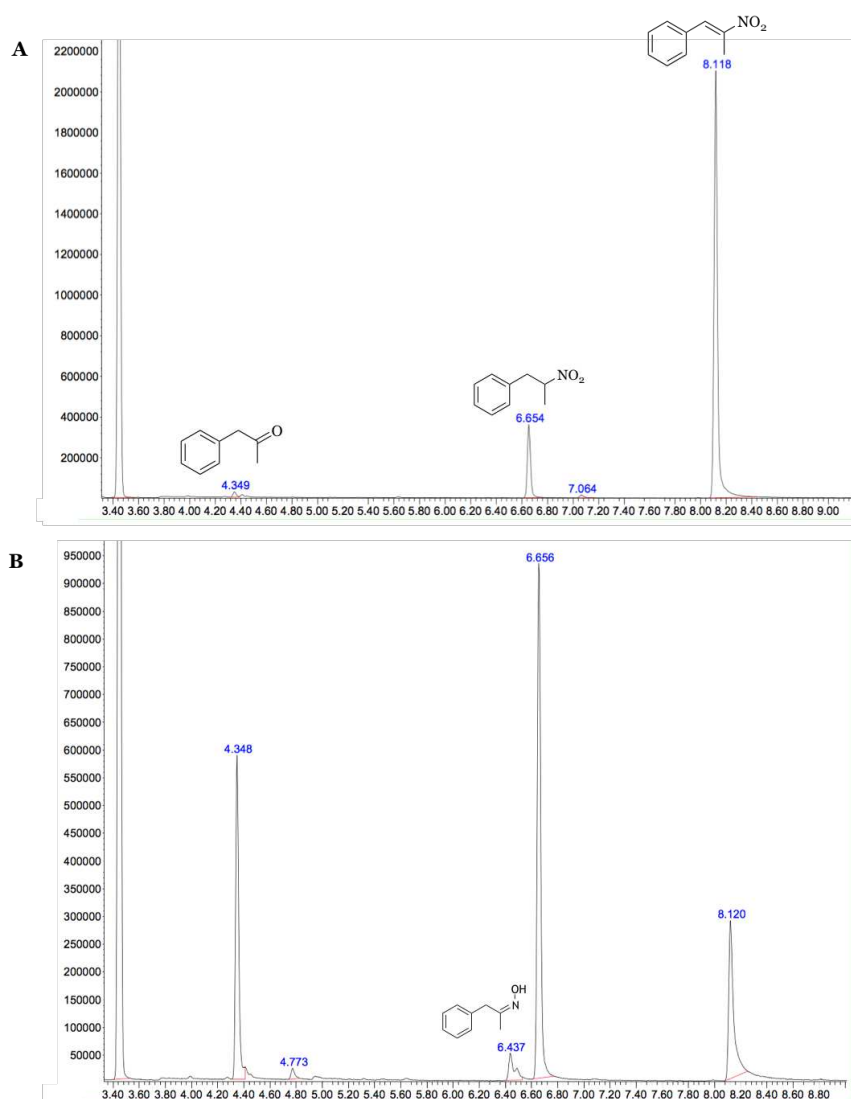


Figure 64. Time study of bio-Nef reaction: samples analyzed by GC-MS after (A) 30 min and (B) over- night reaction, in Tris buffer pH 5.0 and 50 mM glucose.

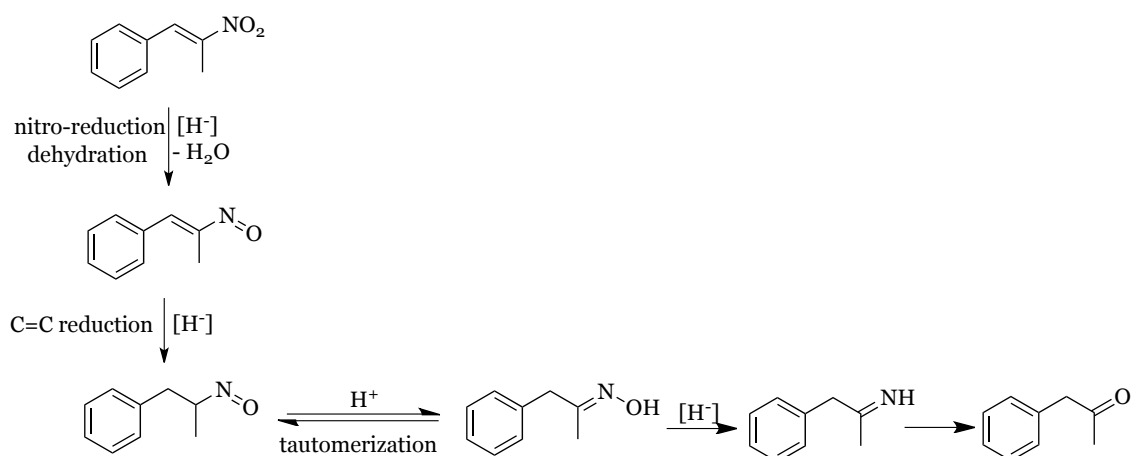


Figure 65. Alternative conversion pathway of nitroalkene combining C=C-bond reduction and nitro-group reduction through bio-Nef-reaction.

In this proposal, an alternative pathway may start with the nitro-group reduction in **17a**, followed by C=C-bond reductive event. As already mentioned, different OYE homologues have a dual activity showing ability to reduce not only C=C-

bonds but also directly nitro-groups [133, 211]. Different structural-activity correlations have been reported to explain this dual nitro- and ene-reductase activity [212]. For more details about *GsOYE* and *CtOYE* crystal structure see Chapter 5.

4.4 Oligomeric state investigation

Members of the OYE family can exist in different oligomeric states depending on the subclass which they belong to (see section 1.4.3 Introduction). OYEs belonging to classical family were found to exclusively occur as monomers or homodimers in solution [63, 66, 68], while thermophilic-like OYEs were found as homodimers and homotetramers [99, 100, 102]. Moreover, for some OYEs belonging to this class such as TOYE [73] and TsOYE (or CrS) [96] higher oligomeric species (*i.e.* octamers and dodecamers) were also detected. However, it has been reported that the equilibrium between the different oligomeric states is influenced by protein concentration [102]. Generally, at higher protein concentration the higher oligomeric species are predominant, whereas at lower protein concentration the equilibrium is shifted towards the dimeric species. Furthermore, the oligomeric state of OYERo2 was found to depend on the interaction with NADPH and thus on the flavin redox state. In fact, in the presence of NADPH, a full dissociation of the enzyme in homodimers was reported [102].

The oligomeric state of all the seven proteins reported in this thesis was investigated by Size Exclusion Chromatography. Moreover, for the thermophilic-like OYEs a native PAGE was also run in order to get more insights on their oligomerization state.

4.4.1 Classical OYEs

Analytical gel filtration revealed that *GsOYE*, *CtOYE* and *BfOYE1* occur as monomers in solution (Fig. 66). More in detail, the molecular weights of the recombinant proteins estimated from this analysis were 1.06, 0.75 and 0.77 times the calculated one from the primary sequence of *GsOYE* (45.5 kDa), *CtOYE* (42.5 kDa) and *BfOYE1* (43.5 kDa), respectively.

AnOYE2 was also analyzed by SEC chromatography revealing a peak corresponding to the monomeric specie (43.3 kDa). In addition to this peak, however, two other peaks were detected at higher and lower molecular weights corresponding to aggregated species and degradation products, respectively (data not shown). The enzyme preparation used for this analysis was stored at -20 °C for 2-months with 20% glycerol and the resulting behavior clearly indicates that the *AnOYE2* protein suffered from degradation and aggregation events. The same

behavior was also observed for OYE3 during crystallization trials (for details see Chapter 5).

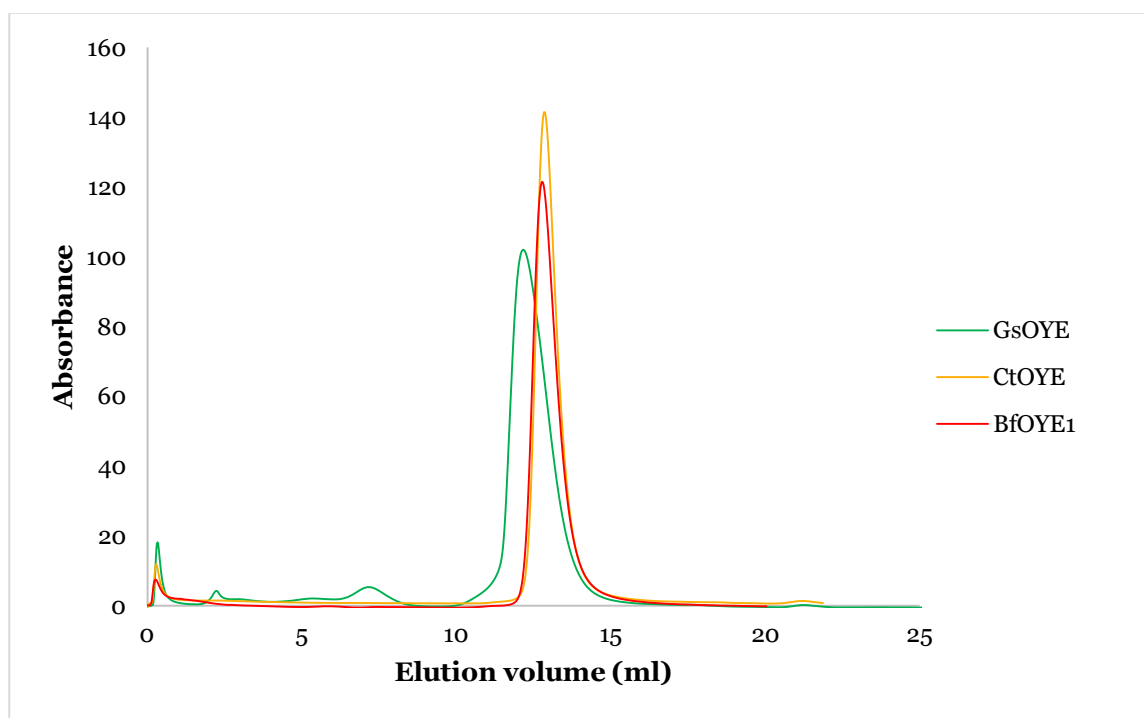


Figure 66. GsOYE (green), CtOYE (orange) and BfOYE1 (red) eluted from a Superose 12 300/GL column. Elution volumes: 12.17 ml, 12.84 ml and 12.77 ml, respectively.

As already mentioned, classical OYEs occur exclusively as monomers or homodimers in solution. The oligomerization state of our proteins was detected to be monomeric from SEC analysis, thus being in line with literature data.

4.4.2 Thermophilic-like OYEs

For the thermophilic-like enzymes, CaOYE and AnOYE8, analytical gel filtration analysis revealed that both occur, surprisingly, as monomers in solution (Fig. 67). More in detail, the molecular weights of the corresponding recombinant proteins were 1.18 and 1.09 times that of the monomeric species for CaOYE (39.9 kDa) and AnOYE8 (47.9 kDa), respectively.

Conversely, BfOYE4 revealed a heterogeneous profile, with different oligomers present in solution detected by SEC analysis. As shown in the chromatogram reported in Figure 68A, two main peaks corresponding to the monomeric and dimeric forms of BfOYE4 were detected. Moreover, others poorly defined oligomeric states at higher molecular weights were found (as a peak shoulder) in lower amounts. The eluted fractions were loaded in an acrylamide SDS-PAGE gel to check their purity and to confirm that all of them contain the desired protein (Fig. 68B).

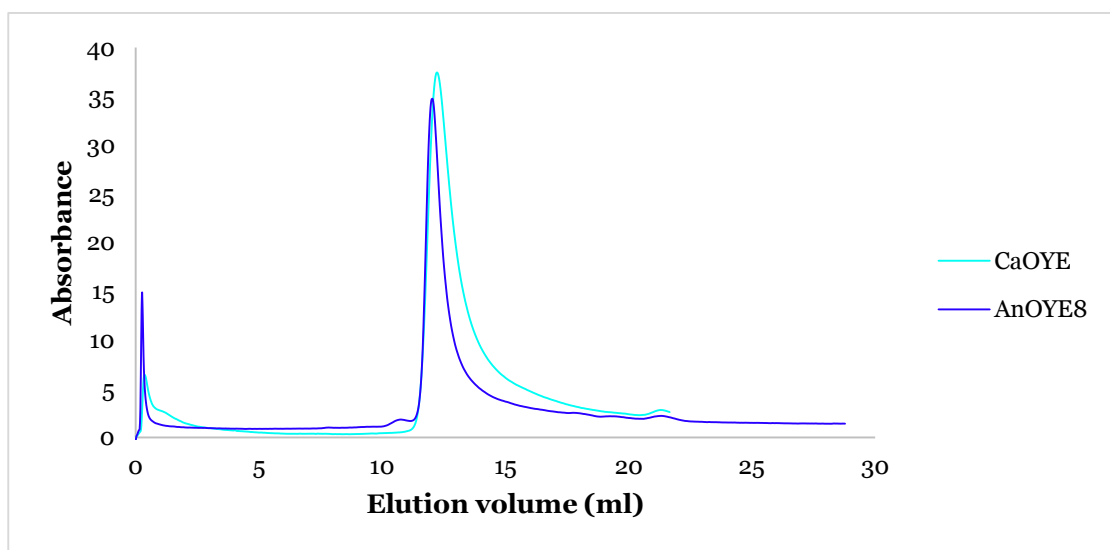


Figure 67. *CaOYE* (cyan) and *AnOYE8* (dark blue) eluted from a Superose 12 300/GL column. Elution volumes: 12.21 ml and 12.04 ml, respectively.

All the eluted fractions contain a major band corresponding to *BfOYE4*. Some impurities at lower molecular weights are also present in all the collected fractions. Moreover, a band at molecular weight slightly higher than 95 kDa, that could correspond to undissociated dimers (98 kDa), is present in the three fractions. Finally, in fraction 5-16 a major contaminant at 60 kDa was detected. Since this enzyme preparation was produced using *E. coli* BL21 (DE3) strain and not the Arctic one (for details see Chapter 3) it is difficult to ascribe this band to a specific protein (*e.g.* chaperons).

In order to better understand the nature of the oligomeric states of *BfOYE4* preparation, a cross-linking experiment was performed using as starting material the fractions 21-25 and 17-20 eluted by size exclusion chromatography. From the gel reported in Figure 69, the concentration of the monomer, in both pools of fractions, decreases with incubation time, while the concentration of dimeric and also higher oligomeric states increases, reaching a maximum after 90 minutes incubation with the cross-linker. In the untreated monomeric fractions, no traces of oligomers both as dimers and higher molecular weight are detectable, since they are dissociated by the denaturing conditions of the gel.

Finally, a native PAGE analysis was performed to get more insights on the oligomeric states of the three enzymes in solution. As shown in Figure 70 *CaOYE* and *AnOYE8* are present as single bands at the corresponding molecular weight of the monomeric species, confirming the results obtained by SEC chromatography. Some degradation is also detected for both proteins. Moreover, for *AnOYE8* a contaminant (present in low amount, red arrow) is observed in the

gel at about 67 kDa, most likely corresponding to the chaperonin Cpn60 over-expressed by the *E. coli* Arctic® strain, used for the production of the protein (see Chapter 3). The electrophoretic run of *BfOYE4* results in a smear; despite the undefined nature of such result, some bands (orange arrows) at distinct molecular weights are detectable suggesting (even if in low amounts) the existence of different oligomeric states *in vitro*, as observed by other techniques.

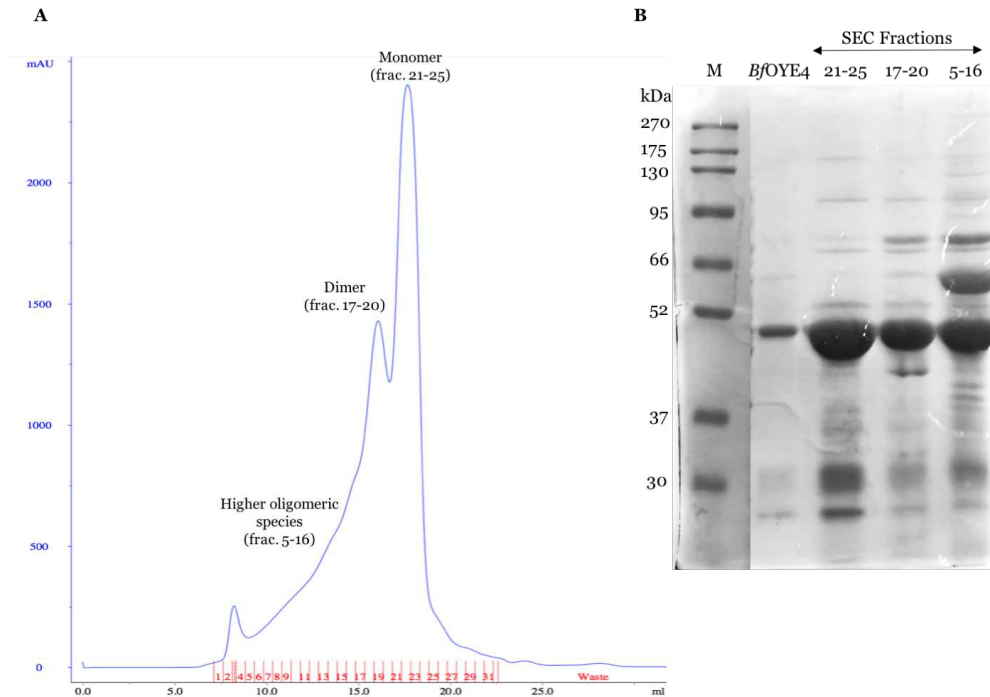


Figure 68. (A) *BfOYE4* eluted from a Superose 6 300/GL column. (B) SDS-PAGE 12% acrylamide showing fractions eluted from SEC: Molecular ladder Mass Sharp VII (M), IMAC purified *BfOYE4* (*BfOYE4*) used as control, SEC fractions: monomer (21-25), dimer (17-20), higher oligomeric states (5-16).

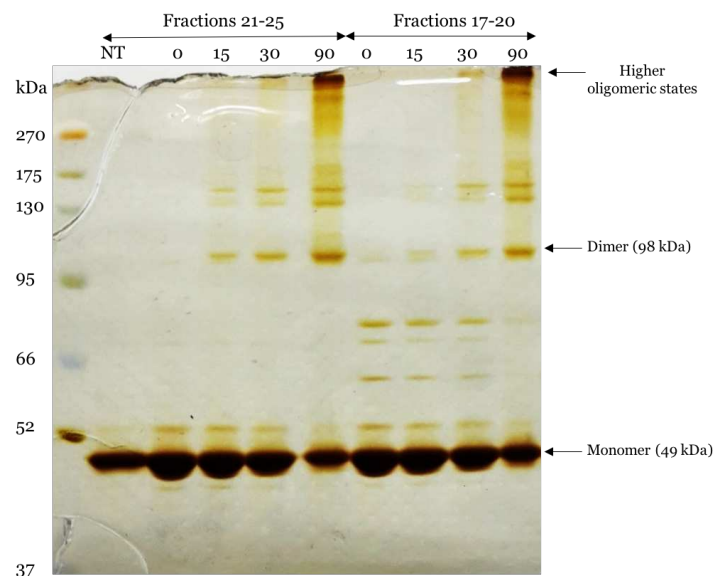


Figure 69. Silver stained SDS-PAGE 10% acrylamide: M molecular ladder MassSharp VII, Non-treated monomeric protein (NT), SEC fractions 21-25 (monomer) and 17-20 (dimer), sampled after different times (0, 15, 30, 90 minutes) of incubation with 25% glutaraldehyde.

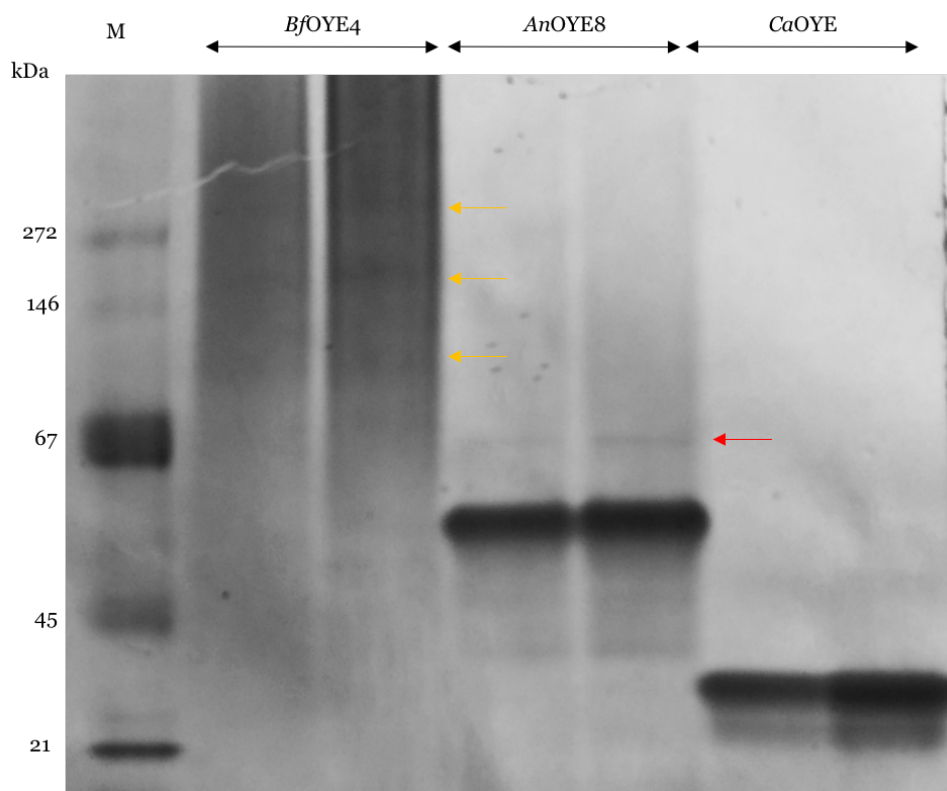


Figure 70. Native-PAGE using precast NuPAGE™ Tris-Acetate 3-8% gel from ThermoFisher: SERVA native marker (M), *BfOYE4*, *AnOYE8* and *CaOYE* samples loaded in two different amounts: 10 µg on the left and 20 µg on the right.

To our knowledge just one enzyme, *i.e.* *RmER*, belonging to the thermophilic-like subclass has been reported to exist as monomer in solution until now [146]. It was hypothesized that the atypical elongated C-terminus of the protein could prevent the Arg-finger interactions involved in dimer formation. However, recently its crystal structure has been solved showing the typical dimer interface [213]. In the crystal structure of *CaOYE* determined in this work the typical dimeric quaternary organization has been observed in the crystal packing (for more details see Chapter 5). As already mentioned, the equilibrium between the oligomeric forms can be concentration dependent and the high concentrations explored by enzymes in the crystallization conditions could promote the dimeric association.

4.5 pH optimum

The effects of pH on OYEs were investigated by monitoring the change in enzyme activity over a pH range of 3.0–12.0 (Fig. 71). The activity-pH profile shows a wide range of pH *optimum* for all the proteins tested.

All OYEs (except *CaOYE*) show a bell-shaped pH profile. *GsOYE* and *CtOYE* maintain their maximum activity for 2-cyclohexen-1-one in a wide range of pH (*i.e.* 5.0–9.0) with *CtOYE* showing an increased activity (about 30%) at basic pH between 9.0 and 10.0. Both enzymes have a decrease in their activity at pH 12.0 with *GsOYE* being completely inactive. Moreover, these enzymes are the only ones that maintain almost half of the maximum activity at pH 3.0. *BfOYE1* shows its maximum activity in a limited pH range between 6.0 and 7.0, compared to *GsOYE* and *CtOYE*. However, the enzyme is still active (even if just 35% of activity is detectable) also at extreme acidic (pH 4.0) and basic (pH 12.0) pH values.

The thermophilic-like OYEs retain 100% of activity in a wide range of pH: from pH 7.0 to almost pH 12.0 and from pH 6.0 to pH 9.0 for *CaOYE* and *BfOYE4*, respectively. Reduced activities are detected however also at acidic pH values (between pH 4.0–6.0) and at basic pH just for *BfOYE4*. Surprisingly, *CaOYE*, is the only enzyme able to maintain 90% of its maximum activity at pH 12.0.

The pH profile of *AnOYE2* and *AnOYE8*, was not investigated as no activity or very low activity with 2-cyclohexen-1-one was registered for both enzymes (see section 4.1 of this Chapter).

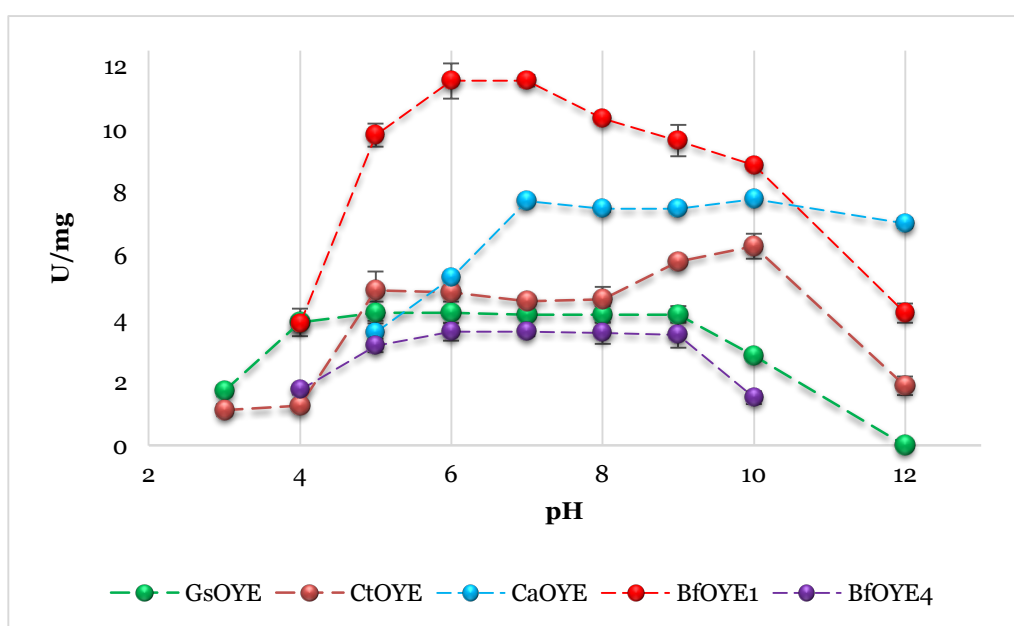


Figure 71. Activity-pH profile of *GsOYE* (green), *CtOYE* (orange), *CaOYE* (cyan), *BfOYE1* (red) and *BfOYE4* (purple).

4.6 Determining unfolding temperatures

Unfolding experiments on all OYEs identified in this PhD work, were performed using the Thermofluor method. Moreover, a screening of different co-solvents was performed in order to evaluate changes in T_m at different percentages of various organic co-solvents.

4.6.1 Classical OYEs

Unfolding temperatures (T_m) of *Gs*OYE (Fig. 72) and *Ct*OYE (Fig. 73), isolated from extremophilic photosynthetic organisms, was 66 °C and 53 °C, respectively. Both enzymes exhibit good tolerance in the presence of 5% to 20% of DMSO, acetonitrile and acetone. A decrease in stability was detected with ethanol and dioxane (reaching a T_m drop of 10 °C in 40% dioxane).

For the enzymes, *Bf*OYE1 (Fig. 74) and *An*OYE2 (Fig. 75), isolated from mesophilic fungi, T_m values of 42 °C and 41.5 °C have been measured.

Both enzymes could tolerate low percentages of organic co-solvents (5%). *An*OYE2 showed good stability in up to 40% DMSO. Decrease of stability was observed in high percentages (10-40%) of the other co-solvents showing dioxane as the worst one. In the 50% co-solvent preparation, a complete denaturation was observed for both enzymes except for *An*OYE2 for which a 32 °C T_m values was registered in 50% acetone.

Classical OYEs are reported as not thermo-resistant biocatalysts, compared to their thermophilic-like counterparts. For some classical ERs isolated from *Pseudomonas putida* (*XenA*, *XenB* and *NemA*, respectively) temperature optimum of 30 °C were reported [151, 153]. Moreover, the standard activity screening used for the vast majority of the identified ERs, are generally performed at 30 °C [82, 106]. However, higher stability was reported for *Chr*-OYE1 ($T_m = 40$ °C) [156] and *Gox* ($T_m = 59$ °C) [145].

Although an accurate comparison is almost impossible due to the different techniques and conditions (such as different buffers and pH values) used for the determination of thermal stability, *Gs*OYE and *Ct*OYE can be considered thermostable and robust biocatalysts. Considering that the source organisms typically grow in extreme environments, this result is not unexpected. On the contrary, the enzymes isolated from mesophilic fungi are characterized by lower T_m values, but, however, comparable with those already reported in literature.

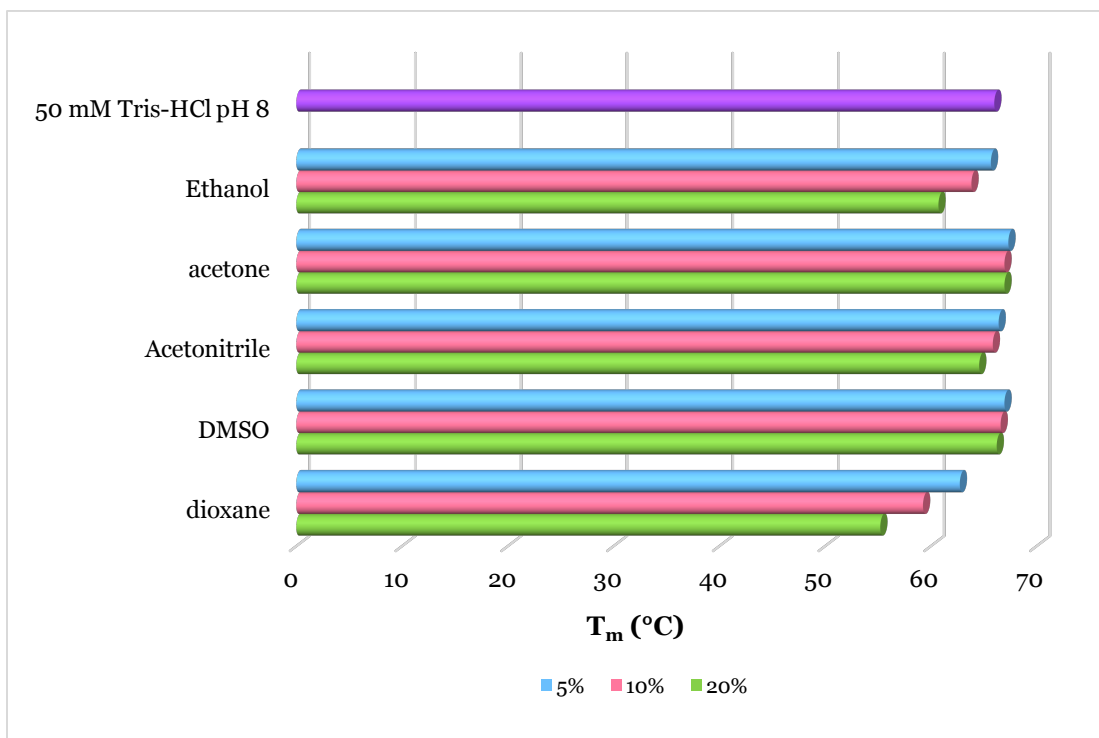


Figure 72. Influence of type and concentration of co-solvents (50 mM Tris-HCl buffer pH 8.0 supplemented with increasing vol% of organic co-solvent) on GsOYE stability.

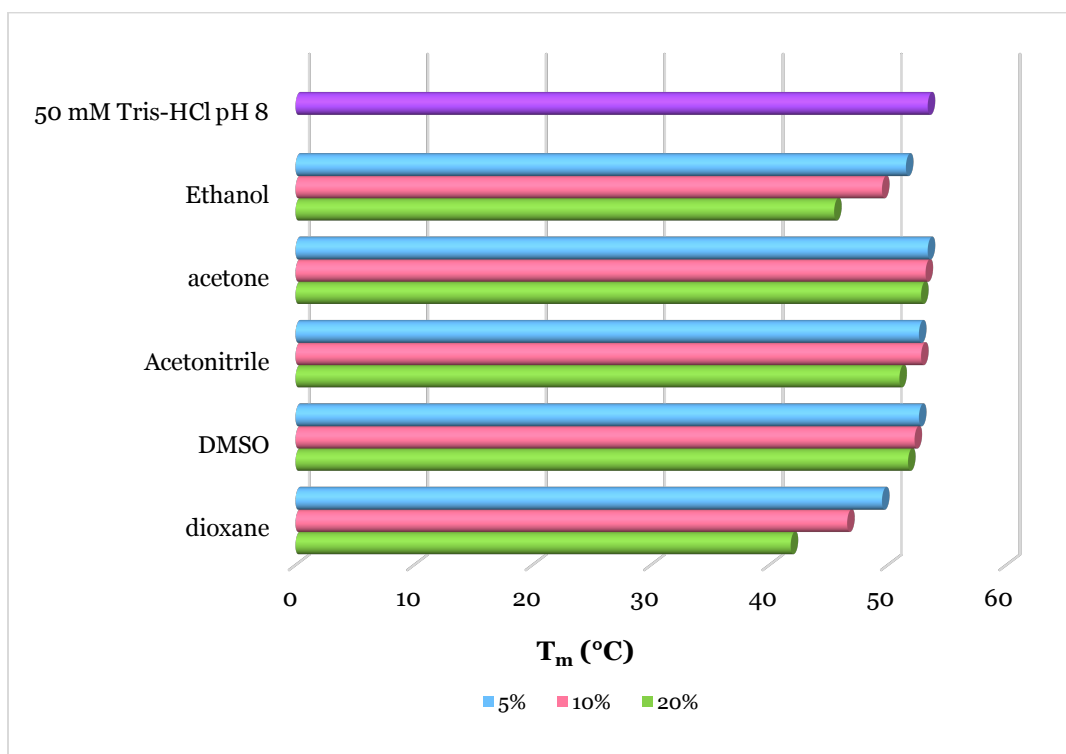


Figure 73. Influence of type and concentration of co-solvents (50 mM Tris-HCl buffer pH 8.0 supplemented with increasing vol% of organic co-solvent) on CtOYE stability.

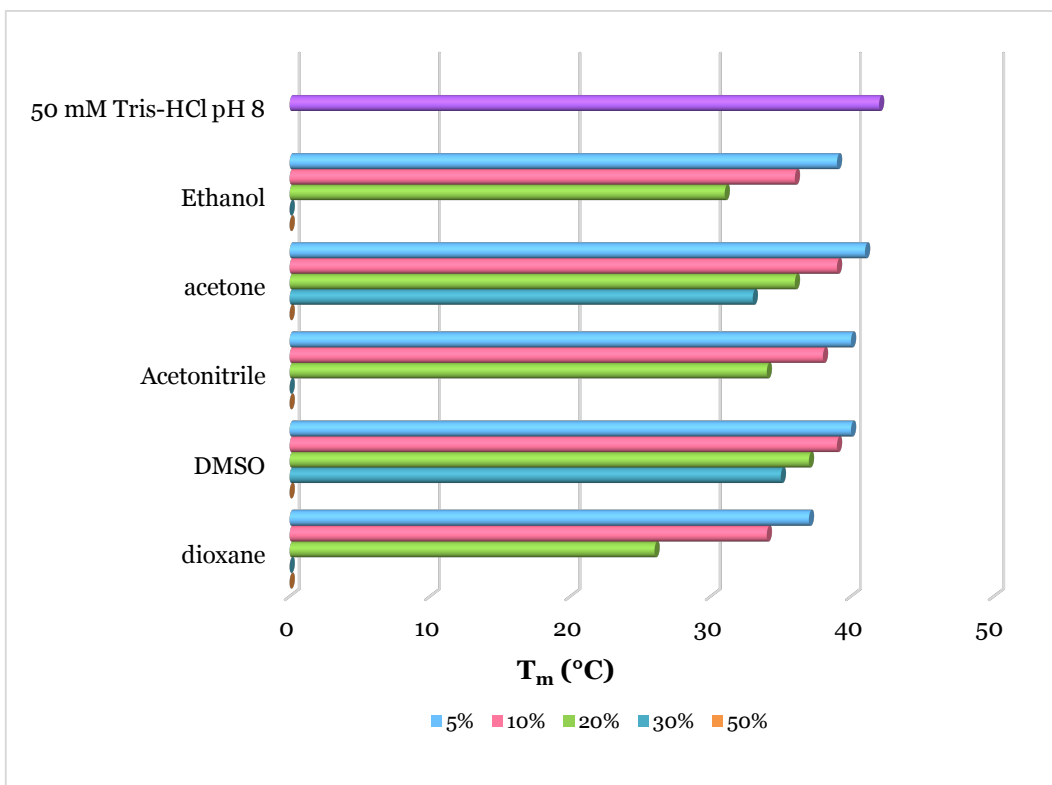


Figure 74. Influence of type and concentration of co-solvents (50 mM Tris-HCl buffer pH 8.0 supplemented with increasing vol% of organic co-solvent) on *BfOYE1* stability.

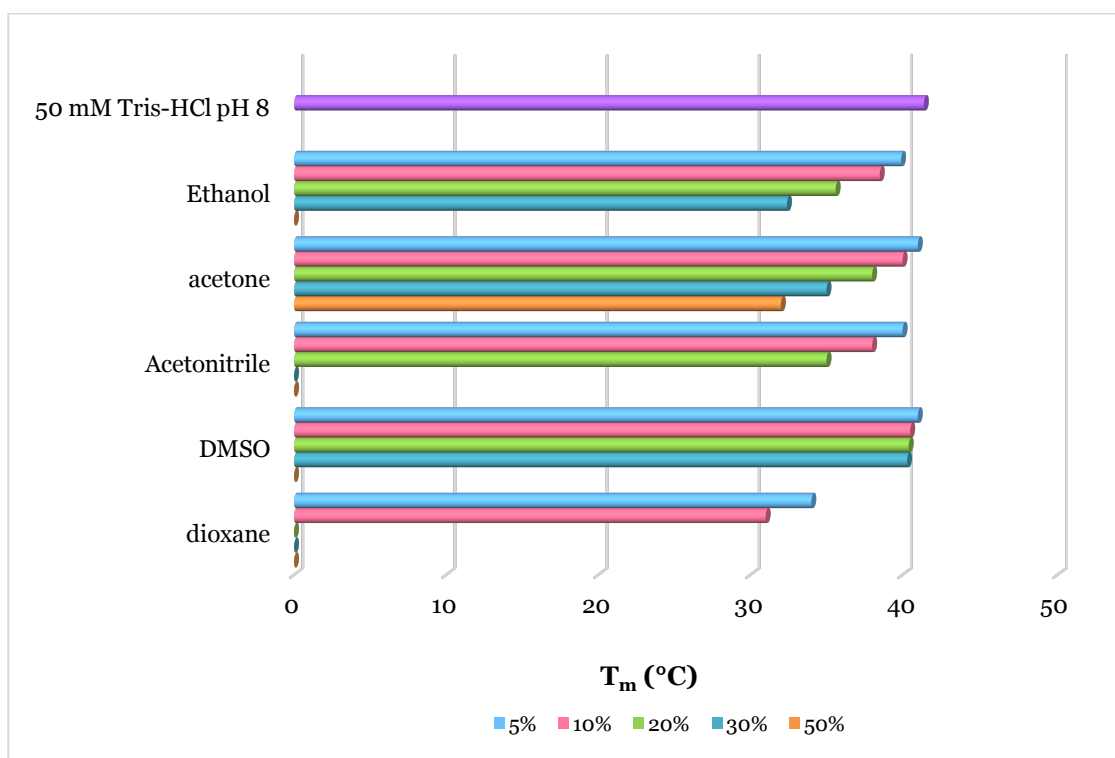


Figure 75. Influence of type and concentration of co-solvents (50 mM Tris-HCl buffer pH 8.0 supplemented with increasing vol% of organic co-solvent) on *AnOYE2* stability.

4.6.2 Thermophilic-like OYEs

The unfolding temperature (T_m) of *CaOYE*, isolated from an extremophilic photosynthetic bacterium, was 79 °C (Fig. 76). Moreover, the enzyme could well tolerate 5-10% of DMSO and acetonitrile but good T_m values were detected also in the presence of higher percentages (up to 40%) of the same organic co-solvents (69.5 °C in DMSO and 55 °C in acetonitrile, respectively). The stability of the protein in ethanol was negatively influenced already at low percentages (T_m = 74 °C in 5% ethanol and 71 °C in 10% ethanol). However, in higher percentages of ethanol the T_m values are comparable with those obtained for the higher percentages of acetonitrile.

BfOYE4 and *AnOYE8* (Fig. 77 and Fig. 78), both isolated from mesophilic fungi, had lower T_m values (43 °C and 44 °C, respectively) compared to *CaOYE*. *BfOYE4* could well tolerate up to 30% of acetone, acetonitrile and DMSO. Conversely, *AnOYE8* was very stable up to 50% DMSO but a decrease in its stability has been measured in all the other co-solvents even in low percentages. The stability of both enzymes in dioxane was lower compared to the other co-solvents, with complete denaturation of the proteins already at 20%.

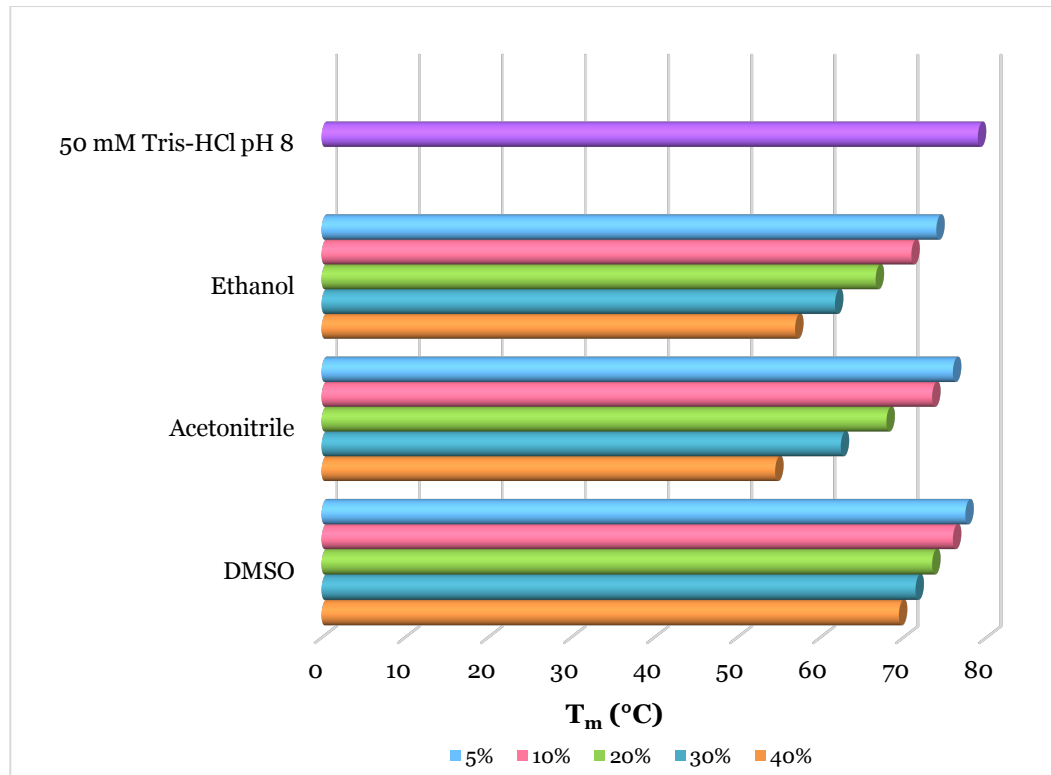


Figure 76. Influence of type and concentration of co-solvents (50 mM Tris-HCl buffer pH 8.0 supplemented with increasing vol% of organic co-solvent) on *CaOYE* stability.

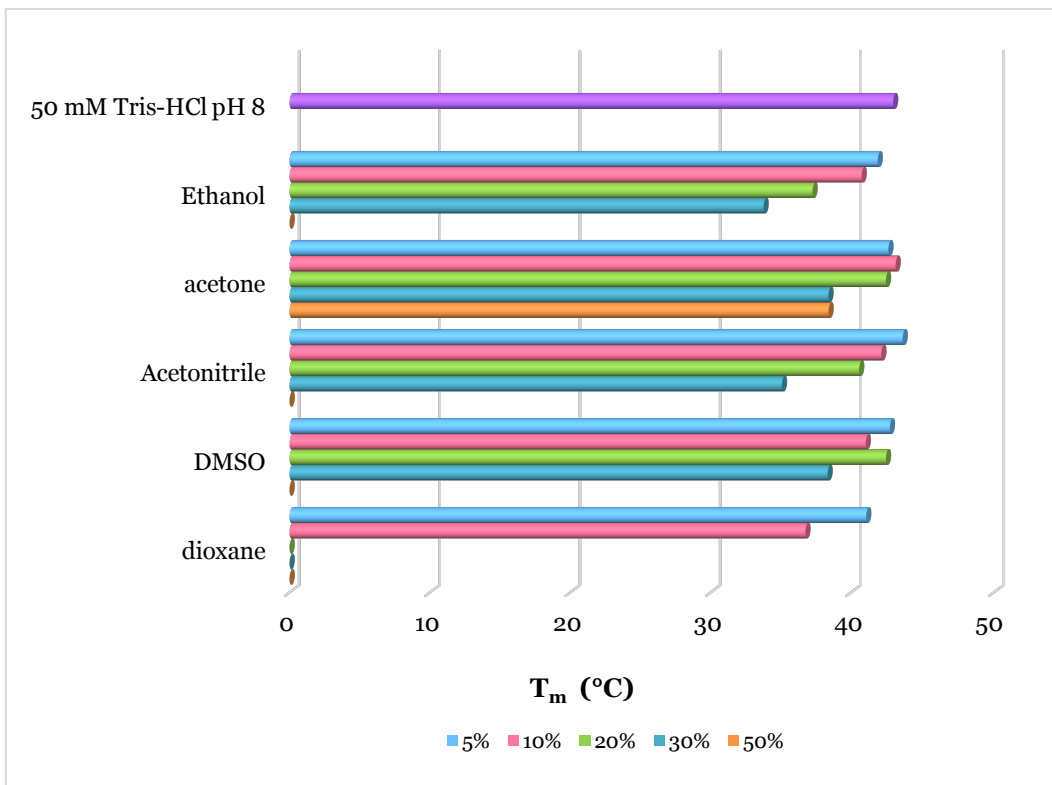


Figure 77. Influence of type and concentration of co-solvents (50 mM Tris-HCl buffer pH 8.0 supplemented with increasing vol% of organic co-solvent) on *BfOYE4* stability.

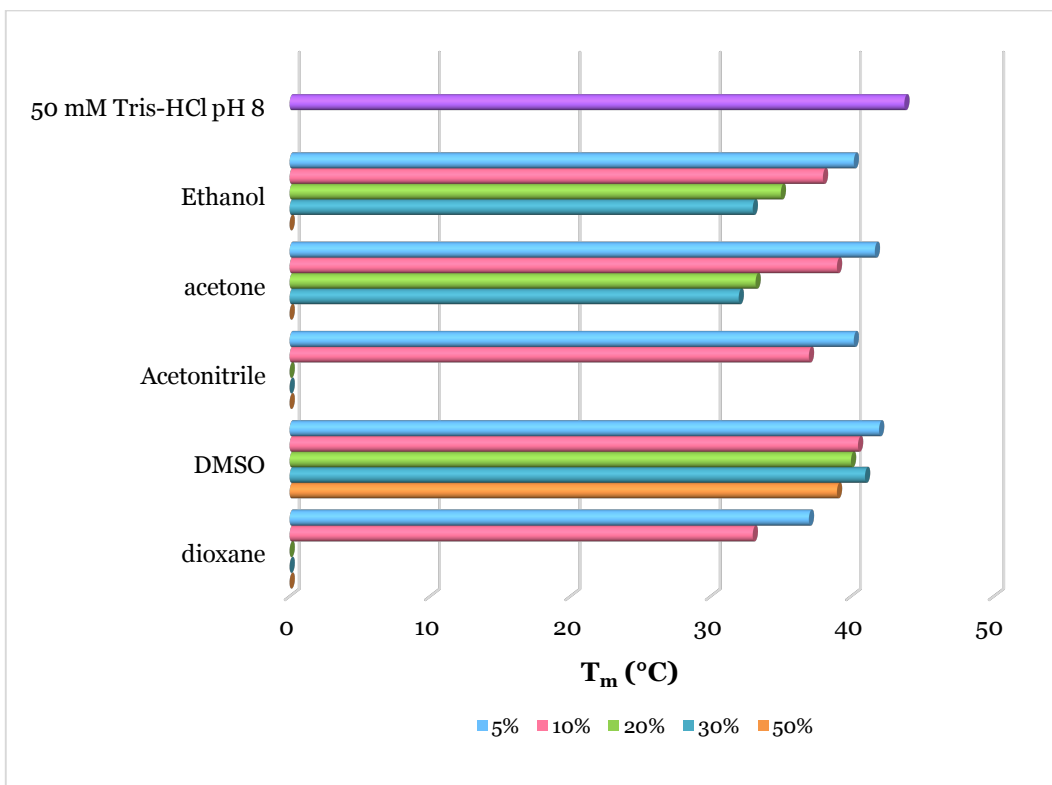


Figure 78. Influence of type and concentration of co-solvents (50 mM Tris-HCl buffer pH 8.0 supplemented with increasing vol% of organic co-solvent) on *AnOYE8* stability.

Generally, thermophilic-like OYEs have an increased thermal stability compared to the classical ones. High melting temperatures were reported for *TsOYE* ($T_{\text{opt}} = 65\text{ }^{\circ}\text{C}$) [96], *TOYE* ($T_{\text{m}} > 70\text{ }^{\circ}\text{C}$) [73], *GkOYE* ($T_{\text{m}} = 76\text{--}82\text{ }^{\circ}\text{C}$) [99], *GeoER* ($T_{\text{opt}} = 70\text{ }^{\circ}\text{C}$) [100], and *FOYE* ($T_{\text{opt}} = 50\text{ }^{\circ}\text{C}$) [101]. This high thermal resistance was assigned to the extra inter-subunit interactions through hydrogen bonding and complex salt bridge networks that are formed at the dimerization interface in the quaternary structure of these enzymes. *CaOYE* is highly thermo-resistant ($T_{\text{m}} = 79\text{ }^{\circ}\text{C}$), with a T_{m} value comparable with that of the most thermo-resistant thermophilic-like ERs reported until now. On the contrary, *BfOYE4* and *AnOYE8* show lower thermal stability ($43\text{ }^{\circ}\text{C}$ and $44\text{ }^{\circ}\text{C}$, respectively) due to the mesophilic origin of the organisms they come from. Other enzymes clustered into the thermophilic-like subclass but isolated from mesophilic organisms are reported in literature as non-thermostable OYEs: *YqjM* ($T_{\text{opt}} = 30\text{ }^{\circ}\text{C}$) [214], *XenA* ($T_{\text{m}} =$ up to $37\text{ }^{\circ}\text{C}$) [153], *OYERo2* ($T_{\text{m}} = 20\text{ }^{\circ}\text{C}$) [102], *RmER* and *DrER* ($T_{\text{opt}} = 35\text{ }^{\circ}\text{C}$ and $30\text{ }^{\circ}\text{C}$) [146].

Concluding remarks

In this Chapter, the biocatalytic potential of newly discovered ene-reductases was demonstrated by characterizing their substrate *spectrum* and biochemical properties, including thermal and organic solvent tolerance, the pH *optimum* and oligomeric state. The ERs under study exhibited moderate to high activities towards maleimide derivatives and enones. *BfOYE1* displayed a remarkably broad substrate *spectrum* in the asymmetric bioreduction being (highly) active with all the substrates tested in the screening. Conversely, *AnOYE2* and *AnOYE8* do not seem very promising biocatalysts due to their limited substrate *spectrum* and/or low activity rates. Singularly, for *GsOYE* and *CtOYE* high reaction rates using NADH as cofactor in maleimide reduction were achieved compared to what reported in literature for other ERs. The highest affinity (K_m from 6 to 69 μM) and activity ($k_{\text{cat}} = 6.78$ to 36.35 s^{-1}) for all the enzymes studied (except *CaOYE*) was observed with maleimide, resulting in catalytic efficiencies in the range of $399 - 1940 \text{ mM}^{-1} \text{ s}^{-1}$. *CtOYE* demonstrates to be the most efficient biocatalyst in the reduction of maleimide.

Biotransformations of carbonyl and nitro-compounds were also set-up with *GsOYE* and *CtOYE* displaying similar behaviors in terms of activities and stereoselectivities. Moreover, the kinetic resolution of 5-phenyl-2-cyclohexenone was here reported for the first time with this substrate.

The oligomeric state investigation confirmed the monomeric states for the classical OYEs identified in this thesis (*i.e.* *GsOYE*, *CtOYE*, *BfOYE1* and *AnOYE2*). For the thermophilic-like OYEs, *CaOYE* and *AnOYE8*, a monomeric state was detected both by SEC chromatography and native PAGE, while for *BfOYE4* the existence of multiple oligomeric species in solution was demonstrated.

The activity-pH profile analysis revealed that all the enzymes have a wide range of pH tolerance with *GsOYE* and *CtOYE* being able to maintain almost half of their maximum activity at pH 3.0 and *CaOYE* being able to retain 90% of its maximum activity also at pH 12.

Finally, the Thermofluor method revealed that the enzymes isolated from extremophilic organisms (*GsOYE*, *CtOYE* and *CaOYE*) show higher thermo-resistance ($T_m = 53 - 79 \text{ }^\circ\text{C}$) compared to the mesophilic counterparts isolated from the fungi *Botryotinia fuckeliana* and *Aspergillus niger* ($T_m = 41.5 - 44 \text{ }^\circ\text{C}$).

5. CRYSTAL STRUCTURE DETERMINATION

Abstract:

The X-ray crystal structures of *GsOYE* and *CtOYE*, two classical OYEs and that of *BfOYE4* and *CaOYE*, two thermophilic-like ERs have been solved with good to moderate resolution and are reported in this Chapter. The different strategies developed for their crystallization and the structural peculiarities of the different ERs subclasses are also discussed. Furthermore, in order to understand *GsOYE* stereoselectivity and the key interactions with substrates and cofactors, its three-dimensional structures in complex with pHBA and 2-methyl-cyclopenten-1-one (MCP) are also reported and discussed here. Finally, preliminary structures of *OYE2* and *OYE3*, two ene-reductases from our collaborators in Graz, have also been solved for the first time and are also shown in this Chapter. The different strategies employed to crystallize *BfOYE1* are briefly discussed even if these attempts have not lead to any crystal hits until now.

5.1 General crystallization strategy

A common crystallization strategy was used for all enzymes in order to get initial crystal hits and subsequently a customized protocol for the optimization of the crystals has been set-up for each enzyme. Recombinant enzymes (16-20 mg/ml in 50 mM Tris-HCl buffer pH 8.0 and 100 mM NaCl) were screened by high-throughput sparse matrix crystallization trials, dispensed by Oryx8 Robot (Douglas Instruments). MRC 96-well two-drops standard plates were adopted both in the initial screenings and following optimization steps. All the conditions were deposited and left equilibrating by vapour diffusion at 293 K. A panel of about 400 crystallization conditions were tested (JCSG, PACT, LMB and MORPHEUS screens, Molecular Dimension Ltd). In the initial screenings drops were prepared by mixing equal volumes (0.3 μ l) of mother liquor and proteins (16-20 mg/mL in 50 mM Tris-HCl pH 8.0 and 100 mM NaCl). Generally, after few days first crystal hits appeared in multiple conditions. For further optimization, the most promising crystals were crushed and used to prepare a seeds stock for the subsequent experiments. The seeds stock was further used for crystals optimization by micro-seeding techniques: drops were prepared by mixing 0.2 μ l of mother liquor, 0.1 μ l seeds suspension and 0.3 μ l protein preparation. For some proteins additives screening was also used during the optimization process.

Different strategies to crystallize *BfOYE1* have been performed: screening of different crystallization kits, different temperature of incubation (4 °C, 12 °C and 20 °C), different protein concentrations (20-80 mg/ml) and cross-seeding. The N-terminal His-tag of the protein was also removed in order to lower the flexibility and promote crystallogenesis. Despite all these attempts we could not get any crystal hits.

Crystals of *GsOYE* in complex with known substrates were prepared by soaking apo-protein crystals with the desired compounds exploring a wide range of concentrations and different incubation times.

Before freezing, the crystals were quickly soaked into an appropriate cryoprotectant solution composed of the precipitant agent, supplemented with 20 % v/v ethylene glycol or glycerol, and flash frozen in liquid nitrogen. X-ray diffraction data were collected at ESRF (Grenoble, France) synchrotron radiation source.

All the diffraction data were processed and analyzed by the automated pipelines feasible at ESRF synchrotron. In particular, we used the data integrated and scaled by EDNA Autoprocessing framework (XDS, XSCALE, Pointless, Aimless; [215]). The obtained data were further cut to appropriate resolution by running aimless through the ccp4i2 suite [216]. The same interface was used in combination with Phenix suite for any of the subsequent steps of phasing and refinement. Briefly, OYE structures were determined by molecular replacement (MOLREP software, [217]) using the most similar structure already reported in literature to build a model by Swiss modelling and use it as template. After few cycles of refinement, the most disordered regions and undefined loops were manually reconstructed with the support of Coot graphic interface [218]. The refinement steps were carried out by Refmac5 [219] and Phenix software Refine [220].

5.2 GsOYE and CtOYE crystal structure

Initial clusters of small, irregular bunches of crystals of N-terminally His₆-tagged GsOYE appeared after 5 days of incubation in multiple conditions (PACT screen n. 22 and 23, Structure screen n. 14, 32 and 42). Most regular ones (Structure screen n.22: 200 mM CaCl₂ dihydrate /100 mM MES, pH 6.0, containing 20 % w/v PEG 6000) were crashed and used to prepare a seeds stock (50 µl) for the subsequent experiments. The seeds stock was further used for crystals optimization by micro-seeding techniques: drops were prepared by mixing 0.2 µl of mother liquor, 0.1 µl seeds suspension and 0.3 µl of GsOYE (20 mg/ml). Thicker and more regular crystals appeared in few days in PACT screen n. 22 and 23 (0.2 M Magnesium chloride hexahydrate or 0.2 M Calcium chloride dihydrate, 0.1M MES pH 6 and 20 % w/v PEG 6000). Seeds stock and the before described crystallization condition were used for any further crystallization trials with slight changes: for 2 µl drops size we added 1 µl mother liquor, 1 µl GsOYE (20 mg/ml) and seeding with catfish. In this last setting, long rod-shaped single crystals appeared in 24 hours and rapidly grew to give high-resolution diffraction quality samples (Fig. 79).

On the contrary, purified CtOYE enzyme was reluctant to crystallize in the initial screenings. Few conditions gave very small irregular bunches of multiple crystals, unsuitable for crystallographic studies. To exclude the interference of His₆-tag in the crystals nucleation and growth we proceeded with tag-cleavage by thrombin treatment. The resulting recombinant enzyme was screened analogously to the previous ones and gave new promising bunches of tiny crystals in multiple conditions. The best results were observed in LMB condition n.93 (0.85 M Sodium citrate tribasic dihydrate, 0.1 M Tris pH 8.0, 0.1 M NaCl) which was used for crystals optimization by seeding techniques. Best crystals were obtained by using LMB condition n.93, micro-seeding from a seed stock prepared and stabilized in the same mother liquor and the addition of Fos-choline additive (Rubic screen, Molecular Dimension Limited), according to the following ratios (0.2 ul protein, 0.1 ul seeds stock, 0.2 ul precipitant agent supplemented with 0.15 mM Fos-Choline 12 detergent) (Fig. 80).

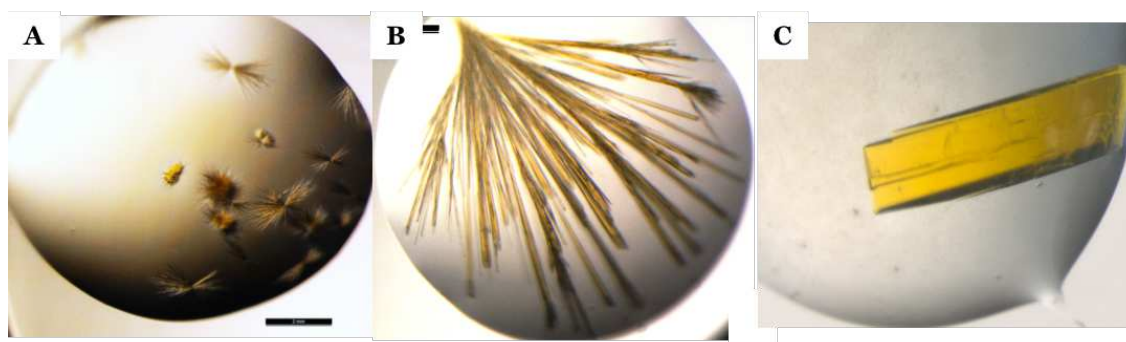


Figure 79. GsOYE crystals optimization: (A) first crystal hits obtained in Structure screen B2; (B) crystals obtained in B10 PACT after micro-seeding techniques; (C) optimized crystals prepared using B10 PACT as seeds and catfish for seeding in larger volume drops.



Figure 80. CtOYE crystals optimization: (A) first crystal hits obtained with N-tagged CtOYE; (B) and (C) crystals obtained after His-tag removal using micro-seeding and Fos-choline as additive.

Crystals of GsOYE in complex with known substrates/inhibitors were prepared by soaking apo-protein crystals with: para- hydroxybenzaldehyde (pHBA, 4-hydroxybenzoic acid), 2-methyl-cyclopente-1-one (MCP), and other substrates/inhibitors exploring a wide range of concentrations and different incubation times. In particular, a clear electron density describing the compounds complexing with GsOYE were obtained for pHBA added in large excess by introducing few grains of powder directly into the drops and left diffusing for 30 minutes, while for MCP the best maps were obtained by incubating the crystals in a 10 mM solution of MCP. Finally, given the affinity of both inorganic and organic monovalent anions towards OYEs active site observed in multiple studies, we introduced a step of “crystals washing” with a 50% PEG 3350 solution before and/or in parallel to compounds soaking to remove such anions and allow the diffusion and binding of substrates of interest.

GsOYE structure was determined by molecular replacement (MOLREP software, [217]) using morphinone reductase (MR) from *Pseudomonas putida* as template (1gwj). One molecule per asymmetric unit and roughly 46 % of solvent define the crystal content. Final model was traced and fully visible from Met 1 to Arg 379, the last two amino acids being poorly defined in the density maps and thus

omitted. Final parameters obtained for the best dataset (1.45 Å resolution) reached Rfactor/Rfree of 0.18/0.19 (for further details see Table 19). Crystal structures of the complexes with substrates pHBA and MCP were collected and processed analogously to the apo enzyme. Data were phased by molecular replacement using the *GsOYE* apo structure as template. Experimental maps obtained in this manner were analyzed to detect the presence of ligands eventually bound to the enzyme. Quite clear electron density not attributable to protein chain or FMN cofactor was observed in the difference maps and allowed to define the binding and orientation of pHBA and of MCP molecules in the active site of the respective complexes. Details of data and models quality are reported in Table 19.

CtOYE data were processed in triclinic space group by EDNA Autoprocessing pipeline and further cut by Aimless to 1.35 Å maximum resolution. Any attempts to process the data with higher symmetry didn't give any improvement and didn't produce a solution. The structure has been determined by Phaser software [221] using as template the model of *CtOYE* enzyme, built by Swiss model server (1gwj structure was used as starting model by the server, <https://swissmodel.expasy.org>). Structure refinement has been performed analogously to what described for *GsOYE*. Final model includes four molecules per cell, 49 % of solvent and its quality reached final parameters Rfactor/Rfree of 0.22/0.25 (further details can be found in Table 19). Protein structure was clear and well defined from residue Thr 3 to Glu 365, except for the fragment from Pro 269 to Glu 283, that was disordered and cannot be traced.

5.2.1 Structural analysis of *GsOYE* and *CtOYE*

The holo structures of *GsOYE* and *CtOYE* have been determined to rich high diffraction resolutions in both cases, 1.45 and 1.32 Å for *GsOYE* and *CtOYE*, respectively. Overall structures of *GsOYE* and *CtOYE* show the expected organization, following the highly conserved eight-stranded ($\alpha\beta$)-barrel fold of triosphosphato isomerase (TIM) and of all the other OYE family members till now described (Fig. 81). Both ones accommodate FMN cofactor lying on top of the β -barrel core, at the C-terminus side, buried inside the active site cavity.

Table 19. X-ray Crystallographic data collection and refinement statistics.

	GsOYE_apo	GsOYE-pHBA	GsOYE-MCP	CtOYE
Data collection statistics				
Wavelength	1.725	0.966	0.966	1.00
Space group	P2 21 21	P2 21 21	P1 21 1	P1
Cell constants				
a, b, c (Å)	56.75 76.66 88.60	57.05 76.29 88.12	56.69 76.42 86.33	49.65 78.17 108.68
a, b, γ (°)	90 90 90	90 90 90	90 93 90	104 100 90
Resolution range for refinement (Å)	45.61 – 1.45 (1.48 – 1.45)	57.05 – 1.63 (1.69 – 1.63)	57.18 – 2.4 (2.48 – 2.40)	48.86 – 1.35 (1.39 – 1.35)
Total reflections	880814 (45283)	300625 (12407)	90684 (9567)	1111221 (105276)
Number of Unique Reflections	69197 (3504)	48778 (4758)	28772 (2856)	312849 (29361)
R _{merge}	0.07 (0.63)	0.21 (0.46)	0.109 (0.114)	0.086 (0.535)
<I / $\sigma(I)$ >	18.0 (3.6)	9.0 (4.9)	14.2 (9.5)	5.76 (1.63)
Completeness (%)	99.8 (99.8)	99.72 (99.12)	99.36 (99.69)	90.89 (85.78)
Multiplicity	18.0 (3.6)	6.2 (5.3)	3.2 (3.2)	3.6 (3.5)
Refinement statistics				
R _{work} / R _{free}	0.18/0.19	0.18/0.21	0.18/0.25	0.22/0.25
RMSD bond lengths (Å)	0.006	0.009	0.008	0.011
RMSD bond angles (°)	1.19	1.35	1.21	1.76
Average B factor	18.59	10.92	11.94	18.25
Main chain B factor	18.14	10.44	12.04	17.26
Ligands B factor	13.10	14.99	5.52	15.10
Water molecules B factor	25.53	15.88	11.61	26.45
No. of non-hydrogen atoms				
Number of protein atoms	3109	3056	6087	10915
Number of ligands atoms	36	85	84	140
Number of water molecules atoms	230	230	94	1379
Ramachandran plot (%)				
Most favoured	96.31	95.49	95.72	95.80
Generously allowed	3.69	4.51	4.28	4.13
Outliers	0.00	0.00	0.00	0.07

GsOYE crystallized in the orthorhombic space group P22121 and one molecule per asymmetric unit (ASU), while *CtOYE* was solved and refined in P1 triclinic space group, with 4 molecules per ASU, not related by peculiar non crystallographic symmetries. In agreement to size exclusion analysis (see Chapter 4) and general behavior for classical OYE enzymes, *GsOYE* and *CtOYE* crystals contacts do not suggest the presence of quaternary structures describing putative oligomers of physiological relevance.

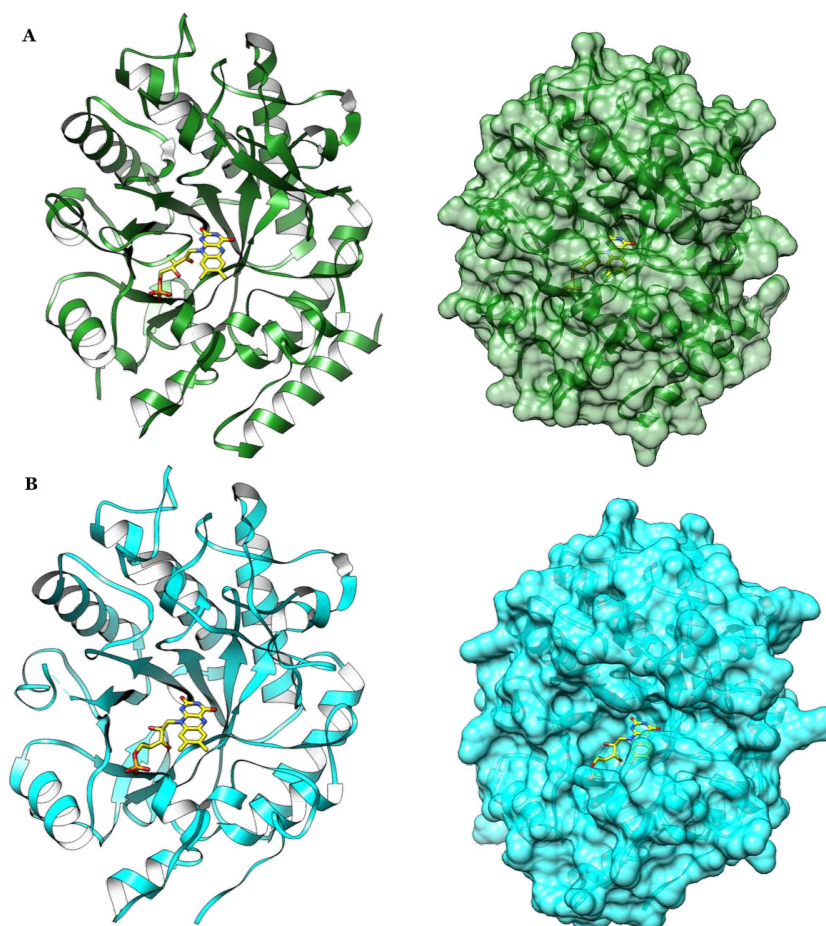


Figure 81. *GsOYE* (green) (A) and *CtOYE* (cyan) (B) overall three-dimensional structure shown as ribbon diagram and surface representation. FMN (yellow) is shown as stick model.

5.2.1.1 Overall *GsOYE* structure

While the overall fold, FMN cofactor binding site and fundamental residues in the catalysis are highly conserved, peculiar features have been disclosed for *GsOYE* enzyme. Indeed, main differences with other family members pertain the loops involved in substrate binding and the lid, where amino acid residues critical for functional divergence are located. OYEs $\beta 6$ loop shows a large variability in terms of size and flexibility, from the very short (7 aa) one of NemaA (3gka), that leaves the active site more accessible and quite open, not contributing to the catalytic properties of the enzyme, to the intermediate size $\beta 6$ loop (12 aa) of MR

(1gwj), which partially protrudes toward the solvent and is still clearly defined, to the very long one reported for SYE1 (2gq9) [222], OYE1 (1oya) [68] and OYE 2.6 (3tjl) [91]. *GsOYE*, analogously to very few examples till now characterized in the OYEs family, has a very long β 6 loop, spanning from Glu264 to Leu279. It assumes an elongated and compact conformation, runs on enzyme surface, reaches active site entrance, with residues from Gly268 to Val271 forming the β hairpin turn directly contributing to size and features of the catalytic cavity (Fig. 82). *GsOYE* Asn270 points its side chain toward the top of the catalytic cavity (β 3 loop), opposite to FMN, analogously to OYE 2.6 [91], and is stabilized in that orientation by a hydrogen bond with Tyr346 of the C-terminal loop, closing the accession to the active site.

On the other side of the catalytic cavity, *GsOYE* shares more similarities toward SYE1 than OYE 2.6. The N-terminus cap subdomain region, defined by the β 3 loop on top of the active site entrance is indeed another hotspot in OYE enzymes family. It has been demonstrated to directly interact with NADH/NADPH and tune the selectivity towards the reducing cofactors [71, 73, 78, 91]. It shows high variability in terms of secondary structure content and size, ranging from α -helices to β -hairpins to largely unstructured turns, often occurring in parallel and in a compensatory manner with β 6 loop variations. Indeed, in *GsOYE*, while the β 6 loop is long and extended till FMN binding core, the lid shows a β -hairpin structure in an open conformation (Fig. 82), very similar to *CtOYE* and SYE1. The presence of acidic residues on the internal side of the lid, specifically Glu135, of MR have been supposed to explain the exclusive NADH specificity to such enzyme, given the binding mode observed for 1,4,5,6-tetrahydroNADH (NADH₄) in the crystallized complex (2r14, [71]) and the repulsion that could occur between negative charges of glutamate and phosphate group of NADPH. Moreover, a peculiar enrichment of acidic or basic residues throughout the lid could contribute to strengthen the selectivity. Enzymes such as PETNR present basic residues in such position (PETNR Arg130 or NerA Lys127 or Nema His135) and show a clear preference toward NADPH as reducing cofactor. *GsOYE*, with its more open and shorter lid but the presence of a Glutamic residue (Glu128), oriented towards the solvent and 4.5 Å apart from the corresponding Glu135 of MR, can accept both NADH and NADPH, but prefer the last as reducing donor. Taken together, the less pronounced acidic nature of β 3 loop, its shorter and more

open conformation and the absence or displacement of acidic residues pointing toward FMN, close to the NADH adenine moiety binding site described in other OYEs, but also the contribution of $\beta 6$ loop from the opposite side of the catalytic cavity, participating in the cofactor binding and orientation, all contribute to the observed preference toward NADPH.

GsOYE is further characterized by an extra unique C-terminal α -helix, about 19 amino acids long (Asp360 to Arg379), never reported in this family (Fig. 82). Such additional component contributes to the globular assembly of the enzyme, packing on one face of TIM barrel and establishing a large number of interactions with other two α -helices (Lys37 to Ser47 and Asp75 to Arg91). An intriguing parallel can be done considering that, differently from classical OYEs, thermophilic-like enzymes are characterized by a C-terminal extension which establishes protein-protein interactions involved in dimers formations. Moreover, C-terminal sequences of thermophilic-like enzymes contribute with the peculiar finger (Arg336 or Trp358 finger as in the case of YqjM and XenA) which reaches the active site of the associated monomer and contribute to define the key features of the catalytic pocket. However, none of these properties have been observed in the case of GsOYE, where such helix contributes to the overall fold and not directly to the catalytic properties of the enzyme.

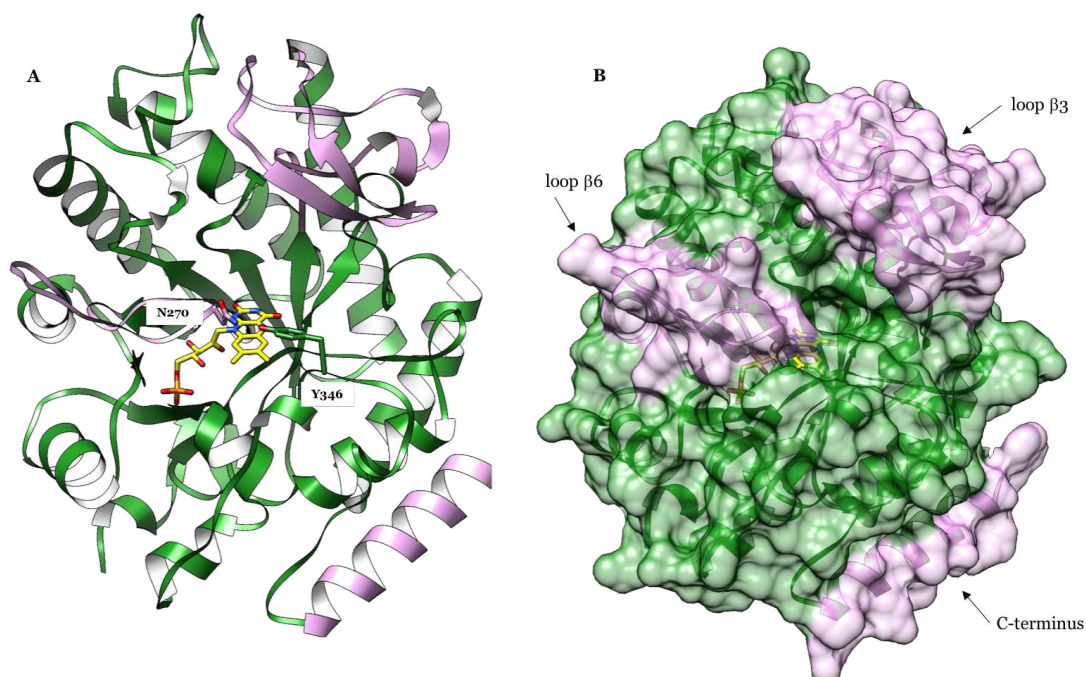


Figure 82. Peculiarities of GsOYE three-dimensional structure: (A) ribbon structure of GsOYE (green) showing the residue N270 of loop $\beta 6$ interacting with Y346 of the C-terminus; (B) GsOYE surface (green) highlighting loops $\beta 3$ and $\beta 6$ (plum) involved in the architecture of the active site and the peculiar extra α -helix at the C-terminus (plum).

The structure of GsOYE has been further elucidated in complex with 4-hydroxy-benzaldehyde (pHBA) inhibitor and the substrate 2-methyl-cyclopenten-1-one (MCP) (Table 19). No changes in the overall structure have been observed in the presence of the substrates. More details on the complexes are reported in the subsequent section.

5.2.1.2 Active site of GsOYE

The overall active site cavity of GsOYE is quite deep and narrow and FMN heavily buried at the bottom of the catalytic tunnel, features mainly due to the extension of loop β_6 inside the active site cavity. However, the catalytic site is slightly more open and accessible from the top side, given the topology and size of loop β_3 , as discussed in detail previously (Fig. 82).

All the key residues coordinating the FMN cofactor and involved in the catalysis are highly conserved in GsOYE enzyme. As other OYEs reported, GsOYE relies on His174/Asn177 dyad for electron-withdrawing group coordination and Tyr179 lying on top of FMN and participating the protonation of the substrate.

As shown in Figure 83 the O4 of the flavin cofactor is interacting with the backbone of Thr25 and Ala56. The N5 of the flavin is also in hydrogen contact with Thr25, a highly conserved residue in classical OYEs known to be involved in the modulation of FMN redox potential. The N3 of the isoalloxazine ring is interacting with the side chain of Gln98. The dimethylbenzene moiety of the flavin isoalloxazine ring is stabilized by different hydrophobic interactions with residues Leu24, Asn270 and Tyr346. The ribityl chain of the cofactor forms one hydrogen bond with Arg226 and different hydrophobic interactions with Gly269 and Pro23. The phosphate group of FMN which has a negative charge is stabilized by the positive charge of Arg319 while the main chain atoms of Gly297 and Gly318 are involved in polar interactions with the phosphate group.

In the active site of the apo GsOYE structure a chloride anion, present in the crystallization solution, was found interacting with both His174 and Asn177 and positioned on the *si*-face of the isoalloxazine ring of FMN, as shown by the difference electron density map $F_o - F_c$ (Fig. 84). In this position, many different anions and small molecules have been already reported also in the structure of other apo OYEs. For example, in OYE1 a chlorine ion was detected [68], acetate in PETNR structure [63], a sulphate ion was modelled in YqjM [94] and TsOYE [96] in the same location. In OYE2.6 malonate was observed [91], as well as

acetate and formate were reported for TOYE [73]. Moreover, also a molecule of ethylene glycol (EDO), used as cryoprotectant was found inside the active site of GsOYE interacting *via* a complex water network with different amino acid residues of the active site cavity (Asn27, Tyr179, Tyr346) (Fig. 84).

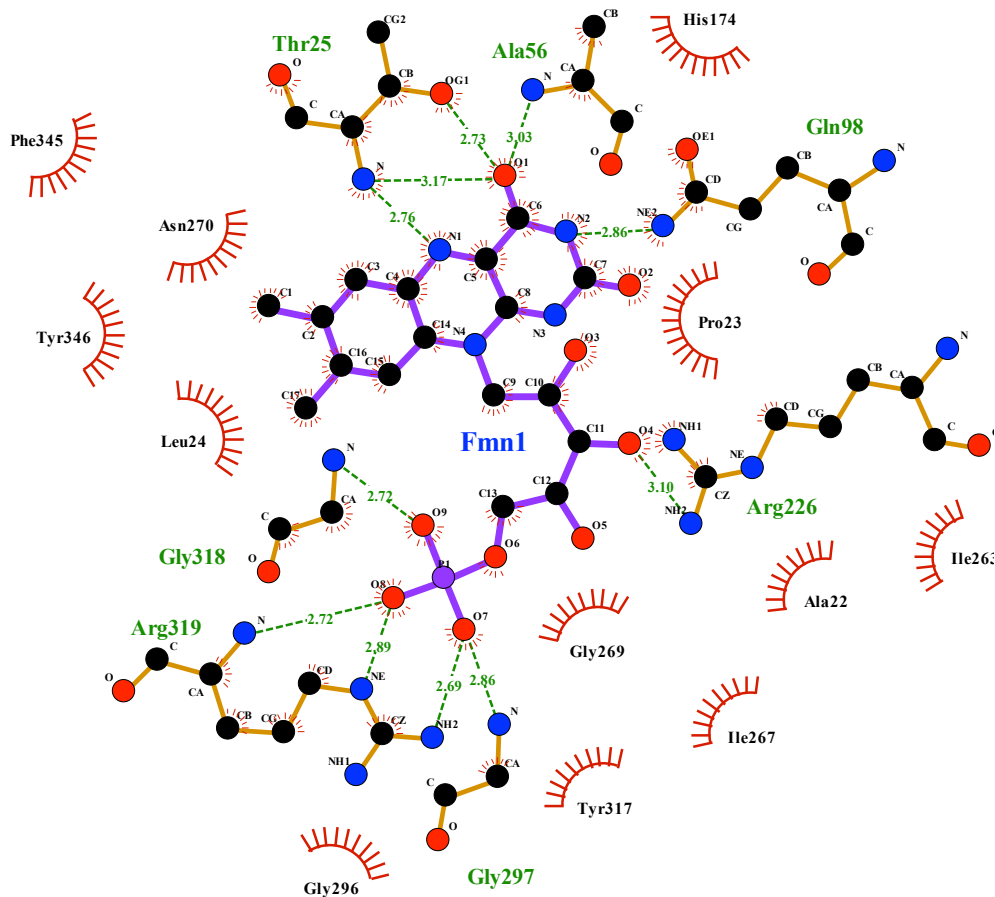


Figure 83. Schematic illustration of the interaction of FMN with active site residues of GsOYE. The thin green dotted lines illustrate hydrogen bonds.

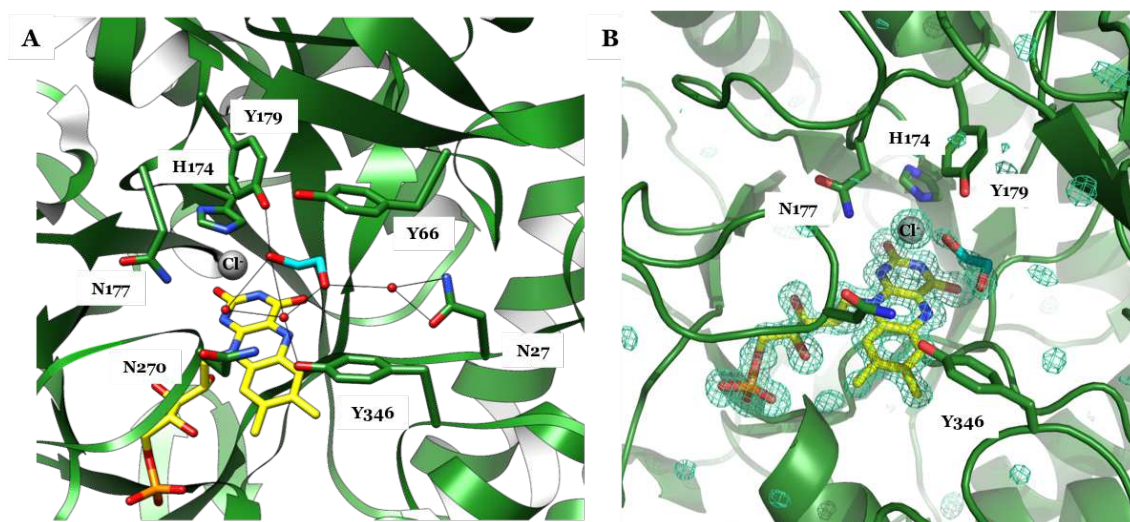


Figure 84. GsOYE active site showing Cl anion (grey) and EDO (cyan) (A) cartoon representation of conserved residues; (B) difference electronic density map $F_o - F_c$ contoured at 4σ .

Both pHBA (Fig. 85) and 2-methyl-cyclopenten-1-one (MCP) (Fig. 86) lie on top of FMN orienting their cyclic core parallel to the cofactor and favorable to establish π -stacking interactions. Both ones are further involved in hydrogen bonding with His174/Asn177 dyad through their hydroxyl and carbonyl groups, respectively.

The difference electron density maps of GsOYE - pHBA complex (Fig. 85 B) suggests it lie on top of FMN in two alternative orientations, that differ only by aldehyde group orientation, either pointing toward Asn270 and Tyr346 and forming hydrogen bonds with them or rotated by 180 degrees and pointing toward the active site entrance. In this second position, it is involved in a network of hydrogen bonding with water molecules and an additional molecule of pHBA bound in a peripheral site at the cavity mouth, between Pro67 and Tyr346. Different OYE structures have been solved in complex with pHBA (such as OYE1 (1oyb), SYE1 (2gq9), SYE4 (5k1k), OYE3 (5v4p) and NerA (4jip)) and the interaction through the hydroxyl group with the His/Asn (His) dyad was reported for all of them but the double conformation was never observed to our knowledge [68, 212, 222, 223]. In *TcOYE* crystal structure (3atz) the two orientations described have been observed but in different asymmetric unit chains [224].

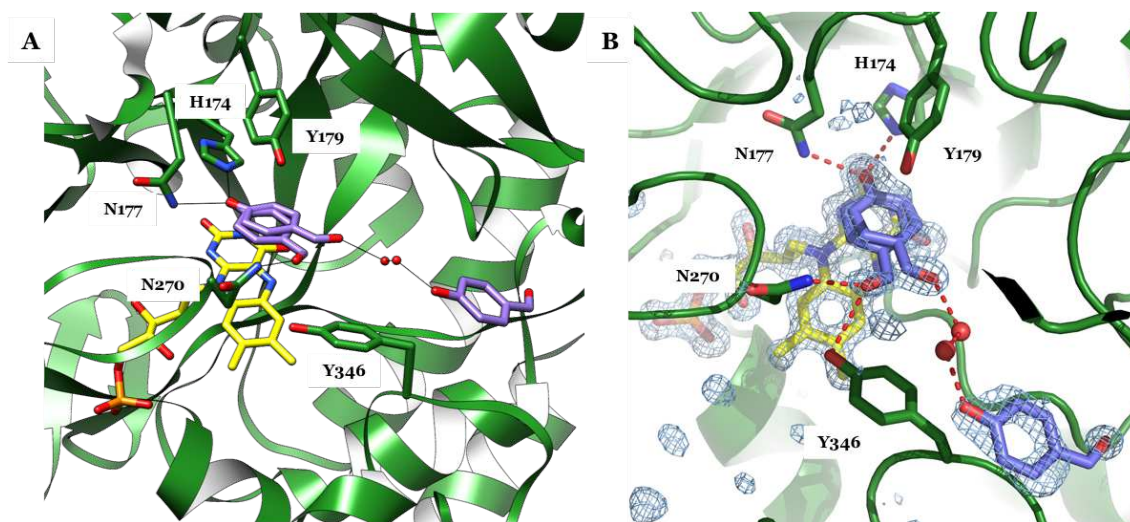


Figure 85. GsOYE active site in complex with pHBA (purple) (A) cartoon representation of conserved residues and their interaction with pHBA through hydrogen bond; (B) difference electronic density map $F_o - F_c$ contoured at 3.2σ .

Analogously to pHBA, MCP binds in two alternative conformations (Fig. 86). These binding modes have been observed not in the same cavity but in each of the two GsOYE molecules present in the asymmetric unit. In both cases MCP binds in the active site, parallel to FMN and trapped with carbonyl group pointing toward His174/Asn177 catalytic binders. The two orientations are roughly

coplanar, differing by a rotation of about 180 degrees around the carbonyl group and such rotation causes the symmetrical repositioning of double bond and methyl group, thus exposing opposite C=C-bond faces to hydride attack. As a consequence, these two alternative orientations could offer an explanation for the moderate stereoselectivity (70% *ee* (*S*)) and low conversion (8% conv.) in the reduction of MCP (see Chapter 4).

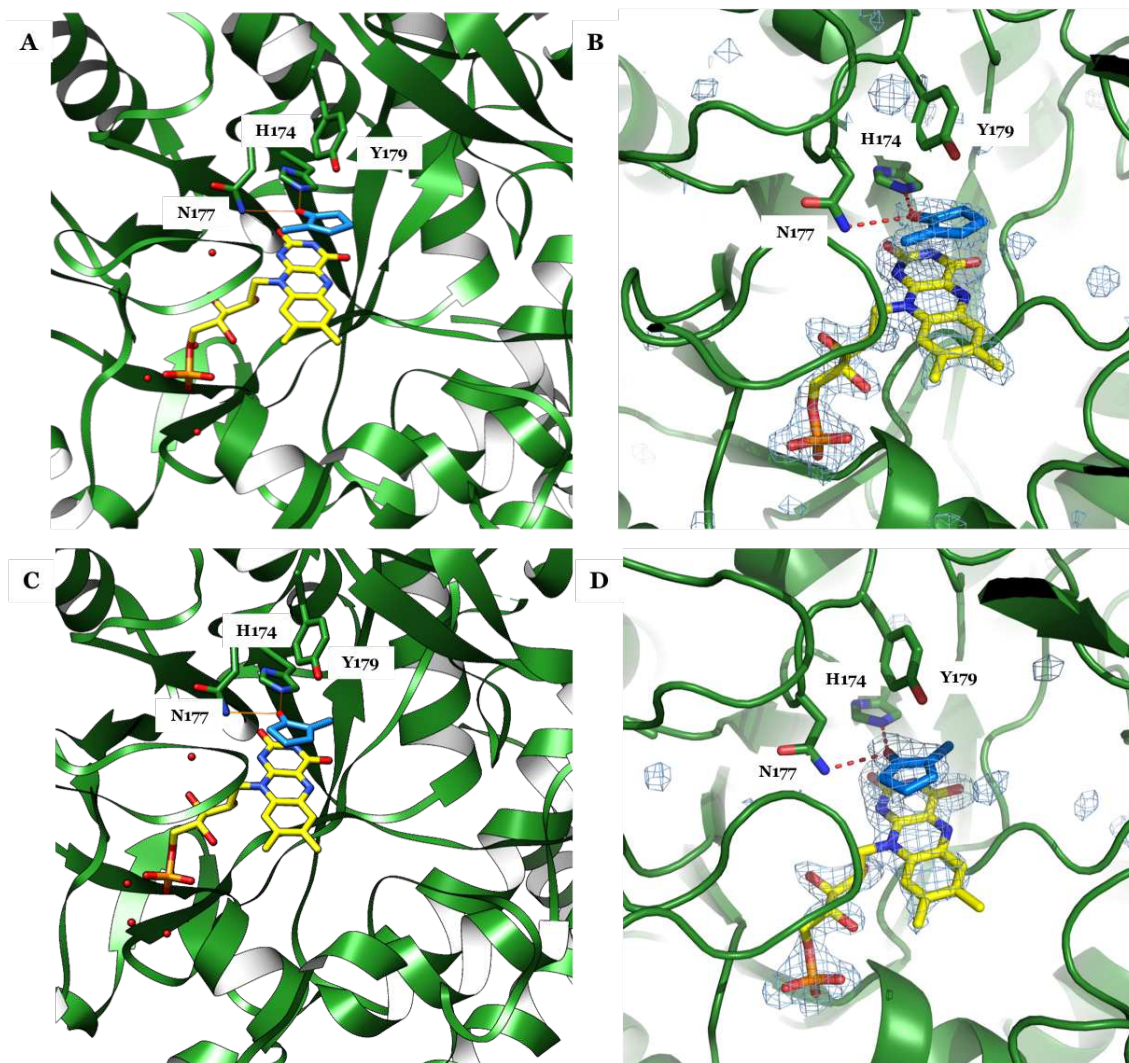


Figure 86. GsOYE active site in complex with MCP (blue) (A, C) cartoon representation of conserved residues and their interaction with MCP through hydrogen bond in two different chains of the asymmetric unit; (B, D) difference electron density map $F_o - F_c$ contoured at 3.5σ .

5.2.1.3 Overall CtOYE structure

CtOYE three-dimensional structure is very similar to GsOYE one due to their high sequence identity and homology (64% sequence identity). However, some peculiarities can be described. The loop β_6 of CtOYE was highly flexible and its residues between Pro269 and Leu284 were disordered and poorly defined in the electron density map thus they could not be traced, as already reported also for other OYE homologues such as OPR1 from tomato (1ics) [225] and OPR3 (1q45)

from *Arabidopsis thaliana* [226]. However, despite disordered and not described in our structural model, *CtOYE* β 6 loop composition is very similar to *GsOYE* one, with a conserved Asn274 (Asn270 in *GsOYE*) as well as a clearly defined and superimposable Tyr351 (Tyr346 in *GsOYE*).

The loop β 3 in *CtOYE* is not organized as α -helices (as reported for *OYE1*) or in β -sheets (as reported for *GsOYE*, *PETNR* or *SYE1*) but it arranges into two largely unstructured turns (as described for the above mentioned *OPR1* and *OPR3*) (Fig. 87). However, compared to *OPR1* and *OPR3*, *CtOYE* β 3 loop is slightly shorter and it has an open orientation leaving the entrance of the active site more accessible to substrates and solvent (Fig. 87). Moreover, its composition is more acidic (6 acidic residues and 3 basic residues) compared to *OPR1* (5 acidic residues and 6 basic residues) and *OPR3* (3 acidic residues and 7 basic residues), influencing its orientation and possibly the NADH/NADPH specificity, as already mentioned. In *CtOYE* the glutamic residue (Glu128 and Glu135 of *GsOYE* and *MR*, respectively) of loop β 3, involved in NADH specificity, is replaced by Met132. *CtOYE* could accept both NADH and NADPH cofactors but it strongly preferred NADPH as source of reducing equivalents (see Chapter 4). Analogous considerations on loop β 3 of *GsOYE* can be applied also to *CtOYE*: the shorter length and more open conformation of β 3 loop and the complete absence of acidic residues pointing toward FMN, close to the NADH adenine moiety binding site described in other classical *OYE*s, as well as the flexibility of β 6 loop from the opposite side of the catalytic cavity, all contribute to the observed preference toward NADPH.

5.2.1.4 Active site of *CtOYE*

The active site cavity of *CtOYE* is apparently more accessible compared to *GsOYE* due to the flexibility of β 6 loop that could not be traced into the crystal structure. However, the length and composition of this loop in *CtOYE* is similar to *GsOYE* one, thus we can assume that *CtOYE* active site cavity is quite closed and narrow, as reported for all classical *OYE*s. Nevertheless, the flexibility of this loop can have a role in substrate accommodation and catalysis. One molecule of FMN cofactor is trapped inside the active site with its isoalloxazine ring forming the bottom of the catalytic tunnel. As already mentioned, *CtOYE* loop β 3 has a slightly more open conformation, thus leaving an accessible entrance to substrates and solvent (Fig. 87).

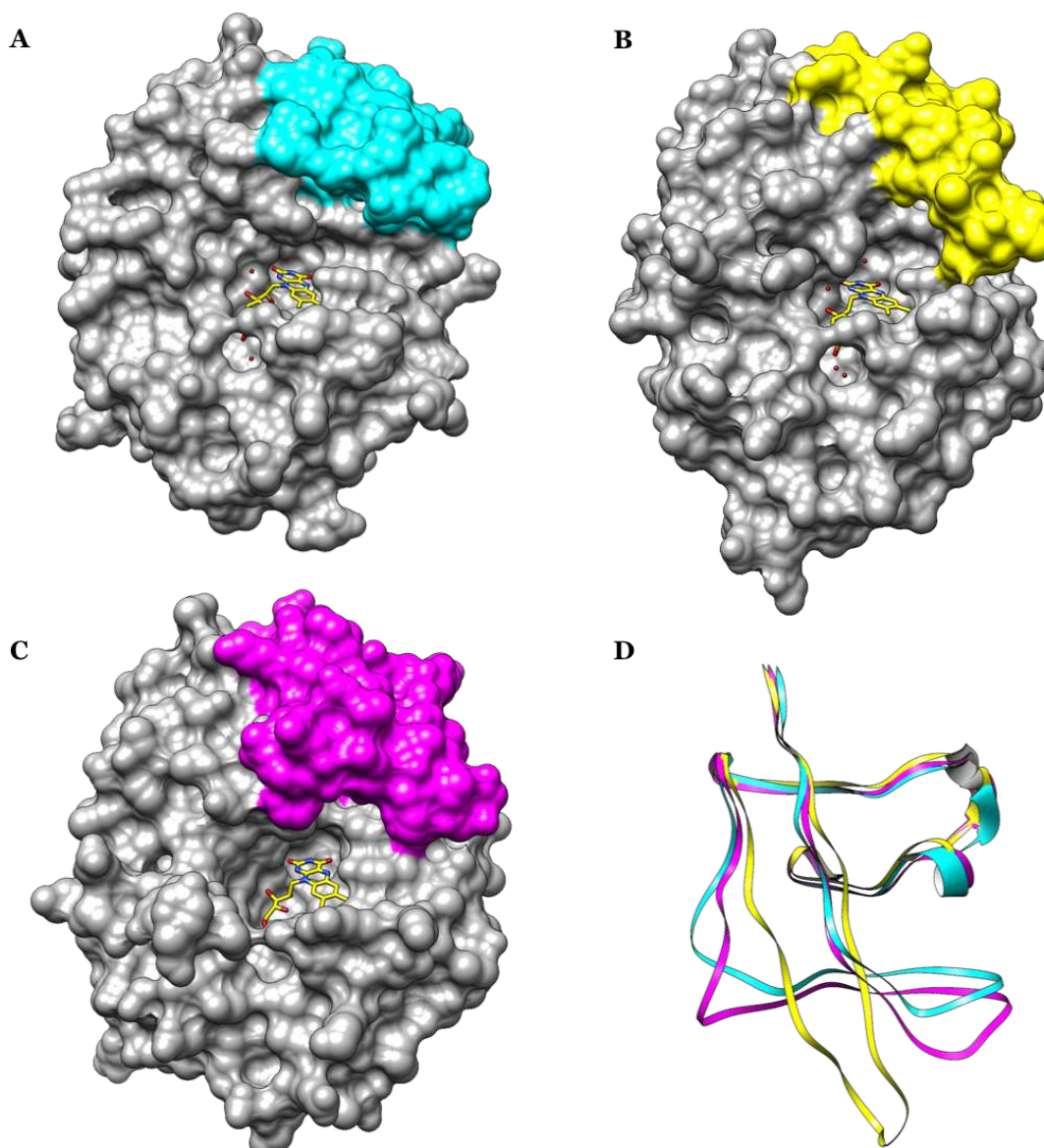


Figure 87. Loop β_3 orientation and its involvement in active site entrance shaping (A) *CtOYE*, (B) OPR1 (1ics) and (C) OPR3 (1q45). (D) Superimposed loop β_3 , represented as cartoon, of the three OYEs analyzed highlighting the different length and orientation.

All the conserved residues into the classical OYEs family that are involved into FMN cofactor binding and in catalysis are highly conserved also in *CtOYE* enzyme. *CtOYE* relies on His178/Asn181 dyad for electron withdrawing group coordination and correct substrate orientation and Tyr183 participating in the protonation of the substrate (Fig 88).

The key interactions involved into FMN coordination in *CtOYE* are depicted in Figure 89. Briefly, the N1 of flavin cofactor is in hydrogen contact with the side chain of Arg230. The O2 atom is also interacting with the same residue Arg230 but it establishes further interactions also with the side chain of Gln101. This residue, Gln101, is interacting as well as with the N3 of the flavin cofactor.

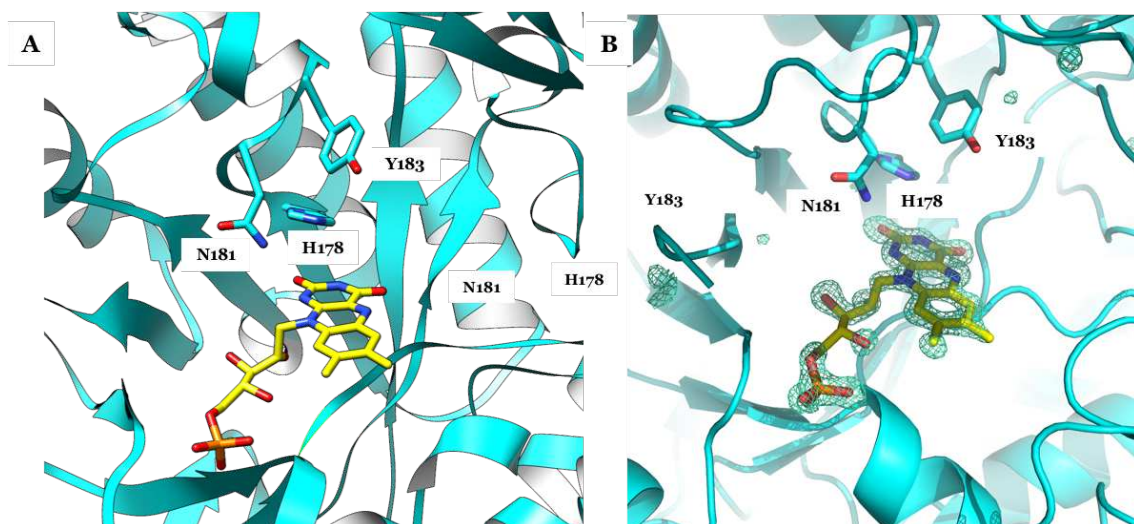


Figure 88. *CtOYE* active site showing the conserved His178/Asn181 dyad and the proton donor Tyr183 residue. The conserved residues and FMN cofactor (yellow) are shown as stick models.

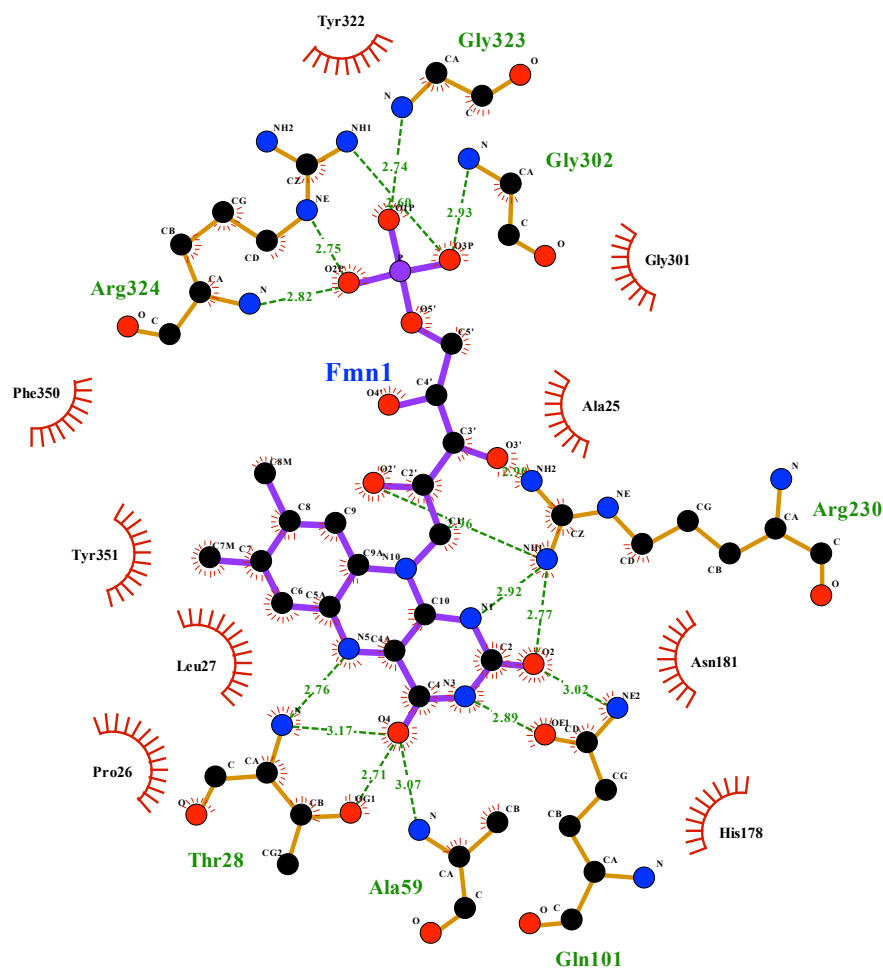


Figure 89. Schematic illustration of the interaction of FMN with active site residues of *CtOYE*. The thin green dotted lines illustrate hydrogen bonds.

The O4 of FMN is coordinated by a complex network of interactions with the backbone of Thr28 and Ala59. The N5 of the flavin is also in hydrogen contact with Thr28, that is supposed to modulate the FMN redox potential in classical OYEs. The dimethylbenzene moiety of the flavin isoalloxazine ring is stabilized

by different hydrophobic interactions with residues Pro26, Leu27 and Tyr351. The ribityl chain of the cofactor forms hydrogen bonds with Arg230 and different hydrophobic interactions with Ala25. The negative charged phosphate group of FMN is stabilized by the interaction with the positive charge of Arg324 while the main chain atoms of Gly302 and Gly323 are involved in polar interactions with the phosphate group.

5.2.2 Overall GsOYE and CtOYE structural comparison

Superposition of models coordinates of GsOYE and CtOYE gives an overall r.m.s. deviation of 0.68 Å, in agreement with the very high sequence identity that reaches 64 % (Pisa software / Gesamt [216]). Similarity searches with DALI server [227] identify the closest structural homologues for both GsOYE and CtOYE within the members of classical OYEs present in the PDB archive. In particular, the five structures most similar to GsOYE are NemaA (r.m.s.d. 0.914 Å; 3gka), MR (0.99 Å, 1gwj), OPR1 (1.02 Å, 1icp), NerA (1.19 Å, 4jip) and PETN reductase (1.15 Å, 5lgx [228] or 1h51). As expected, the structural homology is slightly lower, but still very high, with members of the thermophilic-like OYE subgroup, such as YqjM (1.41 Å and 32.4% sequence identity, 1z41). For CtOYE, the most similar ones resulted: TsOYE (r.m.s.d. 1.46 Å; 5nux), Xena in the reduced form (r.m.s.d. 1.36 Å; 5lnj), OYE 2.6 (r.m.s.d. 2.0 Å; 3tjl), trimethylamine dehydrogenase from *Methylophilus methylotrophus* (r.m.s.d. 1.76 Å; 1djn) and a putative NADH-dependent flavin oxidoreductase from *Staphylococcus aureus* (r.m.s.d. 1.72 Å; 3l5a).

Only the structures of OYE 2.6 from xylose fermenting *Pichia stipitis* [91], SYE1 (2gou) [222] and OYE1 (1oya) [68] show a β6 loop of similar size and active site penetration properties, even if SYE1 and OYE1 largely differ in terms of amino acids composition. Indeed, GsOYE, analogously to OYE 2.6, presents a Glycine and an Asparagine residue (Gly269 - Asn270) in the turn positions, close to FMN cofactor, while SYE1 places Trp274 residue in the same site. Such interaction is conserved in OYE 2.6 but not in SYE1, where both Asn270 and Tyr346 residues are re-placed by Trp274 and Phe350, respectively (Fig. 90). C-terminal loop Tyrosine, Tyr356, of MR has been demonstrated to play a role in both phenolic substrates and NADH binding and β6 loop Trp274 in SYE1 has been supposed to have a compensatory role, given its loss of hydroxyl group due to Tyrosine to Phe350 re-placement [71, 222]. In GsOYE both Asn270 and Tyr346 residues have

the potential to trap the substrate and contribute to reductive half-reaction by hydrogen bonding interactions. OYE1 is characterized by a long β_6 loop, more protruding and accessible to the solvent, with a Phenylalanine (Phe296) and a proline (Pro295) in such loop turn, the last orienting its 5-member ring close to FMN and almost perpendicular to its main plane. *GsOYE* present in loop β_3 a similar tertiary motif as in PETN, SYE1 or MR but its lid subdomain is shorter and in a more open conformation (Fig. 91). On the contrary, in OYE1 as well as in OYE 2.6 fold this β -hairpin lid is totally absent and replaced by a short α -helix quite far from active site entrance.

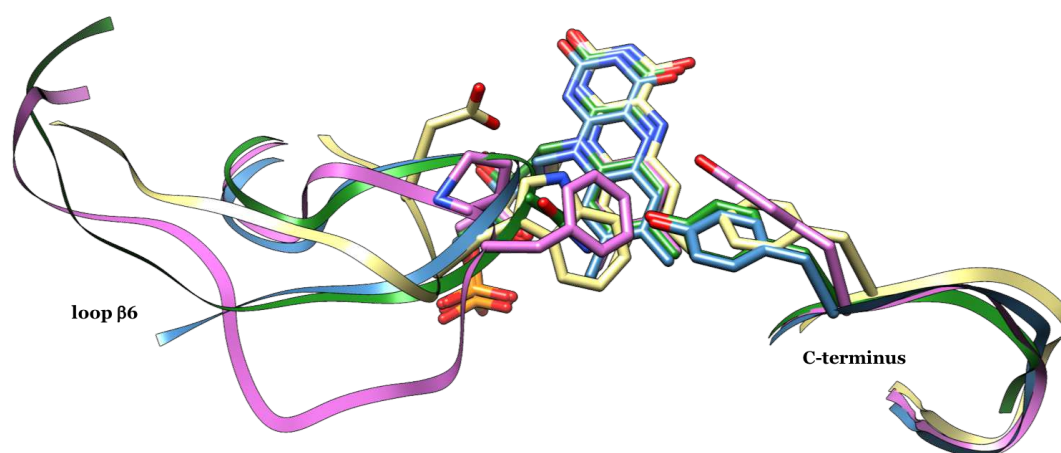


Figure 90. Loop β_6 and C-terminus loop superimposition: *GsOYE* (green), OYE1 (pink), SYE1 (kaki) and OYE 2.6 (blue). FMN and the key residues are shown as stick models.

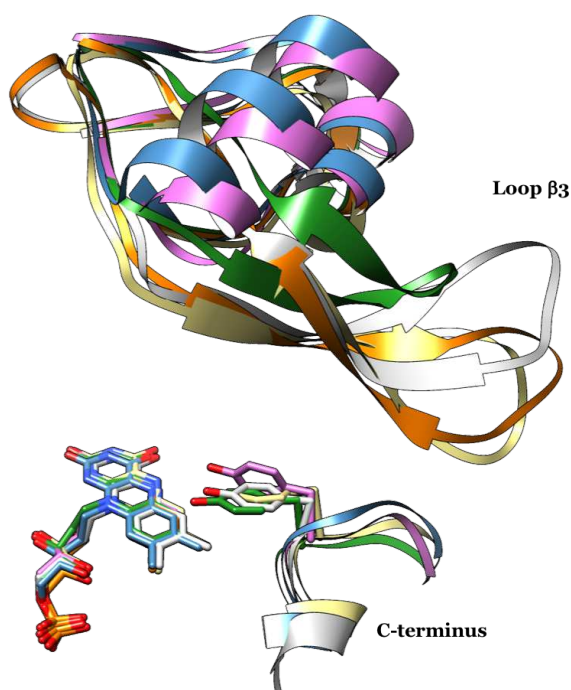


Figure 91. Loop β_3 and C-terminus loop superimposition: *GsOYE* (green), OYE1 (pink), SYE1 (kaki), OYE 2.6 (blue), PETNR (orange) and MR (grey). FMN and the key residues are shown as stick models.

As already discussed, loop β_3 in *CtOYE* arranges into two largely unstructured turns (as described for OPR1, OPR3 and NerA). However, compared to OPR1, OPR3 and NerA, *CtOYE* loop is slightly shorter leaving the entrance of the active site more accessible to substrates and solvent (Fig. 92).

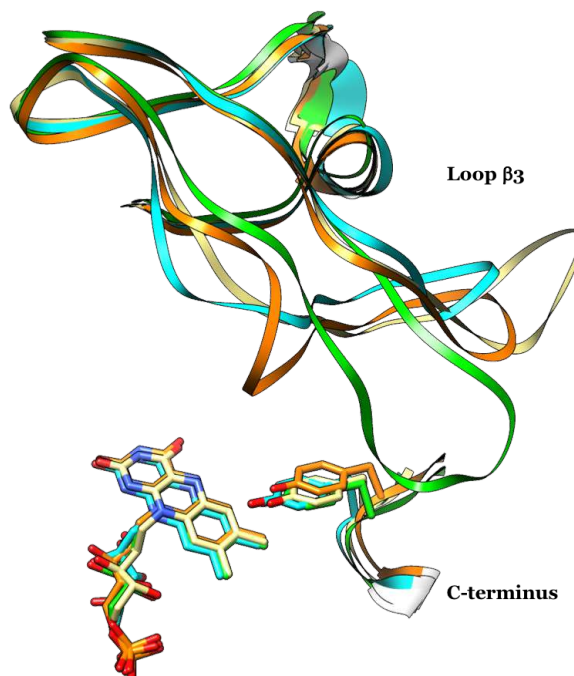


Figure 92. Loop β_3 and C-terminus loop superimposition: *CtOYE* (cyan), OPR1 (green), OPR3 (orange), NerA (kaki). FMN and the key residues are shown as stick models.

GsOYE and *CtOYE* can use both NADH/NADPH cofactors but they show a marked preference for the NADPH cofactor compared to MR which is exclusively NADH selective. The crystal structures of MR (2r14, [71]) and PETNR (3kft, [72]) have been solved in complex with the tetrahydro-NADH₄ analogue and they show different binding modes. The nicotinamide moiety is positioned above the FMN isoalloxazine ring in both structures interacting with His/Asn (His) dyad through its carbonyl-oxygen (Fig. 93) [71]. The adenine and pyrophosphate moiety have different orientations due to the presence of the elongated loop β_3 that force the ribose and adenine moiety of the inhibitor to be exposed on the surface of the protein (Fig. 93). However, loop β_6 could not be traced anymore in PETNR in the presence of the ligand, thus suggesting an involvement in binding due to its flexibility. Looking to the crystal structure, the binding mode of NADH₄ reported for MR and PETNR, is unlikely to occur in *GsOYE* and SYE1 as their loop β_6 is in clashing distance with the ribose moiety of the inhibitor, however this loop seems flexible in OYEs and thus can re-arrange itself in order to accommodate the cofactor. The NADH exclusive specificity of MR has been attributed to Glu135

residue of loop β_3 while the exclusive NADPH specificity of PETNR was imputed to Arg130 residue. However, cofactor specificity cannot be ascribed just to the type of amino acid residue present in position 135 (MR numbering), as already discussed in detail previously.

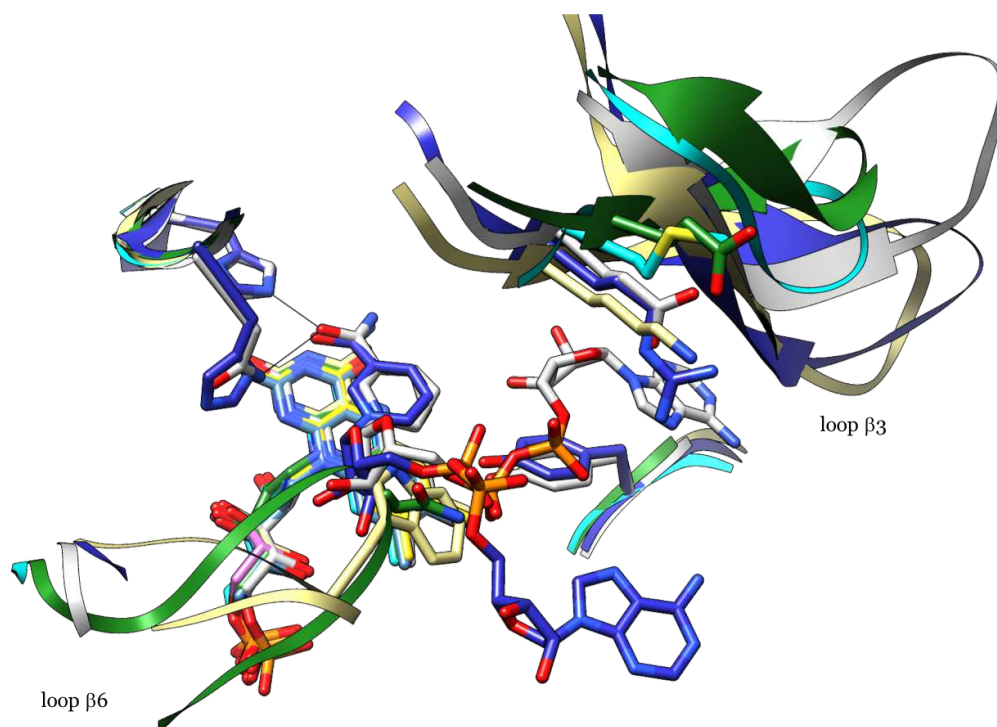


Figure 93. MR in complex with NADH₄ (grey) and PETNR in complex with NADH₄ (blue) superimposed to GsOYE (green), CtOYE (cyan) and SYE1 (kaki). NADH₄, FMN and key residues are shown as stick models.

5.2.3 GsOYE and CtOYE ene-reductase vs nitro-reductase activity

3 clusters of OYEs based on their stereoselectivity in the reduction of 1-nitro-2-phenyl-propene have been identified by Oberdorfer *et al.* [103]. This classification is based on the distance between two “bounding residues” (generally aromatics), involved in shaping the entrance of the active site: OYEs with distances of 8.5 Å exhibit an open binding pocket and exclusive *R*-selectivity; smaller binding sites (distances of 5 Å) correlate with exclusive *S*-selectivity, while intermediate distances (7.5 -7.8 Å) define a fingerprint for the moderate stereoselectivity cluster of enzymes [103, 212].

GsOYE and CtOYE are clustered in this last group exhibiting 7.7 Å distance between their bounding residues (Fig. 94).

In the case of nitro reduction, the hydride has to be transferred directly onto the nitrogen atom. Thus, in OYEs catalyzing the nitro-reduction the existence of different substrate binding modes was hypothesized. However, in the crystal structure of NerA in complex with 1-nitro-2-phenyl-propene, just one binding

mode of the substrate (the one favoring the C=C-bond reduction) has been clearly detected. Comparing the active sites of different OYEs able to catalyze to different extent the nitro-reduction, some common features have been identified and reported [212].

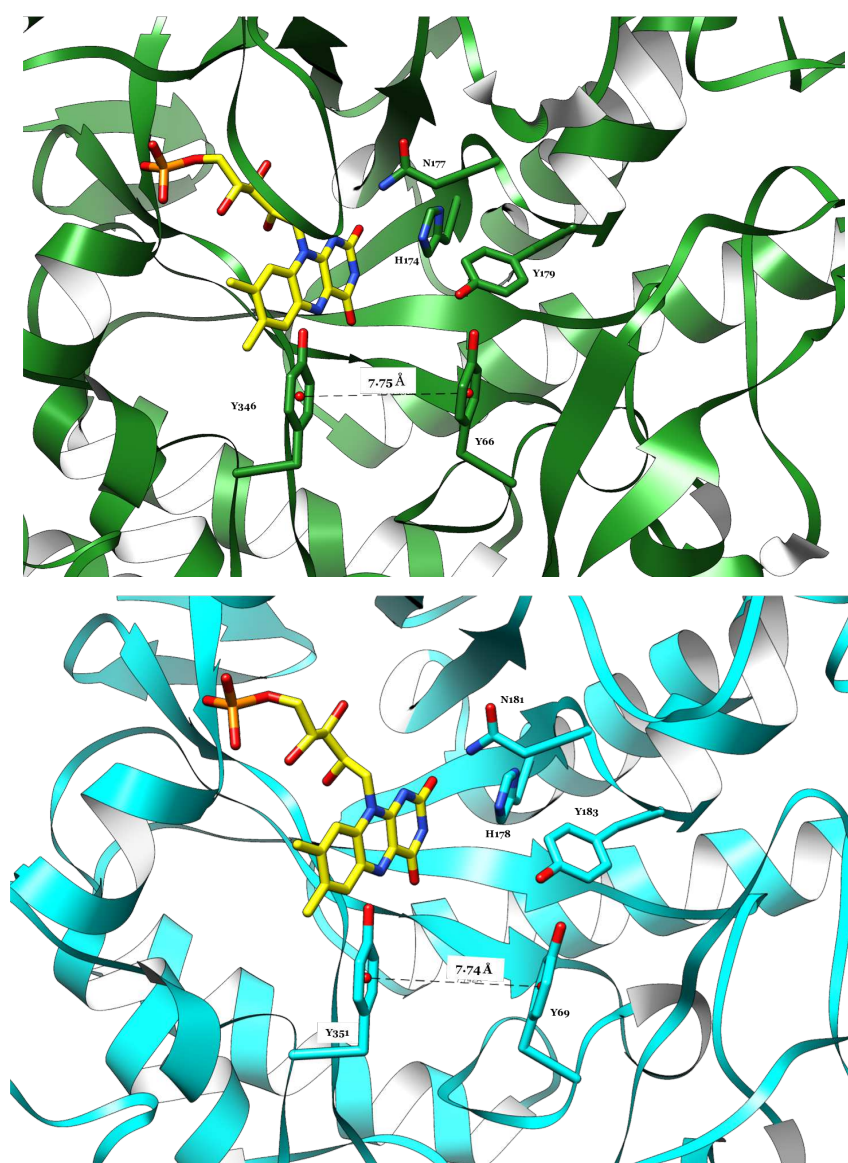


Figure 94. Active site of GsOYE (green) and CtOYE (cyan). The active site residues participating in catalysis are shown as sticks. The distances between the two Tyr bounding residues defining the entrance of the active site are also shown.

For OYE1, which exhibits exclusively ene-reductase activity, a hydrophobic patch was detected between the two bounding residues (Y82 and Y375). This hydrophobic cluster forces the nitro-group of the substrate to interact through hydrogen bonding with the His191/Asn194 dyad, placing in this way the C=C-bond parallel to the FMN isoalloxazine ring, thus favoring the C=C-bond reduction (Fig. 95). For NerA, that shows preferentially C=C-bond reduction activity and just moderate nitro-reductase activity, a small hydrophobic hotspot

located between the bounding residues Y65 and Y356 was identified. In addition, another relatively hydrophobic region was found parallel to the FMN cofactor. These hydrophobic patches can interact with the aromatic part of the substrate, thus orienting the C=C-bond parallel to the FMN and promoting in this way alkene reduction (Fig. 95) [212]. Finally, for XenA, an OYE with remarkable nitro-reductase activity, a hydrophobic area was found in the opposite direction compared to the previous one (formed by loop $\beta 6$ and $\beta 5$) thus favoring a binding mode in which the nitro group is placed in a geometry ideal for direct hydride transfer (Fig. 95) [212].

Both *GsOYE* and *CtOYE* exhibit a hydrophobic hotspot between the bounding residues with an intermediate distance between these residues defining the entrance to the active site cavity. Moreover, as already described in detail, loop $\beta 6$ in *GsOYE* protrudes into the active site cavity placing two hydrophilic residues (Gly269 and Asn270, respectively) in the turn positions, close to FMN cofactor (Fig. 95). For *CtOYE* loop $\beta 6$ was not traced but however it has a similar composition as *GsOYE*, presenting in its turn two hydrophilic residues as well (Gly273 and Asn274). *OYE1* is characterized by a long $\beta 6$ loop exhibiting a hydrophobic Phenylalanine (Phe296) and a proline (Pro295) in such loop turn, the last orienting its 5-member ring close to FMN and almost perpendicular to its main plane. However, its Tyr375 is oriented differently compared to *GsOYE*, *CtOYE* and *NerA*, being almost perpendicular to FMN plane, in order to accommodate the steric hindrance of Phe295 (Fig. 95). The loop $\beta 6$ of *NerA* is shorter compared to *GsOYE* and *OYE1* and it exhibits in its turn two glycine residues (Gly272 and Gly273) (Fig. 95). The active site of the thermophilic-like *XenA* has a different architecture compared to classical OYEs and its loop $\beta 6$ is not protruding inside the active site cavity, but it points toward FMN two Tryptophan residues (Trp278 e Trp302) that delimitate a hydrophobic patch on the opposite side of the active site compared to classical OYEs (Fig. 95).

The superimposition of all the structures described above to *NerA* in complex with 1-nitro-2-phenylpropene confirms the binding mode of the substrate described for *NerA* (4jiiq) also in *GsOYE* and *CtOYE*, both belonging to the intermediate cluster of stereoselectivity (Fig. 95).

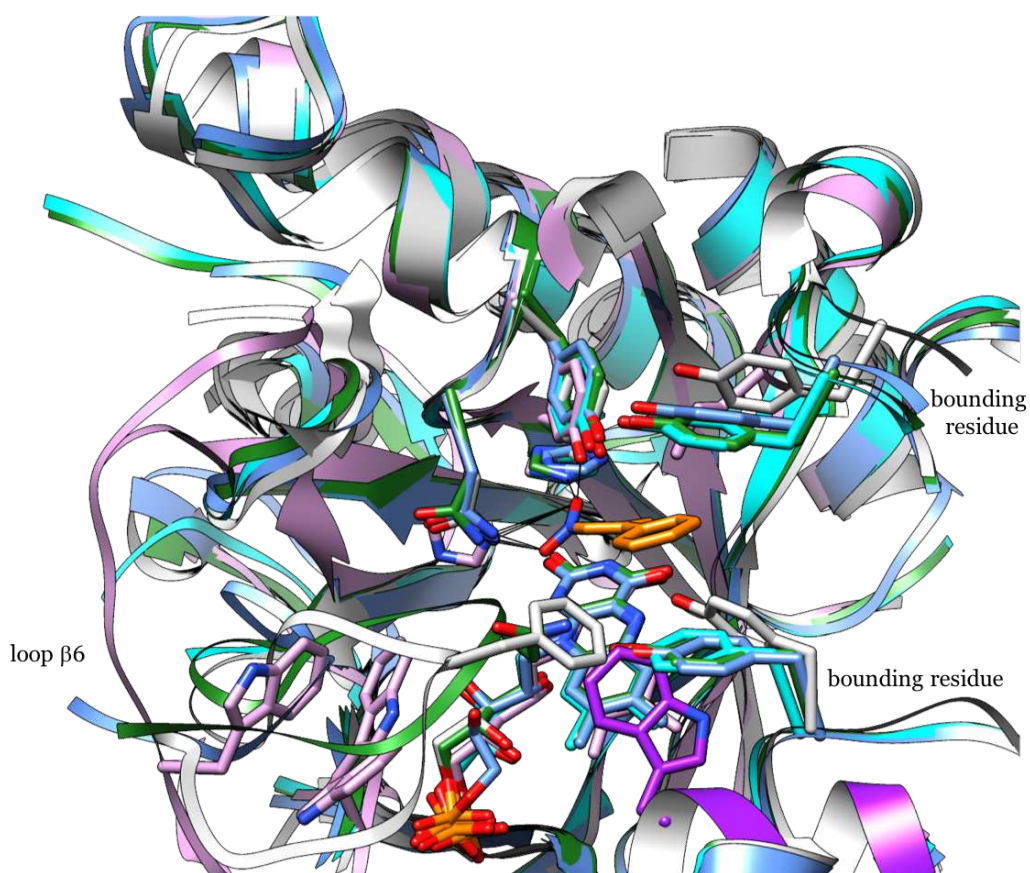


Figure 95. Superimposition of GsOYE (green), CtOYE (cyan), OYE1 (grey), NerA (steel blue) and XenA (plum and Trp358 of the adjacent monomer in purple). The key residues involved in defining the nitro- *vs* ene-reductase activity, the FMN cofactor and 1-nitro-2-phenylpropene (orange) (4jiq) are depicted as sticks.

Moreover, the catalytic activity of PETNR with different nitroalkenes was reported in detail [229]. This enzyme showed excellent conversion in the presence of β -nitrostyrene (> 99% conv.) at neutral pH, as reported also for GsOYE and CtOYE, as well as good conversion (93% conv.) with *trans*- β -methyl- β -nitrostyrene in the same reaction conditions but low ee (14% ee for the (*R*)-enantiomer) similarly to GsOYE and CtOYE. Moreover, for *trans*- β -methyl- β -nitrostyrene and its *p*-Cl substituted analogue apparent nitronate intermediates were detected during the reaction due to the enzyme nitro-reductase activity. A model of PETNR in complex with the (*E*)-isomer of 4-chloro- β -methyl- β -nitrostyrene was build based on the position assumed by 1-nitrocyclohexene in PETNR crystal structure [229]. It has been seen that the nitro-group of the substrate was in hydrogen contact with H181/H184 dyad positioning the aromatic ring of the substrate in van der Waals contact with Y68. Furthermore, the side chain of Y351 was reoriented in order to accommodate the aromatic ring of the substrate [229]. However, this orientation could explain the C=C-bond reduction while no clear evidence for the NO₂ reduction could be deducted.

5.3 **BfOYE4 and CaOYE crystallization and refinement**

BfOYE4 has been successfully crystallized starting from the monomeric fraction isolated by SEC chromatography and concentrated to 16 mg/ml (for more details see Chapter 4). Recombinant *CaOYE* behaves in solution as a homogeneous monomeric preparation as proved by analytical SEC chromatography, and thus it was used without any need for further purification steps (20 mg/ml).

After ten days of incubation at 20 °C, some microcrystals of the N-terminally His₆-tagged *BfOYE4*, grown in solution n. 23 of Structure Screen (100 mM Na-HEPES pH 7.5 containing 28% v/v PEG 400 and 200 mM CaCl₂ x 2H₂O). These microcrystals have been broken and used as seeding for further optimization using micro-seeding techniques. New trials were performed at 4 °C. After a week of incubation, some crystals, suitable for diffraction experiments, have grown in several conditions. The best hits were observed in Morpheus screen (n.74: 100 mM imidazole - MES monohydrate pH 6.5 containing 100 mM carboxylic acids and 50% v/v of the precipitant mix composed by 40% v/v ethylene glycol and 20% w/v PEG 8000) and JCSG screen (n.8: 200 mM ammonium formate and 20% w/v PEG 3350) (Fig. 96).

Flat irregular crystals of N-terminally His₆-tagged *CaOYE* appeared after two weeks of incubation in multiple conditions and the most regular ones (LMB screen n. 64: 100 mM sodium/potassium phosphate, pH 6.2, containing 20 % w/v PEG 4000 and 6% v/v MPD) were crushed and used to prepare a seeds stock for the subsequent optimization experiments. After micro-seeding, thicker and more regular crystals, but still not suitable for X-ray diffraction, appeared in few days in different LMB screen conditions n. 16, n.43, n.57 and n.64. Since all these conditions contain high concentration of salts, we decided to extend our trials to the JCSG kit. After different dilutions of the seed stock, the best crystals were detected in JCSG n.52 (100 mM Tris pH 8.5 containing 1.6 M ammonium sulphate and 200 mM lithium sulphate) and n.70 (100 mM HEPES pH 7.0 containing 1.1 M sodium malonate dibasic monohydrate and 0.5% v/v Jeffamine®-ED2003) (Fig. 97).

Different datasets were collected for both *BfOYE4* and *CaOYE* using the best crystals grown in the different conditions of precipitant. Here we report the best X-ray data which gave us the highest resolution for both proteins: *BfOYE4* grown in A8 JCSG and *CaOYE* grown in F10 JCSG (Table 20).

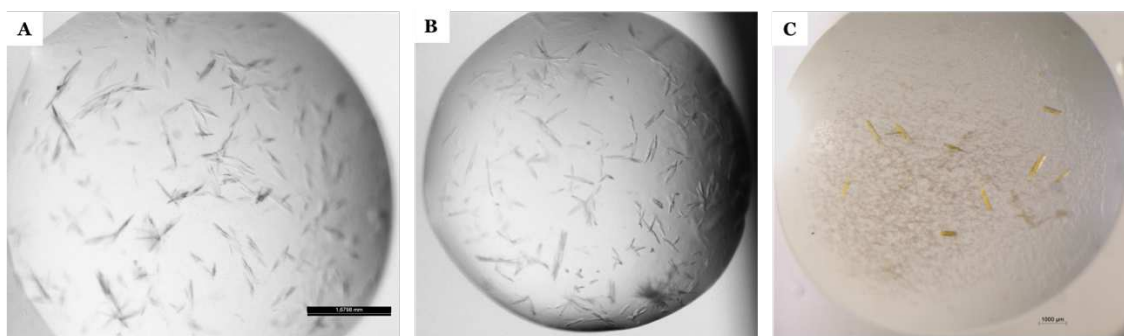


Figure 96. *BfOYE4* crystals in different conditions: (A) crystals grown in n.3 JCSG (B) crystals in n.15 JCSG and (C) crystals obtained in n.8 JCSG.



Figure 97. *CaOYE* crystals optimization: (A) first crystal hits obtained in LMB n64; (B) crystals obtained in n.45 JCSG screen after micro-seeding techniques; (C) optimized crystals obtained in n.70 JCSG.

BfOYE4 structure has been determined by Phaser software [221] using as template the model of *BfOYE4* enzyme, built by Swiss model server (5nux structure was used as starting model by the server, <https://swissmodel.expasy.org>). Final model includes two molecules per cell, 50 % of solvent and final parameters Rfactor / Rfree of 0.18/0.23 (further details can be found in Table 20). Electron density maps and the protein model were clear and well defined from residue Leu24 to Arg433, for chain A, and from Leu23 to Gly431, for chain B, except for the fragment from Val384 to Lys391, that was disordered and cannot be traced for both chains.

CaOYE structure was determined by molecular replacement (MOLREP software, [217]) using as template a model of *CaOYE* enzyme, built by Swiss model server (5nux structure was used as starting model by the server, <https://swissmodel.expasy.org>). Four molecules per asymmetric unit and roughly 50 % of solvent define the crystal content. Final model was traced and fully visible from Met1 to Trp354. Final parameters obtained for the best dataset (2.55 Å) reached Rfactor/Rfree of 0.21/0.26 (for further details see Table 20).

Table 20. X-ray Crystallographic data collection and refinement statistics.

	<i>BfOYE4</i>	<i>CaOYE</i>
Data collection statistics		
Wavelength	0.97	0.97
Space group	P 21 2 21	C 2 2 21
Cell constants		
a, b, c (Å)	62.04 92.061 161.998	108.194 162.274 216.2
a, b, γ (°)	90 90 90	90 90 90
Resolution range for refinement (Å)	49.03 - 2.29 (2.37 - 2.29)	48.38 - 2.55 (2.641 - 2.55)
Total reflections	307939 (31613)	550273 (54843)
Number of Unique Reflections	42603 (4190)	62177 (6179)
R_{merge}	0.12 (0.73)	0.23 (0.67)
$\langle I / \sigma(I) \rangle$	13.5 (3.3)	7.67 (2.55)
Completeness (%)	99.95 (100.00)	99.92 (100.00)
Multiplicity	7.2 (7.5)	8.9 (8.9)
Refinement statistics		
$R_{\text{work}} / R_{\text{free}}$	0.18 / 0.23	0.21 / 0.26
RMSD bond lengths (Å)	0.012	0.009
RMSD bond angles (°)	1.43	1.46
Average B factor	28.80	34.18
Main chain B factor	28.91	34.34
Ligands B factor	25.44	26.88
Water molecules B factor	25.28	30.56
No. of non-hydrogen atoms		
Number of protein atoms	6224	10773
Number of ligands atoms	68	159
Number of water molecules atoms	122	157
Ramachandran plot (%)		
Most favoured	96.36	96.45
Generously allowed	3.64	3.41
Outliers	0.00	0.14

5.3.1 Structural analysis of *BfOYE4* and *CaOYE*

The holo structures of *BfOYE4* (Fig. 98) and *CaOYE* (Fig. 99) have been solved to moderate resolution, 2.29 and 2.55 Å, respectively. Overall structures of *BfOYE4* and *CaOYE* show the typical $\alpha 8/\beta 8$ TIM barrel OYE fold, as already described in the Introduction. Both enzymes accommodate one molecule of FMN cofactor on the top of the β -barrel core, at the C-terminus side. *BfOYE4* crystallized in the orthorhombic space group $P2_122_1$ and two molecules per ASU, while *CaOYE* was solved and refined in $C222_1$ orthorhombic space group, with 4 molecules per ASU. In agreement to size exclusion analysis (for details see Chapter 4) and general behavior for thermophilic-like OYEs enzymes, *BfOYE4* crystals contacts suggest the presence of quaternary structures describing putative dimers of physiological relevance. Also for *CaOYE* crystal contacts suggest a dimeric structure, even though from size exclusion analysis and native gel (see Chapter 4 for details) the protein seem to be monomeric in solution.

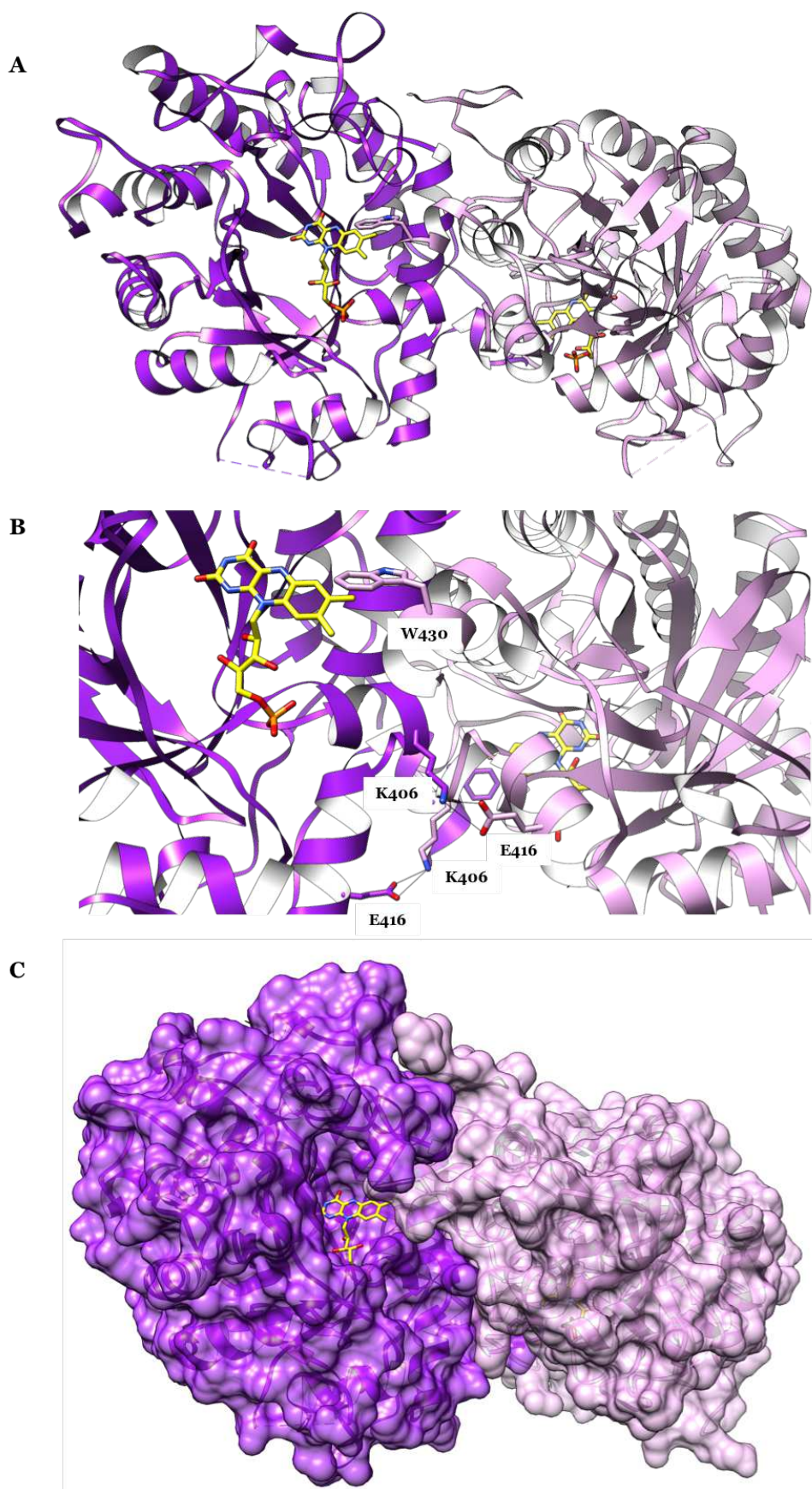


Figure 98. *BfOYE4* dimeric interaction: (A) ribbon diagram (B) zoom in the putative dimeric interface and (C) surface representation. FMN (yellow) and Trp430 finger (plum) are shown as stick models.

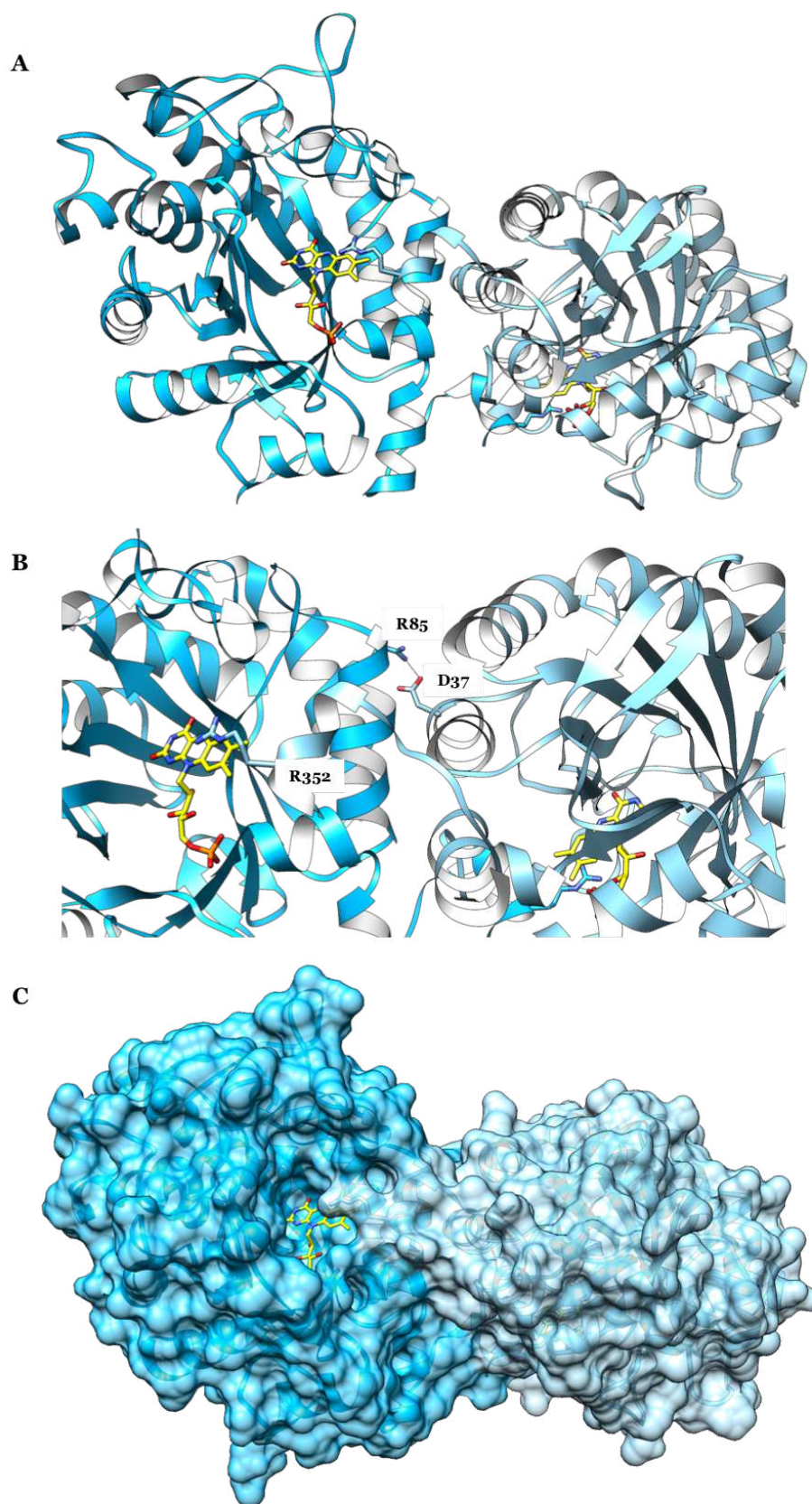


Figure 99. *CaOYE* dimeric interaction: (A) ribbon diagram, (B) zoom into the putative dimeric interface and (C) surface representation. FMN (yellow) and Arg352 (light blue) are shown as stick models.

5.3.1.1 *BfOYE4* structure

BfOYE4 structure presents both typical features of thermophilic-like OYEs and peculiar properties. In the crystals, molecular contacts between symmetrical molecules allowed to identify the functional assembly of the enzyme, that is an elongated dimer with the longest axis of 93.5 Å and mid section of about 39.5 Å. The interaction surface between monomers covers 2283 Å². Both the α 1 helix and loop- β 3 as well as N-terminal and C-terminal loops are involved in the dimerization, the latter ones defining extended protrusions that reciprocally embrace the symmetry mate and contribute to extend the contact surface. The large majority of interactions are hydrophobic contacts (229) followed by 12 hydrogen bonds and 2 salt bridges, between Lys406 and Glu416 of both chains (interactions calculated with the software Profunc <https://www.ebi.ac.uk/thornton-srv/databases/profunc/>).

Generally, thermophilic-like OYEs have shorter sequences if compared to classical ones and a high content of proline residues in their loops. On the contrary, *BfOYE4* is 439 amino acids long and has a 7.1% proline content, compared to *CaOYE* with a sequence of 354 amino acids and 8.2% proline amount.

As already reported for other thermophilic-like OYEs, the C-terminus of each monomer protrudes through an “amino acidic finger” (in our case Trp430) inside the active site of the symmetry mate in the functional dimer, thus contributing to shape the architecture of the active site. This arm places a highly conserved arginine residue in a favorable position to contribute to substrate binding and catalysis in the large majority of the thermophilic-like OYEs, with the exception of *BfOYE4* and XenA enzyme, where the same position is covered by a tryptophan side chain (Fig. 100 C).

An interesting peculiarity of *BfOYE4* is the presence of a longer N-terminal loop, if compared to other thermophilic-like OYEs, that was initially noticed from sequence alignment and captured our attention in the preliminary steps of targets selections (Fig. 100 A). Such extension makes *BfOYE4* 50 residues longer than other OYEs of the same subclass. *AnOYE8*, another enzyme identified in this work, has a long N-terminal loop (almost 30 amino acidic residues), even if shorter than *BfOYE4* one. As both enzymes were identified from fungi, this can be a common feature of enzymes belonging to such organisms and/or a putative

signal peptide targeting the enzyme to appropriate subcellular compartments. Different prediction tools for subcellular localization have been used but contradictory results were found. However, in Nizam and co-workers paper [59] a mitochondrial localization was reported for this protein, and thus the first 22 residues can be involved in directing the protein to this subcellular compartment. As a consequence, the first 22 residues are flexible in the recombinant construct and could not be traced in the structure, given the absence of a clear density in our maps. On the contrary, the next residues, from Leu 23 to Pro 50, define a proline rich loop that interacts with the C-terminal finger of the same chain and protrudes toward the symmetry mate, reaching its active site in the case of the C-term, and contacting the loop between Met 160 and Leu 165, facing the active site cavity, in the case of N-terminus. As mentioned before, such extensions contribute to dimer stabilization mainly by hydrophobic interactions. To our knowledge, this is the first thermophilic-like OYE with such a long N-terminal extension. Recently, a case of an atypical long C-terminal domain was reported for *RmER* [213]. This domain had an average of additional 14 amino acids and its crystal structure revealed that it extends into the active site limiting the active site entrance size. Moreover, it has been seen that in this case the dimerization results in the loss of one FMN molecule of the dimer.

Another peculiar region of *BfOYE4* not identified in none of the other thermophilic-like OYEs is comprised between Met376 and Gly392 and correspond to a negatively charged loop, including six glutamic acid residues (Fig. 100 B). As expected, due to its heavily charged nature and consequent high flexibility, the electron density maps are poorly defined and only partially visible.

Generally thermophilic-like OYEs show great differences in their thermal stability. *XenA* and *YqjM*, that have been isolated from mesophilic organism sources, are not thermo-resistant and it has been observed that their structure is stabilized through salt bridges containing single pairs of charged amino acids [96]. On the contrary, *TsOYE*, a highly thermo-resistant OYE, was found to contain a complex salt bridges network at the dimerization interface [96]. In *TsOYE* this complex five-residues salt bridges pattern defined by Asp37[#] ([#] from adjacent monomer), Glu85, Arg88, Arg89, and Glu92, is responsible for the linkage between helices $\alpha 1^{\#}$ and $\alpha 2$ [96]. Moreover, it has been demonstrated that the introduction of these characteristic intermolecular salt bridges in a non thermo-tolerant OYE homologue could improve its thermal-stability [102].

A		
BfOYE4	MSTPTPHFQHGVPCCGTSTPRPGLLNTAPAGVVFYTPLOSPPSGTALHL---SP	STPKLFT 57
AnOYE8	-----MKDIKVEPAKGISYFPAQETPAGTAANPQTSGK	AIPKLFQ 41
CaOYE	-----	MQPHLFT 7
FOYE	-----	MSLLFS 6
YqjM	-----	MARKLFT 7
TOYE	-----	MSILHM 6
GkOYE	-----	MNTMLFS 7
TsOYE	-----	MALLFT 6
DrER	-----MTVSSAAAPQPASPAAPLLFT	21
RmER	-----	MPHLFD 6
OYERo2	-----	MSVLFE 6
		* .
B		
BfOYE4	RVVGERMLVGTVMIGSGRQAEGLLSG MGGERGVDGEEEEEGKG	TELDLVIIVARGFQKNP 408
AnOYE8	KAVGERMLVATVGHIRDGKLANRLLLE	EGLDVVLVGRGFQKDP 375
CaOYE	R-E-ANIATAAVGLITRPEHADAIVRN-----	GDADLVLLGRELLRDP 330
FOYE	Q-N-VNIPTMAVGLITHTSAQAETILKS-----	EQADMIAIARAALKNP 330
YqjM	E-Q-ADMATGAVGMITDGSMAEEILQN-----	GRADLIFIGRELLRDP 314
TOYE	K-R-CNIKTSVAVGLITPQELAEIILSN-----	ERADLVALLGRELLRNP 314
GkOYE	R-E-ADIPTGAVGLITSGWQAEIILQN-----	GRADLVFLGRELLRNP 314
TsOYE	K-R-VGLRTGAVGLITPQEAETLLQA-----	GSADLVLLGRVLLRDP 325
DrER	RAE-TEISVMAVGLIETGAQAEAILQA-----	GDADLIALGRPFLLRDP 345
RmER	A-E-VGLPTMAVGLITEAQAEAI IAN-----	NEADIIS IARAMLYDP 331
OYERo2	N-E-TTVPAAAVGLITEPEQAERIVES-----	GEAVAVFLGRELLRDP 340
	: . : ** * * : : :	: : . * : *
C		
BfOYE4	GLVWEWAEEELGVR--IMVAHQMRWGFRGKAGGH-----	439
AnOYE8	GLVWTFAQHLDVE--VAMPGQIRWGFQSKQRRGTFVVDPSVYKPSVIE	421
CaOYE	HWPPLRAARALGHD--LAPPQYLRW-----	354
FOYE	HWPWTAALELGDK--PFAPPQYQRRAR-----	354
YqjM	FFARTAAKQLNTE--IPAPVQYERGW-----	338
TOYE	YWVLHTYTSK----EDWPKQYERAFKK-----	337
GkOYE	YWPYAAARELGAK--ISAPVQYERGWRF-----	340
TsOYE	YFPLRAAKALGVA--PEVPPQYQRRGF-----	349
DrER	HWAQRAARELGRLR--PVSIDQYARAGW-----	370
RmER	RWPWHAAAKLGAS--VNAPKQYWRSQPRGLEK--LFKDAH-FGQR---	371
OYERo2	YWPRKAALVLNAQVTPQIPAQYARAY-----	366
	* .	

Figure 100. Sequence alignment of thermophilic-like OYEs. *BfOYE4* (NW_001814538.1); *AnOYE8* (NT_166519.1); *CaOYE* (WP_015941499.1); *FOYE* (WP_056929840); *YqjM* (BAA12619); *TOYE* (YP_001664021); *GkOYE* (YP_148185); *TsOYE* (AM902709); *DrER* (YP_148185); *RmER* (YP_586990); *OYERo2* (KR349311).

BfOYE4 is not a thermo-resistant OYE homologue due to its mesophilic origins (see Chapter 4 for details) and indeed it lacks this characteristic network of interactions that could stabilize its structure. Unfolding temperatures measured for our recombinant enzyme in 50 mM Tris, 150 mM NaCl pH 8.0 buffer assessed a T_m of 42 °C, in line with its structural features.

5.3.1.2 Active site of *BfOYE4*

BfOYE4 is a member of the thermophilic-like subclass of the OYE-family (see Introduction) and it presents the typical features of this subclass. Compared to classical OYEs (*e.g.* *GsOYE*) it has a wider and more accessible active site (Fig. 101). This is mainly due to a different orientation of loop- β 6 (red in Fig. 101), that is not protruding inside the active site almost above the FMN as in the classical OYEs, but is oriented in a different way leaving a more open and accessible active site and higher exposure of FMN isoalloxazine surface. Moreover, compared to

classical OYEs, the loop- β 3 (blue in Fig. 101) is not acting as a lid that covers the active site, thus the active site is more exposed to substrates and solvent.

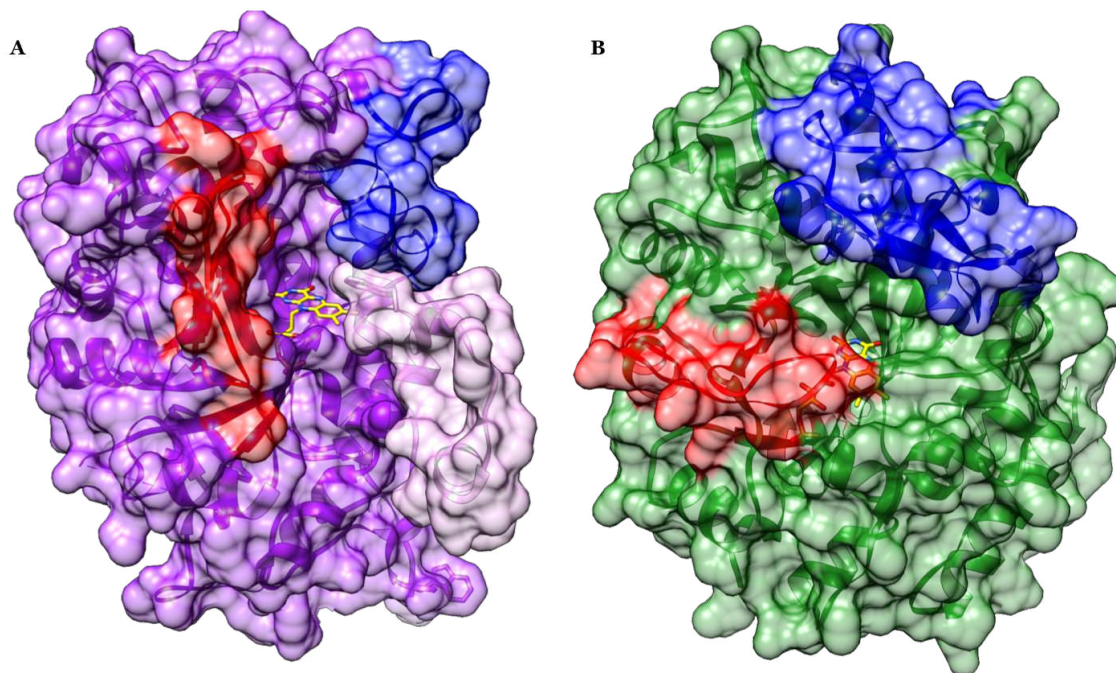


Figure 101. Active site comparison between (A) *BfOYE4* (purple) and (B) *GsOYE* (green). Loop- β 6 and loop- β 3 are colored in red and blue respectively. In *BfOYE4* the Trp430 arm and the C-terminus of the adjacent monomer are also shown in plum.

The active site contains a non-covalently bound FMN molecule placed at the carboxyl-terminal end of the β -barrel. As in all the other OYEs reported, the *si*-face of the FMN is exposed to the solvent while the *re*-face is in contact with the protein backbone. The electron density suggests a 100% occupancy for the FMN in both chains (Fig. 103), compared to other thermophilic-like OYEs such as TOYE [73] and *RmER* [213] for which a lower degree of flavination was seen or to the most recent XdpB that revealed a complete absence of FMN in its crystal structure and its putative binding site occupied by the pentapeptide Thr-Thr-Ser-Asp-Asn from the C-terminus of a symmetry related molecule [230].

The FMN cofactor is bound via extensive hydrogen bonding and hydrophobic interactions with side- as well as main-chains (Fig. 102). Similarly as in other thermophilic-like OYEs, The FMN O(4) occupies a position at hydrogen bonding distance to the main chain amidic nitrogen of Ala108 and the Cys76 sulfhydryl group. This Cys residue, is highly conserved between thermophilic-like OYEs and it has been reported to be involved in the regulation of FMN redox potential. Moreover, other specific interactions between the pyrimidine ring of FMN and a glutamine (Gln150) which interact with N(3) and O(2) as well as an arginine

(Arg283) forming hydrogen bond with the O(2), are also present. The ribityl moiety of the cofactor is anchored to Arg283, Ser73 and Pro74. Like in other OYE enzymes, the FMN phosphate group is embedded in an electropositive groove of the protein that is formed by loops $\beta 7$ and $\beta 8$. Here, the positively charged guanidine group of Arg402 and the main chain atoms of Met362 and Ala401 are involved in an extensive network of polar interactions with the phosphate group.

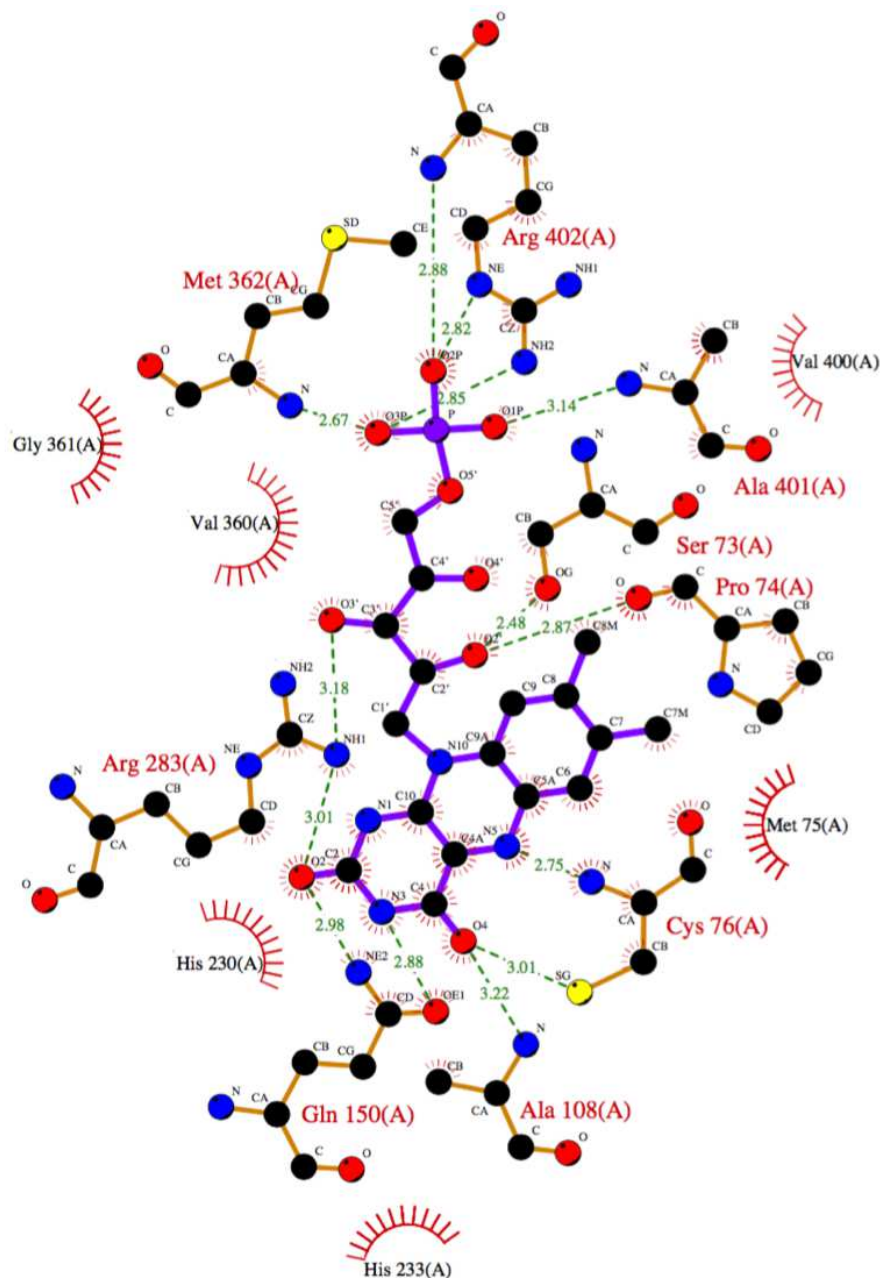


Figure 102. Schematic illustration of the interaction of FMN with active site residues of *BfOYE4*. The thin green dotted lines illustrate hydrogen bonds.

The substrate binding site is located above the *si*-side of the isoalloxazine ring. Similar to other thermophilic-like ERs, *BfOYE4* contains a histidine pair (His230 and His233) involved in the binding and correct orientation of the substrate

through hydrogen bonding with the electron-withdrawing group of the substrate. The proton donor Tyr235 is also highly conserved (Fig. 103 A). As already mentioned, due to dimeric architecture, each monomer is involved in the definition of the active site of the other dimer subunit by the C-terminus finger, contributing each other to the architecture of the catalytic pocket. In particular Trp430 is part of a hydrophobic patch with Pro163 and Trp164 and is positioned about 5.5 Å from the six -carbon aromatic side ring of isoalloxazine group of FMN. The difference electronic density map $F_o - F_c$ shows a small organic molecule, most likely formate anion, present within the crystallization precipitant agents, bound on the *si*-face of the isoalloxazine ring of FMN (Fig. 103 B). In this position, many different anions and small molecules have been reported in the holo structure of OYEs, as already mentioned. In the complex with formate, one carboxylate oxygen of the compound forms two hydrogen bonds with the side chains of the histidine pair His230 and His233, mimicking the interactions they establish with the electron-withdrawing groups of conjugated alkene substrates. Moreover, the other carboxylate oxygen atom is in hydrogen contact with Tyr78 through a water molecule (Fig. 103).

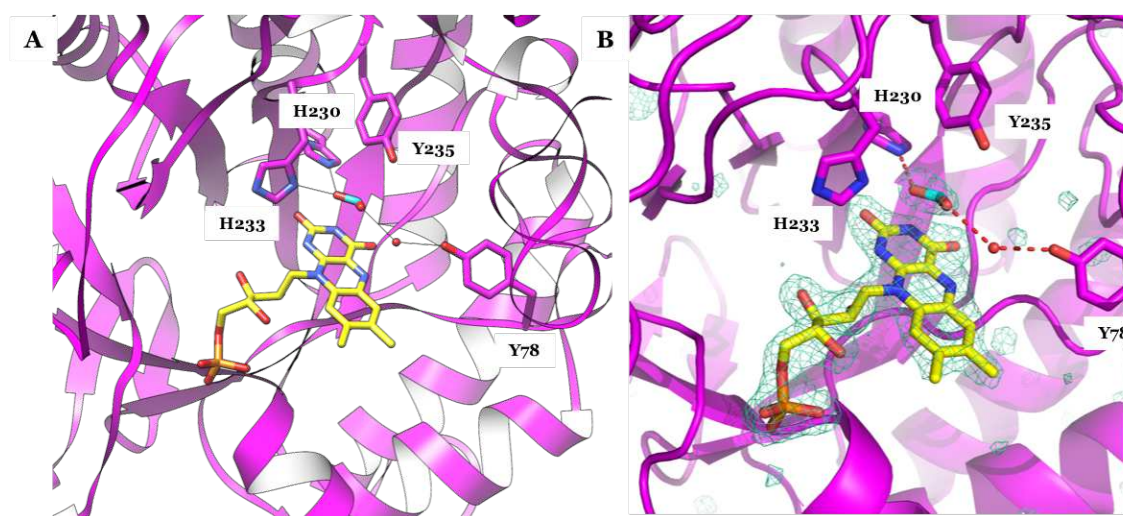


Figure 103. *BfOYE4* active site (A) cartoon representation of conserved residues and their interaction with formate through hydrogen bond; (B) difference map $F_o - F_c$ contoured at 3σ .

5.3.1.3 *CaOYE* structure

CaOYE is a thermostable OYE belonging to the thermophilic-like subclass. Its sequence is shorter (354 amino acid residues) and shows a high content of Proline residues (8.2%) in its turns and loops, compared to the classical OYEs. Even though from oligomeric state investigation (see Chapter 4) this enzyme was monomeric in solution, in the crystal structure it assembles as a functional dimer.

The dimer is elongated and it shows a longest axis of 94.7 Å and a mid section of about 60.6 Å. The interaction surface, between monomers in the functional dimer, covers 1452 Å². The two monomers interact via 2 salt bridges between Asp37 and Arg85 of both chains. Moreover, 17 hydrogen bonds and 186 hydrophobic interactions are also involved in the dimerization interface (interactions calculated with the software Profunc <https://www.ebi.ac.uk/thornton-srv/databases/profunc/>).

As already reported for the other described thermophilic-like OYEs, the C-terminus of one monomer stretches through an “Arg finger” (in our case Arg352) into the active site of the adjacent monomer and interacts with the respective flavin cofactor.

The thermal stability of *TsOYE* was attributed to a complex salt bridge network involved into the formation of the dimerization interface but also to other peculiar characteristics. In *TsOYE* the ratio of Arg/Lys residues is higher (4.6) compared to *YqjM* (0.9) and *XenA* (2.4), in fact, Arginine has a higher pK_a than Lysine and, thus, can maintain ion pairs better at higher temperatures [96]. *CaOYE*, as well, has a higher Arg/Lys content (7.0) compared to *BfOYE4* (1.2) and also *TsOYE* (4.6), however the complex network of interactions, reported in the dimer formation and in the increase of the thermal resistance in *TsOYE*, have not been found in *CaOYE*. As already mentioned, one salt bridge between residue Asp37 of one monomer and Arg85 of the second monomer was observed at *CaOYE* dimer interface. However, the elements responsible for the thermal stability of thermophilic-like OYEs have not been completely elucidated. Taken together, the short amino acid sequence (354 residues), the high content of Proline residues (8.2%) and a surprisingly high ratio of Arg/Lys residues (28 Arg residues *vs* 4 Lys residues) could explain the high thermal resistance observed for *CaOYE* (T_m= 79 °C).

5.3.1.4 Active site of *CaOYE*

The *re*-side of the flavin is facing the protein and is completely hidden from the active site but in contact with strand 1. The *si*-side of the flavin is facing a solvent filled access channel and therefore forms the bottom of a wide-open active pocket. As already mentioned, the redox potential of the FMN cofactor is controlled by different interactions between the protein and the flavin. As shown in Figure 104 the N3 and O2 atoms of the flavin pyrimidine ring are interacting with Gln100,

Cys26 and Ala58 while its O2 with Arg230. The ribityl chain of the flavin is stabilized by Ser23, Pro24 and Arg230. Like in other OYE enzymes, the negative charge of FMN phosphate group is stabilized by the positive charge of Arg324 and the main chain atoms of Gly323 and Leu301 are involved in some polar interactions with the phosphate group.

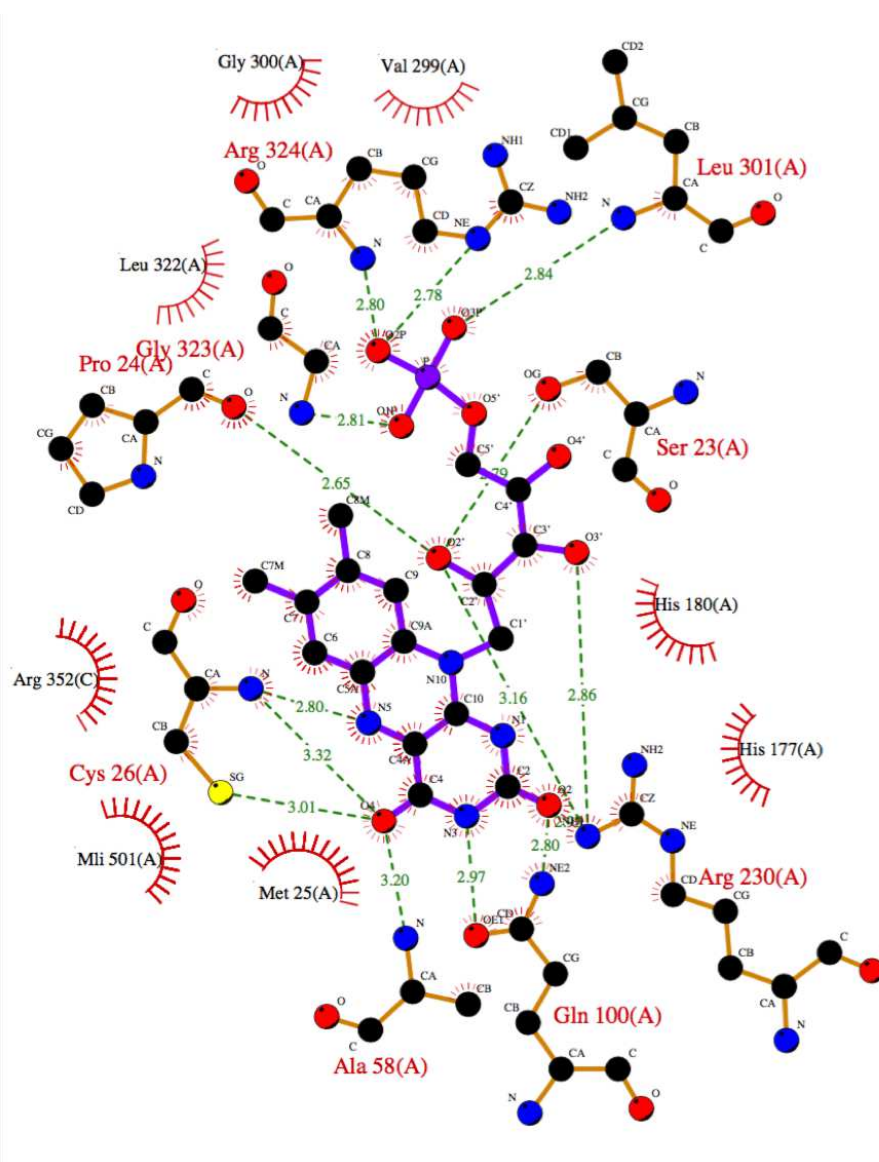


Figure 104. Schematic illustration of the interaction of FMN with active site residues of CaOYE. The thin green dotted lines illustrate hydrogen bonds.

Similar to other thermophilic-like ERs, CaOYE contains a histidine pair (His177 and His180) involved in the binding and correct orientation of the substrate through hydrogen bonding with the electron-withdrawing group of the substrate. The proton donor Tyr182 is also highly conserved (Fig. 105). As already mentioned, due to dimerization the active sites are shared between the two monomers and they are also partially shaped by the C-terminus of the neighboring subunit and in particular Arg352 is positioned near the FMN N5 at

a distance of 5.4 Å closing the active site.

The difference electronic density map $F_o - F_c$ shows an elongated organic molecule, most likely malonate, present within the crystallization precipitant agents, lying above the isoalloxazine ring of FMN (Fig. 105). In the complex with malonate, one carboxylate oxygen of the compound is in hydrogen bonding with the side chains of the histidine His177 but, surprisingly, not with His180. While the other carboxylate moieties are involved into a complex network of hydrogen bonding interacting with Tyr28, the corresponding residue of Tyr346 (*GsOYE* numbering) that was also shown to be involved in substrate binding in classical OYEs [94], with Cys25 and also with Arg352 of the adjacent monomer (Fig 105).

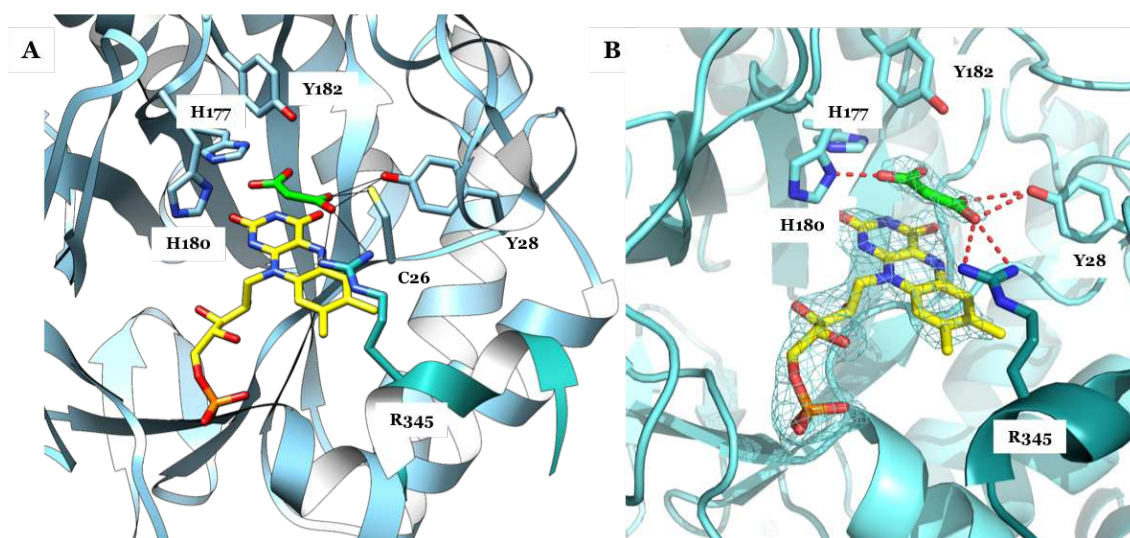


Figure 105. *CaOYE* active site (A) cartoon representation of conserved residues and their interaction with malonate through hydrogen bond. One monomer of *CaOYE* is colored in light blue and the Arg352 finger of the second monomer is shown and colored in dark cyan (B) difference electronic density map $F_o - F_c$ contoured at 3σ .

5.3.2 Overall *BfOYE4* and *CaOYE* structural comparison

Superposition of models coordinates of *BfOYE4* and *CaOYE* gives an overall r.m.s.d. of 1.05 Å (42% sequence identity). The closest structural homologues within the thermophilic-like members family were identified using DALI server [227]. In particular, the two OYE-like structures most similar to *BfOYE4* are *TsOYE* (or CrS) (3hf3, [96]) (r.m.s.d. 1.037 Å, 43% identity) and reduced XenA (5lnj, [231]) (r.m.s.d. 1.2 Å, 39% identity), other structures with low sequence identity (25%) are trimethylamine dehydrogenase from *Methylophilus methylotrophus* (r.m.s.d. 2.7 Å; PDB 1djn) and a putative NADH-dependent flavin oxidoreductase from *Staphylococcus aureus* (r.m.s.d. 1.72 Å; PDB 3l5a). For *CaOYE* the most similar structures were the same reported for *BfOYE4*:

TsOYE (r.m.s.d. 0.79 Å, 57% identity), reduced *XenA* (r.m.s.d. 1.4 Å, 45% identity), trimethylamine dehydrogenase (r.m.s.d. 2.4 Å, 28% identity) and the putative NADH oxidoreductase from *S. aureus* (r.m.s.d. 2.1 Å, 25% identity). Both enzymes show good structural homology (r.m.s.d. roughly 1.5 Å) also with the classical *GsOYE* and *CtOYE* homologues despite their lower sequence identity (between 28% - 34%).

The TIM barrel structures of *BfOYE4* and *CaOYE* are virtually identical to *TsOYE* but small differences in the loops are present. Moreover, in both proteins the angle of interaction between monomers within the functional dimers is slightly different: one monomer is perfectly superimposable to *TsOYE* while the second one is slightly shifted (data not shown).

In general, *BfOYE4* has longer loops (circled in Fig. 106) due to its longer amino acidic sequence (439 vs 349 residues of *TsOYE*), as already mentioned. Another salient difference is its long N-terminus loop, a peculiar characteristic described, to our knowledge, for the first time in a thermophilic-like ene-reductase. This extra loop is very rich in proline residues (14 Pro representing 26.4% of the total composition) and basic amino acids. It is also involved in the formation of the dimeric interface leading to a high surface of contact between the monomers when compared to other thermophilic-like OYEs. The three-dimensional architecture of *CaOYE* is very similar to that of other thermophilic-like OYEs reported in literature (Fig. 106).

For both *BfOYE4* and *CaOYE* loop-β6 is very similar in orientation and length compared to the other thermophilic-like OYEs (Fig. 107) even though it differs quite significantly in composition. The orientation of this loop in thermophilic-like class is completely different compared to classical OYE homologues: while in classical homologues it protrudes inside the active site with its turn positioned above the FMN isoalloxazine ring, in the thermophilic-like homologues it is far from FMN, leaving the entire isoalloxazine ring expose to solvent and substrates. Loop β3 is 5-10 amino acids longer in *BfOYE4*, *CaOYE* and *XenA* compared to *TsOYE*, *YqjM* and *TOYE* (Fig. 107). This loop in the thermophilic-like OYEs closes the active site in a more preponderant manner compared to classical OYEs since the loop β6 has an open conformation thus compensating this effect. Finally, the thermophilic-like OYEs differ in the extra helices αFa and αFb involved in dimer formation (Fig. 107). The orientation and type of the amino acidic arm differs

quite significantly between the homologues: *BfOYE4* has a Tryptophan arm as *XenA* while all the others OYEs have an Arginine residue. Arg351 of *CaOYE* is positioned with a similar orientation as the Arg336 in *YqjM* while the Trp430 of *BfOYE4* differs in orientation compared to Trp358 in *XenA*.

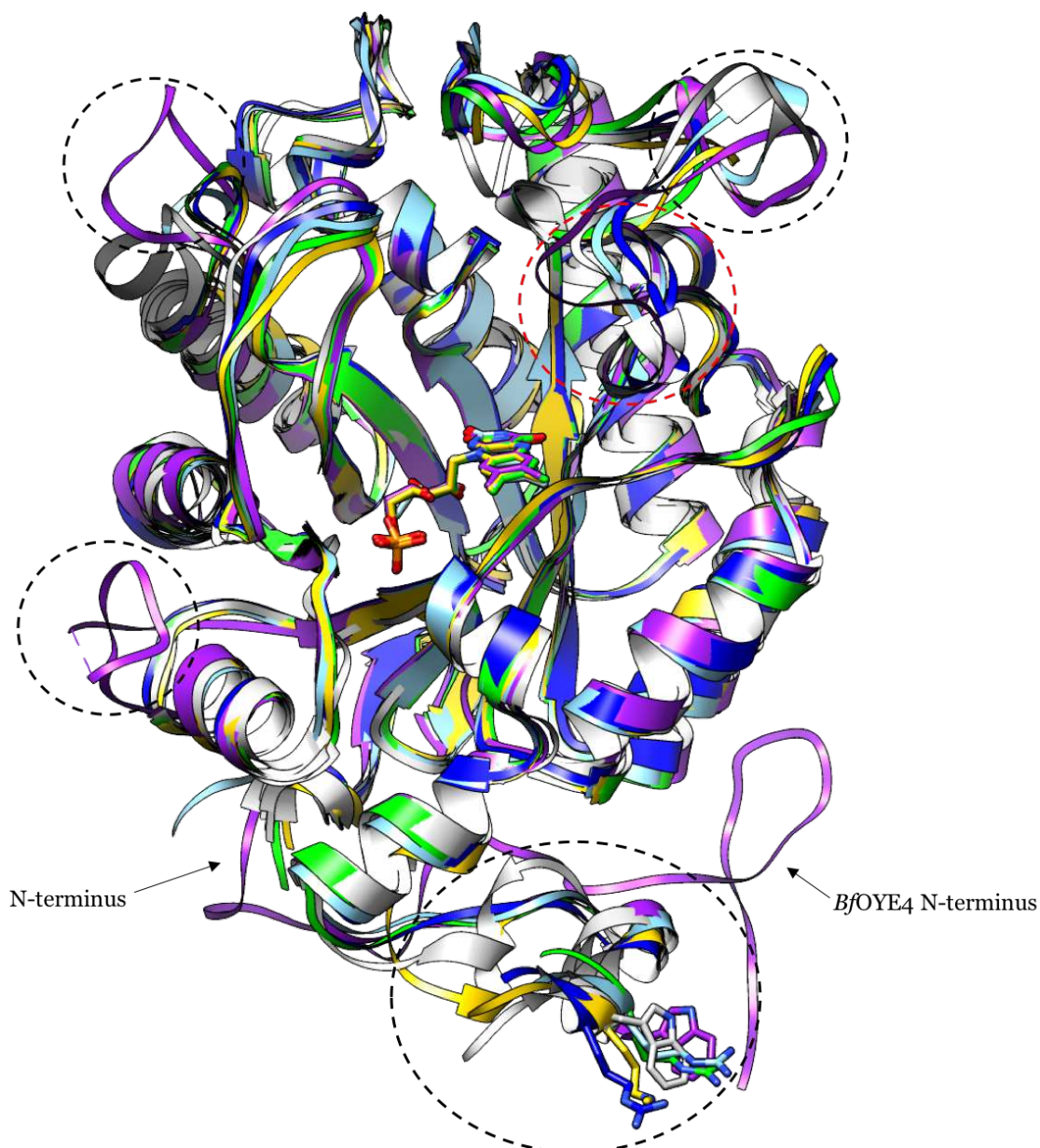


Figure 106. *BfOYE4* (purple) and *CaOYE* (light blue) superimposition with *XenA* (grey) (5lnj), *TsOYE* (blue) (3hf3), *YqjM* (green) (1z14) and *TOYE* (gold) (3kru). FMN and the Arg/Trp finger are shown as stick models.

TOYE and *XenA* have also been co-crystallized in the presence of NAD(P) H_4 analogue (3kru and 5cpm) [73, 78]. For both structures, a clear electronic density and similar position was observed for the nicotinamide moiety while the diphosphate moieties and the adenine were more flexible and disordered.

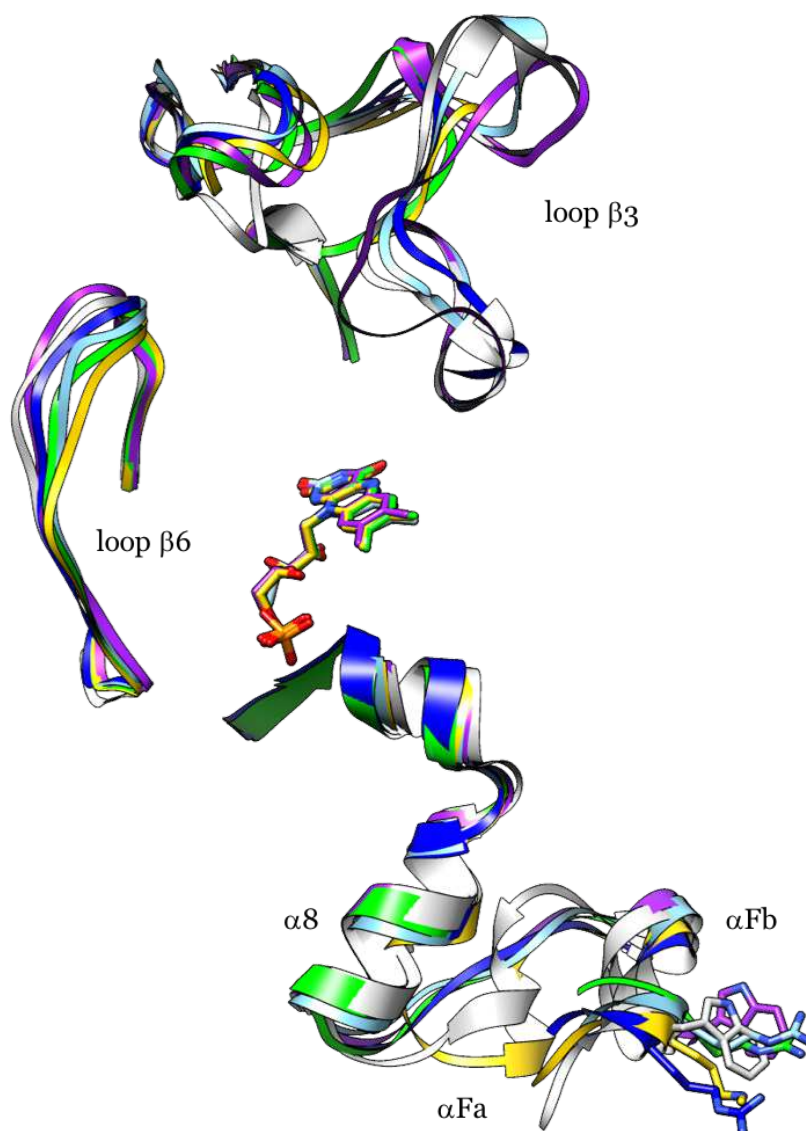


Figure 107. Close view of loop $\beta 6$, $\beta 3$ and C-terminus in *BfOYE4* (purple), *CaOYE* (light blue), *XenA* (grey), *TsOYE* (dark blue), *YqjM* (green) and *TOYE* (gold). FMN and the Arg/Trp finger are shown as stick models.

The nicotinamide moiety binds in a stacked arrangement above the isoalloxazine ring of the FMN cofactor interacting with the dyad His/His through its carbonyl oxygen (Fig. 108) [73, 78]. Moreover, in *TOYE* structure complexed with NADH_4 a rearrangement of the Arg333 finger was observed due to its interaction with the phosphate groups of the inhibitor [73]. *BfOYE4* showed a net preference for NADPH in the reduction of maleimide while no activity was detected with NADH with the same substrate (see Chapter 4). However, for the thermophilic-like OYEs the key residues involved in cofactor specificity have not yet been elucidated.

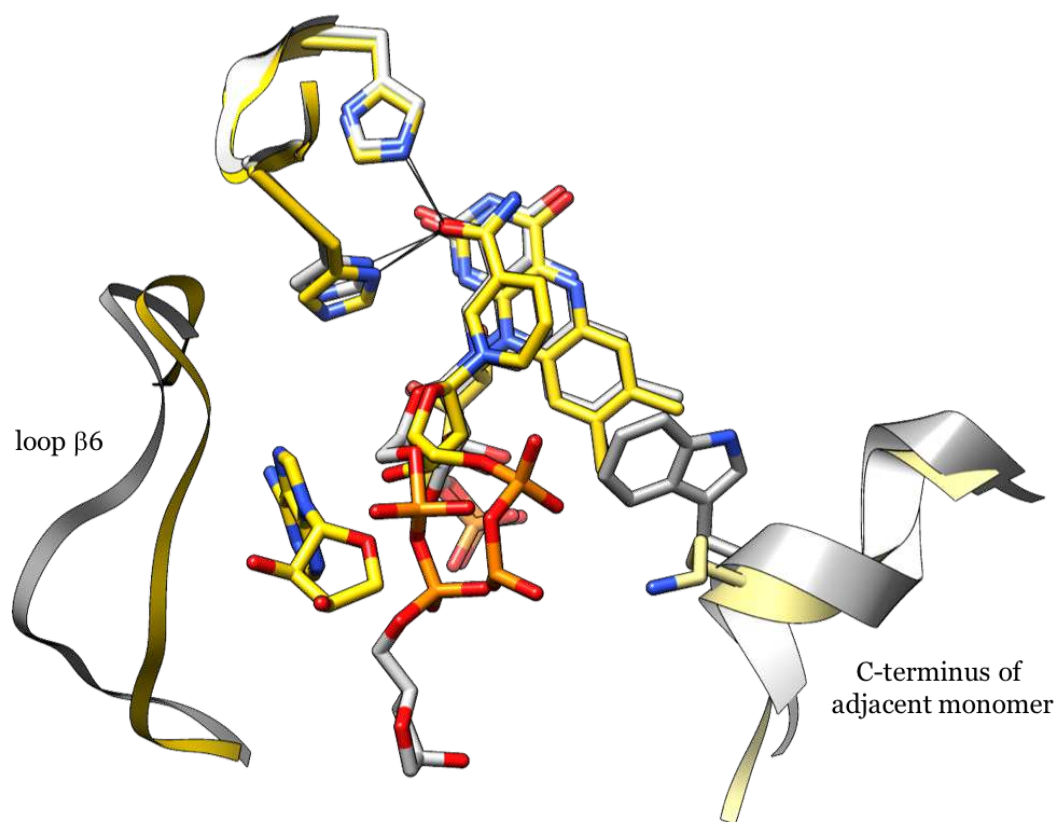


Figure 108. NAD(P)H₄ binding mode in TOYE (gold and kaki) (3kru) and XenA (light and dark grey) (5cpm).

5.4 OYE2 and OYE3 crystal structure

OYE2 and OYE3, together with OYE1, from *Saccharomyces pastorianus* were one of the first ene-reductases produced in recombinant form for biocatalysis applications. Their biocatalytic potential has been extensively investigated during the years [106] and some differences in stereoselectivity as well as substrate acceptance were detected [85, 115, 118, 232]. The crystal structure of OYE1 has been published by Fox and Karplus in 1994 [68] but the structures of OYE2 and OYE3 homologues, have not been investigated when this project was started. Very recently OYE3 crystal structure was deposited in the Protein Data Bank (pdb accession number 5v4v).

In collaboration with Dr. Mélanie Hall, from Graz University, we decided to crystallize the two proteins in order to try to get some insights in their three-dimensional structure that can be linked to their peculiar characteristics. Moreover, even though they have high homology and sequence identity (roughly 80%) they showed different activities and stereoselectivities in the isomerization of α -angelica lactone (for more details see Chapter 6).

After over-night incubation at 20 °C, some bunched microcrystals of the N-terminally His₆-tagged OYE2, grown in solution n. 96 of PACT screen (100 mM Bis-Tris propane pH 8.5 containing 20% w/v PEG 3350 and 200 mM sodium malonate dibasic monohydrate). These microcrystals have been crushed and used as seeding for further optimization using micro-seeding techniques. After six days of incubation, some crystals, still not suited for X-ray diffraction have grown in several conditions of Morpheus screen. The best hits were observed in Morpheus screen (n.90: 100 mM sodium HEPES - MOPS pH 7.5 containing 100 mM amino acids and 50% v/v of the precipitant mix composed by 40% v/v ethylene glycol and 20% w/v PEG 8000). These crystals were also broken and used as new seeding. After two days of incubation thicker yellow sticks were observed in solution n. 92 (100 mM sodium HEPES - MOPS pH 7.5 containing 100 mM amino acids and 50% v/v of the precipitant mix composed by 25% v/v MPD; 25% PEG 1000; 25% w/v PEG 3350) and n.96 (100 mM Tris - Bicine pH 8.5 containing 100 mM amino acids and 50% v/v of the precipitant mix composed by 25% v/v MPD; 25% PEG 1000; 25% w/v PEG 3350) of Morpheus screen and n.35 (100 mM sodium acetate, pH 4.5, containing 8 % w/v PEG 20000, 8 % v/v PEG 500 MME and 250 mM potassium bromide) of LMB screen (Fig. 110). However, OYE2

crystals were not so reproducible and moreover, they were not so stable during time in the precipitant solution becoming jelly and very fragile after less than one month incubation. Different attempts to optimize them were done but without succeeding.

Different crystals of the N-terminally His₆-tagged OYE3, some already optimal for X-ray diffraction experiment, appeared after over-night incubation in multiple conditions of LMB screen (LMB screen n. 36: 100 mM sodium acetate, pH 5.5, containing 8 % w/v PEG 20000, 8 % v/v PEG 500 MME and 200 mM potassium thiocyanate; and LMB screen n. 59: 100 mM sodium citrate, pH 5.2, containing 28 % w/v PEG 4000 and 200 mM ammonium acetate) (Fig. 109). Just fresh enzyme gives us the best crystals. After freezing the protein at -20 °C aggregates were formed (as seen by SEC chromatography) (data not shown) that precipitate immediately in the crystallization conditions.

OYE2 and OYE3 structures have been determined by Phaser software [221] using as template the model of OYE2 and OYE3 enzymes, built by Swiss model server (10ya structure was used as starting model by the server, <https://swissmodel.expasy.org>). Preliminary model of OYE2 includes four molecules per cell, 55 % of solvent and preliminary parameters Rfactor / Rfree of 0.197/0.253 (further details can be found in Table 21). Electron density maps and the protein model were clear and well defined from residue Pro2 to Trp397 with the last three residues not defined by the density. Two molecules per asymmetric unit and roughly 56 % of solvent define the crystal content of OYE3. Final model was traced and fully visible from Met1 to Val393 for chain A and Asp394 for chain B. Final parameters obtained for the best dataset (1.87 Å) reached Rfactor/Rfree of 0.20/0.23 (for further details see Table 21).

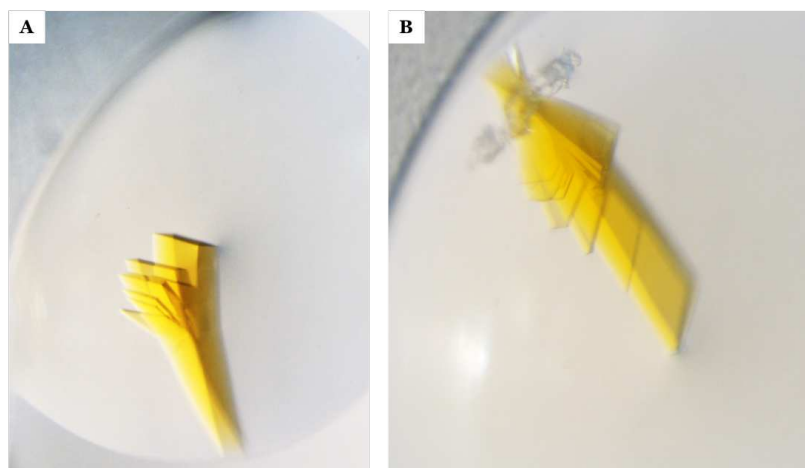


Figure 109. OYE3 crystals: crystals obtained in LMB (A) n.59; (B) n.36.

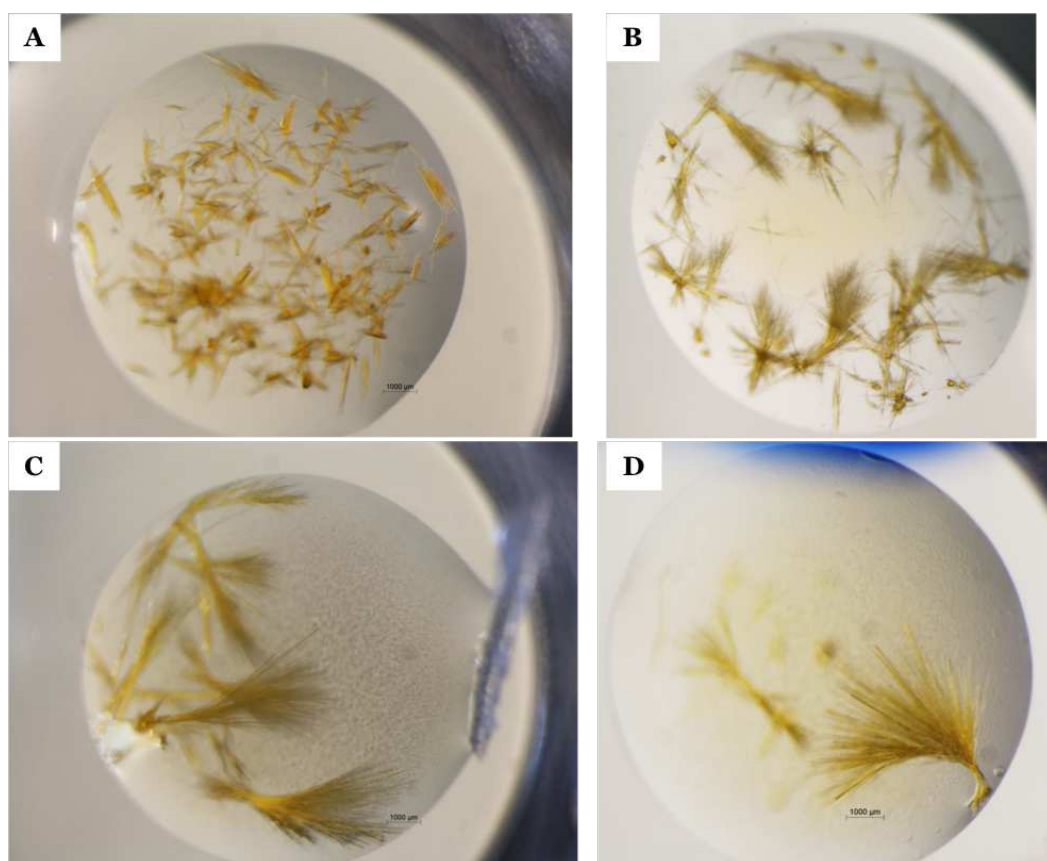


Figure 110. OYE2 crystals optimization: (A) first crystal hits obtained in Morpheus n.88 and (B) Morpheus n.80 after micro-seeding techniques with n.96 seed; optimized crystals obtained in (C) n.92 Morpheus and (D) n.35 LMB after seeding with crystals grown in n.90 Morpheus.

Table 21. X-ray Crystallographic data collection and refinement statistics.

	OYE2	OYE3
Data collection statistics		
Wavelength	0.97	1.073
Space group	P 21 21 21	P 21 21 21
Cell constants		
a, b, c (Å)	105.29 131.98 138	61.99 109.75 141.678
a, b, γ (°)	90 90 90	90 90 90
Resolution range for refinement (Å)	49.19 – 2.52 (2.58 – 2.52)	59.52 - 1.87 (1.94 - 1.87)
Total reflections	362146 (26506)	1050061 (98440)
Number of Unique Reflections	65535 (4564)	80627 (7977)
R_{merge}	0.088 (0.607)	0.14 (0.635)
$\langle I / \sigma(I) \rangle$	12.9 (2.6)	10.0 (3.2)
Completeness (%)	99.9 (100)	99.99 (99.90)
Multiplicity	5.5 (5.8)	13.0 (12.34)
Refinement statistics		
$R_{\text{work}} / R_{\text{free}}$	0.19/0.25	0.20/0.23
RMSD bond lengths (Å)	0.008	0.007
RMSD bond angles (°)	1.36	0.90
Main chain B factor	41.2	28.94
Ligands B factor	34.3	23.90
Water molecules B factor	29.0	34.86
Ramachandran plot (%)		
Most favoured	96.44	97.32
Generously allowed	3.12	2.68
Outliers	0.45	0.00

5.4.1 Structural analysis of OYE2 and OYE3

Both enzymes assemble as an eight stranded $\alpha 8/\beta 8$ barrel covered at the N-terminus by an α, β -hairpin lid, as reported for all OYEs. Moreover, these proteins have high homology and sequence identity (roughly 80%-90%) between them and also with OYE1 (Fig. 111).

OYE2 and OYE3 assemble as a possible functional dimer in the crystal packing with a two-fold axes symmetry as already reported for OYE1 showing a longest axis of 88 Å and a mid section of 59 Å (Fig. 112). The dimer interface area in OYE2 is about 826 Å² and involves 22 residues of helices 4, 5 and 6, that form 11 direct hydrogen bonds and 89 hydrophobic contacts. In OYE3 the area interface is also about 823 Å² and it involves 20 residues which form 8 hydrogen bonds and 79 hydrophobic contacts. In the deposited OYE3 structure (pdb 5v4p) the surface interface is similar to that of the other structures but extra bonds are involved: 2 salt bridges, 9 hydrogen bonds and 90 hydrophobic interactions participate in the formation of the dimerization interface.

However, from SEC analysis both OYE2 and OYE3 seem to be monomeric in solution (data not shown) and also from PISA analysis no quaternary assembly was detected.

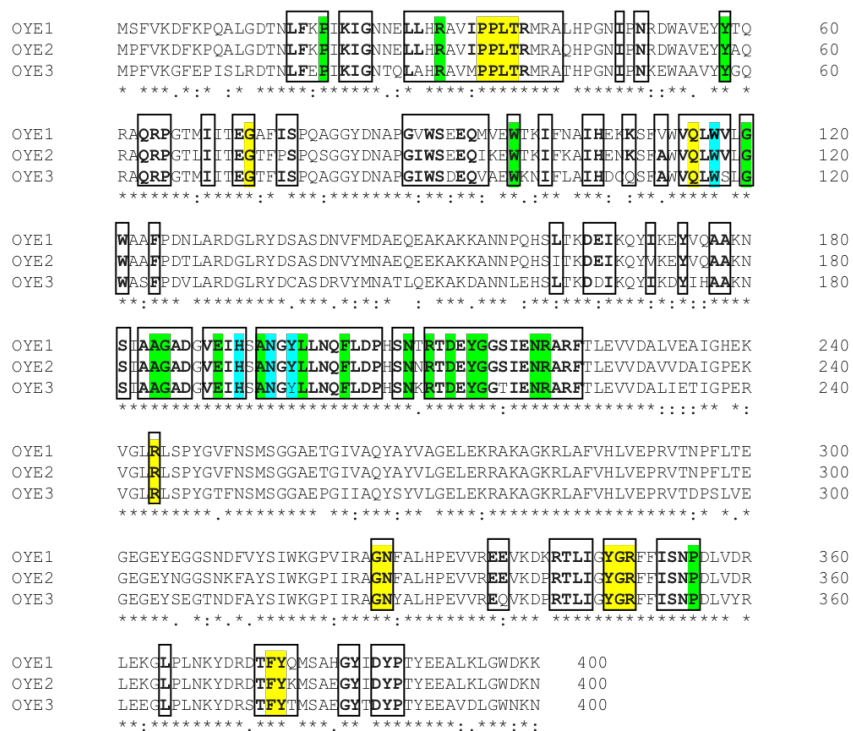


Figure 111. Sequence alignment of OYEs from *Saccharomyces pastorianus*: OYE1 (Q02899.3), OYE2 (Q03558.3) and OYE3 (P41816.2). The boxes shaded in green show the conserved residues, and the unshaded boxes indicate similar residues. Boxes highlighted in cyan and yellow show the sequence conservation of active site residues and FMN binding, respectively.

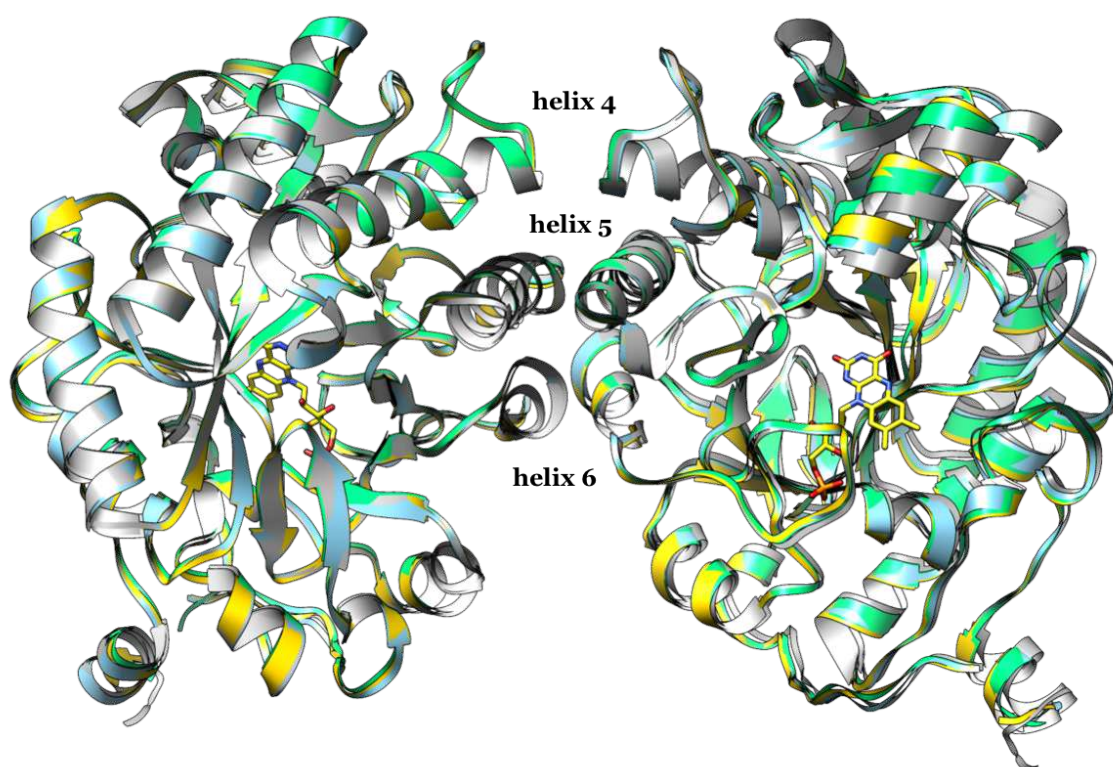


Figure 112. Functional dimer of OYE1 (grey), OYE2 (cyan), OYE3 (green), deposited OYE3 (yellow; 5v4p).

5.4.1.1 OYE2 active site

FMN is non-covalently bound at the bottom of the TIM barrel being mostly buried by the protein environment. Its *si*-side is exposed to the solvent and substrates forming the bottom of the active site pocket while its *re*-side is facing the protein and is completely hidden and not accessible. As shown in Figure 113 the N3 and O2 atoms of the flavin pyrimidine ring are both interacting with Gln115 while its O2 is also interacting with Arg244. N1 is also interacting with Arg244 while O4 of the flavin is in hydrogen bond contact with the OH of the side chain of Thr38. Moreover, the N5 of the flavin is bound to the Thr38, a conserved residue involved in the modulation of FMN redox potential in classical OYEs. The dimethylbenzene moiety of the flavin isoalloxazine ring is also stabilized by different hydrophobic interactions with residues Pro296 and Phe375. The ribityl chain of the flavin forms a complex hydrogen network with Arg244 and different hydrophobic contacts with Pro35 and Gly325. The negative charge of FMN phosphate group is stabilized by the positive charge of Arg349 and the main chain atoms of Gly348 and Asn326 are involved in some polar interactions with the phosphate group. Moreover, Tyr347 is in hydrophobic contact with the phosphate group.

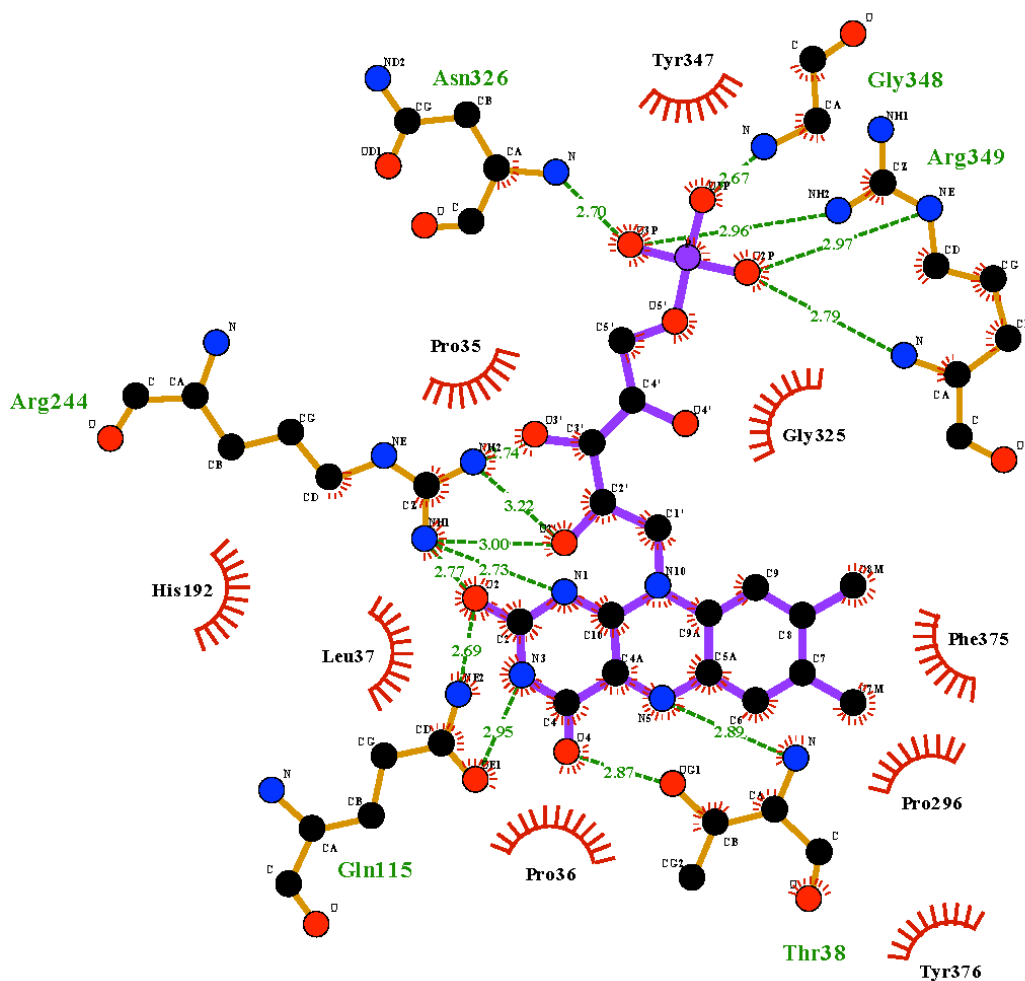


Figure 113. Schematic illustration of the interaction of FMN with active site residues of OYE2. The thin green dotted lines illustrate hydrogen bonds.

The substrate binding site of OYE2 contains the typical Histidine-Asparagine pair (His192 and Asn195) involved in the binding and correct orientation of the substrate through hydrogen bonding with the electron-withdrawing group of the substrate and also the proton donor Tyr197, highly conserved between OYE homologues (Fig. 114A). The difference electronic density map $F_o - F_c$ shows an elongated organic molecule, possibly glycerol, that was used as cryoprotectant, bound above the isoalloxazine ring of FMN (Fig. 114B). In the complex with glycerol, two different hydroxyl groups were in hydrogen bonding with the side chain of His192 and Asn195 while another hydroxyl group formed a hydrogen bond with Tyr376, mimicking the interactions of the substrate inside the active site (Fig. 114A).

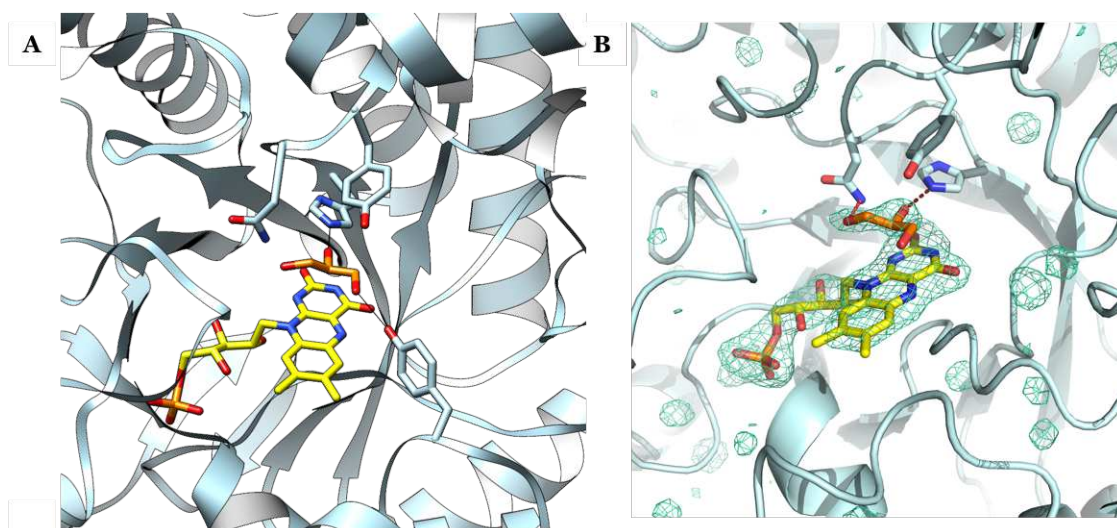


Figure 114. OYE2 active site (A) cartoon representation of conserved residues and their interaction with glycerol through hydrogen bond; (B) difference electronic density map $F_o - F_c$ contoured at 3σ .

5.4.1.2 Active site of OYE3

The FMN is non-covalently bound to the protein backbone through a network of different interactions. As shown in Figure 115 the N3 and O2 atoms of the flavin pyrimidine ring are both interacting with Gln115 while its O2 is also interacting with Arg244. N1 is interacting as well with Arg244 while O4 of the flavin is in hydrogen bond contact with the nitrogen atom of Gly73 and with the OH of the side chain of Thr38. Moreover, the N5 of the flavin is bound to the Thr38, a conserved residue involved in the modulation of FMN redox potential in classical OYEs. The dimethylbenzene moiety of the flavin isoalloxazine ring is stabilized by different hydrophobic interactions with residues Leu37, Pro296 and Phe375. The ribityl chain of the flavin forms a complex hydrogen network with Arg244 by and different hydrophobic contacts with Pro35 and Pro36. Like in other OYE enzymes, the negative charge of FMN phosphate group is stabilized by the positive charge of Arg349 and the main chain atoms of Gly348 and Asn326 are involved in some polar interactions with the phosphate group.

The substrate binding site, located above the *si*-side of the isoalloxazine ring, is similar to other classical ERs. OYE3 contains the typical Histidine-Asparagine pair (His192 and Asn195) involved in the binding and correct orientation of the substrate through hydrogen bonding with the electron-withdrawing group of the substrate and also the conserved proton donor Tyr197 is found in the active site (Fig. 116). A small organic molecule, possibly an acetate, coming from the crystallization condition, was observed from the difference electronic density

map $F_o - F_c$ (Fig. 116B). In the complex with acetate, one oxygen of the carboxylic group was in hydrogen bonding with the side chains of the His192 and Asn195 pair, mimicking the interactions of the substrate inside the active site (Fig. 116).

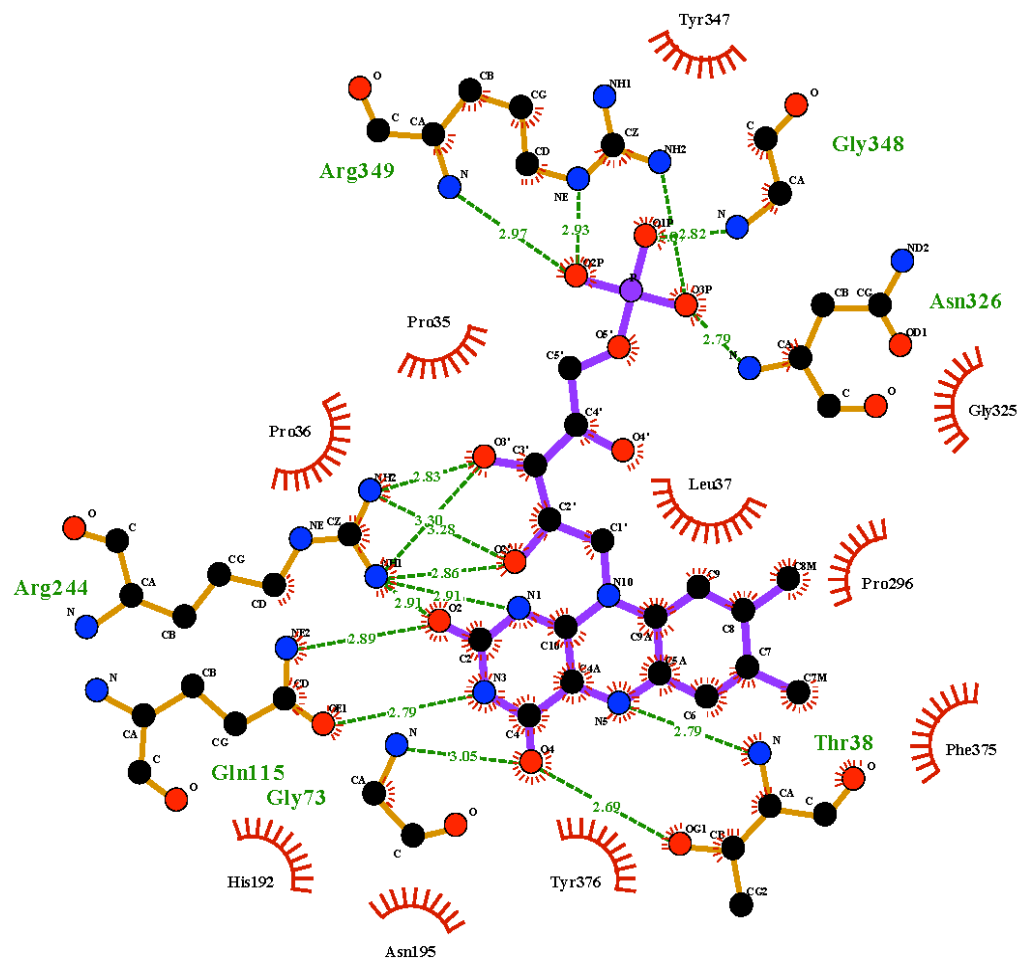


Figure 115. Schematic illustration of the interaction of FMN with active site residues of OYE3. The thin green dotted lines illustrate hydrogen bonds.

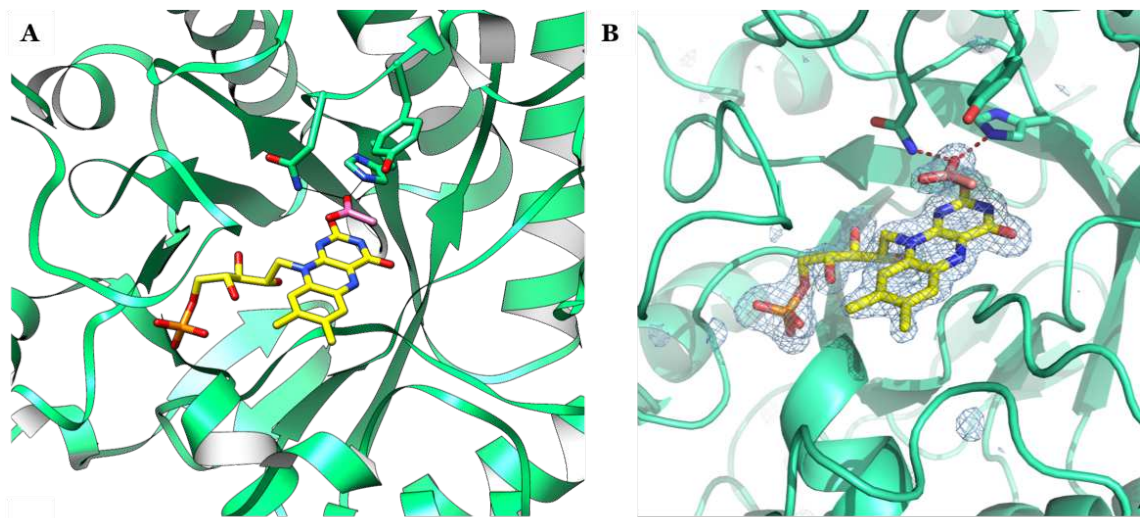


Figure 116. OYE3 active site (A) cartoon representation of conserved residues and their interaction with acetate through hydrogen bond; (B) difference electronic density map $F_o - F_c$ contoured at 3.7σ .

5.4.2 Overall OYE2 and OYE3 structural comparison

OYE2 and OYE3 are close homologues of OYE1 from *Sacharomyces carlsbergensis* (OYE1) (10ya, [68]) with a root-mean-square-deviation (r.m.s.d.) of 0.31 Å (92% identity) and 0.381 Å (80% identity), respectively.

The TIM barrel structures are identical but differ slightly in the architecture and the composition of loop-β3, the one involved in the shaping of the active site entrance (Fig. 117). In OYE1 this loop is composed by two α-helices and two β-sheets but in OYE2 structure just the two α-helices are present while the β-sheets are substituted by loops (Fig. 117). In OYE3 the two β-sheets are present in contrast with OYE2, but one α-helix, due to its different amino acidic composition is not perfectly superimposable to OYE1. In fact, in this α-helix in OYE1 and OYE2 more charged amino acids are present (5 for OYE1 and 6 for OYE2) compared to OYE3 (4 charged residues) (Fig. 111, residues 146-154). Another interesting peculiarity of OYE2 and OYE3 compared to OYE1 is that β-sheet 1 and 2 are shorter (Fig. 117).

Moreover, the entrance of the active sites defined by the bounding residues, reported by Oberdorfer *et al.* [103] is slightly different due to the different orientation of residue Tyr376 (Tyr375 in OYE1): in OYE1 and OYE2 a distance of 8.5 Å and 7.9 Å was detected while for OYE3 a wider access of 9.5 Å has been measured. In OYE3 the residue Tyr376 is parallel to the isoalloxazine moiety of FMN while in OYE2 is perpendicular compared to OYE1 in which an intermediate orientation is assumed (Fig.118).

Moreover, other biochemical differences could explain their different behavior in catalysis: OYE1 and OYE2 have a theoretical isoelectric point (pI) of roughly 6.0 while OYE3 is slightly more acidic with a pI of 5.4 (theoretical pI calculated with ProtParam tool, <https://web.expasy.org/protparam/>).

Finally, all these three homologues isolated from the yeast *S. pastorianus*, have also, as already discussed for the fungal *BfOYE4*, a longer N-terminus (roughly 15 amino acids) compared to other OYEs isolated from other organisms such as bacteria. This N-terminal loop is positioned near the C-terminus of the proteins (Fig. 117), as reported also for *BfOYE4*.

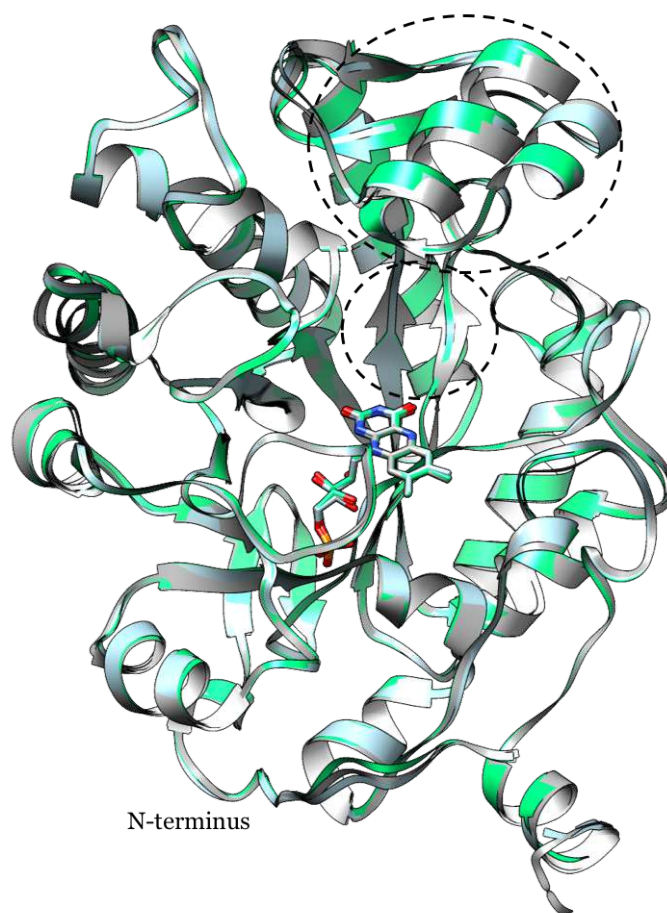


Figure 117. Structural comparison between OYE1 (grey), OYE2 (light blue) and OYE3 (green). The main differences in structure are circled. FMN cofactor is shown as stick model.

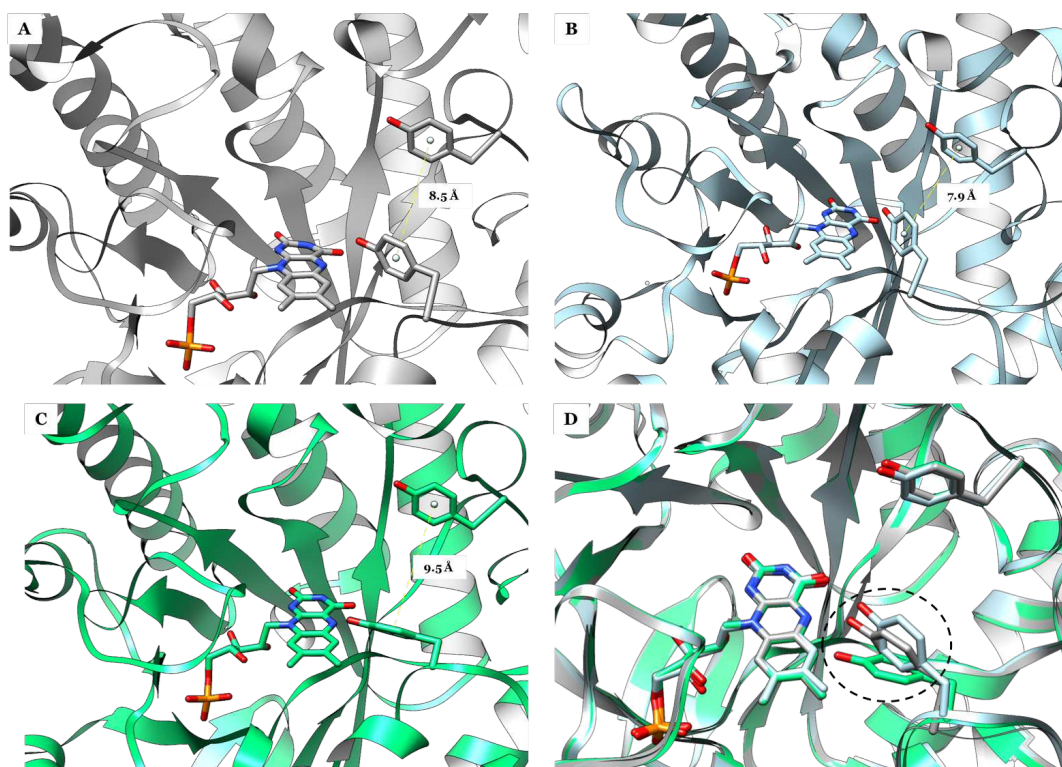


Figure 118. Distances between the bounding residues Tyr83 (in OYE1 Tyr82) and Tyr376 (in OYE1 Tyr375) in (A) OYE1, (B) OYE2 and (C) OYE3. (D) Superimposition of OYE1 (grey), OYE2 (light blue) and OYE3 (green) showing the different orientations of Tyr376 (in OYE1 Tyr375).

Concluding remarks

In this Chapter, we discussed the crystal structures of four of the newly identified ene-reductases belonging either to the classical OYEs subfamily, *i.e.* *GsOYE* and *CtOYE*, or to the thermophilic-like subclass, *i.e.* *CaOYE* and *BfOYE4*. Moreover, the three-dimensional structure of *GsOYE* in complex with the inhibitor pHBA and the substrate 2-methyl-cyclopenten-1-one has also been obtained and the key interactions involved in substrate binding and stereoselectivity were also reported and discussed. Finally, the crystal structure of *OYE2* and *OYE3* were obtained in collaboration with Dr. Mélanie Hall from Graz University. Their structural peculiarities were also described and discussed.

6. Hydride-independent asymmetric isomerization of non-activated C=C-bonds mediated by OYEs

Abstract:

Ene-reductases (ERs) from the Old Yellow Enzyme (OYE) family are versatile flavin-dependent catalysts that have been applied to the asymmetric *trans*-reduction of a broad range of activated C=C-bonds at the expense of NAD(P)H cofactor [35]. Alternative catalytic activities of OYE homologues were also observed [135] such as the hydride-independent isomerization of non-activated C=C-bonds [130].

In this Chapter, we focused on the elucidation of the catalytic mechanism of the isomerization reaction through site-specific mutagenesis, reaction engineering (*e.g.* reaction time and pH) and crystallographic tools. Identification of two stereocomplementary enzymes from the classical and thermophilic-like subclass of OYE homologues revealed likely relevant protein characteristics.

The crystal structure of novel ERs studied in this work was solved with good to moderate resolution. In order to understand the observed stereoselectivity and the key interactions with the substrate, attempts to soak crystals with the substrate α -angelica lactone are also reported.

The design of a two-step enzymatic cascade combining ene-reductase catalyzed stereoselective isomerization of α -angelica lactone to β -angelica lactone [233], with subsequent reduction by a suitable OYE homologue of the enantioenriched β -isomer to (*R*)- γ -valerolactone is also reported.

Angelica lactones (ALs) are usually obtained through dehydration of levulinic acid, which is derived from cellulosic feedstocks and thus represents an important bio-based platform chemical. ALs (Fig. 119) are versatile building blocks in organic synthesis and moreover, they can be further reduced to γ -valerolactone (GVL) (Fig. 119), another platform chemical with broad industrial applications, such as solvent production, fuel additive, precursor of bio-based polymers, building block of natural products and fragrance/flavoring agent [134].

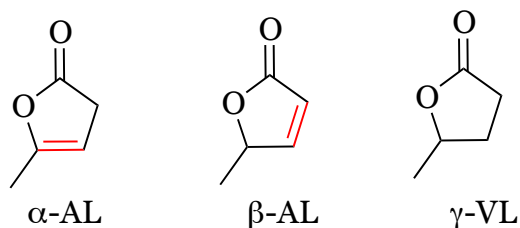


Figure 119. Chemical structure of ALs and GVL.

Different chemical methods for the isomerization of α -angelica lactone (α -AL) to β -angelica lactone (β -AL) and subsequent reduction to γ -valerolactone have been reported in literature. However, most of these approaches require strong acidic and basic catalysts or other harsh reaction conditions producing low yields and racemic products. Recently, the synthesis of enantiomerically enriched β -AL was reported by isomerization of α -AL to β -AL through proton-transfer catalysis in presence of cinchona alkaloid as catalyst. By using 10 mol % of catalyst in dichloromethane at $-20\text{ }^{\circ}\text{C}$ for 60 h 63% yield with 90% ee was obtained [234].

Recently, a biocatalytic alternative was reported by Hall and co-workers [130] using OYE2 ene-reductase for the hydride-independent isomerization of α -AL to β -AL and the subsequent reduction of the intermediate to γ -valerolactone in the presence of NADH (Fig. 120). The isomerization of α -angelica lactone was very fast furnishing 6.3 mM of racemic β -isomer in 15 min at $30\text{ }^{\circ}\text{C}$ in aqueous buffer. Moreover, the reaction was run on semi-preparative scale at 25 mM substrate concentration allowing the isolation of 18 mg of product (32% overall yield and 98% purity) after 45 min of reaction, thus demonstrating the applicability of this process for the valorization of renewable chemicals. However, the product obtained in this case was racemic. As already mentioned in the Introduction, the mechanism of this intriguing and new ene-reductase activity was not fully elucidated although an acid-base mechanism was postulated.

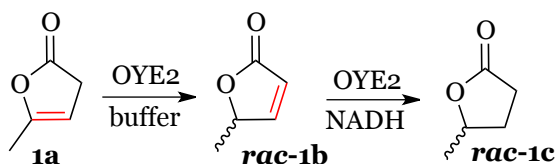


Figure 120. Hydride-independent α -angelica isomerization and subsequent reduction to γ -valerolactone [130].

During my PhD and my stay in Graz, we decided to investigate if other ene-reductases, already reported in literature and the new ones reported in this thesis, were able to perform the isomerization reaction. Focus was also put on elucidating the mechanism of the reaction.

6.1 Stereoselective isomerization of α -AL to β -AL

Different OYE homologues were tested for their ability to isomerize the non-activated C=C-bond of α -AL. The results are reported in Table 22. Almost all the enzymes tested were able to some extent to perform the isomerization reaction and to our surprise in a stereoselective fashion. For OYE2 and OYE1, good conversions were obtained (90 % conversion) but the product was racemic, as already reported by Hall *et al.* [130]. OPR3 was poorly active in the isomerization reaction while for OYE3 and FOYE good conversions and also stereoselectivities were obtained producing both enantiomers with moderate ee values.

Table 22. Screening of new ene-reductases and known ene-reductases in the isomerization of α -angelica lactone to β -angelica lactone (**1a** to **1b**).

	Enzyme	OYE subclass	Reaction time	Conv. %	ee (%)
	GsOYE#	I	ON	59	90 (<i>R</i>)
	CtOYE#	I	ON	20	15 (<i>R</i>)
	CaOYE*	II	5h	7	43 (<i>S</i>)
	BfOYE1	I	ON	55	93 (<i>R</i>)
	BfOYE4	II	ON	29	>99 (<i>S</i>)
	AnOYE2	I	6h	3	-
	AnOYE8*	II	5h	20	88 (<i>S</i>)
	OYE2	I	ON	91	<i>rac</i>
	OYE1	I	ON	91	<i>rac</i>
	OYE3	I	ON	90	57 (<i>R</i>)
	FOYE	II	ON	40	50 (<i>S</i>)
	OPR3	I	ON	16	7 (<i>S</i>)

10 mM **1a**, 200 μ g/mL/* 400 μ g/mL enzyme, ON incubation at 30°C, 50 mM Tris pH 7.0. Conv.% is apparent conversion. Class I = classical OYEs, Class II= thermophilic-like OYEs.

European Patent Application number EP17189155 [233]

The enzymes discovered and produced in this thesis were also active in the isomerization and some of them showed excellent stereoselectivities: GsOYE and BfOYE1 furnished exclusively the *R*-enantiomer (>90% ee and 50% conv.), while BfOYE4 and AnOYE8 produced the *S*-enantiomer (>99 % and 88% ee,

respectively) even though with lower conversion (29 and 20% conv). *CtOYE* and *AnOYE2* were poorly active and/or stereoselective in the isomerization while *CaOYE* showed a modest activity (7% conv.) but good stereoselectivity (43% ee). Interestingly, the stereoselectivity seemed to be related to the different sub-family of OYEs: classical OYEs furnished exclusively the *R*-enantiomer while ERs belonging to the thermophilic-like sub-class produced exclusively the *S*-enantiomer.

6.2 Role of pH in the isomerization reaction

The mechanism of action was not elucidated but an acid-base mechanism has been hypothesized [130], so we decided to investigate the influence of the pH in the catalysis. A screening of different pH values and different reaction times were investigated and the results are shown in Table 22. The isomerization reaction appeared faster at basic pH values compared to acidic pH at which just poor conversion was reached. However, *OYE2* was the only enzyme showing a good conversion also at pH 6.0 (77% conv.) and it was able to maintain its maximum conversion at all the other pH values tested (pH between 7.0 -9.0 almost 90% conv.). For all the other OYE homologues tested, basic pH values led to increased conversion levels (almost 90% conversion). However, at basic pH values, a strong decrease in the product enantiopurity was observed with *GsOYE*, for which 16% ee (*R*) was registered at pH 9.0 compared to 84% ee (*R*) at pH 7.0. Importantly, substrate hydrolysis was observed and was more pronounced at basic pH (data not shown). Surprisingly, in the presence of *BfOYE4*, even after over-night incubation, ee values remained stable.

Two different experiments have been set-up in order to understand whether the racemization of **1b** was spontaneous or enzyme-mediated. First of all, the standard isomerization reaction with *GsOYE* was run at pH 7.0 over-night at 30 °C in order to produce (*R*)-**1b** enantiomer from **1a**. Once (*R*)-**1b** was obtained (84% conv. and 90% ee), the pH of the reaction was adjusted to 8.0 and 9.0 and the reaction was further incubated for 5 h at 30 °C. The results of this experiment are reported in Table 24. After the incubation at basic pH, a decrease in the enantiomeric excess of the product was observed, leading to racemic product at pH 9.0. However, also the total amount (peak area) of the substrate and the product were lower compared to pH 7.0 suggesting a simultaneous hydrolysis/consumption of substrate and product. Since this racemization was not observed with *BfOYE4* even after over-night incubation at pH 9.0 (Table 22),

we suspected that GsOYE enzyme, somehow, was involved in the racemization. We performed again the isomerization reaction in standard conditions (pH 7.0, ON incubation at 30 °C) but, this time, before adjusting the pH to 9.0, we denatured the enzyme by heat and then incubated the reaction for 30 minutes at pH 9.0. In this experiment, no major decrease in ee value was detected (78% conv., 82% ee), indicating the involvement of GsOYE in the apparent racemization. We hypothesized a reversible isomerization, as reported also for the enantioselective chemical isomerization [234]. More in detail, it seems that GsOYE is able to isomerize back preferentially (*R*)-**1b** to **1a**, at basic pH, which is not stable under these conditions and is thus hydrolyzed, leading to reduced ee value of **1b** and an apparent racemization of the β - isomer.

Table 23. pH influence on conversion and stereoselectivity in the isomerization of **1a** to **1b**.

Enzyme	pH	Reaction time	Conv. %	ee (%)
GsOYE	6	ON	5	>99 (<i>R</i>)
	7	ON	41	84 (<i>R</i>)
	8	ON	89	77 (<i>R</i>)
	9	ON	90	16 (<i>R</i>)
CaOYE	7	5 h	0	-
	8	5 h	32	44 (<i>S</i>)
	9	5 h	83	67 (<i>S</i>)
BfOYE4	6	ON	2	>99 (<i>S</i>)
	7	5 h	12	>99 (<i>S</i>)
		ON	31	98 (<i>S</i>)
	8	5 h	78	>99 (<i>S</i>)
		ON	92	>99 (<i>S</i>)
9	5 h	92	>99 (<i>S</i>)	
AnOYE8	9	ON	96	>99 (<i>S</i>)
		5 h	6	>99 (<i>S</i>)
		5 h	65	88 (<i>S</i>)
OYE2	8	5 h	89	90 (<i>S</i>)
	6	ON	77	<i>rac</i>
		ON	92	<i>rac</i>
FOYE	8	ON	90	<i>rac</i>
	9	ON	88	<i>rac</i>
		5 h	17	53 (<i>S</i>)
		5 h	85	49 (<i>S</i>)
9	5 h	90	46 (<i>S</i>)	

10 mM **1a**, 200 μ g/mL enzyme, ON or 5 h incubation at 30 °C, 50 mM Tris pH 6.0-9.0; Conv.%: based on substrate consumption.

Table 24. Role of the pH in the racemization of **1b**.

pH	Conv. %	ee (%)
7	84	90 (<i>R</i>)
8	> 99	60 (<i>R</i>)
9	> 99	<i>rac</i>

10 mM **1a**, 200 μ g/mL GsOYE incubated ON at 30 °C in 50 mM Tris pH 7.0. Once the isomerization reaction was almost complete, the pH was adjusted to pH 8.0 and 9.0 and the reaction was further incubated for 5 h; Conv.%: based on substrate consumption.

6.3 Understanding the mechanism of the isomerization reaction

We focused on the elucidation of the catalytic mechanism of the asymmetric isomerization reaction through site-specific mutagenesis, crystallographic tools and reaction engineering (*e.g.* reaction time and pH).

6.3.1 Mutagenesis

Based on the crystal structure of *GsOYE* and *BfOYE4* (reported in Chapter 5), different positions have been identified for their possible involvement in the catalysis (Fig. 121). Corresponding amino acids have been mutated and these variants were investigated for their ability to catalyze the isomerization reaction. The results are shown in Table 25 together with few mutants of *OYE2* that were already produced in Graz [130].

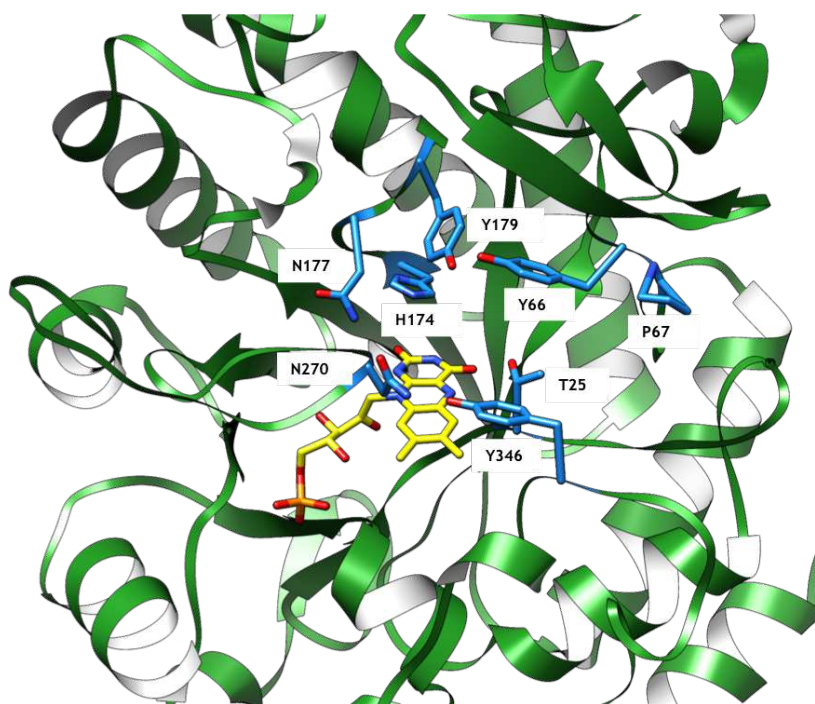


Figure 121. *GsOYE* active site showing the residues for the mutagenesis study.

For *GsOYE*, different conserved residues have been mutated, either those involved in the classical C=C-bond reduction (binding residues H174 and N177 and proton donor Y179) or known residues involved in the shaping of the active site (Y66 and Y346) and in the modulation of redox potential of FMN N5 (T25). It has been reported that the presence of the residue P75 in OPR3 (which corresponds to P67 in *GsOYE*) compared to K79 in OPR1 creates a smaller active site cavity with a flat bottom that forces the substrate 1-nitro-2-phenylpropene to bind in a different mode, leading to an inversion of the stereoselectivity in the reduction reaction [82]. Thus, this position was also targeted as it could influence

the shape of the active site and as a consequence the substrate binding mode. Finally, the residue N270 on loop- β 6 was mutated as it protrudes inside the active site and, by forming a hydrogen bond with Y346, closes the active site preventing the FMN exposure to the substrate. The results of the mutagenesis study are reported in Table 25. From these data, it appeared clear that the residues H174 and N177 are still involved in the binding and correct orientation of the substrate. With the single mutant H174A, a residual activity (8% conv.) was still detected while in the double mutant H174A/N177A the activity was almost completely lost, most likely due to the absence of binding. These data were also confirmed by the mutant H192A in OYE2 that also showed half of its activity, probably because the substrate could still interact with the second binding residue N195. Moreover, the mutation of the proton donor in the reduction reaction (Y179 in GsOYE and Y198 in OYE2) lead to almost complete loss of activity of both proteins suggesting that these residues might act as proton donor also in the isomerization reaction. These three residues are highly conserved between OYEs and also their location in the active site and their orientation is maintained for all ERs (Fig. 122 A). Furthermore, in GsOYE also the mutation of residue Y66 had a dramatic effect on the activity. The importance of this position is revealed by comparing the activity of other wt ERs: AnOYE2 and OPR3 that were poorly active with α -AL have a Valine and a Phenylalanine residue, respectively, in this position.

Table 25. Mutants activity in the isomerization reaction.

Enzyme	Mutant	Reaction time	Conv. %	ee (%)
GsOYE	wt	ON	59	90 (R)
	P67K	4 h	48	89 (R)
	P67A	ON	82	78 (R)
	N270R	5 h	35	70 (R)
	N270A	ON	11	58 (R)
	Y346F	5 h	21	73 (R)
	Y346K	ON	62	60 (R)
	Y66F	5 h	66	73 (R)
	Y66A	ON	N.D.	-
	Y179F	ON	N.D.	-
	H174A	ON	N.D.	-
	H174A/N177A	ON	8	46 (R)
	T25C	ON	2	-
OYE2	wt	15 min	71	81 (R)
	H192A	ON	71	81 (R)
	Y198A	15 min	85	rac
	Y198F	2 h	40	rac
BfOYE4 ^a	wt	ON	N.D.	-
	C76A	ON	15	11 (S)
	C76T	5 h	53*	99 (S)
	Y78F	5 h	43*	93 (S)
		5 h	57	> 99 (S)
		5 h	41	25 (S)

10 mM **1a**, 200 μ g/mL enzyme, ON incubation at 30 °C, 50 mM Tris pH 7.0 (^a: pH 8.0). Conv.% is apparent conversion. * conv.% based on calibration curve of product. N.D. not detected.

Looking at the crystal structure of classical OYEs (Fig. 122 A), it appears that this position differs quite significantly in the orientation of the Tyrosine residue and this could explain the different activities and stereoselectivities observed with the different homologues. Y66, as a residue close to Y179, may be indirectly involved in the protonation step (such as re-protonation of Y179). The mutant Y78F in *BfOYE4*, interestingly maintained its activity but showed lower stereoselectivity, thereby indicating that Y78 might be the selective proton donor of the isomerization reaction. Compared to Y66 of *GsOYE*, the residue Y78 of *BfOYE4* is positioned in the same region of the active site but the ring of Y66 is parallel and above the plane of the flavin while the ring of Y78 in *BfOYE4* but also in *CaOYE* is perpendicular and on the same plane as the flavin (Fig. 122 B). This Tyrosine residue (Y78 *BfOYE4* numbering) is highly conserved in the thermophilic-like ERs.

The residue T25 of *GsOYE* was mutated into a Cysteine and the corresponding C76 of *BfOYE4* was mutated into a Threonine in order to get insights into this position that is highly conserved in classical and thermophilic-like OYEs (involvement in FMN modulation of the redox potential). Moreover, the Cysteine residues of thermophilic-like homologues could act as a base in the deprotonation step. For *GsOYE* the introduction of the Cysteine residue enhanced the conversion (71%) but lowered slightly the stereoselectivity (81% ee) while for *BfOYE4* no detrimental effects were observed neither in conversion nor in stereoselectivity, suggesting that these residues do not play a role in the catalysis. The mutation of the residue P67 in Lysine boosted the conversion (85% conv. vs 59%) but reduced slightly the stereoselectivity (83% ee). This enhancement in the conversion could be explained by the fact that the introduction of a long charged chain into the active site can shape differently the active site cavity, as already reported for OPR1 and OPR3 [82], thus promoting the binding of the substrate in a favorable conformation for the catalysis. In the case of P67A, the conversion is similar to that of the P67K mutant but the ee is lower, maybe because the short chain of Alanine and the loss of the rigidity associated to the Proline can favor different binding modes.

Another region that differs quite significantly between all the classical ERs analyzed but also between the two different subclasses is loop- β 6. As already discussed in Chapter 5, this loop protrudes into the active site of classical OYEs, acting as a cap that covers the surface of exposure of FMN cofactor to the solvent.

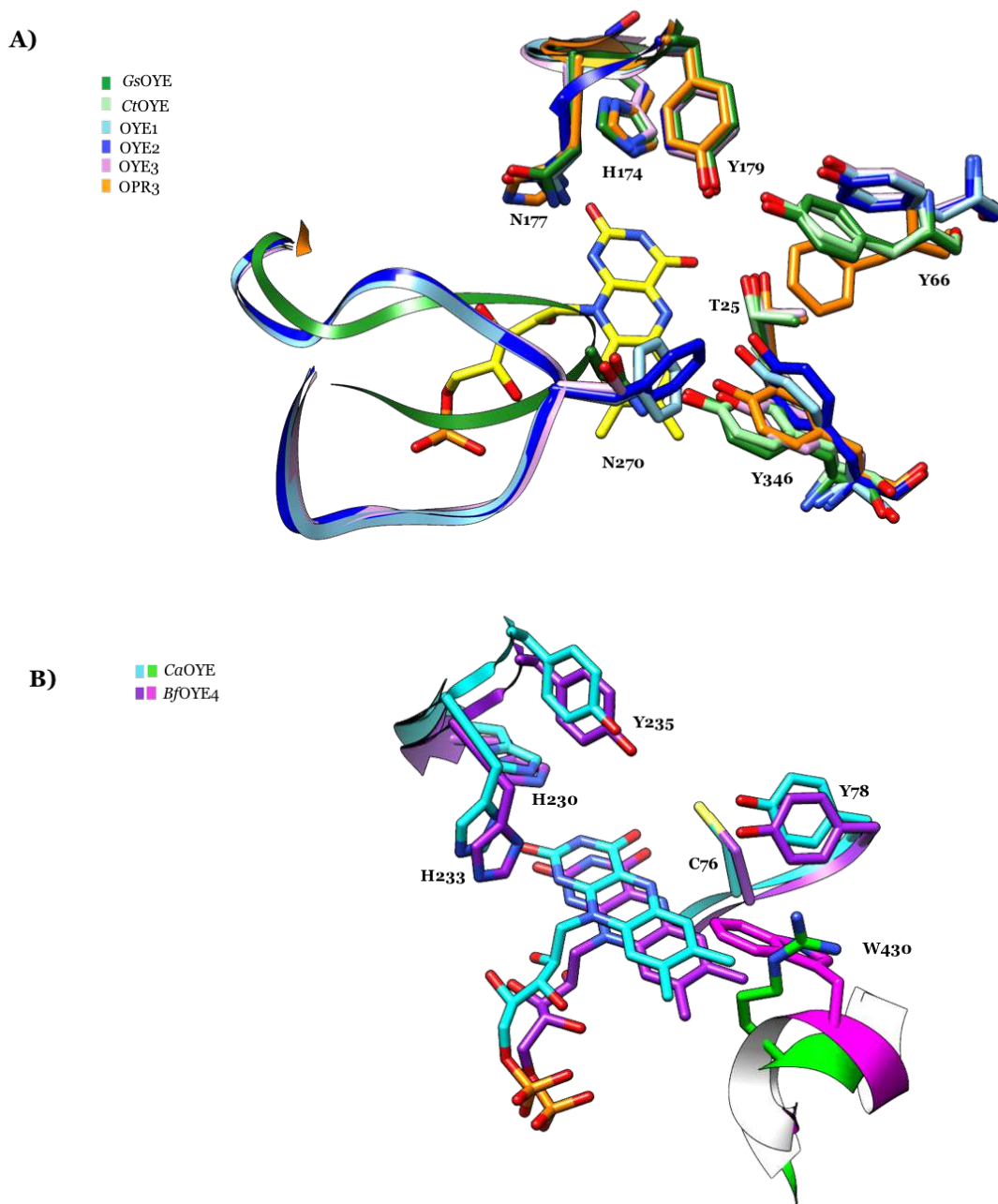


Figure 122. Superimposition of the crystal structures available of ene-reductases active in the isomerization of α -AL to β -AL: (A) classical ERs (*GsOYE* numbering); (B) thermophilic-like ERs (*BfOYE4* numbering).

In thermophilic-like ERs, this loop has a different orientation, leading to a wider opened active site and a major exposure of FMN to solvent and substrate. On the other hand, the thermophilic-like OYEs, due to the dimerization interface and an amino acidic “finger” that protrudes into the active site of each monomer, have a different architecture and entrance of the active site. In *GsOYE*, the N270 residue is in direct hydrogen contact with Y346, closing even more the active site of the protein. When N270 was mutated to an Arginine residue or Alanine the conversion and the stereoselectivity dropped more dramatically in the presence

of Arginine, which has a long charged chain. However, from crystal structure data of this variant, the mutation did not have a dramatic effect on the three-dimensional crystal structure of the protein (see section 6.3.2).

Taken together, these preliminary data suggested us that the residues involved in the binding during the classical C=C-bond reduction (H174 and N177, *GsOYE* numbering) are also involved in the binding of **1a**. These data have also been confirmed from the crystal structure of *GsOYE* in complex with **1a** (see section 6.3.3). Y179 and Y66 in *GsOYE* may act in pair in the protonation step and thus are also responsible for the stereoselectivity while in the thermophilic-like homologues Y78 (*BfOYE4* numbering) seems to be involved in the stereoselective protonation. Other mutations are in progress with *BfOYE4* in order to get more insights in the mechanism of the reaction. However, despite all the efforts, a suitable “base” involved in the deprotonation step could not be identified, thereby suggesting that this step might be spontaneous. Furthermore, as FMN is another conserved element between all the OYEs, its role in the isomerization, even in the oxidized state, needs to be investigated. We are planning stopped-flow experiments in order to get more insights into its possible involvement during the reaction.

6.3.2 Mutants crystal structure

For the mutants Y66F, Y179F, N270R and Y346F the crystal structure was investigated in order to get more insights into their three-dimensional architecture that could explain the variations in catalytic activities reported in the previous section.

The crystallographic details for the best datasets can be found in Table 26.

No evidence of significant changes (*e.g.* loop reorientation or conformational changes in the adjacent residues) was detected after the mutation (Fig. 123). Thus, confirming that the different catalytic activities observed in the mutants could be ascribed just to the chemical properties and/or to the steric hindrance of the amino acidic residues. The Tyrosine residues (Y66, Y179 and Y346) were mutated to Phenylalanine, thereby maintaining the steric hindrance but removing the OH group that is important for catalysis and stereoselectivity.

The mutation of N270 to Arginine influenced both the chemical properties and the steric hindrance. The long charged chain of arginine was extending above the FMN and its guanidine group was protruding deeply into the active site.

Table 26. X-ray Crystallographic data collection and refinement statistics.

Mutant GsOYE	Y66F	Y179F	N270R	Y346F
Data collection statistics				
Wavelength	0.9537	0.9537	0.9537	0.9537
Space group	P 2 21 21	P 1 21 1	P 2 21 21	P 1 21 1
Cell constants				
a, b, c (Å)	56.83 77.21 88.39	56.79 76.64 88.79	56.66 77.02 88.55	56.88 76.89 87.96
a, b, γ (°)	90 90 90	90 92.3 90	90 90 90	90 91.6 90
Resolution range for refinement (Å)	77.21 – 1.52 (1.55 – 1.52)	88.72 – 1.77 (1.81 -1.77)	58.15 – 1.70 (1.73 – 1.7)	48.37 - 1.53 (1.56 - 1.53)
Total reflections	755772 (37939)	494482 (28795)	79329 (4281)	577794 (28720)
Number of Unique Reflections	60609 (2985)	74026 (4194)	41828 (2207)	113789 (5608)
R _{merge}	0.071 (0.587)	0.065 (0.624)	0.178 (0.609)	0.043 (0.595)
<I / sigma(I)>	19.4 (4.3)	16.1 (2.8)	24.9 (4.0)	17.2 (2.3)
Completeness (%)	100 (100)	99.8 (99.5)	96.4 (97.8)	99.7 (99.8)
Multiplicity	12.5 (12.7)	6.7 (6.9)	1.9 (1.9)	5.1 (5.1)
Refinement statistics				
R _{work} / R _{free}	0.171/0.196	0.183/0.217	0.171/0.20	0.188/0.213
RMSD bond lengths (Å)	0.0225	0.0114	0.0128	0.0198
RMSD bond angles (°)	2.178	1.49	1.64	2.01
Main chain B factor	15.9	25.7	20.7	23.20
Ligands B factor	9.0	17.0	13.3	13.6
Water molecules B factor	22.9	25.2	23.5	25.8
Ramachandran plot (%)				
Most favoured	95.78	95.65	95.50	95.78
Generously allowed	3.96	4.22	3.97	3.96
Outliers	0.26	0.13	0.53	0.26

Moreover, its electronic density clearly showed that this residue assumed different conformation/orientation that might prevent the entrance of the substrate into the active site, and thus explaining its lower catalytic activity (Fig. 124 C).

Different attempts to soak the crystals of *GsOYE* mutants with α -AL have been performed but without any success and just partial electronic density was recovered. In the active sites of all mutants a Cl anion, coming from the precipitant solution, was found bound inside the active site and also a molecule of ethylene glycol (EDO), as already mentioned for the apo_ *GsOYE* (see Chapter 5). Moreover, the pH of the precipitant solution was 6.0 and from previous analysis we knew that the reaction at this pH value was very slow. For these reasons in order to obtain the *GsOYE* wt in complex with α -AL, different protocols including washing steps and change of the precipitant solution pH were adopted (see section 6.3.3).

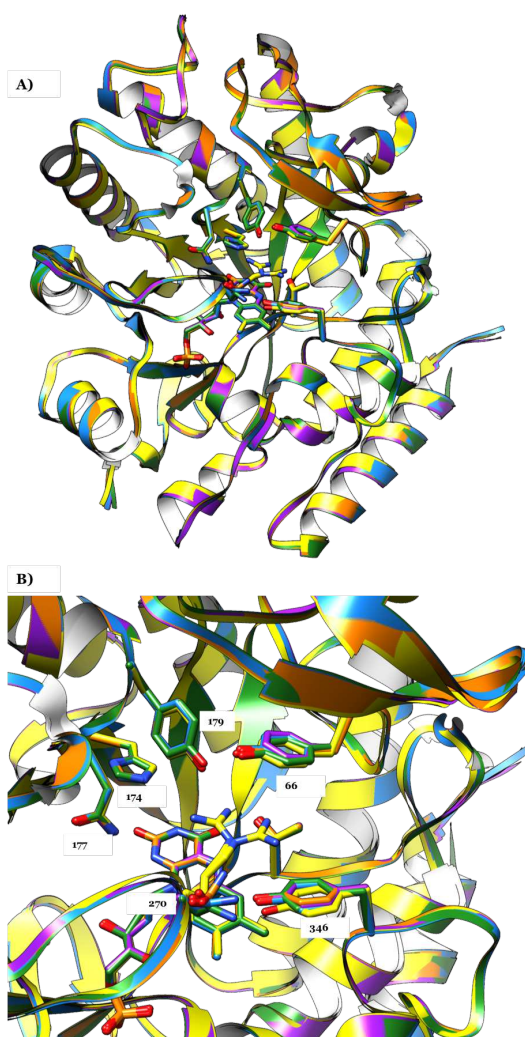


Figure 123. Superimposition of (A) the three-dimensional structure of *GsOYE* wt (green) and the different mutants Y66F (purple), Y179F (blue), N270R (yellow) and Y346F (orange); (B) close-up of the active site and the mutated residues.

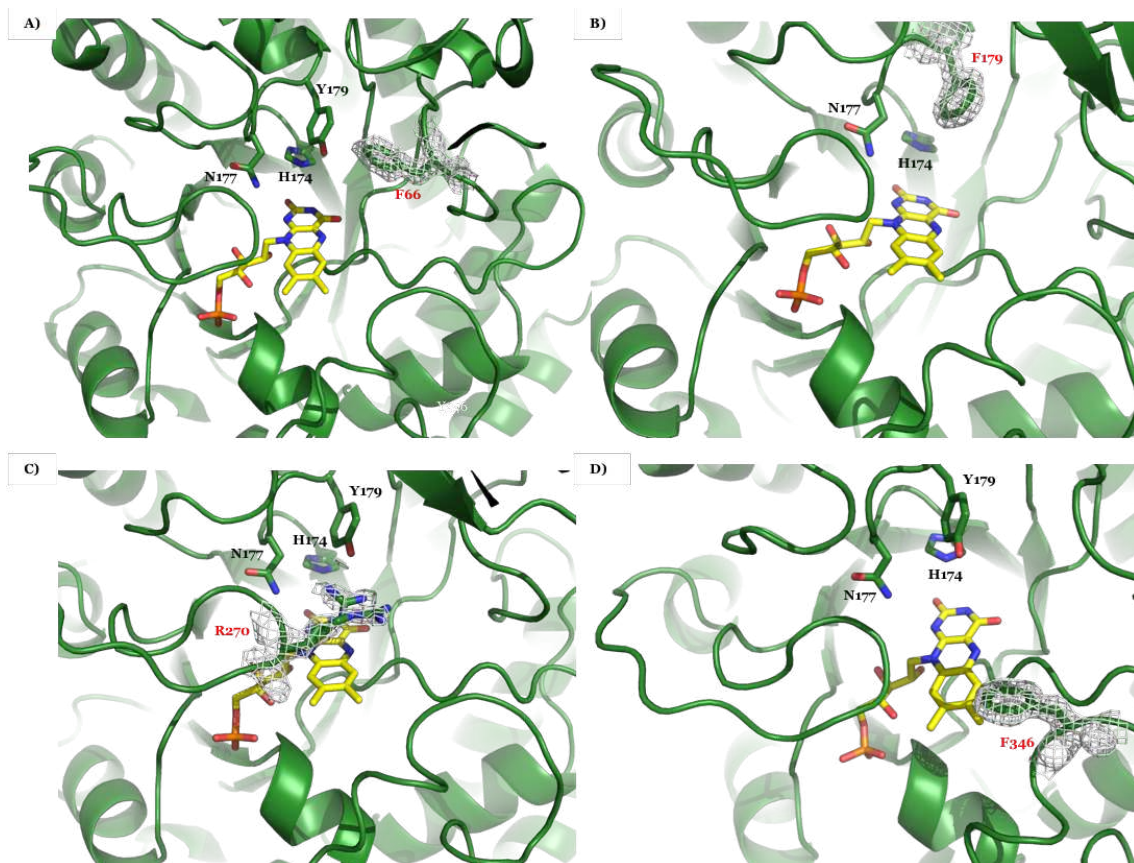


Figure 124. Density map of GsOYE mutants active site: A) Y66F; B) Y179F; C) N270R; D) Y346F.

6.3.3 GsOYE crystal structure in complex with angelica lactones

As already mentioned in the previous section, different strategies and efforts have been employed to get the crystal structure of GsOYE in complex with α -AL in order to get more insights into the interactions of the substrate with the different amino acids of the active site. The substrate has been soaked into the already formed crystals. The co-crystallization strategy was abandoned after few attempts as the reaction could proceed also inside the crystals and the formation of the crystals required an over-night incubation. Different concentrations of α -AL and time incubation were tested but without success in detecting a clear electronic density for the desired substrate. As already anticipated in the apo crystals, a Cl anion, coming from the precipitation solution, and a molecule of ethylene glycol used as cryoprotectant were always found inside the active site of the protein, thus preventing probably the binding of the substrate. A strategy to enhance the formation of the complex while avoiding these drawbacks was set-up and it consisted in changing the pH of the crystallization condition and different steps of back-wash in order to eliminate the Cl anion from the active site. First of all, once the crystals were formed in the standard precipitant solution (50 mM MES pH 6.0, 200 mM MgCl₂ and 20% PEG 6000) they were transferred to a drop

containing the same elements of the standard solution except the buffer and its pH (50 mM Tris + 50 mM MES pH 7.0 or pH 9.0, 200 mM MgCl₂ and 20% PEG 6000). The crystals were let to equilibrate in this solution over-night. The second day, the crystals were transferred again to a back-wash solution (50 mM Tris + 50 mM MES pH 7.0 or pH 9.0, 10% PEG3350 and 20% PEG 6000) in order to eliminate the Cl anion and to furnish already a cryoprotectant different from ethylene glycol. The wash was repeated several times during the day. The crystals exchanged with the buffer at pH 9.0 had some cracks on their surface after the equilibration, so they were not used for further experiments. After the washing was completed to the crystals equilibrated at pH 7.0, 5 mM α -AL was added and let incubated for different times (5 min, 45 min, 3 h, 5 h, 7 h and 24 h). This strategy was successful, allowing to obtain the crystal structure of GsOYE in complex with α -AL (after 45 min incubation) and in complex with (*R*)- β -AL (after 7 h incubation). The crystallographic details for these preliminary datasets are shown in Table 27. For GsOYE- α -AL complex the refinement is still on going as the statistics reported are still not optimal.

Table 27. X-ray Crystallographic data collection and refinement statistics.

	GsOYE-α-AL	GsOYE-β-AL
Data collection statistics		
Wavelength	0.966	0.966
Space group	P 1 21 1	P 1 21 1
Cell constants		
a, b, c (Å)	56.82 76.69 86.93	56.70 76.48 86.07
a, b, γ (°)	90 93 90	90 93 90
Resolution range for refinement (Å)	56.75 – 1.63 (1.66 – 1.63)	48.48 – 1.43 (1.45 – 1.43)
Total reflections	151753 (8377)	330830 (15928)
Number of Unique Reflections	82802 (4540)	132710 (6609)
R _{merge}	0.06 (0.626)	0.045 (0.606)
<I / sigma(I)>	10 (2.0)	9.5 (1.1)
Completeness (%)	89.3 (99.5)	98.1 (98.6)
Multiplicity	1.8 (1.8)	2.5 (2.4)
Refinement statistics		
R _{work} / R _{free}	0.25/0.29	0.23/0.26
RMSD bond lengths (Å)	0.009	0.012
RMSD bond angles (°)	1.445	1.601
Main chain B factor	25	23.0
Ligands B factor	15.1	12.6
Water molecules B factor	23.1	23.6
Ramachandran plot (%)		
Most favoured	95.21	95.60
Generously allowed	4.65	3.87
Outliers	0.13	0.53

α -AL was found bound into the active site of GsOYE in a similar position compared to 2-methyl-cyclopenten-1-one during the classical C=C-bond reduction (for more details see Chapter 5) (Fig. 125). The carbonyl group of α -AL

is in hydrogen bond contact with the conserved H174 and N177. The Y66 and Y179 are pointing to the methyl group of the substrate. Interestingly, T25 assumes a double conformation maybe due to the steric hindrance of the methyl group of the ligand. (*R*)- β -AL was also found bound into the active site of GsOYE after 7 h of incubation in a position prone for the C=C-bond reduction (Fig. 126). Also in this case, the carbonyl group of β -AL is in hydrogen bond contact with the conserved H174 and N177 and again T25 assumes a double conformation. Importantly, the methyl group of the chiral center points toward the flavin, due to the proton newly donated.

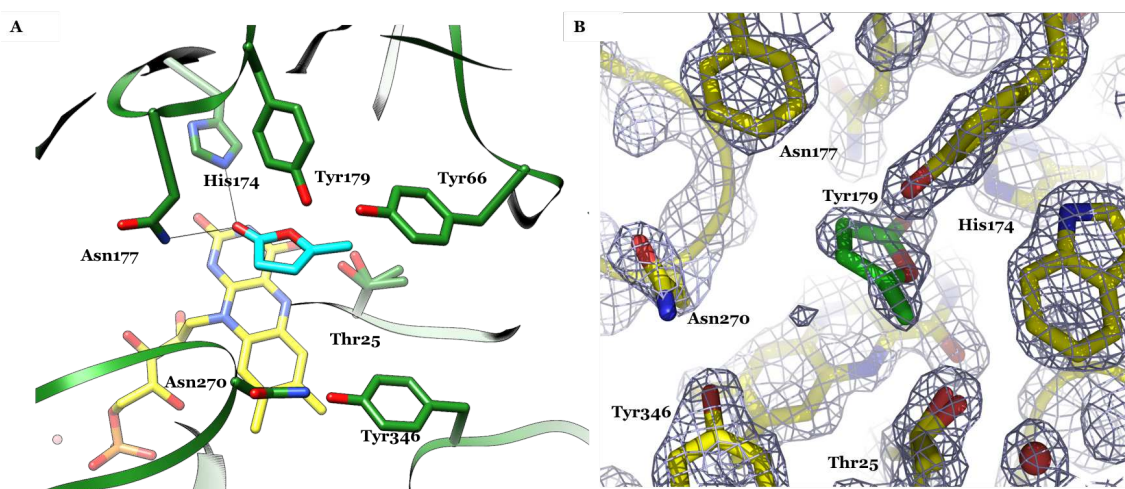


Figure 125. Close view of the structure of GsOYE complexed with α -angelica lactone: (A) GsOYE active site showing the most important residues and the hydrogen bonds between the carboxylic group of α -AL the His174 and Asn197 residues. FMN (yellow) and α -AL (cyan) are shown as stick models; (B) the $F_o - F_c$ difference electron density map before the ligand was fit into the density, contoured at 2.5σ is shown.

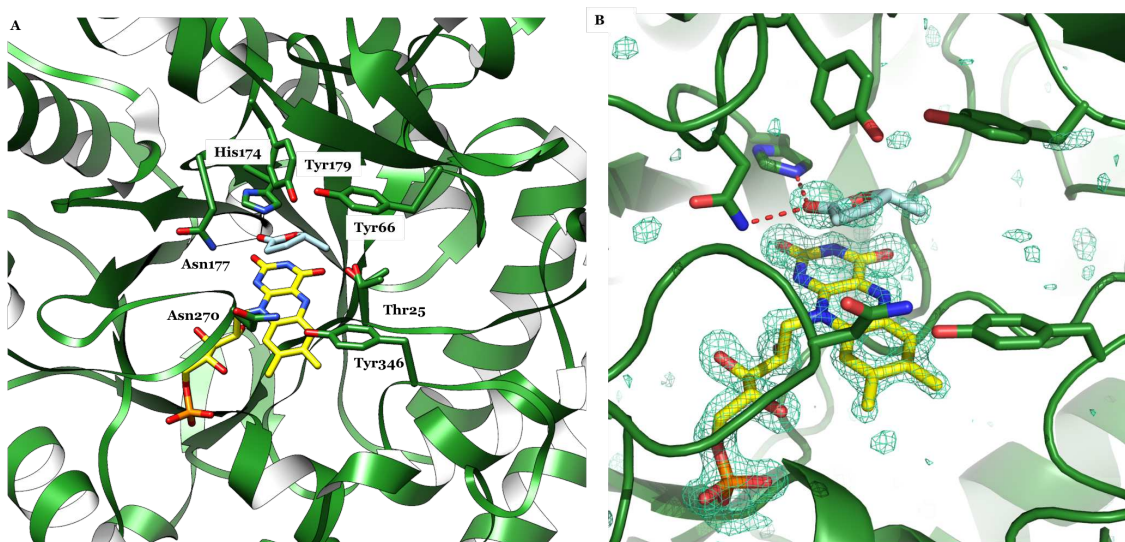


Figure 126. Close view of the structure of GsOYE complexed with (*R*)- β -angelica lactone: (A) GsOYE active site showing the most important residues and the hydrogen bonds between the carbonylic group of β -AL the His174 and Asn197 residues. FMN (yellow) and β -AL (light blue) are shown as stick models; (B) the $F_o - F_c$ difference electron density map before the ligand was fit into the density, contoured at 3σ is shown.

6.3.4 Hypothetical mechanism of reaction in GsOYE

Taken together, all the results obtained from the activity studies and from the crystallographic experiments suggest an acid-base catalysis mechanism, as already hypothesized by Hall and co-workers [130]. The proposed reaction mechanism is depicted in Figure 127. Briefly, a base, still not identified, abstracts a rather acidic proton to the substrate generating an aromatic anion as intermediate, which is subsequently protonated by the couple Tyr66 and Tyr179 in GsOYE. However, it is not yet clear how these two tyrosine residues act together.

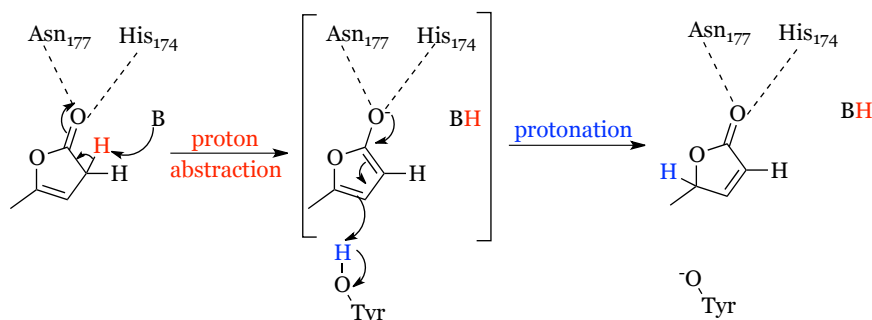


Figure 127. Proposed reaction mechanism for the isomerization of α -AL to β -AL. Residues numbering according to GsOYE sequence.

6.4 Cascades for the reduction of β -AL to γ -valerolactone

Different cascades were set-up in order to obtain also the γ -valerolactone through C=C-bond reduction in high conversion and stereoselectivity. Key reaction parameters were identified that allowed the isomerization and the sequential reduction to run in one-pot (Fig. 128), while avoiding substrate/product spontaneous degradation and racemization (*e.g.*, pH, presence of co-solvents, reaction time).

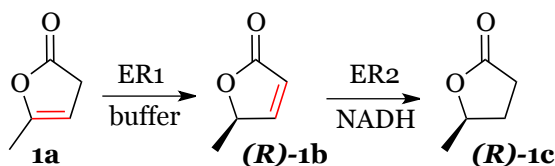


Figure 128. Isomerization of α -AL and sequential reduction of β -AL to GVL mediated by OYEs

6.4.1 Reaction parameters investigation

One of the most important parameters to set-up was the pH of the reaction, as already mentioned. Basic pH could boost conversions but in the meanwhile promoted the degradation of the substrate **1a** through lactone hydrolysis. Moreover, also the reaction time was a key parameter, especially with GsOYE, as at basic pH the ee of **1b** decreased rapidly. A time study at different pHs was

performed in order to fine-tune the conversion and the stereoselectivity during the time of the reaction. The results are shown in Table 28. The reaction was almost complete at pH 9.0 after 30 minutes incubation (92% conv.) compared to the standard reaction run at pH 7.0, which required an over-night incubation (59% conv.).

Another interesting aspect was that at basic pHs but short incubation times the stereoselectivity was maintained and the racemization reduced. Moreover, for long incubation times at basic pH values the spontaneous degradation of substrate and/or product was promoted and the total amount (peak areas) of substrate/product detected into the chromatograms was lower compared to standard neutral conditions. Thus, the isomerization at pH 9.0 and short incubation time (30 minutes) appeared as a good compromise for further studies. Moreover, 10 mM valerolactone were incubated for 3 hours in Tris pH 7.0 and 9.0 in order to evaluate its stability at the different pHs. GVL was stable in all the conditions tested (data not shown).

Table 28. Time study of **1a** isomerization to **1b** mediated by GsOYE at different pHs.

Reaction time (h)	pH 5		pH 8		pH 9	
	Conv. %	ee (%)	Conv. %	ee (%)	Conv. %	ee (%)
0.5	-	-	67	90 (<i>R</i>)	92	81 (<i>R</i>)
2	-	-	> 99 [#]	81 (<i>R</i>)	> 99 [#]	73 (<i>R</i>)
4	N.D.	N.D.	> 99 [#]	63 (<i>R</i>)	> 99 [#]	43 (<i>R</i>)
18	-	-	> 99 [#]	27 (<i>R</i>)	> 99 [#]	30 (<i>S</i>)

10 mM **1a**, 200 µg/mL enzyme, ON incubation at 30 °C, 50 mM Tris pH 5.0-9.0

[#]Conversion as substrate consumption. N.D. = not detected.

In order to prevent substrate/product spontaneous degradation, a by-phasic system was set-up using different percentages of TBME (tert-butyl methyl ether) as co-solvent. First of all, we investigated if the isomerization reaction could still occur in the presence of the co-solvent (Table 29) and secondly, we evaluated also the stability of GVL in the by-phasic system (Table 30).

Table 29. **1a** isomerization to **1b** in the presence of TBME as co-solvent.

% TBME	Conv. %	ee (%)
10	84	74 (<i>R</i>)
25	76	73 (<i>R</i>)
50	66	73 (<i>R</i>)

10 mM **1a**, 200 µg/mL enzyme, 50 mM Tris pH 7.0 with x% TBME, 30 °C, ON.

Presence of traces of racemic **1b** in the starting material not taken into account

Table 30. Stability study of valerolactone (**1c**) in different buffer compositions.

% TBME	Relative recovery (%)	
	pH 7	pH 9
10	100	100
25	65	64
50	61	61

10 mM **1c** incubated in 50 mM Tris pH 7.0 and 9.0 with x% TBME, 30 °C, 3h

As reported in Table 29, the isomerization reaction occurred as in the standard aqueous buffer in the presence of 10% TBME, while the conversion was lower at increasing concentrations of co-solvent. Moreover, **1c** was also stable in 10% TBME both at pH 7.0 and 9.0 (Table 30).

The final reaction parameter analyzed was the presence of NADH (15 mM). During the first trials for the cascades design, we realized that in the presence of NADH, the degradation of the substrate was enhanced, leading to lower amount of recovered material (peak area). We performed some stability studies using **1a** and **1c** in the presence of 15 mM NADH: after over-night incubation of **1a** in Tris pH 7.0 at 30 °C its relative recovery was 65% while that of **1c** was complete after 3 hours incubation. In order to overcome the instability of **1a** in the presence of NADH, we have set-up few cascades using GDH and glucose in order to allow the use of catalytic amounts of nicotinamide.

Once these parameters were optimized, different cascades were designed for the stereoselective synthesis of γ -valerolactone starting from α -angelica lactone.

6.4.2 One-pot one-step cascades

First, one-pot one-step cascades were set-up for the synthesis of GVL starting from α -AL, as already reported for OYE2 [130]. Unfortunately, this set-up using GsOYE for both the isomerization step and subsequent reduction appeared immediately not feasible as the isomerization reaction was too slow (over-night) compared to OYE2 (15 minutes) and thus hydrolysis of the substrate/product was predominant, allowing very low recovery (peak areas) of both substrate and product. Different strategies were employed in order to optimize the cascade such as using GsOYE for the stereoselective isomerization and other OYE homologues for the reduction step in one-pot. From previous data, we knew that YqjM was the most active OYE homologue in the reduction step with very good stereoselectivity. Some examples of the one-pot one step cascades are here reported using GsOYE and YqjM as biocatalysts (Fig. 129). In the first set-up, GsOYE and YqjM were used together in the presence of NADH but very low

recovery for substrate and products was detected (data not shown). In an attempt to optimize the recovery, the NADH cofactor was substituted with the recycling system but also in this case low conversion (< 1%) was detected (data not shown).

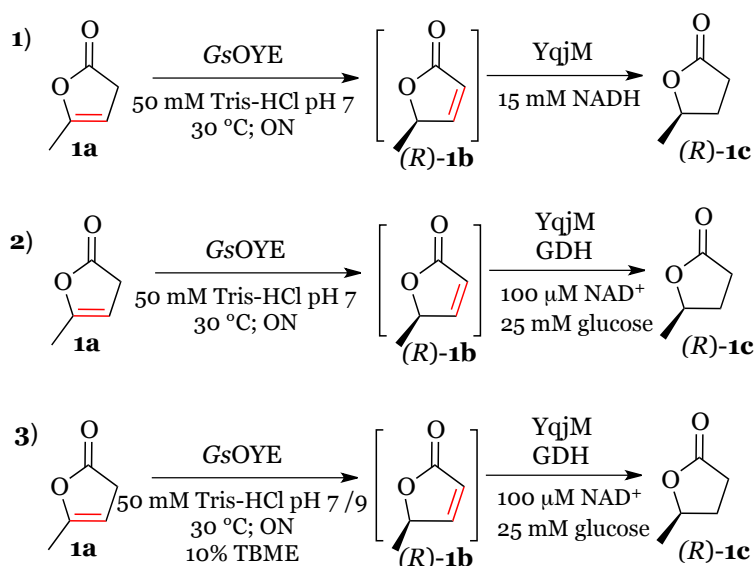


Figure 129. Different design of the one-pot one-step cascades using GsOYE and YqjM for the synthesis of **1c**.

Finally, the by-phasic system (setup 3 in Fig. 129) was tried and the data are reported in Table 31. In this final set-up at pH 7.0 almost no conversion of **1a** was detected neither into **1b** nor **1c**. While at pH 9.0 the isomerization proceeded quite well but however, the degradation and the racemization of the substrate were detected and moreover the reduction reaction was not occurring.

Taken together, these results suggested that the isomerization and the subsequent reduction have to occur as separated steps (sequential cascade).

Table 31. Conversion and stereoselectivity of the one-pot one-step cascade in the final design (design 3 in Figure 129).

pH	Reaction time (h)	Conv. % 1a → 1b	ee % 1b	Conv. % 1b → 1c	ee % 1c
7	3	N.D.	-	0	-
	6	< 1	-	0	-
	18	< 1	-	1	> 99 (<i>R</i>)
9	3	94#	61 (<i>R</i>)	0	-
	6	95#	46 (<i>R</i>)	0	-
	18	98#	<i>rac</i>	0	-

Conv.%: based on substrate consumption

6.4.3 One-pot two-step cascades

Different one-pot two-step cascades were set-up using GsOYE for the stereoselective isomerization of **1a** to **1b** and a second OYE homologue for the subsequent reduction of the β -isomer to **1c**. After isomerization of **1a** by GsOYE, the ability of different OYE homologues to reduce the obtained (*R*)-**1b** into **1c** while maintaining the chiral center formed by GsOYE (formation of (*R*)-**1c**) was investigated. The results of this screening are shown in Table 32.

Table 32. Screening of OYE homologues in the stereoselective reduction of (*R*)-**1b** to **1c** after isomerization of **1a** by GsOYE.

Enzyme	ee % 1b	Conv.%	ee % 1c
1b → 1c			
GsOYE	52 (<i>R</i>)	25	> 99 (<i>R</i>)
	# 12 (<i>R</i>)	47	81 (<i>R</i>)
CtOYE	73 (<i>R</i>)	23	> 99 (<i>R</i>)
OYE2	14 (<i>R</i>)	76	75 (<i>R</i>)
	# 10 (<i>R</i>)	96	69 (<i>R</i>)
OYE1	22 (<i>R</i>)	77	74 (<i>R</i>)
OYE3	70 (<i>R</i>)	17	> 99 (<i>R</i>)
OPR3	62 (<i>R</i>)	26	> 99 (<i>R</i>)
YqjM	40 (<i>R</i>)	67	> 99 (<i>R</i>)
	# 66 (<i>S</i>)	90	91 (<i>R</i>)

In the first step: 10 mM **1a**, 100 μ g/mL GsOYE, 50 mM Tris pH 7.0, 30 °C, ON. For the second step: addition of 100 μ g/ml (# 300 μ g/ml) enzyme and 15 mM NADH, 30 °C, 3 h (# 5 h). Presence of traces of racemic **1b** in the starting material not taken into account.

OYE1 and OYE2 are fast in reducing the β -isomer to **1c** but they are not selective converting both enantiomers of **1b**. The best enzyme for conversion and selectivity in the reduction was YqjM (67% conv.; > 99% ee). In the presence of higher concentration of YqjM (300 μ g/mL) the reaction was even faster reaching 90% conv. after 5 h incubation while maintaining the selectivity. GsOYE was also able to reduce the C=C-bond after the isomerization but it was slower and also less selective compared to YqjM. For further cascades YqjM was used in the reductive step of the cascade.

Two different designs were set-up for the one-pot two-step sequential cascades and they are depicted in Fig. 130. The results of the two different designs are reported in Table 33.

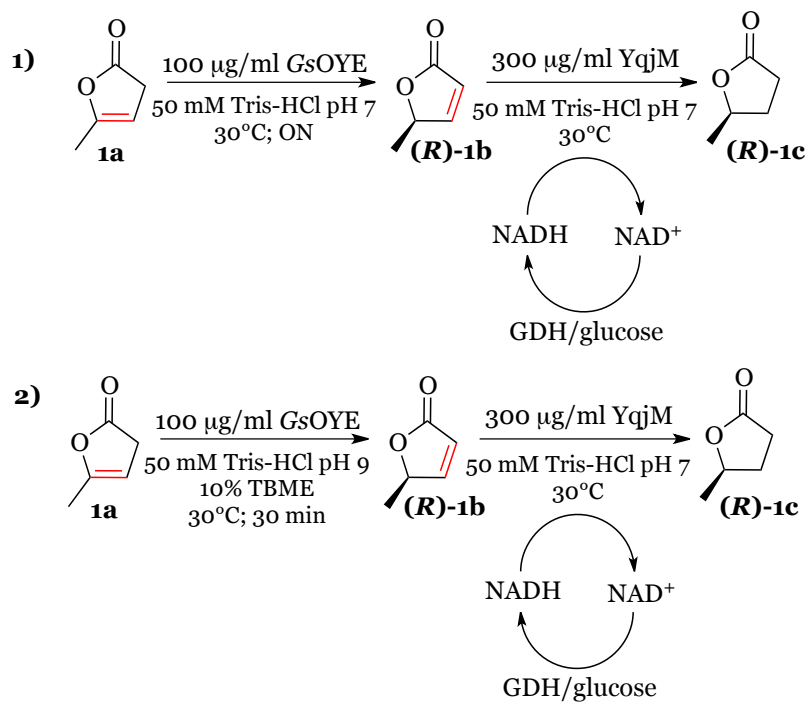


Figure 130. Different design of the one-pot two-step sequential cascade using GsOYE and YqjM for the synthesis of **1c**.

In the final design (2), 3.5 mM of **1c** was formed according to calibration curve with authentic material.

Table 33. Conversion and stereoselectivity of the one-pot two-step cascade.

Set-up	Time (h)	ee % 1b	Conv.% 1b → 1c	ee % 1c
1)	3	45 (<i>R</i>)	47	95 (<i>R</i>)
	6	12 (<i>S</i>)	74	94 (<i>R</i>)
	18	48 (<i>S</i>)	55	91 (<i>R</i>)
2)	3	35 (<i>S</i>)	75	92 (<i>R</i>)
	6	33 (<i>S</i>)	74	92 (<i>R</i>)
	24	29 (<i>S</i>)	72	92 (<i>R</i>)

10 mM **1a**, 50 U/mL GDH, 25 mM glucose, 100 μM NAD⁺
Presence of traces of racemic **1b** in the starting material not taken into account.

Concluding remarks

In this Chapter, we report the first case of stereoselective hydride-independent isomerization of α -angelica lactone to enantioenriched β -angelica lactone catalyzed by different new ene-reductases identified during this PhD work. Moreover, stereocomplementary enzymes from the classical and thermophilic-like subclass of OYE homologues were detected revealing interesting clues into the reaction mechanism characteristics. Furthermore, the efforts for the elucidation of the catalytic mechanism of the isomerization reaction through site-specific mutagenesis, reaction engineering (*e.g.*, pH, presence of co-solvents, reaction time) and crystallographic tools were also reported in detail.

Finally, the design of different enzymatic cascades combining ene-reductase catalyzed stereoselective isomerization of α -angelica lactone to β -angelica lactone, with subsequent reduction by a suitable OYE homologue of the enantioenriched β -isomer to (*R*)- γ -valerolactone allowed the formal asymmetric reduction of non-activated C=C-bonds in one-pot.

7. Summary and Outlooks

7.1 Summing-up

The use of enzymes for the synthesis of a large variety of hard-to-synthesize compound under mild reaction conditions is of great interest from an industrial point of view. Compared to the traditional chemical processes, biocatalysts offer different advantages such as high chemo-, regio- and enantioselectivity as well as mild reaction conditions and low waste generation. Therefore, biocatalysis is a sustainable and enabling technology that can be employed for the production of fine chemicals in processes environmentally friendlier and safer in accordance with the principles of “Green Chemistry”.

Ene-reductases are extremely appealing for industrial application as they catalyze the stereoselective C=C-bond reduction on a wide range of substrates yielding products with a variety of biotechnological and pharmaceutical applications [105]. ERs are flavin- and NAD(P)H-dependent catalysts that have been extensively studied in the last years as attractive tools for alkenes reduction with the potential to generate up to two stereogenic centers [39, 135]. In general ERs have been identified in a large number of organisms such as bacteria, fungi and plants but nevertheless their toolbox is still limited [98].

Nowadays, an increasing number of sequenced genomes are deposited into public databases that are accessible and can be explored using bioinformatics tools for the discovery of novel putative enzymes. In the last years fungi organisms have been identified as a very promising source of ene-reductases, as their genomes encode gene families (from 6 to 22 genes) coding for these enzymes. Moreover, looking carefully in the literature, we have noticed that photosynthetic bacteria and eukaryotes are unexploited sources for this class of enzymes. Thus, by genome mining using OYE1 and YqjM as probe sequences for the classical and thermophilic-like ERs, and searching for the typical “fingerprint” motifs reported in the literature for this class of enzymes, we have identified and selected seven new putative ene-reductases from different organisms: *Galdieria sulphuraria* (GsOYE), *Chroococcidiopsis thermalis* (CtOYE), *Chloroflexus aggregans* (CaOYE), *Botryotinia fuckeliana* (BfOYE1 and BfOYE4) and *Aspergillus niger* (AnOYE2 and AnOYE8).

A common cloning strategy was set-up in order to obtain all the identified putative ene-reductases in recombinant form. The standard pET-28a(+) plasmid was used for the insertion of the different coding sequences after their previous isolation and amplification from the genomic DNA of the different organisms.

The obtained constructs were transformed into *E. coli* BL21 (DE3) and over-expression tests were performed varying different parameters such as expression temperatures and suitable bacterial strains in order to obtain the desired proteins in soluble form. Moreover, for *BfOYE4* other host such as *Pichia pastoris* was also tried in order to enhance its recombinant expression but unfortunately this strategy was not successful. In the end, all the proteins were produced and purified from *E. coli* in good yields (or at least sufficient amounts for further characterization) by IMAC chromatography.

A preliminary biocatalytic characterization of the new ene-reductases was carried out. Moreover, steady-state kinetics parameters were also determined for the most promising enzymes and analytical biotransformations were set-up just for *GsOYE* and *CtOYE* in collaboration with Dr. Mélanie Hall (University of Graz, Austria). Furthermore, also a biochemical characterization in terms of pH *optimum*, thermal stability and oligomeric state investigations has been performed in order to get more insights into the potential of these new biocatalysts.

The crystal structure of *GsOYE* and *CtOYE*, two classical OYEs, and of *CaOYE* and *BfOYE4*, two members of thermophilic-like ERs, has been solved with good to moderate resolution. Moreover, the three-dimensional structures of *GsOYE* in complex with the inhibitor pHBA and the substrate 2-methyl-cyclopenten-1-one have also been solved and are here reported. Finally, *OYE2* and *OYE3* have also been crystallized in collaboration with Dr. Mélanie Hall and their crystal structure is here reported and described for the first time.

To conclude, the hydride-independent isomerization of non-activated C=C-bonds, an alternative catalytic activity reported for some OYE homologues by Hall and co-workers [130], was also tested with the newly identified ene-reductases. The reaction revealed for the first time a case of asymmetric C=C-bond isomerization by OYE homologues, leading to highly enantioenriched product. We have also reported the different attempts to elucidate the mechanism of action of this alternative reaction through site-specific mutagenesis, crystallographic tools and reaction engineering. Moreover, different cascades were also set-up for the subsequent reduction to γ -valerolactone of the β -angelica lactone obtained by the isomerization.

7.2 Outlooks

In the present work, we have discovered new ene-reductases from unexploited sources, contributing to increase the number of available recombinant ERs that could catalyze the reduction of activated C=C-bonds in substrates of industrial relevance.

A preliminary substrate scope and biochemical characterization have been performed for all the new biocatalysts identified in this thesis. In the next future biotransformations using *CaOYE*, *BfOYE1* and *BfOYE4* can be set-up in order to get more insights into their catalytic properties and stereoselectivity profiles. Moreover, for *AnOYE2* and *AnOYE8*, which seemed almost inactive biocatalysts in the preliminary screening, a more detailed biochemical characterization in terms of reaction *medium* engineering, substrate concentration and cofactor preference can be performed with the aim to boost their conversion with the standard substrates tested in this thesis and/or to find other substrates mimicking their natural substrates (which, however, are still unknown for the majority of OYEs).

The crystal structure of four out of the seven enzymes was solved with good to moderate resolution. Further crystal optimization can be performed on *BfOYE4* and *CaOYE* crystals with the goal to obtain structures with better resolution. Efforts to obtain *BfOYE1* structure were not successful in obtaining crystal hits. Other strategies, such as detergent screening, use of inorganic nucleants (*e.g.* Crystallophore No. 1 or Naomi seeds, from Molecular Dimensions), limited proteolysis protocols or mutagenesis of the most flexible parts of the protein, can be tried in order to obtain first crystal hits of *BfOYE1*, which has the highest biocatalytic potential compared to the other enzymes identified in this thesis.

Finally, the mechanism of the hydride-independent isomerization of α -angelica lactone mediated by OYEs was not completely elucidated despite all the strategies reported in this thesis: mutagenesis, reaction engineering and crystallographic tools. In the near future, we plan to investigate the (possible) role of the oxidized FMN cofactor into the catalysis by stopped-flow analysis and/or neutron diffraction and eventually to produce other mutants of *BfOYE4* with the aim to identify the base residue involved in the first deprotonation step of the reaction.

8. MATERIALS AND METHODS

8.1 Materials

All chemicals were purchased from Sigma–Aldrich and Panreac. The antibiotics Kanamycin and Zeocin were purchased from Gene Spin and InvivoGen, respectively. Gentamicine was from Calbiochem®.

BenchTop 1kb DNA Ladder and Loading Dye 6X were from Promega. Gel Stain GELRED™ 10000X was purchased from Biotium. BenchMark™ Unstained Protein Ladder (10-220 kDa) was purchased from ThermoFisher Scientific, Prestained Protein SHARPMASS VII (6.5-270 kDa) Protein MW Marker was from EuroClone. Native ladder was purchased from SERVA and precast Tris-acetate acrylamide gel 3-8% was from ThermoFisher Scientific.

SYPRO® Orange Protein Gel Stain was purchased by Sigma-Aldrich. Acrylamide 40% (acrylamide: bis-acrylamide ratio 37.5:1) was from PanReac AppliChem. PVDF blotting membrane Amersham Hybond (0.45 µm pore size) and Amersham Hyperfilm ECL were from GE Healthcare Life Science and SuperSignal® West Pico Chemiluminescent substrate was from Thermo Scientific. Restriction enzymes, T4 DNA Ligase and Phusion® High-fidelity DNA polymerase were obtained from New England Biolabs (NEB). TSAP (Thermosensitive Alkaline Phosphatase) and GoTaq® DNA polymerase were purchased from Promega. Anti-His-tag antibodies were purchased from Sigma-Aldrich while goat-anti-mouse antibodies labelled with peroxidase were from KPL. Electroporation cuvettes 0.2 cm were purchased from VWR®. IMAC-Select Affinity Gel resin was purchased from Sigma–Aldrich, the Superose 6 10/300 and Superose 12 10/300 GL columns and column derivatized with benzamidine were from GE Healthcare Life Sciences. Vivaspin® centrifugal concentrators (cut off MW 10000 kDa) were purchased from Sartorius. Crystallization kits and MRC plates were from Molecular Dimensions.

8.1.1 Primers

The oligonucleotides were purchased from Sigma-Aldrich and were analyzed by the software OligoAnalyzer Tool. Restriction sites are shown in bold. The mutations introduced to create the restriction sites or to mutate the original sequences are underlined.

	sequence (5'→3')	DNA/Vector	Application
T7_for	TAATACGACTCACTATAGGG	pET28a(+)-OYEs	PCR colony and sequencing
T7_rev	GCTAGTTATTGCTCAGCGG	pET28a(+)-OYEs	PCR colony and sequencing
AOX_for	GACTGGTTCCAATTGACAAGC	pPICZ α -BfOYE4	PCR colony and sequencing
AOX_rev	GCAAATGGCATTCTGACATCC	pPICZ α /pGAPZ α -BfOYE4	PCR colony and sequencing
pGAPZ_for	GTCCCTATTTCAATCAATTGAAC	pGAPZ α -BfOYE4	PCR colony and sequencing
GsOYE1_for	CGTCCGTTGTAGTTAGTGGACGGT	Genomic DNA	External primer for OYE isolation (PCR1)
GsOYE 2_rev	TGCGAGTCATCCAACAGAACAAC	Genomic DNA	External primer for OYE isolation (PCR1)
GsOYE 3_for	TGGACGGTGACATATGTTGAAGC	PCR1 product	Nested primer for NdeI insertion (PCR2)
GsOYE 4_rev	ATAGTTTTGGATCCTTTGTGGAAGAC	PCR1 product	Nested primer for BamHI insertion (PCR2)
GsOYE 5_for	GACCTCGTAGCGTATGGTCGTTG	PCR2 product	Suppression of internal NdeI (PCR3)
GsOYE 6_rev	CAACGACCATACGCTACGAGGTC	PCR2 product	Suppression of internal NdeI (PCR3)
GsOYE 7_for	CCATTGAAAATAGGGCGGAGAATTGTG	PCR3 product	Suppression of predicted N-glycosylation site
GsOYE 8_rev	CACAATTCTCGCCCTATTTTCAATGG	PCR3 product	Suppression of predicted N-glycosylation site
GsOYE_T25C_for	TGATGGCGCCGTTGTGCCGTAACAGAGCAGG	pET28a(+)-GsOYE	Site-specific mutagenesis
GsOYE_T25C_rev	CCTGCTCTGTTACGGCAACGGCGCCATCA	pET28a(+)-GsOYE	Site-specific mutagenesis

GsOYE_Y66F_for	TCTCAACAAGGAATGGGAT <u>TT</u> CCTGATACTCCTGGTATC	pET28a(+)-GsOYE	Site-specific mutagenesis
GsOYE_Y66F_rev	GATACCAGGAGTATCAGGA <u>AA</u> TCCCATTCTTGTGAGA	pET28a(+)-GsOYE	Site-specific mutagenesis
GsOYE_Y66A_for	TCTCAACAAGGAATGGGAG <u>CT</u> CCTGATACTCCTGGTATC	pET28a(+)-GsOYE	Site-specific mutagenesis
GsOYE_Y66A_rev	GATACCAGGAGTATCAGGA <u>GCT</u> CCCATTCTTGTGAGA	pET28a(+)-GsOYE	Site-specific mutagenesis
GsOYE_P67K_for	CAACAAGGAATGGGATAT <u>AAA</u> GATACTCCTGGTATCTAT	pET28a(+)-GsOYE	Site-specific mutagenesis
GsOYE_P67K_rev	ATAGATACCAGGAGTATC <u>TTT</u> TATATCCCATTCTTGTG	pET28a(+)-GsOYE	Site-specific mutagenesis
GsOYE_P67A_for	CAACAAGGAATGGGATAT <u>G</u> CTGATACTCCTGGTATCT	pET28a(+)-GsOYE	Site-specific mutagenesis
GsOYE_P67A_rev	AGATACCAGGAGTATCAG <u>C</u> ATATCCCATTCTTGTG	pET28a(+)-GsOYE	Site-specific mutagenesis
GsOYE_H174A_for	GATGGCATAGAAAT <u>GCG</u> GAGTGC GAATGGTTATC	pET28a(+)-GsOYE	Site-specific mutagenesis
GsOYE_H174A_rev	GATAACCATTCGCACT <u>CGC</u> CAATTTCTATGCCATC	pET28a(+)-GsOYE	Site-specific mutagenesis
GsOYE_N177A_for	AATTGCGAGTGCG <u>GCG</u> GGTTATCTATTGC	pET28a(+)- GsOYE_H174A	Site-specific mutagenesis
GsOYE_N177A_rev	GCAATAGATAACCC <u>CGC</u> CGCACTCGCAATT	pET28a(+)- GsOYE_H174A	Site-specific mutagenesis
GsOYE_Y179F_rev	TCGTGCAATAGAA <u>AA</u> ACCATTTCGCAC	pET28a(+)-GsOYE	Site-specific mutagenesis
GsOYE_Y179K_for	AATTCATAGTGC GAATGGT <u>AAG</u> CTATTGCACGAGTTTCTAG	pET28a(+)-GsOYE	Site-specific mutagenesis
GsOYE_Y179K_rev	CTAGAAACTCGTGCAATAG <u>CTT</u> ACCATTTCGCACTATGAATT	pET28a(+)-GsOYE	Site-specific mutagenesis
GsOYE_N270A_for	GAATCAAAGGA <u>GCT</u> GTGGATGTTG	pET28a(+)-GsOYE	Site-specific mutagenesis
GsOYE_N270A_rev	GAATCAAAGGA <u>GCT</u> GTGGATGTTG	pET28a(+)-GsOYE	Site-specific mutagenesis
GsOYE_N270R_for	CGAGCCAAGAATCAAAGGA <u>CGT</u> GTGGATGTTGAGAAAGAGT	pET28a(+)-GsOYE	Site-specific mutagenesis
GsOYE_N270R_rev	ACTCTTTCTCAACATCCACA <u>CGT</u> CCTTTGATTCTTGGCTCG	pET28a(+)-GsOYE	Site-specific mutagenesis
GsOYE_Y346F_for	GAGCCACATTCT <u>TT</u> TGGTGGTAATGA	pET28a(+)-GsOYE	Site-specific mutagenesis

GsOYE_Y346F_rev	TCATTACCACCA <u>A</u> AGAATGTGGCTC	pET28a(+)-GsOYE	Site-specific mutagenesis
GsOYE_Y346K_for	TTATGATAGAGCCACATTCA <u>A</u> AGGGTGGTAATGAAAAGGGAT	pET28a(+)-GsOYE	Site-specific mutagenesis
GsOYE_Y346K_rev	ATCCCTTTTCATTACCACCTT <u>G</u> AATGTGGCTCTATCATAA	pET28a(+)-GsOYE	Site-specific mutagenesis
CtOYE1_for	CAATTTTCAATCTGGTGGGGTTCGGC	Genomic DNA	External primer for OYE isolation (PCR1)
CtOYE 2_rev	ACAGTTGCGATCGAGTAGGATTCCG	Genomic DNA	External primer for OYE isolation (PCR1)
CtOYE 3_for	CATTTACCCTAGTAAAGC <u>A</u> TATGAATACCAACATCG	PCR1 product	Nested primer for NdeI insertion (PCR2)
CtOYE 4_rev	ATTAGGATCCTCAACCAGCAGCCTGCAATTCCAAAG	PCR1 product	Nested primer for BamHI insertion (PCR2)
CaOYE1_for	ATGATGCAATTAAGCAGCACGTCCG	Genomic DNA	External primer for OYE isolation (PCR1)
CaOYE 2_rev	GCGCGCATGACGAATTTATCGTACC	Genomic DNA	External primer for OYE isolation (PCR1)
CaOYE 3_for	TTCAACTACTGAGAGAGCC <u>A</u> TATGCAACCACATTTATTTAC	PCR1 product	Nested primer for NdeI insertion (PCR2)
CaOYE 4_rev	TATAGGATCCTCACCACGCCGCAAATACTGC	PCR1 product	Nested primer for BamHI insertion (PCR2)
BfOYE1.1_for	ATTCCGCCGAACACCCCACT	Genomic DNA	External primer for OYE isolation (PCR1)
BfOYE 1.2_rev	CTCCCAGGCGCAAAGGCTCT	Genomic DNA	External primer for OYE isolation (PCR1)
BfOYE 1.3_for	TACTAAACAC <u>A</u> TATGTCTCCATCCACAC	PCR1 product	Nested primer for NdeI insertion (PCR2)
BfOYE 1.4_rev	GGTATCTATCTAT <u>G</u> GATCCATGCGTC	PCR1 product	Nested primer for BamHI insertion (PCR2)
BfOYE 1.5_for	CTGGAATGGT <u>G</u> TGTCAGCCCAATTCTC	PCR2 product	Suppression of predicted N-glycosylation site
BfOYE 1.6_rev	GAGAATTGGGCTG <u>A</u> CACCATTCCAG	PCR2 product	Suppression of predicted N-glycosylation site
BfOYE 4.1_for	AGGTGCGGGAGAGATACTTCTTTGT	Genomic DNA	External primer for OYE isolation (PCR1)
BfOYE 4.2_rev	TCTCCTCATCCCCACCCACC	Genomic DNA	External primer for OYE isolation (PCR1)

BfOYE 4.3_for	CACCTGCGCCTGGTGTCCCCTTCTATACCCC	PCR1 product	Removal of intronic sequence (PCR2)
BfOYE 4.4_rev	GGGGTATAGAAGGGGACACCAGGCGCAGGTG	PCR1 product	Removal of intronic sequence (PCR2)
BfOYE 4.5_for	GTATTAGCAAATACATATGTCAACACC	PCR2 product	Nested primer for NdeI insertion (PCR3)
BfOYE 4.6_rev	CACCAAATATTCAAGGATCCAAATCAAC	PCR2 product	Nested primer for BamHI insertion (PCR3)
BfOYE4_C76T_for	GCTCTCTCCAATG ACCCA ATACTCCGC	pET28a(+)- <i>BfOYE4</i>	Site-specific mutagenesis
BfOYE4_C76T_rev	GCGGAGTATTG GGT CATTGGAGAGAGC	pET28a(+)- <i>BfOYE4</i>	Site-specific mutagenesis
BfOYE4_C76A_for	GCTCTCTCCAATG GCACA ATACTCCGC	pET28a(+)- <i>BfOYE4</i>	Site-specific mutagenesis
BfOYE4_C76A_rev	GCGGAGTATTG TGCC CATTGGAGAGAGC	pET28a(+)- <i>BfOYE4</i>	Site-specific mutagenesis
BfOYE4_Y78F_for	CCAATGTGTCAATT T CTCCGCTTCTAAC	pET28a(+)- <i>BfOYE4</i>	Site-specific mutagenesis
BfOYE4_Y78F_rev	GTTAGAAGCGGAG A ATTGACACATTGG	pET28a(+)- <i>BfOYE4</i>	Site-specific mutagenesis
<i>BfOYE4_Pichia_for</i>	ATGGGC ACGTG CCATCATCATCATCAC	pET28a(+)- <i>BfOYE4</i>	Nested primers for PmlI insertion
<i>BfOYE4_Pichia_rev</i>	CAAC GCGGCCG CCTCTAATGTCCCCC	pET28a(+)- <i>BfOYE4</i>	Nested primers for NotI insertion
<i>BfOYE4_int._for</i>	GAAGAATCACCCCTGAAGACAG	pPICZ α /pGAPZ α - <i>BfOYE4</i>	Internal primer for sequencing
AnOYE2.1_for	GGCGTGGAGGTGGTGTGGAGACGC	Genomic DNA	External primer for OYE isolation (PCR1)
AnOYE 2.2_rev	CCACATTCCACGAGTACCGCCTCGAGCGC	Genomic DNA	External primer for OYE isolation (PCR1)
AnOYE 2.3_for	CGCCGGT CCATAT GTGCTCC	PCR1 product	Nested primer for NdeI insertion (PCR2)
AnOYE 2.4_rev	GCGCTTGTAT GGATCC AATATCAGC	PCR1 product	Nested primer for BamHI insertion (PCR2)
AnOYE 8.1_for	CGTTCGAGACTAGGAGGTGCCGCGTGAG	Genomic DNA	External primer for OYE isolation (PCR1)
AnOYE 8.2_rev	CGCCCTGAGTTTTGCCGCTTAGACGGAGG	Genomic DNA	External primer for OYE isolation (PCR1)

AnOYE 8.3_for	GAACCGTCTCGGGGTATCCCAATGTGCCAG	PCR1 product	Removal of intronic sequence (PCR2)
AnOYE 8.4_rev	CTGGCACATTGGGGATACCCGAGACGGTTC	PCR1 product	Removal of intronic sequence (PCR2)
AnOYE 8.5_for	GAAGAGCACAC <u>CATATG</u> AAGGACATCAAGG	PCR2 product	Nested primer for NdeI insertion (PCR3)
AnOYE 8.6_rev	CCCGTCAAGTCTAA <u>AGCTT</u> CGTACATG	PCR2 product	Nested primer for HindIII insertion (PCR3)

All the final constructs were sequenced in order to confirm the presence of the desired gene and/or mutations.

8.1.2 Nutrition media

Nutrition media were autoclaved for 20 minutes at 121 °C and agar (1.5-2 % w/v) was added in order to prepare solid media. Antibiotics and other non autoclavable additives were filtrated (0.2 µm, Minisart, Sartorius).

• *E. coli*:

LB (Luria- Bertani)	LB low-salt (Luria- Bertani low-salt)
1% tryptone 0.5% yeast extract 1% NaCl (+ 1.5% agar) pH 7.5	1% tryptone 0.5% yeast extract 0.5% NaCl (+ 1.5% agar) pH 7.5

• *P. pastoris*:

YPD (<u>Y</u> east Extract <u>P</u> eptone <u>D</u> extrose Medium)	YPDS (<u>Y</u> east Extract <u>P</u> eptone <u>D</u> extrose Medium with <u>S</u> orbitol)
1% yeast extract 2% peptone 2% dextrose (D-glucose) (+ 2% agar)	1% yeast extract 2% peptone 2% dextrose (D-glucose) 1 M sorbitol (+ 2% agar)
BMGY (Buffered glycerol-complex Medium)	BMMY (Buffered Methanol-complex Medium)
1% yeast extract 2% peptone 100 mM Na ₂ HPO ₄ pH 6.0 1.34% YNB 1% glycerol	1% yeast extract 2% peptone 100 mM Na ₂ HPO ₄ pH 6.0 1.34% YNB 0.5% methanol

• *G. sulphuraria*

Cultures of *G. sulphuraria* were grown at 30 °C in Allen Medium pH 1.0 [181] on a rotatory platform shaker at 70 rpm. Light conditions used were 25 mol photons m⁻² sec⁻¹.

M-Allen	A2 trace element stock solution
262 mg (NH ₄) ₂ SO ₄ 54 mg KH ₂ PO ₄ 50 mg MgSO ₄ • 7H ₂ O 14 mg CaCl ₂ • 2H ₂ O 0.2 ml A2 trace element stock solution 99.4 ml distilled water pH 1.0 using 0.5 mol/L H ₂ SO ₄	285 mg H ₃ BO ₃ 180 mg MnCl ₂ • 4H ₂ O 10.5 mg ZnCl ₂ 39 mg Na ₂ MoO ₄ • 2H ₂ O 4 mg CoCl ₂ • 6H ₂ O 4.3 mg CuCl ₂ • 2H ₂ O 100 ml distilled water

After autoclaving, 0.4 ml of A2 Fe stock solution (filter-sterilized) was added. For the preparation of A2 Fe stock solution 700 mg EDTA • 2Na and 400 mg FeCl₃ • 6H₂O were dissolved in 100 ml distilled water.

- ***C. thermalis***

Cells were grown photoautotrophically at 20 °C in BG11 medium. Static cultures were continuously illuminated at 25 mol photons m⁻² sec⁻¹.

BG-11	ml/1 L
1 M TES-KOH pH 8.2	10
100X BG-FPC	10
1000X A	1
1000X B	1
Trace mineral solution	1
99.4 ml MilliQ water	977

Trace mineral solution	100X BG-FPC
2.86 g H ₃ BO ₃	149.58 g Na NO ₃
1.81 g MnCl ₂ • 4H ₂ O	7.49 g MgSO ₄ • 7H ₂ O
0.22 g ZnSO ₄ • 7H ₂ O	3.6 g CaCl ₂ • 2H ₂ O
0.39 g Na ₂ MoO ₄ • 2H ₂ O	0.92 g citric acid
0.05 g Co(NO ₃) • 6H ₂ O	1.12 ml 0.25 M EDTA • 2Na pH 8.0
0.08 g CuSO ₄ • 5H ₂ O	100 ml trace mineral solution
to 1 L with MilliQ water	to 1 L with MilliQ water

For the preparation of 1000X A stock solution 3.05 g K₂HPO₄ and 2 g Na₂CO₃ were dissolved in 100 ml distilled water, while for the stock solution 1000X B 0.6 g ferric ammonium citrate was dissolved in 100 ml distilled water.

- ***A. niger***:

Cells of *A. niger* were grown for 3 days at room temperature on solid malt extract purchased from Sigma Aldrich.

Solid malt extract	g/1 L
Glucose	6
Malt extract	6
Maltose	1.8
Yeast extract	1.2
Agar	15

8.1.3 Bacterial and yeast strains

- **XL-1 Blue:** *E.coli recA1 endA1 gyrA96 thi-1 hsdR17 supE44 relA1 lac [F' proAB lacI^qZΔM15 Tn10 (Tet)]*
- **DH5α ®:** *E. coli fhuA2 (argF-lacZ)U169 phoA glnV44 80 (lacZ)M15 gyrA96 recA1 relA1 endA1 thi-1 hsdR17*

- **BL21 (DE3) ®:** *E. coli fhuA2 [lon] ompT gal (λ DE3) [dcm] ΔhsdS λ DE3 = λ sBamHI ΔEcoRI-B int::(lacI::PlacUV5::T7 gene1) i21 Δnin5*
- **BL21 (DE3) Arctic ®:** *E. coli B F⁻ ompT hsdS (rB – mB –) dcm+ Tetr gal λ(DE3) endA Hte [cpn10 cpn60 Gentr]*
- **OverExpress C41 (DE3) ®:** *E. coli F⁻ ompT hsdSB (rB- mB-) gal dcm (DE3)*
- **OverExpress C43 (DE3) ®:** *E. coli F⁻ ompT hsdSB (rB- mB-) gal dcm (DE3)*
- **X-33:** wild type *Pichia pastoris* strain.

8.1.4 Expression vectors

For the expression of ene-reductase genes in *E. coli* a pET28a vector was used. The vector is composed by a T7lac promoter for the regulated expression of the desired gene after induction with IPTG; a LacI promoter for the transcription of LacI gene and a LacI coding sequence for lac repressor are also present. A multiple cloning site (MCS) where the sequences of the desired ene-reductases genes were cloned using NdeI and BamHI/HindIII restriction sites is also present, followed by a T7 terminator sequence. The plasmid contains also the KanR gene for the resistance to Kanamycin and a bacterial origin of replication (ori) sequence to guarantee the replication of the plasmid inside the bacterial cells (Fig. 131).

For the expression of *BfOYE4* gene in *Pichia pastoris* two different vectors were chosen: pPICZα and pGAPZα.

pPICZα is composed by the following elements (Fig. 132 A): a 5'AOX: alcohol oxidase 1 (*AOX1*) promoter that allows high-level methanol-inducible expression, targeting plasmid integration to the *AOX1* locus and a native *Saccharomyces cerevisiae* α-factor secretion signal that allows for efficient secretion of most recombinant proteins from *Pichia*. Moreover, the multiple cloning site (MCS) permits the insertion of the gene of interest into the expression vector followed by a C-terminal poly-histidine tag used for IMAC purification of the fusion protein and also to detect the fusion protein by the anti-his antibody. A native transcription termination and polyadenylation signal from *AOX1* gene are also present as well as the transcription elongation factor gene promoter (*TEF1*) from

Saccharomyces cerevisiae that drives expression of the *Sh ble* gene in *P. pastoris*, that confers Zeocin resistance. Finally, some elements such as EM7 (synthetic prokaryotic promoter) and the pUC origin that allow the expression of *Sh ble* gene in *E. coli* and the replication and maintenance of the plasmid in *E. coli*, respectively, are also present.

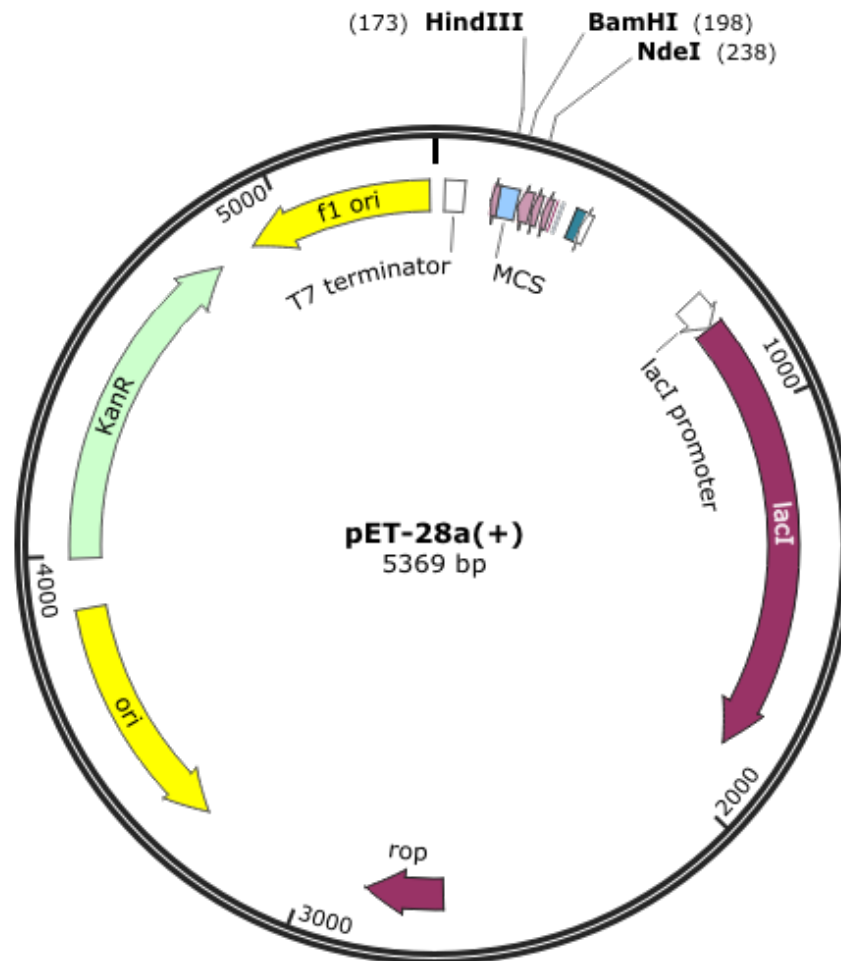


Figure 131. pET28a(+) vector map.

pGAPZ α (Fig. 132 B) was previously built in Professor Bubacco's laboratory from Padova University starting from the expression vector pPICZ α , and substituting the inducible promoter PAOX1 with the constitutive promoter of glyceraldehyde-3-phosphate dehydrogenase (PGAP). It is composed by the same elements of the previously described vector pPICZ α , excluding the promoter that allows high-level constitutive expression and it targets plasmid integration to the *GAP* locus.

Both expression vectors do not contain a yeast origin of replication. Only a recombination event between the plasmid and the genome of *Pichia pastoris* permits the maintenance of the genetic information.

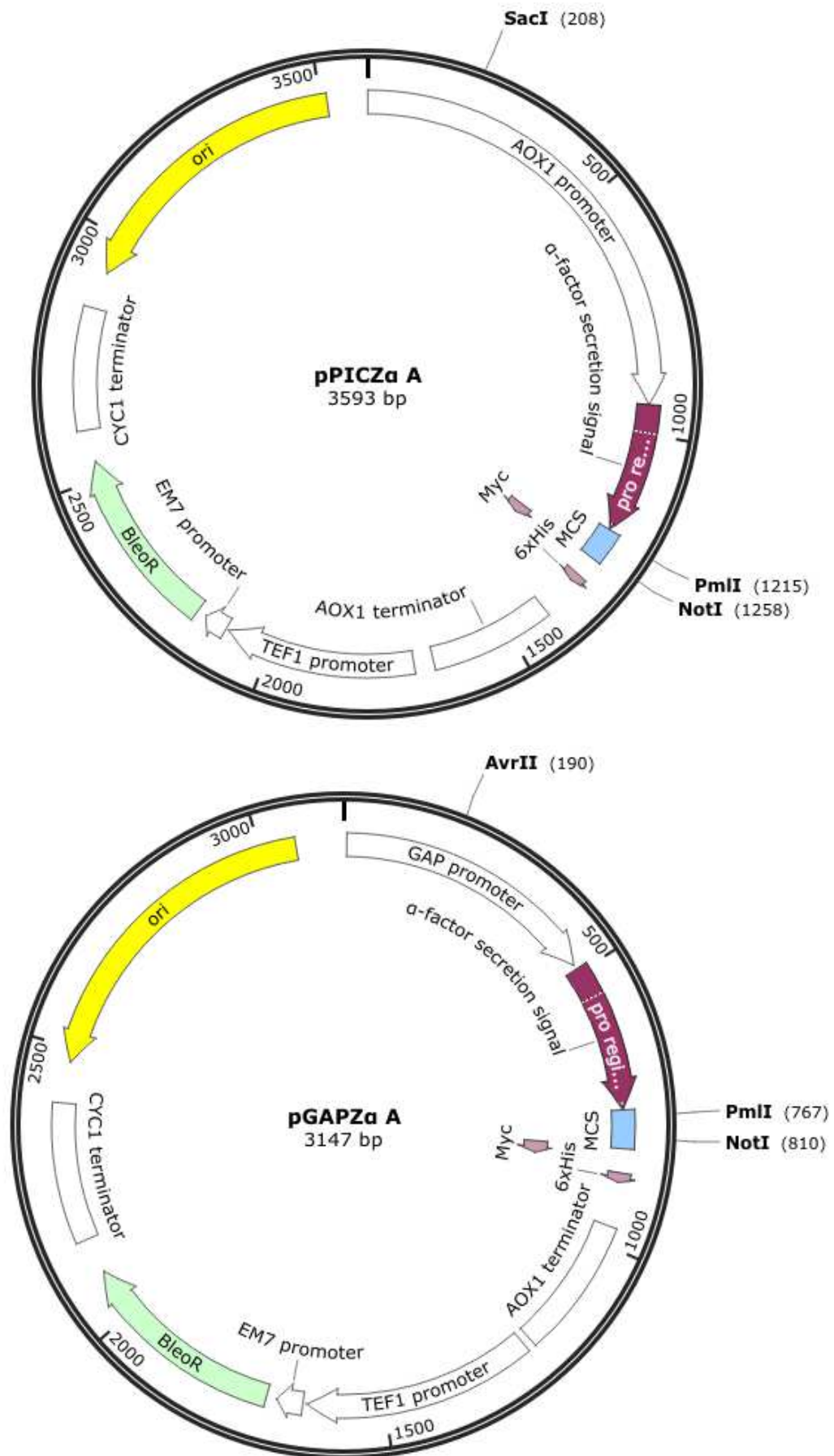


Figure 132. pPICZαA commercial vector map (A) and pGAPZα (B).

8.2 Methods

8.2.1 Cloning

All the PCR reactions used for the amplification of the desired genes or for the screening of positive clones after ligation (PCR colony) were performed following standard protocols and the specifics of each DNA polymerase used reported in the supplier data sheets. The mutations were introduced using the overlap PCR extension technique. Briefly, first a PCR to generate two overlapping gene segments, containing the desired mutation, was performed and subsequently the mutated full-length gene was obtained by another PCR using as template DNA the two fragments previously synthesized and amplified by external primers. The final vector with the desired gene was obtained after digestion and subsequent ligation of the desired gene and plasmid with NdeI (5' end) and BamHI (3' end) (except *AnOYE8* for which HindIII was used) following supplier's data sheet. All the new constructs were sequenced in order to confirm the correct plasmid assembly. The cloning of *GsOYE* is subsequently reported as example of the general cloning strategy used for all constructs.

1) PCR protocols

<u>1) <i>GsOYE</i> isolation from genomic DNA (PCR1 <i>Gs</i>)</u>		T (°C)	time	Cycles
Phusion buffer 5X	10 µl	Initial denaturation	98	30 sec
GS1_for (10 µM)	2.5 µl	Denaturation	98	10 sec
GS2_rev (10 µM)	2.5 µl	Annealing	60	30 sec
dNTPs (10 mM)	1 µl	Extension	72	60 sec
Genomic DNA	0.25 µl (50 ng)	Final extension	72	10 min
Phusion polymerase (2 U/µl)	0.5 µl			
H ₂ O mQ	33.25 µl			
Total volume	50 µl			
<u>2) Insertion of desired restriction sites (PCR2 <i>Gs</i>)</u>		T (°C)	time	Cycles
Phusion buffer 5X	10 µl	Initial denaturation	98	30 sec
GS3_for (10 µM)	2.5 µl	Denaturation	98	10 sec
GS4_rev (10 µM)	2.5 µl	Annealing	50	30 sec
dNTPs (10 mM)	1 µl	Extension	72	40 sec
PCR1 <i>Gs</i>	1 µl	Denaturation	98	10 sec
Phusion polymerase (2 U/µl)	0.5 µl	Annealing	55	30 sec
H ₂ O mQ	32.5 µl	Extension	72	40 sec
Total volume	50 µl	Final extension	72	10 min
<u>3) Elimination internal NdeI site</u>		T (°C)	time	Cycles
PCR1		Initial denaturation	98	30 sec
Phusion buffer 5X	10 µl	Denaturation	98	10 sec
GS3_for (10 µM)	2.5 µl	Annealing	55	30 sec
GS6_rev (10 µM)	2.5 µl	Extension	72	30 sec
dNTPs (10 mM)	1 µl			

PCR2 Gs	0.25 µl	Final extension	72	10 min	
Phusion polymerase (2 U/µl)	0.5 µl				
H ₂ O mQ	33.25 µl				
Total volume	50 µl				
PCR2			T (°C)	time	Cycles
Phusion buffer 5X	10 µl	Initial denaturation	98	30 sec	
GS5_for (10 µM)	2.5 µl	Denaturation	98	10 sec	
GS4_rev (10 µM)	2.5 µl	Annealing	55	30 sec	x 30
dNTPs (10 mM)	1 µl	Extension	72	30 sec	
PCR2 Gs	0.25 µl	Final extension	72	10 min	
Phusion polymerase (2 U/µl)	0.5 µl				
H ₂ O mQ	33.25 µl				
Total volume	50 µl				
PCR3			T (°C)	time	Cycles
Phusion buffer 5X	10 µl	Initial denaturation	98	30 sec	
GS3_for (10 µM)	2.5 µl	Denaturation	98	10 sec	
GS4_rev (10 µM)	2.5 µl	Annealing	55	30 sec	x 30
dNTPs (10 mM)	1 µl	Extension	72	40 sec	
PCR1 dil. 1/10	1 µl	Final extension	72	10 min	
PCR2 dil. 1/10	1 µl				
Phusion polymerase (2 U/µl)	0.5 µl				
H ₂ O mQ	31.5 µl				
Total volume	50 µl				
4) <u>Elimination N-glycosylation site</u>					
PCR1			T (°C)	time	Cycles
Phusion buffer 5X	10 µl	Initial denaturation	98	30 sec	
GS3_for (10 µM)	2.5 µl	Denaturation	98	10 sec	
GS8_rev (10 µM)	2.5 µl	Annealing	53	30 sec	x 5
dNTPs (10 mM)	1 µl	Extension	72	30 sec	
PCR3 dil. 1/10	0.5 µl	Denaturation	98	10 sec	
Phusion polymerase (2 U/µl)	0.5 µl	Annealing	56	30 sec	x 25
H ₂ O mQ	33 µl	Extension	72	30 sec	
Total volume	50 µl	Final extension	72	10 min	
PCR2			T (°C)	time	Cycles
Phusion buffer 5X	10 µl	Initial denaturation	98	30 sec	
GS7_for (10 µM)	2.5 µl	Denaturation	98	10 sec	
GS4_rev (10 µM)	2.5 µl	Annealing	53	30 sec	x 5
dNTPs (10 mM)	1 µl	Extension	72	30 sec	
PCR3 dil. 1/10	0.25 µl	Denaturation	98	10 sec	
Phusion polymerase (2 U/µl)	0.5 µl	Annealing	56	30 sec	x 25
H ₂ O mQ	33.25 µl	Extension	72	30 sec	
Total volume	50 µl	Final extension	72	10 min	
PCR3			T (°C)	time	Cycles
Phusion buffer 5X	10 µl	Initial denaturation	98	30 sec	
GS3_for (10 µM)	2.5 µl	Denaturation	98	10 sec	
GS4_rev (10 µM)	2.5 µl	Annealing	55	30 sec	x 30
dNTPs (10 mM)	1 µl	Extension	72	40 sec	
PCR1 dil. 1/10	1 µl	Final extension	72	10 min	
PCR2 dil. 1/10	1 µl				
Phusion polymerase (2 U/µl)	0.5 µl				
H ₂ O mQ	31.5 µl				
Total volume	50 µl				

2) Digestion with NdeI and BamHI

The amplified and purified GsOYE CDS and the empty pET28a(+) plasmid were digested with NdeI and BamHI enzymes.

	GsOYE CDS	pET28a(+)
isolated OE-PCR product (10 ng/μl)	25 μl	-
pET28a (50 ng/μl)	-	20 μl
NdeI (20 U/μl)	1 μl	1 μl
BamHI-HF (20 U/μl)	1 μl	1 μl
Cut Smart Buffer 10X	5 μl	5 μl
H ₂ O mQ	18 μl	23 μl
Total volume	50 μl	50 μl

The reactions were incubated for 3 hours at 37 °C.

The extremities of the plasmid were dephosphorylated to avoid the reformations of empty circular vectors. Therefore, 1 μl of TSAP enzyme (Thermosensitive Alkaline Phosphatase) (1 U/ μl) were added to the reaction and incubated at 37 °C for 20 minutes. The TSAP enzyme was then inactivated by heating at 74 °C for 20 minutes.

The two digestion reactions have been purified using the EuroGold Gel Extraction kit. 1% w/v agarose gel electrophoresis assay was performed to check the digestion of the plasmid.

3) Ligation of GsOYE CDS into pET28a(+) vector

The digested gene and vector were ligated together using the enzyme T4 DNA ligase, according to the amounts listed below. In the same way, also an auto-ligation reaction was performed, substituting the volume of the gene with water. Ligation and auto-ligation reactions have been incubated overnight at 16 °C.

Purified digested GsOYE gene (10 ng/μl)	5 μl
Purified digested pET28a(+) (50 ng/μl)	1.5 μl
T4 DNA ligase Buffer 10X	2 μl
T4 DNA ligase (400 U/ μl)	1 μl
H ₂ O mQ	10.5 μl
Final volume	20 μl

10 ml of ligation and auto-ligation reactions were used to transform DH5α chemo-competent cells (100 μl). The reaction was kept on ice for 30 minutes, heat shocked at 42 °C for 45 seconds and then placed on ice. After the transformation, 300 μl of LB were added to the reaction, and incubated for 1 hour at 37 °C and 180 rpm. Transformed cells were then plated on LB agar containing 50 μg/ml of kanamycin and incubated overnight at 37 °C.

4) Colonies screening for the identification of recombinant clones

Successful ligation was examined by colony PCR, analytical restriction digestion and sequencing to confirm the correct insertion of the gene and the absence of undesired mutations.

a) Colony PCR screening

10 isolated colonies derived from the ligation reaction, and one colony grown from the auto-ligation reaction (negative control), have been picked and solubilized in 100 μ l of LB. After that, a PCR reaction was performed amplifying the DNA directly from the cells, thus by-passing the plasmid purification step.

Colony solubilized in LB	0.2 μ l		T ($^{\circ}$ C)	time	Cycles
GoTaq Flexi Buffer 5X	6.0 μ l	Initial denaturation	95	2 min	
T7_for (10 μ M)	1.5 μ l	Denaturation	95	1 min	
T7_rev (10 μ M)	1.5 μ l	Annealing	55	1 min	x 25
dNTPs (10 mM)	1.0 μ l	Extension	72	1.5 min	
MgCl ₂ (25 mM)	1.8 μ l	Final extension	72	10 min	
GoTaq polymerase (5 U/ μ l)	0.15 μ l				
H ₂ O mQ	18.25 μ l				
Total volume	30 μ l				

PCR reactions (5 μ L) were checked by 1% w/v agarose gel electrophoresis. Two positive colonies, have been inoculated overnight in LB with 50 μ g/ml kanamycin. The plasmids were purified using an EuroGold Mini prep kit and the DNA concentration was determined measuring the absorbance at 260 nm with a spectrophotometer (Agilent 8453). One absorbance unit corresponds to 50 μ g of DNA in 1 ml.

b) Analytical NdeI and BamHI digestion screening

The pET28a(+):GsoYE vectors purified from positive clones from the previous screening have been analyzed through digestion with NdeI and BamHI to confirm the correct insertion of the gene. Each plasmid has been digested individually with NdeI and BamHI, and using a mixture of both the enzymes

pET28a(+):GsoYE (50 ng/ μ l)	2 μ l	2 μ l	2 μ l
NdeI (20 U/ μ l)	0.2 μ l	-	0.2 μ l
BamHI-HF (20 U/ μ l)	-	0.2 μ l	0.2 μ l
Cut Smart Buffer 10X	1 μ l	1 μ l	1 μ l
H ₂ O mQ	6.8 μ l	6.8 μ l	6.6 μ l
Final volume	10 μ l	10 μ l	10 μ l

The reactions have been incubated for 1 hours at 37 $^{\circ}$ C and then checked by 1% w/v agarose gel electrophoresis.

c) Sequencing

The recombinant plasmid (650 ng) from previously selected positive clones have been dried at 65 °C and sent to BMR Genomics. The complete insert sequencing was carried out using T7_for and T7_rev primers.

8.2.2 Expression in *E. coli*

The pET28a constructs containing the relative ER genes were transformed into *E. coli* BL21 (DE3) or *E. coli* BL21 (DE3) Arctic® cells. Briefly, 100 µl of KCM solution (100 mM KCl, 30 mM CaCl₂ and 50 mM MgCl₂) containing 1 µl of the desired plasmid (50-100 ng/ µl) were added to a BL21(DE3) cell suspension (100 µl). The mix was kept on ice for 30 minutes and then heat shocked at 42 °C for 45 seconds, then immediately put back on ice. After the transformation, 300 µl of LB were added and the cells were incubated at 37 °C for 1 hour. The cells were plated onto selective medium containing 50 µg/ml kanamycin (and 30 µg/ml gentamicin for *E. coli* Arctic®) and incubated overnight at 37 °C.

For small test expression scale cultures were carried out in 25 ml of Luria-Bertani (LB) *medium* containing 50 µg/ml kanamycin (and 30 µg/ml gentamicin for *E. coli* Arctic®) while for purification purposes larger cultures were carried out in 1 L LB *medium*. The cells were grown in a shaking incubator at 37 °C to an optical density at 600 nm (OD₆₀₀) of 0.4–0.6, then riboflavin was added (in 25 µM final concentration) and the cells were induced by addition of isopropyl β-D-1-thiogalactopyranoside (IPTG) to a final concentration of 0.2 mM and cultivated over-night at the optimized temperature of each protein. The cells were harvested by centrifugation (4 °C, 10 min, 5000 × g) and washed with 50 mM Tris-HCl, 150 mM NaCl buffer pH 8.0. Cell disruption was obtained by French Press (Constant Systems Cell Disruptor OneShot; Constant Systems, Kennesaw, GA, USA) and crude extract was centrifuged (4 °C, 30 min, 18000 × g) to separate soluble and insoluble fractions. To enhance the flavination FMN cofactor (at 100 µM final concentration) was added to the crude extract before cell disruption. To verify the expression of the desired ER, different samples corresponding to not induced cells, induced cells, pellet, supernatant were withdrawn, denatured with solubilisation buffer (SB) and used for SDS-PAGE analysis.

Immunoblotting assay was also performed using anti His-tag antibodies in order to verify the identity of the protein.

8.2.3 *BfOYE4* expression in *Pichia pastoris*

BfOYE4 was expressed in *P. pastoris* using two different vectors: one inducible with methanol (pPICZ α) and a constitutive expression system (pGAPZ α).

8.2.3.1 *BfOYE4* expression in *P. pastoris* using the inducible expression vector pPICZ α

Nine clones were chosen for the induction and expression of *BfOYE4* gene. The nine clones and a wild type clone, were picked from the YPD plates + 100 μ g/ml Zeocin and were inoculated in 2 ml of BMGY medium in a 50 ml tube. The inoculums were incubated at 28 °C for 24 hours at 250 rpm. Cells were harvested by centrifugation at 15000 g for 5 minutes at 4 °C. The pellet was washed with 5 ml of BMMY medium. The cellular suspension was centrifuged at 15000 g for 5 minutes at 4 °C and the harvested cells were resuspended into 10 ml of BMMY in a 100 ml flask. The culture was incubated at 28 °C for 96 h and 250 rpm. Samples were collected at different times (0, 24, 48, 72, 96 hours) after the induction with methanol. In particular, 2 ml of culture were collected and centrifuged at 15000 g at 4 °C for 5 minutes. The medium was concentrated 10 times using a Vivaspin concentrator (cut off MW 10000 kDa). The concentrated culture medium and the cellular pellet were stored at -20 °C until polyacrylamide gels and immunoblotting assay were performed. Every 24 hours, the culture was supplemented with 1% methanol and re-incubated at 28 °C and 250 rpm. Besides the methanol, some expression tests were performed also adding 25 μ M FMN to the culture.

8.2.3.2 *BfOYE4* expression in *P. pastoris* using the constitutive expression vector pGAPZ α

Eight clones and a wild type clone, were picked from the YPD plates + 100 μ g/ml Zeocin and were inoculated in 5 ml of YPD medium in a 50 ml tube, and incubated overnight at 28 °C and 250 rpm. A proper amount of the pre-inoculum was used to inoculate 10 ml of YPD in a 100 ml flask, thus obtaining an OD_{600 nm} ~1, and then the culture was incubated at 28 °C and 250 rpm for 96 hours. Samples were collected at different times (0, 24, 48, 72, 96 hours). In particular, 2 ml of culture were collected and centrifuged at 15000 g at 4 °C for 5 minutes. The culture medium was concentrated 10 times using a Vivaspin concentrator (cut off MW 10000 kDa). The concentrated culture media and the cellular pellet were stored at -20 °C until polyacrylamide gels and immunoblotting assay were performed.

8.2.4 SDS-PAGE and UREA-PAGE

The degree of proteins expression and proteins purity was assessed using 12% polyacrylamide gel.

The 12% polyacrylamide gel was prepared following the recipe below.

Stacking Gel		Running Gel	
Composition	Volume	Composition	Volume
Acrylamide 40%	0.5 mL	Acrylamide 40%	3 mL
0.313 M Tris-HCl pH 6.8	625 μ L	3 M Tris-HCl pH 8.8	1.24 mL
SDS 10%	50 μ L	SDS 10%	100 μ L
H ₂ O mQ	3.82 mL	H ₂ O mQ	5.66 mL
Temed	18 μ L	Temed	20 μ L
APS 10%	26 μ L	APS 10%	30 μ L

Urea-PAGE was used to analyze samples from *P. pastoris*. Generally, a 12% polyacrylamide gel was prepared following the recipe below.

Stacking Gel		Running Gel	
Composition	Volume	Composition	Volume
		Urea	3.63 g
Acrylamide 40%	0.375 mL	Acrylamide 40%	3 mL
0.313 M Tris-HCl pH 6.8	1 mL	3 M Tris-HCl pH 8.8	2.67 mL
H ₂ O mQ	1.62 mL	H ₂ O mQ	1.59 mL
Temed	3.5 μ L	Temed	5.5 μ L
APS 10%	35 μ L	APS 10%	55 μ L

Once polymerized, the gel was placed into a Hoefer™ Mighty Small™ II Mini Vertical Electrophoresis Systems (Thermo Fisher Scientific) and covered with the Superior buffer (25 mM Tris-HCl, 192 mM glycine, 0.1% w/v SDS).

The samples were solubilized in solubilization buffer (SB) (10% glycerol, 40 mM Tris pH 6.8, 3% SDS, 0.03 M DTT, 1 mg/ml bromophenol blue) and denatured at 99 °C for 15 minutes. First, an intensity of electric current of 12 mA was applied, allowing the samples to enter the stacking gel and to compact in a sharp band, then the current was increased at 20 mA, allowing the separation of the samples. The gels were stained by Coomassie Blue staining (0.1% Coomassie Blue, 45% methanol, 10% CH₃COOH) for 30 minutes and then destained with a solution composed of 10% methanol and 7.5% CH₃COOH.

For silver staining the gel was incubated over-night with a fixing solution (50% methanol, 12% CH₃COOH, 50 μ l of formaldehyde 37% in 100 ml of water). After fixation, the gel was washed with 50% ethanol (3 times x 20 minutes) and subsequently incubated with the pre-treatment solution (0.02g Na₂S₂O₃ in 100

ml of water) for 1 minute and then washed three times with water. Furthermore, the gel was then incubated for 20 minutes with the silver staining solution (0.2 g AgNO₃, 75 µl of formaldehyde 37% in 100 ml of water) and then washed three times with water. After the staining, the gel was incubated with the development solution (6 g Na₂CO₃, 50 µl of formaldehyde 37%, 2 ml of the pre-treatment solution in a total volume of 100 ml) until dark brown bands appeared. Two fast washes with water were then performed and finally the gel was incubated with the stop solution (50% methanol, 12% ml CH₃COOH) for 10 minutes and washed with a solution of 50% methanol.

8.2.5 Immunoblot assay

After performing a Urea-PAGE or a SDS-PAGE, as already described, the proteins were transferred to a PVDF blotting membrane (GE Healthcare Life Sciences), previously activated by methanol. Sponges, blotting paper, PVDF membrane and the acrylamide gels, were used to assembly a sandwich which was wet by Transfer Buffer (0.01 M NaHCO₃, 0.003 M Na₂CO₃, 10% methanol). The sandwich was loaded into a Hoefer TE22 Mighty Small Transfer Tank and covered by the Transfer Buffer. The transfer operation was performed over-night at 4 °C using 200 mA. After the transfer of the proteins, the membrane was saturated with milk (10% w/v) dissolved in TBS solution (10 mM Tris-HCl, 150 mM NaCl) and incubated for 1 hour in tilting agitation. The excess of milk was washed using TBS solutions (5 washes in 30 minutes). The membrane was then incubated for 2 hours with the primary antibody (murine anti-His tag antibody) diluted 1:6000 in TTBS solution (10 mM Tris-HCl, 150 mM NaCl, 0.05% Tween 20). The excess of antibody was then washed away by 5 washes completed in 30 minutes using TTBS solution. Subsequently, the secondary antibody (goat-anti-mouse antibody) (diluted 1:15000 in TTBS solution) labelled with a peroxidase was added and let incubate for 1 hour. The excess of antibody was washed away (5 washes in 30 minutes with TTBS solution). Finally, the membrane was incubated for 5 minutes with a 1:1 peroxide-luminol solution. A photographic film has been impressed by the chemiluminescence, developed and fixed in the dark room.

8.2.6 Purification and enzymes concentration determination

Overexpressed proteins were purified by immobilized-metal affinity chromatography (IMAC). Soluble fractions obtained from 1 L culture were incubated with the nickel derivatized resin for 30 min at 4 °C and then loaded on

a 10 ml empty Poly-prep® column (Bio-Rad). The column was washed by gravitational flow with five column volumes of 50 mM Tris-HCl, 150 mM NaCl buffer pH 8.0. Elution was performed by five column volumes of 50 mM Tris-HCl pH 8.0 and 250 mM imidazole solution. For the proteins expressed in BL21 (DE3) Arcite® cells a further step of incubation was introduced to remove the impurities due to the chaperonin, as previously reported in [235]. Briefly, after the washing, the resin was incubated for 2 hours at 4 °C, in agitation on the tube revolver with a dissociation buffer (20 mM HEPES pH 7.0, 10 mM MgCl₂, 5 mM ATP, 150 mM KCl). The resin was then loaded again into the column and washed by gravitational flow with five column volumes of 50 mM Tris-HCl, 100 mM NaCl pH 8.0. Elution was performed by five column volumes of 50 mM Tris-HCl pH 8.0, 250 mM imidazole solution. Yellow fractions were collected and pooled together. Excess of imidazole was removed by the addition of 3 volumes of 50 mM Tris-HCl, 150 mM NaCl buffer pH 8.0 during the concentration of the proteins using Vivaspin® concentrators. For crystallization purposes the excess of imidazole was removed by size exclusion chromatography.

Enzyme concentration was measured by spectrophotometry, measuring the concentration of free flavin in a solution of denatured protein and calculated as previously reported [177]. By this approach, the extinction coefficient of the flavin-containing enzyme can be calculated by comparing the absorption spectra before and after protein thermal denaturation. Assuming that the absorption spectrum of the unfolded protein can be compared to that of the free FMN (ϵ_{FMN} , 446 nm = 12.2 mM⁻¹ cm⁻¹), a molar extinction coefficient can be calculated for the native forms of the enzymes.

8.2.7 Activity assay and steady- state kinetics

Ene-reductases activity was determined by an Agilent 8453 spectrophotometer monitoring the consumption of NADPH at 340 nm ($\epsilon = 6.22 \text{ mM}^{-1} \text{ cm}^{-1}$). In case of ketoisophorone, the assay was performed at 365 nm using a molar absorption coefficient of 3.51 mM⁻¹ cm⁻¹ [140]. The standard assay (100 µl) was performed at 25 °C in 50 mM Tris-HCl, 150 mM NaCl pH 8.0 containing 100 µM NADPH and 10 mM of substrate dissolved in 100% DMSO (1% final concentration). The reaction was started through the addition of enzyme to a final concentration of 200 nM and monitored for 60 seconds.

One unit of ene-reductase enzymes (ERs) is defined as the amount of protein that

reduces 1 μmol NADPH per minute at a defined temperature and pH. The following equation was used to calculate the enzymatic activity (U/ml):

$$\frac{U}{\text{ml}} = \frac{m \cdot V_{\text{cell}} \cdot t \cdot d}{\epsilon_{\text{NADPH}} \cdot b \cdot V_{\text{enzyme}}}$$

slope: m

Cell volume: $V_{\text{cell}} = 0.1 \text{ ml}$

Time: $t = 60 \text{ seconds}$

Enzyme dilution: d

Molar absorptivity coefficient: $\epsilon_{\text{NADPH}} = 6.22 \text{ mM}^{-1} \text{ cm}^{-1}$ or $3.51 \text{ mM}^{-1} \text{ cm}^{-1}$

Path length: $b = 1 \text{ cm}$

Volume of enzyme: V_{enzyme}

The specific activity of the enzyme (U/mg) was calculated dividing the enzymatic activity (U/ml) by the initial concentration of the enzyme (mg/ml). The experiment was performed at least in duplicate.

Steady-state kinetic parameters K_M and k_{cat} were determined just for the substrates which were transformed during the previous activity assay. The standard activity assay (100 μl) was performed using different concentrations ranging from 0 to 50 mM of the same substrate.

Steady-state kinetic parameters K_M and k_{cat} were also determined for the cofactors NADPH and NADH. The activity assay (200 μl) was performed using different concentrations of cofactors ranging from 0 to 2 mM, 10 mM of maleimide and 20- 200 nM of enzyme in 50 mM Tris-HCl, 150 mM NaCl pH 8.0.

First the parameter k_{observed} has been calculated as follows:

$$K_{\text{observed}} = \frac{\text{slope}}{\epsilon_{\text{NADPH}} \cdot C_{\text{enzyme}} \cdot b}$$

For the substrates, the b parameter was 1 cm, while for the cofactors was 0.1 cm. ϵ_{NADPH} at 340 nm was $0.00622 \mu\text{M}^{-1} \text{ cm}^{-1}$ and at 365 nm was $0.00351 \mu\text{M}^{-1} \text{ cm}^{-1}$

Second, the k_{observed} data were fitted using the Michaelis–Menten equation by the program Graph-Pad Prism 6.0.

Third, the catalytic efficiency was calculated dividing the k_{cat} (s^{-1}) by the K_M (mM).

8.2.8 Conversions and GC/GC-MS analysis

An aliquot of enzymes (100 µg/ml) (2.5 µM) was added to a Tris-HCl buffer solution (0.5 ml, 50 mM, pH 8.0) containing the substrate (10 mM) and the oxidized form of the cofactor (NAD⁺, 100 µM), the co-substrate (glucose, 20 mM) and the corresponding recycling enzyme (glucose dehydrogenase, 10 U/ml). For substrates **1a**, **2a**, **4a**, **5a**, **7a**, **8a** and **12a** a final concentration of 50 mM was also tested. The reaction mixture consisted of Tris-HCl buffer solution (0.5 ml, 50 mM, pH 8.0) containing the substrate (50 mM) and the oxidized form of the cofactor (NAD⁺, 1 mM), the co-substrate (glucose, 100 mM) and the corresponding recycling enzyme (glucose dehydrogenase, 10 U/ml).

All substrates were added as a 1 M DMSO solution (1% final DMSO concentration) to overcome their poor solubility in water. The mixture was shaken at 30 °C and 140 rpm. After over-night incubation, products were extracted with EtOAc (2 x 0.25 mL for 10 mM substrate and 4 x 0.25 mL for 50 mM substrate) containing 10 mM (*R*)-limonene as internal GC standard. The combined organic phases were dried (Na₂SO₄) and the resulting samples were analyzed on achiral GC. Conversion was estimated based on product formation or substrate depletion, when authenticated GC standard were not available, according to calibration curves. The calibration curves are reported in the Appendix section.

For compounds **15a**, **16a**, **17a** (10 mM) the reaction mixture was composed of Tris-HCl buffer solution (0.5 ml, 50 mM, pH 5.0 - 8.0), the oxidized form of the cofactor (NAD⁺, 500 µM), the cosubstrate (glucose, 20 or 50 mM) and the corresponding recycling enzyme (glucose dehydrogenase, 10 U/ml). All substrates were added as a 1 M DMSO solution (1% final DMSO concentration) to overcome their poor solubility in water. The mixture was shaken at different temperatures (10 °C, 25 °C and 30 °C) and 140 rpm. After over-night incubation, products were extracted with EtOAc (2 x 0.25 mL) containing 10 mM (*R*)-limonene as internal GC standard. The combined organic phases were dried (Na₂SO₄) and the resulting samples were analyzed on GC-MS. Products were identified by comparison with authentic reference materials (which were either commercially available or were independently synthesized) via co-injection on GC-MS.

Analytical procedures for determination of conversion:

GC–MS analyses were performed on a 7890A GC System (Agilent Technologies, Santa Clara, CA, USA), equipped with a 5975C mass selective detector. GC–FID analyses were carried out with GC System (Agilent Technologies, Santa Clara, CA, USA) by using H₂ as a carrier gas (14.5 psi). HPLC analyses were performed by using a Shimadzu LC-20AD HPLC system equipped with a DGU-20 A5 degasser, a SIL-20AC autosampler, SPD-M20A diode array detector and a CTO-20AC column oven.

Conversions for 2-cyclohexen-1-one (**4a**), 2-methyl-cyclohexenone (**5a**) and 5-phenyl-cyclohexenone (**11a**) were analyzed by GC-FID using a 5% phenyl-dimethylpolysiloxane capillary column (HP-5 Agilent, 30 m, 0.32 mm, 0.25 μm), detector temperature 250 °C, split ratio 20:1. Programme for **4a**: 40 °C, hold for 2.0 min, 10 °C min⁻¹ to 280 °C, hold for 1.0 min. Retention times were as follow: cyclohexanone (**4b**) 1.97 min, 2-cyclohexen-1-one (**4a**) 2.16 min. Programme for **5a**: 80 °C, hold for 10 min, 20 °C min⁻¹ to 210 °C, hold for 2.0 min. Retention times were as follows: 2-methyl-cyclohexanone (**5b**) 6.07 min, 2-methyl-cyclohexenone (**5a**) 6.89 min. Programme for **11a**: 80 °C, hold for 2 min, 10 °C min⁻¹ to 280 °C, hold for 1.0 min.

Conversions of 2-cyclopenten-1-one (**1a**), 2-methyl-cyclopentenone (**2a**), 3-methylcyclopentenone (**3a**), 3-methylcyclohexenone (**6a**), 1-acetylcyclohexene (**10a**), citral (**13a**) were determined using a 14% cyanopropylphenyl-dimethylpolysiloxane (DB-column 1701 Agilent, 30 m x 0.25 mm, 0.25 μm), detector temperature 250 °C, split ratio 20:1. Programme: 80 °C, hold for 10 min, 20 °C min⁻¹ to 200 °C, hold for 2.0 min. Retention times were as follow: 2-cyclopentanone (**1b**) 3.59 min, 2-cyclopenten-1-one (**1a**) 4.74 min, 2-methyl-cyclopentanone (**2b**) 4.28 min, 2-methyl-cyclopentenone (**2a**) 6.21 min, 3-methylcyclopentanone (**3b**) 4.57, 3-methylcyclopentenone (**3a**) 10.5 min, 3-methylcyclohexanone (**6b**) 7.9 min, 3-methylcyclohexenone (**6a**) 12.93 min, 1-acetylcyclohexane (**10b**) 11.2 min, 1-acetylcyclohexene (**10a**) 13.01 min, citronellal (**13b**) 13.51 min, neral and geranial (**13a**) 15.21 min and 15.56 min, respectively.

Conversions of ketoisophorone (**7a**), (*S*)-carvone (**8a**), (*R*)-carvone (**9a**), *N*-phenyl-2-methylmaleimide (**12a**) were determined using a 14% cyanopropylphenyl-dimethylpolysiloxane (DB-column 1701 Agilent, 30 m x 0.25 mm, 0.25 μm), detector temperature 250 °C, split ratio 20:1. Programme: 110 °C,

hold for 5.0 min, 20 °C min⁻¹ to 210 °C, hold for 6.0 min. Retention times were as follow: levodione (**7b**) 8.28 min, ketoisophorone (**7a**) 7.52 min, (*S*)-carvone (**8a**) and (*R*)-carvone (**9a**) 8.51 min, *trans*-dihydrocarvone (*trans*-**8b**) 7.85 min, *cis*-dihydrocarvone (*cis*-**8b**) 7.97 min, *N*-phenyl-2-methylsuccinimide (**12b**) 15.27 min, *N*-phenyl-2-methylmaleimide (**12a**) 13.36 min.

Conversions of β -damascone (**14a**) was analysed by GC-MS using a 5% phenyl-dimethylpolysiloxane capillary column (HP-5 Agilent, 30 m x 0.32 mm, 0.25 μ m), detector temperature 250 °C, split ratio 20:1. Programme: 100 °C, hold for 2.0 min, 10 °C min⁻¹ to 280 °C, hold for 4.0 min.

For substrates **1a-10a**, calibration curves were obtained in the range 0 mM to 50 mM for both substrates and products using the internal standard. For substrate **11a**, a calibration curve was generated for the substrate only as the expected product was not available.

Conversions of 1-nitro-1-cyclohexene (**15a**), *trans*- β -nitrostyrene (**16a**), *trans*- β -methyl-nitrostyrene (**17a**) were analyzed by GC-MS using a 5% phenyl-dimethylpolysiloxane capillary column (HP-5 Agilent, 30 m x 0.32 mm, 0.25 μ m), detector temperature 250 °C, split ratio 20:1. Programme for **15a**: 40 °C, hold for 2.0 min, 10 °C min⁻¹ to 180 °C, hold for 1.0 min. Retention times were as follow: **15b** 10.35 min and **15a** 11.74 min. Programme for **16a** and **17a**: 100 °C, hold for 4.0 min, 10 °C min⁻¹ to 180 °C, hold for 1.0 min. Retention times were as follow: **16b** 6.28 min, **16a** 7.63 min, **17b** 6.66, **17a** 8.15 min.

Analytical procedures for determination of enantiomeric excess and absolute configuration:

Enantiomeric excesses of **2b**, **3b**, **6b** were determined using a 2,3-di-*O*-ethyl-6-*O*-*tert*-butyl dimethylsilyl β -cyclodextrin capillary column (Restek Rt-BDEXse, 30 m x 0.32 mm, 0.25 μ m). Detector temperature 200 °C, injector temperature 180 °C, split ratio 25:1. Temperature programme for **2b**: 50 °C hold 5.0 min, 10 °C min⁻¹ to 180 °C hold 1.0 min. Retention times were as follow: (*S*)-**2b** 11.28 min, (*R*)-**2b** 11.46 min, **2a** 12.64 min. Temperature programme for **3b**: 50 °C hold 2.0 min, 5 °C min⁻¹ to 120 °C hold 2.0 min, 15 °C min⁻¹ 180 °C hold 2.0 min. Retention times were as follow: (*R*)-**3b** 12.53 min, (*S*)-**3b** 12.72 min, **3a** 17.01 min. Temperature programme for **6b**: 80 °C hold 10.0 min, 3 °C min⁻¹ to 130 °C, 15 °C min⁻¹ 180 °C hold 2.0 min. Retention times were as follows: (*R*)-**6b** 18.07 min, (*S*)-**6b** 19.21 min, **6a** 28.0 min.

Enantiomeric excess of **5b** was determined using a 2,6-di-*O*-pentyl-3-trifluoroacetyl derivative of β -cyclodextrin capillary column (Chiraldex B-TA 40 m x 0.25 mm, 0.12 μ m). Detector temperature 200 °C, injector temperature 180 °C, split ratio 25:1. Temperature programme for **5b**: 80 °C hold 2.0 min, 5 °C min⁻¹ to 105 °C, 10 °C min⁻¹ to 180 °C hold 4.0 min. Retention times were as follow: (*S*)-**5b** 7.4 min, (*R*)-**5b** 7.8 min.

Enantiomeric excess of **7b** was determined using a modified β -cyclodextrin capillary column (Chirasil DexCB 30 m x 0.25 mm, 0.25 μ m). Detector temperature 200 °C, injector temperature 180 °C, split ratio 25:1. Temperature programme for **7b**: 90 °C hold 2.0 min, 4 °C min⁻¹ to 115 °C, 15 °C min⁻¹ to 180 °C hold 2.0 min. Retention times were as follow: (*R*)-**7b** 8.73 min, (*S*)-**7b** 8.95 min, **7a** 7.86 min.

Enantiomeric excess of **13b** was determined using a modified β -cyclodextrin capillary column (Hydrodex- β -TBMAc, 25 m x 0.25 mm, 0.25 μ m). Detector temperature 200 °C, injector temperature 180 °C, split ratio 20:1. Temperature programme for **13b**: 60 °C hold 10.0 min, 1 °C min⁻¹ to 105 °C, 15 °C min⁻¹ to 180 °C, hold 3.0 min. Retention times: (*S*)-**13b** 52.13 min, (*R*)-**13b** 52.63 min, neral and geranial [(*Z*)- and (*E*)-**13a**] 58.5 min and 59.4 min, respectively.

Enantiomeric excess of **11b** was determined on HPLC using a Chiralcel OD-H column (25 cm x 0.46 cm) and *n*-heptane/*i*-propanol 95:5 (isocratic) at 25 °C, flow 1 ml min⁻¹. Retention times: (*R*)-**11b** 17.53 min, (*S*)-**11b** ND, **11a** 11.27 min.

Enantiomeric excess of **14b** was determined on HPLC using a Chiralcel OJ column (25 cm x 0.46 cm) and *n*-heptane/*i*-propanol 99:1 (isocratic) at 25 °C, flow 0.5 ml min⁻¹. Retention times: (*R*)-**14b** 14.74 min, (*S*)-**14b** 14.9 min, **14a** 13.59 min.

Enantiomeric excess of **17b** was determined on HPLC using a Chiralcel OJ column (25 cm x 0.46 cm) and *n*-heptane/*i*-propanol 90:10 (isocratic) at 25 °C, flow 0.8 ml min⁻¹. Retention times: (*R*)-**17b** 13.22 min, (*S*)-**17b** 14.61 min, **17a** 10.0 min.

8.2.9 Angelica lactone isomerization: conversions and enantiomeric excess determination

For the isomerization reaction an aliquot of enzymes (100 μ g/ml or 200 μ g/ml) was added to a Tris-HCl buffer solution (0.5 ml, 50 mM, pH 5.0-9.0) containing the substrate (10 mM) added as a 1 M DMSO solution (1% final DMSO concentration). The mixture was shaken at 30 °C and 140 rpm. After different

times of incubation, depending on the reaction, products were extracted with EtOAc (2 x 0.25 mL) containing 10 mM 1-decanol as internal GC standard. The combined organic phases were dried (Na_2SO_4) and the resulting samples were analyzed on achiral GC or GC/MS.

For the reduction reaction an aliquot of 200 $\mu\text{g}/\text{ml}$ (if not otherwise specified) of the desired enzyme was added to the previous described reaction (0.5 mL, 50 mM, pH 7.0) containing the substrate β -isomer generated from the isomerization in different concentrations depending on the condition used. The mixture was shaken at 30 °C and 140 rpm. After different times of incubation, depending on the reaction, products were extracted with EtOAc (2 x 0.25 mL) containing 10 mM 1-decanol as internal GC standard. The combined organic phases were dried (Na_2SO_4) and the resulting samples were analyzed on achiral GC or GC/MS.

For conversion, the samples were analyzed by GC-FID using a 5% phenyl-dimethylpolysiloxane capillary column (HP-5 Agilent, 30 m, 0.32 mm, 0.25 μm), detector temperature 250 °C, split ratio 20:1. Programme for **1a**: 40 °C, hold for 1.0 min, 10 °C min^{-1} to 180 °C, hold for 2.0 min. Retention times were as follow: α -angelica lactone (**1a**) 6.4 min, β -angelica lactone (**1b**) 7.66 min.

Enantiomeric excesses of **1b** and **1c** were determined using a 2,3-di-*O*-ethyl-6-*O*-*tert*-butyl dimethylsilyl β -cyclodextrin capillary column (Restek Rt-BDEXse, 30 m x 0.32 mm, 0.25 μm). Detector temperature 200 °C, injector temperature 180 °C, split ratio 25:1. Temperature programme for **1b** and **1c**: 70 °C hold 1.0 min, 5 °C min^{-1} to 100 °C hold 5.0 min, 5 °C min^{-1} to 130 °C hold 0.0 min, 10 °C min^{-1} to 220 °C hold 1.0 min. Retention times were as follow: **1a** 7.8 min, (*R*)-**1b** 11.40 min, (*R*)-**1c** 11.51 min, (*S*)-**1b** 12.59 min, (*S*)-**1c** 12.77 min.

8.2.10 Oligomeric state determination by SEC chromatography

The oligomeric state was determined by analytical SEC. The proteins, from the IMAC purification (100 μg) were loaded onto a Superose™ 12 or a Superose 6 10/300 GL column placed on an ÄKTA purifier system and previously equilibrated with 50 mM Tris-HCl, 150 mM NaCl pH 8.0. The flow rate for protein elution was 0.5 ml/min. Tyreoglobulin (669 kDa), alcohol dehydrogenase (150 kDa), albumin (69 kDa), carbonic anhydrase (29 kDa), ribonuclease A (13.7 kDa) and cytochrome C (12 kDa) were used as molecular mass standards for a calibration curve (Fig. 132 AND 133). Apparent M_r values of enzymes were calculated using the calibration curve where the elution volume (V_e) of the

standard proteins was plotted against $\log M_w$.

$$K_{av} = \frac{V_e - V_o}{V_t - V_o}$$

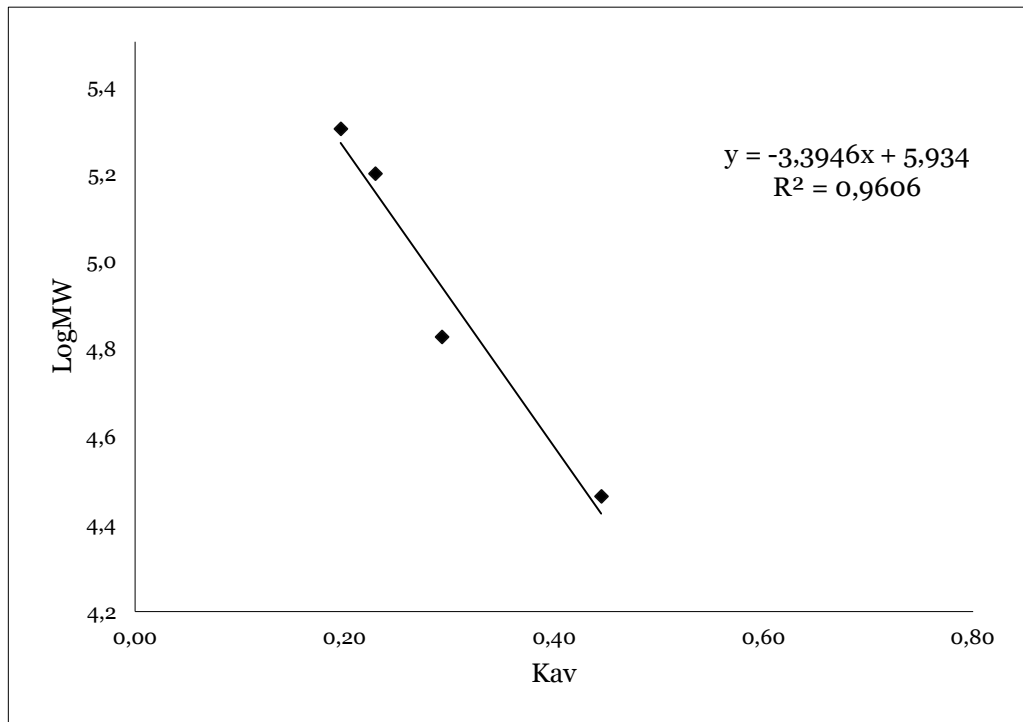


Figure 133. Calibration curve for Superose 12 10/300 GL column

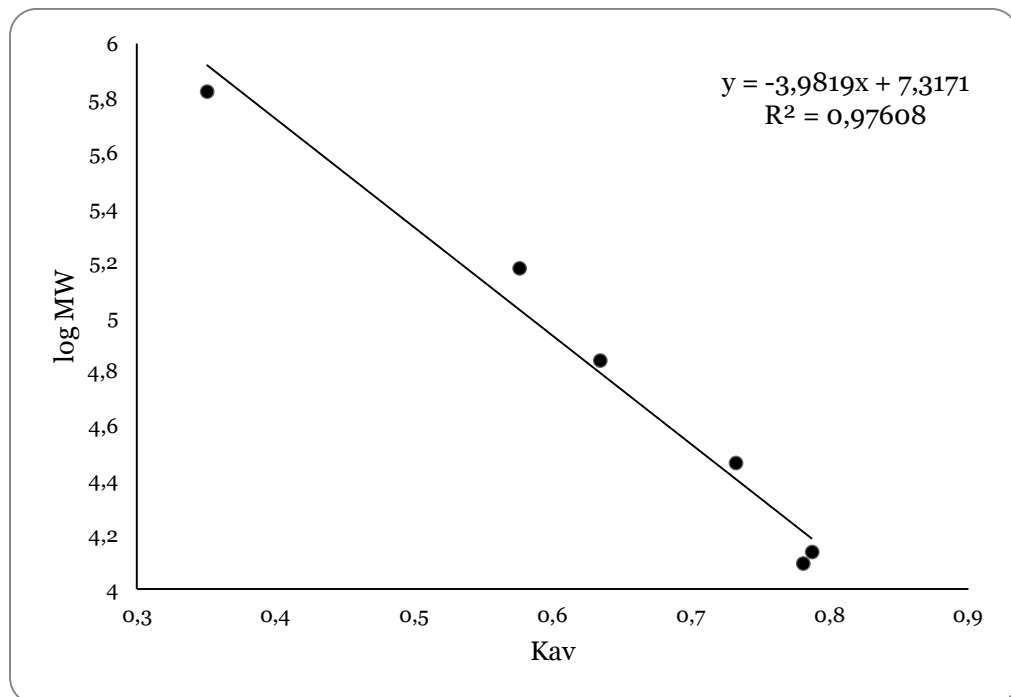


Figure 134. Calibration curve for Superose 6 10/300 GL column

8.2.11 Oligomeric state determination by native PAGE

Native polyacrylamide gel electrophoresis was performed using precast Tris-acetate acrylamide gel 3-8% from ThermoFisher Scientific, excluding SDS and β -mercaptoethanol from buffer and sample buffer. Samples were not boiled before electrophoresis either. The running gel was composed of 25 mM Tris and 19.2 glycine pH 8.5. Gel was run at room temperature and a constant voltage of 150 V for 3 hours.

8.2.12 ThermoFluor assay

The apparent unfolding temperatures of the recombinant enzymes (T_m s), in standard conditions (50 mM Tris-HCl, 150 mM NaCl pH 8.0) and in the presence of different co-solvents (ethanol, acetone, acetonitrile, dimethylsulfoxide and dioxane) present in different percentages (5-50%), were determined using the ThermoFluor method. Briefly, 2 μ l of protein (0.6 mM) (final concentration 5 μ M) in 50 mM Tris-HCl, 150 mM NaCl pH 8.0 added with the different conditions and 3 μ l of Sypro® Orange diluted 1/ 100 were loaded into an Applied Biosystems StepOne Real-Time PCR System (Eppendorf) fitted with a 300–472 nm excitation filter and a Sypro® Orange emission filter (570 nm). A temperature gradient from 20 to 90 °C was applied (0.5 °C/min), and fluorescence data were recorded. A sigmoidal curve was obtained after plotting the fluorescence amount against the temperature. The T_m values were determined as the maximum of the derivative of the obtained sigmoidal curve. Using the software GraphPad Prism 6, the fluorescence values have been interpolated into the Boltzmann function to obtain the first derivative, which corresponds to the melting temperature. Experiments were performed in duplicate.

8.2.13 Activity assay to determine the pH optimum

For the determination of the pH *optimum*, the standard assay (100 μ l) was performed using 10 mM of 2-cyclohexen-1-one as standard substrate. Reactions were started by the addition of 200 nM purified enzyme and measured over 1 minute. A universal buffer of constant ionic strength: 100 mM Tris-HCl, 50 mM MES and 50 mM CH₃COOH adjusted to the following pH values at 25 °C using 5 M NaOH or 5 M HCl: 4.0, 5.0, 6.0, 7.0, 8.0, 9.0, 10.0 and 12.0, was used to determine the specific activity (U/mg) of the enzyme.

8.2.14 Three-dimensional structure determination

Freshly purified recombinant ene-reductases (16-20 mg/ml in 50 mM Tris-HCl buffer pH 8.0 and 150 mM NaCl) were submitted to sparse matrix crystallization trials, applying the isothermal vapour diffusion method, partially automated by Oryx8 Robot (Douglas Instruments). All the conditions were screened using the sitting drop setup on MRC 96-well plates at 293 K.

For *CtOYE* and *BfOYE1* the N-terminal His-tag has been removed using thrombin protease in order to obtain hit crystals. Briefly, 10 mg of protein were digested using 50 μ l of human thrombin (50 U) (Sigma Aldrich) over-night at 4 °C on a rotatory platform. A second IMAC chromatography purification was performed in order to separate the removed His-tag from the protein. A further purification step for the removal of thrombin from the preparation was introduced using a column derivatized with benzamidine.

The crystallogenesi and the data collection and refinement are discussed in detail in Chapter 5 for each protein.

BIBLIOGRAPHY

References

1. Martínez, V.D. *The colors of biotechnology*. 2010 [9-06-2014]; Available from: http://biotechspain.com/en/article.cfm?iid=colores_biotechnologia.
2. Assobiotec-FederChimica. *Il mondo delle biotecnologie: Cosa sono le biotecnologie*. 2010 [24-05-2014]; Available from: <http://assobiotec.federchimica.it/default/mondo-delle-biotecnologie/cosa-sono-le-biotecnologie.aspx>.
3. Soetaert, W. and Vandamme E., *The impact of industrial biotechnology*. *Biotechnol J*, 2006, **1** (7-8), 756-769.
4. Anastas, P.T. and Warner J.C., *Green chemistry: Theory and practice*, 1998, Oxford University Press.
5. Anastas, P. and Eghbali N., *Green Chemistry: Principles and Practice*. *Chem Soc Rev*, 2010, **39**, 301-312.
6. Clark, J.H., et al., *Green chemistry and the biorefinery: A partnership for a sustainable future*. *Green Chem*, 2006, **8** (10), 853-860.
7. Sanders, J., et al., *Bio-refinery as the bio-inspired process to bulk chemicals*. *Macromol Biosci*, 2007, **7** (2), 105-117.
8. Tang, W.L. and Zhao H., *Industrial biotechnology: Tools and applications*. *Biotechnol J*, 2009, **4** (12), 1725-1739.
9. Mohsen, M.D. and Fahime A.J., *Application of alpha-amylase in biotechnology*. *J Biol Today's World*, 2012, **1** (1), 39-50.
10. Houde, A., et al., *Lipases and their industrial applications: An overview*. *Appl Biochem Biotechnol A* 2004, **118** (1-3), 155-170.
11. Ryom, N.M., *Influence of enzymes in the modern laundry sector*. *Tintoria*, 2003, **100** (12), 50-54.
12. Ryom, N.M., *Detergents using enzymes*. *Tintoria*, 2003, **100** (12), 50-54.
13. Lei, X.G., et al., *Supplementing corn-soybean meal diets with microbial phytase maximizes phytate phosphorus utilization by weanling pigs*. *J Animal Sci*, 1993, **71** (12), 3368-3375.
14. Awad, G.A., et al., *A novel phytase enzyme for poultry feed*. *World Appl Sci J*, 2013, **26** (2), 194-199.
15. Reetz, M.T., *Biocatalysis in organic chemistry and biotechnology: Past, present, and future*. *J Am Chem Soc*, 2013, **135** (34), 12480-12496.
16. Straathof, A.J.J., et al., *The production of fine chemicals by biotransformations*. *Curr Opin Biotechnol*, 2002, **13** (6), 548-556.
17. Sheldon, R.A., *The E-Factor: Fifteen years on*. *Green Chem*, 2007, **9** (12), 1273-1283.
18. Sheldon, R.A., et al., *Green Chemistry and Catalysis*. 1st ed, 2007, Wiley-VCH.
19. Schmid, A., et al., *Industrial biocatalysis today and tomorrow*. *Nature*, 2001, **409** (6817), 258-268.
20. Faber, K., *Biotransformations in Organic Chemistry*. 6rd ed, 2011, Heidelberg.
21. Andreas S. Bommarius, B.R.R., *Biocatalysis, Fundamentals and Applications*, 2004, WILEY-VCH.
22. Burton, S.G., et al., *The search for the ideal biocatalyst*. *Nat Biotechnol*, 2002, **20** (1), 37-45.
23. Jemli, S., et al., *Biocatalysts: Application and engineering for industrial purposes*. *Crit Rev Biotechnol*, 2016, **36** (2), 246-258.
24. Uppada, V., et al., *Cofactor regeneration an important aspect of biocatalysis* 2014.

25. Knowles, W.S. and Noyori R., *Pioneering perspectives on asymmetric hydrogenation*. *Acc Chem Res*, 2007, **40** (12), 1238-1239.
26. Toogood, H.S., *et al.*, 7.11 *Reduction: Enantioselective bioreduction of C-C double bonds*, in *Comprehensive Chirality*. 2012, 216-255.
27. Knowles, W.S. and Sabacky M.J., *Catalytic asymmetric hydrogenation employing a soluble, optically active, rhodium complex*. *Chem Comm*, 1968 (22), 1445-1446.
28. Horner, L., *et al.*, *Asymmetric catalytic hydrogenation with an optically active phosphinerhodium complex in homogeneous solution*. *Angew Chem Int Ed*, 1968, **7** (12), 942-942.
29. Noyori, R., *Asymmetric catalysis: Science and opportunities (nobel lecture)*. *Angew Chem Int Ed*, 2002, **41** (12), 2008-2022.
30. Nagendiran, A., *et al.*, *Mild and selective catalytic hydrogenation of the C=C Bond in α,β -Unsaturated carbonyl compounds using supported palladium nanoparticles*. *Eur J Chem*, 2016, **22** (21), 7184-7189.
31. Ouellet, S.G., *et al.*, *Enantioselective organocatalytic hydride reduction*. *J Am Chem Soc*, 2005, **127** (1), 32-33.
32. Jung, W.Y., *et al.*, *Metal-free, organocatalytic asymmetric transfer hydrogenation of α,β -unsaturated aldehydes*. *Angewandte Chemie - International Edition*, 2004, **44** (1), 108-110.
33. Toogood, H.S., *et al.*, *Biocatalytic reductions and chemical versatility of the Old Yellow Enzyme family of flavoprotein oxidoreductases*. *ChemCatChem*, 2010, **2** (8), 892-914.
34. Gatti, F.G., *et al.*, *Synthetic strategies based on C=C bioreductions for the preparation of biologically active molecules*, in *Synthetic Methods for Biologically Active Molecules: Exploring the Potential of Bioreductions*. 2013, 49-84.
35. Nestl, B.M., *et al.*, *New generation of biocatalysts for organic synthesis*. *Angew Chem Int Ed*, 2014, **53** (12), 3070-3095.
36. Faber, K. and Hall M., *Biocatalysis in Organic Synthesis 2*. *Science of Synthesis*, 2015, 213-260.
37. Gall, M., *et al.*, *Enzymatic conversion of flavonoids using bacterial chalcone isomerase and enoate reductase*. *Angew Chem Int Ed*, 2014, **53** (5), 1439-1442.
38. Joo, J.C., *et al.*, *Alkene hydrogenation activity of enoate reductases for an environmentally benign biosynthesis of adipic acid*. *Chem Sci*, 2017, **8** (2), 1406-1413.
39. Toogood, H.S. and Scrutton N.S., *Discovery, characterization, engineering, and applications of ene-reductases for industrial biocatalysis*. *ACS Catal*, 2018, **8** (4), 3532-3549.
40. Mansell, D.J., *et al.*, *Biocatalytic asymmetric alkene reduction: Crystal structure and characterization of a double bond reductase from *Nicotiana tabacum**. *ACS Catalysis*, 2013, **3** (3), 370-379.
41. Steinkellner, G., *et al.*, *Identification of promiscuous ene-reductase activity by mining structural databases using active site constellations*. *Nat Comm*, 2014, **5**.
42. French, C.E., *et al.*, *Biodegradation of explosives by transgenic plants expressing Pentaerythritol Tetranitrate Reductase*. *Nat Biotechnol*, 1999, **17** (5), 491-494.
43. Khan, H., *et al.*, *Kinetic and structural basis of reactivity of pentaerythritol tetranitrate reductase with NADPH, 2-cyclohexenone, nitroesters, and nitroaromatic explosives*. *J Biol Chem*, 2002, **277** (24), 21906-21912.

44. Khan, H., *et al.*, Atomic resolution structures and solution behavior of enzyme-substrate complexes of *Enterobacter cloacae* PB2 Pentaerythritol Tetranitrate Reductase: Multiple conformational states and implications for the mechanism of nitroaromatic explosive degradation. *J Biol Chem*, 2004, **279** (29), 30563-30572.
45. Williams, R.E., *et al.*, Biotransformation of explosives by the Old Yellow Enzyme family of flavoproteins. *Appl Environ Microbiol*, 2004, **70** (6), 3566-3574.
46. Williams, R.E. and Bruce N.C., 'New uses for an old enzyme' - The Old Yellow Enzyme family of flavoenzymes. *Microbiology*, 2002, **148** (6), 1607-1614.
47. Fitzpatrick, T.B., *et al.*, Characterization of YqjM, an Old Yellow Enzyme homolog from *Bacillus subtilis* involved in the oxidative stress response. *J Biol Chem*, 2003, **278** (22), 19891-19897.
48. Ehira, S., *et al.*, A novel redox-sensing transcriptional regulator CyeR controls expression of an Old Yellow Enzyme family protein in *Corynebacterium glutamicum*. *Microbiol*, 2010, **156** (5), 1335-1341.
49. Brigé, A., *et al.*, Comparative characterization and expression analysis of the four Old Yellow Enzyme homologues from *Shewanella oneidensis* indicate differences in physiological function. *Biochem J*, 2006, **394** (1), 335-344.
50. Schaller, F., *et al.*, 12-Oxophytodienoate reductase 3 (OPR3) is the isoenzyme involved in jasmonate biosynthesis. *Planta*, 2000, **210** (6), 979-984.
51. Cheng, J.Z., *et al.*, A role for Old Yellow Enzyme in ergot alkaloid biosynthesis. *J Am Chem Soc*, 2010, **132** (6), 1776-1777.
52. Díaz-Viraqué, F., *et al.*, Old Yellow Enzyme from *Trypanosoma cruzi* exhibits in vivo Prostaglandin F2a synthase activity and has a key role in parasite infection and drug susceptibility. *Front Immunol*, 2018, **9** (MAR).
53. Costa, C.L., *et al.*, An *Arabidopsis* gene induced by wounding functionally homologous to flavoprotein oxidoreductases. *Plant Mol Biol*, 2000, **44** (1), 61-71.
54. Sobajima, H., *et al.*, Cloning and characterization of a jasmonic acid-responsive gene encoding 12-oxophytodienoic acid reductase in suspension-cultured rice cells. *Planta*, 2003, **216** (4), 692-698.
55. Mano, J., *et al.*, Protection against photooxidative injury of tobacco leaves by 2-alkenal reductase. Detoxication of lipid peroxide-derived reactive carbonyls. *Plant Physiol*, 2005, **139** (4), 1773-1783.
56. Vollenweider, S., *et al.*, Fatty acid ketodienes and fatty acid ketotrienes: Michael addition acceptors that accumulate in wounded and diseased *Arabidopsis* leaves. *Plant J*, 2000, **24** (4), 467-476.
57. Kubata, B.K., *et al.*, A key role for Old Yellow Enzyme in the metabolism of drugs by *Trypanosoma cruzi*. *J Exp Med*, 2002, **196** (9), 1241-1251.
58. Yamaguchi, K., *et al.*, Structure of the inhibitor complex of Old Yellow Enzyme from *Trypanosoma cruzi*. *J Synchrotron Radiat*, 2011, **18** (1), 66-69.
59. Nizam, S., *et al.*, Comprehensive genome-wide analysis reveals different classes of enigmatic Old Yellow Enzyme in fungi. *Sci Rep*, 2014, **4**.
60. Romagnolo, A., *et al.*, Old Yellow Enzyme homologues in *Mucor circinelloides*: expression profile and biotransformation. *Sci Rep*, 2017, **7** (1).

61. French, C.E. and Bruce N.G., *Bacterial morphinone reductase is related to Old Yellow Enzyme*. *Biochem J*, 1995, **312** (3), 671-678.
62. Miura, K., *et al.*, *Molecular cloning of the nemA gene encoding N-ethylmaleimide reductase from Escherichia coli*. *Biol Pharm Bull*, 1997, **20** (1), 110-112.
63. Barna, T.M., *et al.*, *Crystal structure of Pentaerythritol tetranitrate reductase: "Flipped" binding geometries for steroid substrates in different redox states of the enzyme*. *J Mol Bio*, 2001, **310** (2), 433-447.
64. Breithaupt, C., *et al.*, *Structural basis of substrate specificity of plant 12-oxophytodienoate reductases*. *J Mol Bio*, 2009, **392** (5), 1266-1277.
65. Chilton, A.S., *et al.*, *Structure of an Aspergillus fumigatus Old Yellow Enzyme (EasA) involved in ergot alkaloid biosynthesis*. *Acta Crystallogr F*, 2014, **70**, 1328-1332.
66. Barna, T., *et al.*, *Crystal structure of bacterial Morphine reductase and properties of the C191A mutant enzyme*. *J Biol Chem*, 2002, **277** (34), 30976-30983.
67. Craig, D.H., *et al.*, *Reductive and oxidative half-reactions of Morphine reductase from Pseudomonas putida M10: A kinetic and thermodynamic analysis*. *Biochemistry*, 1998, **37** (20), 7598-7607.
68. Fox, K.M. and Karplus P.A., *Old yellow enzyme at 2 Å resolution: overall structure, ligand binding, and comparison with related flavoproteins*. *Structure*, 1994, **2** (11), 1089-1105.
69. Basran, J., *et al.*, *H-tunneling in the multiple H-transfers of the catalytic cycle of Morphine reductase and in the reductive half-reaction of the homologous Pentaerythritol Tetranitrate Reductase*. *J Bio Chem*, 2003, **278** (45), 43973-43982.
70. Brown, B.J., *et al.*, *On the active site of Old Yellow Enzyme: Role of histidine 191 and asparagine 194*. *J Bio Chem*, 1998, **273** (49), 32753-32762.
71. Pudney, C.R., *et al.*, *Mutagenesis of Morphine reductase induces multiple reactive configurations and identifies potential ambiguity in kinetic analysis of enzyme tunneling mechanisms*. *J Am Chem Soc*, 2007, **129** (45), 13949-13956.
72. Pudney, C.R., *et al.*, *Evidence to support the hypothesis that promoting vibrations enhance the rate of an enzyme catalyzed H-tunneling reaction*. *J Am Chem Soc*, 2009, **131** (47), 17072-17073.
73. Adalbjörnsson, B.V., *et al.*, *Biocatalysis with thermostable enzymes: Structure and properties of a thermophilic ene-reductase related to Old Yellow Enzyme*. *ChemBioChem*, 2010, **11** (2), 197-207.
74. Paul, C.E., *et al.*, *Mimicking nature: Synthetic nicotinamide cofactors for C=C bioreduction using enoate reductases*. *Org Lett*, 2013, **15** (1), 180-183.
75. Paul, C.E. and Hollmann F., *A survey of synthetic nicotinamide cofactors in enzymatic processes*. *Appl Microbiol Biotechnol*, 2016, **100** (11), 4773-4778.
76. Geddes, A., *et al.*, *Donor-acceptor distance sampling enhances the performance of "better than Nature" nicotinamide coenzyme biomimetics*. *J Am Chem Soc*, 2016, **138** (35), 11089-11092.
77. Löw, S.A., *et al.*, *Enhanced ene-reductase activity through alteration of artificial nicotinamide cofactor substituents*. *ChemCatChem*, 2016, **8** (5), 911-915.

78. Knaus, T., *et al.*, *Better than Nature: Nicotinamide biomimetics that outperform natural coenzymes*. *J Am Chem Soc*, 2016, **138** (3), 1033-1039.
79. Brenner, S., *et al.*, *Experimental approaches towards proton-coupled electron transfer reactions in biological redox systems*, in *RSC Catalysis Series*. 2012. p. 57-88.
80. Kohli, R.M. and Massey V., *The oxidative half-reaction of Old Yellow Enzyme: The role of Tyrosine 196*. *J Biol Chem*, 1998, **273** (49), 32763-32770.
81. Messiha, H.L., *et al.*, *Role of active site residues and solvent in proton transfer and the modulation of flavin reduction potential in bacterial Morphine reductase*. *J Biol Chem*, 2005, **280** (29), 27103-27110.
82. Hall, M., *et al.*, *Asymmetric bioreduction of C=C bonds using enoate reductases OPR1, OPR3 and YqjM: Enzyme-based stereocontrol*. *Adv Synth Catal*, 2008, **350** (3), 411-418.
83. Walton, A.Z., *et al.*, *Residues controlling facial selectivity in an alkene reductase and semirational alterations to create stereocomplementary variants*. *ACS Catal*, 2014, **4** (7), 2307-2318.
84. Oberdorfer, G., *et al.*, *Stereocontrol strategies in the asymmetric bioreduction of alkenes*. *Synlett*, 2012, **23** (13), 1857-1864.
85. Tasnádi, G., *et al.*, *A substrate-driven approach to determine reactivities of α,β -unsaturated carboxylic esters towards asymmetric bioreduction*. *Eur J Chem*, 2012, **18** (33), 10362-10367.
86. Winkler, C.K., *et al.*, *Asymmetric synthesis of O-protected acyloins using enoate reductases: Stereochemical control through protecting group modification*. *Eur J Org Chem*, 2010 (33), 6354-6358.
87. Stueckler, C., *et al.*, *Stereo-controlled asymmetric bioreduction of α,β -dehydroamino acid derivatives*. *Adv Synth Catal*, 2011, **353** (7), 1169-1173.
88. Amato, E.D. and Stewart J.D., *Applications of protein engineering to members of the Old Yellow Enzyme family*. *Biotechnol Adv*, 2015, **33** (5), 624-631.
89. Nett, N., *et al.*, *Revealing additional stereocomplementary pairs of Old Yellow Enzymes by rational transfer of engineered residues*. *ChemBioChem*, 2017, **18** (7), 685-691.
90. Pompeu, Y.A., *et al.*, *X-ray crystallography reveals how subtle changes control the orientation of substrate binding in an alkene reductase*. *ACS Catal*, 2013, **3** (10), 2376-2390.
91. Pompeu, Y.A., *et al.*, *Structural and catalytic characterization of pichia stipitis OYE 2.6, a useful biocatalyst for asymmetric alkene reductions*. *Adv Synth Catal*, 2012, **354** (10), 1949-1960.
92. Rütthlein, E., *et al.*, *Finding the selectivity switch - A rational approach towards stereocomplementary variants of the ene-reductase YqjM*. *Adv Synth Catal*, 2015, **357** (8), 1775-1786.
93. Padhi, S.K., *et al.*, *Site-saturation mutagenesis of Tryptophan 116 of Saccharomyces pastorianus Old Yellow Enzyme uncovers stereocomplementary variants*. *J Am Chem Soc*, 2009, **131** (9), 3271-3280.
94. Kitzing, K., *et al.*, *The 1.3 Å crystal structure of the flavoprotein YqjM reveals a novel class of Old Yellow Enzymes*. *J Biol Chem*, 2005, **280** (30), 27904-27913.
95. Khan, H., *et al.*, *Proton transfer in the oxidative half-reaction of Pentaerythritol Tetranitrate Reductase: Structure of the reduced*

- enzyme-progesterone complex and the roles of residues Tyr186, His181 and His184.* FEBS Journal, 2005, **272** (18), 4660-4671.
96. Opperman, D.J., *et al.*, *Crystal structure of a thermostable Old Yellow Enzyme from Thermus scotoductus SA-01.* Biochem Biophys Res Comm, 2010, **393** (3), 426-431.
 97. Xu, D., *et al.*, *The role of Threonine 37 in flavin reactivity of the Old Yellow Enzyme.* Proc Natl Acad Sci, 1999, **96** (7), 3556-3561.
 98. Scholtissek, A., *et al.*, *Old yellow enzyme-catalysed asymmetric hydrogenation: Linking family roots with improved catalysis.* Catalysts, 2017, **7** (5).
 99. Schittmayer, M., *et al.*, *Old yellow enzyme-catalyzed dehydrogenation of saturated ketones.* Adv Synth Catal, 2011, **353** (2-3), 268-274.
 100. Tsuji, N., *et al.*, *Isolation and characterization of a thermotolerant ene reductase from Geobacillus sp. 30 and its heterologous expression in Rhodococcus opacus.* Appl Microbiol Biotechnol, 2014, **98** (13), 5925-5935.
 101. Scholtissek, A., *et al.*, *A thermophilic-like ene-reductase originating from an acidophilic iron oxidizer.* Appl Microbiol Biotechnol, 2017, **101** (2), 609-619.
 102. Riedel, A., *et al.*, *Functional characterization and stability improvement of a 'thermophilic-like' ene-reductase from Rhodococcus opacus 1CP.* Front Microbiol, 2015, **6** (OCT).
 103. Oberdorfer, G., *et al.*, *Stereopreferences of Old Yellow Enzymes: structure correlations and sequence patterns in enoate reductases.* ChemCatChem, 2011, **3** (10), 1562-1566.
 104. Nizam, S., *et al.*, *Comparative structural modeling of six Old Yellow Enzymes (OYEs) from the necrotrophic fungus Ascochyta rabiei: Insight into novel OYE classes with differences in cofactor binding, organization of active site residues and stereopreferences.* PLoS ONE, 2014, **9** (4).
 105. Winkler, C.K., *et al.*, *Asymmetric bioreduction of activated alkenes to industrially relevant optically active compounds.* J Biotechnol, 2012, **162** (4), 381-389.
 106. Hall, M., *et al.*, *Asymmetric bioreduction of activated C=C bonds using Zymomonas mobilis NCR enoate reductase and Old Yellow Enzymes OYE 1-3 from yeasts.* Eur J Org Chem, 2008 (9), 1511-1516.
 107. Fryszkowska, A., *et al.*, *Asymmetric reduction of activated alkenes by Pentaerythritol Tetranitrate Reductase: Specificity and control of stereochemical outcome by reaction optimisation.* Adv Synth Catal, 2009, **351** (17), 2976-2990.
 108. Bougioukou, D.J., *et al.*, *Towards preparative-scale, biocatalytic alkene reductions.* Chem Comm, 2010, **46** (45), 8558-8560.
 109. Hall, M., *et al.*, *Asymmetric whole-cell bioreduction of an α,β -unsaturated aldehyde (citral): competing prim-alcohol dehydrogenase and C-C lyase activities.* Tetrahedron Asymmetry, 2006, **17** (21), 3058-3062.
 110. Müller, A., *et al.*, *Enzymatic reduction of the α, β -unsaturated carbon bond in citral.* J Mol Catal B, 2006, **38** (3-6), 126-130.
 111. Stueckler, C., *et al.*, *Bioreduction of α -methylcinnamaldehyde derivatives: Chemo-enzymatic asymmetric synthesis of Lilial™ and Helional™.* Dalton Trans, 2010, **39** (36), 8472-8476.
 112. Castiglione, K., *et al.*, *Asymmetric whole-cell bioreduction of (R)-carvone by recombinant Escherichia coli with in situ substrate supply and product removal.* Biochem Eng J, 2017, **117**, 102-111.

113. Winkler, C.K., *et al.*, *Chemoenzymatic asymmetric synthesis of pregabalin precursors via asymmetric bioreduction of β -cyanoacrylate esters using ene-reductases*. *J Org Chem*, 2013, **78** (4), 1525-1533.
114. Musgrave Burrell, A.J., *et al.*, *Process for the preparation of (S)-3-cyano-5-methylhexanoic acid derivatives and of pregabalin*. WO2012025861A1, 2012.
115. Janicki, I., *et al.*, *Asymmetric bioreduction of β -activated vinylphosphonate derivatives using ene-reductases*. *Adv Synth Catal*, 2017, **359** (23), 4190-4196.
116. Waller, J., *et al.*, *Structural insights into the ene-reductase synthesis of profens*. *Org Biomol Chem*, 2017, **15** (20), 4440-4448.
117. Turrini, N.G., *et al.*, *Enzymatic synthesis of optically active lactones via asymmetric bioreduction using ene-reductases from the Old Yellow Enzyme family*. *Adv Synth Catal*, 2015, **357** (8), 1861-1871.
118. Turrini, N.G., *et al.*, *Biocatalytic access to nonracemic γ -oxo esters via stereoselective reduction using ene-reductases*. *Green Chem*, 2017, **19** (2), 511-518.
119. Brenna, E., *et al.*, *Multi-enzyme cascade synthesis of the most odorous stereoisomers of the commercial odorant Muguesia®*. *J Mol Catal B*, 2015, **114**, 37-41.
120. Monti, D., *et al.*, *Cascade coupling of ene-reductases and ω -transaminases for the stereoselective synthesis of diastereomerically enriched amines*. *ChemCatChem*, 2015, **7** (19), 3106-3109.
121. Peters, C., *et al.*, *Fusion proteins of an enoate reductase and a Baeyer-Villiger monooxygenase facilitate the synthesis of chiral lactones*. *Biol Chem*, 2017, **398** (1), 31-37.
122. Agudo, R. and Reetz M.T., *Designer cells for stereocomplementary de novo enzymatic cascade reactions based on laboratory evolution*. *Chem Commun*, 2013, **49** (93), 10914-10916.
123. Jakubczyk, D., *et al.*, *Discovery and reconstitution of the Cycloclavine biosynthetic pathway - enzymatic formation of a cyclopropyl group*. *Angew Chem Int Ed*, 2015, **54** (17), 5117-5121.
124. Biermann, M., *et al.*, *Guerbet Alcohols: From processes under harsh conditions to synthesis at room temperature under ambient pressure*. *ChemCatChem*, 2016, **8** (5), 895-899.
125. Wang, Y., *et al.*, *Combining Rh-catalyzed diazocoupling and enzymatic reduction to efficiently synthesize enantioenriched 2-substituted succinate derivatives*. *ACS Catal*, 2017, **7** (4), 2548-2552.
126. Mansoorabadi, S.O., *et al.*, *The diverse roles of flavin coenzymes - Nature's most versatile thespians*. *J Org Chem*, 2007, **72** (17), 6329-6342.
127. Durchschein, K., *et al.*, *Unusual reactions mediated by FMN-dependent ene- and nitro-reductases*. *Green Chem*, 2013, **15** (7), 1764-1772.
128. Toogood, H.S. and Scrutton N.S., *New developments in ene-reductase catalysed biological hydrogenations*. *Curr Opin Chem Biol*, 2014, **19** (1), 107-115.
129. Sandoval, B.A., *et al.*, *Enantioselective hydrogen atom transfer: Discovery of catalytic promiscuity in flavin-dependent ene-reductases*. *J Am Chem Soc*, 2017, **139** (33), 11313-11316.
130. Turrini, N.G., *et al.*, *Sequential enzymatic conversion of α -angelica lactone to γ -valerolactone through hydride-independent C=C bond isomerization*. *ChemSusChem*, 2016, **9** (24), 3393-3396.

131. Vaz, A.D.N., *et al.*, *Old Yellow Enzyme: Aromatization of cyclic enones and the mechanism of a novel dismutation reaction*. *Biochemistry*, 1995, **34** (13), 4246-4256.
132. Paula, B.R.S., *et al.*, *Bioreduction of α -acetoxymethyl enones: Proposal for an SN2' mechanism catalyzed by ene-reductase*. *Adv Synth Catal*, 2016, **358** (22), 3555-3571.
133. Durchschein, K., *et al.*, *The flavoprotein-catalyzed reduction of aliphatic nitro-compounds represents a biocatalytic equivalent to the Nef-reaction*. *Green Chem*, 2010, **12** (4), 616-619.
134. Lima, C.G.S., *et al.*, *Angelica lactones: From biomass-derived platform chemicals to value-added products*. *ChemSusChem*, 2018, **11** (1), 25-47.
135. Winkler, C.K., *et al.*, *Biocatalytic reduction of activated C=C-bonds and beyond: emerging trends*. *Curr Opin Chem Biol*, 2018, **43**, 97-105.
136. Ni, Y., *et al.*, *An ene reductase from *Clavispora lusitaniae* for asymmetric reduction of activated alkenes*. *Enzyme Microb Technol*, 2014, **56**, 40-45.
137. Domínguez, B., *et al.*, *Reduction of activated carbon-carbon double bonds using highly active and enantioselective double bond reductases*. *Johnson Matthey Technology Review*, 2016, **60** (4), 243-249.
138. Durchschein, K., *et al.*, *Unusual reactions mediated by FMN-dependent ene- and nitro-reductases*. *Green Chemistry*, 2013, **15** (7), 1764-1772.
139. Raddadi, N., *et al.*, *Biotechnological applications of extremophiles, extremozymes and extremolytes*. *Appl Microbiol Biotechnol*, 2015, **99** (19), 7907-7913.
140. Fu, Y., *et al.*, *Comparative characterization of novel ene-reductases from cyanobacteria*. *Biotechnol Bioeng*, 2013, **110** (5), 1293-1301.
141. Romagnolo, A., *et al.*, *Identification of fungal ene-reductase activity by means of a functional screening*. *Fungal Biol*, 2015, **119** (6), 487-493.
142. Romano, D., *et al.*, *Recombinant *S. cerevisiae* expressing Old Yellow Enzymes from non-conventional yeasts: an easy system for selective reduction of activated alkenes*. *Microb Cell Fact*, 2014, **13** (1).
143. Snape, J.R., *et al.*, *Purification, properties, and sequence of Glycerol Trinitrate Reductase from *Agrobacterium radiobacter**. *J Bacteriol*, 1997, **179** (24), 7796-7802.
144. Müller, A., *et al.*, *Asymmetric alkene reduction by yeast Old Yellow Enzymes and by a novel *Zymomonas mobilis* reductase*. *Biotechnol Bioeng*, 2007, **98** (1), 22-29.
145. Richter, N., *et al.*, *Asymmetric reduction of activated alkenes using an enoate reductase from *Gluconobacter oxydans**. *Appl Microbiol Biotechnol*, 2011, **89** (1), 79-89.
146. Litthauer, S., *et al.*, *Heterologous expression and characterization of the ene-reductases from *Deinococcus radiodurans* and *Ralstonia metallidurans**. *J Mol Catal B*, 2014, **99**, 89-95.
147. Liu, Y.J., *et al.*, *Asymmetric bioreduction of activated alkenes by a novel isolate of *Achromobacter* species producing enoate reductase*. *Appl Microbiol Biotechnol*, 2012, **95** (3), 635-645.
148. Wang, H.B., *et al.*, *An enoate reductase *Achr-OYE4* from *Achromobacter* sp. *JA81*: Characterization and application in asymmetric bioreduction of C=C bonds*. *Appl Microbiol Biotechnol*, 2014, **98** (2), 705-715.
149. French, C.E. and Bruce N.C., *Purification and characterization of Morphinone reductase from *Pseudomonas putida* M10*. *Biochem J*, 1994, **301** (1), 97-103.

150. French, C.E., *et al.*, *Sequence and properties of Pentaerythritol Tetranitrate Reductase from Enterobacter cloacae PB2*. J Bacteriol, 1996, **178** (22), 6623-6627.
151. Peters, C., *et al.*, *Identification, characterization, and application of three enoate reductases from Pseudomonas putida in in vitro enzyme cascade reactions*. ChemCatChem, 2014, **6** (4), 1021-1027.
152. Blehert, D.S., *et al.*, *Cloning and sequence analysis of two Pseudomonas flavoprotein Xenobiotic reductases*. J Bacteriol, 1999, **181** (20), 6254-6263.
153. Chaparro-Riggers, J.F., *et al.*, *Comparison of three enoate reductases and their potential use for biotransformations*. Adv Synth Catal, 2007, **349** (8-9), 1521-1531.
154. Khairy, H., *et al.*, *The NADH:flavin oxidoreductase Nox from Rhodococcus erythropolis MI2 is the key enzyme of 4,4'-dithiodibutyric acid degradation*. Lett Appl Microbiol, 2016, **63** (6), 434-441.
155. Husserl, J., *et al.*, *Key enzymes enabling the growth of Arthrobacter sp. Strain JBH1 with nitroglycerin as the sole source of carbon and nitrogen*. Appl Environ Microbiol, 2012, **78** (10), 3649-3655.
156. Pei, X.Q., *et al.*, *Two "classical" Old Yellow Enzymes from Chryseobacterium sp. CA49: Broad substrate specificity of Chr-OYE1 and limited activity of Chr-OYE2*. J Mol Catal B, 2016, **123**, 91-99.
157. Xu, M.Y., *et al.*, *Identification and characterization of a novel "thermophilic-like" Old Yellow Enzyme from the genome of Chryseobacterium sp. CA49*. J Mol Catal B, 2014, **108**, 64-71.
158. Sheng, X., *et al.*, *Identification and characterization of a novel Old Yellow Enzyme from Bacillus subtilis str.168*. J Mol Catal B, 2016, **130**, 18-24.
159. Gao, X., *et al.*, *Biochemical characterization and substrate profiling of a new NADH-dependent enoate reductase from Lactobacillus casei*. Enzyme Microb Technol, 2012, **51** (1), 26-34.
160. Opperman, D.J., *et al.*, *A novel chromate reductase from Thermus scotoductus SA-01 related to Old Yellow Enzyme*. J Bacteriol, 2008, **190** (8), 3076-3082.
161. Fu, Y., *et al.*, *A novel ene-reductase from Synechococcus sp. PCC 7942 for the asymmetric reduction of alkenes*. Process Biochem, 2012, **47** (12), 1988-1997.
162. Magallanes-Noguera, C., *et al.*, *Plant tissue cultures as sources of new ene- and ketoreductase activities*. J Biotechnol, 2017, **251**, 14-20.
163. Saito, K., *et al.*, *The cloning and expression of a gene encoding Old Yellow Enzyme from Saccharomyces carlsbergensis*. J Biol Chem, 1991, **266** (31), 20720-20724.
164. Stott, K., *et al.*, *Old yellow enzyme. The discovery of multiple isozymes and a family of related proteins*. J Biol Chem, 1993, **268** (9), 6097-6106.
165. Niino, Y.S., *et al.*, *A new Old Yellow Enzyme of Saccharomyces cerevisiae*. J Biol Chem, 1995, **270** (5), 1983-1991.
166. Madani, N.D., *et al.*, *Candida albicans estrogen-binding protein gene encodes an oxidoreductase that is inhibited by estradiol*. Proc Natl Acad Sci, 1994, **91** (3), 922-926.
167. Komduur, J.A., *et al.*, *Old yellow enzymes confers resistance of Hansenula polymorpha towards allyl alcohol*. Curr Genet, 2002, **41** (6), 401-406.
168. Kataoka, M., *et al.*, *Old Yellow Enzyme from Candida macedoniensis catalyzes the stereospecific reduction of the C=C bond of ketoisophorone*. Biosci Biotechnol Biochem, 2002, **66** (12), 2651-2657.

169. Kataoka, M., *et al.*, *Cloning and overexpression of the Old Yellow Enzyme gene of Candida macedoniensis, and its application to the production of a chiral compound.* J Biotechnol, 2004, **114** (1-2), 1-9.
170. Patterson-Orazem, A., *et al.*, *Pichia stipitis OYE 2.6 variants with improved catalytic efficiencies from site-saturation mutagenesis libraries.* Bioorg Med Chem, 2014, **22** (20), 5628-5632.
171. Zhang, B., *et al.*, *Characterization of an ene-reductase from Meyerozyma guilliermondii for asymmetric bioreduction of α,β -unsaturated compounds.* Biotechnol Lett, 2016, **38** (9), 1527-1534.
172. Straßner, J., *et al.*, *A homolog of Old Yellow Enzyme in tomato. Spectral properties and substrate specificity of the recombinant protein.* J Biol Chem, 1999, **274** (49), 35067-35073.
173. Straßner, J., *et al.*, *Characterization and cDNA-microarray expression analysis of 12-oxophytodienoate reductases reveals differential roles for octadecanoid biosynthesis in the local versus the systemic wound response.* Plant J, 2002, **32** (4), 585-601.
174. Schaller, F. and Weiler E.W., *Molecular cloning and characterization of 12-oxophytodienoate reductase, an enzyme of the octadecanoid signaling pathway from Arabidopsis thaliana. Structural and functional relationship to yeast Old Yellow Enzyme.* J Biol Chem, 1997, **272** (44), 28066-28072.
175. Biesgen, C. and Weiler E.W., *Structure and regulation of OPR1 and OPR2, two closely related genes encoding 12-oxophytodienoic acid-10,11-reductases from Arabidopsis thaliana.* Planta, 1999, **208** (2), 155-165.
176. Mussig, C., *et al.*, *A novel stress-inducible 12-oxophytodienoate reductase from Arabidopsis thaliana provides a potential link between brassinosteroid-action and jasmonic-acid synthesis.* J Plant Physiol, 2000, **157** (2), 143-152.
177. Fraaije, M.W., *et al.*, *Discovery of a thermostable Baeyer-Villiger monooxygenase by genome mining.* Appl Microbiol Biotechnol, 2005, **66** (4), 393-400.
178. Jain, K., *et al.*, *Extreme features of the Galdieria sulphuraria organellar genomes: A consequence of polyextremophily.* Genome Biol Evol, 2014, **7** (1), 367-380.
179. Schönknecht, G., *et al.*, *Gene transfer from bacteria and archaea facilitated evolution of an extremophilic eukaryote.* Science, 2013, **339** (6124), 1207-1210.
180. Graziani, G., *et al.*, *Microalgae as human food: Chemical and nutritional characteristics of the thermo-acidophilic microalga Galdieria sulphuraria.* Food Funct, 2013, **4** (1), 144-152.
181. Allen, M.M., *Simple conditions for growth of unicellular blue-green algae on plates* J Phycol, 1968, **4** (1), 1-4.
182. Allen, G.C., *et al.*, *A modified protocol for rapid DNA isolation from plant tissues using cetyltrimethylammonium bromide.* Nat Protoc, 2006, **1** (5), 2320-2325.
183. Billi, D., *et al.*, *Gene transfer to the desiccation-tolerant cyanobacterium Chroococcidiopsis.* J Bacteriol, 2001, **183** (7), 2298-2305.
184. Hanada, S., *et al.*, *Chloroflexus aggregans sp. nov., a filamentous phototrophic bacterium which forms dense cell aggregates by active gliding movement.* Int J Sys Bacteriol, 1995, **45** (4), 676-681.
185. Latorre, B.A., *et al.*, *Gray mold caused by Botrytis cinerea limits grape production in Chile.* Cienc Investig Agr, 2015, **42** (3), 305-330.

186. Miroux, B. and Walker J.E., *Over-production of proteins in Escherichia coli: Mutant hosts that allow synthesis of some membrane proteins and globular proteins at high levels*. J Mol Biol, 1996, **260** (3), 289-298.
187. Ferrer, M., et al., *Chaperonins govern growth of Escherichia coli at low temperatures* Nat Biotechnol, 2003, **21** (11), 1266-1267.
188. Huang, C.J., et al., *A proteomic analysis of the Pichia pastoris secretome in methanol-induced cultures*. Appl Microbiol Biotechnol, 2011, **90** (1), 235-247.
189. Joseph, R.E. and Andreotti A.H., *Bacterial expression and purification of Interleukin-2 Tyrosine kinase: Single step separation of the chaperonin impurity*. Protein Expres Purif, 2008, **60** (2), 194-197.
190. Pel, H.J., et al., *Genome sequencing and analysis of the versatile cell factory Aspergillus niger CBS 513.88*. Nat Biotechnol, 2007, **25** (2), 221-231.
191. Svanstrom, A., *Trehalose metabolism and stress resistance in Aspergillus niger*, in *Department of Microbiology*. 2013, Swedish University of Agricultural Sciences Uppsala.
192. Fryszkowska, A., et al., *A surprising observation that oxygen can affect the product enantiopurity of an enzyme-catalysed reaction*. FEBS Journal, 2012, **279** (22), 4160-4171.
193. Massey, V., et al., *The production of superoxide anion radicals in the reaction of reduced flavins and flavoproteins with molecular oxygen*. Biochem Biophys Res Comm, 1969, **36** (6), 891-897.
194. Massey, V., *Activation of molecular oxygen by flavins and flavoproteins*. J Biol Chem, 1994, **269** (36), 22459-22462.
195. Brown, B.J., et al., *The role of glutamine 114 in Old Yellow Enzyme*. J Biol Chem, 2002, **277** (3), 2138-2145.
196. Romero, E., et al., *Same Substrate, Many Reactions: Oxygen Activation in Flavoenzymes*. Chem Rev, 2018, **118** (4), 1742-1769.
197. Khalil, A.E.G.M., et al., *Synthesis and study of some new N-substituted imide derivatives as potential antibacterial agents*. Chem Pap, 2010, **64** (5), 637-644.
198. Lenardão, E.J., et al., *Citronellal as key compound in organic synthesis*. Tetrahedron, 2007, **63** (29), 6671-6712.
199. Caputi, L. and Aprea E., *Use of terpenoids as natural flavouring compounds in food industry*. Recent Patents on Food, Nutrition and Agriculture, 2011, **3** (1), 9-16.
200. Ludwiczuk, A., et al., *Terpenoids*, in *Pharmacognosy: Fundamentals, applications and atrategy*. 2016, 233-266.
201. Yanto, Y., et al., *Asymmetric bioreduction of alkenes using ene-reductases YersER and KYE1 and effects of organic solvents*. Org Lett, 2011, **13** (10), 2540-2543.
202. Mangan, D., et al., *A three-enzyme system involving an ene-reductase for generating valuable chiral building blocks*. Adv Synth Catal, 2012, **354** (11-12), 2185-2190.
203. Bechtold, M., et al., *Biotechnological development of a practical synthesis of ethyl (S)-2-ethoxy-3-(p -methoxyphenyl)propanoate (EEHP): Over 100-fold productivity increase from yeast whole cells to recombinant isolated enzymes*. Org Process Res Dev, 2012, **16** (2), 269-276.
204. C.K. Savile, V.M., X. Zhang, G.W. Huisman, *Enone Reductases*. US Patent Appl. 2015/0,315,613, 2015.

205. Straathof, A.J.J. and Jongejan J.A., *The enantiomeric ratio: Origin, determination and prediction*. *Enzyme Microb Technol*, 1997, **21** (8), 559-571.
206. Green, D. and Johnson T., *Nitroalkane chemistry*. *Chem Technol*, 2000, 79-87.
207. Berner, O.M., *et al.*, *Asymmetric Michael additions to nitroalkenes*. *Eur J Org Chem*, 2002 (12), 1877-1894.
208. Alonso, D.A., *et al.*, *Recent advances in asymmetric organocatalyzed conjugate additions to nitroalkenes*. *Molecules*, 2017, **22** (6).
209. Stuermer, R., *et al.*, *Asymmetric bioreduction of activated C=C bonds using enoate reductases from the Old Yellow Enzyme family*. *Curr Opin Chem Biol*, 2007, **11** (2), 203-213.
210. Burda, E., *et al.*, *Highly enantioselective reduction of α -methylated nitroalkenes*. *Angewandte Chemie - International Edition*, 2013, **52** (35), 9323-9326.
211. Durchschein, K., *et al.*, *Reductive biotransformation of nitroalkenes via nitroso-intermediates to oxazetes catalyzed by xenobiotic reductase A (XenA)*. *Org Biomol Chem*, 2011, **9** (9), 3364-3369.
212. Oberdorfer, G., *et al.*, *The structure of Glycerol Trinitrate Reductase NerA from Agrobacterium radiobacter reveals the molecular reason for nitro- and ene-reductase activity in OYE homologues*. *ChemBioChem*, 2013, **14** (7), 836-845.
213. Opperman, D.J., *Structural investigation into the C-terminal extension of the ene-reductase from Ralstonia (Cupriavidus) metallidurans*. *Proteins: Struct Funct Bioinf*, 2017.
214. Pesic, M., *et al.*, *Characterization of the Old Yellow Enzyme homolog from Bacillus subtilis (YqiM)*. *ChemistrySelect*, 2017, **2** (13), 3866-3871.
215. Kabsch, W., *XDS*. *Acta Crystallogr D*, 2010, **66** (2), 125-132.
216. Winn, M.D., *et al.*, *Overview of the CCP4 suite and current developments*. *Acta Crystallogr D*, 2011, **67** (4), 235-242.
217. Vagin, A. and Teplyakov A., *Molecular replacement with MOLREP*. *Acta Crystallogr D*, 2010, **66** (1), 22-25.
218. Emsley, P. and Cowtan K., *Coot: model-building tools for molecular graphics*. *Acta Crystallogr D*, 2004, **60** (12 Part 1), 2126-2132.
219. Skubak, P., *et al.*, *Direct incorporation of experimental phase information in model refinement*. *Acta Crystallogr D*, 2004, **60** (12 Part 1), 2196-2201.
220. Afonine, P.V., *et al.*, *Towards automated crystallographic structure refinement with phenix.refine*. *Acta Crystallogr D*, 2012, **68** (4), 352-367.
221. McCoy, A.J., *et al.*, *Phaser crystallographic software*. *J App Crystallogr*, 2007, **40** (4), 658-674.
222. Van Den Hemel, D., *et al.*, *Ligand-induced conformational changes in the capping subdomain of a bacterial Old Yellow Enzyme homologue and conserved sequence fingerprints provide new insights into substrate binding*. *J Biol Chem*, 2006, **281** (38), 28152-28161.
223. Elegheert, J., *et al.*, *Structural dissection of Shewanella oneidensis Old Yellow Enzyme 4 bound to a Meisenheimer complex and (nitro)phenolic ligands*. *FEBS Letters*, 2017, **591** (20), 3391-3401.
224. Okamoto, N., *et al.*, *Structural insight into the stereoselective production of PGF₂ α by Old Yellow Enzyme from Trypanosoma cruzi*. *J Biochem*, 2011, **150** (5), 563-568.
225. Breithaupt, C., *et al.*, *X-ray structure of 12-oxophytodienoate reductase 1 provides structural insight into substrate binding and specificity within the family of OYE*. *Structure*, 2001, **9** (5), 419-429.

226. Malone, T.E., *et al.*, *X-ray structure of Arabidopsis At2g06050, 12-oxophytodienoate reductase isoform 3*. *Proteins: Struct Funct Genet*, 2005, **58** (1), 243-245.
227. Holm, L. and Laakso L.M., *Dali server update*. *Nucleic acids Res*, 2016, **44** (W1), W351-W355.
228. Kwon, H., *et al.*, *Combining X-ray and neutron crystallography with spectroscopy*. *Acta Crystallogr D*, 2017, **73** (2), 141-147.
229. Toogood, H.S., *et al.*, *Structure-based insight into the asymmetric bioreduction of the C=C double bond of α,β -unsaturated nitroalkenes by pentaerythritol tetranitrate reductase*. *Adv Synth Catal*, 2008, **350** (17), 2789-2803.
230. Zahradník, J., *et al.*, *The crystal structure of XdpB, the bacterial Old Yellow Enzyme, in an FMN-free form*. *PLoS ONE*, 2018, **13** (4).
231. Werther, T., *et al.*, *Redox-dependent substrate-cofactor interactions in the Michaelis-complex of a flavin-dependent oxidoreductase*. *Nat Comm*, 2017, **8**.
232. Stueckler, C., *et al.*, *Stereo-controlled asymmetric bioreduction of α,β -dehydroamino acid derivatives*. *Advanced Synthesis and Catalysis*, 2011, **353** (7), 1169-1173.
233. Robescu, M.S., *et al.*, *Efficient process for the preparation of (R)-beta angelica lactone and derivatives therefor*. EP17189155, 2017.
234. Wu, Y., *et al.*, *Asymmetric olefin isomerization of butenolides via proton transfer catalysis by an organic molecule*. *J Am Chem Soc*, 2011, **133** (32), 12458-12461.
235. Alegre, K.O. and Law C.J., *Purification of a multidrug resistance transporter for crystallization studies*. *Antibiotics*, 2015, **4** (1), 113-135.

APPENDIX

GsOYE

>native sequence

ATGTTGAAGCTGTTGGAACCGTTTGACTTGAATGGACTAGAACTAGCCAATAGAATGGTGATGGCGCCGTTGACTCGT
AACAGAGCAGGTCCACGCTTTGTGCTACTAAAATGAACGCTTTATATATATGCCCAAAGAAGTGGTTTAGGTCTTATT
ATCACCGAAGCAACTCAAATATCTCAACAAGGAATGGGATATCCTGATACTCCTGGTATCTATACAGATGAACAAGTG
GATGGTTGGCGAATGGTAACCGAAGCAGTCCATCGAAGAGAAGGTTGTATATTTTTACAGTTGTGGCAGCTTGAAGA
GTTTCTCACTCCTCATTTCAACCAAACGGTCAACTACCAGTTGCACCTAGTGCAGATTGCACCGGAAGGTGAAGTAATG
ACTTATGATGGCATCAAACCTTTGAAACACCGAGAGCACTGGAACCGGAGGAAGTTGCCCATATTGTGGAAGACTAT
CGAAAAGCAGCAATTAATGCGAAACGTGCAGGTTTTGATGGCATAGAAATTCATAGTGCGAATGGTTATCTATTGCAC
GAGTTTCTAGAAGATGGCACGAATAAGAGAACCGACCGTTATGGTGGTCCATTGAA**AATAGGACG**GAGAATTGTGTTT
GAAGTTCTCGATGCAGTGTGTAAGTATATCCTTCCCGCAGAGTTGGCATTCTGCTTTCTCCAGATACAGAGTTTATG
AGTATGAGTGACTCTGACAGACCTGCTCTTTATAGTTATTTAGTACAGAGTTGAGTCGACGCGAAGTGGCCTATTTA
CACCTTATCGAGCCAAGAATCAAAGGAAATGTGGATGTTGAGAAAGAGTCTCATTTGAATGTAGAATTTTTCCGTCCC
TTATATAAGGGTGTCTTATCACTGCTGGAGGTTATCAAAGGAAACAGGAGAAGAAAGACTGCAAAAGCAACATGCC
GACCTCGTAG**CATATG**GTCGTTGGGTGATTGCCAACCTGACTTGCCAGCAGATTTGAACAAAATGCACCTCTAAAT
CCTTATGATAGGCCACATTCTATGGTGGTAATGAAAAGGGATACACAGATTATCCATTTTTAGATCCACGAGATTCT
CAAGAAGCATTGAAGGAAGCTGAAGCAGCCGAAAGGAAATGGCGTCTGTTGTAG

>sequence after abolition of the predicted N-glycosylation site & internal NdeI site

ATGTTGAAGCTGTTGGAACCGTTTGACTTGAATGGACTAGAACTAGCCAATAGAATGGTGATGGCGCCGTTGACTCGT
AACAGAGCAGGTCCACGCTTTGTGCTACTAAAATGAACGCTTTATATATATGCCCAAAGAAGTGGTTTAGGTCTTATT
ATCACCGAAGCAACTCAAATATCTCAACAAGGAATGGGATATCCTGATACTCCTGGTATCTATACAGATGAACAAGTG
GATGGTTGGCGAATGGTAACCGAAGCAGTCCATCGAAGAGAAGGTTGTATATTTTTACAGTTGTGGCAGCTTGAAGA
GTTTCTCACTCCTCATTTCAACCAAACGGTCAACTACCAGTTGCACCTAGTGCAGATTGCACCGGAAGGTGAAGTAATG
ACTTATGATGGCATCAAACCTTTGAAACACCGAGAGCACTGGAACCGGAGGAAGTTGCCCATATTGTGGAAGACTAT
CGAAAAGCAGCAATTAATGCGAAACGTGCAGGTTTTGATGGCATAGAAATTCATAGTGCGAATGGTTATCTATTGCAC
GAGTTTCTAGAAGATGGCACGAATAAGAGAACCGACCGTTATGGTGGTCCATTGAA**AATAGGCG**GAGAATTGTGTTT
GAAGTTCTCGATGCAGTGTGTAAGTATATCCTTCCCGCAGAGTTGGCATTCTGCTTTCTCCAGATACAGAGTTTATG
AGTATGAGTGACTCTGACAGACCTGCTCTTTATAGTTATTTAGTACAGAGTTGAGTCGACGCGAAGTGGCCTATTTA
CACCTTATCGAGCCAAGAATCAAAGGAAATGTGGATGTTGAGAAAGAGTCTCATTTGAATGTAGAATTTTTCCGTCCC
TTATATAAGGGTGTCTTATCACTGCTGGAGGTTATCAAAGGAAACAGGAGAAGAAAGACTGCAAAAGCAACATGCC
GACCTCGTAG**CGTATG**GTCGTTGGGTGATTGCCAACCTGACTTGCCAGCAGATTTGAACAAAATGCACCTCTAAAT
CCTTATGATAGGCCACATTCTATGGTGGTAATGAAAAGGGATACACAGATTATCCATTTTTAGATCCACGAGATTCT
CAAGAAGCATTGAAGGAAGCTGAAGCAGCCGAAAGGAAATGGCGTCTGTTGTAG

native	MLKLEPFDLNGLLELANRMVMAPLTRNRAGPRFVPTKMNALYYAQRSGLGLIITEATQIS	60
mutated	MLKLEPFDLNGLLELANRMVMAPLTRNRAGPRFVPTKMNALYYAQRSGLGLIITEATQIS *****	60
native	QQMGYPDTPGIYTDQVDGWRMVTEAVHREGCIFLQLWHVGRVSHSSFQPNGQLPVAP	120
mutated	QQMGYPDTPGIYTDQVDGWRMVTEAVHREGCIFLQLWHVGRVSHSSFQPNGQLPVAP *****	120
native	SAIAPERGEVMTYDGIKPFETPRALETEEVAHIVEDYRKAAINAKRAGFDGIEIHSANGYL	180
mutated	SAIAPERGEVMTYDGIKPFETPRALETEEVAHIVEDYRKAAINAKRAGFDGIEIHSANGYL *****	180
native	LHEFLEDGTDYGGSIENRTRIVFEVLDVAVCKVYPSRRVGRVSPDTEFMSMSDSD	240
mutated	LHEFLEDGTDYGGSIENRTRIVFEVLDVAVCKVYPSRRVGRVSPDTEFMSMSDSD *****	240
native	RPALYSYLVQELSRRELAYLHLIEPRIKGNVDVEKESLNVEFFRPLYKGVLTAGGYQK	300
mutated	RPALYSYLVQELSRRELAYLHLIEPRIKGNVDVEKESLNVEFFRPLYKGVLTAGGYQK *****	300
native	ETGEERLQKHADLVAYGRWVIANPDLPSRFEQNAPLNPDYDRATFYGGNEKGYTDYPFLD	360
mutated	ETGEERLQKHADLVAYGRWVIANPDLPSRFEQNAPLNPDYDRATFYGGNEKGYTDYPFLD *****	360
native	PRDSQEALKEAEEAERKWRRL	381
mutated	PRDSQEALKEAEEAERKWRRL *****	381

>recombinant sequence

atgggcagcagc catcatcatcatcatcac agcagcggc ctggtgccgcgcggcagccat
M G S S H H H H H S S G L V P R G S H
atgttgaagctggttgaaccgtttgacttgaatggactagaactagccaatagaatggtg
M L K L L E P F D L N G L E L A N R M V
atggcgccgttgactcgtaacagagcaggtccacgcgtttgtgcctactaaaatgaacgct
M A P L T R N R A G P R F V P T K M N A
ttatattatgccagagaagtgggttaggtcttattatcaccgaagcaactcaaatact
L Y Y A Q R S G L G L I I T E A T Q I S
caacaaggaatgggatatcctgatactcctgggtatctatacagatgaacaagtggatgg
Q Q G M G Y P D T P G I Y T D E Q V D G
tggcgaatggtaaccgaagcagtcctcgaagagaaggttgatatatttttacagttgtgg
W R M V T E A V H R R E G C I F L Q L W
cacgttgaagagtttctcactcctcatttcaaccaaagggtcaactaccagttgcacct
H V G R V S H S S F Q P N G Q L P V A P
agtgcgattgcaccggaaggtgaagtaatgacttatgatggcatcaaaccctttgaaaca
S A I A P E G E V M T Y D G I K P F E T
ccgagagcactggaaacggaggaagttgcccatattgtggaagactatcgaaaagcagca
P R A L E T E E V A H I V E D Y R K A A
attaatgcgaaacgtgcaggttttgatggcatagaaattcatagtgcgaatggttatcta
I N A K R A G F D G I E I H S A N G Y L
ttgcacgagtttctagaagatggcacgaataagagaaccgaccttatgggtggctccatt
L H E F L E D G T N K R T D R Y G G S I
gaaaatagggcgagaattgtgtttgaagttctcgatgcagtggtgtaaagtatatccttcc
E N R **A** R I V F E V L D A V C K V Y P S
cgcagagttggcattcgtctttctccagatacagagtttatgagtatgagtgactctgac
R R V G I R L S P D T E F M S M S D S D
agacctgctctttatagttatttagtacaagagttgagtcgacgcgaactggcctattta
R P A L Y S Y L V Q E L S R R E L A Y L
caccttatcgagccaagaatcaaaggaaatgtggatggtgagaaagagtcctcattgaat
H L I E P R I K G N V D V E K E S S L N
gtagaatttttccgtcccttatatataaggggtgttcttatcactgctggaggttatcaaaag
V E F F R P L Y K G V L I T A G G Y Q K
gaaacaggagaagaaagactgcaaaagcaacatgctggacctcgtagcgtatggctggttg
E T G E E R L Q K Q H A D L V A Y G R W
gtgattgccaacctgacttgcccagcagatttgaacaaaatgcacctctaaatccttat
V I A N P D L P S R F E Q N A P L N P Y
gatagagccacattctatggtggtaatgaaaagggatacacagattatccattttttagat
D R A T F Y G G N E K G Y T D Y P F L D
ccacgagattctcaagaagcattgaaggaagctgaagcagccgaaaggaaatggcgctcgc
P R D S Q E A L K E A E A A E R K W R R
ttgtagacatttgtcttccacaaaggatcc
L - T F V F H K G S
BamHI

a) Cloning

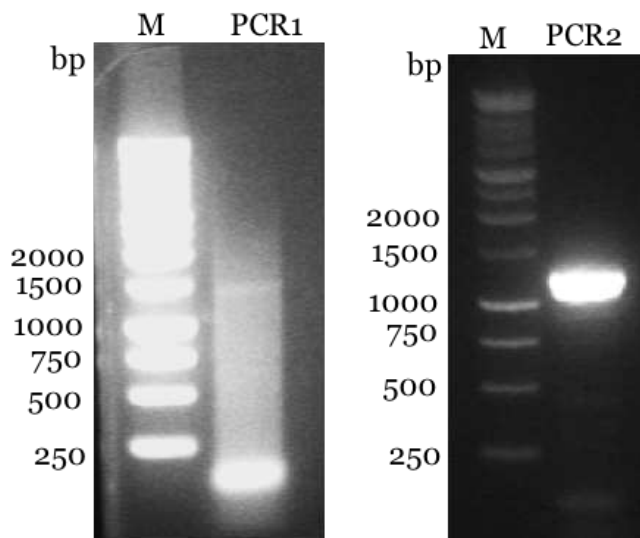


Figure 135. 1% agarose gel analysis of the preliminary 1402 bp and final 1191 bp PCR products (PCR1 and PCR2) for *GsOYE* cloning. M: standard marker (Promega).

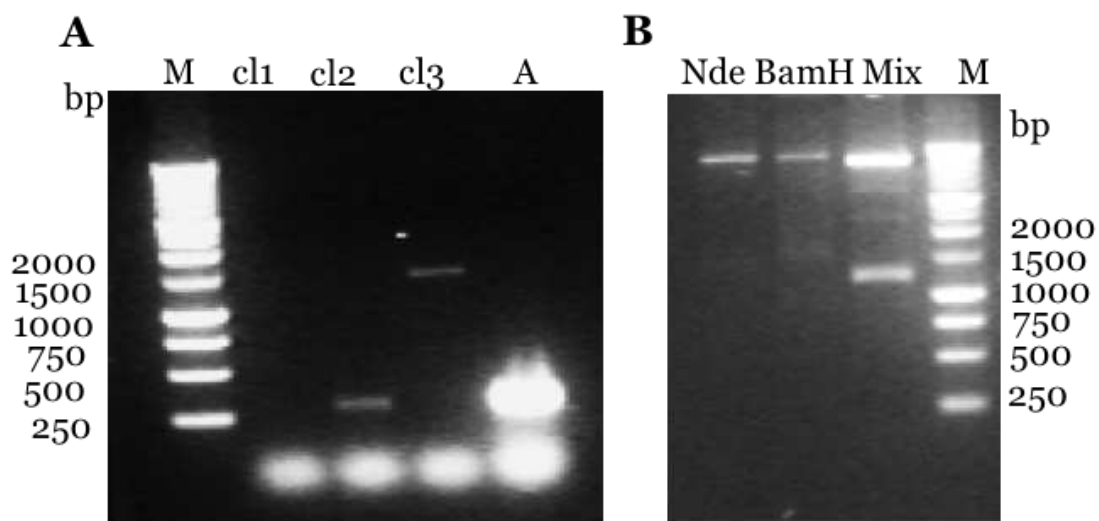
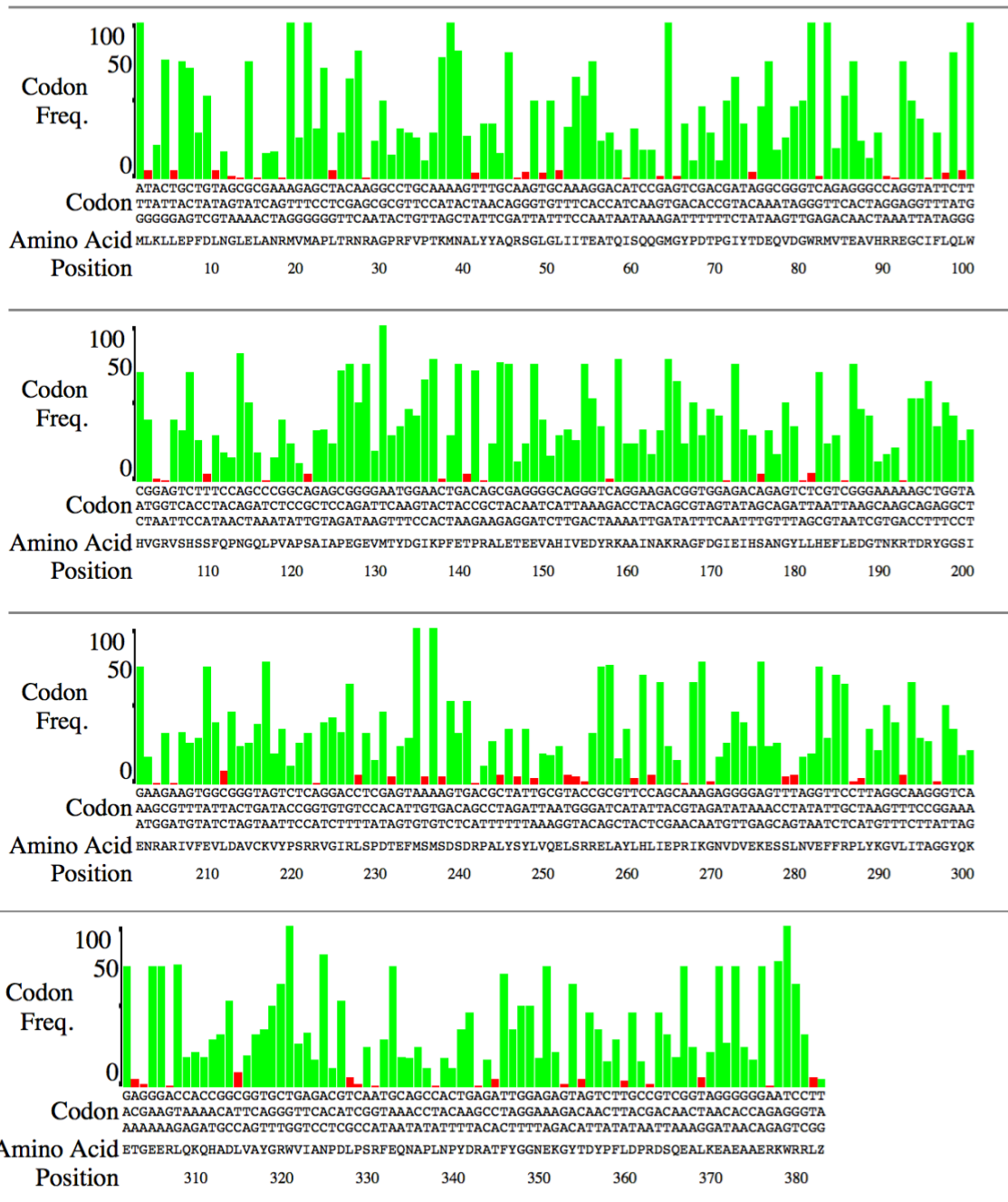
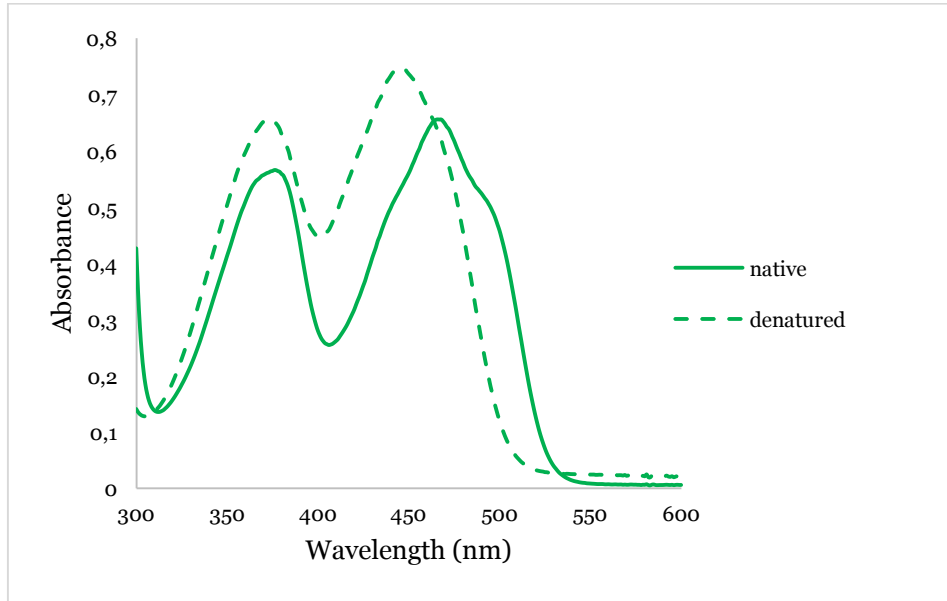


Figure 136. (A) 1% agarose gel analysis of amplimers produced by colony PCR using T7_for and T7_rev primers. A: autoligation. (B) 1% agarose gel analysis of analytical restriction digestion of pET28a-*GsOYE* vector purified from a positive clone. Nde: plasmid digested just with NdeI, BamH: plasmid digested just with BamHI, Mix: plasmid double digested with NdeI and BamHI. M: standard marker (Promega).

b) Codon usage analysis



c) UV/Vis spectrum of native and denatured GsOYE



CtOYE

>native sequence

ATGAATACCAACATCGATCTATTCTCACCCGTTCCGGCTCGGTTCGTTACGAATTACCTAACCGAATGGTGATGGCTCCC
TTAACGCGCAACCGTGGGGAGAGGGTAACGTGCCGAGAGAATTGAATGCAGAATATTACGCCAAAGAGTCTCGGCA
GGACTGATTATTACAGAAGCGACTCAGGTGTGCCACAAGGCTTAGGTTATCCGTTTACCCCTGGTATTCACCTCCCAA
GAACAGGTAGAAGGCTGGCGGCTAGTGACGAAAGCCGTACACGATCGCGGTGGCAAAATTTTTCTCCAGCTATGGCAC
GTCGGGCGAATATCTCACCCCGATTGCAAGTCGATGGAGCATTGCCCGTTGCACCTAGCGCGATCGCGCCATCAGAA
GGTATGGCAGCTACTTACGAAGGAGAAAAGCCTTACGTTACACCCCGCGCCCTAGAAACAGCAGAAATTCAGGAATT
GTAGAACAATATCGCAAGGGGCAAAAAATGCGTTGGCGGCTGGGTTTGTATGGCGTAGAAATTCACAGCGCCAACGGC
TATCTGCTCGATCAATTTCTCCACGATGGCTCCAATCACCGTACAGATGAATATGGTGGCTCGATTGAAAATCGCGCC
CGCTTGCTAATGGAAGTGAAGCAGTCGTTAGTGTGTTGGGGTGCAGATAGAGTGGGAGTCAGACTTTCACCCAGT
GGCACTTTTGGCAGCGTCTACGACTCCGATCTCAAAGCATTGTTTACCTATGTAGTTGATGCGCTCAACCAATTTGAA
TTAGCTTATCTACATTTGGTAGAGCCGAGAGTTGCTGGTAACGAGACAGTAGAAAATCCTACTTCAGAAATGTCATCA
AAATACTTCCGTCGATCTACAAAGGACTCTCATCAGTGTGGCGGCTACGATCGCGAATCGGGAATGCAGTATTA
GCCTCTGGAGATCGCGACTTAGTTGCTTACGGTAGACTGTTTATTTCCAACCCCGACTTACCGCAGCGTTTTGCTCTC
AACGCACAATTAACCCCTACGATCGCTCTAGCTTTTATGGCGGAGACAAGAGGGGTATACAGATTATCCATCTTTG
GAATTGCAGGCTGCTGGTTGAGGATCCGAATTCGAGCTCCGTCGACAAGCTTGGCGGCCACTCGAGCACCA

>recombinant sequence

His₆-tag
Thrombin-site
NdeI

atgggagcagcagc**catcatcatcatcatcac**agcagcgggc**ctgggtgcegcgcgccagccat**
M G S S H H H H H S S G L V P R G S H
atgaataccaacatcgatctattctcaccggttcggctcgggtcggttacgaattacctaac
M N T N I D L F S P V R L G R Y E L P N
cgaatggtgatggctcccttaacgcgcaaccggtgcgggagagggtaacgtgccgagagaa
R M V M A P L T R N R A G E G N V P R E
ttgaatgcagaatattacgccc aaagagtctcggcaggactgattattacagaagcgact
L N A E Y Y A Q R V S A G L I I T E A T
Caggtgtcgccacaaggcttaggttatccggttaccctgggtattcactcccaagaacag
Q V S P Q G L G Y P F T P G I H S Q E Q
gtagaaggctggcggctagtgacgaaagccgtacacgatcgcggtggcaaaatTTTTctc
V E G W R L V T K A V H D R G G K I F L
cagctatggcacgctcgggcaaatatctcaccocgatttgaagtcgatggagcattgccc
Q L W H V G R I S H P D L Q V D G A L P
gttgacactagcgcgatcgcgccatcagaaggtatggcagctacttacgaaggagaaaag
V A P S A I A P S E G M A A T Y E G E K
ccttacgtsacccccgcgccatagaaacagcagaattccaggaattgtagaacaat
P Y V T P R A L E T A E I P G I V E Q Y
cgccaaggggcaaaaaatgcgttggcggctgggtttgatggcgtagaaattcacagcgcc
R Q G A K N A L A A G F D G V E I H S A
aacggctatctgctcgatcaatTTctccacgatggctccaatcaccgtacagatgaatat
N G Y L L D Q F L H D G S N H R T D E Y
gggtggctcgattgaaaatcgcgcccgttgcataatggaagtgactgaagcagtcgtagt
G G S I E N R A R L L M E V T E A V V S
gtttgggggtgcagatagagtgggagtcagactttcaccagtggtcacttttggcagcgtc
V W G A D R V G V R L S P S G T F G S V
tacgactccgatctcaaagcattgTTTtacctatgtagttgatgcgctcaaccaatTTgaa
Y D S D L K A L F T Y V V D A L N Q F E
ttagcttatctacatttggtagagccgagagttgctggtaacgagacagtagaaaatcct
L A Y L H L V E P R V A G N E T V E N P
acttcagaattgtcatcaaaatacttccgtccgatctacaaagggactctcatcagtgct
T S E L S S K Y F R P I Y K G T L I S A
ggcggctacgatcgcgaatcgggaaatgcagattagcctctggagatgcggacttagtt
G G R E S G N A V L A S G D A D L V
gcttacggtagactgtttatTTccaacccccgacttaccgcagcgttttgcctctcaacgca
A Y G R L F I S N P D L P Q R F A L N A
caattaaaccctacgatcgcctctagctTTTTatggcggagacaagaggggttatacagat
Q L N P Y D R S S F Y G G D K R G Y T D
tatccatcttTggaattgcaggctgctggt**tgaggatcc**
Y P S L E L Q A A G - G S
BamHI

a) Cloning

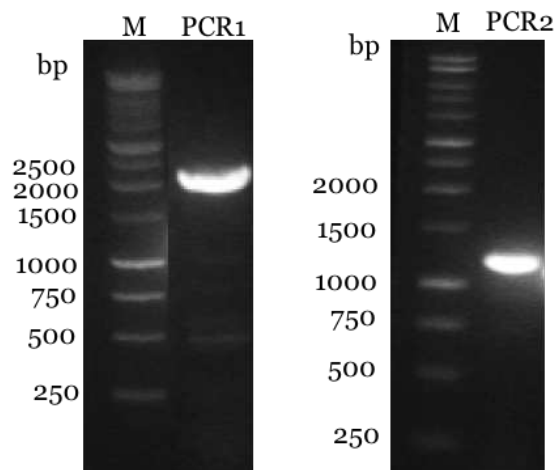


Figure 137. 1% agarose gel analysis of the preliminary 2200 bp and final 1121 bp PCR products (PCR1 and PCR2) for *CtOYE* cloning. M: standard marker (Promega).

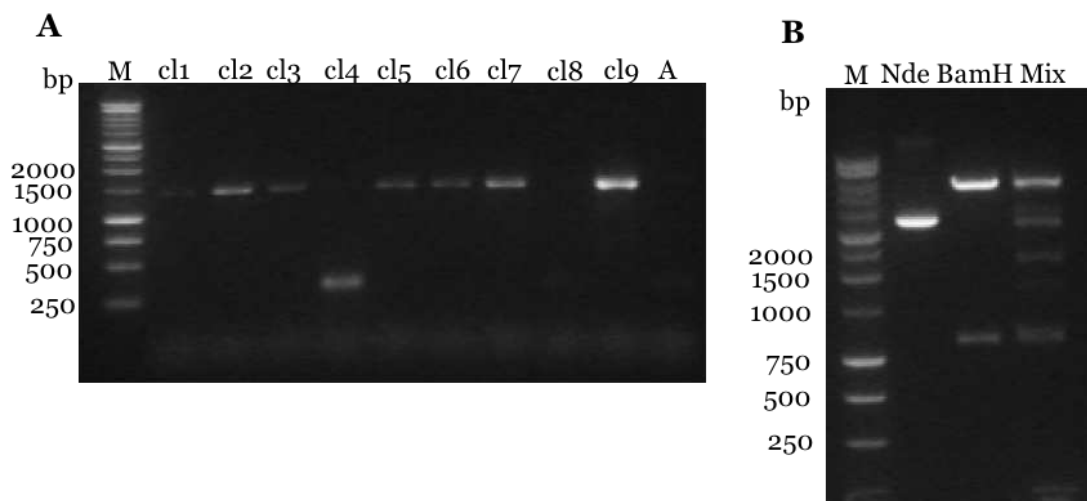
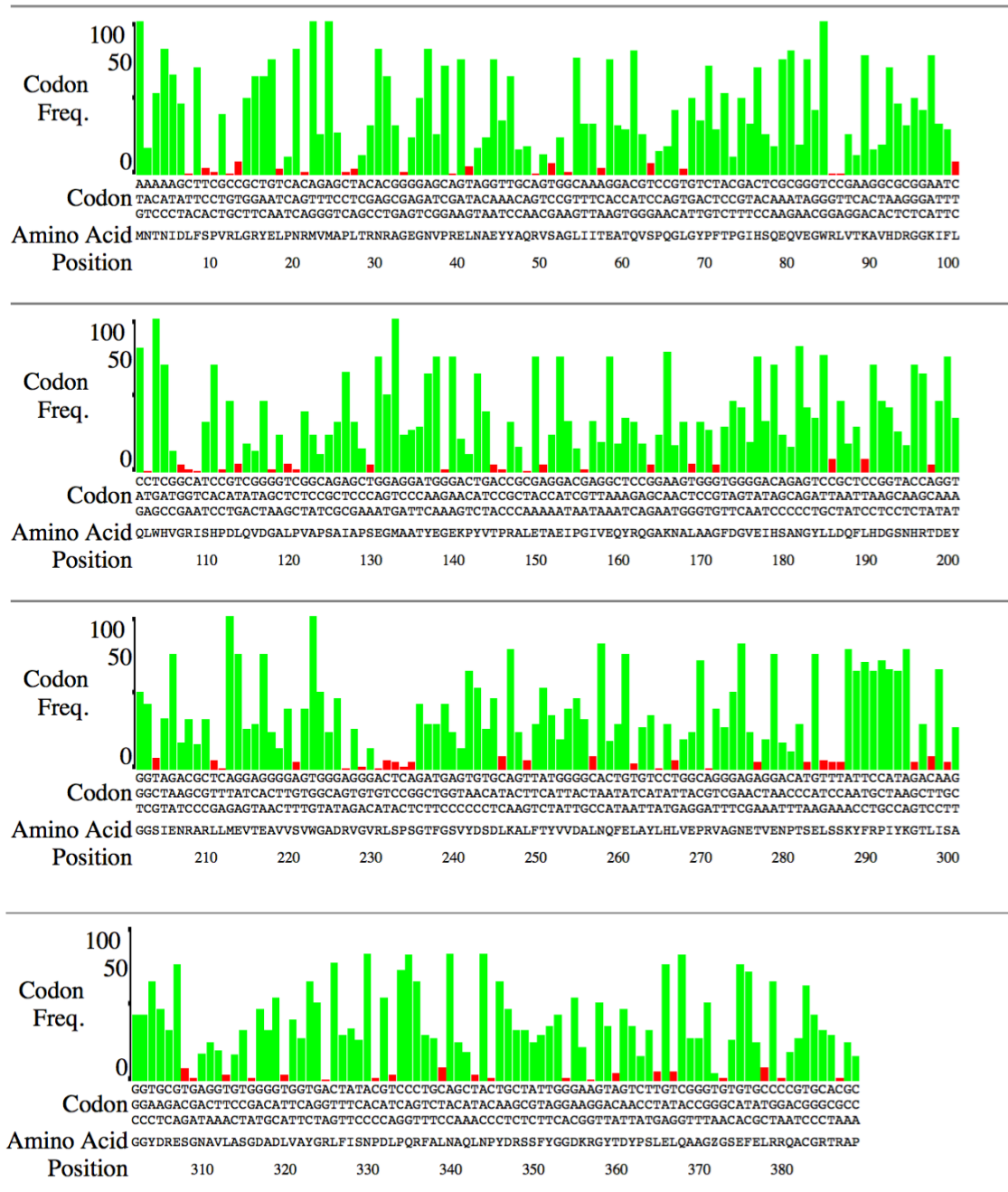
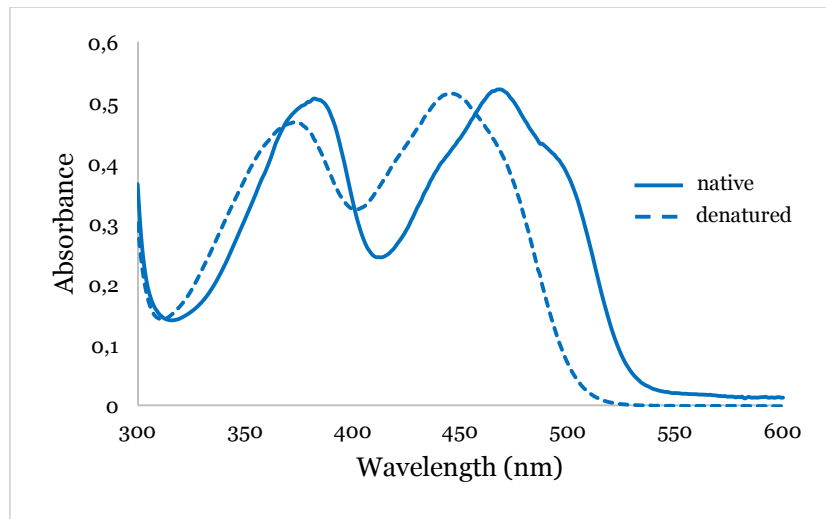


Figure 138. (A) 1% agarose gel analysis of amplimers produced by colony PCR using T7_for and T7_rev primers. A: autoligation. (B) 1% agarose gel analysis of analytical restriction digestion of pET28a-*CtOYE* vector purified from a positive clone. Nde: plasmid digested just with NdeI, BamH: plasmid digested just with BamHI, Mix: plasmid double digested with NdeI and BamHI. M: standard marker (Promega).

b) Codon usage analysis



c) UV/Vis spectrum of native and denatured CtOYE



CaOYE

>native sequence

ATGCAACCACATTTATTACACCGCTGACCATCGGCAGCGTACCCTACGCAATCGGATCGGTATGTCGCCGATGTGT
CAATACAGCGCCGTCGACGGCTTCCAACCGATTGGCATCTGATGCATCTCGGCGCGGGCAGCCGGCGGGTTGGT
CTCATCATCTCGAGGCCACGGCCGTTTCGCCCGAAGGACGGATTTCTCCGTTTCGATTTGGGTATCTGGAGCGATGAT
CACATTGCTGCCCTCTCCCGCATTGTTAAGCTGATCGAGAGTCTTGGTGGGTAGCCGGCATTCAATTAGCGCACGCC
GGACGTAAGCAAGTGTGGTTCGCCGTCGGGAGGGCGCAAACCGATTGCGCCGGCAAACGGCGGCTGGCCGGTAGTC
GGCCGACGGCTGAACCGTTTCGCTCCCGGTTACCCACCCCGATCCCGCTCGATGCAGCCGGTATTGCCAGGGTTGTG
GCCGATTTTGGCACCGCCACCAACGCGCAGAGCTGCCGGTTTCGCTGGATCGAGATCCACGCTGCCATGGCTAC
CTCCTCCACAACCTCCTCTCGCCACTTGGCAATGACCGCAACGACGAGTACGGTGGCGATCTGCGTGAAGAGTGCCT
CTGCTGAGTGAAGTAAACCGCCGAGTGCAGCAGAAATGGCCATCTGATCTGCCACTTGTCTCGCTCTCGTGCAGT
GACTGGACACCGGAAGTTTAAACCATCGCCGATACGGTAGAGGTGGCGCGCATGCTACGTGAACAGGGAGTTGATCTG
ATCGATTGTAGTTCGGCGGGATTGCCCGGCATTACCATCCCGTTCGGAGAGGGGTATCAAGTGCCATTTGCAGCT
CAGGTCCGTGCGGAGGCCAATATCGCCACCGCCGCTGTCGGCCTAATTACCCGGCCGAACACGCCGACGCCATTGTC
CGCAACGGCGACGCCGATCTGGTATTGTTGGGCCGAGAATGCTCCGTGACCCACACTGGCCGCTGCGCGCGGCGGG
CGCTCGGCCACGATCTCGGCCGCCCGCCGAGTATTGCGGGCGTGGTGA

>recombinant sequence

atgggagcagcagc **catcatcatcatcatcac** agcagcgggc **ctggtgcccgcggcgcagc** cat
M G S S H H H H H S S G L V P R G S H
atgcaaccacattttattacaccgctgaccatcggcagcgtcaccctacgcaatcggatc
M Q P H L F T P L T I G S V T L R N R I
ggatgctcgccgatgtgtcaatacagcgcgctcgacggcttcccacccgattggcatctg
G M S P M C Q Y S A V D G F P T D W H L
atgcatctcggcgcgcgggagccggcggggttggctcatcatcctcgaggccacggcc
M H L G A R A A G G V G L I I L E A T A
gtttcgcccgaaggacggattttctcgttcgatttgggtatctggagcgtatgacacatt
V S P E G R I S P F D L G I W S D D H I
gctgcccctctcccgcattgttaagctgatcgagagcttgggtgaggtagccggcattcaa
A A L S R I V K L I E S L G A V A G I Q
ttagcgcagcggacgtaagcaagtgttggctcgcccggtgggagggcggaaccgatt
L A H A G R K A S V G R P W E G G K P I
gcgcccggcaaacggcggctggccggtagtcggcccgcagcgtgaaccgcttccgctcccgg
A P A N G G W P V V G P T A E P F A P G
taccaccccccgatcccgcctcgatgcagcggatattgccagggttggtggccgatatttgcc
Y P T P I P L D A A G I A R V V A D F A
accgccaccaaacgcgacagctgcccgtttccgctggatcgagatccacgctgcccatt
T A T K R A R A A G F R W I E I H A A H
ggctacctcctccacaacttctctcggcacttggcaatgaccgcaacgacgagtagcgtg
G Y L L H N F L S S P L G N D R N D E Y G
ggcgtctgctggaagagtgctgctgagtgaggaaccgcccagtgccgagcagaa
G D L R G R V R L L S E V T A A V R A E
tggccatctgatctgccacttggctgctcctcctcgtgagtgactggacaccggaagg
W P S D L P L A V R L S C S D W T P E G
ttaaccatcgccgatacggtagaggtggcgcgcagtgctacgtgaacagggagttgatctg
L T I A D T V E V A R M L R E Q G V D L
atcgattgtagttccggcgggattgccccggcattaccatcccggctcgagaggggtat
I D C S S G G I A P G I T I P V G E G Y
caagtgccatttgcagctcaggtccgctcgagggccaatatcgccaccgcccgtgtcgcc
Q V P F A A Q V R R E A N I A T A A V G
ctaattaccggcccgaacacgcccagccattgtccgcaacggcgacgcccgatctggta
L I T R P E H A D A I V R N G D A D L V
ttggtggccgagaactgctccgtgacccacactggccgctgcccggcgccggcgctc
L L G R E L L R D P H W P L R A A R A L
ggccacgatctcgccggccgcccagctatattgcccggcggtg **tgaggatcc**
G H D L A P P P Q Y L R A W - G S
BamHI

a) Cloning

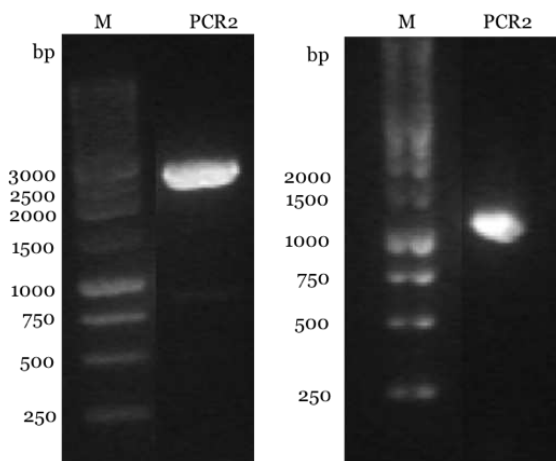


Figure 139. 1% agarose gel analysis of the preliminary 2734 bp and final 1062 bp PCR products (PCR1 and PCR2) for *CaOYE* cloning. M: standard marker (Promega).

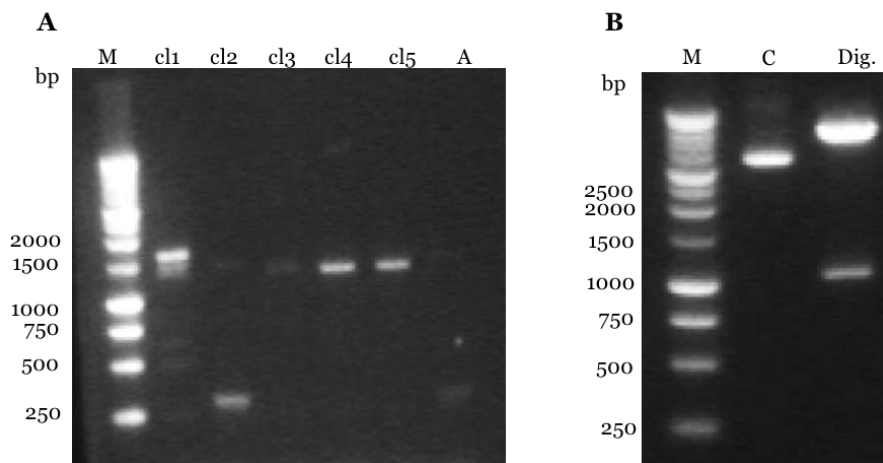
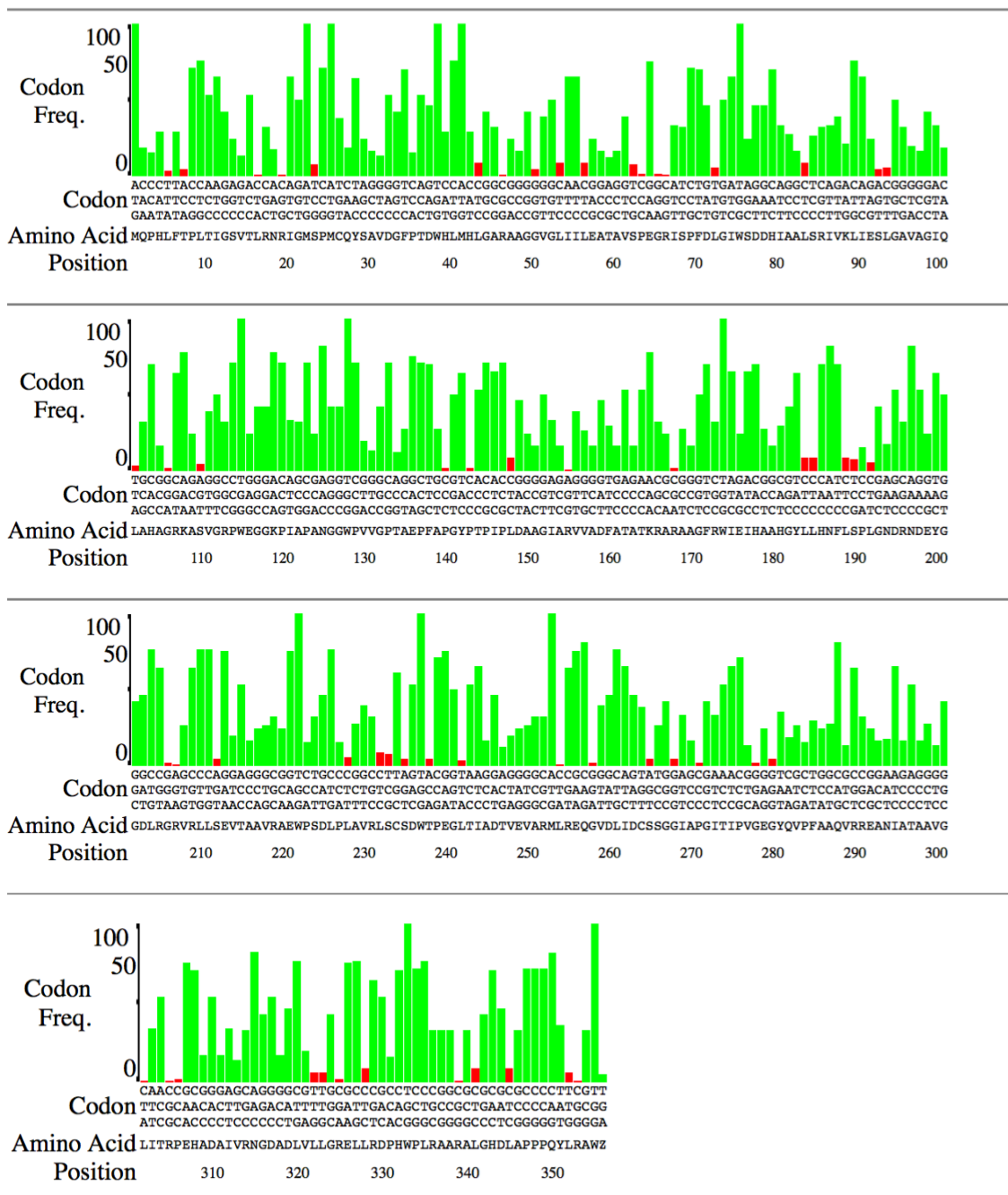
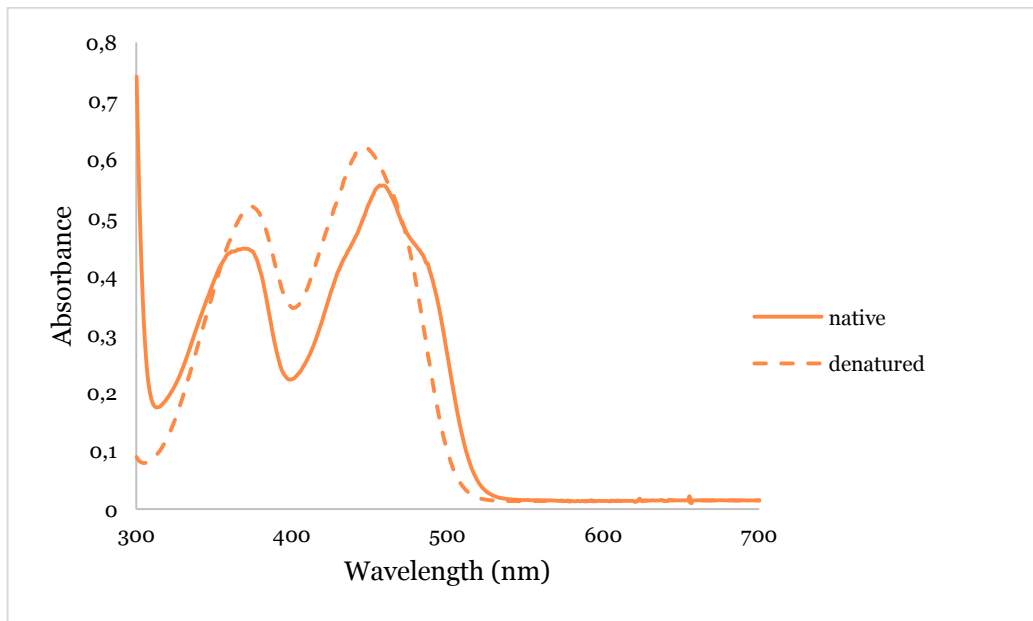


Figure 140. (A) 1% agarose gel analysis of amplimers produced by colony PCR using T7_for and T7_rev primers. A: autoligation. (B) 1% agarose gel analysis of analytical restriction digestion of pET28a-*CaOYE* vector purified from a positive clone. C: non digested plasmid used as control, Dig.: digested plasmid with NdeI and BamHI. M: standard marker (Promega).

b) Codon usage analysis



c) UV/ Vis spectrum of native and denatured *CaOYE*



BfOYE1

>native sequence

ATGTCTCCATCCACACTCTTCACCCCTCTCAAAGTTGGAACCTCTGAGCTCCAACATCGAATTGCCATGGCACCTCTC
ACCCGATTCCGTGCCGATGATAACCACGTACCCCTTCCAATGGTTGCCGAATACTACGCACAACGTGCTTCTGTACCT
GGCACACTGCTCGTCTCTGAAGCTACCTTCATTGCTCCAGAGCCGCCGTTATGCCAATCCCCCTGGTATTTGGAAC
AAAGAACAATTGCCGGATGGAAAAAGGTCACCGACGCCGTTACAGCAAAGAAATCATACATCTGGATGCAACTATGG
GCATTAGGAAGAGCTGCAGACCCATCAGTCTTACAACAAGAAGGTGGTTATAAACTCCAGTCTTCGAGCGATATTGCC
TTCGAGGGAGGTGCCAAGCCAGAACCCTTGACCGAGCCGAGATTAAGGAATATATTGAATTATACACACAAGCTGCC
AAGAACGCAATTGAAGCTGGATTTGACGGTGTGAGATCCACGGAGCAAACGGTTATTTGATCGATCAATTCTTCCAA
GATACCGCAAATCAACGTACCGACTCCTGGGGAGGAAGTGTGAGAACCAGCGCACGTTTTGGCCTTGAGGTTGCCAAA
TCTGTGCTTGAGCTGTTGGTGCCGAGAAGACTTCTATGCGATTGAGTCCATTTTCTCCTTTCCAAGGAATGAAGATG
GCAGATCCTATTCCACAATTTACCTACATCGCTCAAGAGCTTAAGAAATTGAACCTTGCATATCTACACGTTGTCCGAA
TCAAGAATTATCGGAAATGCAGATATCGAAGCAACCAGGAAGGTTGACTTTTTGATCAATATCTGG**AATGGTACC**AGC
CCAATTCTCCTCGCTGGAGGTTTCACAGCCGAATCTGCAAAGAAGGCTGTGCAAGAAGAATACAAAGGAAAGGATATT
GTAATTGTATTCCGACGATACTTCATCACCAACCCAGATCTTCCATTCAGAGTTAAGGAGGGAATCGAGTTCACTCCA
TACGATAGAGATTTCTTTTACAACAAGAAGGAGGCTGAAGGATATACCACTTATCCTTTTCAGCAAGGAGTTTGAGGCC
CAACGAAAGGCCATTGAATCTTCAGCATAA

> sequence after removal of the predicted N-glycosylation site

ATGTCTCCATCCACACTCTTCACCCCTCTCAAAGTTGGAACCTCTGAGCTCCAACATCGAATTGCCATGGCACCTCTC
ACCCGATTCCGTGCCGATGATAACCACGTACCCCTTCCAATGGTTGCCGAATACTACGCACAACGTGCTTCTGTACCT
GGCACACTGCTCGTCTCTGAAGCTACCTTCATTGCTCCAGAGCCGCCGTTATGCCAATCCCCCTGGTATTTGGAAC
AAAGAACAATTGCCGGATGGAAAAAGGTCACCGACGCCGTTACAGCAAAGAAATCATACATCTGGATGCAACTATGG
GCATTAGGAAGAGCTGCAGACCCATCAGTCTTACAACAAGAAGGTGGTTATAAACTCCAGTCTTCGAGCGATATTGCC
TTCGAGGGAGGTGCCAAGCCAGAACCCTTGACCGAGCCGAGATTAAGGAATATATTGAATTATACACACAAGCTGCC
AAGAACGCAATTGAAGCTGGATTTGACGGTGTGAGATCCACGGAGCAAACGGTTATTTGATCGATCAATTTCTTCCAA
GATACCGCAAATCAACGTACCGACTCCTGGGGAGGAAGTGTGAGAACCAGCGCACGTTTTGGCCTTGAGGTTGCCAAA
TCTGTGCTTGAGCTGTTGGTGCCGAGAAGACTTCTATGCGATTGAGTCCATTTTCTCCTTTCCAAGGAATGAAGATG
GCAGATCCTATTCCACAATTTACCTACATCGCTCAAGAGCTTAAGAAATTGAACCTTGCATATCTACACGTTGTCCGAA
TCAAGAATTATCGGAAATGCAGATATCGAAGCAACCAGGAAGGTTGACTTTTTGATCAATATCTGG**AATGGTCTC**AGC
CCAATTCTCCTCGCTGGAGGTTTCACAGCCGAATCTGCAAAGAAGGCTGTGCAAGAAGAATACAAAGGAAAGGATATT
GTAATTGTATTCCGACGATACTTCATCACCAACCCAGATCTTCCATTCAGAGTTAAGGAGGGAATCGAGTTCACTCCA
TACGATAGAGATTTCTTTTACAACAAGAAGGAGGCTGAAGGATATACCACTTATCCTTTTCAGCAAGGAGTTTGAGGCC
CAACGAAAGGCCATTGAATCTTCAGCATAA

native	MSPSTLFTPLKVGTSSELQHRIAMAPLTRFRADDNHVPLPMVAEYYAQRASVPGTLLVSEA	60
mutated	MSPSTLFTPLKVGTSSELQHRIAMAPLTRFRADDNHVPLPMVAEYYAQRASVPGTLLVSEA *****	60
native	TFIAPRAAGYANPPGIWNKEQIAGWKVTDVAHAKKSYIWMQLWALGRAADPSVLQQEGG	120
mutated	TFIAPRAAGYANPPGIWNKEQIAGWKVTDVAHAKKSYIWMQLWALGRAADPSVLQQEGG *****	120
native	YKLQSSSDIAFEGGGKPEPLTEAEIKEYIELYTAQAKNAIEAGFDGVEIHGANGYLIDQF	180
mutated	YKLQSSSDIAFEGGGKPEPLTEAEIKEYIELYTAQAKNAIEAGFDGVEIHGANGYLIDQF *****	180
native	FQDTANQRTDSWGGSVENRARFGLEVAKSVVAAVGAEKTSMLRSPFSPFQGMKMDPIQ	240
mutated	FQDTANQRTDSWGGSVENRARFGLEVAKSVVAAVGAEKTSMLRSPFSPFQGMKMDPIQ *****	240
native	FTYIAQELKKLNLAYLHVESRIIGNADIEATEKVDFLINIWN G TSPILLAGGFTAESAK	300
mutated	FTYIAQELKKLNLAYLHVESRIIGNADIEATEKVDFLINIWN G VSPILLAGGFTAESAK *****	300
native	KAVEEYKGDIVIVFGRYFITNPDLPFRVKEGIEFTPYDRDFYFNKKEAEGYTTYPF	360
mutated	KAVEEYKGDIVIVFGRYFITNPDLPFRVKEGIEFTPYDRDFYFNKKEAEGYTTYPF *****	360
native	EFEAQRKAIESSA 373	
mutated	EFEAQRKAIESSA 373 *****	

>recombinant sequence

atgggcagcagc**catcatcatcatcatcac**agcagcggc**ctggtgccgcgaggcagccat**
M G S S H H H H H S S G L V P R G S H
atgtctccatccacactcttcacccctctcaaagttggaacttctgagctccaacatcga
M S P S T L F T P L K V G T S E L Q H R
attgccatggcacctctcacccgattccgtgcccgatgataaccacgtacccttccaatg
I A M A P L T R F R A D D N H V P L P M
gttgccgaatactacgcacaacgtgcttctgtacctggcacactgctcgtctctgaagct
V A E Y Y A Q R A S V P G T L L V S E A
accttcattgctcccagagccgcccggttatgccaatccccctggatatttggacaaagaa
T F I A P R A A G Y A N P P G I W N K E
caaattgccggatggaaaaaggtcaccgacgccgttcacgcaaagaaatcatacatctgg
Q I A G W K K V T D A V H A K K S Y I W
atgcaactatgggcattaggaagagctgcagaccatcagctttacaacaagaaggtggt
M Q L W A L G R A A D P S V L Q Q E G G
tataaactccagctcttcgagcgatattgccttcgagggaggtggcaagccagaaccttgg
Y K L Q S S S D I A F E G G G K P E P L
accgaggccgagattaaggaatatattgaattatacacacaagctgccagaacgcaatt
T E A E I K E Y I E L Y T Q A A K N A I
gaagctggatttgacggtggttgagatccacggagcaaacggttatttgatcgatcaattc
E A G F D G V E I H G A N G Y L I D Q F
ttccaagataccgcaaatacagtcaccgactcctggggaggaagtggttgagaaccgcga
F Q D T A N Q R T D S W G G S V E N R A
cgttttggccttgaggttgccaaatctgctcgttgccagctggtggcgagaagacttct
R F G L E V A K S V V A A V G A E K T S
atgcgattgagtcattttctcctttccaaggaatgaagatggcagatcctattccacaa
M R L S P F S P F Q G M K M A D P I P Q
tttacctacatcgctcaagagcttaagaaattgaaccttgcatatctacacggttgcgaa
F T Y I A Q E L K K L N L A Y L H V V E
tcaagaattatcggaatgcagatatcgaagcaaccgagaaggttgactttttgatcaat
S R I I G N A D I E A T E K V D F L I N
atctgg**aatggtgtc**agcccaattctcctcgtgaggtttcacagccgaatctgcaaag
I W N G V S P I L L A G G F T A E S A K
aaggctgtcgaagaagaatacaaaaggaaaggatattgtaattgtattcggacgatacttc
K A V E E E Y K G K D I V I V F G R Y F
atcaccaaccagatcttccattcagagttaaggaggggaatcgagttcactccatacga
I T N P D L P F R V K E G I E F T P Y D
agagatttcttttacaacaagaaggaggtgaaggatataccacttatcctttcagcaag
R D F F Y N K K E A E G Y T T Y P F S K
gagtttgaggcgcaacgaaaggccattgaatcttcagca**taa**tttatatatatagaattt
E F E A Q R K A I E S S A - F I Y I E F
tttttatagacgcat**ggatcc**
F F I D A W I
BamHI

a) Cloning

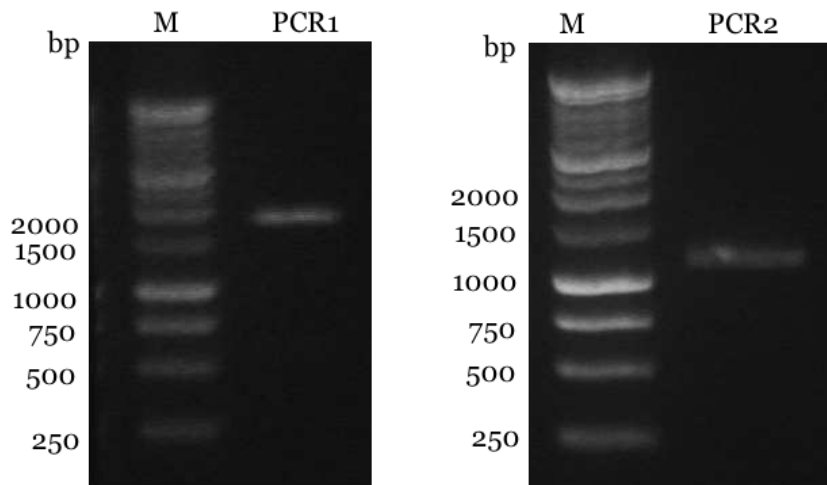


Figure 141. 1% agarose gel analysis of the preliminary 1795 bp and final 1187 bp PCR products (PCR1 and PCR2) for *BfOYE1* cloning. M: standard marker (Promega).

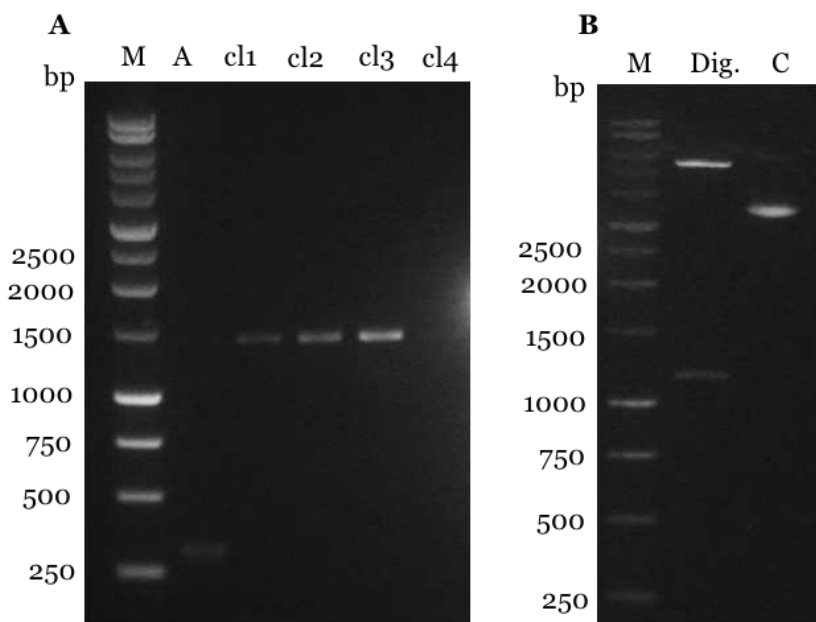
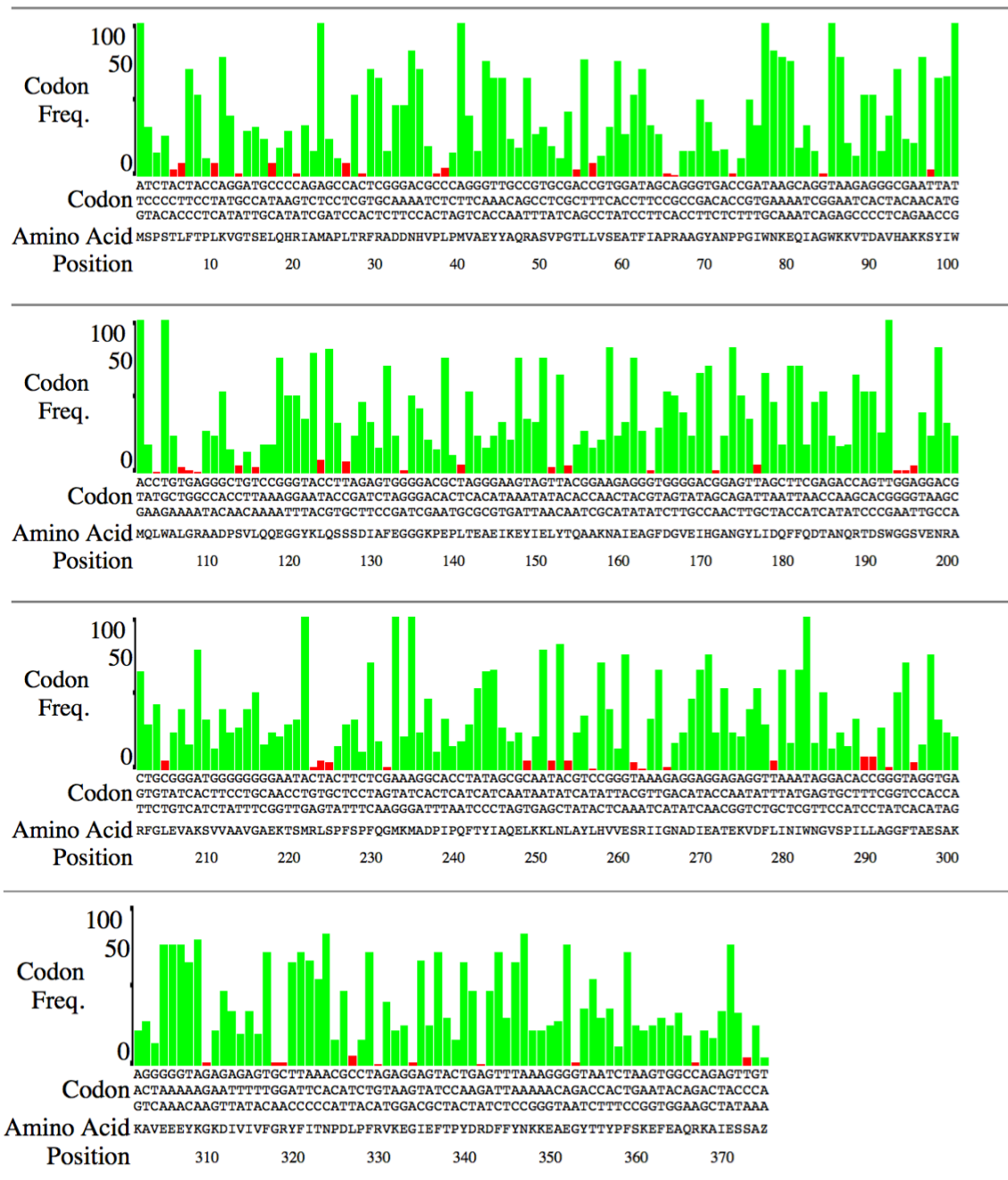
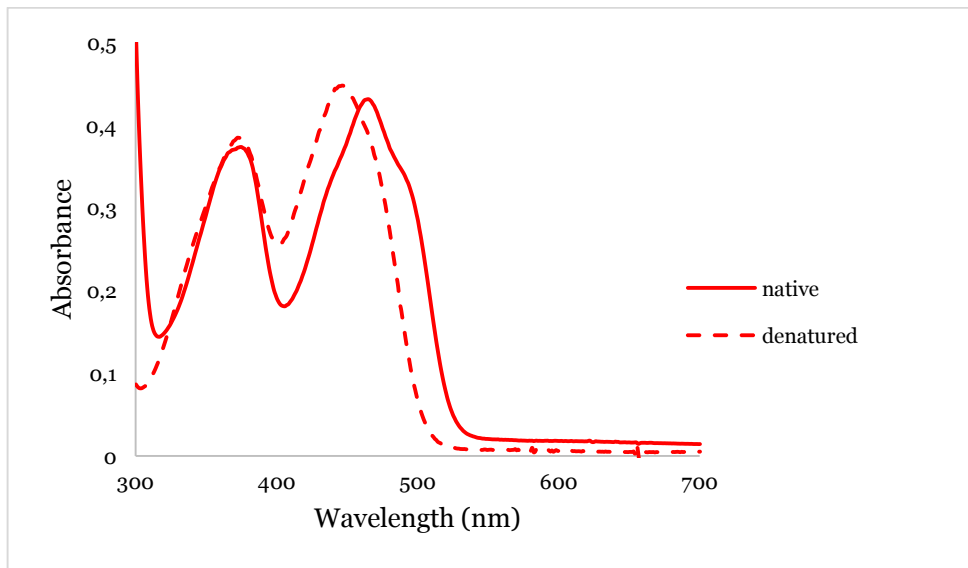


Figure 142. (A) 1% agarose gel analysis of amplimers produced by colony PCR using T7_for and T7_rev primers. A: autoligation. (B) 1% agarose gel analysis of analytical restriction digestion of pET28a-*BfOYE1* vector purified from a positive clone. C: non digested plasmid used as control, Dig.: digested plasmid with NdeI and BamHI. M: standard marker (Promega).

b) Codon usage analysis



c) UV/Vis spectrum of native and denatured *BfOYE1*



BfOYE4

>native sequence

ATGTCAACACCAACACCTCATCCCCAACATGGTGTTCATGTGGTACTAGTACTCCTCGACCAGGTCTTCTTAACACA
CCTGCGCCTGGTGTACGCCGTCCAAGCCCTCTCAAAATAACAGATTATTAACATCATCTAGGTCGCCCTTCTATACCCC
TCTCCAAAGTCTCCCTCGGGCACAGCCCTCCATCTCAGCCCTTCAACTCCCAACTCTTACCCCCCTCAAAATCCGC
TCTCTCACTCTCCAAAATCGCATCATGCTCTCTCCAAATGTGTCAAACCTCCGCTTCTAACGGCCACTTTACTCCTTGGC
ACATGGCTCATCTAGGTGGGATCATCTCCCGCGGTCCGGTCTCTCGATGGTAGAAGCCACCTCTGTTTTACCCGAAGG
AAGAATCACCCCTGAAGACAGCGGATATGGTTAGATCTCAAGGCACAAATTGAAAGAAGTTGTACAATTCGCACA
TTCACAGGGACAGCTAATTGGGATTC AATTGAGCCACGCAGGGAGAAAAGCGAGTATGGTAGCACCATGGCTCGATCG
CTCCGCGTGC AACAGAGGAAGCAGGCGGCTGGCCACCAAAGTCAAAGGACCAAGCGCTATTCCCTACGACGAACA
TCACTACAAACCTTCTGCCATGACACTTGAAGATATTC AAGAATTC AAAGACGCATGGGCCGCGTCTCTCAAACGCGC
ACTCAAAGCTGGATTCGACGTGATAGAAATCCATAACGCGCACGGGTATCTGCTTACGAATTCGTGTCTCCGGTTTC
TAACAAACGCACCGATCAATATGGTGGGAGTTTTGAAAATCGTATTCTGCTCACCCCTTGAGATTGTAGAGATTACGCG
GAAGATTATCCCGAATCTATGCCGCTTTTCTTGGCGATTAGTGCACGGATTGGTTGGATTATGAGGGGTTTGGAGA
GGAGAGTTGGACGGTGGCGGATTCGGCGAGGTTGGCGGGGATTCTGGCGGATAGGGGGTGGATTTAATGGATGTTTC
TTCCGGGGCGAATCATCCGAGACAGAAGATTACGGCAGGGTTGGGATATCAGGCGCCATTTGCGAAGGAGATTAAGAG
GGTGGTGGGGGAGAGATGTTGGTGGGACGGTGGGATGATCGGGAGTGGAAGGCAAGCGGAGGGGCTGTTGAGTGG
AATGGGAGGGGAGAGAGGTGTGGATGAAGGGGAGGAGGAGGGGAAAGGGGACGGAATTAGATTTGGTCATTGTCCG
GCGTGGGTTTCAGAAGAATCCGGGGTGGTGTGGGAGTGGGCGGAGGAATTGGGGTTAGGATTATGGTGGCACATCA
GATGAGGTGGGGTTTAGGGGAAGGCAGGGGGACATTAG

> sequence after of removal of intron

ATGTCAACACCAACACCTCATCCCCAACATGGTGTTCATGTGGTACTAGTACTCCTCGACCAGGTCTTCTTAACACA
CCTGCGCCTGGTGTCCCTTCTATACCCCTCTCCAAAGTCTCCCTCGGGCACAGCCCTCCATCTCAGCCCTTCAACT
CCCAACTCTTACCCCCCTCAAAATCCGCTCTCTCACTCTCCAAAATCGCATCATGCTCTCTCCAATGTGTCAAACCTC
CGCTTCTAACGGCCACTTTACTCCTTGGCACATGGCTCATCTAGGTGGGATCATCTCCCGCGGTCCGGTCTCTCGATG
GTAGAAGCCACCTCTGTTTTACCCGAAGGAAGAATCACCCCTGAAGACAGCGGATATGGTTAGATTC AAGGCGAC
AAATTGAAAGAAGTTGTACAATTCGCACATTCACAGGGACAGCTAATTGGGATTCAATTGAGCCACGCAGGGAGAAAA
GCGAGTATGGTAGCACCATGGCTCGATCGCTCCGCGTGC AACAGAGGAAGCAGGCGGCTGGCCACCAAAGTCAA
GGACCAAGCGCTATTCCCTACGACGAACATCACTACAAACCTTCTGCCATGACACTTGAAGATATTC AAGAATTC AAA
GACGCATGGGCCGCGTCTCTCAAACGCGCACTCAAAGCTGGATTCGACGTGATAGAAATCCATAACGCGCACGGGTAT
CTGCTTACGAATTCGTGTCTCCGGTTTCTAACAAACGCACCGATCAATATGGTGGGAGTTTTGAAAATCGTATTCTG
CTCACCCCTTGAGATTGTAGAGATTACGCGGAAGATTATTC CCGAATCTATGCCGCTTTTCTTGGCGATTAGTGCACG
GATTGGTTGGATTATGAGGGGTTTGGAGAGGAGATTGGACGGTGGCGGATTCGGCGAGGTTGGCGGGGATTCTGGCG
GATAGGGGGTGGATTTAATGGATGTTTCTTCCGGGGCGAATCATCCGAGACAGAAGATTACGGCAGGGTTGGGATAT
CAGGCGCCATTTGCGAAGGAGATTAAGAGGGTGGTGGGGGAGAGGATGTTGGTTGGGACGGTGGGGATGATCGGGAGT
GGAAGGCAAGCGGAGGGGCTGTTGAGTGAATGGGAGGGGAGAGAGGTGTGGATGAAGGGGAGGAGGAGGGGAAAG
GGACGGAATTAGATTTGGTCATTGTCCGCGTGGGTTTCAGAAGAATCCGGGGTGGTGTGGGAGTGGGCGGAGGAA
TTGGGGGTTAGGATTATGGTGGCACATCAGATGAGGTGGGGTTTAGGGGAAGGCAGGGGGACATTAG

>recombinant sequence

atgggcagcagc **catcatcatcatcatcac** agcagcggc **ctggtgccgcgcccagccat**
M G S S H H H H H S S G L V P R G S H
atgtcaacaccaacacctcatccccaacatgggtgttccatgtggtactagtactcctcga
M S T P T P H P Q H G V P C G T S T P R
ccaggtcttcttaacacacctgcgccctgggtgtccccttctatacccctctccaaagtct
P G L L N T P A P G V P F Y T P L Q S P
ccctcgggcacagccctccatctcagcccttcaactcccaaactcttcacccccctcaaa
P S G T A L H L S P S T P K L F T P L K
atccgctctctcactctccaaaatcgcatcatgctctctccaatgtgtcaatactccgct
I R S L T L Q N R I M L S P M C Q Y S A
tctaacggccactttactccttggcacatgggtcatctaggtgggatcatctcccgcggt
S N G H F T P W H M A H L G G I I S R G
cctggctctcgcaggttagaagccacctctgttttaccgaaggaagaatccccctgaa
P G L S M V E A T S V L P E G R I T P E
gacagcggattatgggttagattctcaaggcgacaaattgaaagaagttgtacaattcgca
D S G L W L D S Q G D K L K E V V Q F A
cattcacagggacagctaattgggattcaattgagccacgcagggagaaaagcgagtatg
H S Q G Q L I G I Q L S H A G R K A S M
gtagcaccatggctcgcagctccgcccgcgcaacagaggaagcagggcggtggcccacc
V A P W L D R S A V A T E E A G G W P T
aaagtcaaaggaccaagcgctattccctacgacgaacatcactacaaaccttctgccatg
K V K G P S A I P Y D E H H Y K P S A M
acattgaagatattcaagaattcaagacgcagctgggcccgcgctctctcaaacgcgcactc
T L E D I Q E F K D A W A A S L K R A L
aaagctggattcgcagtgatagaaatccataacgcgcacgggtatctgcttcacgaattc
K A G F D V I E I H N A H G Y L L H E F
gtgtctccggttttctaacaacgcaccgatcaatatgggtgggagttttgaaaatcgatt
V S P V S N K R T D Q Y G G S F E N R I
cgtctcacccttgagattgtagagattacgcggaagattattcccgaatctatgccgctt
R L T L E I V E I T R K I I P E S M P L
ttcttgccgattagtgcgacggattggttgattatgaggggtttggagaggagattgg
F L R I S A T D W L D Y E G F G E E S W
acgggtggcgattcggcgaggttggcggggattctggcggataggggggtggatttaatg
T V A D S A R L A G I L A D R G V D L M
gatgtttcttcggggcgaatcatccgagacagaagattacggcaggggttgggatatcag
D V S S G A N H P R Q K I T A G L G Y Q
gcccatttgcaaggagattaagaggggtgggtgggggagaggatggttggttgggacgggtg
A P F A K E I K R V V G E R M L V G T V
gggatgatcgggagtggaaggcaagcggaggggctggtgagtggaatgggaggggagaga
G M I G S G R Q A E G L L S G M G G E R
ggtgtggatgaaggggaggaggaggaggggaaggggacggaattagatttgggtcattgtc
G V D E G E E E E G K G T E L D L V I V
gcgcgtgggtttcagaagaatccgggggttgggtgtgggagtgggcgagggaattgggggtt
A R G F Q K N P G L V W E W A E E L G V
aggattatgggtggcacatcagatgaggtgggggtttagggggaaggcagggggacat **tag**
R I M V A H Q M R W G F R G K A G G H -
aggcgggaggggtt **ggatcc**
R R E G - F G S
BamHI

a) Cloning

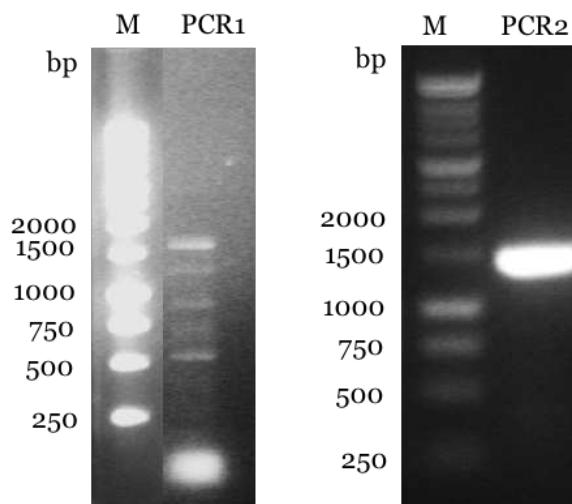


Figure 143. 1% agarose gel analysis of the preliminary 1787 bp and final 1353 bp PCR products (PCR1 and PCR2) for *BfOYE4* cloning. M: standard marker (Promega).

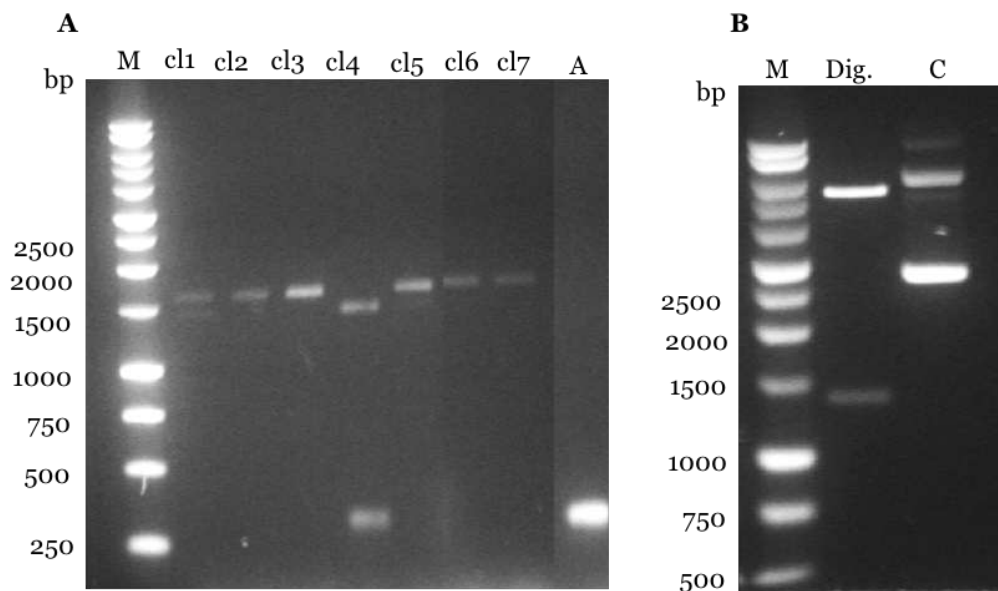
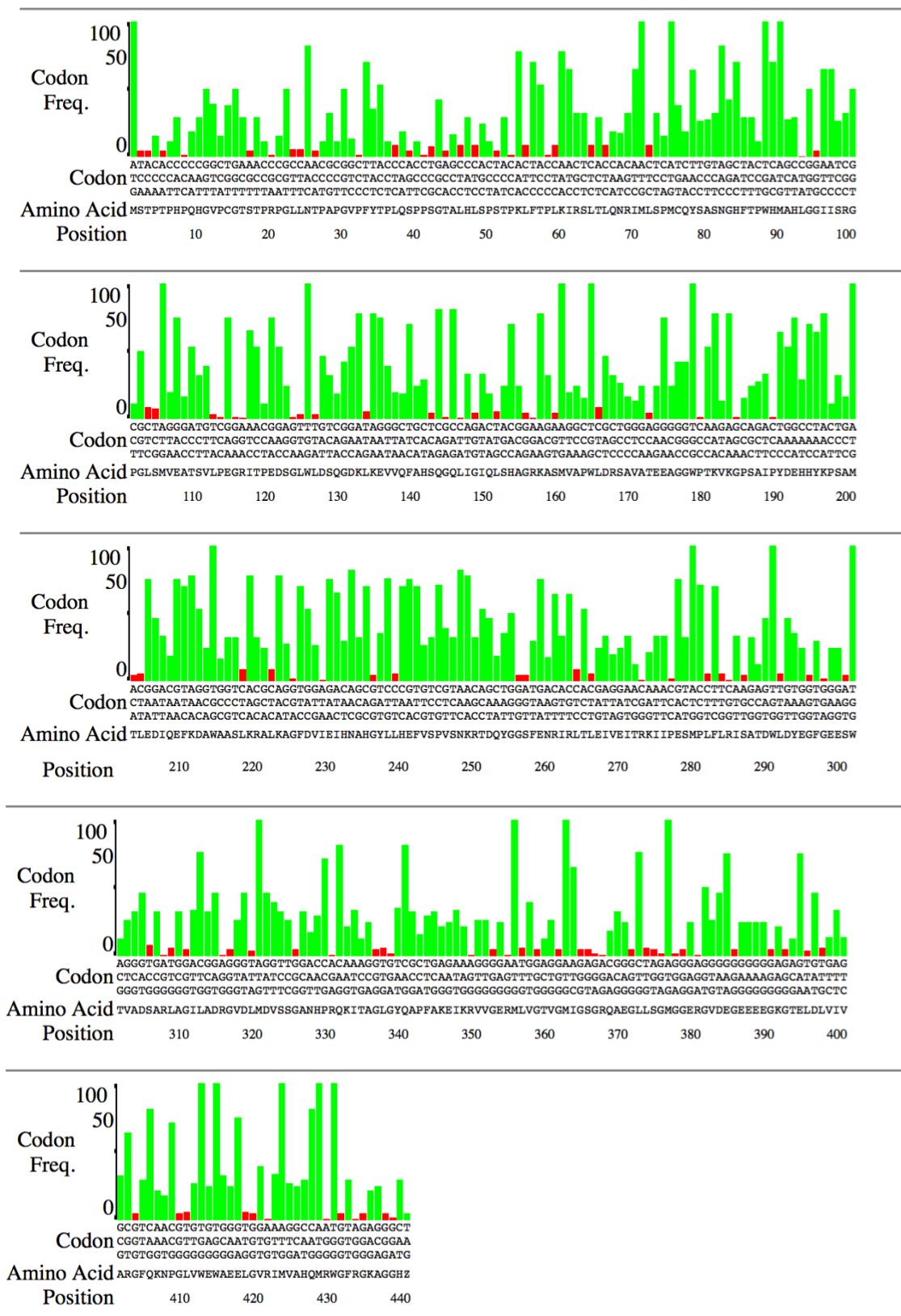
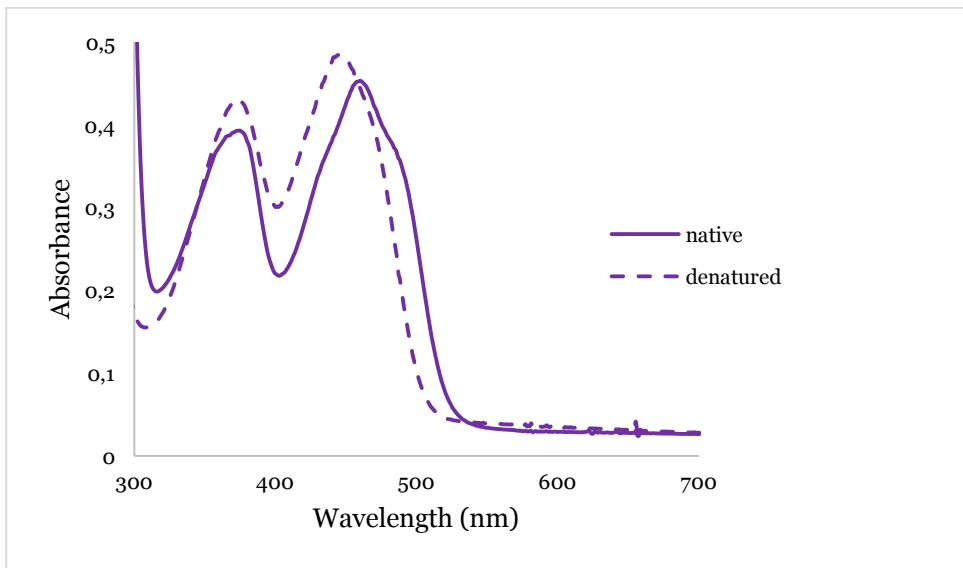


Figure 144. (A) 1% agarose gel analysis of amplimers produced by colony PCR using T7_for and T7_rev primers. A: autoligation. (B) 1% agarose gel analysis of analytical restriction digestion of pET28a-*BfOYE1* vector purified from a positive clone. C: non digested plasmid used as control, Dig.: digested plasmid with NdeI and BamHI. M: standard marker (Promega).

b) Codon usage analysis



c) Vis spectrum of native and denatured *BfOYE4*



AnOYE2

>native sequence

ATGTGCTCCAAACTTTTCAGCCCTTCAGATCGGCCAAAACCAATCTTGAGCACCGAGTAGTCATGGCACCCTCACT
CGATFCCGCGCGGACTCGCAACATGTACCTCTTCCCATGGCAACAACATACTATGAGCAACGTGCTTCGGTTCGGGC
ACCTGCTCATCGCAGAAGCAACACTGATCTACCCTCAGCTGGCGGAGTTTCTCATGCGCCTGGGGTGTGGAGCGAA
GAACAGGTTAACGGCTGAAAAAGATTACTGAAGCGGTGCATAAGAAAGGGAGCTTTATTTTCTGTCAACTAATTGCT
GCTGGCAGAGCTGCTGACCCAGCCAGTTGCATGCAGAAGGTGGTTTTATGCTGCATGCTCCTAGTCCGATTCCCTATT
GAGCCGGGGATGCCGGTACCCAAGGAGCTGGATGAAATCGAAGTGCAGGAAATCATCAATGACTTCGCAATGGCTGCG
AAGAACGCTATTCGTGCTGGTTTTGACGGCGTTGAGATCCACGGGGCTAATGGGTACTTGGTTCGACCAGTTCCTCCAA
GACGTTTCTAATAAGAGAAACGATAAATGGGGTGGTAGCATCCCCAACAGAGCACGATTCGGCTTGGAGGTCGCCAAA
GCAGTGGCCGATGCTATCGGCGCTGACCGACTTGGCTTTCGCTCAGTCCGTGGAACACATGGCAGAGCATGAAAATG
GTCGACCCTGTGCCTCAATTCACCTACTTCGTGGAGCGCCTGCAACAGCTCGGACTGGCCTACCTCCATGTAATTGAG
TCTCGCGTCATCAATAACGTGGACTGCGAAAAGGAGGGCAGTATCAAGTTCCTACTCGACGTTTGGGGGAAATCAGCG
CCTGTGATTGTTGCCGGCGGATATAGACCAGAGAATGTAGAAAATGCTTTGGAGGAAGAATACAAGGACTACAAGGTT
GCAGTCGCCTTTGGTTCGTCATTTTATCGCCAATCCGACTTGCATTTTCGATTCGTCATGATATTTCATCTTAACCTT
TACGACCGAGAGAGTTTTTATACACCTTTGCAAGAGAATGGCTACACGGATTACCCTTTAGTGGCGAATTTATTA
AGCAAAACTAAATGCTGA

>recombinant sequence

atgggcagcagc**catcatcatcatcatcac**agcagcggc**ctggtgcegcgcgccagccat**
M G S S H H H H H S S G L V P R G S H
atgtgtctccaaacttttccagcccttcagatcggcAAAACCAATCTTGAGCACCGAGTAGTCATGGCACCCTCACT
M C S K L F Q P L Q I G K T N L E H R V
gtcatggcaccactcactcgtattccgcgcgggactcgcAACAATGACTTCGCAATGGCTGCG
V M A P L T R F R A D S Q H V P L P M A
acaacatactatgagcaacgtgcttccggttccgggacccctgctcatcgcagaagcaaca
T T Y Y E Q R A S V P G T L L I A E A T
ctgatctcaccctcagctggcggagttcctcatgcgcctgggggtgaggagcgaagaacag
L I S P S A G G V P H A P G V W S E E Q
gttaacggctggAAAAAGATTACTGAAGCGGTGCATAAGAAAGGGAGCTTTATTTTCTGT
V N G W K K I T E A V H K K G S F I F C
caactaattgctgctggcagagctgctgacccagcccagttgcatgcagaaggtggtttt
Q L I A A G R A A D P A Q L H A E G G F
atgctgcatcctcagtcagttcctattgagccggggatgcccgggtaccCAAGGACT
M L H A P S P I P I E P G M P V P K E L
gatgaaatcgaagtgcaggaaatcatcaatgacttcgcaatggctgcaagaacgctatt
D E I E V Q E I I N D F A M A A K N A I
cgtgctggttttgacggcggttgagatccacggggctaattgggtacttggtcgaccagttc
R A G F D G V E I H G A N G Y L V D Q F
ctccaagacgttttctaataagagaaacgataaattgggggtgtagcatccccaacagagca
L Q D V S N K R N D K W G G S I P N R A
cgattcggcttgagggtcgccaaagcagtgccgatgctatcggcgctgaccgacttggc
R F G L E V A K A V A D A I G A D R L G
tttcgcctcagtcctggaacacatggcagagcatgaaaatggctcgaccctgtgcctcaa
F R L S P W N T W Q S M K M V D P V P Q
ttcacctacttcgtggagcgcctgcaacagctcggactggcctacctccatgtaattgag
F T Y F V E R L Q Q L G L A Y L H V I E
tctcgcgtcatcaataacgtggactgcaaaaaggagggcagtatcaagttcctactcgac
S R V I N N V D C E K E G S I K F L L D
gtttgggggaaatcagcgcctgtgattggtgcccggcgatataaccagagaatgtagaa
V W G K S A P V I V A G G Y R P E N V E
aatgctttggaggaagaatacaaggactacaaggttgagtcgcctttggtcgtcattt
N A L E E E Y K D Y K V A V A F G R H F
atcgccaatcccgacttgccatttccgattcgtcatgatattcatcttaacccttacgac
I A N P D L P F R I R H D I H L N P Y D
cgagagagtttttatacacctttgcaagagaatggctacacggattacccttttagtgcg
R E S F Y T P L Q E N G Y T D Y P F S A
gaattttataaaagcaaaactaaatgctgatatt**ggatcc**
E F I K S K T K C - Y W I
BamHI

a) Cloning

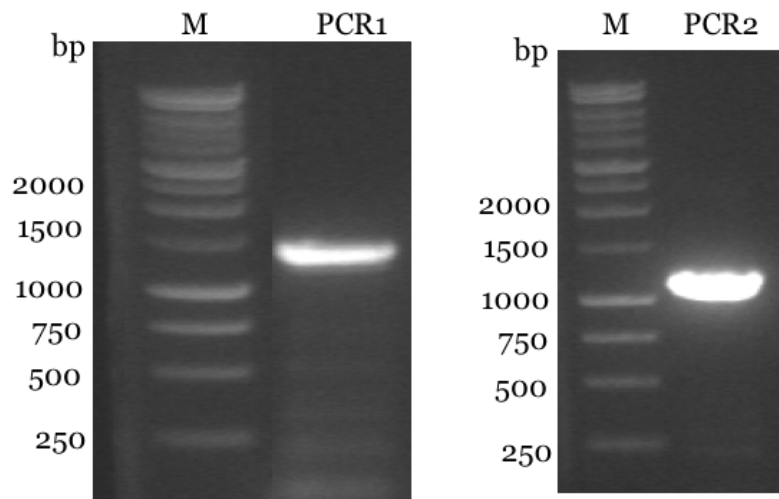


Figure 145. 1% agarose gel analysis of the preliminary 1351 bp and final 1140 bp PCR products (PCR1 and PCR2) for *AnOYE2* cloning. M: standard marker (Promega).

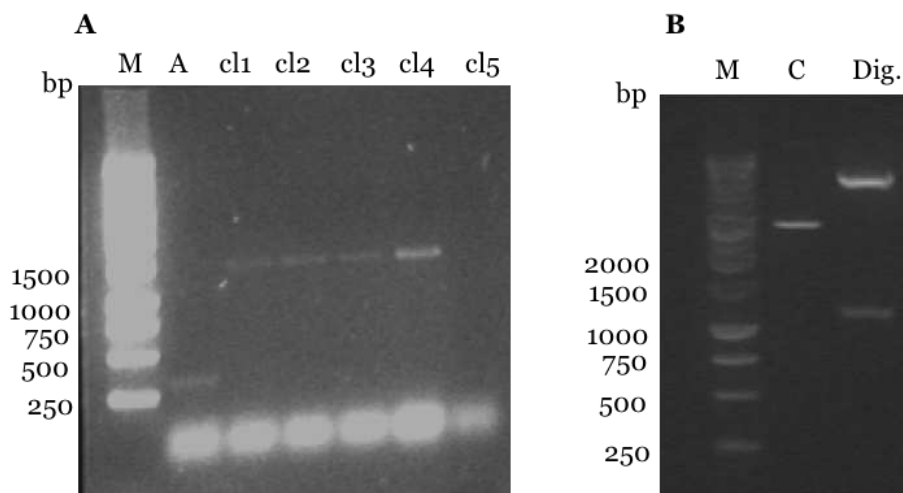
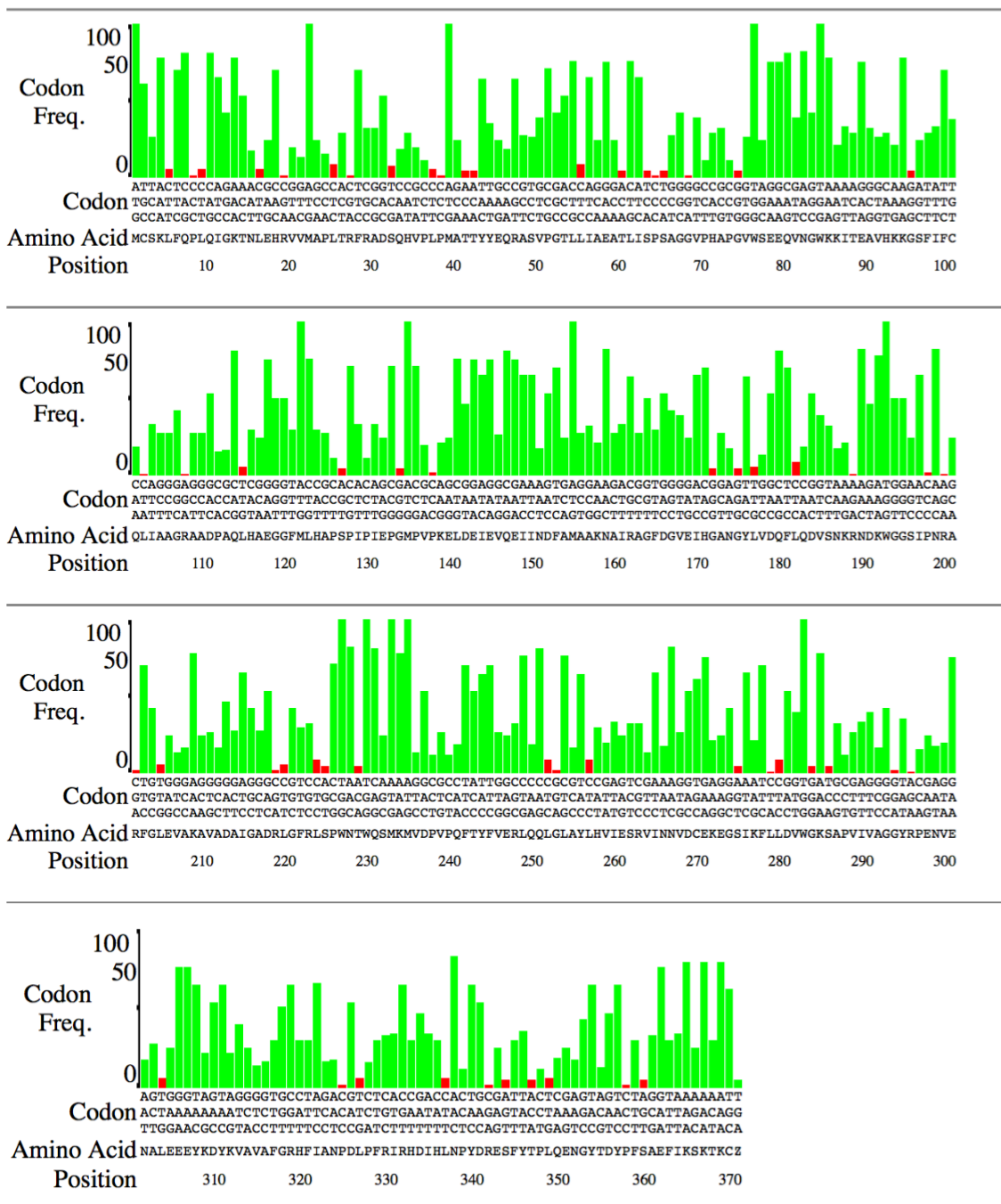
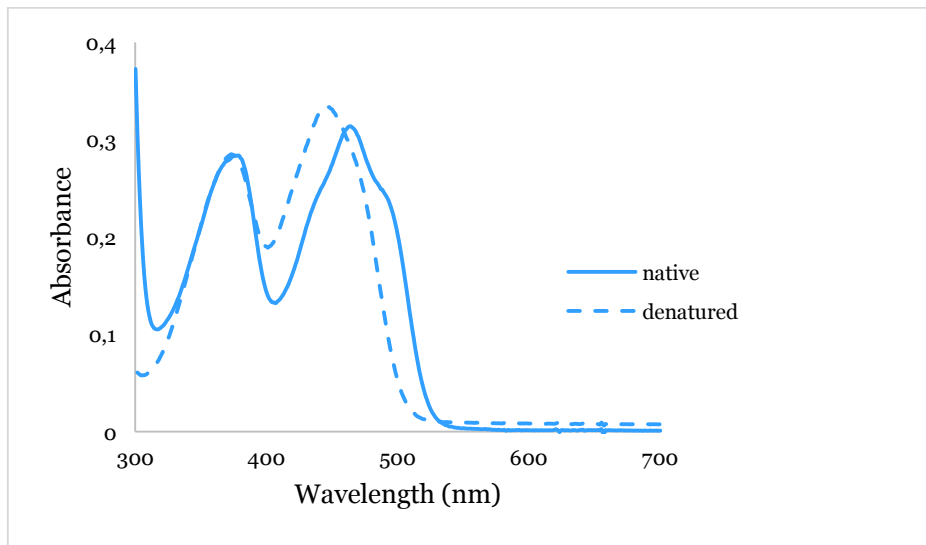


Figure 146. (A) 1% agarose gel analysis of amplimers produced by colony PCR using T7_for and T7_rev primers. A: autoligation. (B) 1% agarose gel analysis of analytical restriction digestion of pET28a-*AnOYE2* vector purified from a positive clone. C: non digested plasmid used as control, Dig.: digested plasmid with NdeI and BamHI. M: standard marker (Promega).

b) Codon usage analysis



c) UV/Vis spectrum of native and denatured *AnOYE2*



AnOYE8

>native

ATGAAGGACATCAAGGTTGAGCCCGCAAAGGGCATTTCCTACTTTACTCCTGCACAAGAAACCCAGCAGGAACAGCA
GCCAACCCGCAGACCAGTGGGAAGGCAATACCAAACTCTTCCAGCCGATTACTATTCGAGGACTAACCTTTCAGAAC
CGTCTCGGGGTAAAATAACCACTCACCCTAGATTACTGGCCTGTGCTGACAACAACCCGGTCTAGGTATCCCAATT
GCCAGTATTCGCGCAGGATGGACACATGACAGACTACCACCTCGCCACCTCGGCGGTATAGCCAGCGAGGCCAG
GCCTTATCATGATCGAGGCCACCGCCGTTCACCAGAGGGTTCGCATCTCGCCGCAGGATGTAGGGCTATGGAAAGACT
CACAAATCGCCCCAATAGCCCGAGTCATCGAGTTCGCGCATAGTCAAGGCCAGAAAATCGGCATTACAGCTTGCACG
CGGGCCGAAAGGCAAGTACTACTGTGCCATGGATGCTGAACCATGGCAGTATAGCAACAGAGAACGTCCGTGGATGGC
CCGATAACGTGAAAGGACCCAGTGATATACCCTTCAGCGAAACATTCCCGCGTCCACGAGCGATGACACAGGATGACA
TCCGCGAGTTCAGGAGGCATGGGTTGCGGCCGCGAAAAGGGCCCTTGTGCGCGGAGCAGATTTTATTGAAATTCATA
ATGCGCATGGGTATCTGCTTGCATCGTTTTTTGACCCCTTACGCAAACAAGCGGACGGATGAGTATGGTGGATCCTTTG
AGAATCGAATGCGATTGCCGTTGAAGATTGCGCAATTGACTCGCGATACGGTGGGTGAGCATGTACCTGTTTTTCTGC
GCCTTTCGGCGTCGGATTGGCTGGGTAGCACTTCGACAGAACTGGGACCTGCAGCATGCGGTGCGATTTGCTGAAG
CATTGGCCGATCAAGGGGCTATCGATCTGGTTGATGTTTCTTCTGGCGGTTTGCATTCCAGTCAAGAGGTGAAATCCG
GGCTGGGTTTCAGGCACCGTTTTGGTATTGCGGTTAAGAAGGCGGTTGGGGAAAGGATGCTTGTGCGACTGTTGGTC
ATATCAGAGACGGGAAGCTGGCAAACCGGCTGCTCGAAGAAGAAGGACTGGATGTAGTCCCTTGTGCGGCGTGGGTTT
AGAAAGATCCCGGATTGGTTTTGGACCTTTGCGCAGCATCTTGATGTCGAGGTTGCTATGCCAGGCCAGATTTCGCTGG
GATTCCTCAAACAAGGACGGAGGGGGACGCCCTTTGTCGATCCGTCGGTCTACAAACCCCTCAGTCATAGAATAA

>sequence after of removal of intron

ATGAAGGACATCAAGGTTGAGCCCGCAAAGGGCATTTCCTACTTTACTCCTGCACAAGAAACCCAGCAGGAACAGCA
GCCAACCCGCAGACCAGTGGGAAGGCAATACCAAACTCTTCCAGCCGATTACTATTCGAGGACTAACCTTTCAGAAC
CGTCTCGGGGTATCCCAATGTGCCAGTATTCGCGCAGGATGGACACATGACAGACTACCACCTCGCCACCTCGGC
GGTATAGCCAGCGAGGCCAGGCCCTTATCATGATCGAGGCCACCGCCGTTCACCAGAGGGTTCGCATCTCGCCGCAG
GATGTAGGGCTATGGAAAGACTCACAAATCGCCCCAATAGCCCGAGTCATCGAGTTCGCGCATAGTCAAGGCCAGAAA
ATCGGCATTACAGCTTGCACGCGGGCCGAAAGGCAAGTACTACTGTGCCATGGATGCTGAACCATGGCAGTATAGCA
ACAGAGAACGTCCGTGGATGGCCGATAACGTGAAAGGACCCAGTATATACCTTCAGCGAAACATTCCTCCGCTCCA
CGAGCGATGACACAGGATGACATCCGCGAGTTCAGGAGGCATGGGTTGCGGCCGCGAAAAGGGCCCTTGTGCGCGGA
GCAGATTTTATTGAAATTCATAATGCGCATGGGTATCTGCTTGCATCGTTTTTTGACCCCTTACGCAAACAAGCGGACG
GATGAGTATGGTGGATCCTTTGAGAAATCGAATGCGATTGCCGTTGAAGATTGCGCAATTGACTCGCGATACGGTGGGT
GAGCATGTACCTGTTTTTCTGCGCCTTTTCGGCGTCGGATTGGCTGGGTAGCACTTCGACAGAACTGGGACCTGCAG
CATGCGGTGCGATTTGCTGAAGCATTGGCCGATCAAGGGGCTATCGATCTGGTTGATGTTTCTTCTGGCGGTTTGCAT
TCCAGTCAAGAGGTGAAATCCGGGCTGGGTTTCAGGCACCGTTTTGGTATTGCGGTTAAGAAGGCGGTTGGGGAAAGG
ATGCTTGTGCGACTGTTGGTCATATCAGAGACGGGAAGCTGGCAAACCGGCTGCTCGAAGAAGAAGGACTGGATGTA
GTCTTGTGCGGCGTGGGTTTCAGAAAGATCCCGGATTGGTTTTGGACCTTTGCGCAGCATCTTGATGTCGAGGTTGCT
ATGCCAGGCCAGATTTCGCTGGGGATTCTCAAACAAGGACGGAGGGGGACGCCCTTTGTCGATCCGTCGGTCTACAAA
CCCTCAGTCATAGAATAA

>recombinant sequence

atgggacgagcagc**catcatcatcatcatcac**agcagcgggc**ctggtgcccgcgcccagccat**
M G S S H H H H H S S G L V P R G S H
atgaaggacatcaaggttagccccgcaaagggcatttcctactttactcctgcacaagaa
M K D I K V E P A K G I S Y F T P A Q E
acccagcaggaacagcagccaaccgcagaccagtgggaaggcaataccaaaactcttc
T P A G T A A N P Q T S G K A I P K L F
cagccgattactattcgaggactaacctttcagaaccgtctcggggatcccccaatgtgc
Q P I T I R G L T F Q N R L G V S P M C
cagtattccgcccagggatggacacatgacagactaccacctcgcccacctcggcggtata
Q Y S A E D G H M T D Y H L A H L G G I
gccagcagggcccaggccttatcatgatcgaggccaccgcccgttcaaccagagggctgc
A Q R G P G L I M I E A T A V Q P E G R
atctcgccgcaggatgtagggctatggaaagactcaciaaatcgccccaatagcccagctc
I S P Q D V G L W K D S Q I A P I A R V
atcgagttcgcgcagatgtaaggccagaaaatcggcattcagcttgcgcacgcccggcca
I E F A H S Q G Q K I G I Q L A H A G R
aaggcaagtactactgtgccatggatgctgaaccatggcagtatagcaacagagaacgctc
K A S T T V P W M L N H G S I A T E N V
ggtaggatggcccagataacgtgaaaggaccagtgatatacccttcagcgaaacattcccc
G G W P D N V K G P S D I P F S E T F P
cgtccacgagcagatgacacaggatgacatccgcccaggttcaaggaggcatggggttcggccc
R P R A M T Q D D I R E F K E A W V A A
gcgaaaagggcccttgctcgccggagcagatttttattgaaattcataatgcgcatgggtat
A K R A L V A G A D F I E I H N A H G Y
ctgcttgcatcggtttttgacccttacgcaaacagcggacggatgagtatgggtggatcc
L L A S F L T P Y A N K R T D E Y G G S
tttgagaatcgaatgagattgcccgttgaagattgcccgaattgactcgcgatacgggtgggt
F E N R M R L P L K I A Q L T R D T V G
gagcatgtacctgtttttctgcgcctttcggcgctggattggctgggttagcacttcgaca
E H V P V F L R L S A S D W L G S T S T
gaaacttgggacctgcagcatgcccgtgagtttctggaagcattggccgatcaaggggct
E T W D L Q H A V R F A E A L A D Q G A
atcgatctgggtgatgtttcttctggcgggtttgcattccagtcagaggtgaaatccggg
I D L V D V S S G G L H S S Q E V K S G
cctgggtttcaggcaccggtttggtattgcccgttaagaaggcgggttggggaaaggatgctt
P G F Q A P F G I A V K K A V G E R M L
gttgcgactgtttggtcatatcagagacgggaagctggcaaacgggctgctcgaagaagaa
V A T V G H I R D G K L A N R L L E E E
ggactggatgtagtccttgctcgggctgggtttcagaaagatccccgattggtttgacc
G L D V V L V G R G F Q K D P G L V W T
tttgccgagcatcttgatgtcaggttgctatgccaggccagattcgtcggggattctcc
F A Q H L D V E V A M P G Q I R W G F S
aaacaaggacggagggggacgcccctttgctgatccgctcgggtctacaaaccctcagtcata
K Q G R R G T P F V D P S V Y K P S V I
gaa**taa**cgtcagatatttatcttttcatgtacga**aagctt**
E - R R V F I F S C T K L
HindIII

a) Cloning

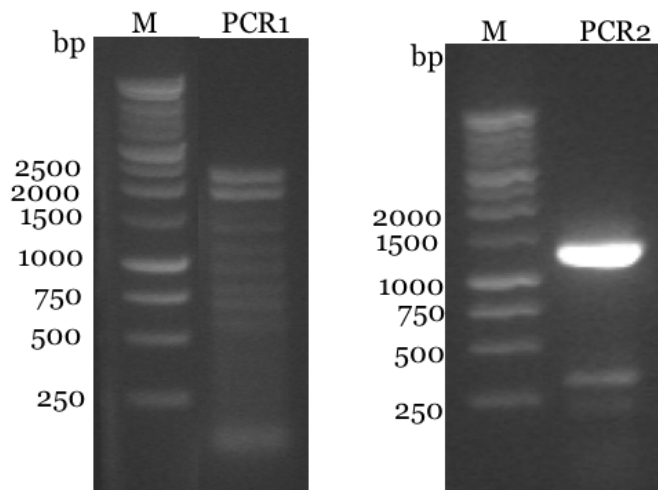


Figure 147. 1% agarose gel analysis of the preliminary 1796 bp and final 1351 bp PCR products (PCR1 and PCR2) for *AnOYE8* cloning. M: standard marker (Promega).

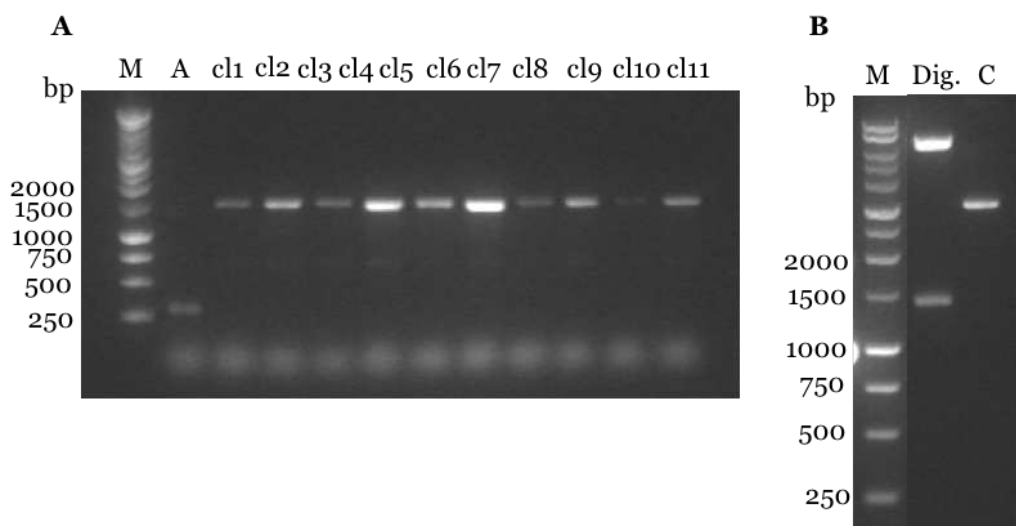
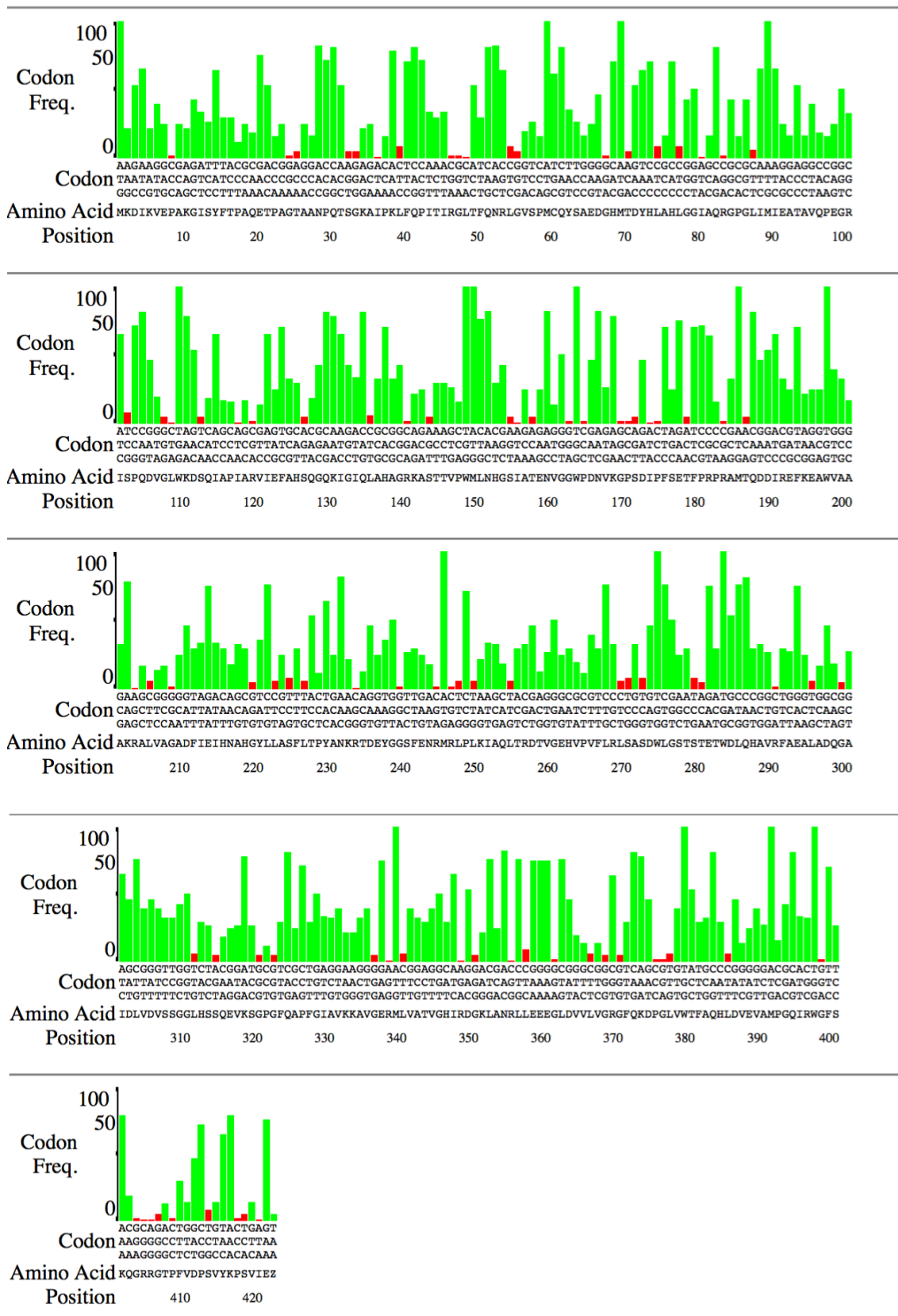
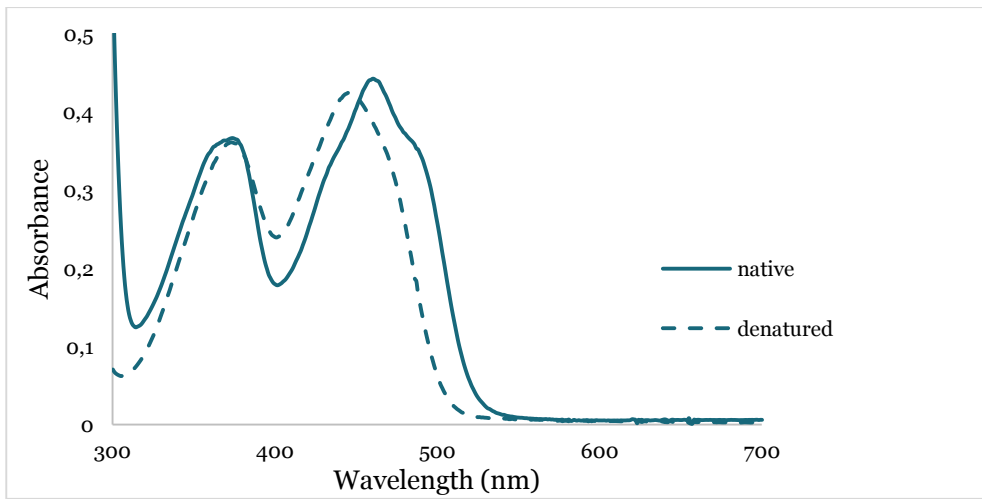


Figure 148. (A) 1% agarose gel analysis of amplimers produced by colony PCR using T7_for and T7_rev primers. A: autoligation. (B) 1% agarose gel analysis of analytical restriction digestion of pET28a-*AnOYE8* vector purified from a positive clone. C: non digested plasmid used as control, Dig.: digested plasmid with NdeI and HindIII. M: standard marker (Promega).

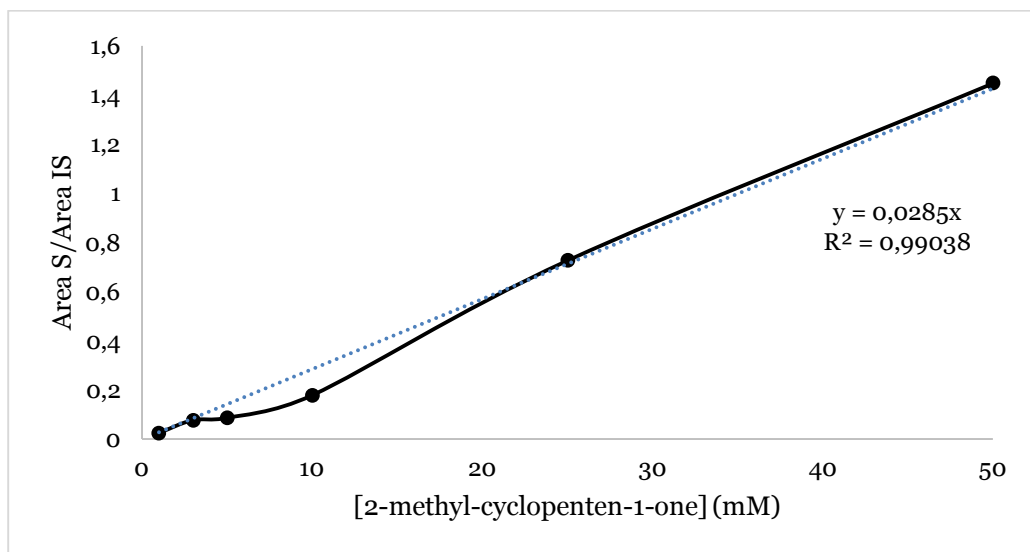
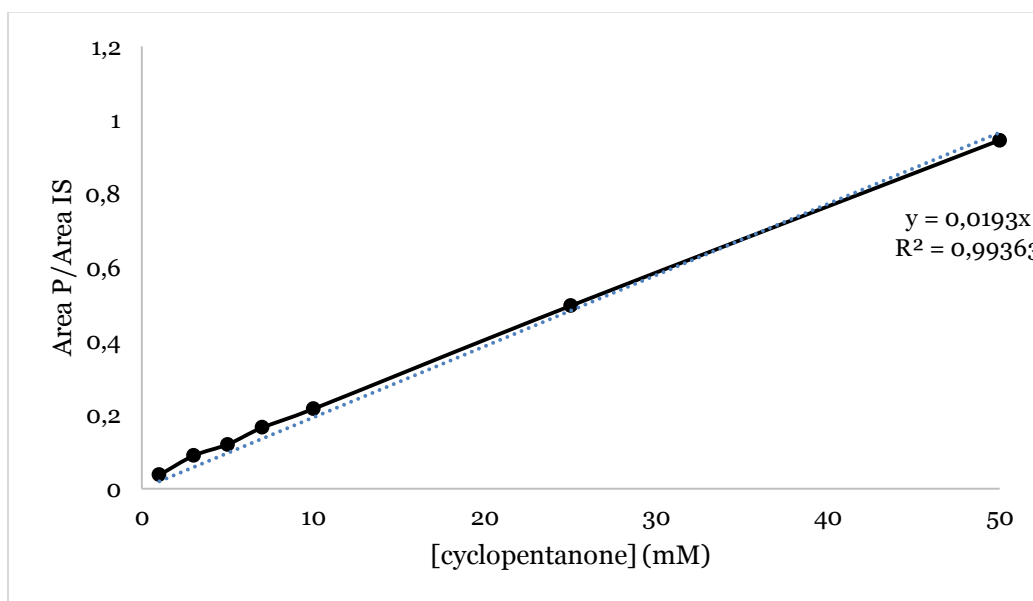
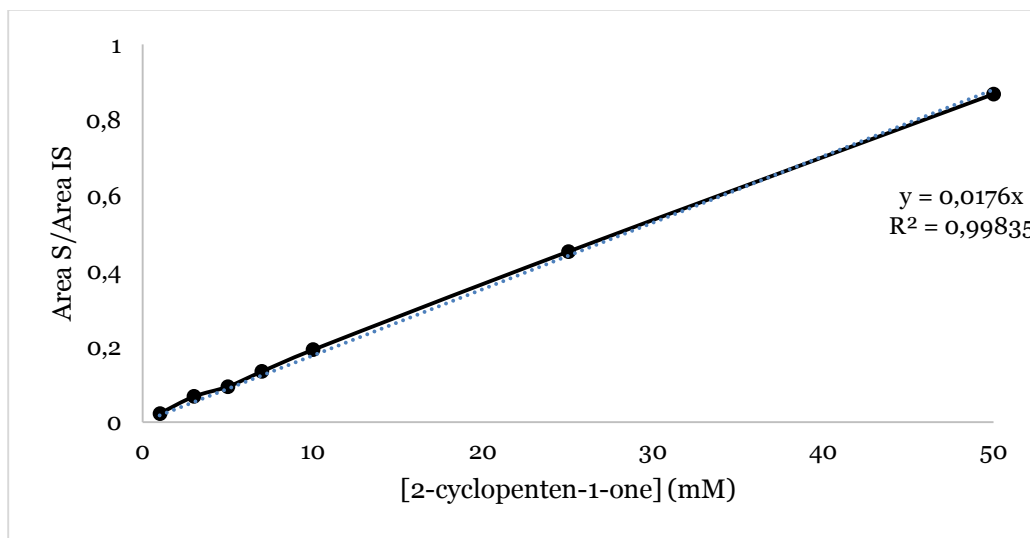
b) Codon usage analysis

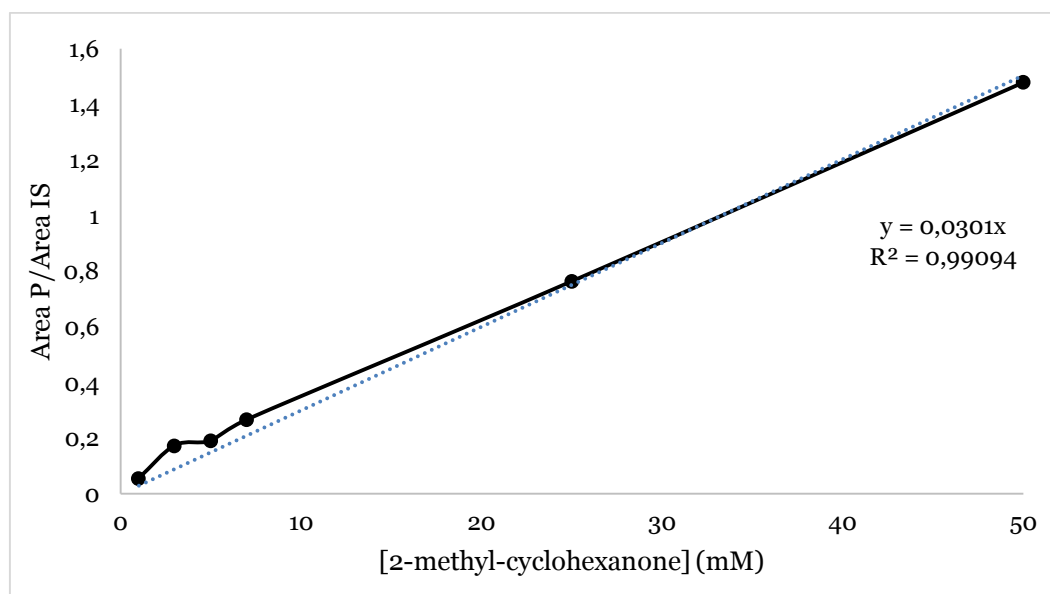
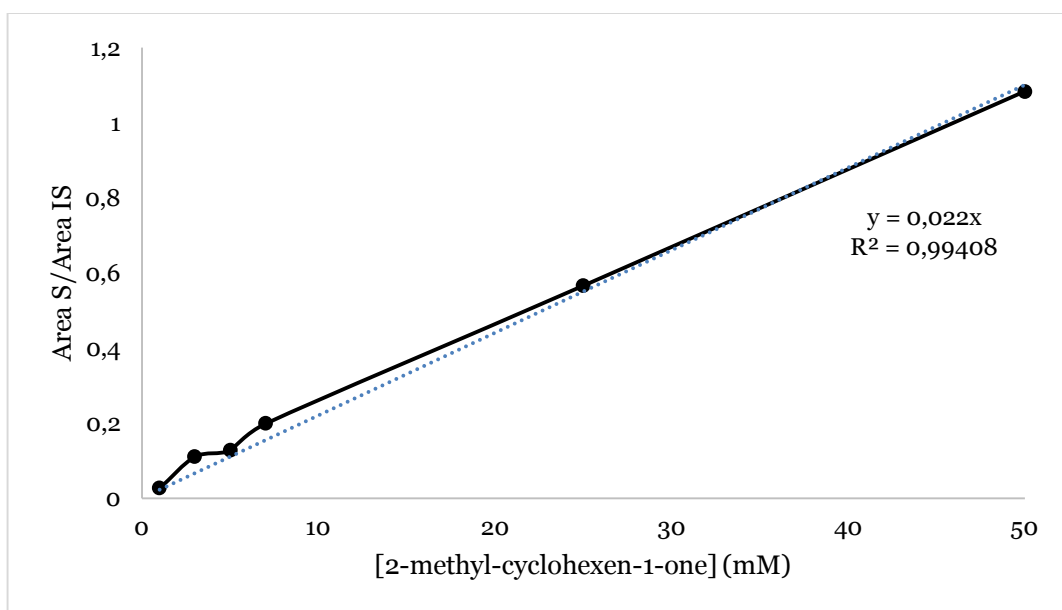
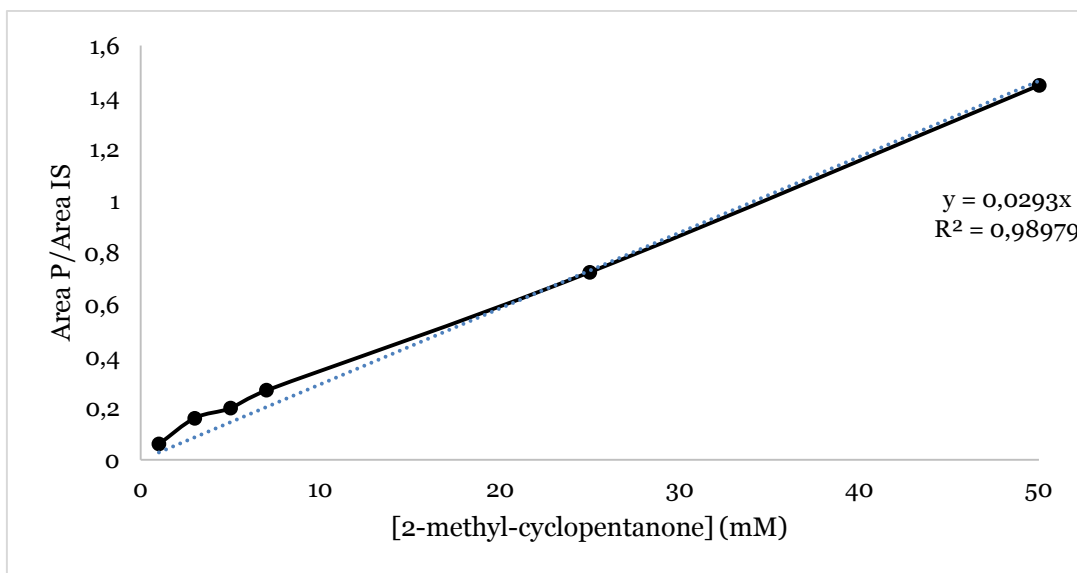


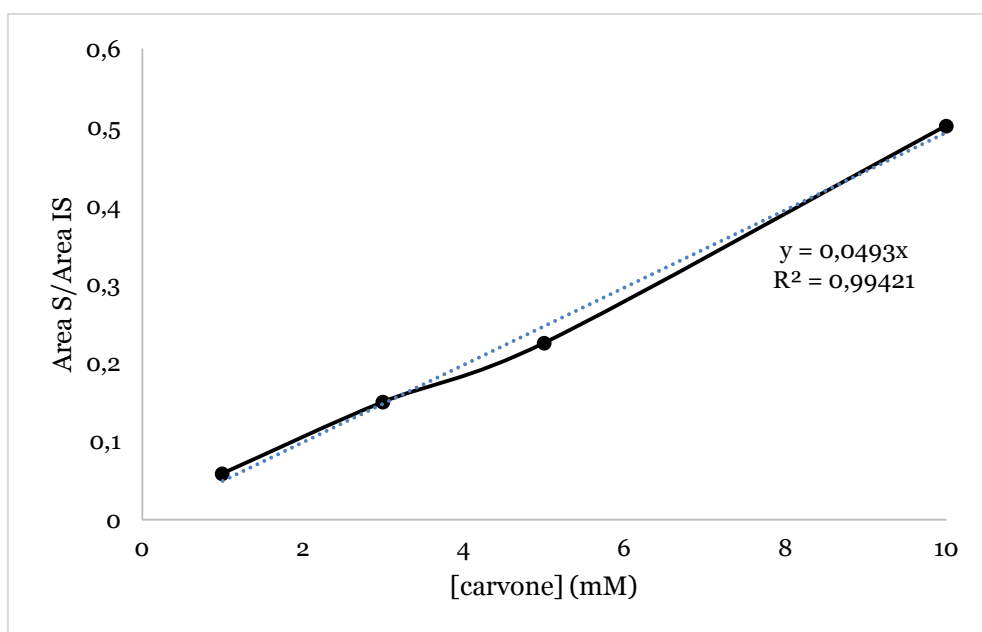
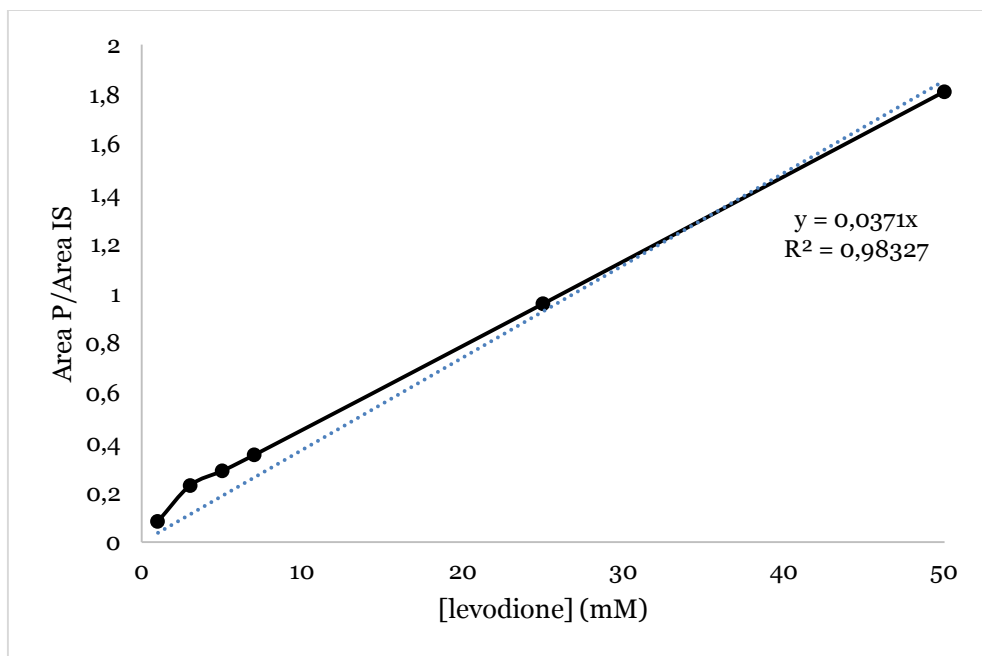
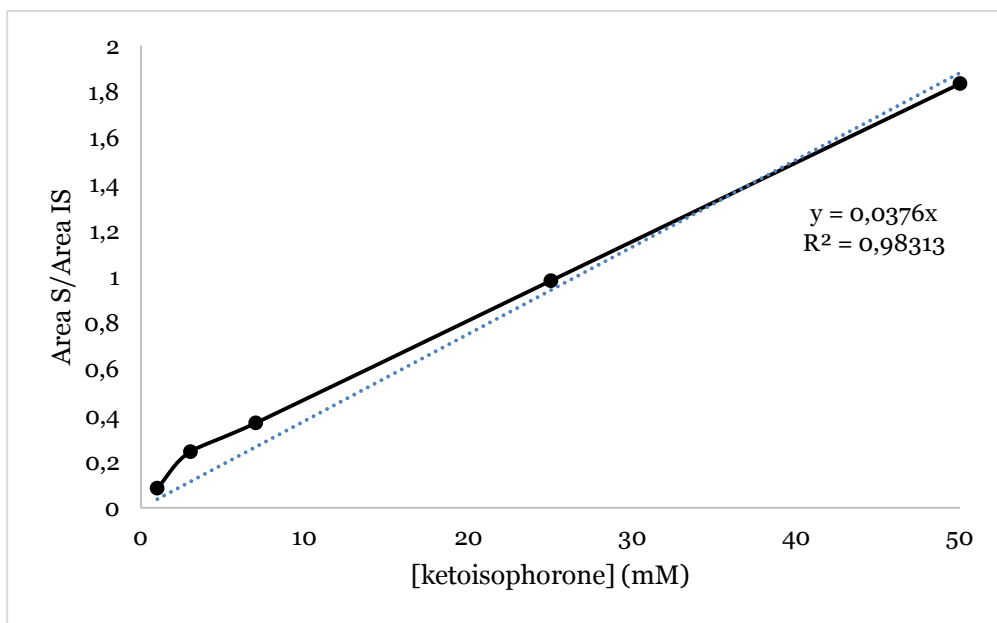
c) UV/Vis spectrum of native and denatured *AnOYE8*

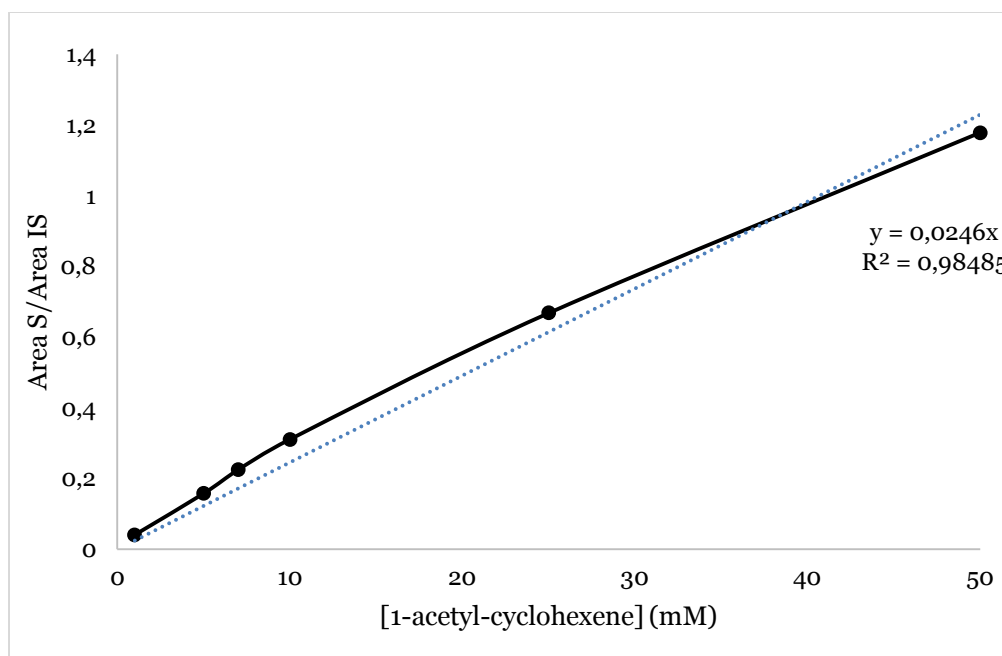
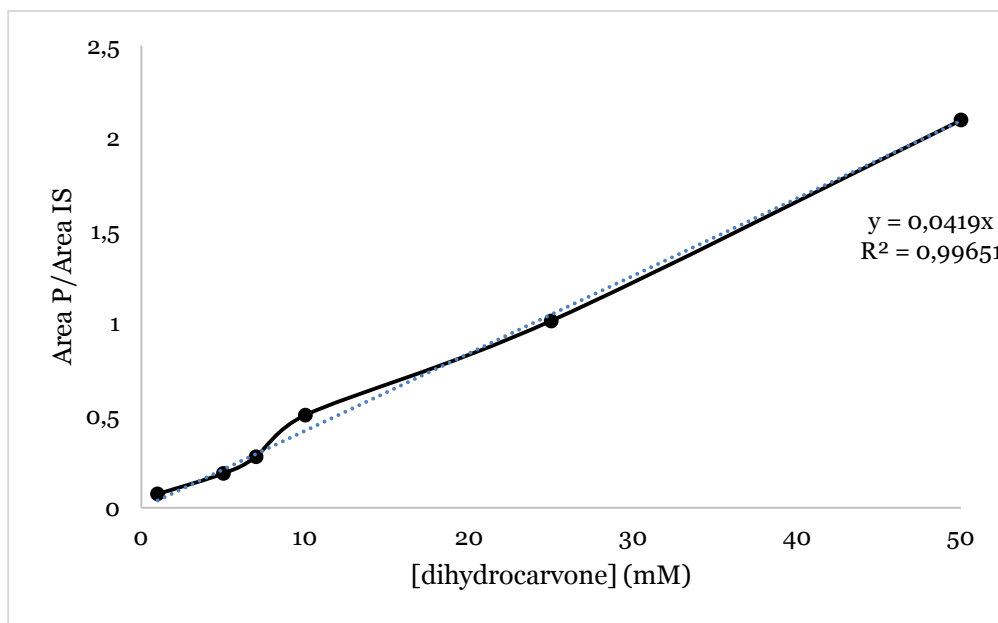


GC calibration curves









Abstract and poster congresses

List of congresses, schools and workshops

- 1) 8th International Congress on Biocatalysis (**biocat 2016**) from 28th August to 1st September, Hamburg, Germany
- 2) 3rd European Summer School on Industrial Biotechnology (**ESSIB 2016**), "Bioprocess design and optimization for the production of recombinant proteins - Concepts, tools, methods and current challenges", from 4th September to 9th September, Barcelona, Spain
- 3) Italian Forum on Industrial Biotechnology and Bioeconomy (**IFIB 2016**), from 22th September to 23th September, Vicenza, Italy ([poster presentation](#))
- 4) "International School on Biological Crystallization" (**ISBC 2017**) (Gran Hotel Luna de Granada, Spain, May 29th - June 2nd, 2017) ([poster presentation](#))
- 5) "13th International Symposium on Biocatalysis and Biotransformations" (**BioTrans 2017**), (ELTE Convention Centre, Budapest, July 9th - July 13th, 2017) ([poster presentation](#))
- 6) "Advanced Methods in Macromolecular Crystallization VIII" (**8th FEBS practical crystallization course**), (Nove Hrady, Czech Republic, June 10th-June 16th, 2018) ([poster presentation](#))
- 7) "9th International Congress on Biocatalysis" (**biocat 2018**) (Hamburg University of Technology, Germany, August 26th - 30th, 2018) ([poster presentation & lightening talk](#))
- 8) **EMBO Workshop** "Enzymes, biocatalysis and chemical biology: the new frontiers" (Pavia, September 9th - 12th 2018) ([poster presentation](#)).

Research periods in other laboratories

1. Visiting PhD Student in Professor Kurt Faber laboratory, Karl-Franzens-Universität Graz, Austria from February to April 2017 (3 months). Substrate scope of two new ene-reductases: conversion & stereoselectivity determination (GC, GC-MS, HPLC), reaction engineering.

Other achievements

- Best poster prize at 8th FEBS practical crystallization course
- Best Oral Communication of the PhD forum awarded by Professors' Jury